# Synthesis and Characterization of Non-conventional Liquid Crystals

**A Dissertation Presented in Partial Fulfillment of the Requirements for the Degree of Doctor of Philosophy at IIT Guwahati**

***by***


## Suraj Kumar Pathak

**Department of Chemistry**
**Indian Institute of Technology Guwahati**
**Guwahati-781039, Assam**
**India**


**August 2016**

*"An expert is a person who has made all*

*the mistakes that can be made in a very narrow field"*

*- Neils Bohr*

*Dedicated to my family and friends.....*

## DECLARATION

I do hereby declare that the research work embodied in this thesis entitled "***Synthesis and Characterization of Non-conventional Liquid Crystals***" has been carried out by me under the supervision of **Dr. A. S. Achalkumar** in the Department of Chemistry, Indian Institute of Technology Guwahati, Assam– 781039, India.

In keeping with the general practice of reporting scientific observations, due acknowledgements have been made wherever the work described is based on the findings of other investigators.

IIT Guwahati
August, 2016

Suraj Kumar Pathak

Dr. A. S. Achalkumar
*Associate Professor*
*Department of Chemistry*
*Indian Institute of Technology Guwahati*
*Guwahati – 781039, Assam, India*
*Phone: +91-361-258-2329*
*Fax: +91-361-258-2349*
*E-mail: achalkumar@iitg.ernet.in*
*achalkumar78@gmail.com*

## CERTIFICATE

This is to certify that the research work presented in this thesis entitled "***Synthesis and Characterization of Non-conventional Liquid Crystals***" is an authentic record of the results obtained from the research work carried out by **Mr. Suraj Kumar Pathak (Roll No. 11612229)** under my supervision in the Department of Chemistry, Indian Institute of Technology Guwahati, India. This work is original and has not been submitted elsewhere for a degree or award.

IIT Guwahati
August, 2016

Dr. A. S. Achalkumar
(Thesis Supervisor)

## ACKNOWLEDGEMENTS

The present thesis is an outcome of the years of experience, ideas generated in the form of knowledge. Over five years of my research career I have been supported and assisted by a large number of people, in regards to whom I want to convey my words for heartfelt thanks. Foremost, I would like to thank Dr. Ammathnadu S. Achalkumar whose enthusiasm and creativity has motivated all of the work in this thesis. He has given me an extraordinary amount of freedom to be creative and to work on the problems that have interested me. I've spent countless hours discussing research and ideas in science with him. Without his patience and guidance, I would not have finished this work. It was one of the best choices I have ever made to choose him as my supervisor. He is the only person who used to make me feel the sayings, “If you rest, you will rust”. He has motivated me always to do good research and to develop an interest for organic chemistry and its application in material Science.

My special thanks to our mother Indian Institute of Technology Guwahati for nurturing our research career. I express my deepest sense of gratitude and heartfelt thanks to the doctoral members Prof. Gopal Das, Dr. C. K. Jana and Dr. Sumana Dutta for their constant support and encouragement. I would like to thank all of the professors at Gauhati University who taught me the M. Sc. courses. Their genuine concern in the teachings of organic chemistry is evident in the synthesis of my liquid crystal molecules. I am greatly indebted to them. I would like to express my sincere thanks to Dr. Chandan Mukherjee for providing me his electrochemical work station for the analysis. I cannot forget the help which I got from my friend Dr. Samir Ghorai for helping in electrochemical analysis and solving single crystal X-ray diffraction data. Also I would like to acknowledge Miss. Monika Gupta, IISER Mohali for helping us with X-ray diffraction analysis and rheological studies. I would like to express my sincere gratitude and thanks to Dr. Santanu Kumar Pal, Associate Professor, IISER Mohali, Prof. D. S. Shankar Rao and Prof. S. K. Prasad, CeNS, Bangalore, for helping me with X-ray Diffraction analysis. I would like to acknowledge Mr. Avishek Banik for helping me to carry out thin film UV

studies. Of course nothing would function properly without our gifted scientific officer, Dr. Babulal Das and other non-teaching staffs, I acknowledge them gratefully. I would like to acknowledge Central Instruments Facility, IIT Guwahati for providing me the analytical facility.

It would have been impossible for me to continue my five years stay of Ph. D research without the help and support of my batchmates; I am greatly indebted to them. I would like to give special acknowledgment to my friend Mr. Subrata Nath with whom I spent many long hours planning and working in the lab and everything which we faced in the long run. He has assisted me in our newly born lab in the initial days and also in my thesis writing. I realize again that when something is done however small it is, it is not done by alone. I express my deep sense of gratitude to all my research colleagues of lab Mr. Balaram Pradhan, Mr. Ravindra Kumar Gupta and Mr. Vinod Kumar Vishwakarma for their support. I would like to thank post-doctoral fellows Dr. Nirmalangshu Chakraborty, Dr. Sachin Kumar Singh and Dr. Srikant Turlapati in sharing their experiences of life and science.

My little steps in science started from my childhood, thanks to the patience of my parents Mr. Umesh Pathak and Mrs. Kalyani Pathak in answering my constant barrage of questions. They encouraged me to pay attention to the world around me and to wonder why and how things work. I express my sincere thanks to my uncle Mr. Binod Pathak and younger brother Ratul Kumar Pathak, who is there with me being supportive all the time irrespective of situations. My deep sense of gratitude to my late grandmother and other relatives for being with me all the time starting from the beginning of my educational career.

Of course everything will go invalid if I forget the blessings of Almighty God without whom nothing will function and I pray him for his blessings.

## Curriculum Vitae of Suraj Kumar Pathak

**Present Address**

C/O: Dr. A. S. Achalkumar
Room No. T41, Brahmaputra Hostel
Department of Chemistry
Indian Institute of Technology Guwahati
Guwahati-781039, Assam, India
Phone: +91 361 2583306
Email: p.suraj@iitg.ernet.in, surajpathak6@gmail.com

**Permanent Address**

S/O: Umesh Pathak
Madhupur
Nagaon-782003
Assam, India
Mobile:+91 8723892294

**Education**

**2016** **Ph.D.** [Thesis submitted in August, 2016]
Thesis Title: Synthesis and Characterization of Non-conventional Liquid Crystals (This work was carried out between July 2011 and August 2016 at the Indian Institute of Technology Guwahati, Guwahati, Assam, 781039, India).

**2009** **Master of Science** (*in Organic Chemistry*)
Gauhati University, Assam, India

**2007** **Bachelor of Science** (*Chemistry Hons.*)
Nowgong College
Gauhati University, Assam, India

**Honors/Awards:**

Qualified GATE 2011, 2012, and SLET, ASSAM (N.E. REGION) DECEMBER 2013.

**List of Conferences/symposiums**

1. Frontiers in Chemical Sciences (FICS)-2014, 4$^{th}$ -6$^{th}$ December, Department of Chemistry, Indian Institute of Technology Guwahati.
2. 2$^{nd}$ Symposium on Advances in Sustainable Polymers (ASP-15), 21-22 January, Department of Chemical Engineering, Indian Institute of Technology Guwahati.

Some of the work described in this thesis has been reported in the following publications.

1. "Columnar self-assembly of star-shaped luminescent oxadiazole and thiadiazole derivatives" **S. K. Pathak**, R. K. Gupta, S. Nath, D. S. Shankar Rao, S. K. Prasad and A. S. Achalkumar, *J. Mater. Chem. C*, 2015, **3**, 2940-2952.

2. "Effect of regioisomerism on the self-assembly and photophysical behavior of 1,3,4-thiadiazole-based polycatenars" **S. K. Pathak**, S. Nath, R. K. Gupta, D. S. Shankar Rao, S. K. Prasad and A. S. Achalkumar, *J. Mater. Chem. C*, 2015, **3**, 8166-8182.

3. "Aromatic π–π driven supergelation, aggregation induced emission and columnar self-assembly of star-shaped 1,2,4-oxadiazole derivatives" **S. K. Pathak**, B. Pradhan, R. K. Gupta, M. Gupta, S. K. Pal and A. S. Achalkumar, *J. Mater. Chem. C*, 2016, **4**, 6546-6561.

4. "Hexacatenars Exhibiting π-π Driven Supergelation, Aggregation Induced Blue Light Emission and Thermochromism" **S. K. Pathak**, M. Gupta, S. K. Pal and A. S. Achalkumar. *Chemistry Select*, 2016, **1**, 5107 – 5120.

5. "Liquid Crystalline Star-shaped Supergelator Exhibiting Aggregation Induced Blue light Emission" **S. K. Pathak**, B. Pradhan, M. Gupta, S. K. Pal and A. S. Achalkumar, *Langmuir*, 2016**, 32,** 9301−9312.

**Articles on results not included in this thesis**

6. "Self-assembly of luminescent N-annulated perylene tetraesters into fluid columnar phases" R. K. Gupta, **S. K. Pathak**, B. Pradhan, D. S. Shankar Rao, S. K. Prasad and A. S. Achalkumar, *Soft Matter*, 2015, **11**, 3629-3636.

7. "Perylo[1,12- b, c, d] Thiophene Tetraesters: A New Class of Luminescent Columnar Liquid Crystals" R. K. Gupta, B. Pradhan, **S. K. Pathak**, M. Gupta, S. K. Pal and A. S. Achalkumar, *Langmuir*, 2015, **31**, 8092-8100.

8. "Bay-Annulated Perylene Tetraesters: A New Class of Discotic Liquid Crystals" R. K. Gupta, **S. K. Pathak**, B. Pradhan, M. Gupta, S. K. Pal, and A. S. Achalkumar, *ChemPhysChem.*, 2016, **17**, 859 – 872.

9. "Star-shaped fluorescent liquid crystals derived from s-triazine and 1,3,4-oxadiazole moieties" B. Pradhan, **S. K. Pathak**, R. K. Gupta, M. Gupta, S. K. Pal and A. S. Achalkumar, *J. Mater. Chem.C*, 2016, **4**, 6117-6130.

10. "Effect of regioisomerism on the mesomorphic and photophysical behavior of oxadiazole-based tris(N-salicylideneaniline)s: Synthesis and characterization". **S. K. Pathak**, M. Gupta, S. K. Pal and A. S. Achalkumar. (Manuscript under preparation)

11. "Columnar self-assembly of tris(N-salicylideneaniline)s based on fluorescent oxadiazole and thiadiazole derivatives" **S. K. Pathak**, M. Gupta, S. K. Pal and A. S. Achalkumar. (Manuscript under preparation)

12. "Columnar self-assembly of tris(N-salicylideneaniline)s based on fluorescent cyano stilbene derivatives" **S. K. Pathak**, M. Gupta, S. K. Pal and A. S. Achalkumar. (Manuscript under preparation)

# CONTENTS

## Chapter IV

## 1,2,4-Oxadiazole based star-shaped mesogens



## Chapter V

## 1,2,4-Oxadiazole based polycatenar mesogens



## Chapter VI

## Stilbene amide based star-shaped mesogens

## GENERAL REMARKS

All commercially obtained chemicals were used as received. As required the solvents were dried as per the standard protocols. Silica gel or neutral alumina used as stationery phase for column chromatography. Aluminium sheets coated with silica gel were used for thin layer chromatography (TLC) to monitor the reactions and column purifications. Infrared spectra were measured on a Perkin Elmer IR spectrometer at room temperature by preparing the KBr pellet. $^{1}H$ and $^{13}C$ NMR spectra were recorded using Varian Mercury 400 MHz (at 298K) or Bruker 600 MHz NMR spectrometer. Mass spectrometry was carried out using MALDI-TOF mass spectrometer (Bruker Autoflex Speed MALDI TOF/TOF Mass spectrometer) or High Resolution Mass Spectrometer. Polarizing optical microscope (POM) (Nikon Eclipse LV100POL) in conjunction with a controllable hot stage (Mettler Toledo FP90) was used for the characterization of mesogens. The phase transitions, associated enthalpy changes were obtained by differential scanning calorimeter (DSC) (Mettler Toledo DSC1). X-ray diffraction (XRD) studies were carried out using image plate and a detector. This setup had CuK$\alpha$ ($\lambda$ =0.15418 nm) radiation from a source (GeniX3D, Xenocs) operating at 50 kV and 0.6 mA in conjunction with a multilayer mirror was used to irradiate the sample. Glass capillaries containing the sample were used for the measurements. The X-ray diffraction data for single crystals were collected at 296 K with MoK$_\alpha$ radiation ($\lambda$ = 0.71073 Å) using a Bruker Nonius SMART APEX II CCD diffractometer equipped with a graphite monochromator. Smart software was used for data collection and also for indexing the reflections and determining the unit cell parameters; the collected data were integrated using SAINT software. The structures were solved by direct methods and refined by full-matrix least-squares calculations using SHELXTL software. All the non-H atoms were refined in the anisotropic approximation. Thermogravimetric analysis (TGA) was accomplished with a thermogravimetric analyzer (Mettler Toledo, model TG/SDTA 851 e). Perkin-Elmer Lambda 750, UV/VIS/NIR spectrometer was used to obtain UV-Vis spectra, while Fluoromax-4 fluorescence spectrophotometer and Perkin Elmer LS 50B spectrometer were used to obtain emission spectra in solution state and solid thin film state respectively. Steady State anisotropy

experiment was performed on Horiba Scientific Fluoromax spectrofluorometer 4. Time resolved lifetime measurements were done on time correlated single photon counter from Horiba Jobin Yvon (excitation by 440 nm laser diode). Cyclic Voltammetry (CV) studies were carried out using a Versa Stat 3 (Princeton Applied Research) instrument. Atomic Force microscopy (AFM) images were obtained for the spin-coated films using Agilent 5500-STM instrument. SEM images were obtained on a JEOL 7600F FESEM instrument. TEM images were obtained on a JEM-2100 Transmission Electron Microscope operating at an accelerating voltage of 200 kV. Rheological data is obtained using Rheometer MCR-302 Anton Paar.

## List of abbreviations used in the text

| | |
|---|---|
| anhyd | anhydrous |
| brd | broad doublet |
| brs | broad singlet |
| Cr | crystal |
| d | doublet |
| dd | doublet of a doublet |
| DMF | *N, N'*-dimethylformamide |
| DMSO | dimethyl sulphoxide |
| DSC | differential scanning calorimetry |
| equiv | equivalents |
| Et | ethyl |
| $Et_2O$ | diethylether |
| $Et_3N$ | triethylamine |
| EtOAc | ethyl acetate |
| Fig | figure |
| g | gram |
| h | hour |
| Hz | hertz |
| I | isotropic |
| ITO | indium-tin oxide |
| IR | infrared |
| J | joules |
| *J* | coupling constant |
| LC | liquid crystal |
| m | multiplet |
| MHz | megahertz |
| min | minutes |
| mmol | milli mole(s) |
| mp | melting point |
| NMR | nuclear magnetic resonance |
| N | nematic |
| N* | chiral nematic |
| p | para |
| POM | polarizing optical microscopy |
| ppm | parts per million |
| q | quartet |
| $R_f$ | retention factor |
| rt | room temperature |
| s | singlet |
| t | triplet |
| TGB | twist grain boundary |
| THF | tetrahydrofuran |
| TMS | tetramethyl silane |

| | |
|---|---|
| TLC | thin layer chromatography |
| UV | ultra violet |
| XRD | X-ray diffraction |

## PREFACE

Liquid crystals (LCs) are unique functional soft materials combining both order and mobility on molecular, supramolecular and macroscopic levels. The shape anisotropic molecules which exhibit this unique behavior are also known as mesogens. They can be organic (forming thermotropic and lyotropic phases), inorganic (metal oxides forming lyotropic phases) or organometallic (metallomesogens) in nature.

Conventionally, the anisometric molecules employed to stabilize thermotropic LC phases are either rod-like (calamitic) or disc-like (discotic). Calamitics form the backbone of the well-established flat panel display industry. Discotic LCs also have made notable progress in recent years, both from scientific and application viewpoints and slowly they are finding a foothold in the main stream of organic molecular electronics. It is also known that LC behavior is realizable with molecules differing in their shape from conventional ones. The general feature of majority of such materials is the molecular structural contrast within a molecule *i.e.*, these molecules are made up of chemically different molecular parts that are incompatible with each other. Some of the important examples of nonconventional systems are oligomers, polycatenars, bent-core molecules, polyhydroxy amphiphiles, octahedral complexes, star shaped molecules, rod-coil molecules and dendrimers. In the case of nonconventional LCs, the main driving force for the self-assembly to form liquid-crystalline (LC) phases is based on the nano-segregation of chemically or physically different building blocks and the tendency to efficiently fill the space in condensed state.

Polycatenars and star-shaped molecules, display a remarkable mesophase behavior. Compared to the synthetic difficulty associated with discotics this molecular design is advantageous due to the inherent synthetic flexibility. Thus, new types of polycatenar and star-shaped materials have been designed, synthesized and characterized. All the synthesized materials have been characterized by the requisite characterization techniques for their structural identity and thermal behavior. The results of these studies

are embodied in the present doctoral thesis, which comprises six chapters, as given below. Throughout the thesis, the potential of the synthesized non conventional liquid crystals for practical applications has been discussed intensively, for it is this prospect that inspired us to design and synthesize several novel molecular systems presented herein and technologically oriented experiments do not fall within the scope of this thesis.

**Chapter 1** This is an introductory chapter to liquid crystals in general describing their classification and their important significance in material science. The chapter focuses in greater detail on the physical properties of nonconventional liquid crystals. Beginning with an overview of thermotropic liquid crystals and their brief history, this chapter mainly focuses the major classes of columnar mesophases formed by non conventional liquid crystals, relevant mesomorphic and physical properties and finally, some applications and perspectives in material science and molecular electronics.

**Chapter 2** This chapter deals with the star shaped liquid crystals. A new class of blue light emitting liquid crystalline star-shaped molecules based on 1,3,4-thiadiazoles have been designed and synthesized. These compounds were investigated by polarizing optical microscopy, differential scanning calorimetry, X-ray diffractometry, cyclic voltammetry and photophysical studies. In comparison to their 1,3,4-oxadiazole counterparts, these thiadiazole-based molecules are promising as they stabilize the hexagonal columnar phases over a broad thermal range. Thermal behavior and photophysical properties of these new star shaped molecules were extremely dependent on the number and types of peripheral tails in the molecular structure. 1,3,4-thiadiazole derivatives exhibit sky blue emission in solution in comparison to the deep blue emission of 1,3,4-oxadiazole derivatives. They also exhibit lowered band gap in comparison to their oxadiazole counterparts and are promising for applications in organic light emitting diodes.

**Chapter 3** presents a new class of polycatenars where the central benzene ring is connected to two arms derived from substituted 1,3,4-thiadiazoles at 1,3- and 1,4-positions. These thiadiazole-based molecules are promising as they stabilize columnar

phases over a wide range in comparison to their oxadiazole analogues. *para*-Substituted polycatenars exhibited columnar hexagonal and/or columnar oblique phase, while *meta*-substituted polycatenars exhibited solely columnar oblique phase. *para*-Substituted polycatenars exhibit green emission in solution and thin film state, while the *meta*-substituted polycatenars exhibited blue emission in solution and film state. Stabilization of broad range columnar phase and luminescence in solid state make these new compounds promising from the viewpoint of applications in emissive displays. The self-assembly and luminescence of these regioisomers was greatly influenced by the molecular structure.

**Chapter 4** focuses on the synthesis and characterization of a new class of star shaped 1,2,4-oxadiazole based molecules with the variation in the number of the flexible peripheral tails. It is interesting to note that the number of peripheral flexible tails dictate the self-assembly and the photophysical behavior. The compound with three flexible tails stabilized a crystalline state with lamellar packing, and did not show organogelation, but showed blue emission in crystalline and thin film state. The compound with six flexible tails stabilized hexagonal columnar liquid crystalline state and it showed gelation in nonpolar solvents at a concentration less than 1 weight percent; qualifying it as a supergelator. The compound forms self-standing moldable gel, exhibiting aggregation-induced emission, which persisted even in xerogel state. X-ray diffraction studies revealed the rectangular columnar self-assembly of the molecules in xerogel. The supergelation driven by π-π interactions is impressive in comparison to earlier reports where this phenomenon required the support of H-bonding interactions. The columnar order and blue light emission in the liquid crystal and xerogel state makes this molecule promising for the application in emissive displays. The increase in the number of flexible tails to nine, enhanced the mesophase range; red shifted the emission in solid state and destabilized the gelation abilities. This shows how a minute structural variation impacts the molecular self-assembly.

**Chapter 5** describes two series of polycatenars comprising five rings, among which two are 1,2,4-oxadiazoles. These two series vary from each other with respect to the position at which these unsymmetrically substituted 1,2,4-oxadiazole moieties are connected to the central benzene ring. It is interesting to note that the number of flexible tails in the periphery dictated the self-assembly (liquid crystallinity and gelation) and the photophysical behavior. Their thermal behavior was analyzed with the help of polarizing optical microscopy, differential scanning calorimetry and X-ray diffraction studies. The compound with four *n*-decyloxy tails was crystalline in both series. In the *para*-substituted series, all the hexacatenars exhibited columar hexagonal phase. It is noteworthy that the hexacatenar with *n*-dodecyloxy chains showed thermochromism. The emissive nature of this compound exhibited a crossover on moving from $Col_h$ phase to Cr phase, where the $Col_h$ phase was highly emissive, while the Cr phase showed quenching of fluorescence. All the compounds of the *p*-substituted series exhibited an ability to gelate in longer chain hydrocarbons. Three of the compounds in this series exhibited supergelation, exclusively promoted by π-π interactions. This is very rare, in comparison to earlier reports where the supergelation is supported by H-bonding interactions. Besides the capability to form self-standing, moldable gel, the hexacatenar with decyloxy chains exhibited aggregation-induced blue light emission. In the *meta*-substituted series, tetracatenar with *n*-decyloxy tails was crystalline and the same is true for the compound with six *n*-octyloxy tails. Compounds with six *n*-decyloxy and *n*-dodecyloxy tails exhibited columnar hexagonal phase. The *meta*-substituted series exhibited reduced tendency to stabilize the mesophase in comparsion to *p*-substituted series. In comparison to hexacatenars based on 1,3,4-oxadiazoles, *p*-substituted hexacatenars exhibit higher ability to show mesophase, while *m*-substituted hexacatenars exhibit lower ability to form the mesophase. This observation shows the impact of the bend angle of these two regioisomeric heterocycles affects liquid crystallinity. The columnar order and emissive nature in the aggregated state makes these molecules promising for the application in emissive displays. This report emphasizes the importance of various non-covalent interactions in deciding the nature of self-assembly. Additionally this report also

highlights the beneficial effect of *p*-substitution in this class of molecules on the stabilization of supramolecular self-assemblies.

**Chapter 6** deals with the synthesis and characterization of star shaped stilbene based molecules containing an amide linkage and the investigation of self-assembly in liquid crystalline and gel state. Interestingly one of the molecules was bimesomorphic exhibiting columnar hexagonal and columnar rectangular phase, while three of them stabilized room temperature columnar hexagonal phase. The self-assembly of these molecules in liquid crystalline and organogel state is extremely sensitive to the position and number of alkoxy tails in the periphery. Two of the compounds exhibited supergelation behavior in higher hydrocarbon solvents. One of these compounds has shown higher stability and moldability in the gel state. The xerogel of this compound was characterized with the help of extensive microscopic and X-ray diffraction studies. The nanofibers in the xerogel are found to consist of molecules arranged in a lamellar fashion. This compound shows very weak emission in solution, but show aggregation induced emission property in the gel state. Considering the dearth of solid-state blue light emitting organic materials, this molecular design is promising where the self-assembly and emission in the aggregated state can be preserved. The introduction of amide bonding helps in lowering the melting point to stabilize the room temperature columnar phase and also helps in organogelation.

# Chapter I

# Introduction to liquid crystals

### 1.1. The liquid crystal state

Liquid crystals are special state of matter formed by the self-assembly of shape anisotropic molecules (mesogens). This is an intermediate state between the crystalline solid and isotropic liquid state and thus possess an intermediate order and mobility in comparison to solid and liquid states. In highly structured solid phase, the constituent molecules have no chance to move and practically reorient themselves with respect to one another and point their axes in one direction. Thus in crystals, molecules usually possess both orientation and three-dimensional positional orders. However if the same solid melts to an isotropic liquid state, the molecules tumble in all possible directions, which result in the loss of all positional and orientational order. On the other hand LC phases possess some kind of either positional or orientational order (tendency of the molecules to point along a common direction called the director **n**) due to anisotropic weak intermolecular interactions between the mesogens. The degree of organization is lesser than the solid crystalline state, but having more degree of organization than in the liquid state. In other words solid usually have both positional and orientational order, which implies that center of mass for molecules is situated at specific location and molecular axes point at certain directions. In case of liquid, there is no specific location for the center of mass of molecules as it varies, since molecules diffuse in all directions as shown in Fig. 1.1. Therefore physical properties not dependent on direction and hence this state called isotropic state. Overall, mesogens are anisotropic ordered fluids and sometimes described as "positionally disordered crystals" or "orientationally ordered liquids".[1] This special state of matter is very sensitive to external perturbations like heat, pressure, electrical and magnetic fields. The molecular mobility and the propensity to self-organize promote the self-healing processes even after the material's responses to these external stimuli. These properties make such compounds fascinating and extremely appealing for applications in materials sciences and biology.[2c-d] The field of liquid crystals started in the year 1888 when a botanist cum chemist, F. Reinitzer for the first time observed "double melting" behavior of cholesteryl benzoate[3] (Fig.1.2). This compound had two melting points, one is at 145 °C where it melted to a cloudy liquid and the other one is at 179 °C where it went

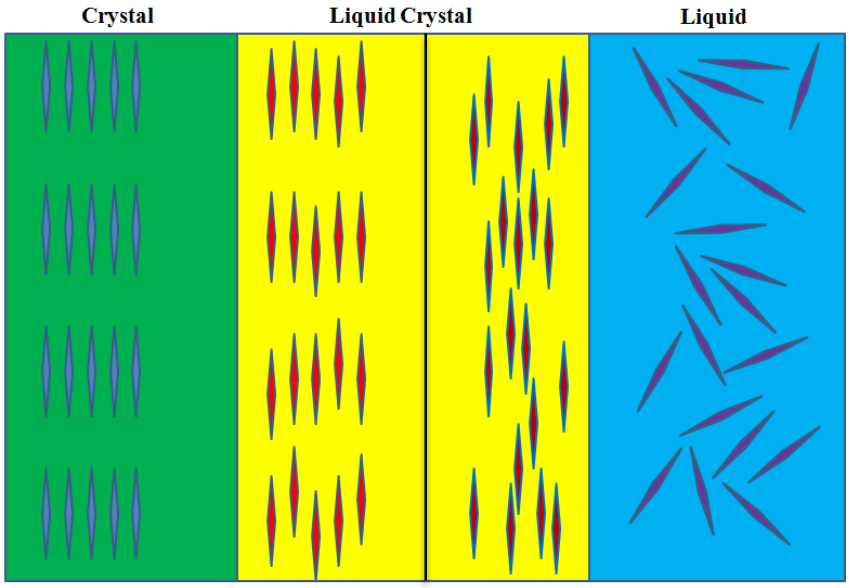


**Figure 1.1.** Basic structural difference among crystalline solid, liquid crystal and isotropic liquid.

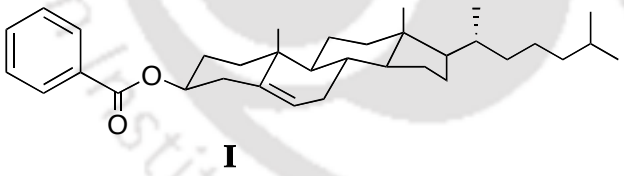


**I**

Cr 146 °C N* 178 °C I

**Figure 1.2.** Structure of cholesteryl benzoate derivatives.

to a transparent liquid. In the beginning, Reinitzer attributed this phenomenon to the presence of impurities in the material, but he observed same behavior after further purification. This behavior was further examined by the German physicist, Otto Lehmann, who was an expert in polarizing optical microscopy.[4] It was concluded that the cloudy liquid was a new state of matter and coined the term '*fluid crystal*' or '*liquid*

*crystal'* to indicate that it was something between a liquid and solid, sharing the essential properties of both.

In 1977, Chandrasekhar and his colleagues accounted that not only rod-like *i.e.* calamitic molecules, but also compounds with disc-like (discotic) molecular shape are capable to form mesophases.[5] Currently more than 3000 discotic liquid crystals are known in the literature. In 1986, liquid crystals formed by board-like (lath-like) were reported.[6] Depending on the relative size of the main axes, these molecules can be derived from rod-like or disc-like molecules. The latest addition in the liquid crystal family is banana-shaped molecules in 1996.[11] Typically, their molecular structure can be regarded as being composed of three units; an angular central unit, two linear rigid cores and terminal chains. The discovery of ferroelectricity in non-chiral banana shaped molecules has led to a very intense research activity in the field. Several hundred bent molecular shape compounds have been synthesized so far. Bent shaped molecules provide access to mesophases with polar order and supramolecular chirality. These and many other non-conventional structures exhibit interesting mesophase morphologies. Among them, one class that has attracted a particular attention is the oligomeric liquid crystals [OLCs].[9] Liquid crystalline oligomers are composed of more than two similar or different mesogenic moieties connected together via fexible spacers. The overall shape of an oligomesogen may vary from linear to star shaped, depending on the molecular topology, that is, the manner in which the mesogenic fragments are connected to each other or one another. Similarly many non-conventional molecular designs were incorporated to stabilize liquid crystallinity, which will be discussed in following sections.

### 1.2. Classification of liquid crystals

Liquid Crystals can be classified as shown in the Fig. 1.3. Broadly they can be classified into lyotropic and thermotropic liquid crystals depending on how the liquid crystalline phase has been obtained whether by adding solvent (lyotropic)[7] or by varying the temperature (thermotropic).[7a] In thermotropic liquid crystals the mesophase formation is temperature dependent, while in the case of lyotropic liquid crystals the mesophase formation is solvent and concentration dependent. Besides, there are some molecules that

exhibit LC phases under the influence of both heat and solvent; such systems have been referred as amphotropic LCs.[7c] Lyotropic LC phases are frequently encountered in everyday life, and most importantly, life itself is critically based on such ordered fluids. Despite the significance of lyotropic LCs, thermotropic LCs have claimed a relatively greater attention, firstly because they are simple to realize and easy to handle, and secondly they serve as an important medium in the fabrication of low-power devices. Since this thesis deals entirely on thermotropic liquid crystals, we limit our discussion to this topic only.

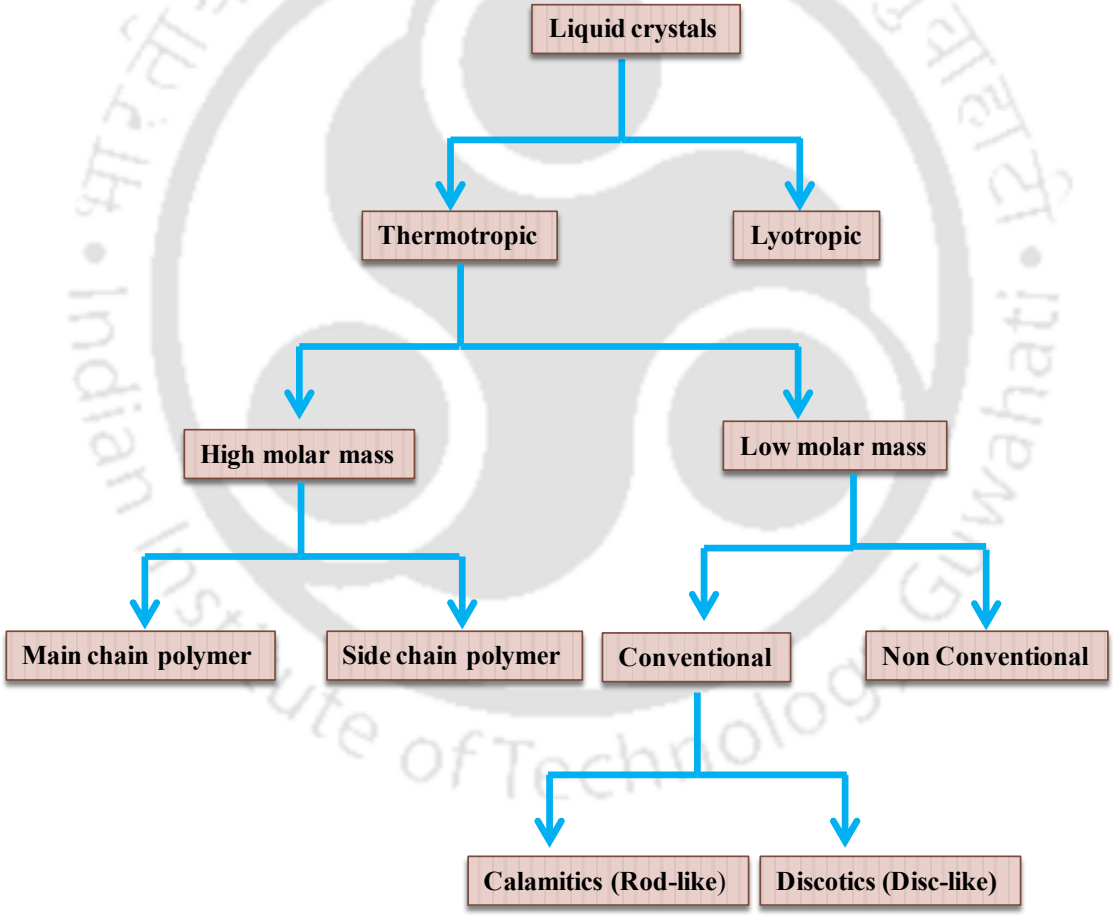


**Figure 1.3.** Schematic representation of general classification of liquid crystals.

### 1.3. Thermotropic liquid crystals

Most of the crystals on heating transform into the isotropic liquid phase by simultaneous loss of the long-range positional and orientational orders. If the molecules possess certain amount of shape anisotropy, then the disappearance in one, two or three dimensions of long-range translational periodicity in the crystals may precede the collapse of the long-range orientational order. Such compounds may show a series of mesomorphic transitions into fluid states that exhibit varying degrees of the structural symmetries. The temperature at which the crystal transforms into mesophase is called melting point, while that from the mesophase to isotropic state is called clearing point. Thermodynamically stable mesophases which appear both on heating and cooling are termed as enantiotropic, while the thermotropic mesophases that appear only on cooling are monotropic. Thermotropic LCs can be either high molar mass (polymeric) or low molar mass. Low molar mass thermotropic LCs can be classified further into conventional and non-conventional liquid crystals. [8]

### 1.4. Conventional liquid crystals

Conventionally, rod-like and disc-shaped mesogens exhibit thermotropic mesomorphism; they are popularly known as calamitics and discotics respectively. For many years it was believed that the molecule has to be long or rod-shaped molecule (Fig. 1.4a) such as 4-methoxybenzylidene-4'-*n*-butylaniline, MBBA (**II**)[9] could be mesogenic. However, in 1977 Chandrasekhar *et.al.*, demonstrated that disk-like molecules (Fig. 1.4b) such as benzene-1,2,3,4,5,6-hexayl hexaoctanoate (**III**) display mesomorphism.[5a]

Rod-like or calamitic molecules have an elongated shape *i.e*. the molecular length (l) is notably greater than the molecular breadth (h) as depicted in Fig. 1.5. The shape anisotropy in combination with microsegregation of incompatible parts in calamitic liquid crystals results in a number of mesophase structures. Most of the rod-shaped meosgenic compounds contain two or more ring structures, linked together directly or through connecting groups. They frequently have terminal hydrocarbon chains and in some cases may contain lateral substituents as well. The representative chemical structure of these molecules can be demonstrated by the general template as shown in Fig. 1.4a, where rigid core units (benzene, naphthalene, biphenyl *etc*.), R and R' are flexible moieties such as

normal and/or branched alkyl groups, X and Y are generally small lateral substituents (-$NO_2$, -$CH_3$, -$OCH_3$, -CN etc.). L is a linking group to the core units. Discotic mesophases shown by those molecules that are classically made of a central rigid conjugated core substituted by saturated aliphatic chains. These materials frequently have two, three, four or six-fold rotational symmetry. However, there are many exceptions and materials with low symmetry, a non-planar, non-aromatic core having shorter number of chains are also documented to display discotic mesophases. The mesomorphism is the result of the microsegregation of the two constituents: the face on interaction between the conjugated rigid cores promotes the crystalline character while the liquid character originates from

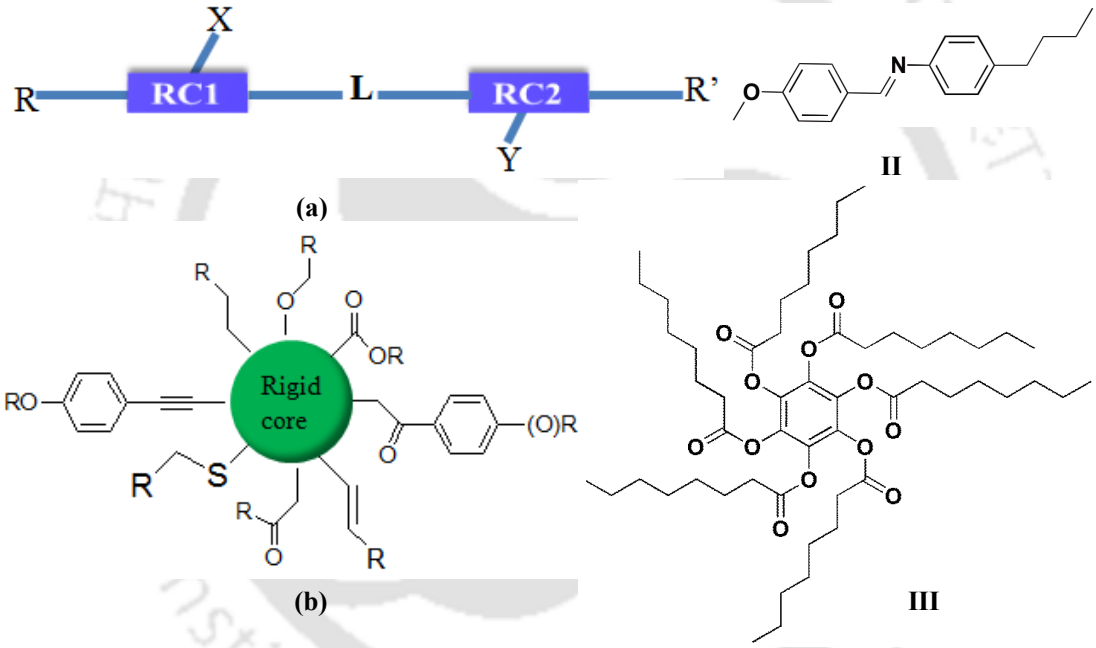


**Figure 1.4.** General templates for the rod-like (a) and disk-shaped (b) mesogens and their respective representative examples **II** and **III**

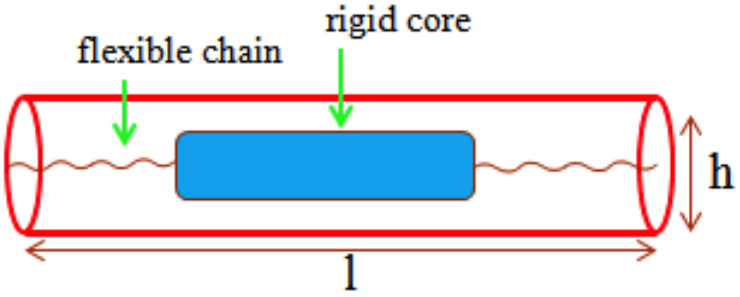


**Figure 1.5.** Representation of calamitic LCs where l >> h

the melting of the saturated peripheral alkyl chains in the mesophase. Contrary to crystalline materials, discotic liquid crystals have capacity of repairing structural defects because of the fact that, molecules in this phase organize spontaneously under the form of one-dimensional columns, which can be oriented easily and possess self-healing properties. The search for such mesophase is mostly regulated by delicate changes in the number, size and nature of the lateral chains in addition to the central core. A general template for discotic mesogens is shown in Fig. 1.4b. Most of the disc-shaped molecules display only one type of mesophase but few examples are known to exhibit polymorphism. Mesophases formed by discotic molecules are primarily of four types: (i) Nematic, (ii) Smectic, (iii) Columnar, (iv) Cubic.[5k] The columnar phase is most common in discotics followed by nematic phase whereas the other phases are rarely observed. The nematic phases of disk-like molecules can be subdivided into four types: (i) discotic nematic ($N_D$), (ii) chiral nematic ($N_D$*), (iii) columnar nematic ($N_{Col}$), and (iv) nematic lateral ($N_L$). The schematics of these nematic phases are shown in Fig. 1.6. Discotic nematic ($N_D$) phase is the least ordered, least viscous, and more symmetric mesophase among the other nematic phases.[5b] In a discotic nematic mesophase, the discotic molecules possess full translational and rotational freedom around their short molecular axis (disk normal) but on an average, the short molecular axes are oriented in a preferred direction called the director, **n**. In other words, the short molecular axes of the molecules orient more or less parallel to each other, while their centers of mass are isotropically distributed in the nematic phase. $N_D$ has the same symmetry as that of calamitic nematic but both are not miscible with one another and hence phase separation occurs owing to the fundamental structural differences. Like chiral nematic or cholesteric phase, chiral discotic nematic phase $N_D$* also exists.[5c] The mesophase occurs in mixtures of discotic nematic and mesomorphic or non-mesomorphic chiral dopants as well as in pure chiral discotic molecules.[5d] The helical structure of the chiral discotic nematic phase is shown in Fig. 1.6b. The columnar nematic phase ($N_{Col}$) is characterized by a columnar stacking of the molecules. However these columns do not form 2D lattice structures.[5e-i] They display a positional short-range order and an orientational long-range order. The columns behave like supramolecular rods and can be regarded as building blocks of the $N_{Col}$ phase instead of single molecules. Recently, another nematic phase has been reported, where the disk-shaped molecules aggregate into large superstructure, and these supramolecular aggregates show a nematic arrangement. The phase is referred as the nematic lateral

phase ($N_L$) due to the strong lateral interactions [5j-l]. Since this thesis deals with non-conventional liquid crystals, we limit our discussion to this topic only.

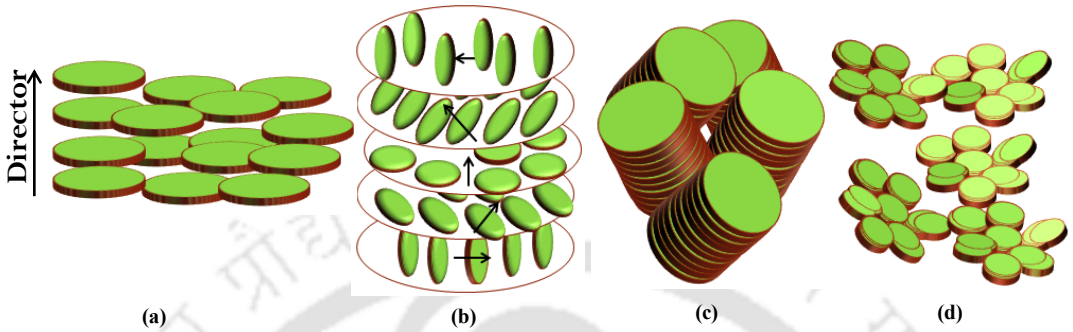


**Figure 1.6.** Structure of various nematic phases exhibited by discotic mesogens: (a) discotic nematic, (b) chiral nematic, (c) columnar nematic, and (d) nematic lateral.

### 1.5. Non-conventional liquid crystals

Driven by curiosity and also in a quest to obtain novel mesophases, a great deal of attention has been paid to the design and synthesis of several different novel molecular architectures wherein the anisometric shape deviates from the conventional rod or disc forms; they are collectively known as 'non-conventional liquid crystals'.[8] The general feature of majority of such materials is the molecular structural contrast within a molecule *i.e.*, these molecules are made up of chemically different molecular parts that are incompatible with each other. Some of the important examples of non conventional systems (Fig. 1.7) are oligomers (**IV**),[9] Polycatenars (**V**),[10] bent-core molecules (**VI**), [11] polyhydroxy amphiphiles (**VII**),[8c,d,e,12] octahedral complexes (**VIII**),[13] star shaped molecules (**IX**),[14] rod-coil molecules[15] (**X**) and dendrimers (**XI**).[16] Conventionally, mesogens are designed with shape anisotropic rigid cores, such as rods or discs, decorated with flexible chains. Whereas the latter lend the material fluidity, the first is believed to induce the anisotropic properties. In contrast, non-conventional mesogens, which have become very popular in recent years, lack such shape-anisotropy of the core unit. The driving force for the self-assembly of these molecules in liquid-crystalline (LC) phases is

based on the nanosegregation of chemically or physically different building blocks and the tendency to efficiently fill space in condensed matter. [8b,c, 17]

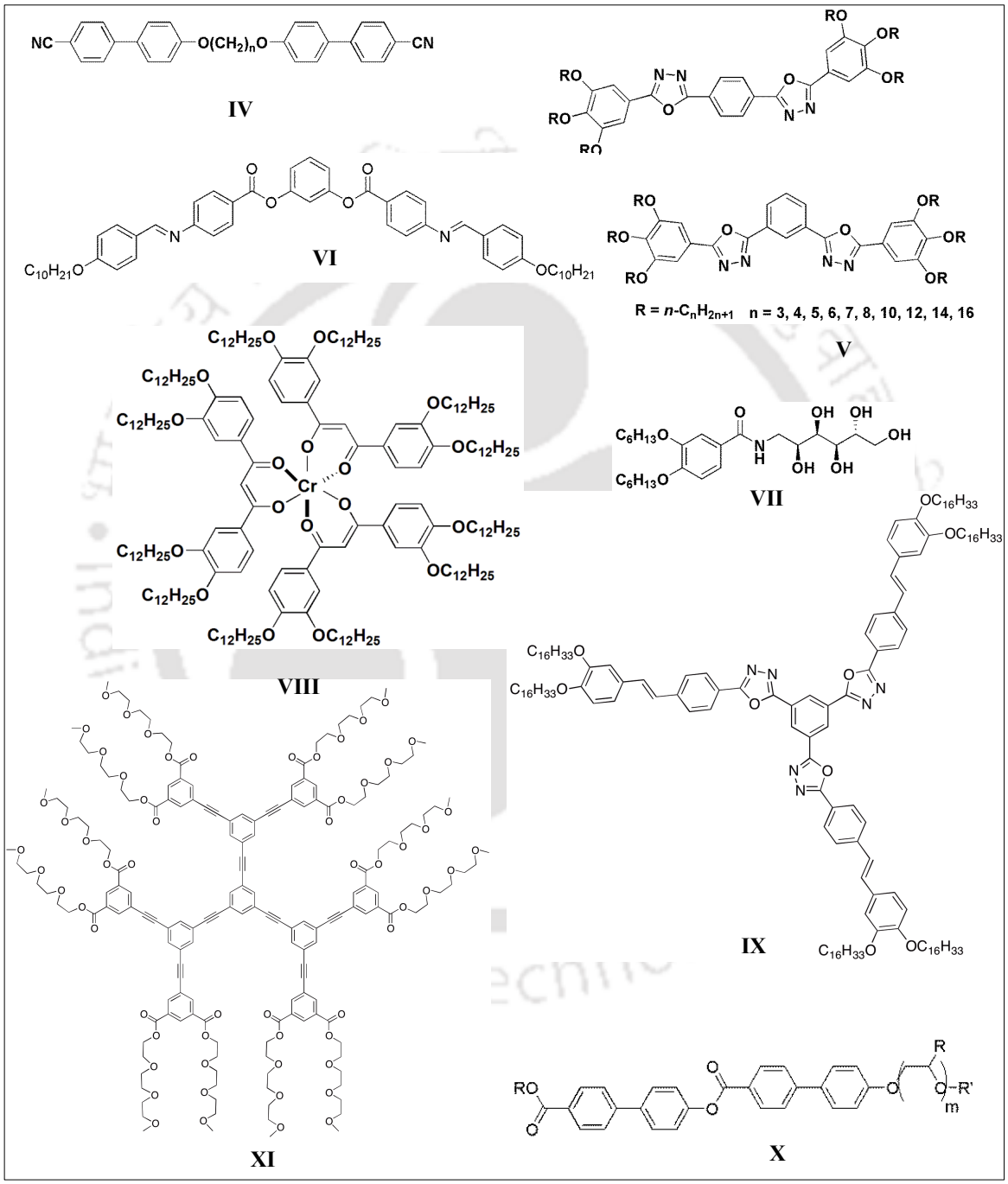


**Figure 1.7.** Molecular structures of different types of non-conventional LCs.

### 1.6. Bent-core mesogens

Though conventional thermotropic liquid crystals (LCs) are commonly made up of calamitic and disk-like molecules, the liquid crystalline phase is demonstrated by molecules with unconventional molecular structures also. One example of such a molecular architecture is a banana-shaped one, with a bend in the middle of the mesogenic part.[11] Niori *et al*.[11a] first reported the phenomenon of ferroelectricity in a smectic liquid crystalline phase which was created from achiral banana-shaped molecules. Since then, several other research groups have reported banana-shaped molecules that exhibited ferroelectric properties in the mesophase.[11n] The ferroelectricity is attributed to the polar packing of molecules with $C_{2v}$ symmetry where the molecules are packed in the same direction.

Banana-shaped mesogens are also called as bent core liquid crystals. Generally, these compounds are composed of a bent central aromatic part (*i.e.* a 1,3-disubstituted benzene) and two flexible tails. The curve in the middle of rigid core of the banana shaped compounds causes a reduction of the rotational disorder of the molecules about their long axes. The reduced symmetry of the rigid segments of such molecules leads to a directed packing of the molecules within layers. The main outcome of the directed packing of such molecules is the occurrence of a polar order parallel to the smectic layers. In order to escape from a macroscopic polarization, the layer structures are modified, and this leads to new mesophase morphologies. Bent core molecules are the first examples, which have experimentally shown that antiferroelectric switching with large spontaneous polarization in a liquid crystal phase composed of non-chiral materials. This inherent chirality can lead to mesophases with chiral supramolecular structures even though the molecules themselves are achiral. The happening of superstructural chirality in the mesophase of bent-core compounds without having any chiral auxiliary in the molecules is not only of fundamental scientific interest but also of industrial application as this chirality can be switched in response to external electric fields. Various new applications of these materials include nonlinear optics, flexoelectricity, photoconductivity, molecular

electronics and the design of biaxial nematic phase. Fig. 1.8 shows a general template of banana liquid crystal molecules.

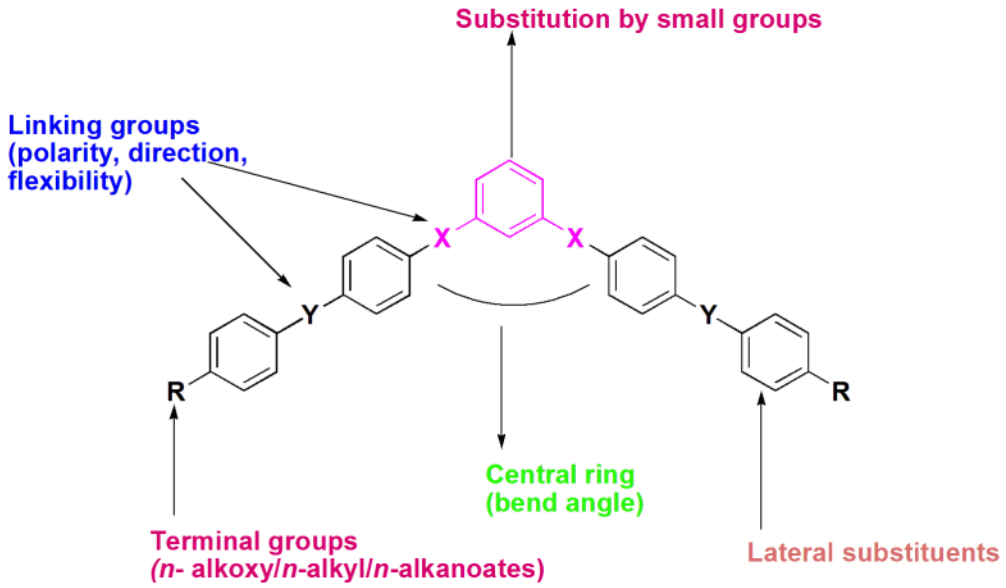


**Figure 1.8.** General template for banana liquid crystals.

## 1.7. Oligomers

Oligomeric liquid crystals (OLCs) are supramolecular liquid crystals formed by the linking of two or more than two mesogenic (functional) segments by flexible spacers. Again the individual mesogenic units can be connected axially, laterally or radially. Among them, the linear oligomeric liquid crystals (LOLCs) having the individual mesogenic segments axially connected through paraffinic spacer/s[9c] are getting increasing attention. The reasons are obvious: firstly, it is a practical approach towards the attainment of multifunctional material with increased order and processability.[9h-k] Secondly, these macromolecules can exhibit the properties related to polymers, while retaining the fluidity and viscosity of low molar mass LCs. Thirdly, if the molecule is monodisperse it will lead to well defined properties unlike in polymers. Apart from these benefits, they will provide a platform to understand the supramolecular chemistry involved in the self-assembly of shape anisotropic macromolecules and this knowledge is of great importance in material sciences. A linear addition of one more mesogenic unit to a dimer through an alkylene spacer results in the next higher LOLC namely, trimer.

Further addition of mesogenic segments results in tetramer, pentamer or hexamers and so on. Depending on the similarity of the molecular structure of the individual mesogenic units, these LOLCs can be classified as (i) symmetrical LOLCs- all the mesogenic units are identical, (ii) partially identical or $C_2$ symmetric LOLCs – some of the mesogenic units are identical and (iii) unsymmetrical LOLCs – none of the mesogenic units are identical (Fig. 1.9). The mesogenic units can be either rod like or disc like or any unconventional shape like bent systems.

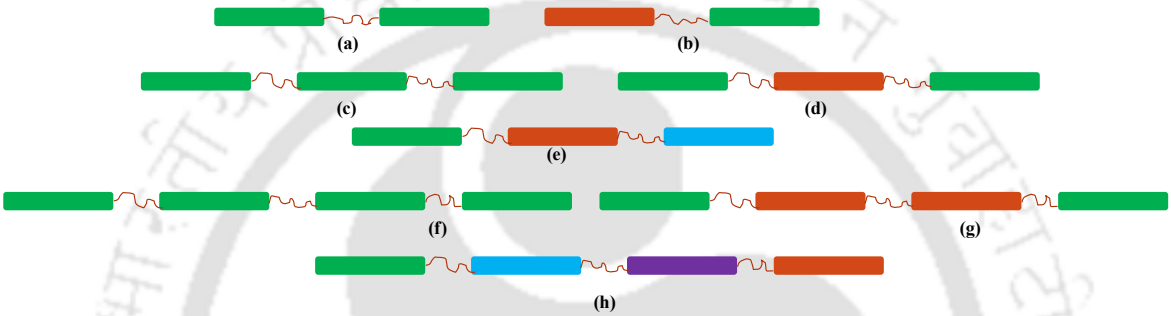


**Figure 1.9.** Schematic representation of various LOLCs: (a) symmetrical dimer, (b) unsymmetrical dimer, (c) symmetrical trimer, (d) $C_2$ symmetric or partially identical trimer, (e) unsymmetrical trimer, (f) symmetrical tetramer, (g) $C_2$ symmetric tetramer and (h) unsymmetrical tetramer. (Rectangular blocks in general represent the mesogenic segments)

## 1.8. Star-shaped mesogens (Hekates)

Conventional mesogens are designed with rod and disc shaped anisotropic rigid cores decorated with flexible chains. In contrast, star shaped liquid crystals has lack of shape anisotropy in the core unit, but this lack of shape anisotropy to exhibit mesophases is compensated by the nanophase segregation of chemically or physically different molecular subunits and their tendency of efficient space filling. The simplest multiarm mesogens that donot fall in the category of rod shaped mesogens, dimers or bananas are molecules with three arms symmetrically linked with core units, which possess $C_3$ symmetry where all arms are identical are frequently known as star-shaped mesogens or hekates[14e] as shown in Fig. 1.10. The star mesogens can be divided into three subgroups; star with three promesogens and mesogens linked to the central core with flexible spacers (**XII**) (subgroup I);[22] stars with semiflexible scaffold (**XIII**) (subgroup II)[23] and shape

persistent star shaped mesogens are obtained on connecting the three rigid arms to central core through linkers (**XIV**) (subgroup III)[14e, 24] as shown in Fig. 1.11-1.12.

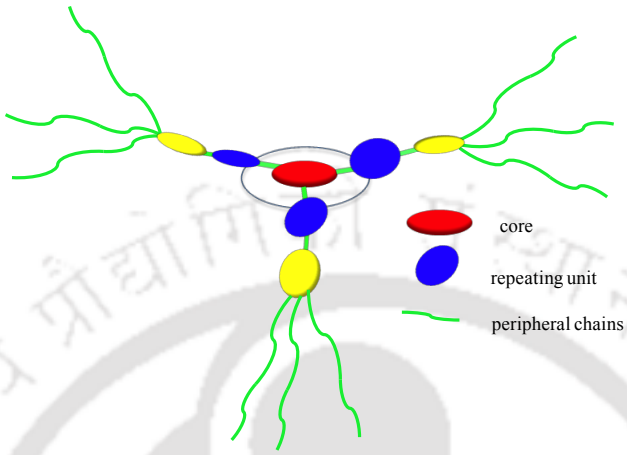


**Figure 1.10.** General structure of star shaped mesogens with three arms

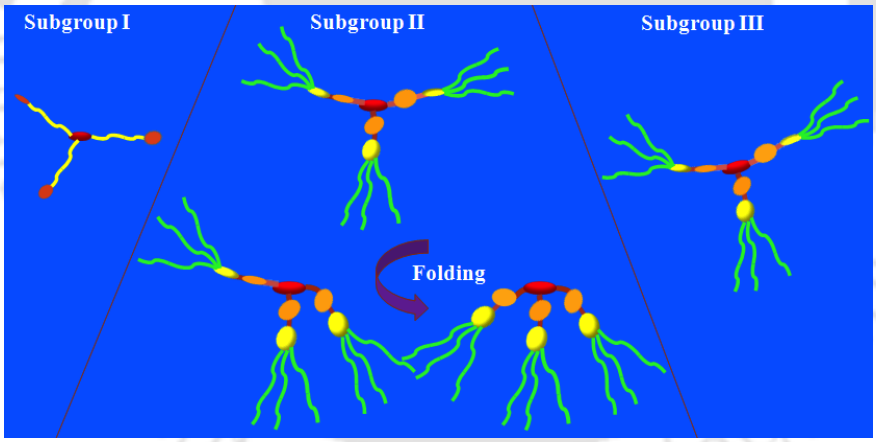


**Figure 1.11.** Classification of star-shaped three-arm mesogens

Compared to the synthetic difficulty associated with discotics this molecular design is advantageous due to the inherent synthetic flexibility. Thus the Col phases can be incorporated with other functional properties like hole or electron transport, nonlinear optical activity or fluorescence. Apart from this aspect, star shaped molecules are capable

of exhibiting a rich variety of mesophases like nematic, columnar, cubic or soft crystal phases, because of their peculiar structure and tunable molecular design. The presence of

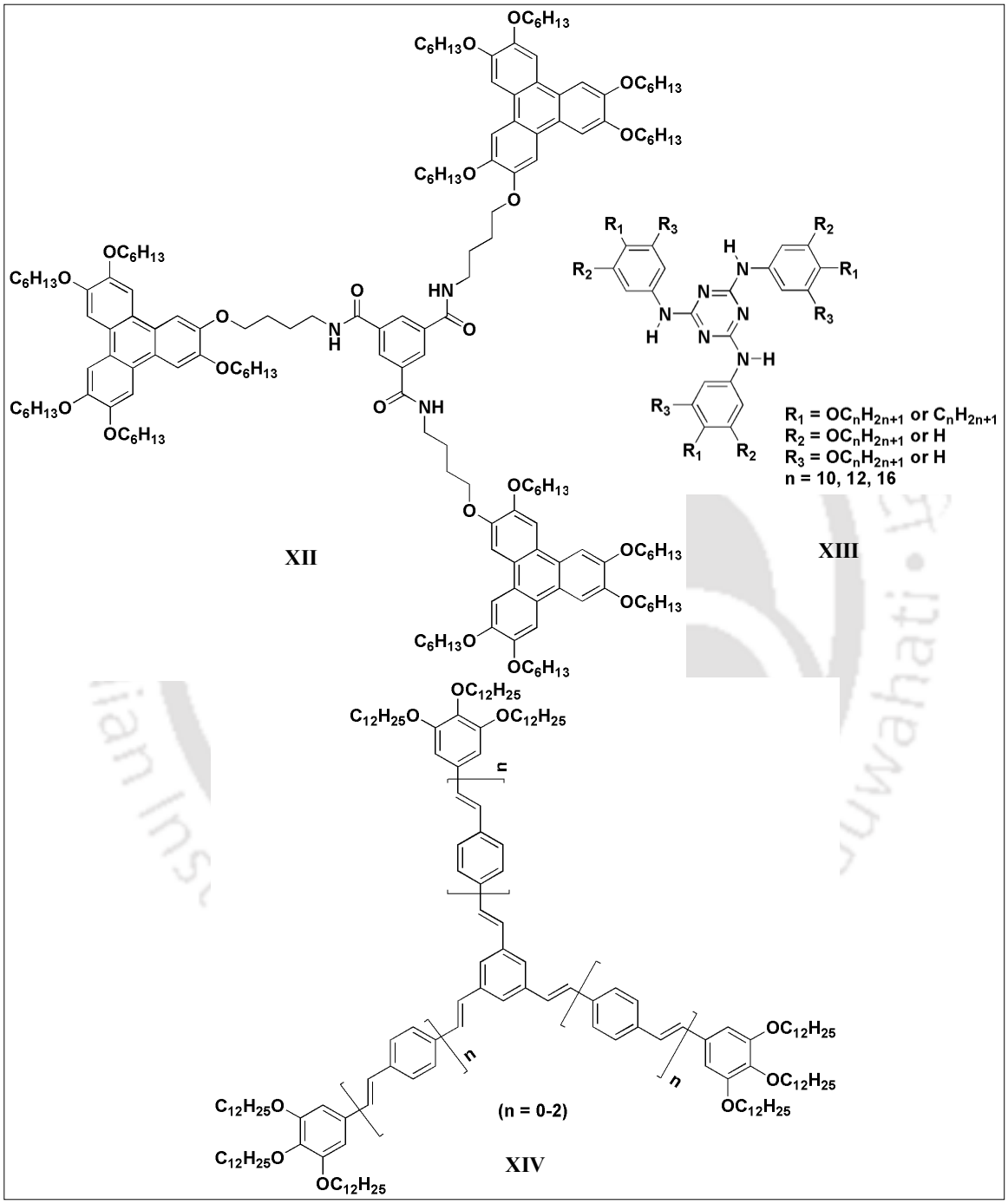


**Figure 1.12.** Flexible hekates (subgroup I)(**XII**); semiflexible hekates (subgroup II)(**XIII**); and shape persistent hekates (subgroup III)(**XIV**).

the voids between the arms of the molecular structure helps to avoid the crystallization of mesophases and promote the glassy state with the simultaneous restriction of ionic impurities. There is large void between the individual arms that has to be filled in condensed phases. Thus, a priori, one would not expect these molecules to form mesophases based on nanosegregation, since space-filling would likely lead to a mixing of core and periphery of the stars, especially in the subgroup of shape-persistent molecules (Subgroup III). The void could be used advantageously by incorporating larger chromophores in the arm scaffold by covalent bonds or guest molecules by supramolecular interactions. Complementary hydrogen-bond donors and acceptors can interact to give planar disc-shaped aggregates due to the available void between the arms of the three-armed structure. Hekates afforded Janus-type complexes (**XV**, **XVI**) (Fig. 1.13) that self-assemble to form complex columnar hexagonal structures.[14e, 25]

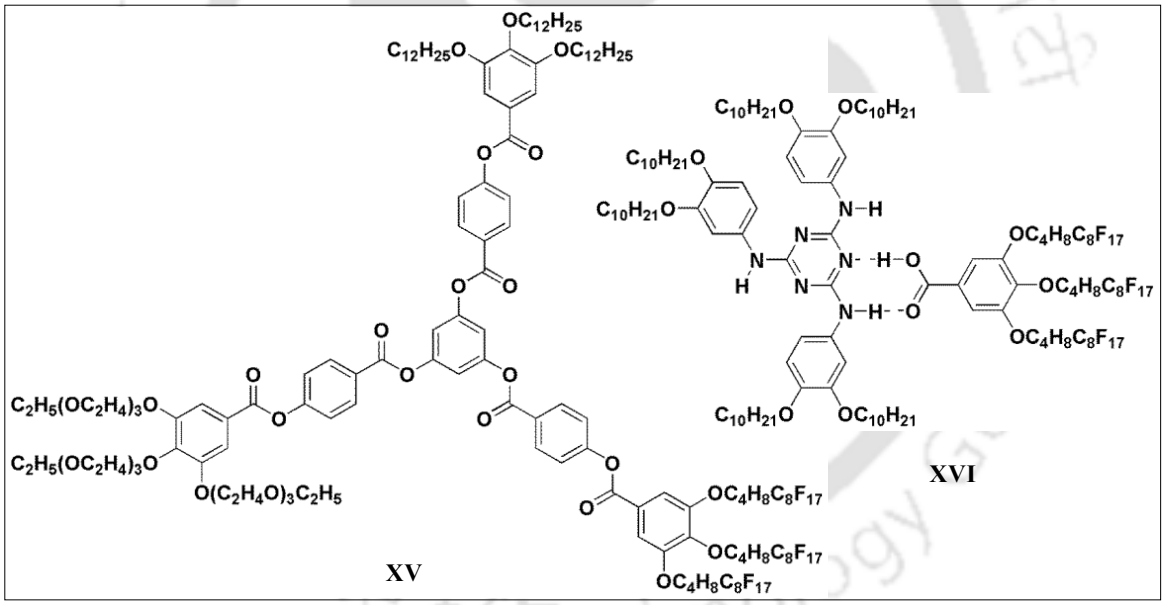


**Figure 1.13.** Janus-type hekates with incompatible peripheral chains (**XV**); Janus-type hekate forming a 1:1 host-guest complex with semi-perfluorinated chains (**XVI**).

## 1.9. Polycatenars

Over the years there are many unconventional designs that stabilize Col LC phase has been reported that vary from the conventional disc like design. Polycatenar mesogens

or phasmids are regarded as the connecting link between conventional rod like (calamitics) and disc like (discotics) mesogens as they possess the structural features and exhibit rich mesomorphic behavior common to both class of conventional LCs as shown in Fig. 1.14.[10, 26] With regard to the stabilization of Col phase this class of molecules are advantageous due to their lower melting/clearing point which helps in the alignment and the inherent synthetic flexibility to incorporate various functionalities, in comparison to discotics.

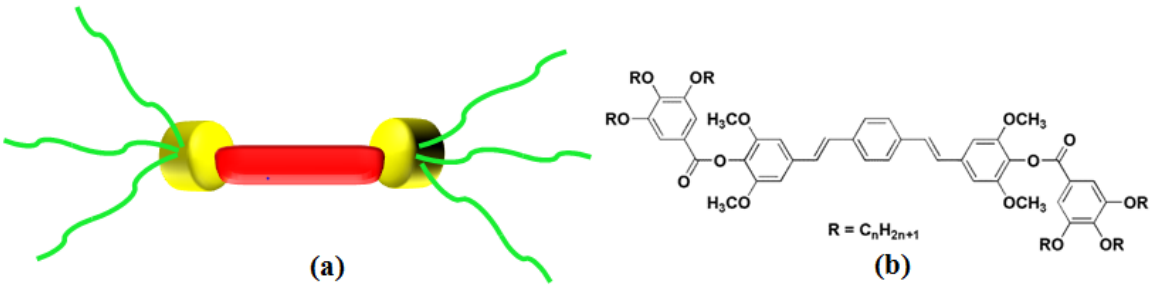


**Figure 1.14.** General structure of polycatenar mesogens (a) hexacatenar compound reported by Gin *et.al.* (b).

These molecules self-assemble into different LC phases due to the nanosegregation of aromatic units and flexible chains. Since polycatenars share the structural features of both calamitic and discotic LCs, they exhibit various LC phases like nematic, smectic (lamellar), cubic, and columnar phases, depending on the number of peripheral tails. Recently it was reported that some polycatenars based on an indigoid system (**XVIII**) even exhibited mesophases similar to bent core LC phases.[27] This synthetically flexible molecular motif can incorporate many functional moieties, so as to develop multifunctional LCs. Incorporation of an extended π-conjugated aromatic system in the polycatenar molecular structure is very important from the viewpoint of charge carrier and luminescence properties.[28] Gin *et. al.* reported a polycatenar system (**XVII**) with photophysical functions.[10g] Yelamaggad *et. al.* incorporated hydrogen-bonding oligopeptides (**XIX**) in the polycatenar structure, which stabilized a Columnar phase.[10t] Prasad *et. al.* introduced a photoisomerizable azobenzene unit (**XX**) in the polycatenar structure.[29c] There are many reports on luminescent polycatenar LCs.[28d-i]

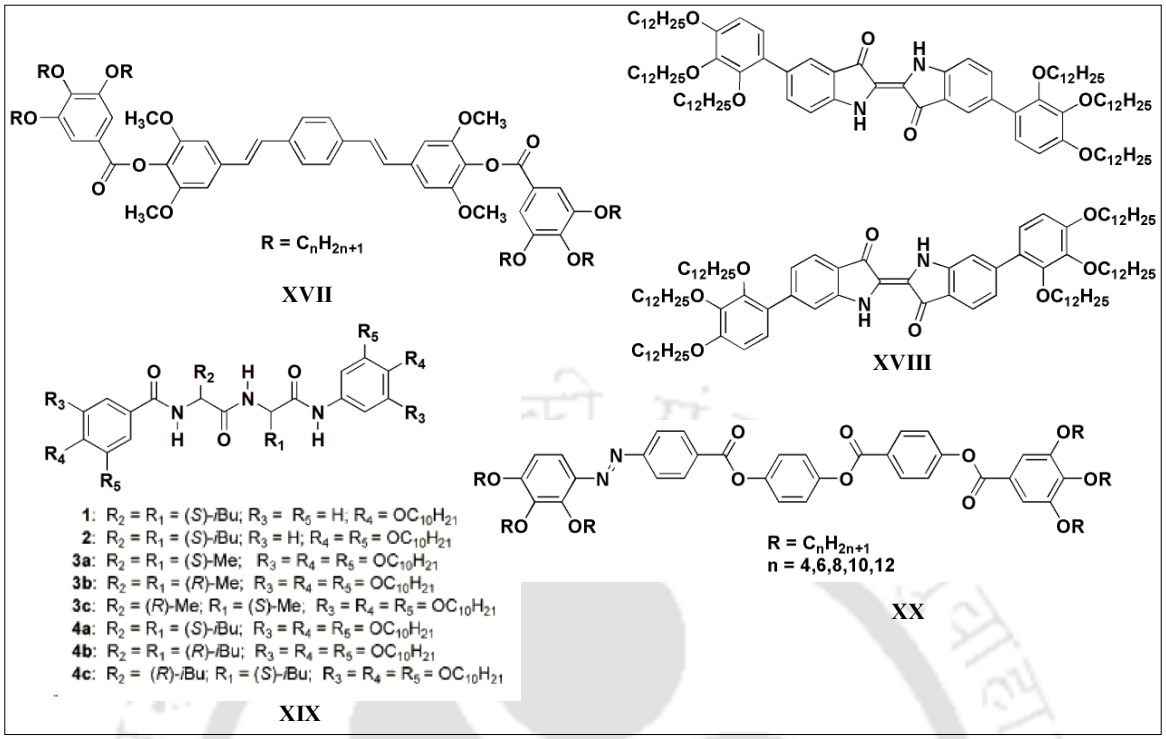


**Figure 1.15.** Molecular structures of different types of polycatenar mesogens.

## 1.10. Mesophase morphologies of thermotropic liquid crystals

Depending on the chemical structure and the shape of the constituent molecules and external parameters such as temperature and pressure, a rich variety of LC phases have been observed. In this section, columnar mesomorphism exhibited by conventional and non conventional molecules are discussed.

## 1.11. Columnar phases of conventional and non-conventional liquid crystals: phase types and structures

Depending on the degree of order in the molecular stacking, orientation of the molecules along the columnar axis, the dynamics of the molecules within the columns and the two-dimensional lattice symmetry of the columnar packing, the columnar mesophases may be classified into seven classes. (i) Columnar hexagonal mesophase ($Col_h$), (ii) Columnar rectangular mesophase ($Col_r$), (iii) Columnar oblique phase ($Col_{ob}$), (iv) Columnar plastic

phase ($Col_p$), (v) Columnar square (tetragonal) phase ($Col_{sq}$ or $Col_{tet}$), (vi) Columnar helical (H) phase, (vii) Columnar lamellar phase ($Col_L$).

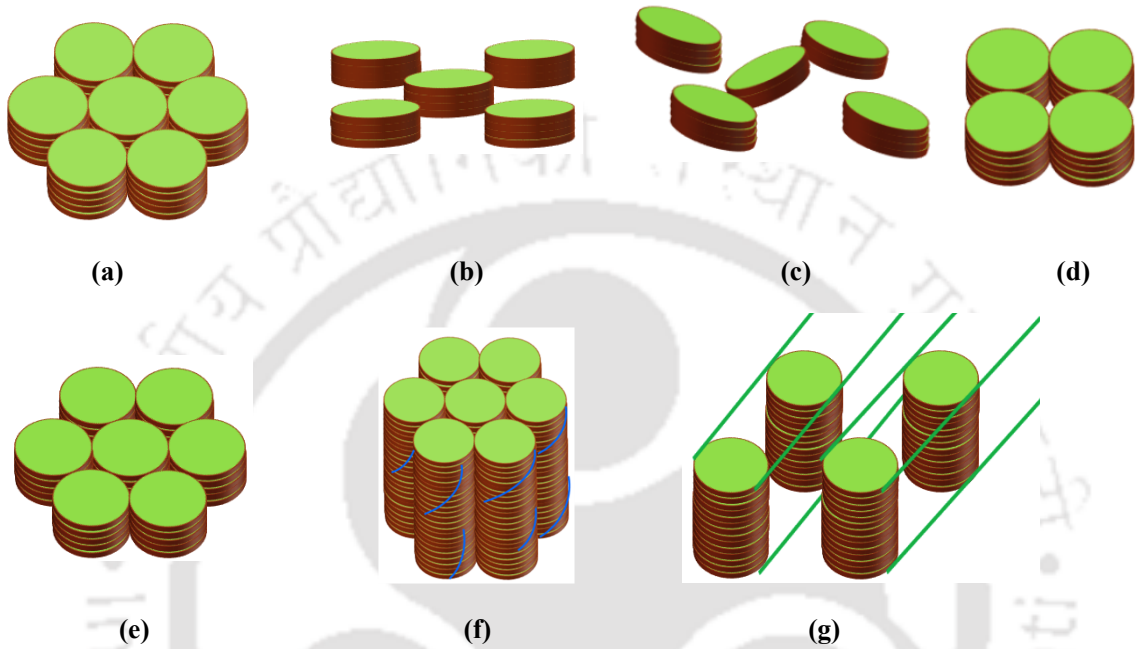


**Figure 1.16.** Schematic representation of (a) columnar hexagonal phase, (b) columnar rectangular phase, (c) columnar oblique phase, (d) columnar square phase, (e) columnar plastic phase, (f) columnar helical phase, (g) columnar lamellar phase

### (i) Columnar hexagonal mesophase ($Col_h$)

Columnar hexagonal mesophase is characterized by a hexagonal packing of the molecular columns as shown in Fig. 1.16a and Table 1.1. Hexagonal mesophases are often denoted as $Col_{ho}$ or $Col_{hd}$ where "h" stands for hexagonal and "o" and "d" for ordered or disordered stacking of the molecules. In both cases, fluidity exists; only the correlation lengths are different and, therefore, it is recommended to discontinue o and d subscripts. The recommended abbreviation for columnar hexagonal phase is "$Col_h$." The planar space group of a hexagonal columnar mesophase is *p6mm*.

The X-ray scattering profiles of a columnar hexagonal phase are given as follows. In the small-angle region, the columnar hexagonal phase generally exhibits four peaks

whose spacings are in the ratio 1:1/√3:1/√4:1/√7 along with two broad peaks in the wide-angle region. However, geometric considerations suggest that the $Col_h$ phase can, in principle, display more reflections in the small-angle region. Out of the two wide-angle reflections, one corresponds to the liquid-like packing of flexible alkyl chains and the other one, which is relatively narrow, corresponds to the intracolumnar stacking of discotic cores.[32]

**(ii) Columnar rectangular mesophase ($Col_r$)**

Columnar rectangular phase is denoted as $Col_r$ and here the columns are arranged in a rectangular pattern as shown in Fig. 1.16b and Table 1.1. The two-dimensional space group of rectangular columnar phase are *p*2*mm, c*2*mm*, *p*2*gg* and *p*2*mg* depends on the direction of the principle symmetry axis, that is direction of columns. The molecules are elliptically placed in the plane, which results in the deviation of symmetry of $Col_r$ from a proper hexagonal arrangement. For that reason, strong core-core interactions are needed for the formation of the columnar rectangular phase because the cores of one column must be tilted with respect to cores of neighbouring columns. Therefore with increasing of side-chain length, cross over from columnar rectangular to columnar hexagonal has been observed.[18]

**(iii) Columnar oblique phase ($Col_{ob}$)**

The arrangement of the columns in a columnar oblique ($Col_{ob}$) mesophase, in which the tilted columns are represented by elliptic cross sections as shown in Fig. 1.16c and Table 1.1. The symmetry of this 2D lattice corresponds to the space group *p*1. Examples of columnar oblique mesophases are rare because of strong core–core interactions.[18b,19b] Since *p*1 is a primitive planar space group, there are no reflection conditions like columnar hexagonal and rectangular phases and therefore all peaks are allowed. Hence, the assignment of the oblique mesophase by X-ray diffraction study is not so straightforward. Fan-shaped textures and spiral textures are characteristic for $Col_{ob}$ phase.[18b,19]

**(iv) Columnar plastic phase ($Col_p$)**

Columnar plastic phase is denoted as $Col_p$. This phase is characterized by 3D crystal-like order of the center of mass of the molecules, but the columns are arranged in a 2D hexagonal lattice, while the disks within the columns are able to rotate about the column axis as shown in Fig. 1.16e. In the case of $Col_h$ phase, structural disorders such as nonparallel arrangement of the disks, longitudinal and lateral displacements, and rotation around the columnar axis occur, while the motional freedom of disks in the $Col_p$ phase is restricted. The X-ray diffraction pattern of $Col_p$ phase exhibits low-angle reflections that can be indexed to a 2D hexagonal lattice. In addition, the profile for the plastic phase has reflections having mixed indices. The presence of the diffuse peak due to the alkyl chains differentiates this phase from a truly crystalline phase. The wide angle core–core reflection, which is usually diffused in the columnar phase, becomes very sharp and splits into two peaks.[20]

**(v) Columnar square (tetragonal) phase ($Col_{tet}$)**

The columnar square phase is also known as tetragonal phase ($Col_{tet}$). The structure of this phase is represented in Fig. 1.16d and Table 1.1. In this mesophase the columns are upright and they are arranged in a square lattice. Similar to columnar hexagonal phase, this phase also exhibit spontaneous homeotropic alignment of the columns. This phase is reported in few sugar molecules, phthalocyanines and supramolecular fluorinated liquid crystals.[33]

**(vi) Columnar helical (H) phase**

This exceptional mesophase structure with helical order was observed in a triphenylene derivative namely hexahexylthiotriphenylene (HHTT).[34a,b] In these helical columns, hydrocarbon chains interdigitate in groups of three columns. X-ray diffraction experiments have proved that the helical H phase is distinctive to HHTT and certain mixtures of compounds with an average chain length close to 6 carbons.[34c] The H phase found in HHTT is shown in Fig. 1.16f.

**Table 1.1.** Two-dimensional space groups of columnar liquid crystals with corresponding cross-section area and number of discoids (disc or ellipsoid) $Z_{disc}$ in a cross section.[36]

| **Type (notation)** | **Space group** | **Extinction rules** | **Cross section** | | | **Three dimensional representation** |
|---|---|---|---|---|---|---|
| | | | Schematic | Area | Discoid number | |
| Columnar hexagonal ($Col_h$) | *p6mm* | No conditions | 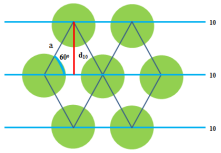 | $S = a^2 sin60^o$ | $Z_{disc} = 1$ |  |
| Columnar tetragonal ($Col_{tet}$) | *p4mm* | No conditions | 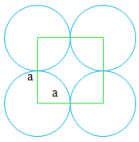 | $S = a^2$ | $Z_{disc} = 1$ |  |
| Columnar rectangular ($Col_r$) | *p2mm* | No conditions | 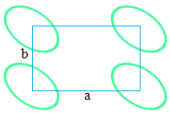 | $S = ab$ | $Z_{disc} = 1$ | 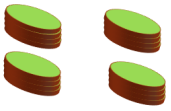 |
| | *c2mm* | *hk*: $h + k = 2n$, *h*0: $h = 2n$, 0*k*: $k = 2n$ | 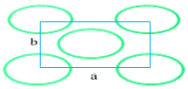 | | $Z_{disc} = 2$ | 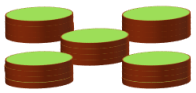 |
| | *p2gg* | *hk*: no conditions, *h*0: $h = 2n$, 0*k*: $k = 2n$ | 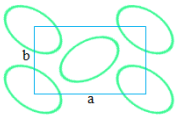 | | $Z_{disc} = 2$ | 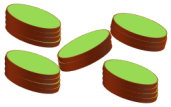 |
| | *p2mg* | *hk*: no conditions, *h*0: no conditions, 0*k*: $k = 2n$ | 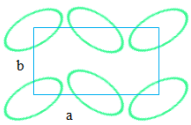 | | $Z_{disc} = 2$ | 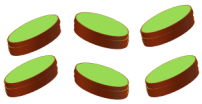 |
| | | | 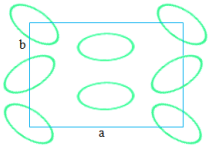 | | $Z_{disc} = 4$ | 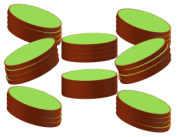 |
| Columnar oblique ($Col_o$) | *p*1 | No conditions | 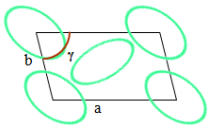 | $S = absin\gamma$ | $Z_{disc} = 2$ | 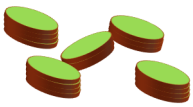 |

**(vii) Columnar lamellar phase ($Col_L$)**

A layered structure with columnar organization is known to exist for mesophases of certain discotic compounds.[21,35] Such a columnar lamellar mesophase, which is denoted by the symbol $Col_L$, is shown in Fig. 1.16g. In this phase, discotic molecules stack to form columns and these columns are arranged in layers, where the columns in layers can slide but the columns in different layers do not possess any positional (translational) correlation. The X-ray profile of this phase in the low angle region displays reflections whose spacings are in the ratio 1:2:3 suggesting the lamellar organization of the columns and there appears a wide angle reflection corresponding to a distance of intracolumnar separation suggesting columnar organization of molecules in the layers.

All the classical columnar mesophases included in this report are summarized in Table 1.1 with related schematics and structural parameters. The number of molecules per unit cell (or cross section) ($z$) can be estimated according to $z = \rho N_A S h_o / M$ where $\rho$ is the density of the liquid crystal phase, $N_A$ is Avogadro's constant, $S$ is the columnar cross-section area, $h_o$ is the height of the columnar slice and $M$ is the molecular weight of the constitutive molecule. $S$ can be easily calculated from the cell parameters, keeping in mind that its expression depends on the geometry of the cell (see Table 1.1). The number of discoids present in the unit cell ($Z_{disc}$) is characteristic of the lattice geometry and the proposed model (see Table 1.1). Consequently, the number of molecules per discoid ($N$) is easily accessible by dividing the number of molecules in the cross section ($z$) by the corresponding $Z_{disc}$ value. Therefore, a hypothesis on how mesogen molecules are eventually organized to form the discoidal shape can be formulated.

## 1.12. Identification of thermotropic mesophases

As discussed in previous sections, till date a number of liquid crystalline phases have been discovered. The structural differences between these phases are quite narrow and therefore the precise characterization of LC phases generally requires the use of different techniques.[1] The most commonly used device to identify the LC phases is the polarizing optical microscope (POM) that reveals the characteristic optical texture of a

mesophase.[1, 2a] The textures are usually examined between crossed polarizers, in white light under orthoscopic illumination; the sample is taken in the form of thin layer held between a glass slide and cover slip; the substrates are either chemically treated for homogeneous/homeotropic alignment or used without any pretreatment. Calorimetric study using differential scanning calorimetry (DSC) is a complementary tool to microscopic studies to know the precise phase transition temperature and the enthalpy change associated with the transition. However there are limitations in mesophase characterization by either of these methods as the optical textures of different smectic or columnar phases are difficult to distinguish and the enthalpy values cannot be so characteristic for different phase transitions. Sometimes miscibility studies, in which a well known liquid crystal phase is physically mixed with an unknown phase to ascertain the nature of the phase, are carried out based on the criterion of complete miscibility of identical phases.[2b] For unambiguous identification of mesophases, structural information such as relative molecular positions, the presence of long-range positional order, the quality of preferred molecular orientation *etc*., can be obtained from diffraction studies. X-ray, electron and neutron radiations are suitable for diffraction studies. X-rays are probably the most convenient and widely used whereas electrons and neutrons have advantages in particular situations. Other experimental techniques such as electro-optic measurements and nuclear magnetic resonance (NMR) spectroscopy are also in use for the characterization of mesophases.

### 1.13. Application and prospects of columnar phases

Columnar phase is of great importance because it allows the possibility to combine different physical properties (optical, conductive) with orientational control of the molecular order, self-healing of structural defects and ease of processability. Most importantly all these properties can be tailored by careful molecular engineering. Currently the solar cells used for the direct conversion of light into electricity by the photovoltaic effect are fabricated from inorganic semiconductors; in particular, they are based on the single or polycrystalline silicon cells. On the other hand, organic thin-film

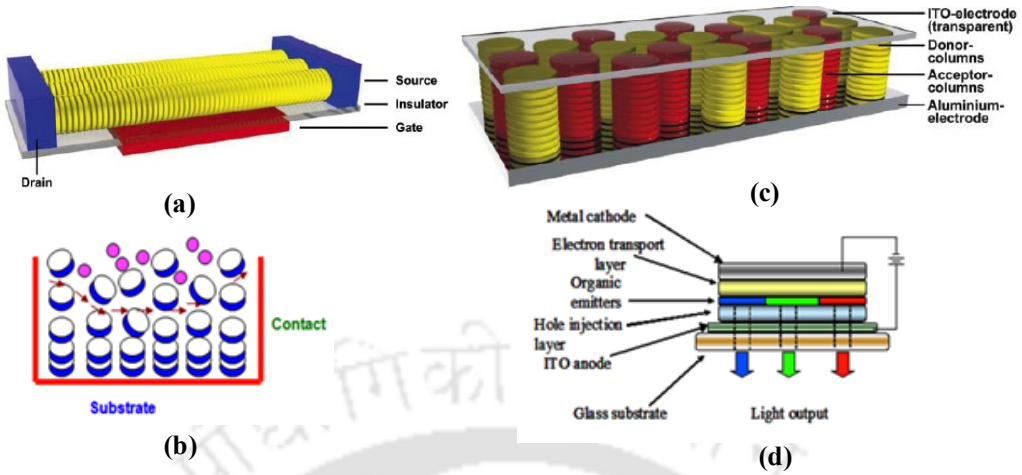


**Figure 1.17.** Schematic representations of molecular electronic devices from columnar mesophases [adopted from ref. 29a]: (a) field effect transistor; (b) gas sensors; (c) photovoltaic or solar cells and (d) organic light emitting diodes.

solar cells having single crystalline organic material are also promising for flat–plate photovoltaic technology based on either of these two materials is rather difficult and expensive. Most importantly, the large quantity of inorganic semiconductors used in such a technology is hazardous to the environment. Thus for the solar cell applications, new organic materials with low cost and good processability, large absorption coefficient, efficient photogeneration of charge and good charge carrier mobility are needed. In this context columnar phases formed by the electron rich/poor discotic mesogens appear to be promising given the fact that their structure resembles the aromatic stacking in single crystalline conductors (Fig. 1.17). The "edge on" orientation of the Col phases can be translated into field effect transistors (FET), which are the vital components in molecular electronic devices. The high mobility for photo induced charge carriers in the Col phases also make them suitable for their use as active charge transport layer in fast and high resolution xerographic and laser printing applications.[29] The Col phase has a unique conductive surface and changes as soon as the surface is disturbed. The carrier mobility along the surface is fluctuation assisted and the tunneling rates are exponentially dependent on the molecular core spacings. The core-core separation fluctuates with the surface and changes as soon as surface is disturbed. The electrical conductivity of this surface is, therefore, very sensitive to the absorption of molecules. Thus columnar liquid

crystals can be used as sensitive to the sensors for both polar and nonpolar molecules.[30] Recently Col phases are gaining importance in the construction of organic light emitting diodes (OLEDs) as they can act as good emitting and conductive materials with proper design. Columnar phase with a combination of hole/electron transport and luminescence properties is an ideal material for the fabrication of OLEDs.[31]

## 1.14. References


1. (a) S. Chandrasekhar, in *Liquid Crystals*, 2nd ed.; Cambridge University Press: New York, 1994; (b) *Handbook of Liquid Crystals: Fundamentals*, ed. J. W. Goodby, P. J. Collings, T. Kato, C. Tschierske, H. Gleeson and P. Raynes, Wiley-VCH: Weinheim, Germany, 2014, *Vol.* **1**; (c) T. Geelhaar, K. Griesar and B. Reckmann, *Angew. Chem. Int. Ed.*, 2013, **52**, 8798-8809; (d) P. J. Collings and M. Hird, *Introduction to Liquid Crystals Chemistry and Physics*, Taylor and Francis Ltd. London, 1997; (e) B. Bahadur, *Liquid Crystals: Application and Uses. Vol.1-3,* World Scientific, Singapore, 1990; (f) G. W. Gray, *Molecular structure and the properties of liquid crystals.*, Academic press, London and New York, 1962; (g) D. Demus, and L. Richter, *Textures of liquid crystals*, 2nd Ed. Deutscher Verlag f. Grundstoffindustrie Leipzig, 1978; (h) G. W. Gray, in *Handbook of liquid crystals*, *Vol-1*, Eds: D. Demus, J. W. Goodby, G. W. Gray, H. -W. Spiess, and V. Vill, Wiley-VCH, Germany, 1998; (i) G. W. Gray, and J. W. Goodby, *Smectic Liquid crystalline Textures and Structures*, Leonard Hill, Philadelphia, 1984; (j) P. G. de Gennes, and J. Prost, *The Physics of Liquid Crystals*, Oxford Science Publication, Oxford, 1993; (k) S. Kumar, *Liquid Crystals: Experimental Study of Physical Properties and Phase Transitions*; Cambridge University Press, 1st Ed. 2001.
2. (a) I. Dierking, *Textures of Liquid Crystals*, Wiley-VCH, Weinheim, 2003; (b) H. Sackmann, and D. Demus, *Mol. Cryst. Liq. Cryst*., 1973, **21**, 239; (c) T. Kato, N. Mizoshita and K. Kishimoto, Angew. Chem., 2006, **118**, 44-74; (d) T. Kato, N. Mizoshita and K. Kishimoto, *Angew. Chem. Int. Ed.*, 2006, **45**, 38-68.
3. (a) F. Reinitzer, *Monatsh. Chem.*, 1888, **9**, 421; (b) F. Reinitzer, *Liq. Cryst*., 1989, **5**, 7-18.
4. O. Lehmann, *Z. Phys. Chem.*, 1889, **4**, 462-72.
5. (a) S. Chandrasekhar, B. K. Sadashiva and K. A. Suresh, *Pramana*, 1977**, 9**, 471-480; (b) H. K. Bisoyi, and S. Kumar, *Chem. Soc. Rev*., 2010, **39**, 264–285; (c) M. Langner, K. Praefcke, D. Kruerke, and G. Heppke, *J. Mater. Chem*., 1995, **5**, 693–699; (d) H. Ringsdorf, R. Wustefeld, E. Zerta, M. Ebert and J. H. Wendorff, *Angew. Chem. Int. Ed*., 1989, **28**, 914–918; (e) A. Grafe, D. Janietz, T. Frese and J. H. Wendorff, *Chem. Mater*., 2005, **17**, 4979–4984; (f) P. H. J. Kouwer, W. F. Jager, W. J. Mijs and S. J. Picken, *Macromolecules*, 2000, **33**, 4336–4342; (g) A. Stracke, J. H. Wendorff, D. Janietz and S. Mahlstedt, *Adv. Mater*., 1999, **11**, 667–670; (h) S. Mahlstedt, D. Janietz, A. Stracke and J. H. Wendorff, *Chem. Commun*., 2000, 15–16; (i) P. H. J. Kouwer, W. F. Jager, W. J. Mijs and S. J. Picken,

*Macromolecules*, 2001, **34**, 7582–7584; (j) P. H. J. Kouwer, W. F. Jager, W. J. Mijs and S. J. Picken, *Macromolecules*, 2002, **35**, 4322–4329; (k) P. H. J. Kouwer, O. van den Berg, W. F. Jager, W. J. Mijs, and S. J. Picken, *Macromolecules*, 2002, **35**, 2576–2582; (l) S. Kumar, *Chemistry of Discotic Liquid Crystals: From Monomers to Polymers*; CRC Press: Boca Raton, FL, 2010.

6. O. H. Schönherr, J. H. Wendorff, H. Ringsdorf and Peter Tschirner, *Makromol. Chem. Rap. Commu.*, 1986, **7**, 791.
7. (a) P. G. de Gennes and J. Prost, *The physics of Liquid Crystals*, *2nd ed.* (Oxford: Clarendon Press), 1993; (b) Y. Hendrikx, J. Charvolin, M. Rawiso and M. C. Holmes, *J. Phys. Chem.*, 1983, **87**, 3991; (c) C. Tschierske, *C. Curr. Opin. Colloid Interface Sci.*, 2002, **7**, 355-370.
8. (a) D. Demus, *Liq. Cryst.*, 1989, **5**, 75-110; (b) C. Tschierske, *J. Mater. Chem*., 1998, **8**, 1485-1508; (c) C. Tschierske, *J. Mater. Chem*., 2001, **11**, 2647-2671; (d) C. Tschierske, *Annu. Rep. Prog. Chem*. *Sect. C*, 2001, **97**, 191-267; (e) C. Tschierske, *Curr. Opin. Colloid Interface Sci*., 2002, **7**, 69-80.
9. (a) H. Kelker and B. Scheurle, *Angew. Chem.*, 1969, **81**, 903-904; (b) C. T. Imrie and G. R. Luckhurst, in *Handbook of liquid crystals*, *Vol-2B*, Eds.; D. Demus, J. W. Goodby, G. W. Gray and H. -W. Spiess, V. Vill, Wiley-VCH, Germany, 1998, part – III, p.799; (c) C. T. Imrie and P. A. Henderson, *Curr. Opin. Colloid Interface Sci*., 2002, **7**, 298-311; (d) C. T. Imrie in *Structure and Bonding - Liquid crystals, II*, Ed: D. M. P. Mingos, Springer-Verlag, 1999, p.149; (e) N. Tamaoki, *Adv. Mater*., 2001, **13**, 1135-1147; (f) C. V. Yelamaggad, G. Shanker, U. S. Hiremath, and S. K. Prasad, *J. Mater. Chem.*, 2008, **18**, 2927-2949; (g) A. S. Achalkumar, U. S. Hiremath, D. S. Shankar Rao and C. V. Yelamaggad, *Liq. Cryst.*, 2011, **38**, 1563-1589; (h) E. Allard, F. Oswald, B. Donnio, D. Guillon, J.U. Delgado, F. Langa and R. Deschenaux, *Org. Lett*., 2005, **7**, 383 and the references cited there; (i) C. V. Yelamaggad, S. A. Nagamani, U. S. Hiremath, D. S. S. Rao and S. K. Prasad *Liq. Cryst*., 2002, **29**, 231; (j) C. T. Imrie, F. E. Karasz and G. S. Attard, *Macromolecules*, 1993, **26**, 545; (k) C. T. Imrie, P. A. Henderson and J. M. Seddon, *J. Mater. Chem.*, 2004, **14**, 2486-2488.
10. (a) J. Tang, R. Huang, H. Gao, X. Cheng, M. Prehm, and C. Tschierske, *RSC Adv.*, 2012, **2**, 2842-2847; (b) X. Yang, H. Dai, Q. He, J. Tang, X. Cheng, M. Prehm, and C. Tschierske, *Liq. Cryst.*, 2013, **40**, 8, 1028-1034; (c) J. Malthete, A. M. Levulut and N. H. Tinh, *J. Phys. Lett.*, 1985, **46**, 875-880; (d) J. Malthete, H. T. Nguyen and C. Destrade, *Liq. Cryst.*, 1993, **13**, 171-187; (e) H.-T. Nguyen, C. Destrade and J. Malthete, *Adv. Mater.*, 1997, **9**, 375–388; (f) K. E. Rowe and D. W. Bruce, *J. Mater. Chem.*, 1998, **8**, 331-341; (g) B. P. Hoag and D. L. Gin, *Adv. Mater.*, 1998, **10**, 1546-1551; (h) T. Yasuda, K. Kishimoto and T. Kato, *Chem. Commun.*, 2006, 3399-3401; (i) J. Seo, S. Kim, S. H. Gihm, C. R. Park and S. Y. Park, *J. Mater. Chem.*, 2007, **17**, 5052-5057; (j) S.-J. Yoon, J. H. Kim, K. S. Kim, J. W. Chung, B. Heinrich, F. Mathevet, P. Kim, B. Donnio, A.-J. Attias, D. Kim and S. Y. Park, *Adv. Funct. Mater.*, 2012, **22**, 61-69; (k) V. N. Kozhevnikov, B. Donnio and D. W. Bruce, *Angew. Chem. Int. Ed.*, 2008, **47**, 6286-6289; (l) C. Alstermark, M. Eriksson, M. Nilsson, C. Destrade and H. T. Nguyen, *Liq Cryst.*, 1990, **8**, 75-80; (m) D. Fazio, C. Mongin, B. Donnio, Y. Galerne D. Guillon and

D.W. Bruce. *J. Mater. Chem*., 2001, **11**, 2852-2863; (n) D. M. Huck, H. L. Nguyen, P. N. Horton, M. B. Hursthouse, D. Guillon, B. Donnio and D. W. Bruce, *Polyhedron*, 2006, **25**, 307-324; (o) A. I. Smirnova and D. W. Bruce, *J. Mater. Chem*., 2006, **16**, 4299-4306; (p) E. Gorecka, D. Pociecha, J. Mieczkowski, J. Matraszek, B. Donnio and D. Guillon, *J. Am. Chem. Soc.*, 2004, **126**, 15946-15947; (q) C. Tschierske, *Angew. Chem. Int. Ed.*, 2000, **39**, 2454-2458; (r) E. Gorecka, D. Pociecha, J. Matraszek, J. Mieczkowski, Y. Shimbo, Y. Takanishi and H. Takezoe, *Phys. Rev. E.*, 2006, **73**, 31704-31708; (s) J. Barbera, E. Cavero, M. Lehmann, J. L. Serrano, T. Sierra and J. T. Vazquez, *J. Am. Chem. Soc.*, 2003, **125**, 4527-4533; (t) D. Pucci, *Liq Cryst.*, 2011, **38**, 1451-1465; (u) K. Han and B.-K. Cho, *Soft Matter*, 2014, **10**, 7588-7594; (v) C. V. Yelamaggad, G. Shanker, R. V. R. Rao, D. S. S. Rao, S. K. Prasad, and V. V. S. Babu, *Chem. Eur. J.*, 2008, **14**, 10462-10471.

11. (a) T. Niori, T. Sekine, J. Watanabe, T. Furukawa and H. Takezoe, *J. Mater. Chem*., 1996, **6**, 1231-1233; (b) R. A. Reddy and C. Tschierske, *J. Mater. Chem*., 2006, **16**, 907-961; (c) H. Takezoe and Y. Takanishi, *Jpn. J. of App. Phys*., 2006, **45**, No. 2A, 597-625; (d) G. Pelzi, S. Diele and W. Weissflog, *Adv. Mater.*, 1999, **11**, 707-724; (e) M. B. Ros, J. L. Serrano, M. R. de la Fuente, C. L. Folcia, *J. Mater. Chem*., 2005, **15**, 5093-5098; (f) C. Tschierske and G. Dantlgraber, *Pramana*, 2003, **61**, 455; (g) J. Etxebarria and M. B. Ros, *J. Mater. Chem*., 2008, **18**, 2919-2926; (h) M. Lehmann, J. Seltmann, A. A. Auer, E. Prochnow and U. Benedikt, *J. Mater. Chem.*, 2009, **19**, 1978-1988; (i) M. Lehmann and J. Seltmann, *Beilstein J. Org. Chem*., 2009, **5**, 73 (1-9); (j) T. Niori, T. Sekine, J. Watanabe, T. Furukawa and H. Takezoe, *Mol. Cryst. Liq. Cryst.*, 1997, **301**, 337-342; (k) T. Sekine, Y. Takanishi, T. Niori, J. Watanabe and T. Takezoe, *J. Mater. Chem*., 1997, **7**, 1307-1309; (l) Y. Matsunaga and S. Miyamoto, *Mol. Cryst. Liq. Cryst.*, 1993, **237**, 311-317; (m) R. Cai and E. Samulski, *Liq. Cryst.*, 1991, **9**, 617-634.
12. (a) K. Borisch, S. Diele, P. Goring, H. Muller and C. Tschierske, *Liq. Cryst.*, 1997, **22**, 427-443; (b) K. Borisch, S. Diele, P. Goring, H. Kresse and C. Tschierske, *J. Mater. Chem*., 1998, **8**, 529-543; (c) F. Liu, R. Kieffer, X. Zeng, K. Pelz, M. Prehm, G. Ungar and C. Tschierske, *Nature Communications*, 2012, **3**, 1104-1107; (d) C. Tschierske, *Isr. J. Chem.*, 2012, **52**, 935-959.
13. (a) H. Zeng and T. M. Swager, *J. Am. Chem. Soc*., 1994, **116**, 761-762; (b) T. M. Swager and H. Zeng, *Mol. Cryst. Liq. Cryst.*, 1995, **260**, 301-306.
14. (a) A. Pegenau, P. Goring and C. Tschierske, *Chem. Commun.*, 1996, 2563-2564; (b) M. Lehmann, R. I. Gearba, M. H. J. Koch, and D. A. Ivanov, *Chem. Mater.*, 2004, **16**, 374-376; (c) M. Lehmann and M. Jahr, *Chem. Mater.*, 2008, **20**, 5453-5456; (d) H. Detert, M. Lehmann and H. Meier, *Materials*, 2010, **3**, 3218–3330; (e) M. Lehmann, *Chem. Eur. J.*, 2009, **15**, 3638–3651; (f) S. Varghese, N. S. S. Kumar, A. Krishna, D. S. S. Rao, S. K. Prasad and S. Das, *Adv. Funct. Mater*., 2009, **19**, 2064-2073.
15. M. Lee, D. -W. Lee and B. -K. Cho, *J. Am. Chem. Soc*., 1998, **120**, 13258-13259.
16. (a) J. H. Cameron, A. Facher, G. Lattermann and S. Diele, *Adv. Mater*., 1997, **9**, 398-403; (b) A. Pegenau, T. Hegmann, C. Tschierske and S. Diele, *Chem. Eur. J.*,

1999, **5**, 1643-1660; (c) S. I. Stupp, M. Keser and G. N. Tew, *Polymer*, 1998, **39**, 4505-4508; (d) H. Meier, M. Lehmann, and U. Kolb, *Chem. Eur. J.*, 2000, **6**, 2462-2469; (e) V. Percec, A. E. Dulcey, V. S. K. Balagurusamy, Y. Miura, J. Smidrkal, M. Peterca, S. Nummelin, U. Edlund, S. D. Hudson, P. A. Heiney, H. Duan, S. N. Magonov, and S. A. Vinogradov, *Nature*, 2004, **430**, 764-768; (f) M. Lehmann, C. Köhn, H. Meier, S. Renker and A. Oehlhof, *J. Mater. Chem.*, 2006, **16**, 441-451; (g) B. M. Rosen, C. J. Wilson, D. A. Wilson, M. Peterca, M. R. Imam, and V. Percec, *Chem Rev.*, 2009, **109**, 6275-6540; (h) B. Donnio, *Inorganica Chimica Acta*, 2014, **409**, 53-67; (i) D. J. Pesak and J. S. Moore, *Angew. Chem. Int. Ed*., 1997, **36**, 1636-1639.

17. A. Skoulios and D. Guillon, *Mol. Cryst. Liq. Cryst*., 1988, **165**, 317 –332.
18. (a) F. C. Frank and S. Chandrasekhar, *J. Phys*., 1980, **41**, 1285-1288; (b) C. Destrade, P. Foucher, H. Gesparoux, H. T. Nguyen, A. M. Levelut, J. Malthete, *Mol. Cryst. Liq. Cryst*., 1984, **106**, 121-146.
19. (a) F. Morale, R. W. Date, D. Guillon, D. W. Bruce, R. L. Finn, C. Wilson, A. J. Black, M. Schroder and B. Donnio, *Chem. Eur. J*., 2003**, 9**, 2484-2501; (b) C. Destwde, N. H. Tinh, L. Mamlok, and J. Malthete, *Mol. Cryst. Liq. Cryst*., 1984, **114**, 139–150.
20. B. Glusen, W. Heitz, A. Kettner and J. H. Wendorff, *Liq. Cryst*., 1996, **20**, 627-633.
21. (a) K. Ohta, H. Muroki, A. Takagi, K. I. Hatada, H. Ema, I. Yamamoto and K. Matsuzaki, *Mol. Cryst. Liq. Cryst*., 1986, **140**, 131-152; (b) H. Sakashita, A. Nishitani, Y. Sumiya, H. Terauchi, K. Ohta and I. Yamamoto, *Mol. Cryst. Liq. Cryst*., 1988, **163**, 211-219.
22. a) G. H. Mehl, A. J. Thornton and J. W. Goodby, *Mol. Cryst. Liq. Cryst.*, 1999, **332**, 455 – 461; b) S. Kumar and M. Manickam *Liq. Cryst.*, 1999, 26, 939 – 941; c) L. Wilson, *Liq. Cryst.*, 1994, **18**, 1005 – 1014.
23. a) J. Barber, L. Puig, J.-L. Serrano and T. Sierra, *Chem. Mater.*, 2004, **16**, 3308 – 3317; b) D. Goldmann, D. Janietz, C. Schmidt and J. H. Wendorff, *Liq. Cryst.*, 1998, **25**, 711 – 719; c) K. P. Van den Hout, R. Martín-Rapffln, J. A. J. M. Vekemans and E. W. Meijer, *Chem. Eur. J.* 2007, **13**, 8111 – 8123; d) J. J. van Gorp, J. A. J. M. Vekemans and E. W. Meijer, *Mol. Cryst. Liq. Cryst.*, 2003, **397**, 191 –205.
24. a) R. Christiano, D. M. Pereira de Oliveira Santos and H. Gallardo, *Liq. Cryst*., 2005, **32**, 7– 14; b) C.-H. Lee and T. Yamamoto, *Mol. Cryst. Liq. Cryst.*, 2002, **378**, 13–21; c) B. G. Kim, S. Kim and S. Y. Park, *Tetrahedron Lett*., 2001, **42**, 2697 –2699; d) J. C. Chang, J. R. Yeon, Y. S. Chin, M. J. Han and S.-K. Hong, *Chem. Mater.*, 2000, **12**, 1076 –1082; e) J. C. Chang, J. H. Baik, C. B. Lee, M. J. Han and S.-K. Hong, *J. Am. Chem. Soc.*, 1997, **119**, 3197 –3198.
25. (a) A. Kohlmeier and D. Janietz, *Liq. Cryst.*, 2007, **34**, 289 –294; b) D. Janietz, *J. Mater. Chem.*, 1998, **8**, 265 – 274; c) D. Goldmann, D. Janietz, C. Schmidt and J. H. Wendorff, *J. Mater. Chem.*, 2004, **14**, 1521 – 1525; (d) D. Goldmann, D. Janietz, C. Schmidt and J. H. Wendorff, *Liq. Cryst.*, 1998, **25**, 711 –719.
26. C. Tschierske, *Angew. Chem. Int. Ed*., 2013, **52**, 8828 – 8878.
27. J. H. Porada and D. Blunk, *J. Mater. Chem.*, 2010, **20**, 2956- 2958.

28. (a) K. Mullen and G. Wegner, *Electronic Materials: The Oligomer Approach*; Wiley-VCH: Weinheim, 1998; (b) R. E. Martin and F. Diederich, *Angew. Chem. Int. Ed.*, 1999, **38**, 1350-1377; (c) F. S. Precup-Blaga, J. C. Garcia-Martinez, A. P. H. J. Schenning and E. W. Meijer, *J. Am. Chem. Soc.*, 2003, **125**, 12953-12960; (d) F. Lincker, P. Bourgun, P. Masson, P. Didier, L. Guidoni, J.-Y. Bigot, J.-F. Nicoud, B. Donnio, and D. Guillon, *Org. Lett.*, 2005, **7**, 1505-1508; (e) M. O'Neill and S.M. Kelly. *Adv Mater.*, 2003, **15**, 1135-1146; (f) A. Contoret, A. Eastwood, S. Farrar, S. M. Kelly, E Nicholls, M. O'Neill, G. Richards and C. Wu, *Mol. Cryst. Liq. Cryst.*, 2001, **368**, 271-278; (g) N. H. Sultana, S.M. Kelly, B. Mansoor and M. O'Neill, *Liq Cryst*., 2007, **34**, 1307-1316; (h) A. P. Sivadas, N. S. S. Kumar, D. D. Prabhu, S. Varghese, S. K. Prasad, D. S. S. Rao, and S. Das, *J. Am. Chem. Soc.*, 2014, **136**, 5416-5423.
29. (a) C.D. Simpson, J. Wu, M.D. Watson, and K. Mullen, *J. Mater. Chem*., 2004, **14**, 494-504; (b) S. Laschat, A. Baro, N. Steinke, F. Giesselmann, C. Hägele, G. Scalia, R. Judele, E. Kapatsina, S. Sauer, A. Schreivogel and M. Tosoni *Angew. Chem.Int. Ed*., 2007, **46**, 4832- 4887; (c) N. G. Nagaveni, M. Gupta, A. Roy, and V. Prasad, *J. Mater. Chem.*, 2010, **20**, 9089-9099.
30. N. Boden, R. Bissel, J. Clements, and B. Movaghar, *Current science*, 1996, **71**, 599-601.
31. T. Christ, B. Glusen, A. Greiner, A. Kettner, R. Sander, V. Stumpflen, V. Tsukruk and J.H. Wendorff, *Adv. Mater*.,1997, **9**, 48-52.
32. S. K. Prasad, D. S. S. Rao, S. Chandrasekhar and S. Kumar *Mol. Cryst. Liq. Cryst*., 2003, **396**, 121-139.
33. (a) T. Vlad-Bubulak, J. Buchs, A. Kohlmeier, M. Bruma, and D. Janietz, *Chem. Mater.*, 2007**, 19**, 4460-4466; (b) K. Ohta, T. Watanabe, H. Hasebe, Y. Morizumi, T. Fujimoto and I. Yamamoto, *Mol. Cryst. Liq. Cryst*., 1991, **196**, 13-26; (c) K. Hatsusaka, K. Ohta, I. Yamamoto and H. Shirai, *J. Mater. Chem*., 2001, **11**, 423-433;(d) M. Ichihara, A. Suzuki, K. Hatsusaka and K. Ohta, *Liq. Cryst*., 2007, **34**, 555-567; (e) K. Praefcke, P. Marquard, B. Kohne, W. Stephan, A. -M. Levelut and E. Watchtel, *Mol. Cryst. Liq. Cryst*., 1991, **203**, 149-158; (f) Md. A. Alam, J. Motoyanagi, Y. Yamamoto, T. Fukushima, J. Kim, K. Kato, M. Takata, A. Saeki, S. Seki, S. Tagawa, T. Aida, *J. Am. Chem. Soc.*, 2009, **131**, 17722-17723.
34. (a) E. Fontes, P. A. Heiney and W. H. De Jeu, *Phys. Rev. Lett.*, 1988, **61**, 1202-1205; (b) P. A. Heiney, E. Fontes, W. H. De Jeu, A. Riera, P. Carroll and A. B. Smith III, *J. Phys. France*, 1989, **50**, 461-483; (c) S. H. J. Idziak, P. A. Heiney, J. P. McCauley, Jr. P. Carroll and A. B. Smith III, *Mol. Cryst. Liq. Cryst*., 1993, **237**, 271-275.
35. (a) S. Mery, D. Haristoy, J. F. Nicoud, D. Guillon, S. Diele, H. Monobe, and Y. Shimizu, *J. Mater. Chem*., 2002, **12**, 37–41; (b) P. Davidson, A. M. Levelut, H. Strzelecka, and V. Gionis, *J. Phys. Lett*., 1983, **44**, 823–828.
36. N. Godbert, A. Crispini, M. Ghedini, M. Carini, F. Chiaravalloti and A. Ferrise, *J. Appl. Cryst.*, 2014, **47**, 668–679.

# Chapter II

# 1,3,4-Oxadiazole/thiadiazole based star-shaped mesogens

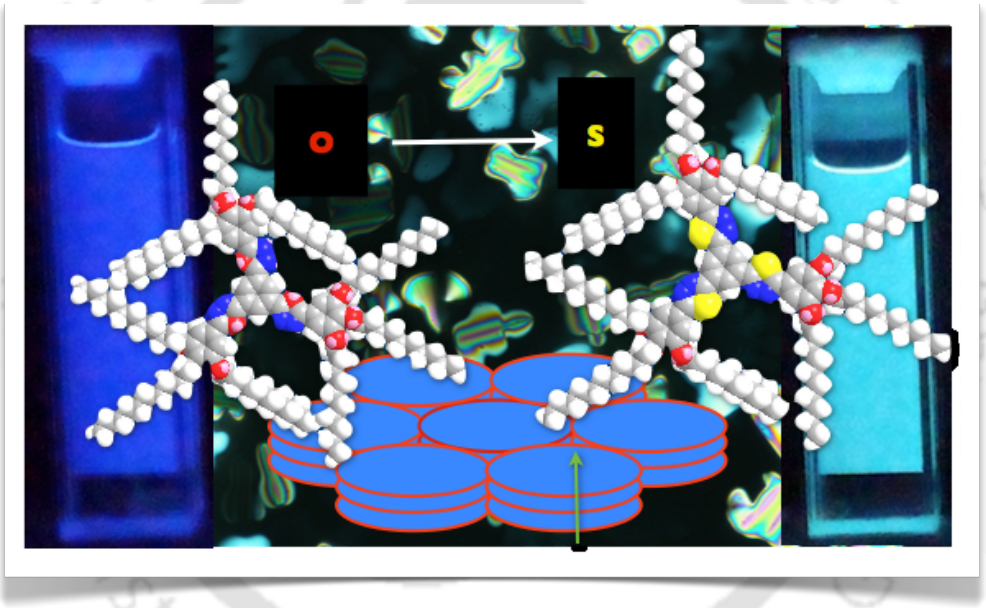


Results have been published in *J. Mater. Chem. C*, 2015, **3**, 2940-2952.

## 2.1. Introduction

The Spontaneous self-assembly of shape anisotropic molecules into liquid crystalline (LC) phase/s is a subject that has attracted a great deal of curiosity in recent years. This unique combination of order and fluidity in the LC state is very important from the viewpoint of basic research as well as future application.[1] Reinitzer's discovery of this phenomenon in cholesterol benzoate (calamitic/rod-like molecule) in 1888, aroused curiosity in the scientific community[2] and almost a century later, calamitic LCs became the mainstay of display technology.[3] The discovery of discotic LCs (DLCs) by Chandrasekhar *et. al.*[4] in 1977 provided a completely new dimension and research in the last four decades on DLCs has shown a bright and promising potential in the area of organic electronics.[5] These disc-like molecules either align with long-range orientation to the stabilize nematic (N) phase or stack one above the other to form the columnar (Col) phase.[1] Discotic nematic materials have been used in the fabrication of optical compensation films for wide viewing angle liquid crystal displays (LCDs)[6] and also tested as active components in LCD devices.[7,8] Columnar phases formed from the strong overlap of central discotic cores with the insulating mantle of the peripheral tails can act as molecular wires and may help in one-dimensional (1D) charge migration.[9] This property is of importance in the fabrication of optoelectronic devices like organic photovoltaic (OPV) cells,[10] organic light emitting diodes (OLEDs),[11] organic field effect transistors (OFETs)[12], gas sensors[13] and lubricants.[14]

The general design template of DLCs include the combination of a central rigid core connected to the peripheral tails with linking groups.[1,5] The central core is chosen in such a way that it can be either electron rich (p-type) or electron deficient (n-type) depending on the requirement. Recently, there has been a surge in the introduction of heterocylces in the molecular architecture because of the immense variety of the structures available, as well as because of the tunability in the corresponding properties.[15] The presence of hetero atoms like N, O and S in the molecular structure reduces the symmetry and causes a strong polar induction (lateral and/or longitudinal dipoles). When the electron-deficient heterocylic rings are attached to aromatic rings, it leads to donor-acceptor interactions within the molecules. All these properties in turn affect the electronic and mesophase behavior.[15d] Therefore, mesogenic heterocyclic derivatives are finding a strong foothold in the area of

OLEDs as they provide a wide choice of luminescence colors. They also enable polarized emission from oriented mesogens.[16] 1,3,4-Oxadiazoles are one such class of heterocycles, which are known for their advantageous features, including their hydrolytic and thermal stability as well as their resistance to oxidative degradation. They are also known for their high fluorescence quantum yield and electron transporting properties. Because of these properties they are widely used as electron transporting/hole blocking and emissive layers in OLEDs.[15,17] Liquid crystalline oxdiazole derivatives have been extensively explored over the years. A vast number of 1,3,4-oxadiazole-based calamitics,[18] discotics,[19] polycatenars,[20] V-shaped mesogens,[21a] supramolecular LCs,[21] ionic LCs,[22] bent core mesogens,[23] dimeric[24] and polymeric[25] mesogens have been reported. Despite the inherent advantages of oxadiazole-based mesogens, there are certain drawbacks such as high melting point, high clearing point and narrow mesophase range, which limits their applications.[26] 1,3,4-thiadiazoles are analogues of 1,3,4-oxadiazole derivatives, in which the oxygen atom is replaced with sulfur. This leads to properties that are strikingly different than those of the 1,3,4-oxadiazole derivatives; e.g., higher melting and clearing temperatures, higher viscocity, efficient packing and larger dipole moments.[15c, 27] The larger atomic size of the sulfur in the case of hexahexylthiotriphenylene (HHTT), imparted an increased order in columnar packing and thus enhances conductivity as compared to that exhibited by hexaalkoxytriphenylene.[28] Unlike the large number of 1,3,4-oxadiazole-based mesogens, reports on 1,3,4-thiadiazole based mesogens are scarce. This is partly attributed to the difficult synthesis and low yields. Very few reports on calamitic mesogens,[29] banana mesogens[30] , hydrogen bonded LCs,[31] polymerics,[32] and polycatenars [26, 33] based on 1,3,4-thiadiazole are found in previous studies. Recently, there are few reports of bent molecules stabilizing smectic and nematic phases[34a] and star shaped molecules bearing 1,3,4-thiadiazole unit stabilizing the Col phase .[34b]

As part of our research program on the synthesis of luminescent LCs, we were interested in synthesizing 1,3,4-oxadiazole- and 1,3,4-thiadiazole-based star shaped LCs to understand their structure-property relationship. We wanted to optimize a simple route for the realization of hitherto unreported 1,3,4-thiadiazole-based star shaped LCs. Because of the use of a common intermediate, we could prepare some of the 1,3,4-oxadiazole-based

star shaped LCs. [19] In this study we report the syntheses, characterization and thermal behavior of 1,3,4-oxadiazole- and 1,3,4-thiadiazole-based star-shaped LCs (Fig. 2.1).

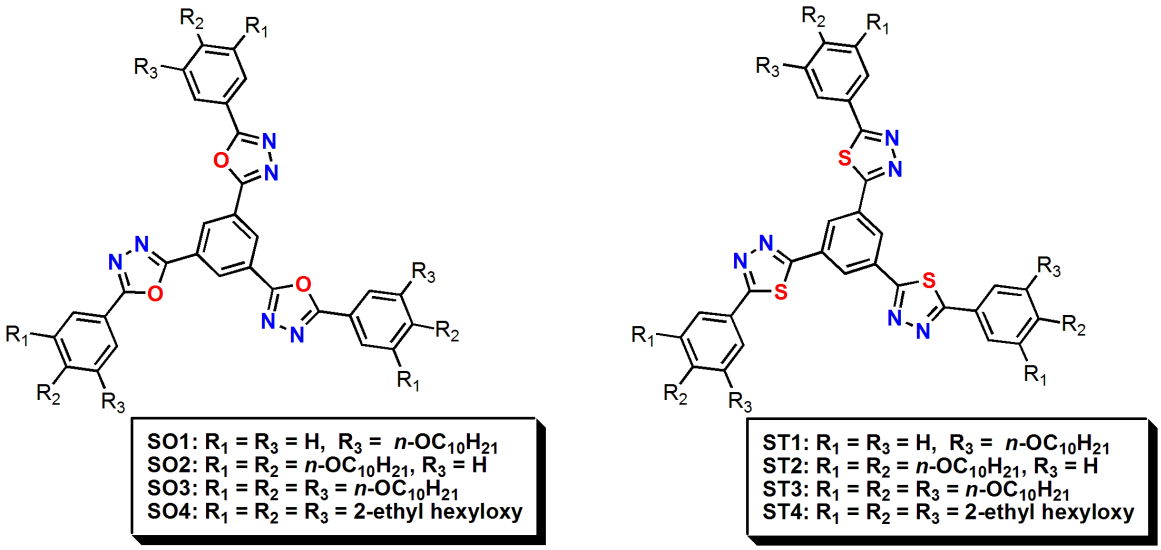


**Figure 2.1.** The molecular structures of star-shaped 1,3,4-oxadiazole and 1,3,4-thiadiazole derivatives.

## 2.2. Results and discussion

### 2.2.1. Synthesis and Characterization

The synthetic route for the preparation of target molecules and their precursors is depicted in scheme 2.1. The general procedures for the syntheses of ethyl gallate, 3,4,5-trialkoxy ethyl gallates, ethyl 3,4-dialkoxy benzoate are same as reported earlier.[35a] These alkoxy esters (**1a-d**) obtained by Williamson's protocol were converted to their respective hydrazides (**2a-d**) by treating with hydrazine hydrate and with ethanol or *n*- butanol as the solvent.[20k] Hydrazides **2a-d** were then refluxed with trimesic acid chloride in THF in the presence of triethylamine to obtain tri-*N*-benzoylbenzohydrazides **3a-d**.[19a] Compounds **3a-d** were subjected to $POCl_3$ mediated dehydrocyclization to obtain trioxadiazoles **SO1-4**.[19a] Similarly, compounds **3a-d** on refluxing with Lawesson's reagent[35b] in toluene yielded corresponding trithiadiazoles **ST1-4**.[31] The use of $P_2S_5$ did not provide good yield because of the incomplete reactions. The structures of all the intermediates and target molecules were confirmed using $^1$H NMR, $^{13}$C NMR, IR spectroscopy as well as with ESI-HRMS or

MALDI-TOF analysis. The $^{1}$H NMR spectra of the oxadiazole derivatives **SO1-4** exhibited low field signals corresponding to aromatic hydrogens as compared to their thiadiazole derivatives **ST1-4**. The $^{13}$C NMR of the oxadiazole derivatives exhibited signals at δ values 166 ppm and 163 ppm for the carbons in the heterocycle in comparison to the δ values 169 ppm and 166 ppm of the thiadiazole derivatives. (See experimental part presented in section 2.4 for the details and Fig. 2.2). As representative cases from each series, $^{1}$H NMR and $^{13}$C NMR spectra of the star-shaped 1,3,4-oxadiazole **SO3** and star-shaped 1,3,4-thiadiazole **ST3** are presented in Fig. 2.2.

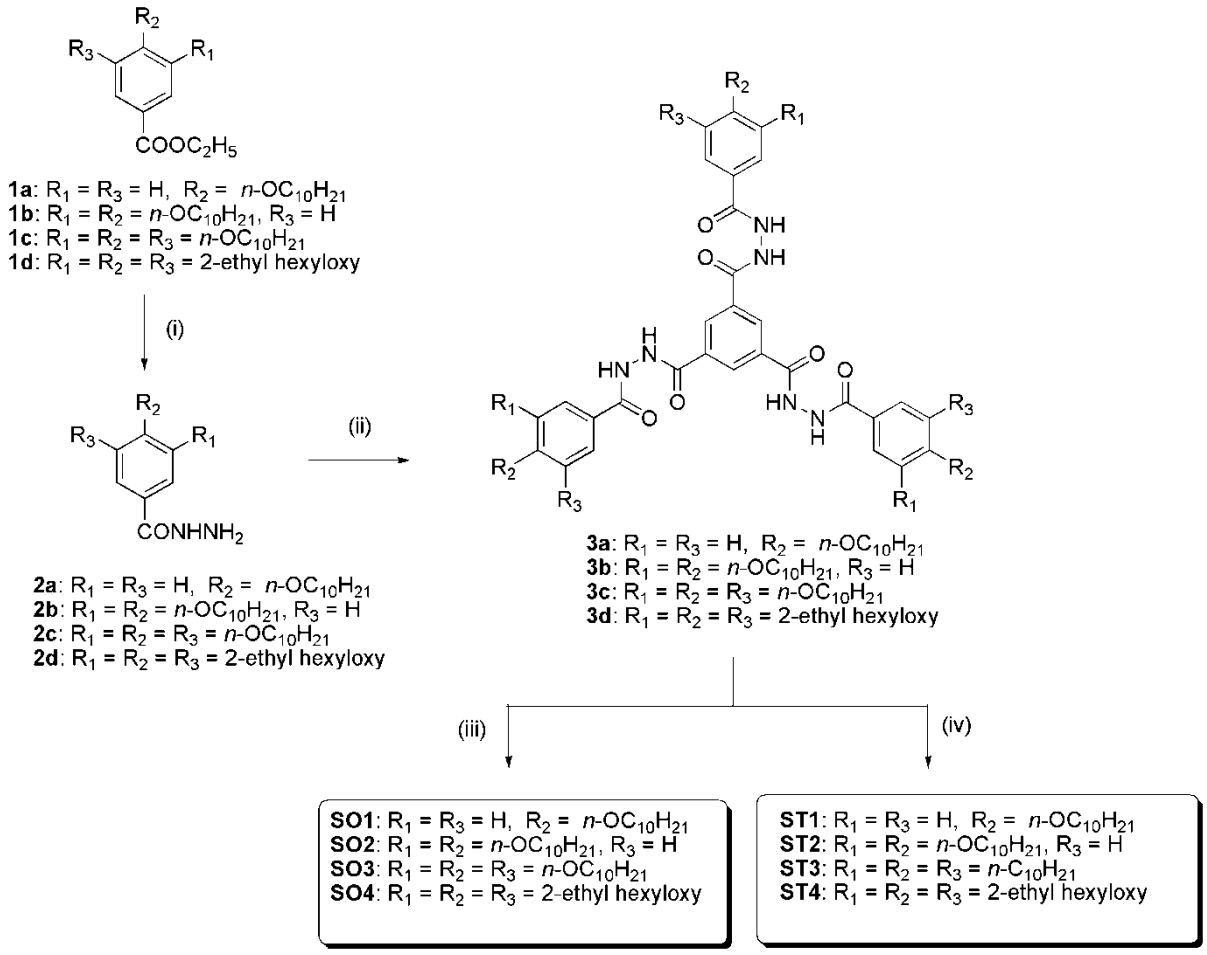


**Scheme 2.1.** Synthesis of 1,3,4-oxadiazole- and 1,3,4-thiadiazole-based star- shaped LCs. (i) $NH_2NH_2{\cdot}H_2O$, Ethanol or butanol, reflux, 48 h (65-80%); (ii) Trimesic acid chloride, THF, Triethylamine, 6 h, reflux; (iii) $POCl_3$, reflux, 17 h (31-36%); (iv) Lawesson's reagent, toluene, reflux, 17 h (31-49%).

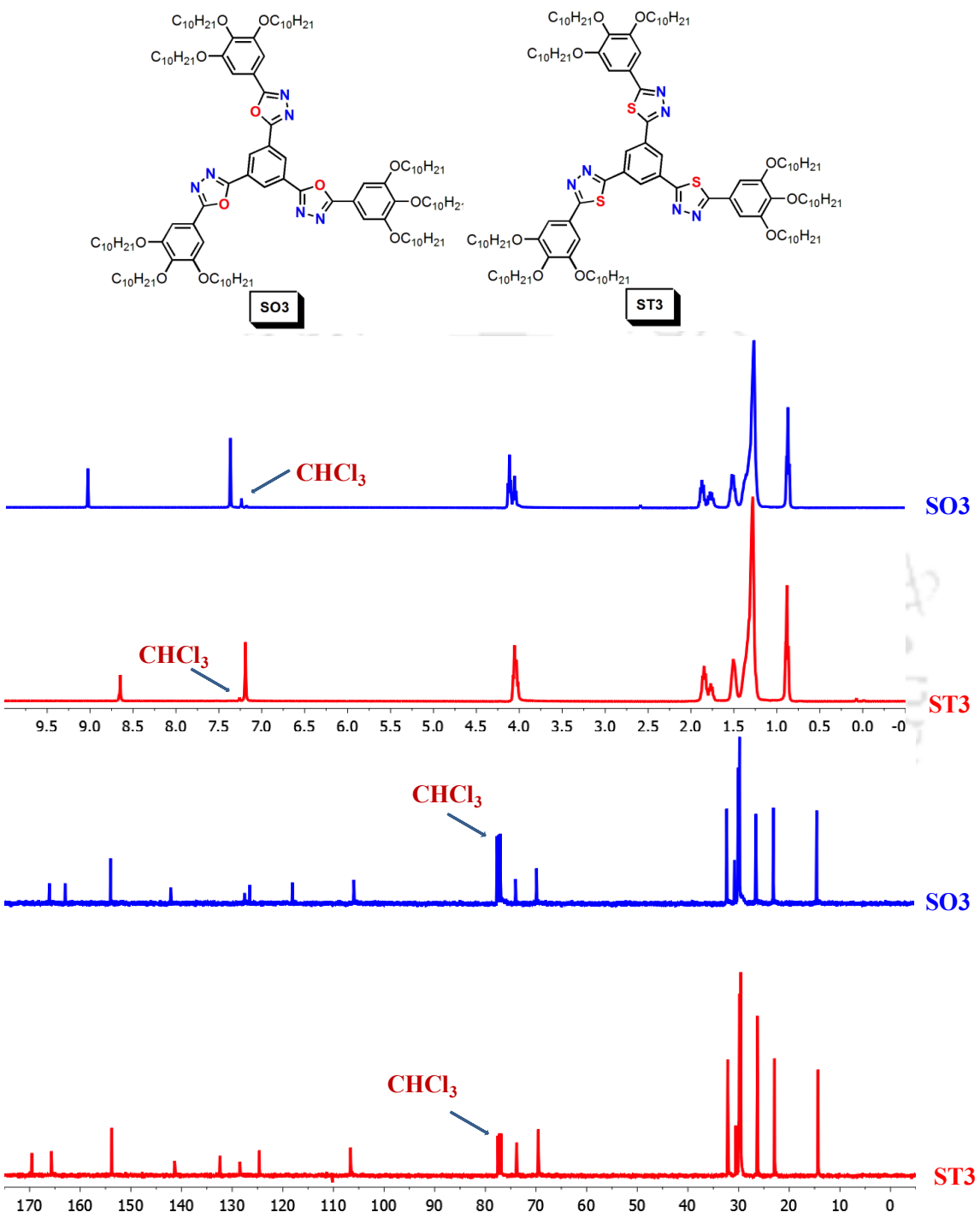


**Figure 2.2.** $^{1}$H NMR (400 MHz) and $^{13}$C NMR (100 MHz) spectra of **SO3** and **ST3** in $CDCl_3$.

### 2.2.2. Thermal behavior

All the compounds were investigated with the help of thermogravimetric analysis (TGA), polarizing optical microscopy (POM) and differential scanning calorimetry (DSC). Oxadiazole-based compounds **SO1-4** were stable at least upto ≈ 330 °C and complete degradation occurs at around 650 °C, as evidenced by TGA. (Fig. 2.3). The phase transition temperatures and enthalpy changes obtained are presented in Table 2.1. Oxadiazole-based star-shaped molecule **SO1** with three *n*-decyloxy tails,[19b] exhibited monotropic columnar hexagonal ($Col_h$) phase over a very short thermal range (4 degrees) with a grainy texture (Fig 2.4).

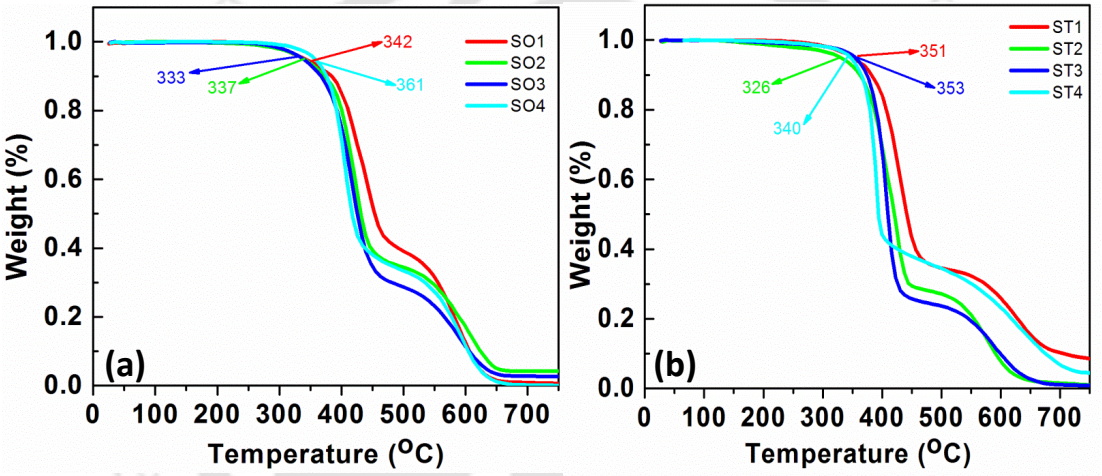


**Figure 2.3.** TGA curves of the compounds **SO1-4** (a) and **ST1-4** (b) carried out at a rate of 10 °C/min.

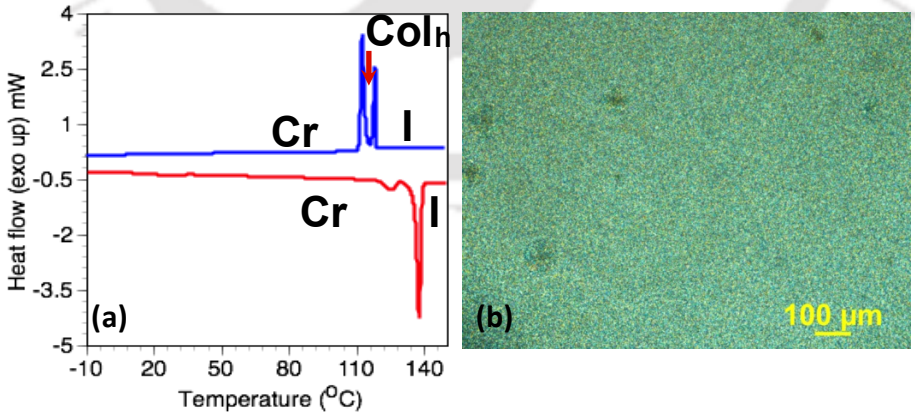


**Figure 2.4.** DSC traces obtained for the first cooling (upper trace) and second heating (lower trace) cycles of **SO1** at a rate of 5 °C $min^{-1}$(a) Photomicrograph of texture as seen by POM for the $Col_h$ phase at 108 °C (b)

Compound **SO2** with six *n*-decyloxy tails showed an increased mesophase range (68 degrees) as compared to **SO1**, with an isotropic temperature around 176 °C. On cooling, a isotropic liquid dendritic texture develops, which soon transforms into small pseudo focal conics and straight linear defects interspersed with homeotropic domains. This pattern is consistent with the texture for Col phases reported in literature.[5b,36] Around 84 °C, the DSC thermogram showed a mesophase-crystal transition with an enthalpy change of 25 kJ/mol, whereas the texture almost remained same, except for a decrease in the birefringence and fluidity. There were some changes in the color of pseudofocal conic fans, accompanied by the appearance of defects in the homeotropic region (Fig. 2.5a and b).

**Table 2.1.** Phase transition temperatures [a] (°C) and corresponding enthalpies (kJ/mol) of star shaped LCs

| | Heating | Cooling |
|---|---|---|
| **SO1** | $Cr_1$ 125.2 (13.8) $Cr_2$ 137.6 (98.3) I | I 117.9 (27) $Col_h$ [b] 113.1(69) Cr |
| **SO2** | $Cr_1$ 51.1 (92.7) $Cr_2$ 83.4 (188.6) $Cr_3$ 107.1 (266.9) $Col_h$ 175.6 (18.4) I | I 174.5 (16.4) $Col_h$ 83.7 (25) $Cr_2$ 63.2 (14.2) $Cr_1$ |
| **SO3** | Cr 45.6 (86.2) Col 169 (15.5) I | I 168 (12.1) $Col_{h1}$ 47 (71) $Col_{h2}$ [c] |
| **SO4** | Cr 111.8 (43.3) I | I 99.5 (38.6) Cr |
| **ST1** | $Cr_1$ 28 (10.7) $Cr_2$141.4 (81.8) $Col_h$ 170.2 (80.3) I | I 166.1 (75) $Col_h$ 122 (72) Cr |
| **ST2** | Cr 93 (466.8) $Col_h$ 155.3 (24.9) I | I 153.1 (18.1) $Col_h$ [c] 65 |
| **ST3** | $Cr_1$ 38 (24.1) $Cr_2$ 48.8 (11.2) $Col_h$ 206.1 (34.9) I | I 205.8 (28) $Col_{h1}$ 46.6 (22.5) $Col_{h2}$ [c] |
| **ST4** | Cr 98.7 (49.8) $Col_h$ 146.3 (15.8) I | I 140.8 (11.1) $Col_h$ 84.2 (77.5) Cr |

[a]Peak temperatures in the DSC thermograms obtained during the first heating and cooling cycles at 5 °C/min. [b] The phase observed is monotropic. [c] The mesophase is not crystallizing up to -20 °C; $Col_h$ = Columnar hexagonal phase.

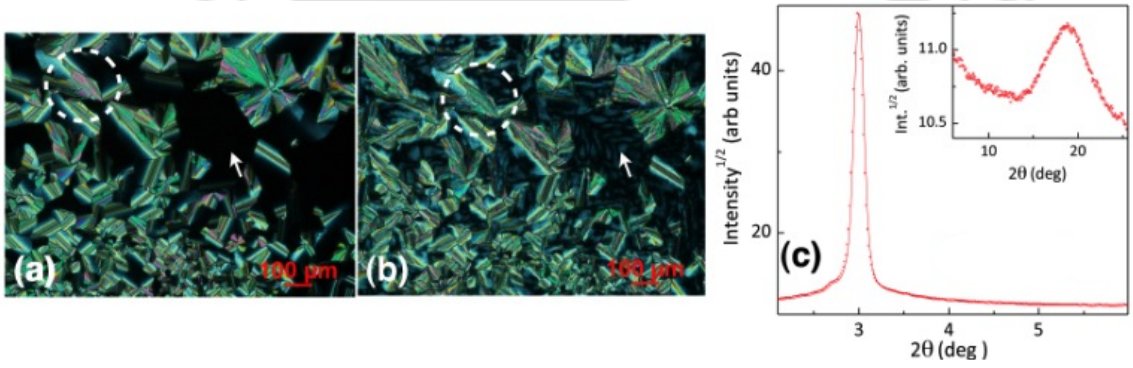


**Figure 2.5.** Photomicrographs of the textures as seen by POM for the $Col_h$ phase (a) at 154 °C and for the crystalline phase (b) at 74 °C of the compound **SO2** (circled region and arrow indicates the change in texture); (c) XRD profiles depicting the intensity against the 2θ obtained for the $Col_h$ phase of compound **SO2** at 150 °C.

Powder XRD measurements were carried out to determine the symmetry of the thermodynamically stable Col phase formed by compound **SO2** at temperature 150 $^{o}$C. The results of indexing the sharp reflections of these profiles to the lattice of the Col phase are summarized in Table 2.2.

**Table 2.2.** Results of the (*hkl*) indexation of the XRD profiles of the compounds at a given temperature (T) of the mesophases[a].

| Compounds (*D*/Å) | Phase (T/$^{o}$C) | $d_{obs}$ (Å) | $d_{cal}$ (Å) | Miller indices *hkl* | Lattice parameters (Å), lattice area S (Å$^2$), molecular volume V (Å$^3$) |
|---|---|---|---|---|---|
| **SO2** (47.68) | $Col_h$ (150) | 29.44<br>4.67($h_a$) | 29.44 | 100 | $a$ = 33.99, S = 1000.9,<br>V = 4674.5,[b] Z = 1.93 [b] |
| **SO3** (47.66) | $Col_h$ (160) | 28.64<br>4.63($h_a$) | 28.64 | 100 | $a$ = 33.07, S = 947.3,<br>V = 4384.3, [b] Z = 1.38 [b] |
| | $Col_h$ (100) | 29.11<br>4.53($h_a$) | 29.11 | 100 | $a$ = 33.61, S = 978.6,<br>V = 4428.2, [b] Z = 1.39 [b] |
| | $Col_h$ (30) | 29.97<br>4.43($h_a$) | 29.97 | 100 | $a$ = 34.60, S = 1036.9,<br>V = 4595.7, [b] Z = 1.44 [b] |

[a]The diameter (D) of the disk (estimated from Chem 3D Pro 8.0 molecular model software from Cambridge Soft). $d_{obs}$: spacing observed; $d_{cal}$: spacing calculated (deduced from the lattice parameters; a for $Col_h$ phase). The spacings marked $h_a$ and $h_c$ correspond to diffuse reflections in the wide-angle region arising from correlations between the alkyl chains and core regions, respectively. Z indicates the number of molecules per columnar slice of thickness $h_c$, estimated from the lattice area S and the volume V. [b]In the absence of core-core peak, the spacings of the alkyl chain stacking ($h_a$) is taken for these calculations.

The X-ray profile of the Col phase showed (Figure 2.5c) a single strong reflection corresponding to a Bragg spacing *d* of 29.44 Å at the low-angle region, besides a diffuse peaks at about 4.64 Å in the wide angles. The presence of a single maximum at low angles precludes an explicit structural assignment; however, as often found in the literature,[35a, 37] such a pattern assigned to the Col phase has been ascribed to a minimum in the form factor. The presence of a sharp peak in the low angle provides the distance between the adjacent (100) lattice planes $d_{10}$, from which the lattice parameter '*a*' can be calculated. The intercolumnar distance for this phase was found to be 34 Å, which is substantially lower than the molecular diameter 47.7 Å. This may be due to the substantial free space available for the aliphatic chains. The diffuse halo found at 4.67 Å is typical of the liquid-like order within the plane. The presence of this peak indicates that this is an ordered

columnar hexagonal phase. To confirm whether the phase lying below 84 °C is a crystalline or a liquid crystalline/glassy state, we carried out XRD studies at 76 °C. The XRD profile showed several sharp reflections in the entire region ($2^o < 2\theta < 30°$), confirming that the phase in question is indeed crystalline.

Compound **SO3** with nine *n*-decyloxy tails showed an increment in the thermal range of mesophase (123 degrees), with a transition from crystal to mesophase at ≈ 46 °C, and with an enthalpy change of 86.2 kJ/mol, finally converting into an isotropic liquid at ≈ 169 °C. After the isotropic liquid cools down, it appears at 168 °C and shows the growth of small batonnets (Fig. 2.6a). Further cooling results in the growth of these batonnets and the coalescence of anisotropic domains into a mosaic texture. This Col phase persists till ≈ 47

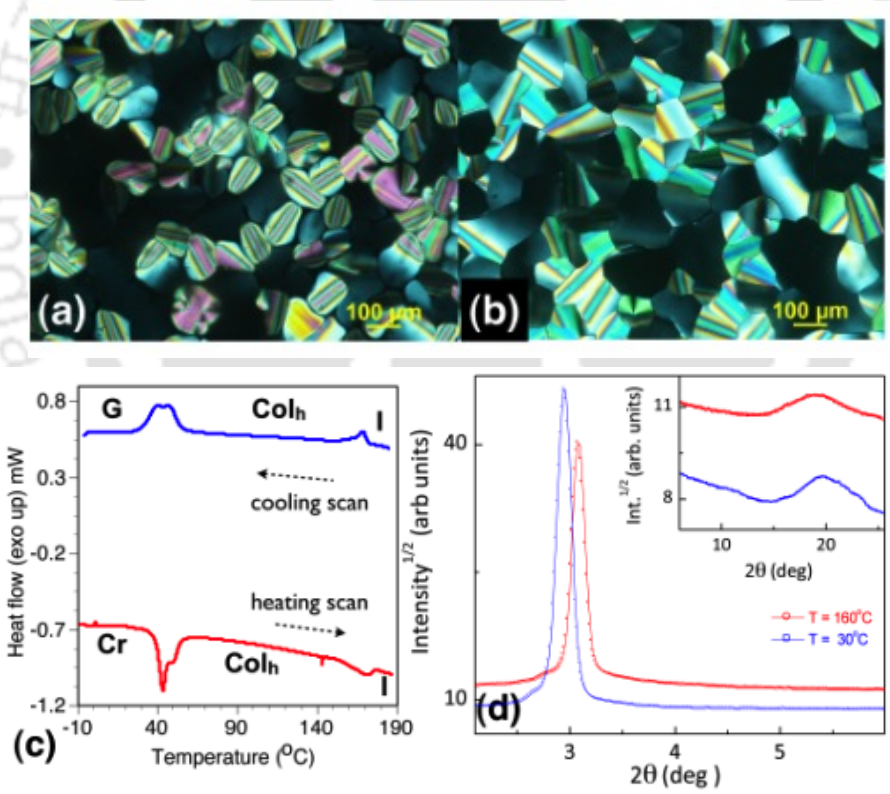


**Figure 2.6.** Photomicrographs of textures as seen by POM for the Col$_h$ phase of compound **SO3** (a) at 152 °C and (b) at 30 °C; (c) DSC traces obtained for the first cooling (upper trace) and second heating (lower trace) cycles of **SO3** at a rate of 5 °C min$^{-1}$; (d) XRD profiles depicting the intensity against the 2θ obtained for the Col$_h$ phase of compound **SO3** at T = 160°C. (red trace) and T = 30°C (blue trace).

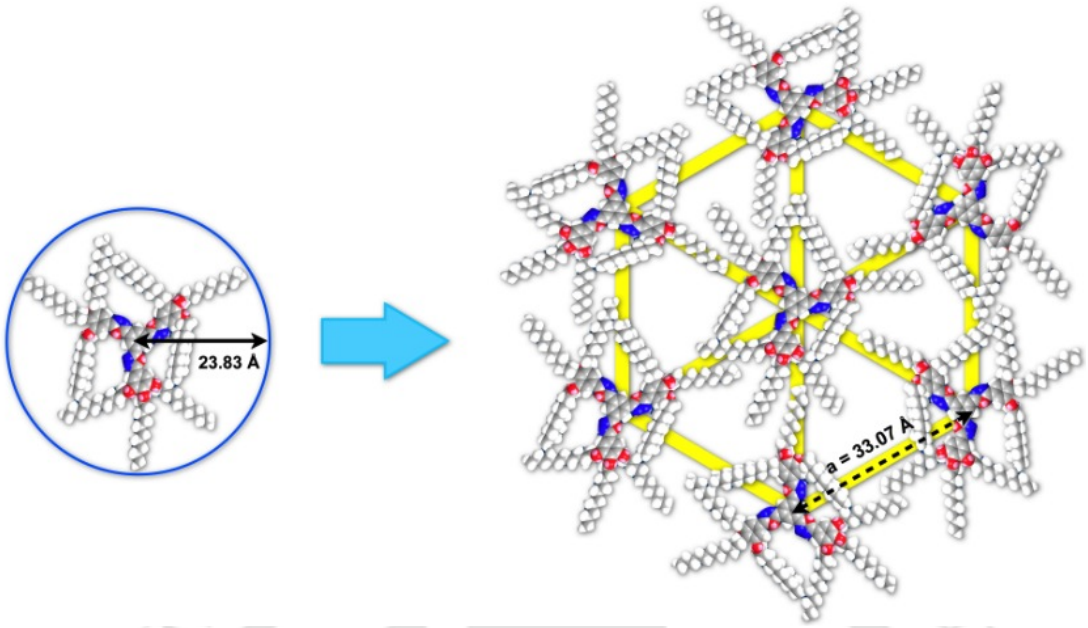


**Figure 2.7.** Schematic showing the self-organization of compound **SO3** into hexagonal columnar ($Col_h$) lattice with inter-digitation of alkyl tails. Space filling energy minimized (all-trans) molecular model of **SO3** derived from molecular mechanics (MM2) method.

$^{o}$C and undergoes a transition, as evidenced by DSC with an enthalpy change of 71 kJ (Fig. 2.6c). Even though this transition is observed in DSC, the texture remains intact without any sign of crystallization (Fig. 2.6b). Fig. 2.6d indicates the 1D intensity versus 2$\theta$ XRD profiles obtained for the high (160 °C; red trace) and low (30 °C; blue trace) temperature Col phases of compound **SO3**. The patterns obtained at both the temperatures are qualitatively similar, with a sharp single peak at low angles and a diffuse maximum at wide angles. The spacings are however different with 28.64 Å and 4.63 Å at high-temperature, and 29.97 Å and 4.43 Å at low temperature. As in the case of compound **SO2**, we assign the $Col_h$ structure at both temperatures. A feature that differentiates the low temperature scenario from the high temperature one is the nonshearability of the sample and the unchanged optical texture of the mesophase below 63 $^{o}$C. In conjunction with the qualitatively identical XRD pattern, this suggests that the $Col_h$ phase supercools into a glassy state. The marginal increase in the *d* value at low angle may be attributed to the stretching of the peripheral alkyl chains, and to the decrease in the temperature. Once again, the intercolumnar distance is substantially smaller than the molecular diameter (47.7 Å) estimated by the molecular model. While this could be due to the free space available

for the chains as explained for compound **SO2**, it cannot fully explain the situation for the following reason. The diameter of the molecule estimated from the molecular model is the same for both **SO2** and **SO3**, but the intercolumnar distance is about 1 Å smaller for the later compound. Because compound **SO3** has more chains, the free volume available for each chain must be smaller than that for compound **SO2**. Thus, the decreased spacing for SO3 could be attributed to the intercalation of the peripheral alkyl tails into the regions of the neighboring molecule, as shown in Fig. 2.7.

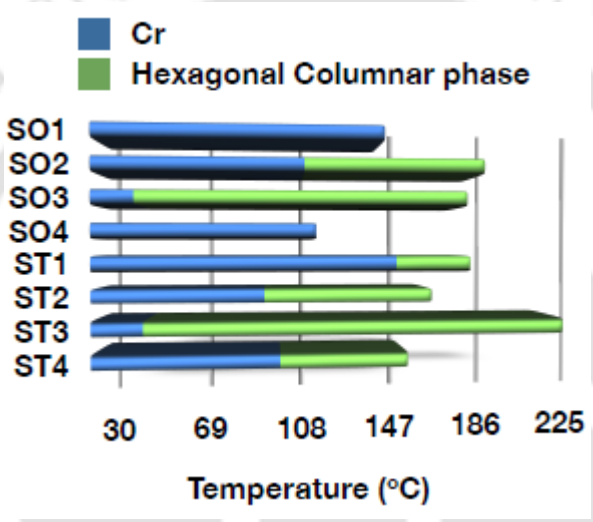


**Figure 2.8.** Bargraph summarizing the thermal behavior of compounds **SO1-4** and **ST1-4** (heating cycle).

In the case of compound **SO4**, with nine branched tails we expected a huge decrease in the melting point. This was expected because of the increased disorder at the periphery of these discotics caused by branching,[39] but surprisingly compound **SO4** melted into an isotropic liquid at 112 $^{o}$C without any LC phase. No mesophase was seen in the cooling mode either; instead, the crystallization occurred with large fan like domains (Fig. 2.9). It is to be noted that a similar oxadiazole derivative with six 2-ethylhexyloxy branched tails exhibited a $Col_h$ phase.[19g] From these studies and as depicted in Fig. 2.8, it is evident that with the increase in the number of tails from **SO1** to **SO3**, the stability and range of the mesophase increased (See Fig. 2.8). Compound **SO4**, with the branched tails turned out to be crystalline, showing that the introduction of branching in the periphery is not favorable

in enhancing the mesophase range, as evident in the case of conventional disc-shaped LCs.[39]

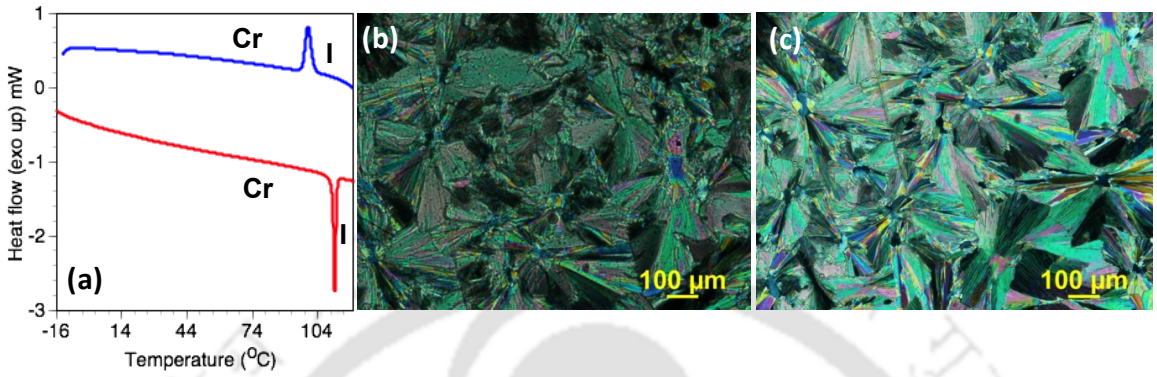


**Figure 2.9.** DSC traces obtained for the first cooling (upper trace) and second heating (lower trace) cycles of **SO4** at a rate of 5 °C $min^{-1}$(a) Photomicrographs of textures as seen by POM at 97 °C (b) and at 71°C (c).

The thermal stability of the thiadiazole derivatives **ST1-4** was studied with the help of TGA under nitrogen atmosphere, and it was found that all the compounds were stable at least upto ≈ 325 °C, with complete degradation occurring at around 650 °C. (Fig. 2.3). Thiadiazole-based star-shaped molecule **ST1,** with three *n*-decyloxy tails showed an enantiotropic mesophase. This is significant when compared to the short-range monotropic behavior of **SO1**. Heating the sample sandwiched between the glass slides exhibited a Cr-Cr transition at a temperature of 28 °C and entered a mesophase at around 141 °C. The mesophase converted to isotropic liquid around 170 °C. The mesophase range of 30 degrees for compound **ST1** is substantial, unlike that for its oxadiazole analogue **SO1** that bears three alkoxy tails.

Upon cooling the viscous isotropic liquid, a fern-like texture develops, which is consistent with the $Col_h$ phase (Fig.2.10a). Further cooling leads to the coalescence of these patterns into a mosaic texture. The mesophase crystallizes at 122 °C with an enthalpy change of 72 kJ/mol (Fig. 2.10b). Thus, it is evident that the presence of sulphur in the molecular structure is responsible for the enhanced mesophase range. The mesophase was

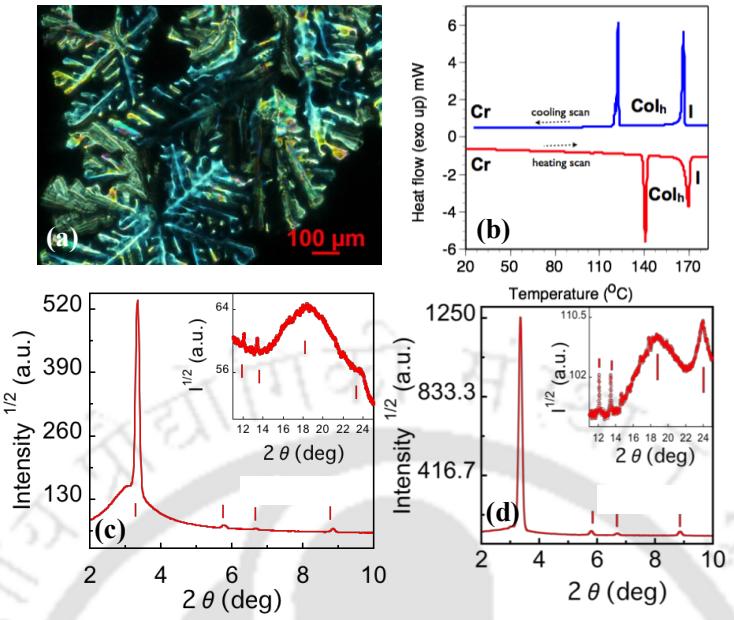


**Figure 2.10.** Photomicrograph of texture as seen by POM for the Col$_h$ phase at 163 °C (a); DSC traces obtained for the first cooling (upper trace) and second heating (lower trace) cycles of **ST1** at a rate of 5 °C min$^{-1}$ (b); XRD profiles depicting the intensity against 2θ obtained for the Col$_h$ phase of compound **ST1** at 155 °C (c) and at 140 °C (d).

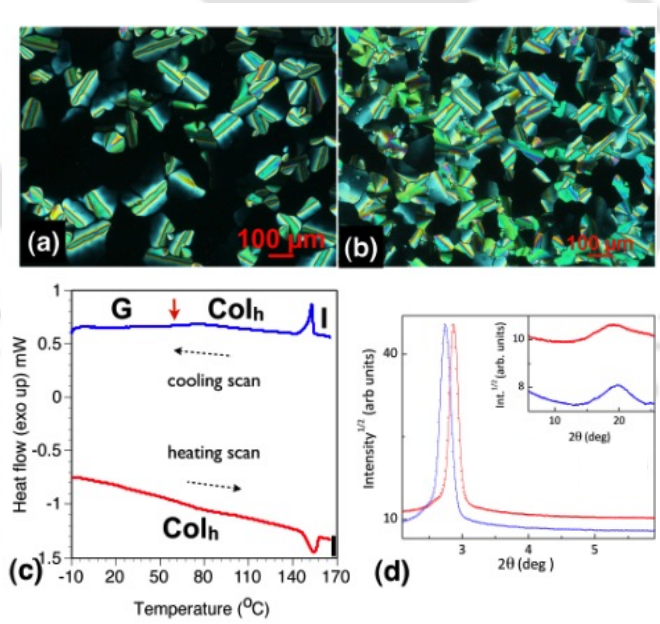


**Figure 2.11.** Photomicrographs of textures as seen by POM for the Col$_h$ phase (a) at 150 °C and (b) at 27 °C of the compound **ST2**; (c) DSC traces obtained for the first cooling (upper trace) and second heating (lower trace) cycles of **ST2** at a rate of 5 °C min$^{-1}$; (d) XRD profiles depicting the intensity against 2θ obtained for the Col$_h$ phase of compound **ST2** at 140 °C and 30°C .

investigated with XRD studies at different temperatures confirms that it is a hexagonal columnar phase (Table 2.3). The XRD profile at 155 $^{o}$C (Fig. 2.10c) exhibits a sharp intense peak corresponding to a *d* spacing of 26.4 Å along with other weaker peaks centered at smaller spacings in the ratio 1: 1/√3: 1/√4: 1/√7: 1/3:1/√12. These values could be indexed to (100), (2-10), (200), (3-10), (310) and (400) reflections of the $Col_h$ mesophase. In the wide-angle region, two diffuse peaks are found at *d*-spacings of 4.69 Å and 3.79Å; moreover, the feature becomes clearer at a low temperature (Fig. 2.10d). The first one is due to the packing of the alkyl tails, while the second one corresponds to the stacking of the molecular cores within the column. The latter is stronger than the former, thereby indicating that the discs are well-ordered within the column.

Thiadiazole derivative **ST2** with six *n*-decyloxy tails, exhibits a Col mesophase over a broad range from 93 $^{o}$C to 155 $^{o}$C during the heating cycle. On cooling the isotropic liquid, the mesophase appears in the form of small batonnets (Fig. 2.11a), which have grown in size and finally coalesced. The mesophase did not show any signs of crystallization even at room temperature as observed under POM (Fig. 2.11b). No signs of crystallization were observed in the DSC scan even up to a temperature of -10 $^{o}$C, thus confirming the presence of a frozen Col structure. (Fig. 2.11c) The XRD profile confirmed the hexagonal columnar structure right down to room temperature. Although these two profiles depict a single peak at low angles, the XRD pattern obtained at 100 $^{o}$C shows more reflections at higher angles, fitting into a $Col_h$ lattice. However, the reflection at wide angles corresponding to the core-core stacking was not observed, indicating a loose packing of the discs within the column (Fig. 2.11d and Table 2.3).

Compound **ST3** with nine *n*-decyloxy tails exhibited an increased thermal range for the Col phase from 49 $^{o}$C to 206 $^{o}$C. Upon cooling from the isotropic liquid, the mesophase appeared with a mosaic texture specific to the Col phase, which remained unchanged at room temperature (Fig. 2.12a). In the DSC scan, there was a phase transition around 47 $^{o}$C, with an enthalpy change of 22.5 kJ/mol (Fig. 2.12b), but no change in the optical texture. The nonshearability of the compound with the unchanged texture confirms the glassy

**Table 2.3.** Results of (hkl) indexation of XRD profiles of the compounds at a given temperature (T) of mesophases[a]

| Compounds ($D$/Å) | Phase (T/°C) | $d_{obs}$ (Å) | $d_{cal}$ (Å) | Miller indices *hkl* | Lattice parameter (Å), lattice area S (Å$^2$), molecular volume V (Å$^3$) |
|---|---|---|---|---|---|
| **ST1** (48.45) | $Col_h$ (155) | 26.40 | 26.42 | 100 | $a$ = 30.51; S = 806.2; V = 3058.2; Z = 1.79 |
| | | 15.27 | 15.26 | 2-10 | |
| | | 13.23 | 13.21 | 200 | |
| | | 9.99 | 9.99 | 3-10 | |
| | | 7.33 | 7.33 | 310 | |
| | | 6.61 | 6.61 | 400 | |
| | | 4.69 ($h_a$) | | | |
| | | 3.79 ($h_c$) | | | |
| | $Col_h$ (140) | 26.36 | 26.37 | 100 | $a$ = 30.45; S = 803.0; V = 2985.3; Z = 1.75 |
| | | 15.23 | 15.22 | 2-10 | |
| | | 13.20 | 13.19 | 200 | |
| | | 9.97 | 9.97 | 3-10 | |
| | | 7.32 | 7.31 | 4-30 | |
| | | 6.60 | 6.59 | 400 | |
| | | 4.74 ($h_a$) | | | |
| | | 3.72 ($h_c$) | | | |
| **ST2** (48.43) | $Col_h$ (140) | 30.72 | 30.72 | 100 | $a$ =35.47; S = 1089.7; V = 5058.2;[b] Z = 2.04[b] |
| | | 4.64 ($h_a$) | | | |
| | $Col_h$ (100) | 31.40 | 31.44 | 100 | $a$ = 36.3; S = 1141.3; V = 5242.1;[b] Z = 2.1[b] |
| | | 18.13 | 18.15 | 2-10 | |
| | | 15.84 | 15.72 | 200 | |
| | | 4.59 ($h_a$) | | | |
| | $Col_h$ (30) | 32.12 | 32.12 | 100 | $a$ = 37.09; S = 1191.3; V = 5306.7;[b] Z = 2.14[b] |
| | | 4.45 ($h_a$) | | | |
| **ST3** (48.42) | $Col_h$ (190) | 29.35 | 29.35 | 100 | $a$ = 33.89; S = 994.8; V = 4138.8;[b] Z = 1.27[b] |
| | | 4.16 ($h_a$) | | | |
| | $Col_h$ (130) | 29.73 | 29.73 | 100 | $a$ = 34.33; S = 1020.8; V = 4323.5;[b] Z= 1.33[b] |
| | | 4.24 ($h_a$) | | | |
| | $Col_h$ (30) | 31.80 | 31.8 | 100 | $a$ = 36.72; S = 1168.0; V = 4951.6;[b] Z = 1.52[b] |
| | | 4.24 ($h_a$) | | | |
| **ST4** (37.99) | $Col_h$ (180) | 26.03 | 26.03 | 100 | $a$ = 30.06; S = 782.5; V = 3034.3; Z = 1.07 |
| | | 4.63 ($h_a$) | | | |
| | | 3.88 ($h_c$) | | | |
| | $Col_h$ (108) | 26 | 26.0 | 100 | $a$ = 30.02; S = 780.3; V = 3086.4; Z = 1.09 |
| | | 4.54 ($h_a$) | | | |
| | | 3.96 ($h_c$) | | | |

[a]The diameter (D) of the disk (estimated from Chem 3D Pro 8.0 molecular model software from Cambridge Soft). $d_{obs}$: spacing observed; $d_{cal}$: spacing calculated (deduced from the lattice parameters; [a] for $Col_h$ phase). The spacings marked $h_a$ and $h_c$ correspond to diffuse reflections in the wide-angle region arising from correlations between the alkyl chains and core regions, respectively. Z indicates the number of molecules per columnar slice of thickness $h_c$, estimated from the lattice area S and the volume V. [b]In the absence of core-core peak, the spacings of the alkyl chain stacking ($h_a$) is taken for these calculations.

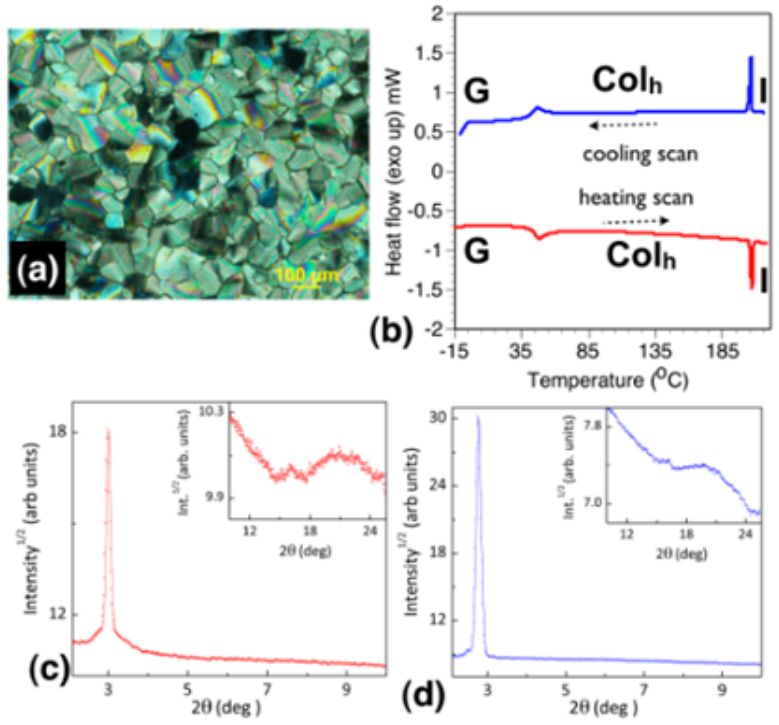


**Figure 2.12.** Photomicrograph of textures as seen by POM for the Col$_h$ phase (a) at 30 °C; (b) DSC traces obtained for the first cooling and second heating cycles of **ST3** at a rate of 5 °C min$^{-1}$; The intensity *vs* 2θ profiles extracted from the XRD patterns of the Col$_h$ phase (c) at 190 $^o$C and (d) at 30 $^o$C for compound **ST3**.

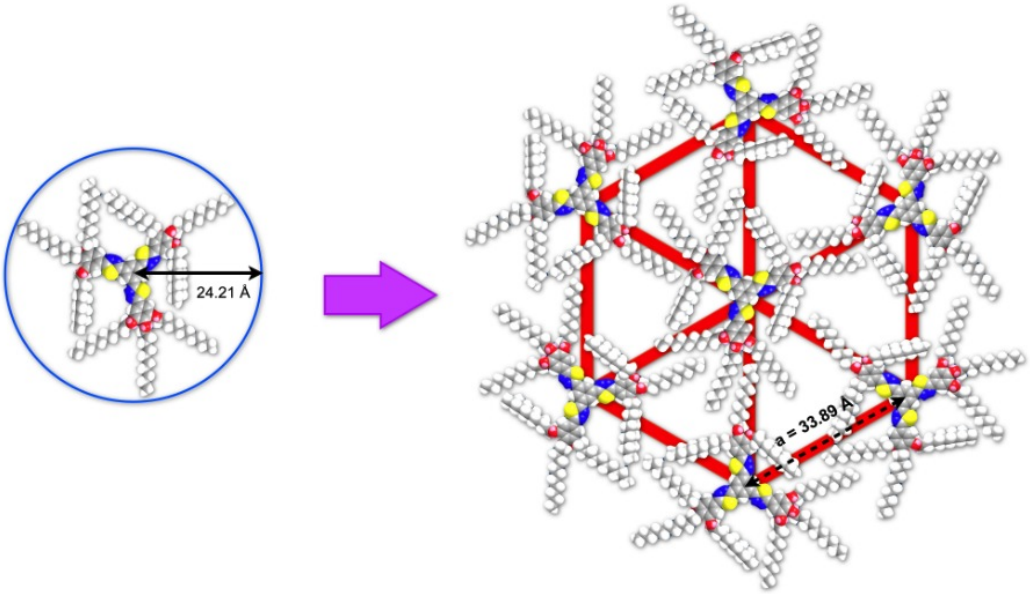


**Figure 2.13.** Self-organization of compound **ST3** in hexagonal columnar (Col$_h$) lattice. Space filling energy minimized (all-*trans*) molecular model of **ST3** derived from molecular mechanics (MM2) method.

nature of the structure. X-ray diffraction studies carried out at 190 $^{o}$C show that the mesophase is columnar with a $D_{6h}$ symmetry and with an intercolumanr distance of 33.9 Å. A Similar pattern was observed for the XRD carried out at 130 $^{o}$C and 30 $^{o}$C, showing that the $Col_h$ phase is of a broad thermal range, freezing into a glassy state at low temperatures. This feature is favorable for charge migration with a concomitant freezing of ionic impurities.[38] The molecular packing could be again of the intercalating type shown in Fig. 2.13.

Compound **ST4** with nine branched tails did not show any abrupt decrease in melting point as expected, but exhibited a hexagonal columnar mesophase over a thermal range of 48 degrees, as confirmed from the POM, DSC and XRD studies. This behavior is in contrast to that of its oxadiazole counterpart **SO4**. These studies on the compounds **ST1-4** again showed the same trend as that in the case of the oxadiazole derivatives **SO1-4** (Fig. 2.8). The mesophase range increases with the number of tails, whereas the branching in the peripheral tails shows an effect that is opposite to the one observed in the case of **ST4**. Overall, the thiadiazole derivatives exhibit an enhanced mesophase range as compared to the oxadiazole derivatives. This is more evident in the case of compound **ST1** with a mesophase range of 31 degrees; as compared to monotropic compound **SO1**. Similarly, the enhanced mesophase range of compound **ST4** with respect to the crystalline compound **SO4** is an example, reiterating the propensity of the thiadiazole ring in improving the thermal behavior. We can assign this enhancement solely to the presence of thiadiazole moiety.

### 2.2.3. Photophysical properties

The Photophysical properties of these star-shaped molecules in solution are depicted in Table 2.4. The absorption and fluorescence spectra of the compounds **SO1-4** and **ST1-4** were taken in micromolar solutions in THF. As evident, the absorption spectra obtained for the solutions of **SO1-4** showed a single absorption maximum in the range of 312-324 nm, whereas the absorption spectra of **ST1-4** showed a bathochromic shift. The absorption maximum of the compounds **ST1-4** was centered in the range of 335-350 nm. Both the

series of molecules show large values of the molar absorption coefficients, thus showing that these are highly conjugated systems ($\varepsilon \geq 25000\ M^{-1}\ cm^{-1}$). Based on their similarity to previous 1,3,4-oxadiazole-based systems, the single absorption band of these systems is attributed to the spin-allowed $\pi$- $\pi^*$ transition of the aromatic system.

The emission spectra of compounds **SO1-4** obtained by exciting the solutions of these compounds at their absorption maxima showed that the emission maxima centers in the range of 388-458 nm (Fig. 2.14a). It is surprising to see that compound **SO2** with six alkyl tails showed a large shift in the emission with an emission maximum at 434 nm, with a large Stoke's shift of 110 nm. Such a large shift in the emission maximum accounts for the large delocalization of the electron cloud as compared to that in the case of compound **SO1**. Compound **SO3** exhibited an emission maximum centered at 461 nm, with a Stoke's shift of 143 nm. Compound **SO4** was similar to **SO3**, except for the branched alkoxy tails. As expected, compound **SO4** exhibits an emission maximum (458 nm, Stoke's shift 139 nm) that did not differ much from compound **SO3**. This shows that the number of alkoxy tails on the aromatic moiety, rather than the nature of these tails, show a significant effect

**Table 2.4.** Photophysical[a] and electrochemical[a,b] properties of star shaped molecules

| Entry | Absorption (nm) | Emission[c] (nm) | Stokes shift nm ($cm^{-1}$) | Quantum Yield[i] | $\lambda_{onset\ (nm)}$ | $\Delta E^{d,e}_{g,\ opt}$ | $E^{f}_{1red}$ | $E^{d,g}_{HOMO}$ | $E^{d,h}_{LUMO}$ |
|---|---|---|---|---|---|---|---|---|---|
| **SO1** | 312 | 388 | 76 (6378) | 0.45 | 357 | 3.48 | -1.24 | -6.52 | -3.04 |
| **SO2** | 324 | 434 | 110 (7822) | 0.43 | 371 | 3.35 | -1.13 | -6.50 | -3.15 |
| **SO3** | 318 | 461 | 143 (9755) | 0.48 | 370 | 3.36 | -1.34 | -6.3 | -2.94 |
| **SO4** | 319 | 458 | 139 (9514) | 0.47 | 369 | 3.37 | -1.45 | -6.2 | -2.83 |
| **ST1** | 335 | 416 | 81 (5812) | 0.25 | 383 | 3.24 | -1.27 | -6.19 | -2.95 |
| **ST2** | 350 | 447 | 97 (6200) | 0.29 | 403 | 3.08 | -1.21 | -6.15 | -3.07 |
| **ST3** | 345 | 471 | 126 (7755) | 0.31 | 398 | 3.12 | -1.07 | -6.33 | -3.21 |
| **ST4** | 345 | 470 | 125 (7709) | 0.26 | 400 | 3.11 | -1.25 | -6.14 | -3.03 |

[a]micromolar solutions in THF; [b] the excited at the respective absorption maxima; [c] Experimental conditions: $Ag/AgNO_3$ as reference electrode, Glassy carbon working electrode, Platinum rod counter electrode, TBAP (0.1 M) as a supporting electrolyte, room temperature, [d] In electron volts (eV), [e] Band gap determined from the red edge of the longest wave length in the UV-vis absorption spectra, [f] In volts (V), [g] Estimated from the formula $E_{HOMO} = E_{LUMO} - E_{g,\ opt,}$ [h]Estimated from the onset reduction peak values by using $E_{LUMO} = -(4.8 - E_{1/2,\ Fc,Fc^+} + E_{red,\ onset})$ eV. [i] Relative quantum yield calculated with respect to quinine sulphate solution in 0.1 M $H_2SO_4$ with a quantum yield of 0.54.

on the emission properties. The emission spectra of compounds **ST1-4** obtained by exciting them at their absorption maxima showed an emission maxima centered in the range 416-471 nm (Fig. 2.14b). Similar to compounds **SO1-4**, we observed a bathochromic shift in the emission with an increase in the number of tails as we move from **ST1** to **ST3**, whereas the emission of compound **ST4** does not differ much from that of compound **ST3**. The observed red shift in the absorption and emission of the thiadiazole derivatives is due to the higher polarizability and basic nature of the sulphur in the thiadiazole moiety. Quantum yields of these compounds were measured with respect to Quinine sulphate solution (in 0.1 M $H_2SO_4$, with quantum yield of 0.54). Oxadiazole-based compounds **SO1-4** showed quantum yields in the range 0.43 to 0.48, whereas thiadiazole-based compounds showed slightly lesser quantum yields ranging from 0.25 to 0.31. As can be seen in the Fig. 2.14c, the blue light is visually perceivable in the emissive state for both the series of compounds. Oxadiazole derivatives exhibited deep blue emission, whereas thiadiazole derivatives exhibited a sky-blue emission. This seems promising, because the blue light emitting materials are not only limited but also their energy levels are high; moreover, they provide an efficient approach for fine-tuning the mission wavelength and for combining with another dopant emitters during the construction of white OLEDs.[40]

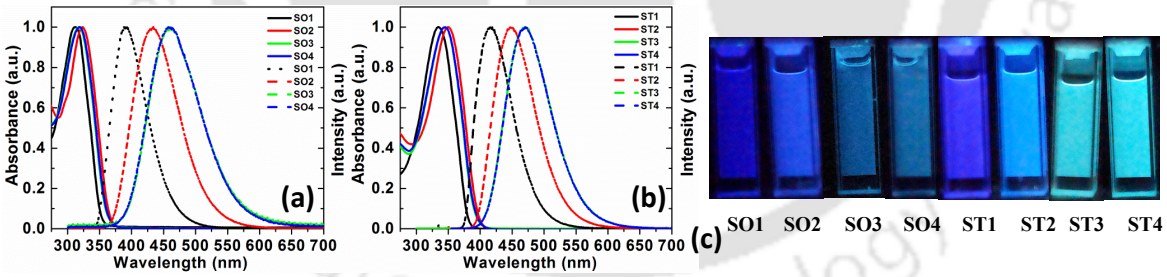


**Figure 2.14.** Normalized absorption (solid line) and emission spectra (dotted line) in THF solution obtained for **SO1-4** (a) and **ST1-4** (b) Pictures of micromolar solutions of compounds **SO1-4** and **ST1-4** in THF as seen with the illumination of 365 nm light (c).

### 2.2.4. Electrochemical properties

Cyclic voltammetry (CV) gives valuable information and allows the estimation of the HOMO and LUMO levels of the organic materials. All the star-shaped molecules were

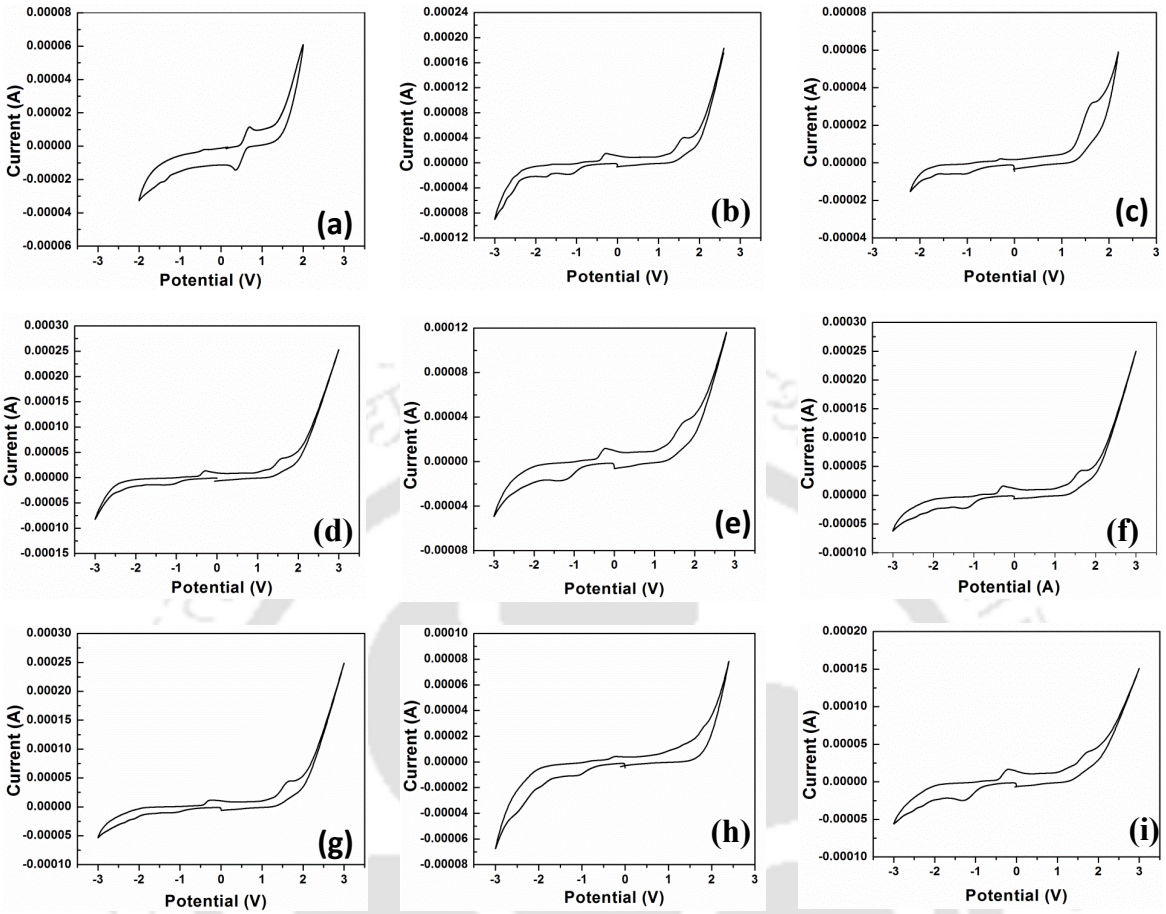


**Figure 2.15.** Cyclic voltammograms of the compounds **SO1-4** (b-e) and **ST1-4** (f-i) in anhydrous THF solution of tetra-n-butylammonium perchlorate (0.1 M) at a scanning rate 0.5mV/s.

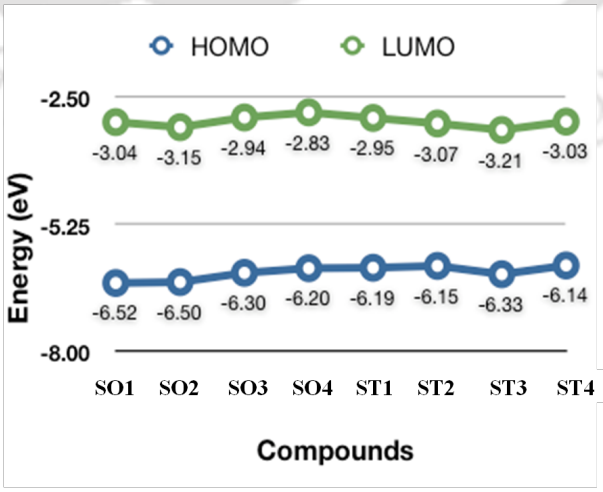


**Figure 2.16.** The HOMO and LUMO energy levels obtained for compounds **SO1-4** and **ST1-4.**

investigated for their electrochemical behavior by carrying out cyclic voltammetry studies in an anhydrous micromolar THF solution. The energy levels and band gaps calculated from these studies are tabulated in Table 2.4. A 0.1 M solution of tetrabutylammonium perchlorate (TBAP) was used as a supporting electrolyte in deoxygenated THF. A single compartment cell equipped with $Ag/AgNO_{3\ (0.1M)}$ reference electrode, platinum rod counter electrode and glassy carbon working electrode was used for the experiments. The reference electrode was calibrated with the ferrocene/ferrocenium ($Fc/Fc^{+}$) redox couple (absolute energy level of –4.80 eV to vacuum).[41] The cyclic voltammograms were recorded with a scanning rate of 0.05 $mVs^{-1}$. All the compounds exhibited well-defined irreversible oxidation and reduction waves (See Fig. 2.15). The optical band gap $E_{g,opt}$ was estimated from the red edge of the absorption spectra.

Oxadiazole derivatives **SO1-4** exhibited higher band gaps, when compared to thiadiazoles **ST1-4** (Table 2.4). The energy levels LUMO were determined by using the formula $E_{LUMO} = -(4.8 - E_{1/2,\ Fc,Fc^{+}} + E_{red\ onset})$ eV, whereas the HOMO energy levels were determined by using the formula $E_{HOMO} = E_{LUMO} - E_{g,\ opt.}$ Oxadiazole-based compounds **SO1-4** exhibited LUMO levels -3.04 eV, -3.15 eV, -2.94 eV and -2.83 eV, whereas the thiadiazole based compounds **ST1-4** exhibited the LUMO levels -2.95 eV, -3.07 eV, -3.21 eV and -3.03 eV respectively (Fig. 2.15 and Fig. 2.16).

### 2.3. Conclusions

In summary, we have synthesized two series of star shaped molecules based on the 1,3,4-oxadiazole and 1,3,4-thiadiazole moieties, varying in the number and nature of the peripheral flexible chains. These two different series of molecules were synthesized through a common intermediate, thus demonstrating the simplicity of the abovementioned method. These compounds were thoroughly characterized and investigated for their thermal, photophysical and electrochemical properties. The thermal behavior was studied with the help of POM, DSC and powder XRD studies. The series based on 1,3,4-thiadiazole moiety is a new class of molecules stabilizing Col phases. We have compared this new series of molecules with their 1,3,4-oxadiazole counterparts to arrive at a

structure-property correlation. 1,3,4-thiadiazole-based LCs exhibited broad mesophase range, with some of them showing close to room temperature crystal to liquid crystal transitions. Many of these molecules exhibit a glassy Col phase, which is beneficial for one-dimensional conductivity. The number and type of the peripheral tails exert a significant effect on the stabilization of the liquid crystallinity of these molecules. Both the series exhibited blue luminescence in solution. Oxadiazole derivatives showed a deep blue emission, whereas the thiadiazole derivatives exhibited a sky-blue emission in solution state. The number and type of the peripheral tails did not have much effect on the absorption maxima, although it showed a significant shift in the emission maxima of these compounds. Thiadiazole derivatives exhibited slightly lower quantum yields as compared to oxadiazole derivatives. Thiadiazole derivatives are new entrants to the limited member family of blue emitting self-assembling materials. These blue light emitting materials are technologically important for the fine-tuning of emission wavelengths upon combining with another dopant emitter during the construction of white OLEDs. Cyclic Voltammetry studies have shown that thiadiazole derivatives show a lower band gap than their oxadiazole counterparts. These 1,3,4-thiadiazole-based star-shaped molecules are promising because of the ease in synthesis, the stabilization of the wide range hexagonal columnar phase, emission tunabilty, and the low band gap, thus have a potential to be used in OLEDs.

## 2.4. Experimental Section

In this section the detailed synthetic procedures and the molecular structural characterization data have been presented for the intermediates and target compounds mentioned in the scheme.

Procedure for the synthesis of ethyl 4-(*n*-decyloxy) benzoate (**1a**):

A mixture of ethyl 4-hydroxybenzoate (18.1 mmol, 1equiv.), anhyd. $K_2CO_3$ (119.2 mmol, 6.6 equiv.), *n*-bromodecane (21.7 mmol, 1.2 equiv.) were taken in dry DMF (20 ml) and heated at 80 $^oC$ for 17 h under nitrogen atmosphere. Then the reaction mixture was poured into ice-water and extracted with $CH_2Cl_2$. The combined extract was washed with water and brine. Dried over anhyd. $Na_2SO_4$ and concentrated. The crude product was purified by

column chromatography on neutral alumina. Elution with hexanes followed by 5% ethyl acetate-hexanes yielded the desired product.

$R_f$ = 0.46 (10% EtOAc-hexanes); colorless liquid, yield: 80%; IR (KBr pellet): $\nu_{max}$ in $cm^{-1}$ 2981, 2928, 2856, 1715, 1579, 1511, 1468, 1436, 1366, 1313, 1254,1167, 1103, 770, 647; $^1$H NMR ($CDCl_3$, 400 MHz): δ 7.97 (d, 2H, *J* = 2.4 Hz, Ar), 6.89(d, 2H, *J* = 2 Hz, Ar), 4.34 (q, 2H, *J* =7.2 Hz, $COOCH_2$), 4.0 (t, 2H, *J* = 6.8 Hz, $OCH_2$), 1.79 (m, 2H, $CH_2$), 1.27-1.47 ( m, 14H, 7 × $CH_2$), 0.86-0.89 (m, 6H, 2 × $CH_3$); $^{13}$C NMR ($CDCl_3$, 100 MHz): 166.69, 163.12, 131.72, 122.90, 114.24, 68.43, 60.80, 32.11, 29.76, 29.58, 29.52, 29.34, 26.20, 22.89, 14.60, 14.31; HRMS (ESI) exact mass calculated for $C_{19}H_{31}O_3$ (M+1) : 307.2268, Found: 307.2276

Procedure for the synthesis of ethyl 3,4,-bis(decyloxy)benzoate (**1b**):

A mixture of ethyl 3,4-dihydroxybenzoate (16.5 mmol, 1equiv.), anhyd. $K_2CO_3$ (108.9 mmol, 6.6 equiv.), *n*-bromodecane (36.2 mmol, 2.2 equiv.) were taken in dry DMF (20 ml) and heated at 80 $^o$C for 17 h under nitrogen atmosphere. Then the reaction mixture was poured into ice-water and extracted with $CH_2Cl_2$. The combined extract was washed with water and brine. Dried over anhyd. $Na_2SO_4$ and concentrated. The crude product was purified by column chromatography on neutral alumina. Elution with hexanes followed by 5-10% ethylacetate-hexanes yielded the desired product.

$R_f$ = 0.54 (10% EtOAc-hexanes); Low melting white solid, yield: 70%; IR (KBr pellet): $\nu_{max}$ in $cm^{-1}$2921, 2850, 1710, 1596, 1517, 1466, 1424, 1338, 1212, 1104, 761, 628; $^1$H NMR ($CDCl_3$, 400 MHz): δ 7.63 (dd, 1H, $J_1$= 2 Hz, $J_2$= 2 Hz, Ar), 7.53 (d, 1H, *J* = 2 Hz, Ar), 6.86 (d, 1H, *J* = 8Hz, Ar), 4.34 (q, 2H, *J* =7.2 Hz, $COOCH_2$), 4.02-4.05 (m, 4H, 2 × $OCH_2$), 1.83 (m, 4H, 2 × $CH_2$), 1.27-1.48 (m, 28H, 14 × $CH_2$), 0.86-0.89 (m, 9H, 3 × $CH_3$). $^{13}$C NMR ($CDCl_3$, 100 MHz): 166.79, 153.38, 148.74, 123.69, 123.02, 114.60, 112.20, 69.55, 69.26, 60.92, 32.14, 29.85, 29.82, 29.80, 29.63, 29.60, 29.56, 29.43, 29.31, 26.23, 26.19, 22.91, 14.63, 14.32. HRMS (ESI) exact mass calculated for $C_{29}H_{51}O_4$ (M+1): 463.3782, Found: 463.3708.

Procedure for the synthesis of ethyl 3,4,5-tris(decyloxy)benzoate (**1c**):

A mixture of ethyl gallate (15.1 mmol, 1equiv.), anhyd. $K_2CO_3$ (99.9 mmol, 6.6 equiv.), *n*-bromodecane (48.4 mmol, 3.2 equiv.) were taken in dry DMF (20 ml) and heated at 80 $^o$C for 17 h under nitrogen atmosphere. Then the reaction mixture was poured into ice-water and extracted with $CH_2Cl_2$. The combined extract was washed with water and brine. Dried over anhyd $Na_2SO_4$ and concentrated. The crude product was purified by column chromatography on neutral alumina. Elution with hexanes followed by 5-10% ethylacetate-hexanes yielded the desired product.

$R_f$ = 0.58 (10% EtOAc-hexanes); Low melting white solid; yield: 70%; IR (KBr pellet): $\nu_{max}$ in $cm^{-1}$2920, 2850, 1710, 1597, 1516, 1466, 1424, 1347, 1213, 1103, 760, 613; $^1$H NMR ($CDCl_3$, 400 MHz): δ 7.26 (s, 2H, Ar), 4.35-4.36 (m, 2H, $COOCH_2$), 4.01 (m, 6H, 3 ×

$OCH_2$), 1.27-1.81 (m, 48H, 24 × $CH_2$), 0.87 (m, 12H, 4 × $CH_3$), $^{13}C$ NMR ($CDCl_3$, 100 MHz): 166.67, 152.99, 145.31, 125.24, 108.19, 73.68, 69.37, 61.14, 32.12, 30.53, 29.93, 29.84, 29.79, 29.60, 29.56, 26.29, 22.89, 14.30. HRMS (ESI) exact mass calculated for $C_{39}H_{71}O_5$ (M+1): 619.5296, Found: 619.5218

Procedure for the synthesis of ethyl 3,4,5-tris(2-ethylhexyloxy) benzoate (**1d**):

A mixture of ethyl gallate (12.6 mmol, 1equiv.), anhyd $K_2CO_3$ (83.2 mmol, 6.6 equiv.), 3-(bromomethyl)heptanes (41.6 mmol, 3.3 equiv.) were taken in dry DMF (20 ml) and heated at 80 $^oC$ for 17 h under nitrogen atmosphere. Then the reaction mixture was poured into ice-water and extracted with $CH_2Cl_2$. The combined extract was washed with water and brine. Dried over anhyd $Na_2SO_4$ and concentrated. The crude product was purified by column chromatography on neutral alumina. Elution with hexanes followed by 5-10% ethylacetate-hexanes yielded the desired product.

$R_f$ = 0.56 (10% EtOAc-hexanes); colorless liquid, yield: 70%; IR (KBr pellet): $\nu_{max}$ in $cm^{-1}$2959, 2931, 2873, 1718, 1588, 1499, 1462, 1429, 1331, 1214, 1105, 765, 593; $^1H$ NMR ($CDCl_3$, 400 MHz): δ 7.25 (s, 2H, Ar), 4.36 (q, 2H, *J* = 6.8 Hz, $COOCH_2$), 3.88 (m, 6H, 3 × $OCH_2$), 1.31-1.77 (m, 27H, 12 × $CH_2$, 3 × CH), 0.91 (21H, 7 × $CH_3$), $^{13}C$ NMR ($CDCl_3$, 100 MHz): 166.81, 153.23, 142.58, 125.14, 107.72, 76.22, 71.56, 61.16, 40.88, 39.85, 30.79, 30.67, 29.52, 29.35, 24.09, 23.91, 23.34, 23.29, 14.63, 14.32, 14.28, 11.34. HRMS (ESI) exact mass calculated for $C_{33}H_{59}O_5$ (M+1): 535.4357, Found: 535.4280.

Procedure for the synthesis of 4-(decyloxy) benzhydrazide (**2a**):

A mixture of ethyl 4-(decyloxy) benzoate (19 mmol, 1equiv.), excess hydrazine hydrate (19 mL), *n*-butanol (20 mL) was refluxed for 40 h. Water (100 mL) was added and resulting precipitate was collected, dried under vacuum, and recrystallized from ethanol to yield pure **2a** as a white solid.

$R_f$ = 0.25 (30% EtOAc-hexanes); white solid, m.p.: 93-95 $^oC$ yield: 75%; IR (KBr pellet): $\nu_{max}$ in $cm^{-1}$3111, 3077, 1719, 1667, 1571, 1472, 1349, 1253, 1113, 986, 888, 717, 505.; $^1H$ NMR ($CDCl_3$, 400 MHz): δ 7.69 (d, 2H, *J* = 7.2 Hz, Ar), 7.31 (br s, 1H, CONH), 6.92 (d, 2H, *J* = 7.2 Hz, Ar), 4.07 (br s, 2H, $NH_2$), 3.99 (s, 2H, 1× $OCH_2$), 1.27-1.79 ( m, 16H, 8 × $CH_2$), 0.88 (m, 3H, 1× $CH_3$). $^{13}C$ NMR ($CDCl_3$, 100 MHz): 168.62, 162.33, 128.83, 124.81, 114.64, 68.44, 32.08, 29.74, 29.55, 29.50, 29.31, 26.18, 22.87, 14.29. HRMS (ESI) exact mass calculated for $C_{17}H_{29}N_2O_2$ (M+1): 293.2224, Found: 293.2153.

Procedure for the synthesis of 3,4,-bis(decyloxy) benzhydrazide (**2b**):

A mixture of ethyl 3,4,-bis(decyloxy)benzoate (10.2mmol, 1equiv.), excess hydrazine hydrate (11 mL), *n*-butanol (11 mL) was refluxed for 40 h. Water (100 mL) was added and resulting precipitate was collected, dried under vacuum, and recrystallized from ethanol to yield pure **2b** as a white solid.

$R_f$ = 0.25 (20% EtOAc-hexanes); white solid, m.p.: 118-120 $^oC$; yield: 70%; IR (KBr pellet): $\nu_{max}$ in $cm^{-1}$ 3279, 2921, 2851, 1618, 1580, 1509, 1468, 1332, 1268, 1146, 987, 873, 717, 512; $^1H$ NMR ($CDCl_3$, 400 MHz): δ 7.4 (br s, 1H, CONH), 7.34 (s, 1H, Ar), 7.23 (d, 1H, *J* = 8 Hz, Ar), 6.85 (d, 1H, *J* = 8.4 Hz, Ar), 4.08 (br s, 2H, $NH_2$), 4.02 (t, 4H, 2 × $OCH_2$), 1.26 – 1.82 (m, 32H, 16 × $CH_2$), 0.87 (m, 6H, 2 × $CH_3$); $^{13}C$ NMR ($CDCl_3$, 100 MHz): 168.78, 152.55, 149.32, 125.21, 119.73, 112.77, 112.65, 69.61, 69.37, 32.12, 29.83, 29.82, 29.79, 29.78, 29.62, 29.60, 29.55, 29.42, 29.33, 26.22, 26.19, 22.89, 14.31. HRMS (ESI) exact mass calculated for $C_{27}H_{49}N_2O_3$ (M+1): 449.3743, Found: 449.3664.

Procedure for the synthesis of 3,4,5-tris(decyloxy)benzhydrazide (**2c**):

A mixture of ethyl 3,4,5-tri-*n*-decyloxybenzoate (10 mmol, 1equiv.), excess hydrazine hydrate (10 mL), *n*-butanol (20 mL) was refluxed for 40 h. Water (100 mL) was added and resulting precipitate was collected, dried under vacuum, and recrystallized from ethanol to yield pure **2c** as a white solid.

$R_f$ = 0.45 (20% EtOAc-hexanes); white solid, m.p.: 114-115$^oC$; yield: 80%; IR (KBr pellet): $\nu_{max}$ in $cm^{-1}$ 3475, 2923, 2852, 1746, 1640, 1580, 1499, 1467, 1347, 1238, 1120, 1019, 826, 719, 523; $^1H$ NMR ($CDCl_3$, 400 MHz): δ 7.33 (br s, 1H, CONH), 6.92 (s, 2H, Ar), 3.99 (m, 8H, 1× $NH_2$, 3 × $OCH_2$), 1.27– 1.80 (m, 48H, 24×$CH_2$) 0.88 (m, 9H, 3×$CH_3$); $^{13}C$ NMR ($CDCl_3$, 100 MHz): 168.91, 153.37, 141.60, 127.61, 105.71, 73.70, 69.50, 32.10, 30.50, 29.91, 29.83, 29.77, 29.59, 29.53, 26.26, 22.87, 14.28. HRMS (ESI) exact mass calculated for $C_{37}H_{69}N_2O_4$ (M+1): 605.5252, Found: 605.5171.

Procedure for the synthesis of 3,4,5-tris(2-ethylhexyloxy) benzhydrazide (**2d**):

A mixture of ethyl 3,4,5-tris(2-ethylhexyloxy) benzoate (6.7 mmol, 1 equiv.), excess hydrazine hydrate (8 mL), *n*-butanol (20 mL) was refluxed for 40 h. Water (100 mL) was added and resulting precipitate was collected, dried under vacuum, and recrystallized from ethanol to yield pure **2d** as a white solid.

$R_f$ = 0.29 (20% EtOAc-hexanes); colorless viscous liquid, yield: 65%; IR (KBr pellet): $\nu_{max}$ in $cm^{-1}$ 3314, 2959, 2932, 2874, 1632, 1580, 1494, 1463, 1343, 1227, 1006, 862, 769, 647; $^1H$ NMR ($CDCl_3$, 400 MHz) 7.38 (br s, 1H, CONH), 6.93 (s, 2H, Ar), 3.83 - 3.87 (m, 8H, 1× $NH_2$, 3 × $OCH_2$), 1.25– 1.76 (m, 27H, 3×CH, 12×$CH_2$) 0.92 (m, 18H, 6 × $CH_3$); $^{13}C$ NMR ($CDCl_3$, 100 MHz): 169.04, 153.65, 141.58, 127.50, 105.10, 76.21, 71.67, 40.81, 39.80, 30.69, 30.64, 29.50, 29.29, 24, 23.87, 23.33, 23.28, 14.33, 14.29, 11.38, 11.29. HRMS (ESI) exact mass calculated for $C_{31}H_{57}N_2O_4$(M+1): 521.4313, Found: 521.4240

Procedure for the synthesis of 1,3,5-tris(5-(4-(decyloxy)phenyl)-1,3,4-oxadiazole-2-yl) benzene (**SO1**):

1,3,5-benzenetricarboxylic acid (2.5mmol) in 6 ml of thionyl chloride and DMF (catalytic amount) was refluxed for 4 h. The excess of thionyl chloride was removed by distillation, the crude product (1,3,5-benzenetricarbonyl trichloride) was dried in vacuo and

used for the next reaction without further purification and characterization. A solution of 1,3,5-benzenetricarbonyl trichloride (2.2 mmol, 1equiv.) in THF (5 mL) was added dropwise into a solution of 4-(decyloxy) benzohydrazide (6.8 mmol, 3.05equiv.) and triethylamine (6.6mmol, 3equiv.) in THF (20mL). The reaction mixture was refluxed for 12 h. After cooling, THF was evaporated in rotavapor and the residue was extracted with dichloromethane. The extract was washed with water and brine. Dried over anhyd. $Na_2SO_4$ and concentrated. The resulting crude product (**3a**) was directly used for next reaction.

The crude product **3a** (0.3mmol, 1equiv.) was dissolved in phosphorus oxychloride ($POCl_3$) (6 mL) and refluxed for about 12 h. Excess $POCl_3$ was distilled out and the residue was slowly added to ice water and extracted with dichloromethane. After removal of solvent *in vacuo*, the crude product was further purified through column chromatography on neutral alumina. Elution with 10-20% ethylacetate-hexanes yielded the desired product.

$R_f$ = 0.69 (40% EtOAc-hexanes); white solid, yield: 44%; IR (KBr pellet): $\nu_{max}$ in $cm^{-1}$ 3447, 2924, 2853, 1611, 1497; $^1$H NMR ($CDCl_3$, 400 MHz): δ 8.95 (s, 3H, Ar), 8.12 (d, 6H, *J* = 7.6 Hz, Ar), 7.04 (d, 6H, *J* = 8Hz, Ar), 4.04 (br s, 6H, 3×$OCH_2$), 1.29-1.82 (m, 48H, 24×$CH_2$), 0.89 (m, 9H, 3×$CH_3$); $^{13}$C NMR ($CDCl_3$, 100 MHz): 165.64, 162.59, 162.50, 129.21, 126.91, 126.47, 115.71, 115.30, 68.57, 32.10, 29.89, 29.85, 29.78, 29.76, 29.60, 29.52, 29.35, 26.21, 22.88, 14.30. MALDI TOF MS ($LD^+$): *m/z* for $C_{60}H_{79}N_6O_6$ [M+1], Calcd: 979.6056, Found: 979.6091.

Procedure for the synthesis of 1,3,5-tris(5-(4-(decyloxy)phenyl)-1,3,4-thiadiazole-2-yl) benzene (**ST1**):

The crude product **3a** (0.5mmol, 1equiv.) in dry toluene (8 mL) was added dropwise to a solution of Lawesson's reagent (1.7 mmoL, 3.6 equiv.) in toluene at room temperature under Argon atmosphere and refluxed for 24 h. After the reaction, toluene was removed by distillation. After removal of solvent *in vacuo*, the crude product was further purified through column chromatography on neutral alumina. Elution with 10-20% ethyl acetate-hexanes yielded the desired product.

$R_f$ = 0.71 (40% EtOAc-hexanes); off white solid, yield: 36%; IR (KBr pellet): $\nu_{max}$ in $cm^{-1}$ 3447, 2923, 2852, 1605, 1497; $^1$H NMR ($CDCl_3$, 400 MHz): δ 8.72 (s, 3H, Ar), 7.97 (d, 6H, *J* =8.8 Hz, Ar), 7.01(d, 6H, *J* =8.8 Hz, Ar), 4.04 (m, 6H, 3×$OCH_2$), 1.28-1.83 (m, 48H, 24×$CH_2$), 0.87 (m, 9H, 3×$CH_3$); $^{13}$C NMR ($CDCl_3$, 100 MHz): 169.07, 165.17, 161.96, 132.34, 129.77, 128.19, 122.36, 115.22, 68.50, 32.11, 29.89, 29.79, 29.64, 29.54, 29.39, 26.23, 22.89, 14.31. MALDI TOF MS ($LD^+$): *m/z* for $C_{60}H_{79}N_6O_3S_3$[M+1], Cald: 1027.5370, Found: 1027.5376

Procedure for the synthesis of 1,3,5-tris(5-(3,4-bis(decyloxy)phenyl)-1,3,4-oxadiazole-2-yl) benzene (**SO2**):

1,3,5-benzenetricarboxylic acid (1.6 mmol) in 6 ml of thionyl chloride and DMF (catalytic amount) was refluxed for 4 h. The excess of thionyl chloride was distilled off and

the crude product (1,3,5-benzenetricarbonyl trichloride) was dried *in vacuo* and used for the next reaction without further purification. The solution of 1,3,5-benzenetricarbonyl trichloride (1.4mmol, 1equiv.) in THF was added dropwise to a solution of 3,4,-bis(decyloxy) benzhydrazide (4.4 mmol, 3.05 equiv.) and triethylamine (4.4 mmol, 3 equiv.) in THF (20 mL) and refluxed for 12h. After cooling, THF was removed through distillation and the residue was extracted with dichloromethane. The extract was washed with water and brine. Dried over $Na_2SO_4$ and concentrated. The resulting crude product (**3b**) was directly used for next reaction.

The crude product **3b** (0.4 mmol, 1equiv.) was dissolved in $POCl_3$ (6 mL) and refluxed for about 12 h. Excess $POCl_3$ was distilled out and the residue was slowly added into ice water and extracted with dichloromethane. After removal of solvent *in vacuo*, the crude products were further purified through column chromatography on neutral alumina. Elution with 10-20% ethylacetate-hexanes yielded the desired product.

$R_f$ = 0.61 (90% DCM-hexanes); off white solid, yield: 35%; IR (KBr pellet): $\nu_{max}$ in $cm^{-1}$ 3447, 2923, 2852, 1605, 1503; $^1$H NMR ($CDCl_3$, 400 MHz): δ 8.96 (s, 3H, Ar), 7.73 (d, 3H, *J* =8 Hz, Ar), 7.66 (s, 3H, Ar), 6.99 (d, 3H, *J* =8.4 Hz, Ar), 4.13 (t, 6H, 3 × $OCH_2$), 4.08(t, 6H, 3 × $OCH_2$), 1.28-1.92 (m, 96H, 48×$CH_2$), 0.87 (m, 18H, 6 × $CH_3$); $^{13}$C NMR ($CDCl_3$, 100 MHz): 165.82, 162.63, 152.94, 149.68, 127.05, 126.47, 121.09, 115.80, 113.10, 111.93, 69.74, 69.35, 32.11, 29.84, 29.83, 29.79, 29.78, 29.66, 29.62, 29.56, 29.46, 29.34, 26.27, 26.21, 22.88, 14.28. MALDI TOF MS ($LD^+$): *m/z* for $C_{90}H_{139}N_6O_9$[M+1], Calculated: 1448.0598. Found: 1448.0602.

Procedure for the synthesis of 1,3,5-tris(5-(3,4-bis(decyloxy)phenyl)-1,3,4-thiadiazole-2-yl)benzene (**ST2**):

The solution of crude product **3b** (0.3 mmol, 1equiv.) in dry toluene (8 mL) was added dropwise to a solution of Lawesson's reagent (1.1 mmol, 3.6 equiv.) in toluene at room temperature and refluxed for a day under Argon atmosphere. Toluene was removed by distillation. After the removal of solvent *in vacuo*, the crude products were further purified through column chromatography on neutral alumina. Elution with 10-20% ethyl acetate-hexanes yielded the desired product.

$R_f$ = 0.68 (70% DCM-hexanes); off white solid, yield: 42%; IR (KBr pellet): $\nu_{max}$ in $cm^{-1}$ 3433, 2909, 2845, 1598, 1523; $^1$H NMR ($CDCl_3$, 400 MHz): δ 8.7 (s, 3H, Ar), 7.65 (s, 3H, Ar), 7.47 (d, 3H, *J* =7.6 Hz, Ar), 6.94 (d, 3H, *J* =8.4 Hz, Ar), 4.07-4.11 (m, 12H, 6×$OCH_2$), 1.29-1.88 (m, 96H, 48×$CH_2$), 0.89 (m, 18H, 6×$CH_3$); $^{13}$C NMR ($CDCl_3$, 100 MHz): 169.52, 165.44, 152.37, 149.70, 132.57, 128.54, 122.67, 122.13, 113.36, 112.45, 69.65, 69.44, 32.15, 29.87, 29.85, 29.83, 29.81, 29.66, 29.64, 29.59, 29.44, 29.36, 26.26, 26.23, 22.92, 14.33. MALDI TOF MS ($LD^+$): *m/z* for $C_{90}H_{139}N_6O_9S_3$[M+1], Calculated: 1495.9913. Found: 1495.9918.

Procedure for the synthesis of 1,3,5-tris(5-(3,4,5-tris(decyloxy)phenyl)-1,3,4-oxadiazole-2-yl) benzene (**SO3**):

1,3,5-benzenetricarboxylic acid (1.1 mmol) in 6 ml of thionyl chloride and DMF (catalytic amount) was refluxed for 4 h. The excess of thionyl chloride was removed by distillation and the crude product (1,3,5-benzenetricarbonyl trichloride) was dried in vacuo. This is used for the next reaction without further purification. The solution of 1,3,5-benzenetricarbonyl trichloride (0.9 mmol, 1equiv.) in THF was added dropwise to a solution of 3,4,5-tri-*n*-decyloxy benzohydrazide (2.8 mmol, 3.05 equiv.) and triethylamine (2.7 mmol, 3 equiv.) in THF (20 mL). The reaction mixture was refluxed for 12 h. After cooling, THF was evaporated under reduced pressure and the residue was extracted with dichloromethane. The extract was washed with water and brine. Dried over anhyd. $Na_2SO_4$ and concentrated. The resulting crude product (**3c**) was directly used for next reaction.

The crude product **3c** (0.3mmol, 1equiv.) was dissolved in $POCl_3$ (7 mL) and refluxed for about 12 h. Excess $POCl_3$ was distilled off and the residue was slowly added into ice water and extracted with dichloromethane. After removal of solvent *in vacuo*, the crude product was further purified through column chromatography on neutral alumina. Elution with 10-20% ethylacetate-hexanes yielded the desired product.

$R_f$ = 0.58 (10% EtOAc-hexanes); yellow solid, yield: 31 %; IR (KBr pellet): $\nu_{max}$ in $cm^{-1}$ 3430, 2923, 2852, 1592, 1494; $^1$H NMR ($CDCl_3$, 400 MHz): $^1$H NMR ($CDCl_3$, 400 MHz) 9.06 (s, 3H, Ar), 7.39 (s, 6H, Ar), 4.13 (t, $J$ =6.4 Hz, 12H, 6 × $OCH_2$), 4.07 (t, $J$ =6.4 Hz, 6H, 3 × $OCH_2$), 1.28-1.90 (m, 144H, 72 × $CH_2$), 0.87 (m, 27H, 9 × $CH_3$). $^{13}$C NMR ($CDCl_3$, 100 MHz): 166.08, 162.97, 153.98, 142.10, 127.49, 126.47, 118.02, 105.87, 73.89, 69.74, 32.13, 30.58, 29.95, 29.89, 29.86, 29.80, 29.65, 29.61, 29.57, 26.36, 26.30, 22.89, 14.31 MALDI TOF MS ($LD^+$): *m/z* for $C_{120}H_{200}N_6O_{12}$[M+2], Calculated: 1917.5213, Found: 1917.5244.

Procedure for the synthesis of 1,3,5-tris(5-(3,4,5-tris(decyloxy)phenyl)-1,3,4-thiadiazole-2-yl) benzene (**ST3**):

The solution of crude product **3c** (0.2mmol, 1equiv.) in dry toluene (8 mL) was added dropwise to a solution of Lawesson's reagent (0.9 mmoL, 3.6 equiv.) in toluene at room temperature under Argon atmosphere and refluxed for 24 h. After the reaction, toluene was evaporated under reduced pressure. After removal of solvent *in vacuo*, the crude product was further purified through column chromatography on neutral alumina. Elution with 10-20% ethylacetate-hexanes yielded the desired product.

$R_f$ = 0.61 (10% EtOAc-hexanes); green waxy solid, yield: 49%; IR (KBr pellet): $\nu_{max}$ in $cm^{-1}$ 3436, 2924, 2853, 1584, 1509; $^1$H NMR ($CDCl_3$, 200 MHz): $^1$H NMR ($CDCl_3$, 400 MHz) 8.65 (s, 3H, Ar), 7.19 (s, 6H, Ar), 4.02-4.07 (m, 18H, 9× $OCH_2$), 1.28 -1.88 (m, 144H, 72 × $CH_2$), 0.87 (m, 27H, 9 × $CH_3$). $^{13}$C NMR ($CDCl_3$, 100 MHz): 169.59, 165.71, 153.78, 141.38, 132.40, 128.48, 124.65, 106.64, 73.83, 69.56, 32.13, 30.59, 29.96, 29.87, 29.83, 29.67, 29.58, 26.32, 22.90, 14.31. MALDI TOF MS ($LD^+$): *m/z* for $C_{120}H_{200}N_6O_9S_3$[M+2], Calculated: 1965.4528, Found: 1965.4528.

Procedure for the synthesis of 1,3,5-tris(5-(3,4,5-tris((2-ethylhexyl)oxy)phenyl)-1,3,4-oxadiazole-2-yl)benzene (**SO4**):

1,3,5-benzenetricarboxylic acid (1.3mmol) in 7 ml of thionyl chloride and DMF (catalytic amount) was heated under reflux for 4 h. The excess of thionyl chloride was removed by distillation, the crude product (1,3,5-benzenetricarbonyl trichloride) was dried *in vacuo* and used for the next reaction without further purification. The solution of 1,3,5-benzenetricarbonyl trichloride (1.2 mmol, 1equiv.) in THF (5 mL) was added dropwise to a solution of 3,4,5-tris(2-ethylhexyloxy) benzohydrazide (3.8 mmol, 3.05 equiv.) and triethylamine (3.7mmol, 3equiv.) in THF (15 mL). The reaction mixture was refluxed for 12 h. After cooling, THF was removed through distillation and the residue was extracted with dichloromethane. The extract was washed with water and brine, finally dried over anhyd $Na_2SO_4$ and concentrated. The resulting crude product (**3d**) was directly used for next reaction.

The crude product **3d** (0.3mmol, 1equiv.) was dissolved in $POCl_3$, (8mL) and refluxed for about 12 h. Excess $POCl_3$ was distilled out and the residue was slowly added into ice water and extracted with dichloromethane. After removal of solvent *in vacuo*, the crude product was further purified through column chromatography on neutral alumina. Elution with 5-10% ethylacetate-hexanes yielded the desired product.

$R_f$ = 0.62 (10% EtOAc-hexanes); off white solid, yield: 32%; IR (KBr pellet): $\nu_{max}$ in $cm^{-1}$ 3441, 2933, 2874, 1591, 1490; $^1$H NMR ($CDCl_3$, 400 MHz): 9.07 (s, 3H, Ar), 7.39 (s, 6H, Ar), 4.01 (t, $J$ =6.4 Hz,12H, 6× $OCH_2$), 3.96 (t, $J$ =6.4 Hz, 6H, 3× $OCH_2$), 1.34-1.83 (m, 81H, 9 × CH, 36 × $CH_2$), 0.91-0.99 (m, 54H, 18 × $CH_3$). $^{13}$C NMR ($CDCl_3$, 100 MHz): 166.24, 163.03, 154.14, 142.01, 127.56, 126.50, 117.90, 105.28, 76.35, 71.66, 40.87, 39.91, 30.80, 30.66, 29.51, 29.38, 24.07, 23.89, 23.34, 23.27, 14.32, 14.29, 11.44, 11.41. MALDI TOF MS ($LD^+$): *m/z* for $C_{102}H_{164}N_6O_{12}$ [M+2], Calculated: 1665.2396, Found: 1665.2361.

Procedure for the synthesis of 1,3,5-tris(5-(3,4,5-tris((2-ethylhexyl)oxy)phenyl)-1,3,4-thiadiazole-2-yl) benzene (**ST4**):

The solution of crude product **3d** (0.4mmol, 1equiv.) in dry toluene (8 mL) was added dropwise to a solution of Lawesson's reagent (1.6 mmoL, 3.6 equiv.) in toluene at room temperature under Argon atmosphere and refluxed for 24h. After the reaction, toluene was evaporated under reduced pressure. After removal of solvent *in vacuo*, the crude product was further purified through column chromatography on neutral alumina. Elution with 5-10% ethylacetate-hexanes yielded the desired product.

$R_f$ = 0.65 (10% EtOAc-hexanes); greenish waxy solid, yield: 31%; IR (KBr pellet): $\nu_{max}$ in $cm^{-1}$3434, 2963, 2876, 1583, 1460; $^1$H NMR ($CDCl_3$, 400 MHz): 8.77 (s, 3H, Ar), 7.27 (s, 6H, Ar), 3.98 (m, 18H, 9× $OCH_2$), 1.26-1.84 (m, 81H, 9 × CH, 36 × $CH_2$), 0.97 (m, 54H, 18 × $CH_3$). $^{13}$C NMR ($CDCl_3$, 100 MHz): 169.78, 165.77, 154.04, 141.40, 132.57, 128.66, 124.61, 106.20, 76.33, 71.75, 40.84, 39.81, 30.71, 30.66, 29.51, 29.31, 24.03, 23.89, 23.34,

23.30, 14.34, 14.31, 11.40, 11.32. MALDI TOF MS ($LD^+$): *m/z* for $C_{102}H_{164}N_6O_9S_3$ [M+2], Calculated: 1713.1711, Found: 1713.1674.

## 2.5. References


1. (a) S. Chandrasekhar, in *Liquid Crystals*, 2nd ed.; Cambridge University Press: New York, 1994; (b) J. W. Goodby, I. M. Saez, S. J. Cowling, V. Görtz, M. Draper, A. W. Hall, S. Sia, G. Cosquer, S. –E. Lee and E. P. Raynes, *Angew. Chem. Int. Ed.*, 2008, **47**, 2754-2787; (c) T. Geelhaar, K. Griesar and B. Reckmann, *Angew. Chem. Int. Ed.*, 2013, **52**, 8798-8809; (d) C. Tschierske, *Angew. Chem., Int. Ed.*, 2013, **52**, 8828-8878; (e) *Handbook of Liquid Crystals: Fundamentals*, eds. J. W. Goodby, P. J. Collings, T. Kato, C. Tschierske, H. Gleeson and P. Raynes, Wiley-VCH: Weinheim, Germany, 2014, Vol. **1**.
2. (a) F. Renitzer, *Monatsch. Chem.*, 1888, **9**, 421-441. (b) F. Reinitzer, *Liq. Cryst.*, 1989, **5**, 7–18.
3. G. W. Gray, K. J. Harrison and J. A. Nash, *Electron. Lett.*, 1973, **9**, 130-131.
4. S. Chandrasekhar, B. K. Sadashiva and K. A. Suresh, *Pramana*, 1977, **9**, 471-480.
5. (a) S. Sergeyev, W. Pisula and Y.H. Geerts, *Chem. Soc. Rev*., 2007, **36**, 1902−1929; (b) S. Laschat, A. Baro, N. Steinke, F. Giesselmann, C. Hagele, G. Scalia, R. Judele, E. Kapatsina, S. Sauer, A. Schreivogel and M. Tosoni, *Angew. Chem., Int. Ed*., 2007, **46**, 4832−4837; (c) W. Pisula, M. Zorn, J. Y. Chang, K. Müllen and R. Zentel, *Macromol. Rapid Commun.*, 2009, **30**, 1179−1202; (d) S. Kumar, *Chemistry of Discotic Liquid Crystals: From Monomers to Polymers*, CRC Press: Boca Raton, FL, 2010; (e) B. R. Kaafarani, *Chem. Mater*., 2011, **23**, 378−396; (f) R. J. Bushby and K. Kawata, *Liq. Cryst*., 2011, **38**, 1415 – 1426; (g) Q. Li, *Self-Organized semiconductors: From Materials to Device Applications*, John Wiley & Sons: New York, 2011; (h) S. Kumar, *Isr. J. Chem.*, 2012, **52**, 820 – 829; (i) Q. Li, *Nanoscience with Liquid Crystals: From Self-Organized Nanostructures to Applications*, Ed., Springer, Heidelberg, 2014; (j) X. Zhou, S. Kang, S. Kumar, R. Kulkar, S. Z. D. Cheng and Q. Li, *Chem. Mater.*, 2008, **20**, 3551-3553; (k) X. Zhou, S. Kang, S. Kumar and Q. Li, *Liq. Cryst.*, 2009, **3**, 269-274.
6. K. Kawata, *Chem. Rec.*, 2002, **2**, 59 – 80.
7. S. Chandrasekhar, S. K. Prasad, G. G. Nair, D. S. S. Rao, S. Kumar and M. Manickam, *EuroDisplay-99, The 19th Intl. Display Res. Conf. Late-News Papers* 1999, pp. 9–11.
8. G. G. Nair, D. S. S. Rao, S. K. Prasad, S. Chandrasekhar and S. Kumar, *Mol. Cryst. Liq. Cryst.*, 2003, **397**, 245 – 252.
9. V. S. K. Balagurusamy, S. K. Prasad, S. Chandrasekhar, S. Kumar, M. Manickam and C. V. Yelamaggad, *Pramana*, 1999, **53**, 3 – 11.
10. (a) L. S. Mende, A. Fechtenkotter, K. Mullen, E. Moons, R. H. Friend and J. D. MacKenzie, *Science* 2001, **293**, 1119 – 1122; (b) H. C. Hesse, J. Weickert, M. Al-Hussein, L. Dössel, X. Feng, K. Mullen and L. S. Mende, *Solar Energy Mater.*

*Sol. Cells*, 2010, **94**, 560–567; (c) Q. Sun, L. Dai, X. Zhou, L. Li and Q. Li, *Applied Physics Letters* 2007, **91**, 253505.

11. (a) A. Bacher, I. Bleyl, C. H. Erdelen, D. Haarer, W. Paulus and H. W. Schmidt, *Adv. Mater.*, 1997, **9**, 1031 – 1035; (b) A. Bacher, C. H. Erdelen, W. Paulus, H. Ringsdorf, H. W. Schmidt and P. Schuhmacher, *Macromolecules,* 1999, **32**, 4551–4557; (c) I. Seguy, P. Destruel, and H. Bock, *Synth. Met.*, 2000, **111**, 15–18. (d) T. Hassheider, S. A. Benning, H. S. Kitzerow, M. F. Achard and H. Bock, *Angew. Chem., Int Ed.*, 2001, **40**, 2060–2063; (e) S. Alibert-Fouet, S. Dardel, H. Bock, M. Oukachmih, S. Archambeau, I. Seguy, P. Jolinat, and P. Destruel, *ChemPhysChem*, 2003, **4**, 983–985; (f) M. O'Neill and S. M. Kelly, *Adv. Mater.*, 2011, **23**, 566-584; (g) J. Eccher, G. C. Faria, H. Bock, H. von Seggern and I. H. Bechtold, *ACS Appl Mater Interfaces,* 2013, **5***,* 11935–11943.
12. (a) A. M. van de Craats, N. Stutzmann, O. Bunk, M. M. Nielsen, M. Watson, K. Mullen, H. D. Chanzy, H. Sirringhaus and R. H. Friend, *Adv. Mater.*, 2003, **15**, 495 – 499; (b) S. Cherian, C. Donley, D. Mathine, L. LaRussa, W. Xia and N. Armstrong, *J. Appl. Phys.*, 2004, **96**, 5638 – 5643; (c) B. A. Jones, M. J. Ahrens, M.-H Yoon, A. Facchetti, T. J. Marks and M. R. Wasielewski, *Angew. Chem., Int. Ed*., 2004, **43**, 6363–6366; (d) I. O. Shklyarevskiy, P. Jonkheijm, N. Stutzmann, D. Wasserberg, H. J. Wondergem, P. C. M. Christianen, A. P. H. J. Schenning, D. M. de Leeuw, Z. Tomovic, J. Wu, K. Mullen and J. C. Maan, *J. Am. Chem. Soc.*, 2005, **127**, 16233 –16237; (e) W. Pisula, A. Menon, M. Stepputat, I. Lieberwirth, U. Kolb, A. Tracz, H. Sirringhaus, T. Pakula and K. Mullen, *Adv. Mater.*, 2005, **17**, 684 – 689; (f) S. Xiao, M. Myers, Q. Miao, S. Sanaur, K. Pang, M. L. Steigerwald and C. Nuckolls, *Angew. Chem. Int. Ed.*, 2005, **44**, 7390 – 7394; (g) J. -Y. Cho, B. Domercq, S. C. Jones, J. Yu, X. Zhang, Z. An, M. Bishop, S. Barlow, S. R. Marder and B. J. Kippelen, *J. Mater. Chem*., 2007, **17**, 2642 – 2647; (h) Y. Shimizu, K. Oikawa, K. I. Nakayama and D. Guillon, *J. Mater. Chem.*, 2007, **17**, 4223 – 4229; (i) H. N. Tsao, H. J. Rader, W. Pisula, A. Rouhanipour and K. Mullen, *Phys. Status Solidi A,* 2008, **205**, 421 – 429; (j) J. P. Bramble, D. J. Tate, D. J. Revill, K. H. Sheikh, J. R. Henderson, F. Liu, X. Zeng, G. Ungar and R. J. Bushby, S. D. Evans, *Adv. Funct. Mater.,* 2010, 20, 914–920.
13. (a) J. D. Wright, P. Roisin, G. P. Rigby, R. J. M. Nolte, M. J. Cook and S. C. Thorpe, *Sens. Actuators, B*, 1993, **13**, 276 – 280; (b) J. Clements, N. Boden, T. D. Gibson, R. C. Chandler, J. N. Hulbert and E. A. Ruck-Keene, *Sens. Actuators B*, 1998, **47**, 37–42; (c) N. Boden, R. J. Bushby, J. Clements and B. Movaghar *J. Mater. Chem.,* 1999, **9**, 2081–2086; (d) V. Bhalla, A. Gupta, M. Kumar, D. S. S. Rao and S. K. Prasad, *ACS Appl. Mater. Interfaces,* 2013, **5**, 672–679.
14. (a) D. D. L. Chung, *J. Mater. Sci.*, 2002, **37**, 1475 – 1489; (b) A. Venu Gopal and P. Venkateswara Rao, *Mater. Manuf. Processes,* 2004, **19**, 177 – 186; (c) K. Kawata and O. Nobuyosi, *Fujifilm Res. Dev*., 2006, **51**, 80 – 85.
15. (a) V. V. Titov and A. I. Pavlyuchenko, *Chem. Heterocycl. Compd.,* 1980, **16**, 1 – 13; (b) M. P. Aldred, P. Vlachos, D. Dong, S. P. Kitney, W. C. Tsoi, M. O. Neill and S. M. Kelly, *Liq. Cryst*., 2005, **32**, 951 – 965; (c) A. Seed, *Chem. Soc. Rev.*, 2007, **36**, 2046 – 2069; (d) B. Roy, N. De and K. C. Majumdar, *Chem. -Eur. J.,* 2012, **18**, 14560–14588; (e) J. Han, *J. Mater. Chem. C*, 2013, **1**, 7779-7797.

16. A. C. Grimsdale, K. Leok Chan, R. E. Martin, P. G. Jokisz and A. B. Holmes, *Chem. Rev*., 2009, **109**, 897–1091.
17. (a) C. S. Wang, G. Y. Jung, Y. L. Hua, C. Pearson, M. R. Bryce, M. C. Petty, A. S. Batsanov, A. E. Goeta and J. A. K. Howard, *Chem. Mater.*, 2001, **13**, 1167 – 1173; (b) A. P. Kulkarni, C. J. Tonzola, A. Babel and S.A. Jenekhe, *Chem. Mater.,* 2004, **16**, 4556–4573.
18. (a) D. Acierno, S. Concilio, A. Diodati, P. Iannelli, S. P. Piotto and P. Scarfato *Liq. Cryst*., 2002, **29**, 1383 – 1392; (b) H. H. Sung, H. C. Lin and H. C. *Liq. Cryst*., 2004, **31**, 831–840; (c) R. Cristiano, F. Ely and H. Gallardo, *Liq. Cryst.,* 2005, **32**, 15–25; (d) J. Han, S. S. Y. Chui and C. M. Che, *Chem. -Asian J.*, 2006, **1**, 814 – 825.
19. (a) Y. D. Zhang, K. G. Jespersen, M. Kempe, J. A. Kornfield, S. Barlow, B. Kippelen and S. R. Marder, *Langmuir,* 2003, **19**, 6534 – 6536; (b) R. Cristiano, D. M. P. D. O Santos and H. Gallardo, *Liq. Cryst.,* 2005, **32**, 7–14; (c) S. Varghese, N. S. S. Kumar, A. Krishna, D. S. S. Rao, S. K. Prasad and S. Das, *Adv. Funct. Mater*., 2009, **19**, 2064 – 2073; (d) C. V. Yelamaggad, A. S. Achalkumar, D. S. S. Rao and S. K. Prasad, *J. Org. Chem.*, 2009, **74**, 3168 – 3171; (e) E. Westphal, I. H. Bechtold and H. Gallardo, *Macromolecules*, 2010, **43**, 1319–1328; (f) D. D. Prabhu, N. S. S. Kumar, A. P. Sivadas, S. Varghese and S. Das, *J. Phys. Chem. B*, 2012, **116**, 13071–13080; (g) E. Girotto, J. Eccher, A. A. Vieira, I. H. Bechtold and H. Gallardo, *Tetrahedron*, 2014, **70**, 3355–3360.
20. (a) J. Bettenhausen and P. Strohriegl, *Macromol. Rapid Commun.*, 1996, **17**, 623 – 631; (b) T. Christ, B. Glüsen, A. Greiner, A. Kettner, R. Sander, V. Stümpflen, V. Tsukruk and J. H. Wendorff, *Adv. Mater*., 1997, **9**, 219-222; (c) J. Bettenhausen, M. Greczmiel, M. Jandke and P. Strohriegl, *Synth. Met.*, 1997, **91**, 223–228; (d) A. C. Sentman and D. L. Gin, *Adv. Mater.*, 2001, **13**, 1398–1401; (e) B. G. Kim, S. Kim and S. Y. Park, *Tetrahedron Lett.*, 2001, **42**, 2697 – 2699; (f) C. K. Lai, Y.-C. Ke, J.–C. Su, C. Shen and W. –R. Li, *Liq. Cryst.*, 2002, **29**, 915–920; (g) B. G. Kim, S. Kim, J. Seo, N.–K. Oh, W.–C. Zin and S. Y. Park, *Chem. Commun.*, 2003, 2306–2307; (h) S. Qu and M. Li, *Tetrahedron,* 2007, **63**, 12429–12436; (i) J. Seo, S. Kim, S. H. Gihm, C. R. Park and S. Y. Park, *J. Mater. Chem.,* 2007, *17*, 5052–5057; (j) H. Wang, F. Zhang, B. Bai, P. Zhang, J. Shi, D. Yu, Y. Zhao, Y. Wang and M. Li, *Liq. Cryst*., 2008, **35**, 905 – 912; (k) J. Tang, R. Huang, H. Gao, X. Cheng, M. Prehm and C. Tschierske, *RSC Adv*., 2012, **2**, 2842 – 2847; (l) E. Westphal, M. Prehm and I. H. Bechtold, *J. Mater. Chem. C*, 2013, **1**, 8011–8022.
21. (a) P. J. Martin and D. W. Bruce, *Liq. Cryst.,* 2007, **34**, 767–774; (b) A. A. Vieira, H. Gallardo, J. Barbera, P. Romero, J. L. Serrano and T. Sierra, *J. Mater. Chem.*, 2011, **21**, 5916 – 5922; (c) J. Han, Q. Geng, W. Chen, L. Zhu, Q. Wu and Q. Wang, *Supramol. Chem*., 2012, **24**, 157–164.
22. (a) D. Haristoy D. Tsiourvas, *Chem. Mater.,* 2003, **15**, 2079–2083; (b) E. Westphal, D. H. D. Silva, F. Molin and H. Gallardo, *RSC Adv.,* 2013, **3**, 6442-6454.
23. (a) P. I. C. Teixeira, A. J. Masters and B. M. Mulder, *Mol. Cryst. Liq. Cryst.,* 1998, **323**, 167–189; (b) C. F. He, G. T. Richards, S. M. Kelly, A. E. A. Contoret

and M. O'Neil, *Liq. Cryst.,* 2007, **34**, 1249-1267; (c) M. L. Parra, E. Y. Elgueta, V. Jimenez and P. I. Hidalgo, *Liq. Cryst*., 2009, **36**, 301-317; (d) L.-R. Zhu, F. Yao, J. Han, J. M.-L. Pang and J.-B. Meng, *Liq. Cryst*., 2009, **36**, 209-213; (e) T. J. Dingemans, L. A. Madsen, O. Francescangeli, F. Vita, D. J. Photinos, C.-D. Poon and E. T. Samulski, *Liq. Cryst.,* 2013, **40**, 1655–1677.

24. (a) J. Han, M. Zhang, F. Wang and Q. Geng, *Liq. Cryst.*, 2010, **37**, 1471–1478; (b) K. C. Majumdar, P. K. Shyam, D. S. S. Rao and S. K. Prasad, *J. Mater. Chem.*, 2011, **21**, 556-561.
25. (a) P. E. Cassidy and N. C. Fawcett, *J. Macromol. Sci., Rev. Macromol. Chem. Phys.,* 1979, **C17**, 209–266; (b) X. C. Li, A. Kraft, R. Cervini, G. C. W. Spencer, F. Cacialli, R. H. Friend, J. Gruener, A. B. Holmes, J. C. DeMello and S. C. Moratti, *Mater. Res. Soc. Symp. Proc.,* 1996, **413**, 13–22; (c) H. H. Sung and H. C. Lin, *Macromolecules*, 2004, **37**, 7945 – 7954; (d) M. Sato, Y. Tada, S. Nakashima, K. I. Ishikura, M. Handa and K. Kasuga, *J. Polym. Sci. Part A*: *Polym.Chem.,* 2005, **43**, 1511 – 1525; (e) M. Sato, Y. Matsuoka and I. Yamaguchi, *J. Polym. Sci., Part A: Polym. Chem.,* 2007, **45**, 2998 – 3008.
26. J. Han, X. Y. Chang, L. R. Zhu, M.-L. Pang, J. B. Meng, S. S.-Y. Chui, S. W. Lai and V. A. L. Roy, *Chem. -Asian J,* 2009, **4**, 1099–1107.
27. Y. Hu, C.-Y. Li, X.-M. Wang, Y.-H. Yang and H.-L. Zhu, *Chem. Rev.,* 2014, **114**, 5572–5610.
28. D. Adam, P. Schuhmacher, J. Simmerer, L. Hayssling, K. Siemensmeyer, K. H. Etzbach, H. Ringsdorf and D. Haarer, *Nature,* 1994, **371**, 141-143.
29. (a) M. Parra, S. Hernandez, J. Alderete and C. Zuniga, *Liq. Cryst*., 2000, **27**(8), 995-1000; (b) Y. Xu, W. Lu, Z. Tai, *Mol. Cryst. Liq. Cryst. Sci. Technol., Sect. A,* 2000, **350**, 151–159; (c) A. A. Kiryanov, P. Sampson, A. J. Seed, *J. Org. Chem.,* 2001, **66**, 7925-7929; (d) M. W. Schroder, S. Diele, G. Pelzl, N. Pancenko and W. Weissflog, *Liq. Cryst.,* 2002, **29**, 1039 – 1046; (e) M. Parra, J. Alderete and C. Zuniga, *Liq. Cryst.,* 2004, **31**, 1531–1537; (f) T. Hegmann, B. Neumann, R. Wolf and C. Tschierske, *J. Mater. Chem.,* 2005, **15**, 1025–1034; (g) M. Parra, J. Vergara, P. Hidalgo, J. Barbera and T. Sierra, *Liq. Cryst.,* 2006, **33**, 739 – 745; (h) B. P. Sybo, A. Bradley, S. Grubb, K. Miller, J. W. Proctor, L. Clowes, M. R. Lawrie, P. Sampson and A. J. Seed, *J. Mater. Chem*., 2007, **17**, 3406 – 3411; (i) C. F. He, G. J. Richards, S. M. Kelly, A. E. A. Contoret and M. O. Neill, *Liq. Cryst*., 2007, **34**, 1249 – 1267; (j) J. Han, X. Y. Chang, L. R. Zhu, Y. M. Wang, J. B. Meng, S. W. Lai and S. S.-Y. Chui, *Liq. Cryst*., 2008, **35**, 1379–1394; (k) J. H. Tomma, I. H. Rou'il and A. H. Al-Dujaili, *Mol. Cryst. Liq. Cryst*., 2009, **501**, 3–19; (l) M. C. McCairn, T. Kreouzis and M. L. Turner, *J. Mater. Chem.,* 2010, **20**, 1999-2006; (m) A. K. Prajapati and V. Modi, *Liq. Cryst*., 2011, **38**, 191–199; (n) Q. Song, D. Nonnenmacher, F. Giesselmann and R. P. Lemieux, *J. Mater. Chem. C*, 2012, **1**, 343-350; (o) P. Tuzimoto, D. M. P. O. Santos, T. D. S. Moreira, R. Cristiano, I. H. Bechtold and H. Gallardo, *Liq. Cryst.,* 2014, **41**, 1097–1108; (p) R. C. Tandel and N. K. Patel, *Liq. Cryst.,* 2014, **41**, 495–502.
30. (a) M. Lehmann, J. Seltmann, A. Auer, E. Prochnow and U. Benedikt, U. *J. Mater. Chem.,* 2009, **19**, 1978–1988; (b) M. Lehmann and J. Seltmann, *Beilstein J. Org. Chem*. 2009, **5**, 73.

31. M. L. Parra, E. Y. Elgueta, J. A. Ulloa, J. M. Vergara and A. I. Sanchez, *Liq. Cryst.,* 2012, **39**, 917–925.
32. (a) M. Sato, *Macromol Rapid Commun*., 1999, **20**, 77–80; (b) M. Sato and Y. Uemoto, *Macromol. Rapid Commun.,* 2000, **21**, 1220-1225; (c) M. Sato, M. Notsu, S. Nakashima and Y. Uemoto, *Macromol. Rapid Commun.,* 2001*,* **22**(9), 681–686; (d) M. Sato, M. Mizoi and Y. Uemoto, *Macromol*. *Chem. Phys*., 2001, **202**, 3634–3641; (e) M. Sato, S. Nakashima and Y. Uemoto, *J. Polym. Sci. A: Polym. Chem.*, 2003, **41**, 2676 –2687; (f) N. S. Al-Muaikel, *Polym. Int.*, 2004, **53**, 301–306; (g) M. Sato, Y. Tada, S. Nakashima, K.-I. Ishikura, M. Handa and K. Kasuga, *J. Polym. Sci. A: Polym. Chem.*, 2005, **43**, 1511–1525; (h) M. Sato, Y. Matsuoka and I. Yamaguchi, *Liq. Cryst.,* 2012, **39**, 1071–1081.
33. (a) M. Parra, S. Villouta, V. Vera, J. Belmar, C. Zuniga and H. Z. Zunza, *Naturforsch., B: J. Chem. Sci.,* 1997, **52**, 1533–1538; (b) M. Sato, R. Ishii, S. Nakashima, K. Yonetake and J. Kido, *Liq. Cryst.,* 2001, **28**, 1211 – 1214; (c) C. F. He, G. J. Richards, S. M. Kelly, A. E. A. Contoret and M. O'Neill, *Liq. Cryst.*, 2007, **34**, 1249–1267; (d) J. H. Tomma, I. H. Rou'il and A. H. Al-Dujaili, *Mol. Cryst. Liq. Cryst.,* 2009, **501**, 3–19.
34. (a) K.-T. Lin, H.-M. Kuo, H.-S. Sheu and C. K. Lai, *Tetrahedron,* 2013, **69**, 9045-9055; (b) K. S. Mustafa, K. S. Al-Malki, A. S. Hameed and A. H. Al-Dujaili, *Mol. Cryst. Liq. Cryst.,* 2014, **593**, 34–42.
35. (a) A. S. Achalkumar, U. S. Hiremath, D. S. Shankar Rao, S. Krishna Prasad and C. V. Yelamaggad, *J. Org. Chem.,* 2013, **78**, 527−544; (b) I. Thomsen, K. Clausen, S. Scheibye and S.-O. Lawesson, *Organic Syntheses,* 1990*,* **7***,* 372-373.
36. S. Chandrasekhar, In *Advances in Liquid Crystals*; ed. G. H. Brown, Academic Press: New York, 1982; **Vol. 5**, p 47.
37. (a) C. Carfagna, A. Roviello and A. Sirigu, *Mol. Cryst. Liq. Cryst.,* 1985, **122**, 151−160; (b) E. F. Gramsbergen, H. J. Hoving, W. H. de Jeu, K. Praefcke and B. Kohne, *Liq. Cryst.,* 1986, **1**, 397−400; (c) H. Metersdorf and H. Ringsdorf, *Liq. Cryst.,* 1989, **5**, 1757−1772; (d) H. Zeng, P. J. Carroll and T. M. Swager, *Liq. Cryst*., 1993, **14**, 1421− 1429; (e) C. F. Van Nostrum, A. W. Bosman, G. H. Gelinck, P. G. Schouten, J. M. Warman, A. P. M. Kentgens, M. A. C. Devillers, A. Meijerink, S. J. Picken, U. Sohling, A.-J. Schouten and R. J. M. Nolte, *Chem. -Eur. J.,* 1995, **1**, 171−182; (f) J. Barbera, R. Gimenez and J. L. Serrano, *Chem. Mater*., 2000, **12**, 481−489; (g) J. L. Serrano and T. Sierra, *Chem. -Eur. J*., 2000, **6**, 759−766; (h) S. Ito, M. Ando, A. Nomura, N. Morita, C. Kabuto, H. Mukai, K. Ohta, J. Kawakami, A. Yoshizawa and A. Tajiri, *J. Org. Chem.,* 2005, **70**, 3939−3949; (i) A. Hayer, V. de Halleux, A. Kohler, A. El-Garoughy, E. W. Meijer, J. Barbera, J. Tant, J. Levin, M. Lehmann, J. Gierschner, J. Cornil and Y. H. Geerts, *J. Phys. Chem. B,* 2006, **110**, 7653−7659; (j) L. Alavarez, J. Barbera, L. Puig, P. Romero, J. L. Serrano and T. Sierra, *J. Mater. Chem.,* 2006, **16**, 3768−3773; (k) C. V. Yelamaggad, A. S. Achalkumar, D. S. S. Rao and S. K. Prasad, *J. Mater. Chem.,* 2007, **17**, 4521−4529; (l) C. V. Yelamaggad, A. S. Achalkumar, D. S. S. Rao and S. K. Prasad, *J. Org. Chem.,* 2007, **72**, 8308−8318; (m) C. V. Yelamaggad, A. S. Achalkumar, D. S. S. Rao, M. Nobusawa, H. Akutsu, J. Yamada and S. Nakatsuji, *J. Mater. Chem.,* 2008, **18**, 3433−3437.

38. V. Percec, M. Glodde, T. K. Bera, Y. Miura, I. Shiyanovskaya, K. D. Singer, V. S. K. Balagurusamy, P. A. Heiney, I. Schnell, A. Rapp, H.-W. Spiess, S. D. Hudsonk and H. Duank, *Nature,* 2002, **419**, 384-387.
39. (a) D. M. Collard and C. P. Lillya, *J. Am. Chem. Soc.,* 1987, **109**, 7544-7545; (b) R. Festag, R. Kleppinger, M. Soliman, J. H. Wendorff, G. Lattermann and G. Staufer, *Liq. Cryst*., 1992, **11**, 699-710; (c) R. Kleppinger, C. P. Lillya and C. Yang, *J. Am. Chem. Soc.,* 1997, **119**, 4097-4102; (d) C. V. Yelamaggad and A. S. Achalkumar, *Tetrahedron Lett.,* 2012, **53**, 7108-7112.
40. (a) C. Adachi, T. Tsutui and S. Saito, *Appl. Phys. Lett.,* 1990, **56**, 799-801; (b) H. Antoniadis, M. Inbasekaran and E. P. Woo, *Appl. Phys. Lett.,* 1998, **73**, 3055-3057; (c) N. –X. Hu, M. Esteghamatian, S. Xie, Z. Popovic, Ah.-M. Hor and O. Beng, S. Wang, S. *Adv. Mater.,* 1999, **11**, 1460–1463; (d) S. Tao, Z. Peng, P. Wang, C. –S. Lee and S. –T. Lee, *Adv. Funct. Mater.,* 2005, **15**, 1716–721.
41. (a) Y. Li, Y. Cao, J. Gao, D. Wang, G. Yu and A. J. Heeger, *Synth. Met*., 1999, **99**, 243–248; (b) L. Dou, J. You, J. Yang, C.–C. Chen, Y. He, S. Murase, T. Moriarty, K. Emery, G. Li and Y. Yang, *Nat. Photonics,* 2012, **6**, 180–185; (c) P. Deng, L. Liu, S. Ren, H. Li and Q. Zhang, *Chem. Commun.,* 2012, **48**, 6960–6962; (d) C. V. Yelamaggad, A.S. Achalkumar, D. S. Shankar Rao and S. K. Prasad, *Org. Lett.,* 2007, **9**, 2641–2644.

# Chapter III

# 1,3,4-Thiadiazole based polycatenar mesogens

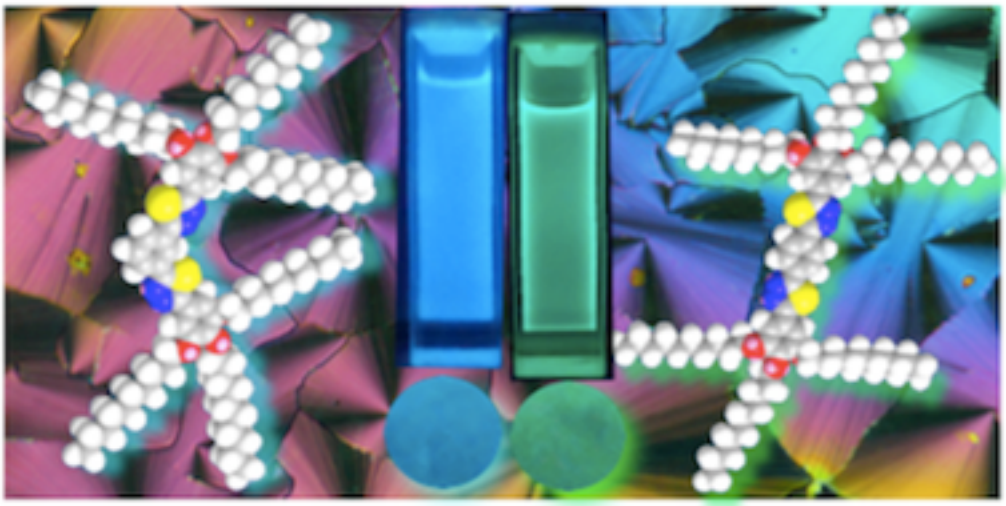

Results have been published in *J. Mater. Chem. C*, 2015, **3**, 8166-8182.

### 3.1. Introduction

Liquid crystal (LC) self-assembly of shape anisotropic molecules is a subject that has attracted huge interest in recent years. This unique state of matter, with the combination of order and fluidity, leads to special inherent properties that are important from the view points of basic and applied research.[1] Liquid crystals can be broadly classified as conventional and non-conventional, based on their shape.[2] Conventional LCs are comprised of two classes; calamitic (rod-like), [3] or discotic (disc-like).[4] Shape anisotropic molecules which stabilize mesophases, that are neither calamitic nor discotic, fall under the class of non-conventional LCs.[2] Scientific curiosity, in a quest to explore novel mesophases and applications, has led to a flurry of activity in the design and synthesis of several different shape aniotropic molecules which deviate from the conventional rod or disc shapes.[2,5-12] Some of the important examples of non-conventional systems are oligomers,[5] bent-core molecules,[6] polyhydroxy amphiphiles, [2c-e,7] octahedral complexes,[8] star shaped molecules,[9] rod-coil molecules,[10] dendrimers[11] and polycatenars.[12]

Polycatenars or phasmid-like LCs, are one such class of non-conventional LCs, comprising a central long aromatic rod connected to two terminal semi-discs with multiple flexible chains.[12a-c] These molecules self-assemble into different LC phases due to the nanosegregation of aromatic units and flexible chains. Since polycatenars share the structural features of both calamitic and discotic LCs, they exhibit various LC phases like nematic, smectic (lamellar), cubic, and columnar phases, depending on the number of peripheral tails. Recently it was reported that some polycatenars based on an indigoid system even exhibited mesophases similar to bent-core LC phases.[13] This synthetically flexible molecular motif can incorporate many functional moieties, so as to develop multifunctional LCs. Incorporation of an extended π-conjugated aromatic system in the polycatenar molecular structure is very important from the viewpoint of charge carrier and luminescence properties.[14] Gin *et. al.* reported a polycatenar system with photophysical functions.[12e] Yelamaggad *et. al.* incorporated hydrogen-bonding oligopeptides in the polycatenar structure, which stabilized a Columnar phase.[15] Prasad *et.al.* introduced a photoisomerizable azobenzene unit in the polycatenar structure.[16] There are many reports on luminescent polycatenar LCs.[14d-i]

The discovery of columnar self-assembly of discotics[4] opened up a fascinating research area because of the various potential applications.[18-22] This is because Col phases formed from discotics resemble molecular wires, due to the one-dimensional stacking of central rigid discs with an insulating sheath of peripheral tails, which help in one-dimensional carrier migration.[17] Columnar phases have the potential to realize many optoelectronic devices like photovoltaics,[18] light-emitting diodes,[19] field-effect transistors,[20] gas sensors[21] and lubricants.[22] Considering the synthetic difficulty and the rigidity for structural tuning in discotic liquid crystals (DLCs), polycatenar LCs seems to be a simpler alternative, as they can also stabilize Col phases.

Recently there is a renewed interest in the incorporation of heterocycles in the molecular design of mesogens, due to the wide variety of structures and, hence, resultant properties.[23] Heteroatoms like nitrogen, oxygen and sulfur provide a reduced molecular symmetry, strong lateral and/or longitudinal dipoles and a donor-acceptor interaction within the molecule, which in turn affects the LC self-assembly and electronic behavior of the mesogens.[23] Mesogens with heterocyclic moieties in their molecular structures provide emission color tunability and also enable a polarized emission. This is an important property, which finds application in the area of OLEDs.[24] Many polycatenar LCs bearing a heterocyclic moiety in their molecular structures have thus been reported. There have been relatively more reports on 1,3,4-Oxadiazole derivatives in comparison to their sulfur analogues, 1,3,4-thiadiazole derivatives.[26, 27]

1,3,4-Oxadiazole-based molecules are known for their high luminescence efficiency, n-type behavior (electron transporting) and resistance to oxidative degradation, hydrolytic and thermal stability. Hence they have found application as n-type electroluminescent layers in organic light-emitting diodes.[23a-c, 25] Unfortunately, oxadiazole-based mesogens have a few drawbacks, like high melting and clearing temperatures, narrow mesophase ranges and poor solubility, which limits their applications.[26] Reports on their sulfur analogues, *i.e.* 1,3,4-thiadiazole-based mesogens, are limited in number. It is expected that substitution of oxygen with sulfur will increase the dipole moments, packing of molecules, viscosity, melting and clearing temperatures.[23c,27] In addition to this notion, partly the synthetic difficulty, coupled with

low yields, has curtailed attempts in this direction. Calamitic LCs,[28] banana-shaped LCs,[29] hydrogen-bonded LCs,[30] and polymeric LCs[31] based on 1,3,4-thiadiazole have been reported. Very recently, a few polycatenar LCs[26,32] and star-shaped mesogens[33a] stabilizing a columnar phase have been reported.

As part of our efforts to combine luminescence with liquid crystalline order, we were interested in synthesizing polycatenar liquid crystals, in particular hexacatenars based on 1,3,4-thiadiazole derivatives (Fig. 3.1). We were also interested in comparing their properties with polycatenars based on 1,3,4-oxadiazole derivatives (Fig. 3.2).[34] Additionally, this also gives information on the effects of structure on the self-assembly process on going from hexacatenars to star-shaped molecules. In this paper we report the synthesis of hexacatenars comprised of five rings, among which two are 1,3,4-thiadiazoles. These two thiadiazole rings are interconnected by *para*- or *meta*-substituted benzene rings, and have six alkyl chains attached equally to two terminal benzene rings.

## 3.2. Results and discussion

### 3.2.1. Synthesis and molecular structural characterization

The synthetic strategy to prepare the hexacatenars is presented in scheme 3.1. Ethyl gallate was *O*-alkylated by heating with appropriate *n*-bromoalkanes in the presence of anhydrous $K_2CO_3$ and anhydrous DMF. The synthetic routes to obtain ethyl gallate and its alkoxy derivatives were reported previously.[35a] These alkoxy esters (**1c**, **4b-c**) were refluxed with hydrazine hydrate in *n*-butanol to obtain the respective hydrazides (**2c**, **5b-c**).[33b,34] The hydrazides **2c**, **5b-c** were then coupled with terephthalic acid chloride to get 1,4-di-*N*-benzoylbenzohydrazides **6a-c**.[34] Similarly, hydrazides **2c**, **5b-c,** on coupling with isophthalic acid chloride, yielded 1,3-di-*N*-benzoylbenzohydrazides **7a-c**. Compounds **6a-c** and **7a-c,** on refluxing with Lawesson's reagent[35b] in toluene, yielded polycatenars **PT1-3** and **MT1-3**.[33b] Molecular structural characterization was carried out using $^1$H NMR, $^{13}$C NMR, IR spectroscopy and ESI-HRMS. (See experimental part presented in section for the details and Fig. 3.3). As representative cases from each series, $^1$H NMR and $^{13}$C NMR spectra of the polycatenar *para*-1,3,4-thiadiazole **PT1** and *meta*-1,3,4-thiadiazole **MT1** are presented in Fig. 3.3.

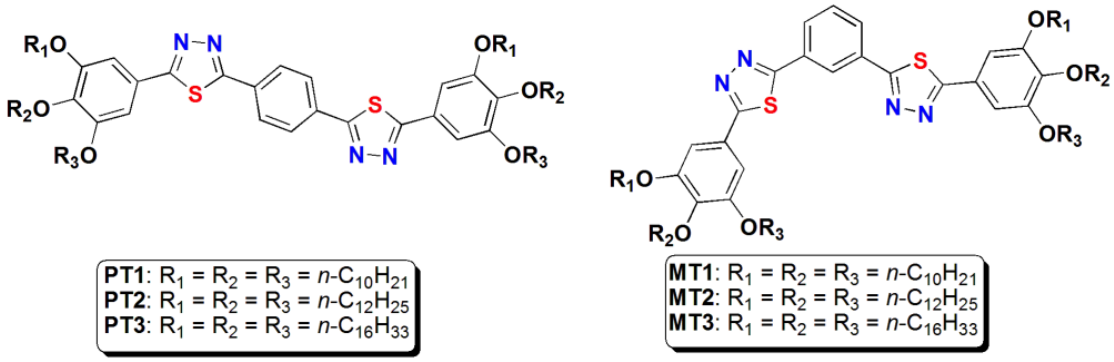


**Figure 3.1.** The molecular structures of compounds **PT1-3** and **MT1-3**.

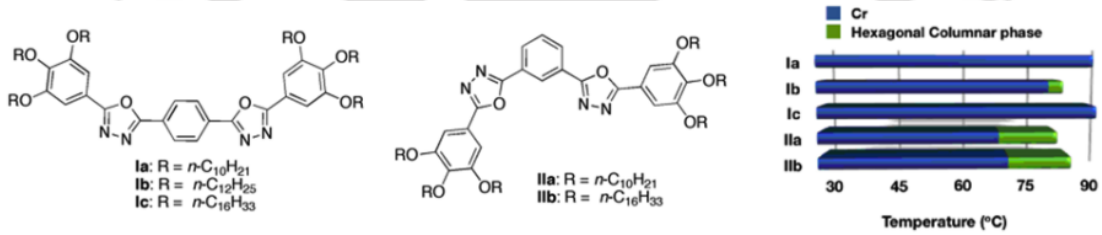


**Figure 3.2.** Polycatenars based on 1,3,4-oxadiazoles (**Ia-Ic**[34b] and **IIa-IIb**[34a]) that are comparable to the 1,3,4-thiadiazole based polycatenars **PT1-3** and **MT1-3** of the present work; a bar graph showing the thermal behavior of compounds **Ia-Ic** and **IIa-IIb** (in heating cycle).

### 3.2.2. Thermal behavior

The liquid crystalline properties of these new hexacatenars belonging to two different series were investigated by polarizing optical microscopy (POM), thermogravimetric analysis (TGA), differential scanning calorimetry (DSC) and X-ray diffraction (XRD) studies. The liquid crystalline nature of the polycatenar LCs was identified by the observation of the strong birefringent and fluidic nature of the materials under POM. Furthermore, the assignments of the LC phases were made by correlating the typical textural patterns with the data obtained from XRD studies. The peak temperatures obtained in DSC traces due to phase transitions were found to be in accordance with POM observations. The transition temperatures, mesophase sequence and the

corresponding enthalpy changes are summarized in Table 3.1. The bar graph provided in Fig. 3.5 summarizes the thermal behavior of these compounds in the first heating cycle. The thermal stabilities of the compounds were analyzed by TGA, which showed that all the compounds were thermally stable upto ≈ 250 °C and that complete degradation occurred at around 600 °C. (See the Fig. 3.4).

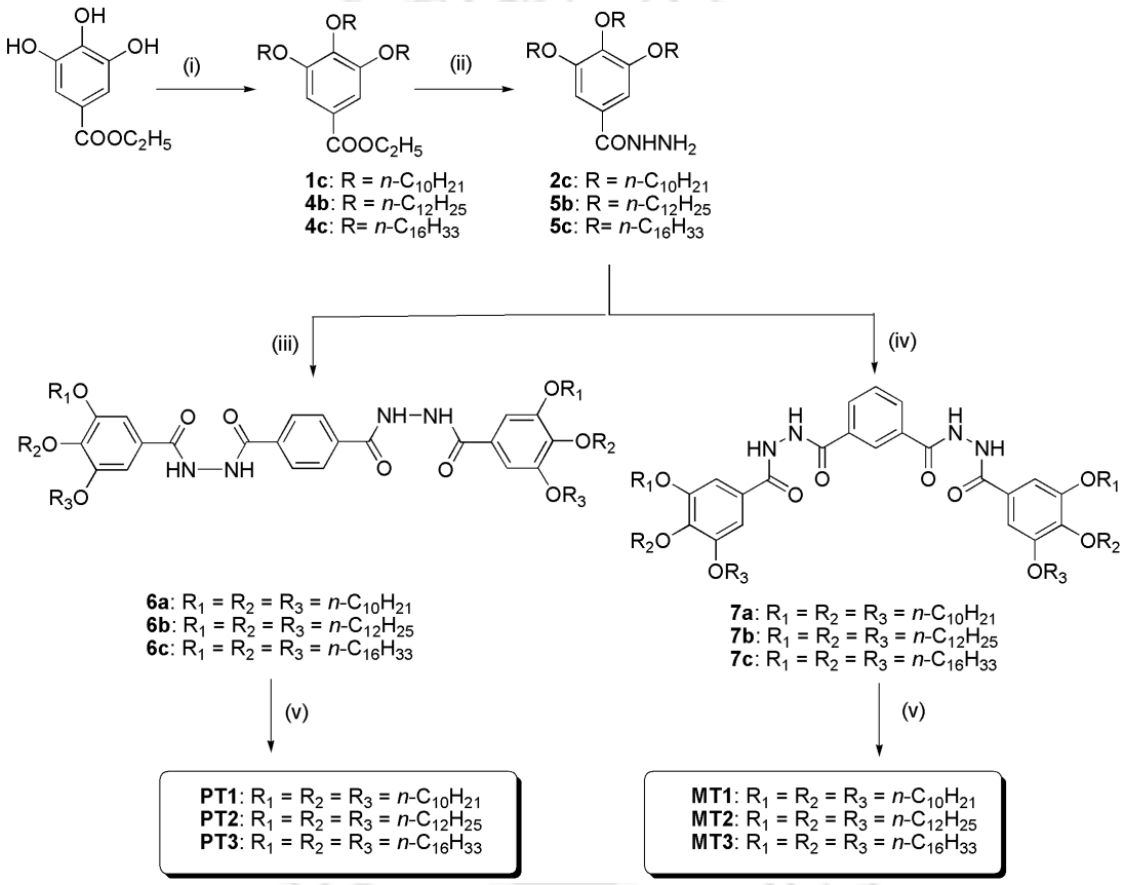


**Scheme 3.1.** Synthesis of 1,3,4-thiadiazole-based polycatenars. Reagents and conditions: (i) *n*-bromoalkanes, anhydrous $K_2CO_3$, DMF, 80 °C, 24 h (70-90 %); (ii) $NH_2NH_2.H_2O$, *n*-butanol, reflux, 48 h (71-80 %); (iii) (a) 1,4-benzene dicarboxylic acid, $SOCl_2$, reflux, 6 h; (b) **2c**, **5b-c**, THF, triethylamine, 12 h, reflux; (iv) (a) 1,3-benzene dicarboxylic acid, $SOCl_2$, reflux, 6 h; (b) **2c**, **5b-c**,THF, triethylamine, 12 h, reflux; (v) Lawesson's reagent, toluene, reflux, 17 h (40-45 %).

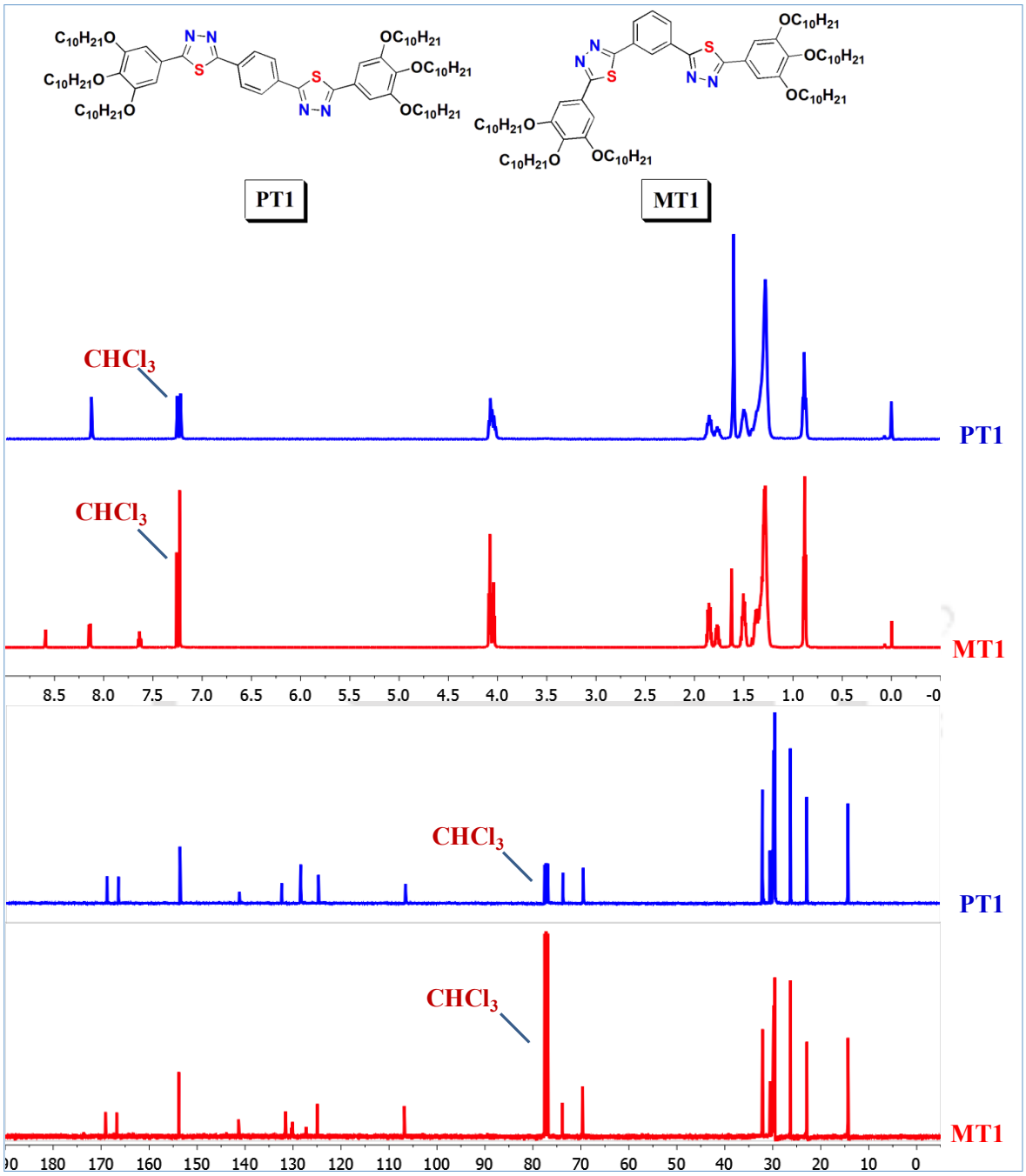


**Figure 3.3.** $^{1}$H NMR (400MHz) and $^{13}$C NMR (100MHz) spectra of **PT1** and $^{1}$H NMR (600MHz) and $^{13}$C NMR (100MHz) spectra of **MT1** in $CDCl_3$.

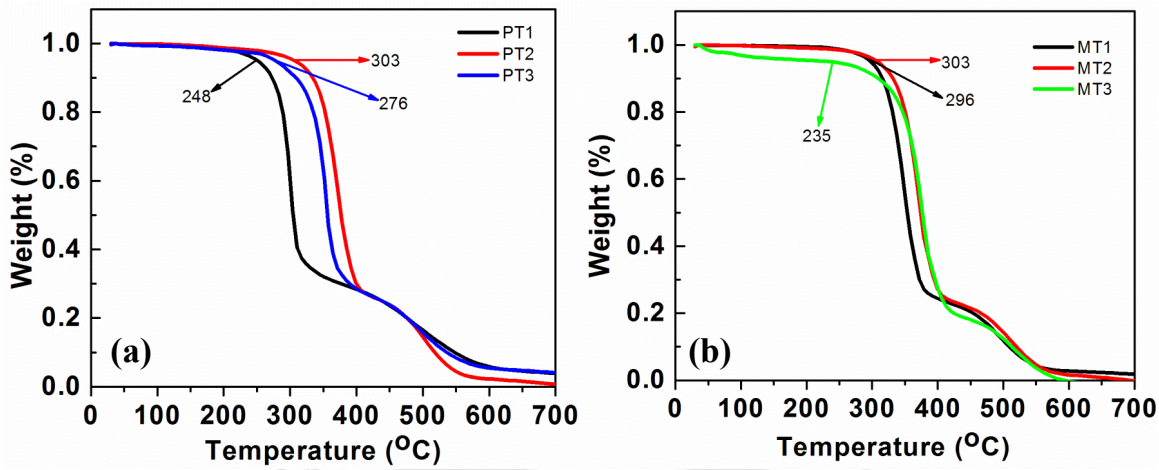


**Figure 3.4.** TGA curves of the compounds **PT1-3 (a)** and **MT1-3 (b)** carried out at a rate of 10 °C/min.

In the following sections, we discuss the LC behavior of the thiadiazole-based polycatenars using the above-mentioned complementary techniques. From the bar graph shown in Fig. 3.5, it is evident that in the case of *p*-substituted polycatenars, the melting temperature decreases with the increase in chain length, while the decrease in clearing point is not regular. The mesophase range is wider for compound **PT2** with a medium chain length, while it is short for compound **PT3** with the highest chain length. In the case of *m*-substituted polycatenars, there is no such trend in the variation of melting points with respect to chain length, but they show a constant decrease in the clearing point. Again, as in the case of *p*-substituted polycatenars, compound **MT2** with a medium chain length shows a wide range of mesophase, while compound **MT3** shows the shortest mesophase width. Thus from this information we can infer that for this class of polycatenars, the appropriate length of peripheral chains is an important factor in deciding the mesophase width. In the cooling cycle, both series of compounds showed a common trend, *i.e.* a constant decrease in the mesophase width with the increase in chain length.

Thiadiazole-based *p*-substituted polycatenar molecule **PT1,** with the shortest chain, exhibited an enantiotropic columnar mesophase spanning a thermal range of 16 degrees in the heating cycle, after passing through two Cr-Cr transitions at ≈ 45 °C and 52 °C with an enthalpy change of 10.3 kJ/mol and 120.7 kJ/mol, respectively, as evidenced

by DSC thermograms. Further heating shows that around 80 °C, a transition to a birefringent fluidic liquid crystalline phase was observed, which stays upto 96 °C before

**Table 3.1.** Phase transition temperatures [a] (°C) and corresponding enthalpies (kJ/mol) of DLCs

| Compound | Phase sequence | |
|---|---|---|
| | Heating | Cooling |
| **PT1** | $Cr_1$ 45.3 (10.3) $Cr_2$ 51.5 (120.7) $Cr_3$ 79.5 (266.5) $Col_h$ 95.9 (11.3) I<br>$Cr_1$ 34.8 (205.3)[c] $Cr_2$ 78.3 (358.1) $Col_h$ 95.9 (20.2) I | I 94.6 (11.3) $Col_h$ 28.4 (13.7) Cr<br>I 94.6 (20.2) $Col_h$ 28.5 (24.8) Cr |
| **PT2** | $Cr_1$ 55.6 (76.5) $Cr_2$ 67.6 (14.8) $Cr_3$ 78.1 (131) $Col_{ob}$ 98.9 (7.1) I<br>$Cr_1$ 53 (269)[c] $Cr_2$ 76.4 (365) $Col_{ob}$ 98.4 (15.7) I | I 97.3 (7.2) $Col_{ob}$ 44 (19.1) Cr<br>I 97.3 (16.4) $Col_{ob}$ 44 (45.4) Cr |
| **PT3** | Cr 70.2 (202.5) $Col_h$ 83.5 (1.5) I<br>$Cr_1$ 55.5 (502) $Cr_2$ 63.99 (78.1) $Cr_3$ 73.2 (6.2) $Col_h$ 81.7 (17) I | I 80.4 (5.3) $Col_h$ 51 $Col_{ob}$ [b] 46.1 (142.3) Cr<br>I 80.6 (17.6) $Col_h$ 51 $Col_{ob}$ [b] 46.1 (262) Cr |
| **MT1** | $Cr_1$ 42.2 (10.6) $Cr_2$ 62 (22.5) $Col_{ob}$ 97.9 (12.6) I<br>$Cr_1$ 25.03 (62.2) $Cr_2$ 62 (49) $Col_{ob}$ 97.8 (20.2) I | I 96.9 (11.5) $Col_{ob}$ 53.4 (25) $Cr_2$ 19.7 (29.9) $Cr_1$<br>I 96.9 (20.1) $Col_{ob}$ 53.51 (45.2) $Cr_2$ 19.8 (54.5) $Cr_1$ |
| **MT2** | Cr 57.2 (135.7) $Col_{ob}$ 94.4 (11.7) I<br>$Cr_1$ 48.4 (97.7) $Cr_2$ 55.8 (103.3) $Cr_3$ 59.9 (24.8) $Col_{ob}$ 94.3 (25) I | I 93.4 (10.8) $Col_{ob}$ 54.9 (20.4) $Cr_1$ 41.8 (71.7) $Cr_2$<br>I 93.4 (24.6) $Col_{ob}$ 54.9 (48.6) $Cr_2$ 41.8 (161.9) $Cr_1$ |
| **MT3** | $Cr_1$ 75.6 (147.3) $Col_{ob}$ 87 (8) I<br>$Cr_1$ 75.7 (499.6) $Col_{ob}$ 87 (27) I | I 86 (8.2) $Col_{ob}$ 64.6 (151.7) Cr<br>I 86 (28.4) $Col_{ob}$ 64.5 (516.5) Cr |

[a]Peak temperatures in the DSC thermograms obtained during the first and second heating-cooling cycles at 5 °C/min. [b]The phase observed is monotropic. $Col_h$ = columnar hexagonal phase; $Col_{ob}$ = columnar oblique phase. [c]Exothermic crystallization.

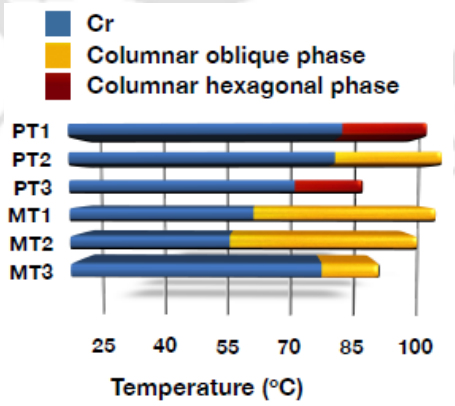


**Figure 3.5.** Bar graph summarizing the thermal behavior of compounds **PT1-3** and **MT1-3** (first heating cycle).

passing to an isotropic liquid. On cooling from isotropic liquid state, small spherulites developed from the homeotropic dark field of view (Fig. 3.6a and b), which persisted untill 28 °C. The compound crystallizes below this temperature (Fig. 3.6c).

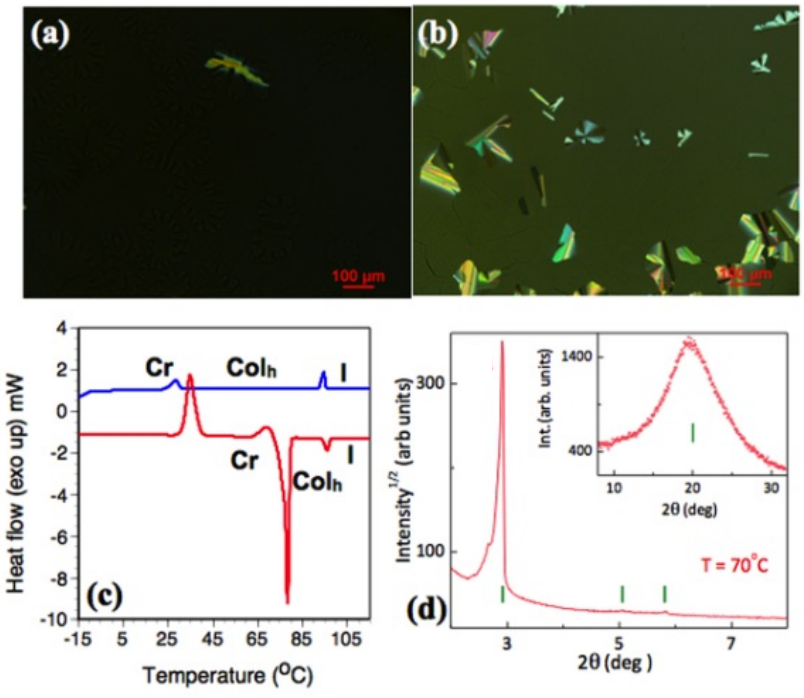


**Figure 3.6.** Photomicrographs of textures as seen by POM for the $Col_h$ phase of compound **PT1** (a) at 90 °C; (b) at 70 °C; DSC traces obtained for the first cooling (blue trace) and second heating (red trace) cycles of compound **PT1** at a rate of 5 °C $min^{-1}$ (c); XRD profiles depicting the intensity against the 2$\theta$ obtained for the $Col_h$ phase of compound **PT1** at 70 °C (d).

Powder X-ray diffraction studies on compound **PT1** at different temperatures were done to determine the symmetry of the enantiotropic columnar mesophase. The results of indexing the reflections of the XRD profiles are tabulated in Table 3.2. The X-ray profile of compound **PT1** at 90 °C showed three reflections in the small-angle region, corresponding to the *d*-spacings 29.94 Å, 17.27 Å and 15 Å, which can be indexed into the Miller indices 100, 110 and 200 respectively. In the wide-angle region, a relatively diffused peak corresponding to the *d* spacing of 4.47 Å was observed. The first three

**Table 3.2.** Results of (*hkl*) indexation of XRD profiles of the compounds at a given temperature (T) of mesophases[a]

| Compounds (*D*/Å) | Phase (T/°C) | $d_{obs}$ (Å) | $d_{cal}$ (Å) | Miller indices (*hkl*) |
|---|---|---|---|---|
| **PT1** (48.3) | $Col_h$ (90) | 29.94<br>17.27<br>15.00<br>4.47 ($h_a$) | 29.95<br>17.29<br>14.97 | 100<br>110<br>200 |
| | $Col_h$ (70) | 30.30<br>17.49<br>15.21<br>4.43 ($h_a$) | 30.31<br>17.50<br>15.16 | 100<br>110<br>020 |
| **PT2** (53.3) | $Col_{ob}$ (90) | 34.23<br>33.39<br>32.21<br>4.49 ($h_a$) | 34.23<br>33.39<br>32.21 | 010<br>100<br>110 |
| **PT3** (63.4) | $Col_h$ (70) | 35.88<br>20.75<br>4.51($h_a$) | 35.90<br>20.73 | 100<br>110 |
| | $Col_{ob}$ (50) | 40.00<br>37.81<br>21.89<br>18.71<br>13.92<br>10.42<br>7.51<br>6.07<br>4.20 ($h_a$)<br>4.19 ($h_c$) | 40.00<br>37.81<br>21.89<br>18.91<br>14.02<br>10.40<br>7.56<br>6.17 | 010<br>110<br>-110<br>220<br>-210<br>420<br>550<br>-430 |

[a] The average diameter (*D*) of the polycatenars (estimated from Chem 3D Pro 8.0 molecular model software from Cambridge Soft). $d_{obs}$: spacing observed; $d_{cal}$: spacing calculated (deduced from the lattice parameters; *a* for the $Col_h$ phase; *a* and *b* for the $Col_{ob}$ phase). The spacings marked $h_a$ and $h_c$ correspond to diffuse reflections in the wide-angle region arising from correlations between the alkyl chains and core regions, respectively.

reflections follow the reciprocal spacing ratio of 1 : 0.58 : 0.5 of a hexagonal lattice. The diffuse peak at wide angle region corresponds to the packing of flexible alkyl tails in the columnar phase. A peak corresponding to the stacking of cores was not observed, showing that the intermolecular interactions are not that strong. The hexagonal lattice parameter '*a*' calculated was found to be 34.58 Å, while the lattice area and molecular volume were found to be 1035.04 $Å^2$, and 4627.7 $Å^3$ respectively. From these values, the number of molecules present in a unit cell was derived and found to be 2.1. This can be explained as below. In principle, we can consider both dumbell-like and hemidisc-like conformations of *p*-substituted polycatenar **PT1**, formed due to the different orientations

of the two thiadiazole rings (Fig. 3.7). Among these conformations, the dumbell-like conformer (Fig. 3.7a) is somewhat straight, while the hemidisc-like conformer (Fig. 3.7b) is a little bent and all alkyl chains are towards one side. In spite of these conformations, these molecules do not differ much in their molecular diameter, as obtained from the

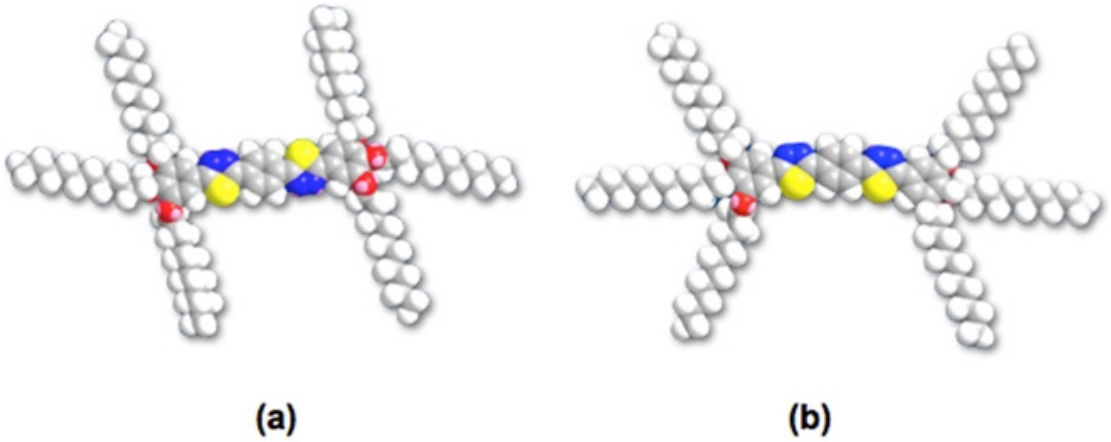


**Figure 3.7.** Molecular models showing the 'dumbell-like' conformation (a) and the hemidisc-like conformation (b) for compound **PT1**.

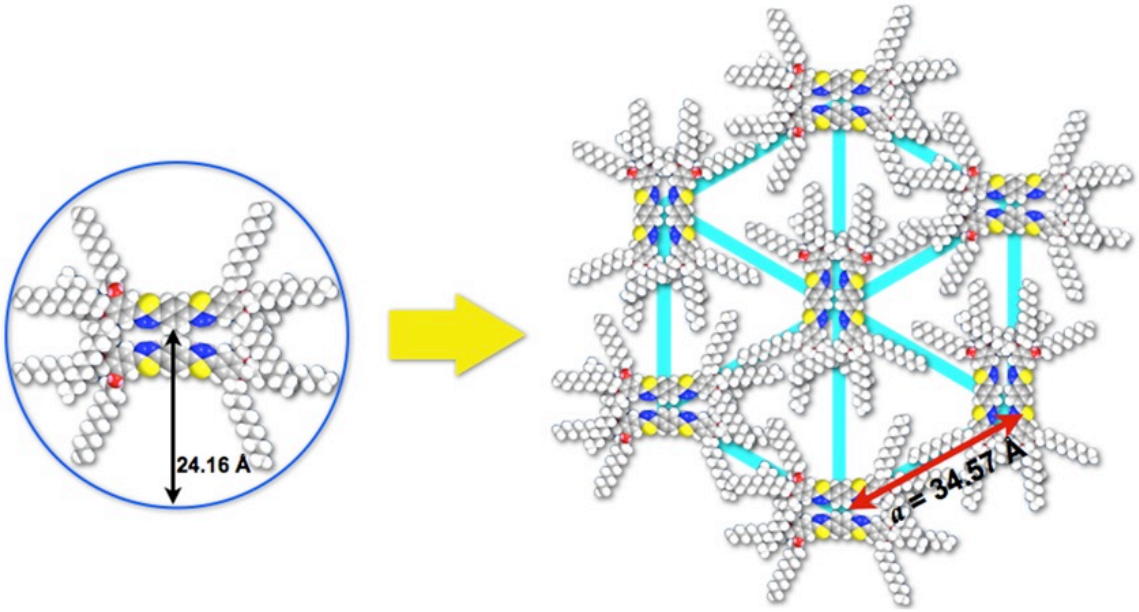


**Figure 3.8.** Schematic showing the self-organization of hexacatenar **PT1** into a hexagonal columnar ($Col_h$) lattice with inter-digitation of alkyl tails. The space filling energy-minimized (all-*trans*) molecular model of **PT1** was derived from a molecular mechanics (MM2) method.

molecular models (Table 3.2). This is because of the larger atomic size of sulfur, which leads to a larger bending angle. From the XRD studies, it is evident that a columnar slice with a thickness of 4.47 Å consists of two molecules.

Thus among the two conformations, it is reasonable to assume that two hemidisc-shaped conformers (Fig. 3.7b) can pack side by side to form a disc with efficient space filling. Furthermore, the voids were filled by the felxible chains (interdigitation) of polycatenars from the adjacent columns or by chain folding. Even though the discs formed by these polycatenars look slightly elliptical in shape, their time and space averaging results in a circular shape (Fig. 3.8). A similar packing arrangement has been reported for analogous oxadiazole-based polycatenars.[34b] These discs, in turn, self-assemble to form a columnar phase with hexagonal symmetry (Fig. 3.8). The hexagonal cell parameter '*a*' obtained from XRD studies was found to be 30% less than the molecular diameter calculated from the software Chem 3D Pro 8.0. This points to the interdigitation or folding of alkyl tails of polycatenars in adjacent columns. X-ray diffraction carried out at lower temperature (70 $^{o}$C) also showed a similar pattern, with a slight increase in the lattice parameter '*a*' (Fig. 3.6d and Table 3.2).

Compound **PT2** also showed a slightly higher isotropic temperature than compound **PT1**, which, on cooling from the isotropic melt, showed the formation of a columnar phase with the appearance of a mosaic texture (Fig. 3.9a). At some regions, spherulitic texture was also seen (Fig. 3.9b). Both of these textures have, in some cases, been reported for the $Col_h$ phase, but mosaic texture is often seen for the $Col_r$ phase.[36,37] Even columnar oblique phase ($Col_{ob}$) also sometimes show fan-shaped textures.[35a] Since there are minor differences in the structures of these different columnar phases, assignment of the symmetry of the mesophase exclusively based on textures is often misleading. The diffraction pattern obtained from the powder XRD studies of the unaligned sample cooled from the isotropic liquid state at 90 $^{o}$C is explained below. Indexing of the one-dimensional (1D) intensity *vs* 2$\theta$ profile deduced from the powder 2D pattern at 90 $^{o}$C shows three strong reflections at the low-angle region ($0 < 2\theta < 5^{o}$) with the respective spacing ratio of 1 : 0.97 : 0.94, which could be assigned to the (010), (100)

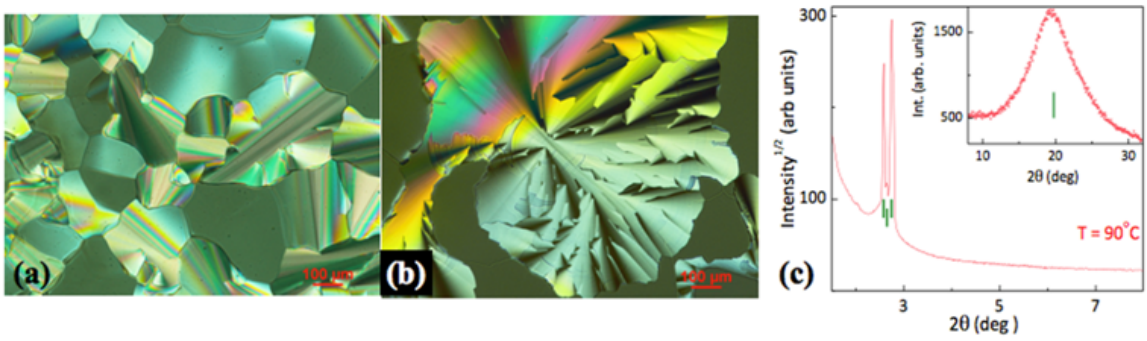


**Figure 3.9.** Photomicrographs of textures as seen by POM for the $Col_{ob}$ phase of compound **PT2** (a) at 90 °C; (b) at 65 °C; XRD profiles depicting the intensity against the $2\theta$ obtained for the $Col_{ob}$ phase of compound **PT2** at 90 °C (c).

and (110) reflections from a $Col_{ob}$ lattice (Fig. 3.9c). This belongs to a primitive planar space group $P_1$, and hence there are no reflection conditions, as in the case of $Col_h$ or $Col_r$. In the wide-angle region, a broad diffused peak corresponding to the packing of flexible alkyl tails was noticed at a *d* spacing of 4.49 Å. The oblique lattice had the cell parameters *a* = 37.38 Å and *b* = 38.31 Å, with the angle between the two-dimensional (2D) lattice directions, *i.e.* γ, being 26.7°. Thus the shape of the 2D lattice is a parallelogram.

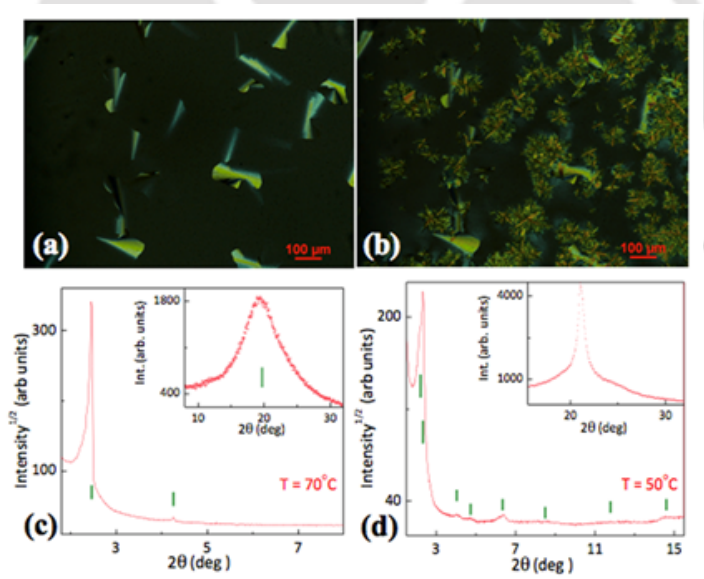


**Figure 3.10.** Photomicrographs of textures as seen by POM for the $Col_h$ phase of compound **PT3** (a) at 70 °C; (b) the $Col_{ob}$ phase at 50 °C; XRD profiles depicting the intensity against the $2\theta$ obtained for the $Col_h$ phase of compound **PT3** at 70 °C (c) and the $Col_{ob}$ phase at 50 °C

The polycatenar molecule **PT3,** with the longest chains in this series, showed a reduced mesophase range of around 13 degrees in the heating cycle with an isotropic temperature of 84 $^{o}$C. The Crystal-to-mesophase transition was observed as a broad peak in the DSC thermogram with an enthalpy change of 202.5 kJmol$^{-1}$. In the cooling cycle, the $Col_h$ phase appeared, with a characteristic texture of large homeotropic regions with some bright defects interspersed (Fig. 3.10a). This was also corroborated by XRD studies carried out at 70 $^{o}$C, with a characteristic pattern commonly observed for the $Col_h$ phase. Around 51 $^{o}$C, the small needles grew over the mosaic pattern and covered the entire area (Fig. 3.10b). Such a needle-like texture has previously been reported for the $Col_r$ phase.[37] XRD studies carried out at 50 $^{o}$C showed several peaks from the low-angle to mid-angle region ($0 < 2\theta < 15$ $^{o}$), in addition to two diffused peaks in the wide-angle region. The *d*-spacings obtained for these reflections correspond to the Miller indices (010), (110), (-110), (220), (-210), (420), (550) and (-430). Lattice parameters derived from these reflections were found to be $a$ = 41.68 Å and $b$ = 46.21 Å, with the angle between them being $\gamma = 30.04^{o}$. Since the value of $\gamma \neq 90^{o}$, we can conclude that the phase under investigation is $Col_{ob}$.

It is interesting to note that all the three molecules showed different thermal behavior, *i.e.* compound **PT1** showed the $Col_h$ phase exclusively, compound **PT2** showed only the $Col_{ob}$ phase, while compound **PT3** showed both the columnar phases, even though the $Col_{ob}$ phase observed was a monotropic phase. Besides the chain length, there is no other modification, thus the chain length is an important factor in deciding the symmetry of the Col phase observed here. In the case of discotics, with an increase in peripheral chain length, it is usual to predict a crossover from rectangular to a hexagonal columnar phase.[36,38] However, such a tendency is not seen in this class of polycatenars. It is to be noted that the corresponding oxadiazole-based polycatenars exhibited either a crystalline or $Col_h$ phase, and the mesophase stabilization is limited to a certain chain length. In the case of the present series of thiadiazoles, all the compounds were liquid crystalline, and the medium chain length compound **PT2** exhibited a broad mesophase range in the heating cycle. In the cooling cycle, a different trend was observed; with the

increase in chain length, a decrease in the mesophase width was observed. Oxygen to sulphur substitution in the molecular structure definitely improved the mesophase width of these compounds with respect to their oxadiazole counterparts.[34b]

The thiadiazole-based *m*-substituted polycatenar **MT1** showed a Cr-Cr transition at ≈ 42 $^{o}$C on heating, before passing to a birefringent fluidic mesophase at 62 $^{o}$C. This compound, on further heating, showed a mesophase to isotropic state transition at ≈ 98 $^{o}$C, with an enthalpy change of 13 kJmol$^{-1}$. On cooling from the isotropic melt, a large pseudofocal fan-shaped texture with spherulitic domains developed, with the concurrent occurrence of homeotropic domains (Fig. 3.11a). On further cooling, this remained unchanged except for a change in color and loss of fluidity, even though a mesophase to crystal transition with an enthalpy change of 25 kJmol$^{-1}$ at ≈ 54 $^{o}$C was observed in DSC (Fig. 3.11b). Powder XRD studies carried out at 90 $^{o}$C and 70 $^{o}$C (Fig. 3.11c) showed that the phase under investigation is the $Col_{ob}$ phase (Table 3.3). XRD studies at 90 $^{o}$C showed three relatively sharp peaks at low angle, followed by two diffused peaks at wide angle. The first three reflections, with *d* spacings of 32.41 Å, 31.03 Å and 15.52 Å, correspond to Miller indices (010), (110) and (-110), respectively. These *d*-spacings were in the ratio of 1: 0.96: 0.48, with lattice parameters *a* and *b* found to be 31.52 Å and 41.39 Å, respectively, with g = 38.47 $^{o}$. The first diffused peak observed, with a *d* spacing of 4.57 Å, corresponds to the packing of flexible alkyl tails, while the second peak, with a *d*-spacing of 3.77 Å, corresponds to the core-core distance. The number of molecules present in a unit cell was found to be 2.2. The XRD studies carried out at 70 $^{o}$C also showed a similar pattern, as shown in Fig. 3.11c.

The packing of two molecules in a columnar slice can be described as below. The *m*-substituted polycatenar **MT1** can exist in two possible conformations, as shown in Fig. 3.12. As the XRD data suggests that on average two molecules must be packed inside the unit cell, they must then arrange side by side to ensure space filling. These sets of two molecules, forming a disc, later self-assemble to form columns, and these columns in turn self-organize to form a 2D lattice of parallelogram lattice (Fig. 3.13). Polycatenars **MT2** and **MT3** showed enantiotropic monomesomorphic behavior. Pseudofocal conic fan-

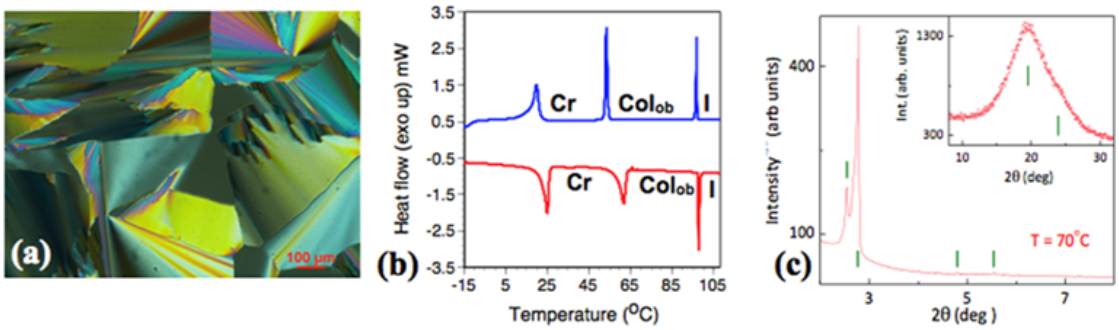


**Figure 3.11.** Photomicrograph of texture as seen by POM for the $Col_{ob}$ phase of compound **MT1** at 70 °C (a); DSC traces obtained for first cooling (blue trace) and second heating (red trace) cycles of compound **MT1** at a rate of 5 $^{o}$C min$^{-1}$ (b); XRD profiles depicting the intensity against the 2$\theta$ obtained for the $Col_{ob}$ phase of compound **MT1** at 70 °C (c).

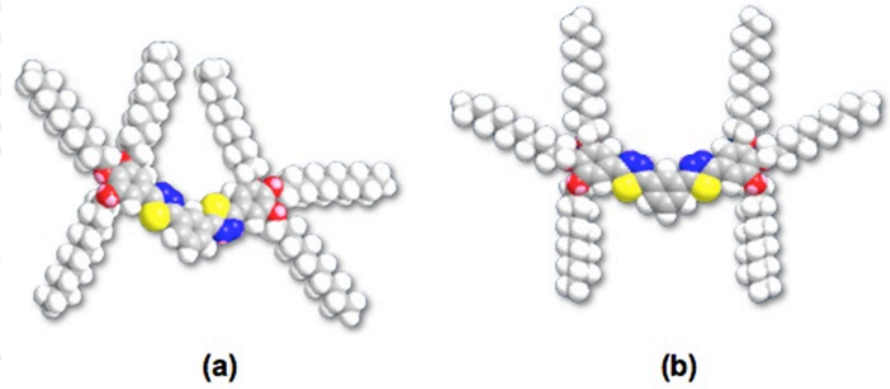


**Figure 3.12.** Molecular models obtained from Chem 3D showing the possible molecular conformations of compound **MT1.**

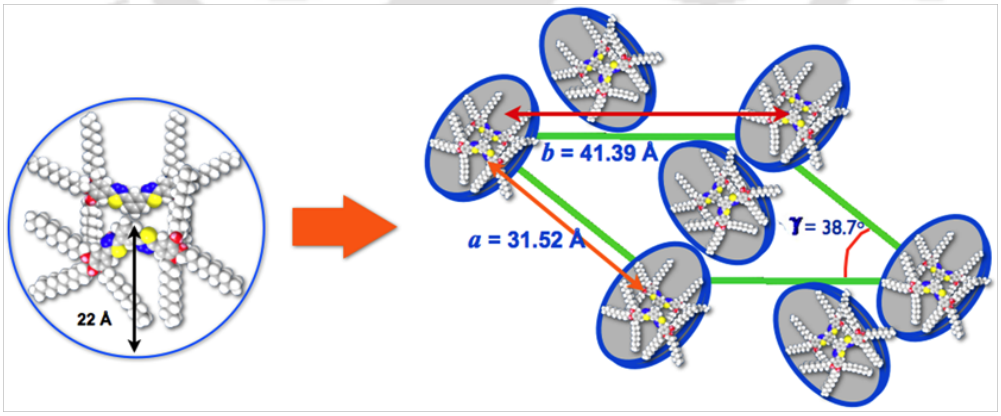


**Figure 3.13.** Schematic showing the self-organization of hexacatenar **MT1** into a columnar oblique ($Col_{ob}$) lattice. The space filling energy minimized (all-*trans*) molecular model of **MT1** was derived from a molecular mechanics (MM2) method. Ellipses denote tilted discs with respect to the columnar axis.

shaped texture was observed for both of these compounds (Fig. 3.14). Powder XRD investigations suggested that these compounds stabilize $Col_{ob}$ phase (Table 3.3).

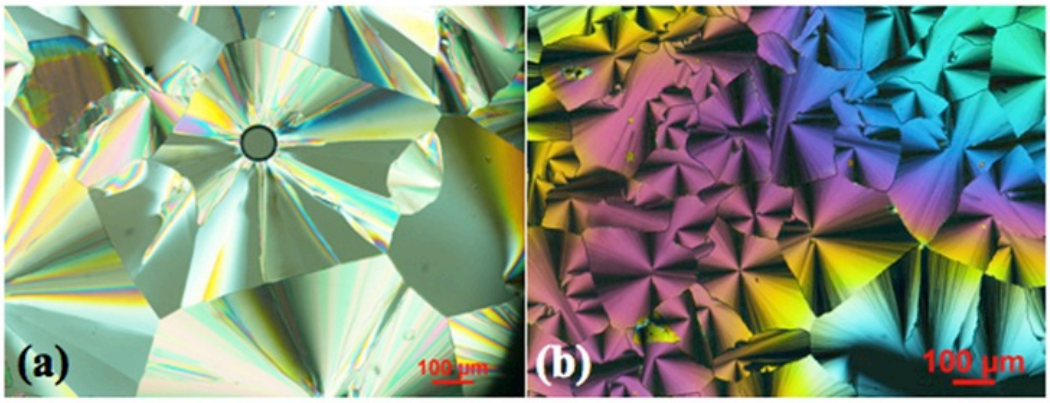


**Figure 3.14.** Photomicrograph of texture as seen by POM for the $Col_{ob}$ phase of compound **MT2** at 80 °C (a), and for compound **MT3** at 84 °C (b).

In the first series, of *p*-substituted polycatenars, the reduction in isotropic temperature is not regular in the heating cycle, while in the second series, of *m*-substituted polycatenars, there is a gradual reduction in the isotropic temperature with the increase in chain length (Fig. 3.5). Both series of molecules showed a reduction in the thermal range with the increase in chain length. When compared to the *p*-substituted polycatenars **PT1-3**, which exhibited $Col_h$ and/or $Col_{ob}$ phases, the *m*-substituted polycatenars **MT1-3** showed broader mesophase ranges, and stabilized the $Col_{ob}$ phase exclusively. We need to recall here that among the *p*-substituted polycatenars from the first series, the peak corresponding to core-core stacking was absent. On the contrary, all the *m*-substituted polycatenars show the reflection corresponding to core-core stacking, suggesting that there is an enhanced core-core interaction in this series of compounds. It is understandable that for the stabilization of the $Col_{ob}$ phase, enhanced core-core interactions are essential because the tilt of the cores in one column must be related to the tilt of cores in another column in certain way.[36]

**Table 3.3.** Results of (*hkl*) indexation of XRD profiles of the compounds at a given temperature (T) of mesophases[a].

| Compounds ($D$/Å) | Phase (T/°C) | $d_{obs}$ (Å) | $d_{cal}$ (Å) | Miller indices *hkl* |
|---|---|---|---|---|
| **MT1** (44.01) | $Col_{ob}$ (90) | 32.41<br>31.03<br>15.52<br>4.57 ($h_a$)<br>3.77 ($h_c$) | 32.41<br>31.03<br>15.52 | 010<br>110<br>-110<br><br>001 |
| | $Col_{ob}$ (70) | 34.74<br>31.90<br>18.42<br>15.96<br>4.54 ($h_a$)<br>3.72 ($h_c$) | 34.74<br>31.90<br>18.42<br>15.95 | 010<br>110<br>-110<br>020<br><br>001 |
| **MT2** (48.5) | $Col_{ob}$ (80) | 36.10<br>34.82<br>33.55<br>4.55 ($h_a$)<br>3.71 ($h_c$) | 36.10<br>34.82<br>33.55 | 010<br>110<br>100<br><br>001 |
| **MT3** (58.8) | $Col_{ob}$ (82) | 40.98<br>38.40<br>37.03<br>21.38<br>4.59 ($h_a$)<br>3.75 ($h_c$) | 40.98<br>38.40<br>37.03<br>21.23 | 010<br>100<br>110<br>210<br><br>001 |

[a] The diameter ($D$) of the polycatenar (estimated from Chem 3D Pro 8.0 molecular model software from Cambridge Soft). $d_{obs}$: spacing observed; $d_{cal}$: spacing calculated (deduced from the lattice parameters; $a$ for the $Col_h$ phase; $a$ and $b$ for the $Col_{ob}$ phase). The spacings marked $h_a$ and $h_c$ correspond to diffuse reflections in the wide-angle region arising from correlations between the alkyl chains and core regions, respectively.

The mesomorphic behavior of thiadiazole-based polycatenars **PT1-3**, **MT1** and **MT3** of the present work can be compared to their oxadiazole counterparts **Ia-c**[34b] and **IIa-b,**[34a] which were reported earlier (Fig. 3.2). On comparing the thermal behavior, it is evident that thiadiazole-based *p*-substituted polycatenars stabilize the $Col_h$ and/or $Col_{ob}$ phases, while their oxadiazole counterparts **Ia-c**[34b] stabilized crystal/ $Col_h$ phases. It is to be noted that analogous *m*-substituted polycatenars based on 1,3,4-oxdiazoles exhibited the $Col_h$ phase exclusively, irrespective of the chain length (Fig. 3.2).[34a] This also supports the enhanced core-core interactions in the case of these thiadiazole-based *m*-substituted polycatenars. The sulphur heteroatom in the molecular structure is another

contributing factor due to the attractive S···S interactions, which is a well-known fact in the case of chalcogen-based semiconductors.[39]

The mesophase width was increased in the case of thiadiazole derivatives in comparison to their oxadiazole analogues. This behavior is in line with the recently reported behavior of star shaped 1,3,4-thiadiazole derivatives, where star-shaped 1,3,4-thiadiazoles exhibited a wide range enantiotropic $Col_h$ phase in comparison to their oxadiazole counterparts.[33b] Thus the thiadiazole moiety enhances the mesogenic behavior due to favorable interactions. Polycatenar thiadiazoles exhibited reduced mesophase ranges when compared to the star shaped thiadiazole derivatives.

### 3.2.3. Photophysical properties

Photophysical properties of the polycatenars **PT1-3** and **MT1-3** in solution are depicted in Table 3.5. It is expected that due to the difference in the substitution pattern between the two series, there must be a considerable difference in the photophysical properties. Absorption and fluorescence spectra of the compounds **PT1-3** and **MT1-3** were taken in THF (Fig. 3.15).

As can be seen, the absorption spectra for the solutions of the *p*-substituted polycatenars **PT1-3** showed single absorption maxima in a range of 360-365 nm. The absorption maxima of the *m*-substituted polycatenars **MT1-3** exhibited a hypsochromic shift, with absorption maxima centered at around 335-337 nm. Large values of the molar extinction coefficients showed that these are highly delocalized electronic systems ($\varepsilon \geq 18{,}650\ M^{-1}\ cm^{-1}$). Based on the similarity to reported 1,3,4-oxadiazole- and thiadiazole-based systems,[33b] the single absorption band of these systems is attributed to a $\pi$-$\pi^*$ transition of the aromatic system. Optical bandgaps of these systems were calculated from the absorption onset values. Compounds **PT1-3** showed a band gap of 3 eV, while compounds **MT1-3** showed a slightly higher bandgap of 3.23 eV. This shows that the $\pi$ electron cloud is delocalized to a greater extent in the case of the *p*-substituted compounds (**PT1-3**), in comparison to the *m*-substituted compounds (**MT1-3**). Compared to their star-shaped analogue, *i.e.* a 1,3,5-benzene-trisubstituted thiadiazole derivative

(optical band gap of 3.1 eV) with nine decyloxy chains, compounds **PT1-3** showed a bathochromic shift of 20 nm in the absorption maximum, while compounds **MT1-3** showed a hypsochromic shift of 10 nm. When compared to the corresponding oxadiazole derivatives, the *p*- and *m*-substituted thiadiazole derivatives showed a red shift of 26 nm.[34]

The emission spectra of compounds **PT1-3** exhibited a single emission maxima centered at around 480-483 nm, with a large Stokes shift of 115-121 nm. Compounds **MT1-3** showed emission with their maxima centered around 446-450 nm, with a Stoke's shift of 111-114 nm. As can be seen from the table, there was no much difference in the absorption and emission properties with respect to the chain length.[33b,34,37] When compared to their star-shaped analogue with nine decyloxy chains, compounds **PT1-3** showed a bathochromic shift of 9 nm in the emission maximum, while compounds **MT1-3** showed a hypsochromic shift of 24 nm. As can be seen in the Fig. 3.15, green light was observed in the emissive state for compounds **PT1-3**, while blue light was observed for compounds **MT1-3** on irradiation with the UV light of 365 nm wavelength.

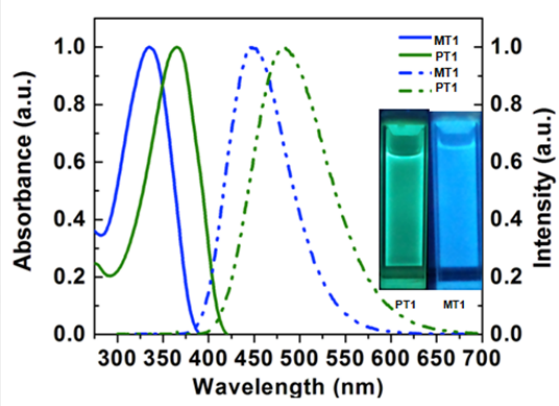


**Figure 3.15.** Normalized absorption (solid trace) and emission spectra (dotted trace) in THF solution obtained for **PT1** (green trace) and **MT1** (blue trace). Pictures of micromolar solutions of compounds **PT1** and **MT1** in THF, as seen with the illumination of 365 nm UV light (inset).

When compared to the corresponding oxadiazole derivatives, the *p*-substituted thiadiazole derivatives showed a red shift of 15 nm, while *m*-substituted thiadiazole

derivatives showed a red shift of 21 nm.[34] As a representative case, we measured the relative quantum yield for compounds **PT1** and **MT1** with respect to quinine sulphate solution (0.1 M $H_2SO_4$ with a quantum yield of 0.54). Compound **PT1** showed a relative quantum yield of 0.4, while compound **MT1** had a silghtly lesser value (0.35) (see Fig. 3.16). These compounds showed slightly higher quantum yields than their star shaped analogue **III** (0.31).[33b] Quantum yield was measured according to established procedure by using quinine sulfate in 0.1 M $H_2SO_4$ solution as the standard. Absolute values were calculated according to the following equation: $Q_S = Q_R \times (m_S / m_R) \times (n_S / n_R)^2$ Where, Q: Quantum yield, m: Slope of the plot of integrated fluorescence intensity *vs* absorbance n: refractive index (1.407 for THF and 1.33 for distilled water).The subscript R refers to the reference fluorophore *i.e.* quinine sulphate solution in 0.1 M $H_2SO_4$ and subscript S refers to the sample under investigation. In order to minimize re-absorption effects, absorbance was kept below 0.15 at the excitation wavelength of 347 nm. Quantum Yield of quinine sulphate is 0.54. Simplified equation for the calculation after substituting the appropriate values is given below and values obtained are given in Table 3.4.

$$Q_S = 0.54 \times (m_S / 2.71) \times (1.407/1.33)^2 = 0.223 \times m_S$$

**Table 3.4.** Quantum yield of polycatenars[a]

| Entry | $m_S$ | $m_R$ | $Q_s$[a,b,c] |
|---|---|---|---|
| **PT1** | $1.78\times10^9$ | $2.71\times10^9$ | 0.40 |
| **MT1** | $1.58\times10^9$ | $2.71\times10^9$ | 0.35 |

[a] Measured in THF; [b]Excited at absorption maxima; [c]Standard quinine sulphate ($\mathbf{Q_f}$ = 0.54) in 0.1M $H_2SO_4$.

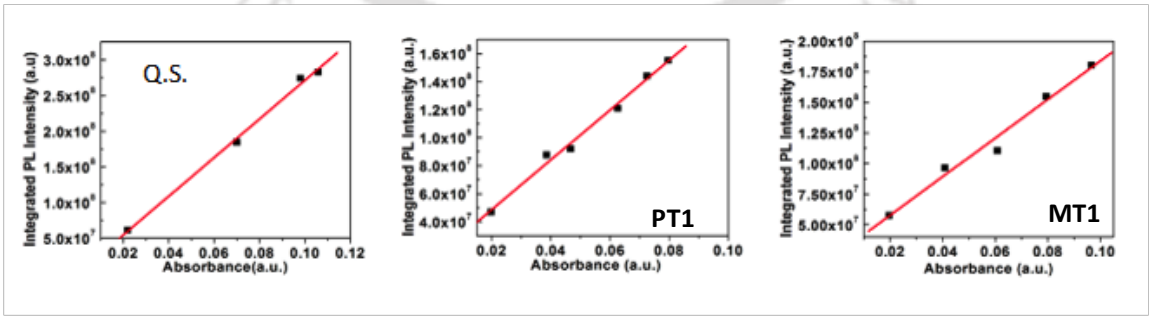


**Figure 3.16.** Plots of integrated photoluminescence intensity *vs* absorbance of Quinine sulphate (0.1M $H_2SO_4$ solution), compounds **PT1** and **MT1** (micromolar THF solution)

**Table 3.5.** Photophysical properties of polycatenars[a]

| Entry | Absorption (nm) | Emission[b] (nm) | Stokes shift nm ($cm^{-1}$) | $\lambda_{onset}$ (nm) | $\Delta E^{c,d}_{g,\ opt}$ |
|---|---|---|---|---|---|
| **PT1** | 365 | 480 | 115(6564) | 414 | 3.0 |
| **PT2** | 360 | 483 | 118(7075) | 414 | 3.0 |
| **PT3** | 360 | 481 | 121 (6987) | 412 | 3.02 |
| **MT1** | 335 | 446 | 111 (7429) | 383 | 3.24 |
| **MT2** | 336 | 450 | 114 (7540) | 385 | 3.23 |
| **MT3** | 337 | 449 | 112 (7402) | 385 | 3.23 |

[a]micromolar solutions in THF; [b] Excited at the respective absorption maxima; [c] Band gap determined from the red edge of the longest wave length ($\lambda_{onset}$) in the UV-vis absorption spectra; [d] In volts (V)

Dilution of these micromolar solutions in THF did not produce any variation in the absorption and emission maxima, showing that these polycatenars are not aggregating at these concentrations. When the concentration is gradually increased from micromolar solution to milimolar solution, the absorption maximum shows a slight blue shift (Fig. 3.17a). The emission spectra in the solutions of increasing concentration did not show any shift in the emission maxima (Fig. 3.17b), but showed a gradual increase in the fluorescence intensity upto a certain concentration (Fig. 3.17c). Further increase in concentration reduced the fluorescence intensity due to aggregation quenching (Fig. 3.17d). Similar behavior was observed in the case of compound **MT1** (Fig. 3.18). At higher concentration the absorption spectra showed a slight blue shift, while the emission spectra did not show any change. As in the case of compound **PT1**, up to a certain concentration there was an increase in the fluorescence intensity, after which there was a decrease in the intensity (Fig. 3.18d). This decrease may be due to aggregation quenching. Fluorescence life-time decay profiles obtained for compounds **PT1** and **MT1,** at concentrations corresponding to their highest fluorescence intensity, exhibited a monoexponential decay with lifetime values of 1.73 and 1.44 ns, respectively, confirming the presence of solvated monomers (Fig. 3.19).

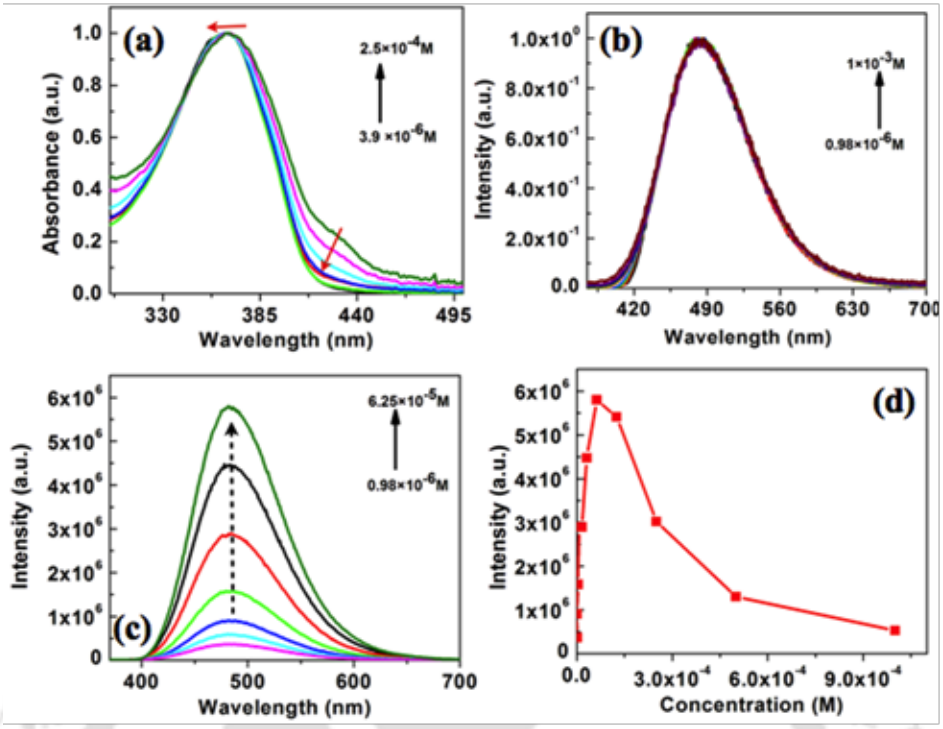


**Figure 3.17.** Normalized absorption (a) and emission (b) spectra obtained for compound **PT1** as a function of concentration; enhancement of luminescence in solution on increasing the concentration (c); a graph showing the variation of luminescence intensity with respect to concentration (d).

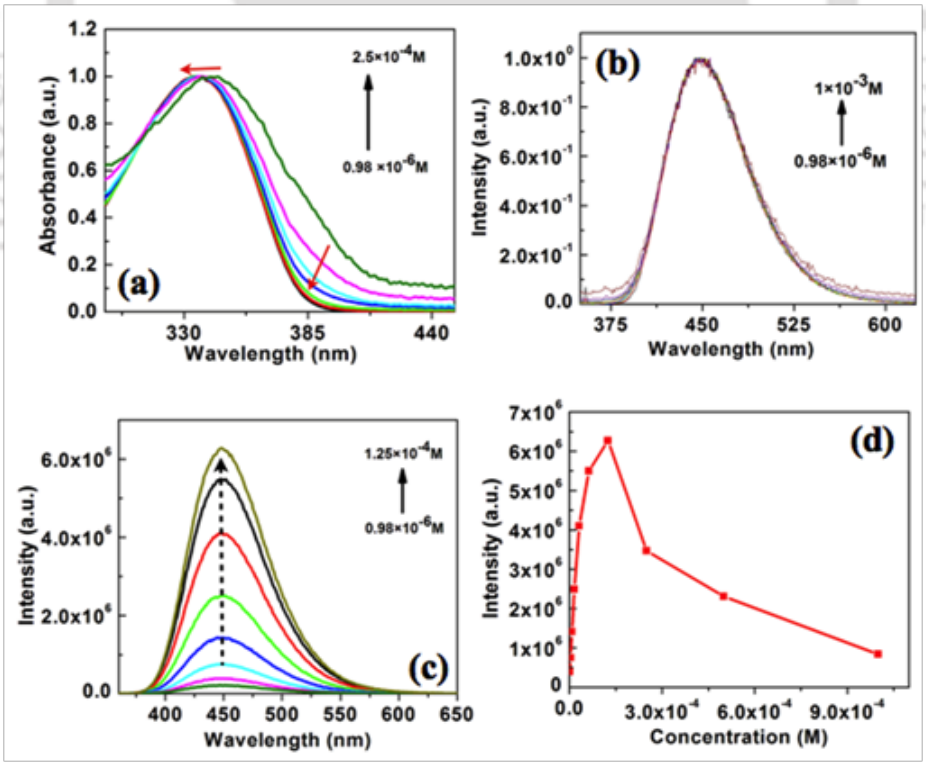


**Figure 3.18.** Normalized absorption (a) and emission (b) spectra obtained for compound **MT1** as a function of concentration; enhancement of luminescence in solution on increasing the concentration (c); a graph showing the variation of luminescence intensity with respect to concentration (d).

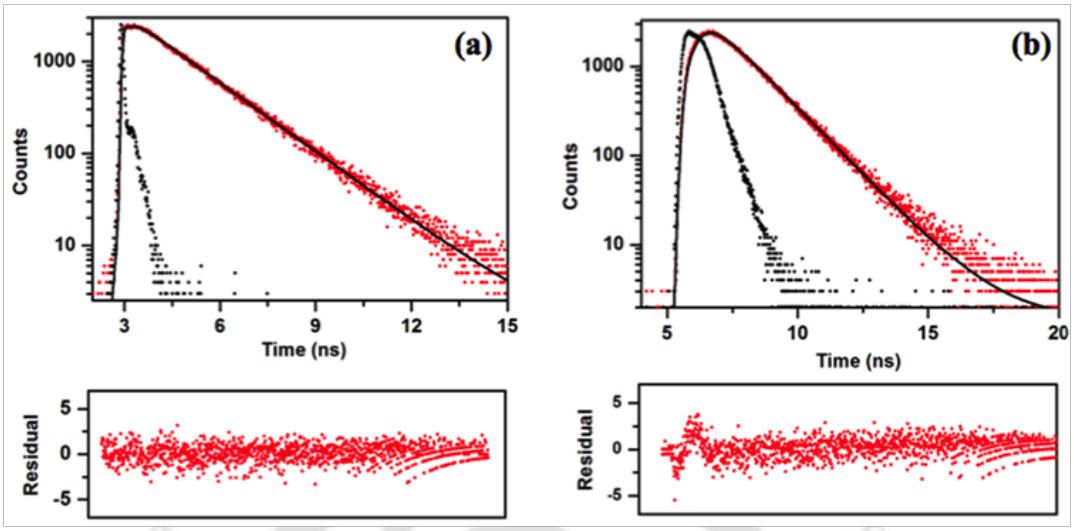


**Figure 3.19.** (a) The fluorescence decay of compound **PT1** in THF ($6.25 \times 10^{-5}$M, $\lambda_{exc}$ = 375 nm); (b) the fluorescence decay of compound **MT1** in THF ($1.25 \times 10^{-4}$M, $\lambda_{exc}$ = 336 nm). (The red traces correspond to the decay profiles, and the black traces correspond to the instrument response functions; the residual plots are shown below the decay plot).

We were interested in studying the emissive nature of these molecules in the solid state. Thin films of these molecules were prepared on glass slides by drop casting the millimolar solutions in toluene. The absorption spectra of compounds **PT1** and **MT1** showed structured absorption bands. Compound **PT1** showed two absorption maxima centered at 301 and 385 nm, while compound **MT1** also showed two absorption maxima, centered at 301 and 371 nm (Fig.3.20). In comparison to their structure less solution-state absorption spectra, these absorption spectra showed two absorption maxima and a blue shift. Emission spectra obtained by exciting the solutions at their absorption maxima found to be broadened with a slight red shift. Compound **PT1** showed an emission maximum centered at 485 nm, while compound **MT1** showed an emission maximum centered at 463 nm. Thus compound **PT1** showed a red shift of 5 nm, while compound **MT1** showed a red shift of 13 nm with respect to their solution-state spectra. However, under UV light of long wavelength (365 nm), these films showed similar visually perceivable emisssion as in the solution state for compounds **PT1** and **MT1** (Fig. 3.16 and Fig. 3.20b). The blue shift in the absorption bands observed for thin films, in comparison to the solution state, indicates that the emission is arising from the molecular

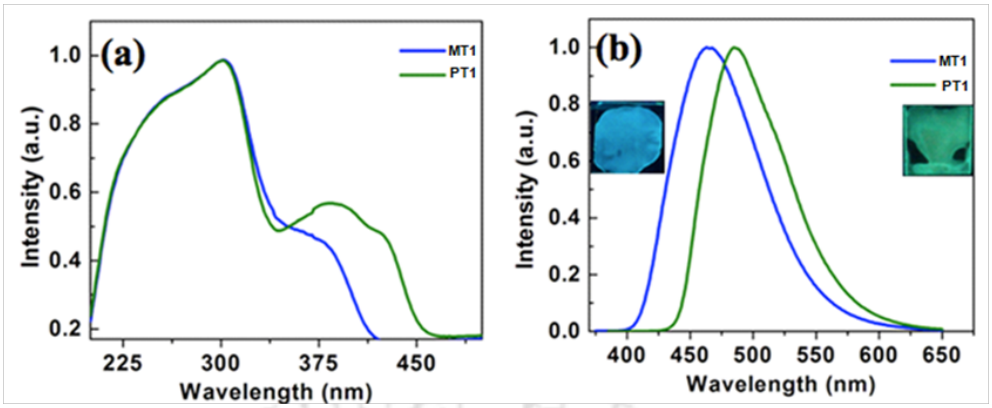


**Figure 3.20.** Normalized absorption spectra obtained for compounds **PT1** (green trace) and **MT1** (blue trace) in the thin film state prepared from drop casting (a); normalized emission spectra obtained for compounds **PT1** and **MT1** in the thin film state (b). The inset shows the thin films of compounds **PT1** and **MT1** on illumination of 365 nm UV light.

aggregates, in which the molecules are stacked one above the other in a cofacial manner ( denoted as H-aggregates).[40] We have also attempted to see these compounds form gel in various solvents, but found that the π-π interaction between the aromatic cores alone was not sufficient for gelation. We have also prepared thin films of the samples by heating the sandwiched samples between glass slides to the isotropic state. These films were suddenly cooled in their liquid crystalline state. Polarizing optical images have shown that compound **PT1** was crystallized during this sudden cooling (Fig. 3.21c), while compound **MT1** retained the texture of the $Col_{ob}$ phase (Fig. 3.21f). Both of the films showed good transparency (Fig. 3.21a and d). It is interesting to note that the thin film prepared from compound **PT1** turned opaque and formed a green-colored film slowly, while compound **MT1** still retained the transparency and liquid crystalline texture even after 7 days (Fig. 3.21g). Thus it can be understood that the molecular structures of the *p*-substituted polycatenars are more conducive to crystallization, while those of the *m*-substituted polycatenars prevent crystallization and favor a glassy state. A glassy columnar structure helps in charge migration with the simultaneous freezing of ionic impurities, which is a favorable feature for applications in organic electronic devices.[41]

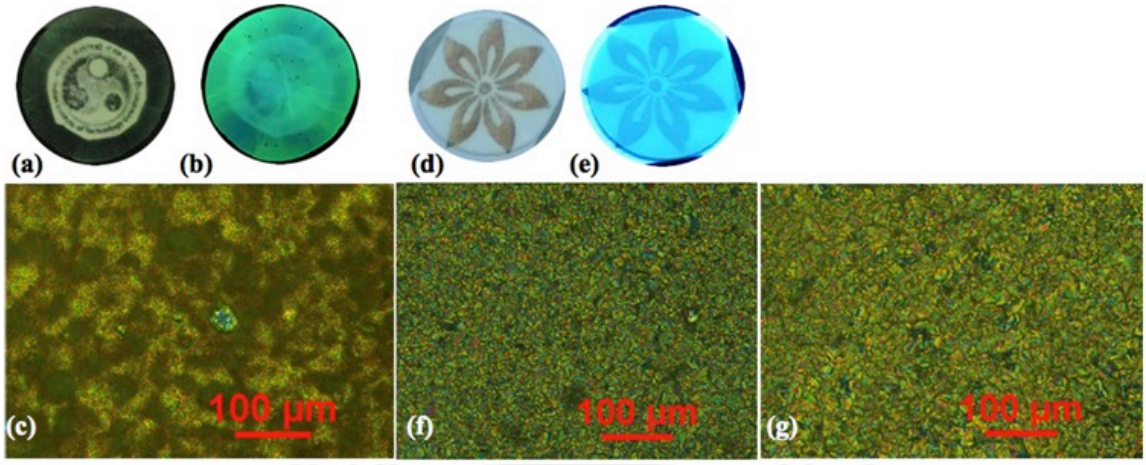


**Figure 3.21.** A thin film prepared from compound **PT1** by annealing the isotropic liquid under (a) day light and (b) 365 nm UV light; a POM image of the same film showing crystallization (c); a thin film prepared from compound **MT1** by annealing the isotropic liquid under (d) day light and (e) 365 nm UV light; a POM image of the same film showing the freezing of $Col_{ob}$ phase (f); a POM image of the film after 7 days showing the stable glassy state (g).

### 3.2.4. Electrochemical properties

The energy levels of the HOMO and the LUMO and the band gap of the polycatenars were obtained by cyclic voltammetry (CV), and the data are tabulated in Table 3.6. We have chosen compounds **PT1** and **MT1** for carrying out CV studies. Both the compounds exhibited irreversible oxidation and reduction waves (See Fig. 3.22).

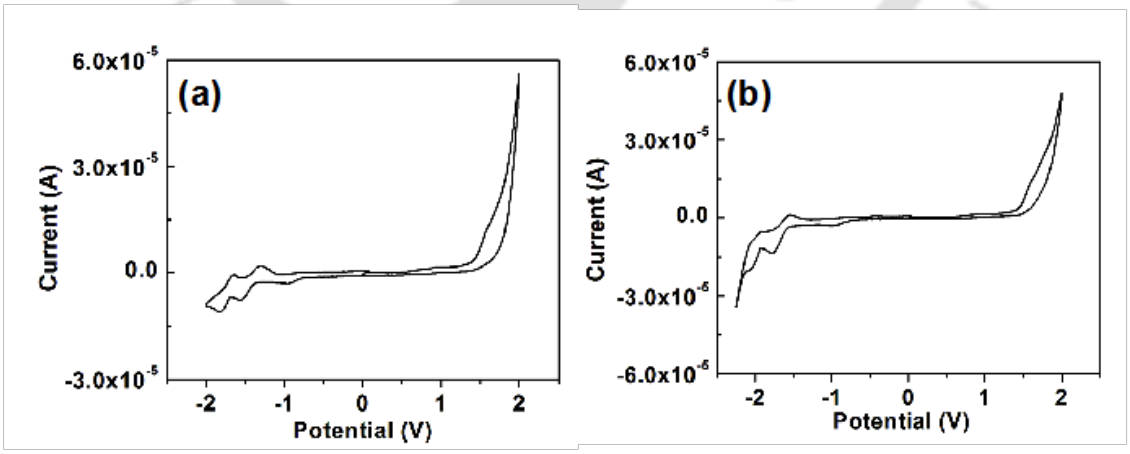


**Figure 3.22.** Cyclic voltammograms of the compounds **PT1** (a) and **MT1** (b) in anhydrous THF solution of tetra-*n*-butylammonium perchlorate (0.1 M) at a scanning rate 0.5mV/s

The optical band gap $E_{g,opt}$ was estimated from the red edge of the absorption spectra. The *p*-Substituted compound **PT1** exhibited a lower band gap when compared to the *m*-substituted compounds **MT1-3**. The LUMO and HOMO energy levels were determined by using the formulae $E_{LUMO} = -(4.8 - E_{1/2,\ Fc,Fc^+} + E_{red,\ onset})$ eV and $E_{HOMO} = (4.8 - E_{1/2,\ Fc,Fc^+} + E_{ox,\ onset})$ eV. The *p*-Substituted compound **PT1** exhibited a LUMO level at -3.31 eV and a HOMO level at -5.87 eV, while the *m*-substituted compound **MT1** exhibited a LUMO level at -3.29 eV and a HOMO level at -5.98 eV. Thus the band gaps estimated from CV by using the above formulae have values of -2.56 eV for compound **PT1** and -2.69 eV for compound **MT1**. These values are slightly less than their respective optical band gap values (Table 3.5). When compared to their star-shaped analogues, the polycatenars exhibit slightly lower LUMO and higher HOMO levels. As a result, there is a reduction in the band gap of the polycatenars when compared to their star-shaped analogue[33b] (Fig. 3.23).

**Table 3.6.** Electrochemical[a,b] properties of the polycatenars

| Entry | $E^{d}_{1red}$ | $E^{d}_{1oxd}$ | $E^{c,e}_{HOMO}$ | $E^{c,f}_{LUMO}$ | $\Delta E^{c,g}_{CV}$ |
|---|---|---|---|---|---|
| **PT1** | -0.93 | 1.63 | -5.87 | -3.31 | 2.56 |
| **MT1** | -0.95 | 1.74 | -5.98 | -3.29 | 2.69 |

[a]Micromolar solutions in THF. [b] Experimental conditions: $Ag/AgNO_3$ as the reference electrode, glassy carbon working electrode, platinum rod counter electrode, TBAP (0.1 M) as a supporting electrolyte, room temperature, scanning rate of 0.05 $mVs^{-1}$. [c]In electron volts (eV). [d] In volts (V). [e] Estimated from the onset oxidation peak values by using the formula $E_{HOMO} = (4.8 - E_{1/2,\ Fc,Fc^+} + E_{ox,\ onset})$ eV. [f]Estimated from the onset reduction peak values by using $E_{LUMO} = -(4.8 - E_{1/2,\ Fc,Fc^+} + E_{red,\ onset})$ eV. [g]Estimated from the formula $\Delta E_{CV} = E_{LUMO} - E_{HOMO}$ eV.

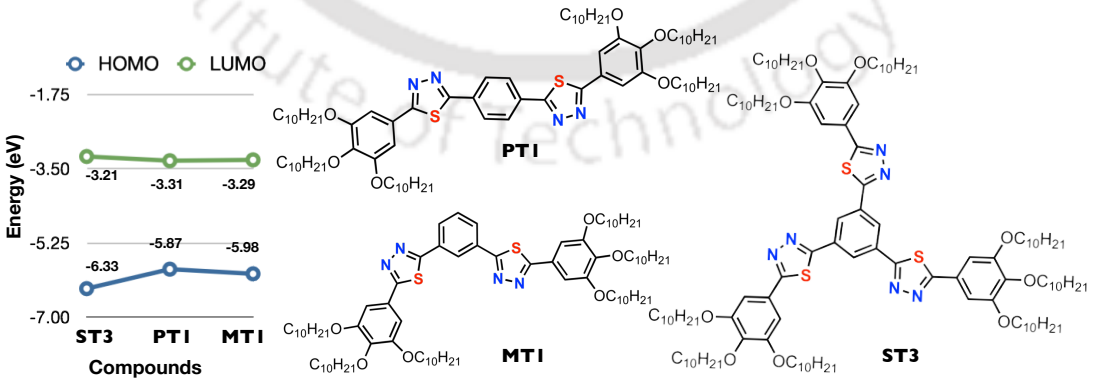


**Figure 3.23**. Comparison of the frontier molecular orbitals for compounds **PT1**, **MT1** and **ST3.**

### 3.3. Conclusions

In summary, we have synthesized two series of polycatenars containing a 1,3,4-thiadiazole moiety in their molecular structure. The main difference between the two series is the position at which the 1,3,4-thiadiazole moiety is connected to a central benzene ring. In the first series, the thiadiazole moieties are connected to the central benzene ring at the 1,4 positions (*p*-substituted), while in the second series, the thiadiazole moieties are connected at the 1,3 positions (*m*-substituted) to the central benzene ring. The thermal behavior was studied with the help of POM, TGA, DSC and powder XRD studies. Both the series stabilized an enantiotropic columnar phase. The *p*-substituted polycatenars stabilized the $Col_h$ and/or $Col_{ob}$ phases, while the *m*-substituted polycatenars exhibited the $Col_{ob}$ phase exclusively. The *m*-substituted polycatenars showed enhanced core-core interactions in comparison to the *p*-substituted polycatenars. In both the series, the mesophase range decreased with the increase in the chain length. Incorporation of sulphur in the molecular structure enhanced the thermal range of the mesophases with respect to the oxadiazole counterparts. The polycatenar thiadiazoles exhibited a reduced mesophase range when compared to the star-shaped thiadiazole derivatives.

Both the series exhibited luminescence in solution. The *p*-substituted compounds showed green emission, while the *m*-substituted compounds exhibited blue emission in the solution state. Thus the substitution plays a very important role in the luminescence properties of these molecules. Most importantly, the thin films prepared by drop casting or by annealing from the isotropic state showed similar visually perceivable emission. The length of the peripheral tails did not have much effect on the absorption and emission behavior of these compounds. Cyclic voltammetry studies have shown that the *p*-substituted polycatenars showed lower bandgaps than the *m*-substituted compounds. Both the polycatenar types exhibited a lower band gap than their star-shaped analogue. Thus in this chapter we have shown that regioisomerism has a significant effect on the self-assembly and photophysical behavior of 1,3,4-thiadiazole-based polycatenars.

### 3.4. Experimental Section

In this section the detailed synthetic procedures and the molecular structural characterization data have been presented for the intermediates and target compounds mentioned in the scheme 3.1. Some of the intermediates such as **1c** and **2c** are reported and characterized in the second chapter.

Procedure for the synthesis of ethyl 3,4,5-tri(dodecyloxy) benzoate (**4b**)

A mixture of ethyl gallate (10.1 mmol, 1equiv.), anhyd. $K_2CO_3$ (66.6 mmol, 6.6 equiv.), *n*-bromododecane (33.3 mmol, 3.3 equiv.) were taken in dry DMF (20 ml) and heated at 80 $^oC$ for 17 h under nitrogen atmosphere. Then the reaction mixture was poured into ice-water and extracted with $CH_2Cl_2$. The combined extract was washed with water and brine. Dried over anhyd. $Na_2SO_4$ and concentrated. The crude product was purified by column chromatography on neutral alumina. Elution with hexanes followed by 5-10% ethylacetate-hexanes yielded the desired product.

$R_f$ = 0.61(10% EtOAc-hexanes); Low melting colorless solid; yield: 90%; IR (KBr pellet): $\nu_{max}$ in $cm^{-1}$ 2924, 2853, 1716, 1590, 1504, 1465, 1432, 1333, 1222, 1119; $^1H$ NMR ($CDCl_3$, 600 MHz): δ 7.25 (s, 2H, Ar), 4.35 (q, 2H, *J* = 6 Hz, $COOCH_2$), 4.01 (m, 6H, 3 × $OCH_2$), 1.23-1.83 ( m, 60H, 30 × $CH_2$), 0.87-0.89 (m, 12H, 4 × $CH_3$); $^{13}C$ NMR ($CDCl_3$, 150 MHz): 166.66, 153.01, 142.57, 125.26, 108.24, 73.68, 69.40, 61.14, 32.14, 30.54, 29.95, 29.92, 29.85, 29.79, 29.61, 29.54, 26.30, 22.90, 14.30; HRMS (ESI+) exact mass calculated for $C_{45}H_{83}O_5$ (M+1): 703.6235, Found: 703.6199.

Procedure for the synthesis of ethyl 3,4,5-tri(hexadecyloxy) benzoate (**4c**)

A mixture of ethyl gallate (10.1 mmol, 1equiv.), anhyd. $K_2CO_3$ (66.6 mmol, 6.6 equiv.), *n*-bromohexadecane (33.3 mmol, 3.3 equiv.) were taken in dry DMF (20 ml) and heated at 80 $^oC$ for 17 h under nitrogen atmosphere. Then the reaction mixture was poured into ice-water and extracted with $CH_2Cl_2$. The combined extract was washed with water and brine. Dried over anhyd. $Na_2SO_4$ and concentrated. The crude product was purified by column chromatography on neutral alumina. Elution with hexanes followed by 2 - 5% ethylacetate-hexanes yielded the desired product.

$R_f$ = 0.81(10% EtOAc-hexanes); colorless solid, m.p.: 54-56 $^oC$; yield: 85%; IR (KBr pellet): $\nu_{max}$ in $cm^{-1}$ 2922, 2850, 1716, 1584, 1469, 1427, 1331, 1219, 1110; $^1H$ NMR ($CDCl_3$, 400 MHz): δ 7.25 (s, 2H, Ar), 4.35 (q, 2H, *J* = 7.2 Hz, $COOCH_2$), 4.01 (t, 6H, 3 × $OCH_2$), 1.25-1.82 ( m, 84H, 42 × $CH_2$), 0.86-0.89 (m, 12H, 4 × $CH_3$); $^{13}C$ NMR ($CDCl_3$, 100 MHz): 166.70, 153.04, 142.61, 125.28, 108.29, 73.72, 69.44, 61.17, 33.05, 32.16, 30.56, 29.94, 29.89, 29.87, 29.80, 29.63, 29.60, 29.57, 26.32, 26.29, 22.92, 14.63, 14.33. HRMS (ESI+) exact mass calculated for $C_{57}H_{107}O_5$ (M+1): 871.8113, Found: 871.8031.

Procedure for the synthesis of 3,4,5-tri-*n*-dodecyloxy benzohydrazide (**5b**)

A mixture of ethyl 3,4,5-tri-*n*-dodecyloxybenzoate (9.7 mmol, 1equiv.), excess hydrazine hydrate (19.4 mL), *n*-butanol (20 mL) was refluxed for 40 h. Water (100 mL) was added and resulting precipitate was collected, dried under vacuum, and recrystallized from ethanol to yield pure **5b** as a colorless solid.

$R_f$ = 0.46 (20% EtOAc-hexanes); colorless solid, m.p.: 114-116$^o$C; yield: 71%; IR (KBr pellet): $\nu_{max}$ in cm$^{-1}$ 3244, 2923, 2851, 1646, 1581, 1500, 1467, 1237, 1122; $^1$H NMR ($CDCl_3$, 400 MHz): δ 7.32 (br s, 1H, CONH), 6.92 (s, 2H, Ar), 3.99 (m, 8H, 1× $NH_2$, 3 × $OCH_2$), 1.26 – 1.83(m, 60H, 30×$CH_2$), 0.86-0.89(m, 9H, 3×$CH_3$); $^{13}$C NMR ($CDCl_3$, 100 MHz):168.96, 153.44, 141.69, 127.66, 105.71, 73.75, 69.57, 32.14, 30.52, 29.94, 29.91, 29.87, 29.85, 29.78, 29.60, 29.57, 29.54, 26.28, 22.90, 14.31. HRMS (ESI+) exact mass calculated for $C_{43}H_{81}N_2O_4$ (M+1): 689.6191, Found: 689.6189.

Procedure for the synthesis of 3,4,5-tri-*n*-hexadecyloxy benzhydrazide (**5c**)

A mixture of ethyl 3,4,5-tri-*n*-hexadecyloxybenzoate (9.2 mmol, 1equiv.), excess hydrazine hydrate (18.4 mL), *n*-butanol (20 mL) was refluxed for 40 h. Water (100 mL) was added and resulting precipitate was collected, dried under vacuum, and recrystallized from ethanol to yield pure **5c** as a colorless solid.

$R_f$ = 0.52 (20% EtOAc-hexanes); colorless solid, m.p.: 102-104 $^o$C; yield: 75%; IR (KBr pellet): $\nu_{max}$ in cm$^{-1}$ 3449, 3248, 2922, 2851, 1635, 1580, 1466, 1428, 1239, 1122; $^1$H NMR ($CDCl_3$, 600 MHz): δ 7.22 (br s, 1H, CONH), 6.92 (s, 2H, Ar), 4.07 (s, 2H, $NH_2$), 3.99 (m, 6H, 3 × $OCH_2$), 1.26 – 1.80 (m, 84H, 42×$CH_2$), 0.88 (m, 9H, 3×$CH_3$); $^{13}$C NMR ($CDCl_3$, 150 MHz): 168.70, 153.54, 141.92, 127.68, 105.74, 69.60, 30.53, 29.97, 29.95, 29.88, 29.60, 26.30, 22.92 and 14.33. HRMS (ESI+) exact mass calculated for $C_{55}H_{105}N_2O_4$ (M+1): 857.8069, Found: 857.8151.

Procedure for the synthesis of 1,3-bis(5-(3,4,5-tris(decyloxy)phenyl)-1,3,4-thiadiazol-2-yl)benzene (**MT1**)

Isophthalic acid (1mmol) in 4.5 ml of thionyl chloride and DMF (catalytic amount) was heated under reflux for 4 h. The excess of thionyl chloride was removed by distillation, the crude product (Isophthaloyl dichloride) was dried *in vacuo* and used for the next reaction without further purification and characterization. The solution of Isophthaloyl dichloride (0.9 mmol, 1equiv.) in THF was added dropwise to a solution of 3,4,5-tri-*n*-decyloxy benzohydrazide (1.85 mmol, 2.05 equiv.) and triethylamine (1.8 mmol, 2 equiv.) in THF (20 mL). The reaction mixture was stirred at 55 $^o$C for 12 h. After cooling, THF was evaporated and the residue was extracted with dichloromethane. The extract was washed with water and brine. Dried over $Na_2SO_4$ and concentrated. The resulting crude product (**7a**) was directly used for next reaction. The solution of crude product **7a** (0.4 mmol, 1equiv.) in dry toluene (8 mL) was added dropwise to a solution of Lawesson's reagent (1 mmol, 2.4 equiv.) in dry toluene at room temperature under Argon

atmosphere and refluxed for 24 h. After removal of solvent *in vacuo*, the crude products were further purified through column chromatography on neutral alumina. Elution with 10-20% ethylacetate-hexanes yielded the desired product.

$R_f$ = 0.3 (20% EtOAc-hexanes); colorless solid, yield: 40%; IR (KBr pellet): $\nu_{max}$ in $cm^{-1}$ 2924, 2853, 1589, 1512, 1187; $^1$H NMR ($CDCl_3$, 600 MHz): $^1$H NMR ($CDCl_3$, 400 MHz): δ 8.59 (s, 1H, Ar), 8.15 (d, 2H, *J* =6Hz, Ar), 7.64 (t, 1H, Ar), 7.23 (s, 4H, Ar), 4.08 (t, 8H, 4× $OCH_2$), 4.04 (t, 4H, 2× $OCH_2$), 1.24 – 1.88 (m, 96H, 48 × $CH_2$), 0.87 – 0.89 (m, 18H, 6 × $CH_3$); $^{13}$C NMR ($CDCl_3$, 100 MHz): 169.11, 166.77, 153.83, 141.38, 131.55, 130.29, 130.13, 127.29, 124.93, 106.81, 73.89, 69.65, 32.16, 32.14, 30.56, 29.95, 29.89, 29.86, 29.81, 29.63, 29.57, 26.31, 22.90, 14.32. HRMS (ESI+) exact mass calculated for $C_{82}H_{135}N_4O_6S_2$(M+1): 1335.9818, Found: 1335.9711.

Procedure for the synthesis of 1,3-bis(5-(3,4,5-tris(dodecyloxy)phenyl)-1,3,4-thiadiazol-2-yl)benzene (**MT2**)

Isophthalic acid (0.9 mmol) in 4.2 ml of thionyl chloride and DMF (catalytic amount) was heated under reflux for 4 h. The excess of thionyl chloride was removed by distillation, the crude product (Isophthaloyl dichloride) was dried in vacuo and used for the next reaction without further purification and characterization. The solution of Isophthaloyl dichloride (0.8 mmol, 1equiv.) in THF was added dropwise to a solution of solution of 3,4,5-tri-*n*-dodecyloxy benzhydrazide (1.6 mmol, 2.05 equiv.) and triethylamine (1.6 mmol, 2 equiv.) in THF (20 mL). The reaction mixture was stirred at 55 $^oC$ for 12 h. After cooling, THF was removed through distillation and the residue was extracted with dichloromethane. The extract was washed with water and brine. Dried over $Na_2SO_4$ and concentrated. The resulting crude product (**7b**) was directly used for next reaction. The solution of crude product **7b** (0.6 mmol, 1equiv.) in dry toluene (12 mL) was added dropwise to a solution of Lawesson's reagent (1.4 mmol, 2.4 equiv.) in dry toluene at room temperature under Argon atmosphere and refluxed for 24 h. Toluene was removed by distillation. After removal of solvent *in vacuo*, the crude products were further purified through column chromatography on neutral alumina. Elution with 10-20% ethylacetate-hexanes yielded the desired product.

$R_f$ = 0.59 (20% EtOAc-hexanes); colorless solid, yield: 45%; IR (KBr pellet): $\nu_{max}$ in $cm^{-1}$ 2923, 2852, 1589, 1512, 1124; $^1$H NMR ($CDCl_3$, 400 MHz): $^1$H NMR ($CDCl_3$, 400 MHz): δ 8.58 (t, 1H, *J* = 1.6 Hz, Ar), 8.14 (dd, 2H, *J* =6.4 Hz, *J* =1.6 Hz, Ar), 7.63 (t, 1H, Ar), 7.22 (s, 4H, Ar), 4.02 – 4.09 (m, 12H, 6× $OCH_2$), 1.27 – 1.89 (m, 120H, 60 × $CH_2$), 0.86 – 0.89 (m, 18H, 6 × $CH_3$). $^{13}$C NMR ($CDCl_3$, 100 MHz): 169.10, 166.75, 153.81, 141.35, 131.53, 130.28, 130.11, 127.25, 124.93, 106.78, 77.88, 69.63, 32.14, 30.56, 29.92, 29.86, 29.80, 29.63, 29.58, 26.30, 22.91, 14.38. HRMS (ESI+) exact mass calculated for $C_{94}H_{159}N_4O_6S_2$(M+1): 1504.1696, Found: 1504.1878.

Procedure for the synthesis of 1,3-bis(5-(3,4,5-tris(hexadecyloxy)phenyl)-1,3,4-thiadiazol-2-yl)benzene (**MT3**)

Isophthalic acid (0.8 mmol) in 3.6 ml of thionyl chloride and DMF (catalytic amount) was heated under reflux for 4 h. The excess of thionyl chloride was removed by distillation, the crude product (Isophthaloyl dichloride) was dried in vacuo and used for the next reaction without further purification and characterization. The solution of Isophthaloyl dichloride (0.7 mmol, 1equiv.) in THF was added dropwise to a solution of solution of 3,4,5-tri-*n*-hexadecyloxy benzhydrazide (1.4 mmol, 2.05 equiv.) and triethylamine (2.1 mmol, 3 equiv.) in THF (20 mL). The reaction mixture was stirred at 55 $^{o}$C for 12 h. After cooling, THF was removed through distillation and the residue was extracted with dichloromethane. The extract was washed with water and brine. Dried over $Na_2SO_4$ and concentrated. The resulting crude product (**7c**) was directly used for next reaction. The solution of crude product **7c** (0.5mmol, 1equiv.) in dry toluene (8 mL) was added dropwise to a solution of Lawesson's reagent (1.2 mmoL, 2.4 equiv.) in dry toluene at room temperature under Argon atmosphere and refluxed for 24 h. After the reaction, toluene was evaporated under reduced pressure. After removal of solvent *in vacuo*, the crude product was further purified through column chromatography on neutral alumina. Elution with 10-20% ethylacetate-hexanes yielded the desired product.

$R_f$ = 0.68 (20% EtOAc-hexanes); colorless solid, yield: 44%; IR (KBr pellet): $\nu_{max}$ in $cm^{-1}$ 2921, 2852, 1586, 1510, 1122; $^1$H NMR ($CDCl_3$, 400 MHz): $^1$H NMR ($CDCl_3$, 400 MHz): δ 8.60 (s, 1H, Ar), 8.15(d, 2H, *J* =8Hz, Ar), 7.64 (t, 1H, Ar), 7.23(s, 4H, Ar), 4.02 – 4.09 (m, 12H, 6 × $OCH_2$), 1.25 – 1.85 (m, 168H, 84 × $CH_2$), 0.86 – 0.89 (m, 18H, 6 × $CH_3$). $^{13}$C NMR ($CDCl_3$, 150 MHz): 169.11, 166.76, 153.83, 141.37, 131.55, 130.29, 130.12, 127.27, 124.93, 106.80, 73.89, 69.65, 32.15, 30.56, 29.94, 29.88, 29.81, 29.64, 29.59, 26.32, 22.91, 14.32. HRMS (ESI+) exact mass calculated for $C_{118}H_{207}N_4O_6S_2$(M+1): 1840.5452, Found: 1840.5558.

Procedure for the synthesis of 1,4-bis(5-(3,4,5-tris(decyloxy)phenyl)-1,3,4-thiadiazol-2-yl)benzene (**PT1**)

Terephthalic acid (1.7mmol) in 8 ml of thionyl chloride and DMF (catalytic amount) was heated under reflux for 4 h. The excess of thionyl chloride was removed by distillation, the crude product (terepthaloyldichloride) was dried *in vacuo* and used for the next reaction without further purification and characterization. The terepthaloyldichloride (1.6 mmol, 1equiv.) was added dropwise to a solution of 3,4,5-tri-*n*-decyloxy benzhydrazide (3.3 mmol, 2.05 equiv.), triethylamine (3.2mmol, 2equiv.) in THF. The reaction mixture was stirred at 55 $^{o}$C for 12 h. After cooling, THF was removed through distillation and the residue was extracted with dichloromethane. The extract was washed with water and brine. Dried over $Na_2SO_4$ and concentrated. The resulting crude product (**6a**) was directly used for next reaction. The solution of crude product **6a** (0.6mmol, 1equiv.) in dry toluene (12 mL) was added dropwise to a solution of Lawesson's reagent (1.4 mmol, 2.4 equiv.) in dry toluene at room temperature under Argon atmosphere and refluxed for 24 h. After the reaction, toluene was evaporated under reduced pressure. After removal of solvent *in vacuo*, the crude product was further purified through column chromatography on neutral alumina. Elution with 5-10% ethylacetate-hexanes yielded the desired product.

$R_f$ = 0.38 (20% EtOAc-hexanes); yellowish green solid, yield: 50%; IR (KBr pellet): $\nu_{max}$ in $cm^{-1}$ 2922, 2851, 1583, 1510, 1127; $^1H$ NMR ($CDCl_3$, 400 MHz): δ 8.13 (s, 4H, Ar), 7.23 (s, 4H, Ar), 4.02 - 4.09(m, 12H, 6 × $OCH_2$), 1.28 – 1.87 (m, 96H, 48 × $CH_2$), 0.88 (m, 18H, 6 × $CH_3$). $^{13}C$ NMR ($CDCl_3$, 100 MHz): 168.91, 166.55, 153.70, 141.28, 132.44, 128.49, 124.79, 106.61, 73.75, 69.51, 32.08, 30.53, 29.91, 29.85, 29.82, 29.77, 29.60, 29.57, 29.53, 26.26, 22.84, 14.24. HRMS (ESI+) exact mass calculated for $C_{82}H_{135}N_4O_6S_2$(M+1): 1335.9818, Found: 1335.9850.

Procedure for the synthesis of 1,4-bis(5-(3,4,5-tris(dodecyloxy)phenyl)-1,3,4-thiadiazol-2-yl)benzene (**PT2**):

Terephthalic acid (0.9 mmol) in 4.1 ml of thionyl chloride and DMF (catalytic amount) was heated under reflux for 4 h. The excess of thionyl chloride was removed by distillation, the crude product (terepthaloyldichloride) was dried *in vacuo* and used for the next reaction without further purification and characterization. The terepthaloyldichloride (0.8 mmol, 1equiv.) was added dropwise to a solution of 3,4,5-tri-*n*-dodecyloxy benzhydrazide (1.6 mmol, 2.05 equiv.), triethylamine (1.6mmol, 2equiv.) in THF. The reaction mixture was stirred at 55 $^oC$ for 12 h. After cooling, THF was removed through distillation and the residue was extracted with dichloromethane. The extract was washed with water and brine. Dried over $Na_2SO_4$ and concentrated. The resulting crude product (**6b**) was directly used for next reaction. The solution of crude product **6b** (0.6mmol, 1equiv.) in dry toluene (12 mL) was added dropwise to a solution of Lawesson's reagent (1.4 mmoL, 2.4 equiv.) in dry toluene at room temperature under Argon atmosphere and refluxed for 24 h. After the reaction, toluene was evaporated under reduced pressure. After removal of solvent *in vacuo*, the crude product was further purified through column chromatography on neutral alumina. Elution with 5-10% ethylacetate-hexanes yielded the desired product.

$R_f$ = 0.62 (20% EtOAc-hexanes); yellowish green solid, yield: 55%; IR (KBr pellet): $\nu_{max}$ in $cm^{-1}$ 2923, 2851, 1585, 1511, 1121; $^1H$ NMR ($CDCl_3$, 400 MHz): δ 8.11 (s, 4H, Ar), 7.21 (s, 4H, Ar), 4.02 - 4.08 (m, 12H, 6 × $OCH_2$), 1.27 – 1.88 (m, 120H, 60 × $CH_2$), 0.88 (m, 18H, 6 × $CH_3$). $^{13}C$ NMR ($CDCl_3$, 100 MHz): 168.84, 166.49, 153.59, 141.15, 132.38, 128.43, 124.68, 106.54, 73.65, 69.41, 31.92, 30.34, 29.74, 29.70, 29.66, 29.64, 29.58, 29.41, 29.39, 29.37, 29.34, 26.09, 22.69, 14.10. HRMS (ESI+) exact mass calculated for $C_{94}H_{159}N_4O_6S_2$(M+1): 1504.1696, Found: 1504.1868.

Procedure for the synthesis of 1,4-bis(5-(3,4,5-tris(hexadecyloxy)phenyl)-1,3,4-thiadiazol-2-yl)benzene (**PT3**):

Terephthalic acid (0.8mmol) in 3.6 ml of thionyl chloride and DMF (catalytic amount) was heated under reflux for 4 h. The excess of thionyl chloride was removed by distillation, the crude product (terepthaloyl dichloride) was dried *in vacuo* and used for the next reaction without further purification and characterization. The

terepthaloyldichloride (0.7 mmol, 1equiv.) was added dropwise to a solution of 3,4,5-tri-*n*-hexadecyloxy benzhydrazide (1.4 mmol, 2.05 equiv.), triethylamine (1.4mmol, 2equiv.) in THF. The reaction mixture was stirred at 55 $^{o}$C for 12 h. After cooling, THF was removed through distillation and the residue was extracted with dichloromethane. The extract was washed with water and brine. Dried over $Na_2SO_4$ and concentrated. The resulting crude product (**6c**) was directly used for next reaction. The solution of crude product **6c** (0.2mmol, 1equiv.) in dry toluene (4 mL) was added dropwise to a solution of Lawesson's reagent (0.5 mmoL, 2.4 equiv.) in dry toluene at room temperature under Argon atmosphere and refluxed for 24h. After the reaction, toluene was evaporated under reduced pressure. After removal of solvent *in vacuo*, the crude product was further purified through column chromatography on neutral alumina. Elution with 5-10% ethylacetate-hexanes yielded the desired product.

$R_f$ = 0.69 (20% EtOAc-hexanes); yellowish green solid, yield: 56%; IR (KBr pellet): $\nu_{max}$ in cm$^{-1}$ 2922, 2851, 1587, 1507, 1121; $^1$H NMR ($CDCl_3$, 400 MHz): δ 8.13 (s, 4H, Ar), 7.23 (s, 4H, Ar), 4.02 - 4.09 (m, 12H, 6 × $OCH_2$), 1.26 – 1.87 (m, 168H, 84 × $CH_2$), 0.86 – 0.89 (m, 18H, 6 × $CH_3$). $^{13}$C NMR ($CDCl_3$, 100 MHz): 169.09, 166.73, 153.83, 141.40, 132.64, 128.69, 124.93, 106.81, 73.88, 69.65, 32.15, 30.57, 29.95, 29.88, 29.81, 29.63, 29.60, 26.32, 22.92, 14.33. HRMS (ESI+) exact mass calculated for $C_{118}H_{207}N_4O_6S_2$ (M+1): 1840.5452, Found: 1840.5267.

### 3.5. References


1. (a) S. Chandrasekhar, in *Liquid Crystals*, 2nd ed.; Cambridge University Press: New York, 1994; (b) T. Geelhaar, K. Griesar and B. Reckmann, *Angew. Chem. Int. Ed.*, 2013, **52**, 8798-8809; (c) C. Tschierske, *Angew. Chem. Int. Ed.*, 2013, **52**, 8828-8878; (d) *Handbook of Liquid Crystals: Fundamentals*, ed. J. W. Goodby, P. J. Collings, T. Kato, C. Tschierske, H. Gleeson and P. Raynes, Wiley-VCH, Weinheim, Germany, 2014, Vol. 1.
2. (a) D. Demus, *Liq. Cryst.*, 1989, **5**, 75-110; (b) C. Tschierske, *J. Mater. Chem*., 1998, **8**, 1485-1508; (c) C. Tschierske, *J. Mater. Chem*., 2001, **11**, 2647-2671; (d) C. Tschierske, *Annu. Rep. Prog. Chem. Sect. C*, 2001, **97**, 191-267; (e) C. Tschierske, *Curr. Opin. Colloid Interface Sci*., 2002, **7**, 69-80.
3. (a) F. Renitzer, *Monatsch. Chem.*, 1888, **9**, 421-441; (b) F. Reinitzer, *Liq. Cryst.*, 1989, **5**, 7–18.
4. S. Chandrasekhar, B. K. Sadashiva and K. A. Suresh, *Pramana*, 1977, **9**, 471-480.
5. (a) C. T. Imrie and G. R. Luckhurst, in *Handbook of liquid crystals*, ed. D. Demus, J. W. Goodby, G. W. Gray and H. -W. Spiess and V. Vill, Wiley-VCH, Germany, 1998, vol. 2B, part – III, p.799; (b) C. T. Imrie and P. A. Henderson, *Curr. Opin. Colloid Interface Sci*. 2002, **7**, 298-311; (c) C. T. Imrie in *Structure and Bonding - Liquid crystals, II*, ed. D. M. P. Mingos, Springer-Verlag, 1999, p.149; (d) N. Tamaoki, *Adv. Mater*., 2001, **13**, 1135-1147; (e) C. V.

Yelamaggad, G. Shanker, U. S. Hiremath, and S. K. Prasad, *J. Mater. Chem.*, 2008, **18**, 2927-2949; (f) A. S. Achalkumar, U. S. Hiremath, D. S. Shankar Rao and C. V. Yelamaggad, *Liq. Cryst.*, 2011, **38**, 1563-1589; (g) V. Borshch, Y. K. Kim, J. Xiang, M. Gao, A. Jakli, V. P. Panov, J. K. Vij, C. T. Imrie, M. G. Tamba, G. H. Mehl and O. D. Lavrentovich, *Nature Commun.*, 2013, **4**, 1-8.

6. (a) T. Niori, T. Sekine, J. Watanabe, T. Furukawa and H. Takezoe, *J. Mater. Chem*., 1996, **6**, 1231-1233; (b) R. A. Reddy and C. Tschierske, *J. Mater. Chem*., 2006, **16**, 907-961; (c) H. Takezoe and Y. Takanishi, *Jpn. J. of App. Phys*., 2006, **45**, No. 2A, 597-625.
7. (a) K. Borisch, S. Diele, P. Goring, H. Muller and C. Tschierske, *Liq. Cryst.*, 1997, **22**, 427-443; (b) K. Borisch, S. Diele, P. Goring, H. Kresse and C. Tschierske, *J. Mater. Chem*., 1998, **8**, 529-543; (c) F. Liu, R. Kieffer, X. Zeng, K. Pelz, M. Prehm, G. Ungar and C. Tschierske, *Nature Commun.*, 2012, **3**, 1104-1107; (d) C. Tschierske, *Isr. J. Chem.*, 2012, **52**, 935-959.
8. (a) H. Zeng and T. M. Swager, *J. Am. Chem. Soc*., 1994, **116**, 761-762; (b) T. M. Swager and H. Zeng, *Mol. Cryst. Liq. Cryst.*, 1995, **260**, 301-306.
9. (a) A. Pegenau, P. and Tschierske, *Chem. Commun.*, 1996, 2563-2564; (b) M. Lehmann, R. I. Gearba, M. H. J. Koch, and D. A. Ivanov, *Chem. Mater.*, 2004, **16**, 374-376; (c) M. Lehmann and M. Jahr, *Chem. Mater.*, 2008, **20**, 5453-5456; (d) H. Detert, M. Lehmann and H. Meier, *Materials*, 2010, **3**, 3218–3330; (e) M. Lehmann, *Chem. -Eur. J.*, 2009, **15**, 3638–3651.
10. M. Lee, D. -W. Lee and B. -K. Cho, *J. Am. Chem. Soc*., 1998, **120**, 13258-13259.
11. (a) J. H. Cameron, A. Facher, G. Lattermann and S. Diele, *Adv. Mater*., 1997, **9**, 398-403; (b) A. Pegenau, T. Hegmann, C. Tschierske and S. Diele, *Chem. -Eur. J.* 1999, **5**, 1643-1660; (c) S. I. Stupp, M. Keser and G. N. Tew, *Polymer*, 1998, **39**, 4505-4508; (d) H. Meier, M. Lehmann, and U. Kolb, *Chem. -Eur. J.*, 2000, **6**, 2462-2469; (e) V. Percec, A. E. Dulcey, V. S. K. Balagurusamy, Y. Miura, J. Smidrkal, M. Peterca, S. Nummelin, U. Edlund, S. D. Hudson, P. A. Heiney, H. Duan, S. N. Magonov, and S. A. Vinogradov, *Nature*, 2004, **430**, 764-768; (f) M. Lehmann, C. Köhn, H. Meier, S. Renker and A. Oehlhof, *J. Mater. Chem.*, 2006, **16**, 441-451; (g) B. M. Rosen, C. J. Wilson, D. A. Wilson, M. Peterca, M. R. Imam, and V. Percec, *Chem Rev.*, 2009, **109**, 6275-6540; (h) B. Donnio, *Inorg. Chim. Acta*, 2014, **409**, 53-67.
12. (a) J. Malthete, A. M. Levulut and N. H. Tinh, *J. Phys. Lett.*, 1985, **46**, 875-880; (b) J. Malthete, H. T. Nguyen and C. Destrade, *Liq. Cryst.*, 1993, **13**, 171-187; (c) H.-T. Nguyen, C. Destrade and J. Malthete, *Adv. Mater.*, 1997, **9**, 375–388; (d) K. E. Rowe and D. W. Bruce, *J. Mater. Chem.*, 1998, **8**, 331-341; (e) B. P. Hoag and D. L. Gin, *Adv. Mater.*, 1998, **10**, 1546-1551; (f) T. Yasuda, K. Kishimoto and T. Kato, *Chem. Commun.*, 2006, 3399-3401; (g) J. Seo, S. Kim, S. H. Gihm, C. R. Park and S. Y. Park, *J. Mater. Chem.*, 2007, **17**, 5052-5057; (h) S.-J. Yoon, J. H. Kim, K. S. Kim, J. W. Chung, B. Heinrich, F. Mathevet, P. Kim, B. Donnio, A.-J. Attias, D. Kim and S. Y. Park, *Adv. Funct. Mater.*, 2012, **22**, 61-69; (i) V. N. Kozhevnikov, B. Donnio and D. W. Bruce, *Angew. Chem. Int., Ed.* 2008, **47**, 6286-6289; (j) C. Alstermark, M. Eriksson, M. Nilsson, C.

Destrade and H. T. Nguyen, *Liq Cryst.*, 1990, **8**, 75-80; (k) D. Fazio, C. Mongin, B. Donnio, Y. Galerne D. Guillon and D.W. Bruce. *J. Mater. Chem*., 2001, **11**, 2852-2863; (l) D. M. Huck, H. L. Nguyen, P. N. Horton, M. B. Hursthouse, D. Guillon, B. Donnio and D. W. Bruce, *Polyhedron*, 2006, **25**, 307-324; (m) A. I. Smirnova and D. W. Bruce, *J. Mater. Chem*., 2006, **16**, 4299-4306; (n) E. Gorecka, D. Pociecha, J. Mieczkowski, J. Matraszek, B. Donnio and D. Guillon, *J. Am. Chem. Soc.*, 2004, **126**, 15946-15947; (o) C. Tschierske, *Angew. Chem. Int. Ed.*, 2000, **39**, 2454-2458; (p) E. Gorecka, D. Pociecha, J. Matraszek, J. Mieczkowski, Y. Shimbo, Y. Takanishi and H. Takezoe, *Phys. Rev. E: Stat., Nonlinear, Soft Matter Phys*., 2006, **73**, 31704-31708; (q) J. Barbera, E. Cavero, M. Lehmann, J. L. Serrano, T. Sierra and J. T. Vazquez, *J. Am. Chem. Soc.*, 2003, **125**, 4527-4533; (r) D. Pucci, *Liq Cryst.* 2011, **38**, 1451-1465; (s) K. Han and B.-K. Cho, *Soft Matter*, 2014, **10**, 7588-7594.

13. J. H. Porada and D. Blunk, *J. Mater. Chem.*, 2010, **20**, 2956- 2958.
14. (a) K. Mullen and G. Wegner, *Electronic Materials: The Oligomer Approach*, Wiley-VCH, Weinheim, 1998; (b) R. E. Martin and F. Diederich, *Angew. Chem. Int. Ed.*, 1999, **38**, 1350-1377; (c) F. S. Precup-Blaga, J. C. Garcia-Martinez, A. P. H. J. Schenning and E. W. Meijer, *J. Am. Chem. Soc.*, 2003, **125**, 12953-12960; (d) F. Lincker, P. Bourgun, P. Masson, P. Didier, L. Guidoni, J.-Y. Bigot, J.-F. Nicoud, B. Donnio, and D. Guillon, *Org. Lett.*, 2005, **7**, 1505-1508; (e) M. O'Neill and S.M. Kelly. *Adv Mater.*, 2003, **15**, 1135-1146; (f) A. Contoret, A. Eastwood, S. Farrar, S. M. Kelly, E Nicholls, M. O'Neill, G. Richards and C. Wu, *Mol. Cryst. Liq. Cryst.*, 2001, **368**, 271-278; (g) N. H. Sultana, S.M. Kelly, B. Mansoor and M. O'Neill, *Liq Cryst*., 2007, **34**, 1307-1316; (h) C. Gadermaier, G. Lanzani, G. Cerullo, M. Zavelani-Rossi, U. Theissel, B. Hoag, G. Leising, S. De Selvestri and D. L. Gin. *Synth Met.*, 2001, **121**, 1323-1324; (i) A. P. Sivadas, N. S. S. Kumar, D. D. Prabhu, S. Varghese, S. K. Prasad, D. S. S. Rao, and S. Das, *J. Am. Chem. Soc.*, 2014, **136**, 5416-5423.
15. C. V. Yelamaggad, G. Shanker, R. V. R. Rao, D. S. S. Rao, S. K. Prasad, and V. V. S. Babu, *Chem. -Eur. J.*, 2008, **14**, 10462-10471.
16. N. G. Nagaveni, M. Gupta, A. Roy, and V. Prasad, *J. Mater. Chem.*, 2010, **20**, 9089-9099.
17. V. S. K. Balagurusamy, S. K. Prasad, S. Chandrasekhar, S. Kumar, M. Manickam and C. V. Yelamaggad, *Pramana,* 1999, **53**, 3-11.
18. (a) B. A. Gregg, M. A. Fox, and A. J. Bard, *J. Phys. Chem*., 1990, **94**, 1586-1598; (b) K. Petritsch, R. H. Friend, A. Lux, G. Rozenberg, S. C. Moratti, and A. B. Holmes. *Synth. Met*., 1999, **102**, 1776- 1777; (c) L. S. Mende, A. Fechtenkotter, K. Mullen, E. Moons, R. H. Friend and J. D. MacKenzie, *Science*, 2001, **293**, 1119 – 1122; (d) N. Tchebotareva, X. Yin, M. D. Watson, P. Samori, J. P. Rabe, and K. Mullen. *J. Am. Chem. Soc*., 2003, **125**, 9734-9739; (e) P. Samori, X. Yin, N. Tchebotareva, Z. Wang, T. Pakula, F. Jäckel, M. D. Watson, A. Venturini, K. Müllen, and J. P. Rabe. *J. Am. Chem. Soc*., 2004, **126**, 3567-3575; (f) Q. Sun, L. Dai, X. Zhou, L. Li and Q. Li, *Applied Physics Letters*, 2007, **91**, 253505; (g) H. C. Hesse, J. Weickert, M. Al-Hussein, L. Dössel, X. Feng, K. Mullen and L. S. Mende, *Solar Energy Materials & Solar Cells*, 2010,

**94**, 560-567; (h) X.-Y. Liu, T. Usui, H. Iino and J. –I. Hanna, *J. Mater. C.*, 2013, **1**, 8186-8193.

19. (a) A. Bacher, I. Bleyl, C. H. Erdelen, D. Haarer, W. Paulus and H. W. Schmidt, *Adv. Mater.*, 1997, **9**, 1031-1035; (b) T. Christ, B. Glusen, A. Greiner, A. Kellner, R. Sander, V. Stumpflen, V. Tsukruk, and J. H. Wendorff, *Adv. Mater.*, 1997, **9**, 48-51; (c) I. H. Stapff, V. Stu¨mpflen, J. H. Wendorff, D. B. Spohn and D. Mo¨bius. *Liq. Cryst.*, 1997, **23**, 613-617; (d) A. Bacher, C. H. Erdelen, W. Paulus, H. Ringsdorf, H. W. Schmidt and P. Schuhmacher, *Macromolecules,* 1999, **32**, 4551-4557; (e) I. Seguy, P. Destruel, and H. Bock, *Synth. Met.*, 2000, **111**, 15-18; (f) T. Hassheider, S. A. Benning, H. S. Kitzerow, M. F. Achard and H. Bock, *Angew. Chem. Int. Ed.*, 2001, **40**, 2060-2063; (g) S. Alibert-Fouet, S. Dardel, H. Bock, M. Oukachmih, S. Archambeau, I. Seguy, P. Jolinat, and P. Destruel, *ChemPhysChem*, 2003, **4**, 983-985; (h) C. R. McNeill and N. C. Greenham, *Adv. Mater.*, 2009, **21**, 1-11; (i) M. O'Neill and S. M. Kelly, *Adv. Mater.*, 2011, **23**, 566-584; (j) J. Eccher, G. C. Faria, H. Bock, H. von Seggern and I. H. Bechtold, *ACS Appl Mater Interfaces,* 2013, **5***,* 11935-11943.
20. (a) P. R. L. Malenfant, C. D. Dimitrakopoulos, J. D. Gelorme, L. L. Kosbar, T. O. Graham, A. Curioni and W. Andreoni, *Appl. Phys. Lett.*, 2002, **80**, 2517; (b) A. M. van de Craats, N. Stutzmann, O. Bunk, M. M. Nielsen, M. Watson, K. Mullen, H. D. Chanzy, H. Sirringhaus and R. H. Friend, *Adv. Mater.*, 2003, **15**, 495-499; (c) S. Cherian, C. Donley, D. Mathine, L. LaRussa, W. Xia and N. Armstrong, *J. Appl. Phys.*, 2004, **96**, 5638- 5643; (d) R. J. Chesterfield, J. C. McKeen, C. R. Newman, P. C. Ewbank, D. A. da Silva Filho, J. L. Bredas, L. L. Miller, K. R. Mann, and C. D. Frisbie. *J. Phys. Chem. B.*, 2004, **108**, 19281-19292; (e) I. O. Shklyarevskiy, P. Jonkheijm, N. Stutzmann, D. Wasserberg, H. J. Wondergem, P. C. M. Christianen, A. P. H. J. Schenning, D. M. de Leeuw, Z. Tomovic, J. Wu, K. Mullen and J. C. Maan, *J. Am. Chem. Soc.*, 2005, **127**, 16233-16237; (f) W. Pisula, A. Menon, M. Stepputat, I. Lieberwirth, U. Kolb, A. Tracz, H. Sirringhaus, T. Pakula and K. Mullen, *Adv. Mater.*, 2005, **17**, 684-689. (g) S. Xiao, M. Myers, Q. Miao, S. Sanaur, K. Pang, M. L. Steigerwald and C. Nuckolls, *Angew. Chem. Int. Ed.*, 2005, **44**, 7390-7394; (h) H. Sirringhaus, *Adv. Mater.*, 2005, **17**, 2411-2425; (i) J. Y. Cho, B. Domercq, S. C. Jones, J. Yu, X. Zhang, Z. An, M. Bishop, S. Barlow, S. R. and J. Kippelen, *J. Mater. Chem.*, 2007, **17**, 2642-2647. (j) Y. Shimizu, K. Oikawa, K. Nakayama, and D. Guillon, *J. Mater. Chem.*, 2007, **17**, 4223-4229; (k) H. N. Tsao, H. J. Rader, W. Pisula, A. Rouhanipour and K. Mullen, *Phys. Status Solidi A.*, 2008, **205**, 421-429; (l) H. N. Tsao, W. Pisula, Z. Liu, W. Osikowicz, W. R. Salaneck, and K. Mu¨llen. *Adv. Mater.*, 2008, **20**, 2715-2719; (m) R. Schmidt, J. H. Oh, Y. S. Sun, M. Deppisch, A. M. Krause, K. Radacki, H. Braunschweig, M. Konemann, P. Erk, Z. Bao and F. Wurthner, *J. Am. Chem. Soc.*, 2009, **131**, 6215-6228; (n) J. P. Bramble, D. J. Tate, D. J. Revill, K. H. Sheikh, J. R. Henderson, F. Liu, X. Zeng, G. Ungar, R. J. Bushby and S. D. Evans, *Adv. Funct. Mater.,* 2010, **20**, 914-920; (o) J. Cattle, P. Bao, J. P. Bramble, R. J. Bushby, S. D. Evans, J. E. Lydon and D. J. Tate, *Adv. Funct. Mater.*, 2013, **23**, 5997-6006.
21. (a) J. D. Wright, P. Roisin, G. P. Rigby, R. J. M. Nolte, M. J. Cook and S. C.

Thorpe, *Sens. Actuators B.*, 1993, **13**, 276-280; (b) J. Clements, N. Boden, T. D. Gibson, R. C. Chandler, J. N. Hulbert and E. A. Ruck-Keene, *Sens. Actuators B.*, 1998, **47**, 37-42; (c) N. Boden, R. J. Bushby, J. Clements and B. Movaghar, *J. Mater. Chem.*, 1999, **9**, 2081-2086; (d) V. Bhalla, A. Gupta, M. Kumar, D. S. S. and K. Prasad, *ACS Appl Mater Interfaces,* 2013, **5**, 672-679.

22. (a) D. D. L. Chung, *J. Mater. Sci.*, 2002, **37**, 1475-1489; (b) A. Venkateswara Rao, *Mater. Manuf. Processes*, 2004, **19**, 177 – 186; (c) K. Kawata and O. Nobuyosi, *Fujifilm Res. Dev*., 2006, **51**, 80-85.
23. (a) A. Seed, *Chem. Soc. Rev.*, 2007, **36**, 2046- 2069; (b) B. Roy, N. De and K. C. Majumdar, *Chem. -Eur. J.*, 2012, **18**, 14560-14588; (c) J. Han, *J. Mater. Chem. C.*, 2013, **1**, 7779-7797.
24. A. C. Grimsdale, K. Leok Chan, R. E. Martin, P. G. Jokisz and A. B. Holmes, *Chem. Rev*., 2009, **109**, 897-1091.
25. (a) C. S. Wang, G. Y. Jung, Y. L. Hua, C. Pearson, M. R. Bryce, M. C. Petty, A. S. Batsanov, A. E. Goeta and J. A. K. Howard, *Chem. Mater.*, 2001, **13**, 1167-1173; (b) A. P. Kulkarni, C. J. Tonzola, A. Babel and S.A. Jenekhe, *Chem. Mater.*, 2004, **16**, 4556-4573;
26. J. Han, X. Y. Chang, L. R. Zhu, M.-L. Pang, J. B. Meng, S. S.-Y. Chui, S. W. Lai and V. A. L. Roy, *Chem. -Asian J.*, 2009, **4**, 1099-1107.
27. Y. Hu, C.-Y. Li, X.-M. Wang, Y.-H. Yang and H.-L. Zhu, *Chem Rev.*, 2014, **114**, 5572-5610.
28. (a) M. Parra, S. Hernandez, J. Alderete and C. Zuniga, *Liq. Cryst*., 2000, **27**, 8, 995-1000; (b) A. A. Kiryanov, P. Sampson and A. J. Seed, *J. Org. Chem*., 2001, **66**, 7925-7929; (c) M. W. Schroder, S. Diele, G. Pelzl, N. Pancenko and W. Weissflog, *Liq. Cryst.*, 2002, **29**, 1039-1046; (d) M. Parra, J. Alderete and C. Zuniga, *Liq. Cryst.*, 2004, **31**, 1531-1537; (e) T. Hegmann, B. Neumann, R. Wolf and C. Tschierske, *J. Mater. Chem.*, 2005, **15**, 1025-1034; (f) M. Parra, J. Vergara, P. Hidalgo, J. Barbera and T. Sierra, *Liq. Cryst.*, 2006, **33**, 739-745; (g) B. Sybo, P. Bradley, A. Grubb, S. Miller, K. J. W. Proctor, L. Clowes, M. R. Lawrie, P. Sampson and A. J. Seed, *J. Mater. Chem*., 2007, **17**, 3406-3411; (h) C. F. He, G. J. Richards, S. M. Kelly, A. E. A. Contoret and M. O. Neill, *Liq. Cryst*., 2007, **34**, 1249-1267; (i) J. Han, X. Y. Chang, L. R. Zhu, Y. M. Wang, J. B. Meng, S.W. Lai and S. S.-Y. Chui, *Liq. Cryst*., 2008, **35**, 1379-1394; (j) J. H. Tomma, I. H. Rou'il and A. H. Al-Dujaili, *Mol. Cryst. Liq. Cryst*., 2009, **501**, 3-19; (k) M. C. McCairn, T. Kreouzis and M. L. Turner, *J. Mater. Chem.*, 2010, **20**, 1999-2006; (l) A. K. Prajapati and V. Modi, *Liq. Cryst*., 2011, **38**, 191-199; (m) Q. Song, D. Nonnenmacher, F. Giesselmann and R. P. Lemieux, *J. Mater. Chem.*, *C*, 2013, **1**, 343-350; (n) P. Tuzimoto, D. M. P. O. Santos, T. D. S. Moreira, R. Cristiano, I. H. Bechtold and H. Gallardo, *Liq. Cryst.*, 2014, **41**, 1097-1108; (o) R. C. Tandel and N. K. Patel, *Liq. Cryst.*, 2014, **41**, 495-502.
29. (a) M. Lehmann, J. Seltmann, A. A. Auer, E. Prochnow and U. Benedikt, *J. Mater. Chem.*, 2009, 19, 1978-1988; (b) M. Lehmann and J. Seltmann, *Beilstein J. Org. Chem*., 2009, **5**, 73.
30. M. L. Parra, E. Y. Elgueta, J. A. Ulloa, J. M. Vergara and A. I. Sanchez, *Liq.*

*Cryst.*, 2012, **39**, 917-925.

31. (a) M. Sato, *Macromol. Rapid Commun*., 1999, **20**, 77-80; (b) M. Sato and Y. Uemoto, *Macromol. Rapid Commun.*, 2000, **21**, 1220-1225; (c) M. Sato, M. Notsu, S. Nakashima and Y. Uemoto, *Macromol. Rapid Commun.*, 2001, **22**, 681-686; (d) M. Sato, M. Mizoi and Y. Uemoto, *Macromol*. *Chem. Phys*., 2001, **202**, 3634-3641; (e) M. Sato, S. Nakashima and Y. Uemoto, *J. Polym. Sci., part A: Polym. Chem.*, 2003, **41**, 2676-2687; (f) N. S. Al-Muaikel, *Polym. Int.*, 2004, **53**, 301-306; (g) M. Sato, Y. Tada, S. Nakashima, K.-I. Ishikura, M. Handa and K. Kasuga, *J. Polym. Sci. A Polym. Chem.*, 2005, **43**, 1511-1525; (h) M. Sato, Y. Matsuoka and I. Yamaguchi, *Liq. Cryst.*, 2012, **39**, 1071-1081.
32. (a) M. Parra, S. Villouta, V. Vera, J. Belmar, C. Zuniga and H. Zunza, *Z. Naturforsch., B: J. Chem. Sci.*, 1997, **52**, 1533-1538; (b) M. Sato, R. Ishii, S. Nakashima, K. Yonetake and J. Kido, *Liq. Cryst.*, 2001, **28**, 1211-1214; (c) C. F. He, G. J. Richards, S. M. Kelly, A. E. A. Contoret and M. O'Neill, *Liq. Cryst.*, 2007, **34**, 1249-1267; (d) J. H. Tomma, I. H. Rou'il and A. H. Al-Dujaili, *Mol. Cryst. Liq. Cryst.*, 2009, **501**, 3-19.
33. (a) M. K. S. Al-Malki, A. S. Hameed and A. H. Al-Dujaili, *Mol. Cryst. Liq. Cryst.*, 2014, **593**, 34-42; (b) M. L. Parra, E. Y. Elgueta, J. A. Ulloa, J. M. Vergara, A. I. Sanchez, *Liq. Cryst.*, 2012, **39**, 917–925
34. (a) J. Tang, R. Huang, H. Gao, X. Cheng, M. Prehm, and C. Tschierske, *RSC Adv.*, 2012, **2**, 2842-2847; (b) X. Yang, H. Dai, Q. He, J. Tang, X. Cheng, M. Prehm, and C. Tschierske, *Liq. Cryst.*, 2013, **40**(8) 1028-1034.
35. (a) A. S. Achalkumar, U. S. Hiremath, D. S. Shankar Rao, S. Krishna Prasad and C. V. Yelamaggad, *J. Org. Chem.*, 2013, **78**, 527-544; (b) I. Thomsen, K. Clausen, S. Scheibye and S.-O. Lawesson, *Org. Synth.,* 1990, **7**, 372-373.
36. S. Laschat, A. Baro, N. Steinke, F. Giesselmann, C. Hägele, G. Scalia, R. Judele, E. Kapatsina, S. Sauer, A. Schreivogel, and M. Tosoni, *Angew. Chem. Int. Ed.*, 2007, **46**, 4832–4887.
37. C. V. Yelamaggad, A. S. Achalkumar, D. S. Shankar Rao, and S. Krishna Prasad, *J. Org. Chem.*, 2007, **72**, 8308-8318.
38. (a) H. Zheng, C. K. Lai and T. M. Swager, *Chem. Mater.*, 1995, **7**, 2067 –2077; (b) C. Destrade, P. Foucher, H. Gesparoux, H. T. Nguyen, A. M. and Malthete, *Mol. Cryst. Liq. Cryst.*, 1984, **106**, 121 – 146. (c) F. Morale, R. W. Date, D. Guillon, D. W. Bruce, R. L. Finn, C. Wilson, A. J. Blake, M. Schröder and B. Donnio, *Chem. -Eur. J.*, 2003, **9**, 2484 – 2501; (d) C. K. Lai, C. -H. Tsai and Y.-S. Pang, *J. Mater. Chem.*, 1998, **8**, 1355– 1360. (e) S. Chandrasekhar, *Adv. Liq. Cryst.*, 1982, **5**, 47 – 48.
39. A. Patra and M. Bendikov, *J. Mater. Chem*., 2010, **20**, 422–433,
40. (a) D. D. Prabhu, N. S. S. Kumar, A. P. Sivadas, S. Varghese, and S. Das, *J. Phys. Chem. B*, 2012, **116**, 13071–13080. (b) M. Kasha, H. R. Rawls and M. A. El- Bayoumi, *Pure Appl. Chem.*, 1965, **11**, 371. (c) F. C. Spano, *Acc. Chem. Res.*, 2010, **43**, 429–439.
41. V. Percec, M. Glodde, T. K. Bera, Y. Miura, I. Shiyanovskaya, K. D. Singer, V. S. K. Balagurusamy, P. A. Heiney, I. Schnell, A. Rapp, H.-W. Spiess, S. D. Hudsonk, H. Duank, *Nature*, 2002, **419**, 384-387.

# Chapter IV

# 1,2,4-Oxadiazole based star-shaped mesogens

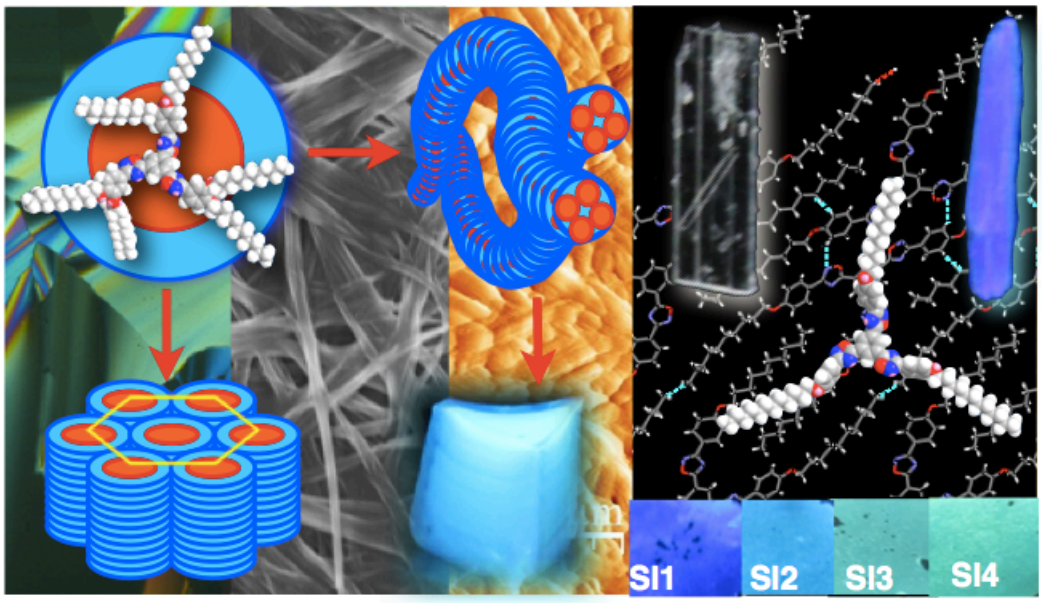


Results have been published in *J. Mater. Chem. C*, 2016, **4**, 6546-6561.

## 4.1. Introduction

The self-assembly of organic molecules into well-defined hierarchical superstructures that perform various functions require a 'bottom-up' approach from the molecular level. Incorporation of functional units in the molecular structure alone will not guarantee the anticipated outcome. In order to have a preferred outcome, the behavior of the molecular aggregates in bulk or in a medium matters. Liquid crystals (LC) are one such example of engineered molecular materials, which are the result of the spontaneous self-assembly of shape anisotropic molecules. This state of matter possesses an intermediate order and mobility between solids and liquids.[1] The driving force for such assembly is mainly nanophase segregation between the incompatible molecular subunits in addition to other secondary interactions like H-bonding, π-π interactions, ionic, hydrophilic or hydrophobic interactions. With a careful molecular design one can predict the outcome of the self-assembly of such shape anisotropic molecules. Gelators are another class of molecules with specific structural features, which immobilize large amount of solvents when they self-assemble.[2] They may gelate organic or aqueous solvents. The self-assembly of such molecules to form gels is assisted by weak forces like H-bonding, π-π interactions, hydrophobic-hydrophilic or van der Waals interactions. This class of materials shows promise for application in optoelectronics,[3] templates for the growth of inorganic nanostructures,[4] fluorescent sensors[5] and controlled release systems. Usually the ability of organogelators to gelate a large volume of solvent comes from the presence of certain functional groups like amide, alcohol, carboxylic acid, aromatic units, steroid moieties, aliphatic chains etc.[2] Gelation brings about drastic changes in the electronic and optical properties. For example, fluorescent molecules that are emissive as monomers may not be emissive in the aggregated state due to the aggregation induced quenching of fluorescence. Organogels which show aggregation induced emission (AIE) due to their supramolecular self-assembly in the gel state form an important class of materials from the view point of solid state lighting.[6] Though there are several reports on AIE active molecules which emit across the whole visible region,[7] there is a dearth of solid state blue emitters. Blue light emitters form an integral part of full color display devices and also

form a vital cog in white light emitting devices.[8] Hence a lot of efforts have been devoted to the building of solid-state blue light emitters by the introduction of functional moieties which will help to generate AIE.[9] Among gelators, there is a class of supergelators which at very low concentration (less than 1 wt %) yield self-standing, self-healing and moldable gels.[10] A common structural feature of these molecules is their ability to form strong H-bonding.[11] There has been a single report so far on a polycatenar type supergelator without such H-bonding but mainly stabilized by π-π interaction.[12] The presence of two heterocyclic (1,3,4-oxadiazole) units might have increased the intermolecular π-π interactions to stabilize the aggregation. This observation encouraged us to incorporate heterocyclic moieties in our molecular design that might enhance the π-π interactions to stabilize gelation.[12] Synthesis of such supergelators is challenging, as there is no proven design principle.

Integration of heterocyclic moieties in the molecular architecture of thermotropic liquid crystals is a rewarding task as it can bring about a large change in their thermal and physical properties. This stems from the polarizability of heteroatoms like nitrogen, oxygen and sulfur atoms. There is increasing interest in the design of highly π-conjugated liquid crystals bearing heterocycles[13] due to the enormous possibilities they offer. Liquid crystalline self-assemblies derived from electron deficient heteroaromatic rings are potential candidates for organic light-emitting diodes (OLEDs),[14] by offering good charge-transport properties and strong fluorescence. In particular 1,3,4-oxadiazole moieties are well-known for their excellent electron-accepting behavior and fluorescence and hence have been incorporated in the core structure of calamitic and discotic LCs, to obtain the conductive smectic or columnar mesophases respectively.[13] In spite of the good emissive nature and high thermal endurance of the 1,2,4-oxadiazole unit, the reports on its incorporation in LC design are scarce, unlike its 1,3,4-isomer. This is probably due to the synthetic difficulty in comparison to 1,3,4-oxadiazole derivatives. The asymmetric ring of 1,2,4-oxadiazole moieties provides a strong lateral dipole, which leads to the stabilization of different LC phases than those obtained from corresponding 1,3,4-isomers.[15,17-24] Asymmetrical substitution of 1,2,4-oxadiazole could be another tuning handle to modify

their material properties. In comparison to 1,2,5- and 1,3,4-oxadiazole derivatives, asymmetrically substituted 1,2,4-oxadiazole derivatives are known for their high band gap and known to possess high $S_1$ and $T_1$ energies, which are beneficial for the design of high triplet energy host materials for efficient phosphorescent OLEDs (PHOLEDs).[16] PHOLEDs are known for their higher efficiency in comparison to OLEDs as they harvest both the singlet and triplet excitons. According to the literature 1,2,4-oxadiazole derivatives have moderate thermal stability (decompose around 300 $^{o}$C) compared to their 1,3,4-oxadiazole isomers, [17] but they exhibit lower melting points and a wider mesophase range.[18] There are many reports on banana shaped liquid crystals,[19] bent shaped liquid crystals, [17,20,21,22] supramolecular liquid crystals,[23] and chiral calamitic liquid crystals [24] based on 1,2,4-oxadiazole derivatives. In the case of bent compounds the bending angle provided by the 1,2,4-oxadiazole core is 140$^{o}$ which is slightly more than that of the 1,3,4-oxadiazole core (134$^{o}$) and hence they are anticipated to show some interesting properties like biaxial nematic behavior.[19a] Apart from the bent polycatenars reported by Gallardo *et. al.*,[20a] there are no reports on molecules based on 1,2,4-oxadiazoles exhibiting columnar phases. Though columnar (Col) phases formed by the one-dimensional stacking of disc-like molecules were discovered in 1977,[25] consequently many different non-conventional molecular designs like polycatenars, dendrimers, metallomesogens, bent shaped molecules, oligomers, polymers, macrocycles and star shaped molecules were identified to stabilize Col phases.[1] Columnar phases are of technological importance in recent times because of their potential application in organic electronic devices like solar cells, field effect transistors and OLEDs as they provide one-dimensional pathway for the movement of charge carriers along the columns. [26]

Star shaped mesogens or 'hekates' are formed by the covalent linking of three arms symmetrically to a central core.[27] Shape-persistent star shaped mesogens are obtained by connecting the three rigid arms to the central core through linkers. The lack of shape anisotropy to exhibit mesophases is compensated by the nanophase segregation of chemically or physically different molecular subunits and their tendency of efficient space filling. Compared to the synthetic difficulty associated with discotics this molecular

design is advantageous due to the inherent synthetic flexibility. Thus the Col phases can be incorporated with other functional properties like hole or electron transport, nonlinear optical activity or fluorescence. Apart from this aspect, star shaped molecules are capable of exhibiting a rich variety of mesophases like nematic, columnar, cubic or soft crystal phases, because of their peculiar structure and tunable molecular design. The presence of the voids between the arms of the molecular structure helps to avoid the crystallization of mesophases and promote the glassy state. Columnar phases with glassy nature are important as they allow the movement of charge carriers through them with the simultaneous restriction of ionic impurities.[28] In the context of the application of Col phases to OLEDs, it is important to prepare molecules, which stabilize Col phase along with the preserved solid-state luminescence. This is because the aggregation-induced quenching of luminescence in the Col phase is detrimental to the device performance.

In this chapter we report the first examples of star shaped molecules containing three 1,2,4-oxadiazole heterocyclic moieties attached to the 1, 3 and 5 positions of the central benzene ring. These molecules exhibit $Col_h$ phase over a wide range. Most importantly one of these molecules shows supergelation in hydrocarbon solvents. Gels and xerogels show aggregation-induced emission behavior with blue emission, while the dilute solutions containing solvated monomers are weakly emissive.

## 4.2. Results and discussion

### 4.2.1. Synthesis and Characterization

The synthetic method for the preparation of the target molecules is presented in scheme 4.1. The synthetic methods for ethyl gallate, 3,4,5-trialkoxyethyl gallate are the same as reported earlier.[29a-c] 3,4,5-trialkoxy ethyl gallates (**1c**), **(4b)** and 3,4-dialkoxy benzaldehyde **(9b)** were obtained by the *O*-alkylation of ethyl gallate and 3,4-dihydroxy benzaldehyde, respectively, following Williamson's protocol. Compounds **1c** and **4b** were reduced to their respective 3,4,5-trialkoxy benzyl alcohols **(8c-d)** by lithium aluminium hydride (LAH) in dry THF. Further oxidation of 3,4,5-trialkoxy benzyl alcohols **(8c-d)** using pyridinium chlorochromate (PCC) gave 3,4,5-trialkoxy

benzaldehydes **(9c-d)**.[29b] These benzaldehyde derivatives **(9b-d**) were converted to their respective nitriles **(10b-d)** upon heating with hydroxylamine hydrochloride in DMSO at 100 $^{o}$C for 3h.[30] *p*-Hydroxy benzonitrile was converted to *p*-alkoxy benzonitrile **(10a)** by Williamson's protocol. Further reflux of nitrile **(10a-d)** with hydroxylamine hydrochloride in ethanol led to benzamidoxime intermediates **(11a-d)**, which upon further refluxing with trimesylchloride in pyridine afforded 1,3,5-benzene substituted 1,2,4-oxadiazole derivatives **SI1-4**.[31] The structures of all the intermediates and target molecules were confirmed using $^{1}$H NMR, $^{13}$C NMR, IR spectroscopy and ESI-HRMS or MALDI-TOF analysis.

The $^{1}$H NMR spectra of oxadiazole derivatives **SI1-4** exhibited low field signals ($\delta$ = 9.27 ppm for **SI3**) for the protons on central benzene ring in comparison with that of the chapter 2 star shaped molecules with 1,3,4-oxadiazole arms ($\delta$ = 9.06 ppm), which is due to the more electron withdrawing nature of 1,2,4-oxadiazole units. Similarly, the $^{13}$C NMR of 1,2,4-oxadiazole derivatives **SI1-4** exhibited low field signals at 173 ppm and 169 ppm for the heterocyclic carbons in comparison to the heterocyclic carbons of the 1,3,4-oxadiazole derivatives (signals at 169 ppm and 165 ppm) (See the experimental section for the details). As a comparison between 1,3,4- and 1,2,4-oxadiazole based star shaped LCs, $^{1}$H NMR and $^{13}$C NMR spectra of the representative compounds **SO3** and **SI3** are presented in Fig. 4.1.

### 4.2.2. Thermal behavior

The target molecules were probed for their thermal behavior with the help of thermogravimetric analysis (TGA), Polarizing Optical Microscopy (POM) and Differential Scanning Calorimetry (DSC). The TGA studies of compounds **SI1-4** showed good thermal stability at least upto $\approx$ 300 $^{o}$C and complete degradation occurred at around 600 $^{o}$C, as evidenced by TGA (See the Fig. 4.2). The thermotropic LC behavior of the compounds is summarized in Table 4.1. A comparison between the thermal behaviors of the earlier reported regioisomers of the present series is furnished in Fig. 4.3.

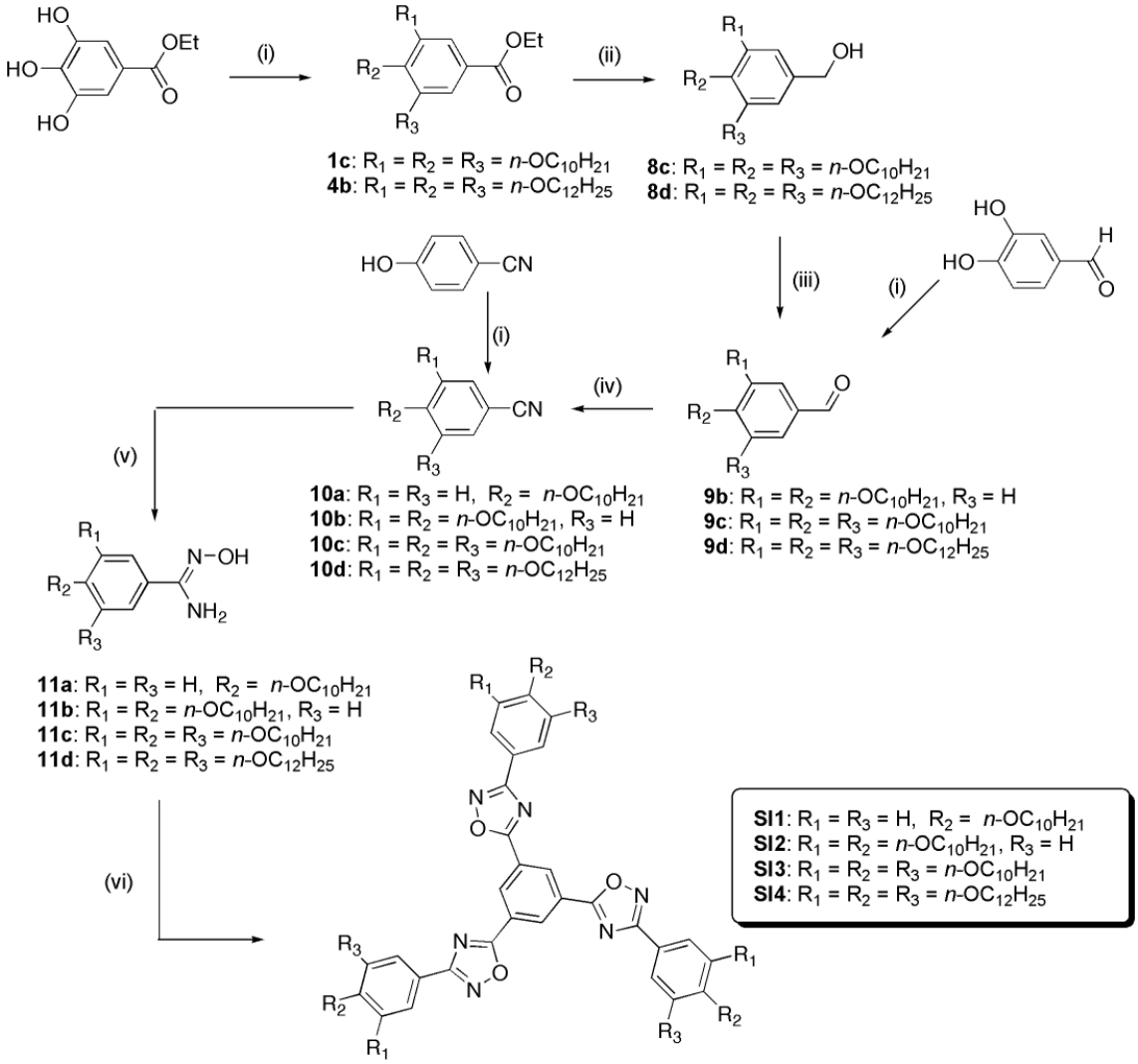


**Scheme 4.1.** Synthesis of star shaped 1,2,4-oxadiazole derivatives. Reagents and conditions: (i) 1-Bromoalkanes, anhyd. $K_2CO_3$, DMF, 80 $^oC$, 12 h (70-90%); (ii) LAH, THF, 0 $^oC$ to rt, 12 h (75-80%); (iii) PCC, DCM, rt, 1 h (70-81%); (iv) $NH_2OH{\cdot}HCl$, DMSO, reflux, 3 h (70-80%); (v) $NH_2OH{\cdot}HCl$, triethylamine, $C_2H_5OH$, reflux, 24 h (70-85%); (vi) trimesic acid chloride, pyridine, 6 h, reflux (55-60%).

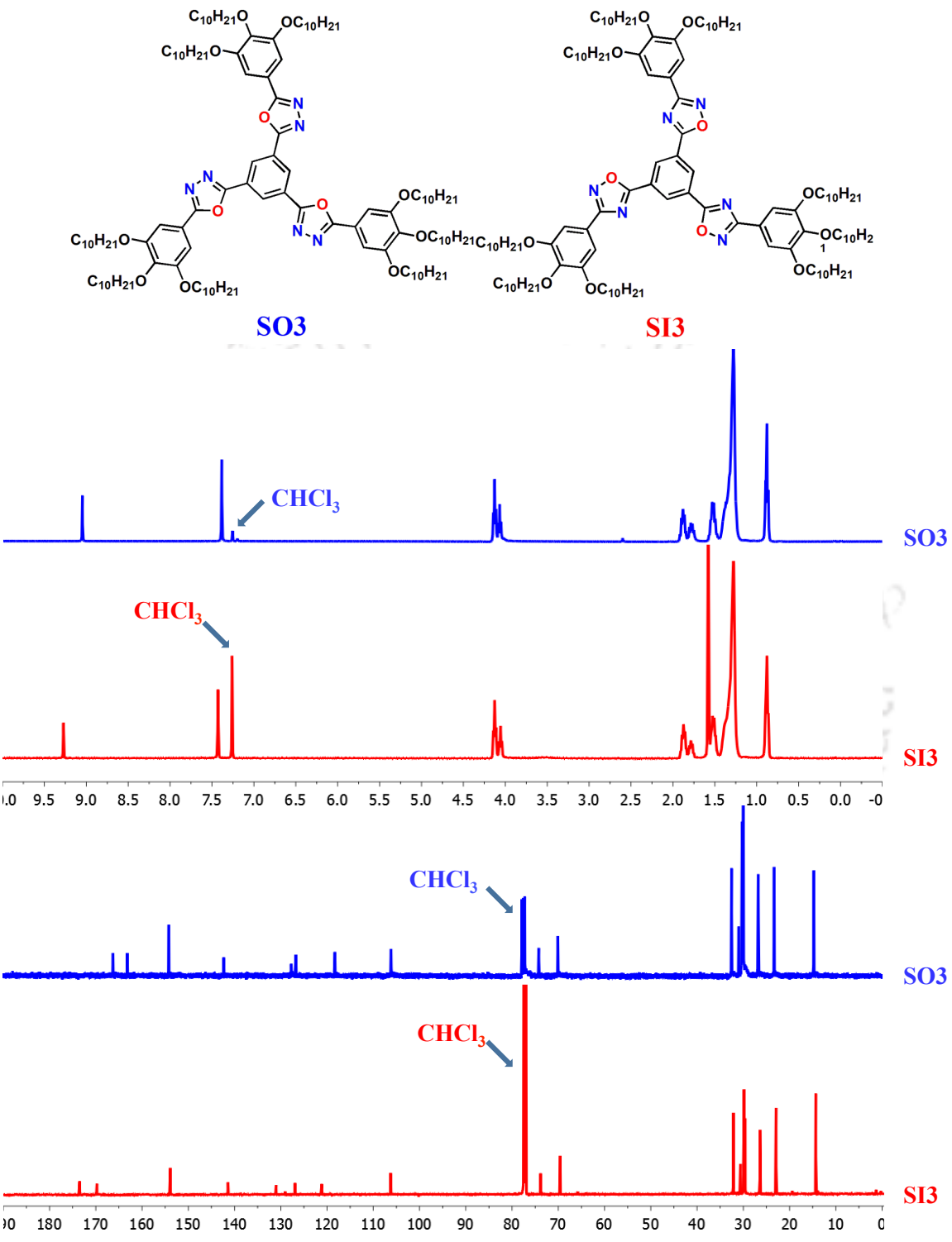


**Figure 4.1.** $^{1}H$ NMR (400MHz) and $^{13}C$ NMR (100MHz) spectra of compound **SO3** and $^{1}H$ NMR (400MHz) and $^{13}C$ NMR (150MHz) spectra of compound **SI3** in $CDCl_3$.

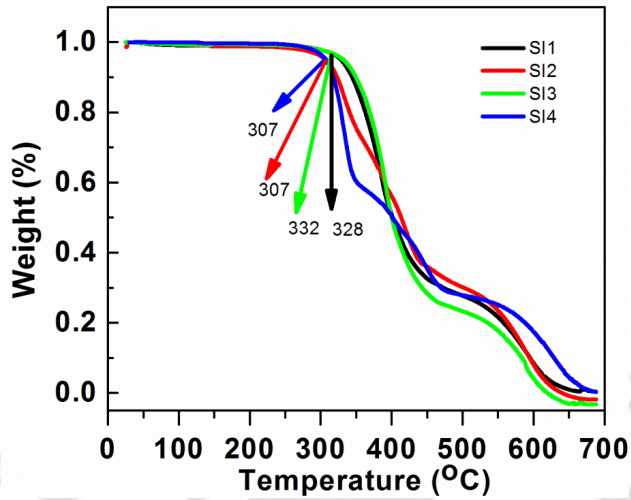


**Figure 4.2.** TGA curves of the compounds **SI1-4** carried out at a rate of 10 °C/min

**Table 4.1.** Phase transition temperatures [a] (°C) and corresponding enthalpies (kJ mol$^{-1}$) of DLCs

| | Phase sequence | |
|---|---|---|
| | 2nd Heating | 1st Cooling |
| **SI1** | Cr 128.8 (375.6) I | I 82.9 (332.3) Cr |
| **SI2** | Cr 106.7 (340.2) $Col_h$ 112.4 (13.8) I | I 111.4 (15.1) $Col_h$ 75.8 (349) Cr |
| **SI3** | Cr 12.9 (100.2) $Col_h$ 160.0 (26.5) I | I 158.9 (26.3) $Col_h$ 3.8 (42.8) Cr |
| **SI4** | $Cr_1$ 22.0 (137.4) $Cr_2$ 42.0 (607.6) $Cr_3$ 60.0 (751.2) $Col_h$ 150.6 (40.0) I | I 149.3 (40) $Col_h$ 12.1 (65.1) Cr |

[a] Peak temperatures in the DSC thermograms obtained during the second heating and first cooling cycles at 5 °C min$^{-1}$. Cr = crystal phase; $Col_h$ = columnar hexagonal phase; I = isotropic phase.

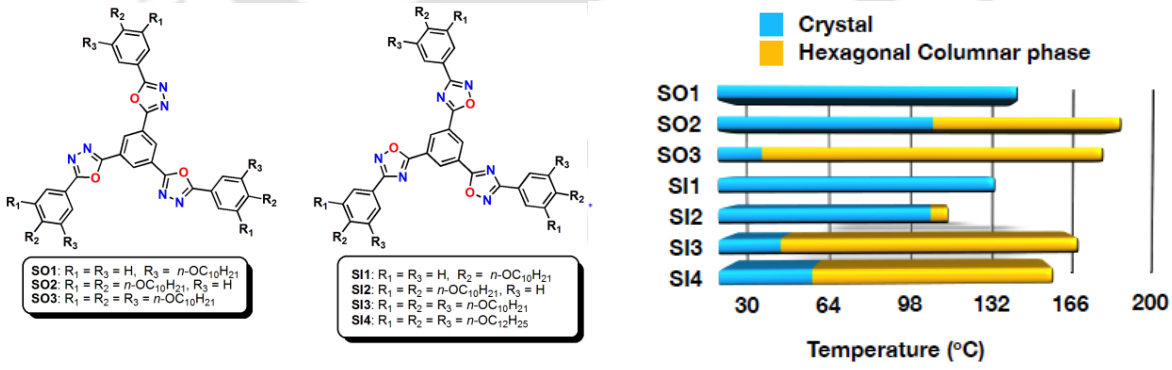


**Figure 4.3.** Bar graph summarizing the thermal behavior of compounds **SO1-3** and **SI1-4** (first heating cycle, the temperature range of the $Col_h$ phase is mentioned on the bars).

Compound **SI1** with three *n*-decyloxy tails turned out to be a crystalline compound, as in the case of corresponding 1,3,4-oxadiazole derivative **SO1** as in chapter 2. The flexibility provided by three alkoxy tails is not sufficient to stabilize liquid crystalllinity. Compound **SI2** with six *n*-decyloxy tails exhibited an improved thermal behavior with an enantiotropic columnar hexagonal phase ($Col_h$) phase over a short thermal range (6 degrees in the heating cycle). Upon cooling from the isotropic liquid state, a mosaic texture interspersed with the homeotropic domain (Fig. 4.4a) was found, before reaching crystallization at ≈ 76$^o$ (Fig. 4.4b).

The compound was investigated further with the help of XRD studies to understand the symmetry of the mesophase. Powder XRD patterns obtained at 100 $^o$C and at 85 $^o$C (Fig. 4.4c) were almost similar. The XRD pattern obtained at 100 $^o$C exhibited a sharp single peak at a low angle ($2\theta \approx 3^o$), along with two diffused peaks at a wide angle ($2\theta \approx$ 16-28$^o$). The first diffused peak corresponds to the packing of flexible alkyl tails, while the second one corresponds to the packing of discs within the column, *i.e.* intracolumnar distance. The intracolumnar distance was found to be 3.29 Å, which was quiet low without any secondary interactions.[3] It is to be noted that in chapter 2, the regioisomeric compounds **SO2-3** did not show any peak corresponding to core-core stacking, thus confirming the enhanced core-core interaction in the case of 1,2,4-

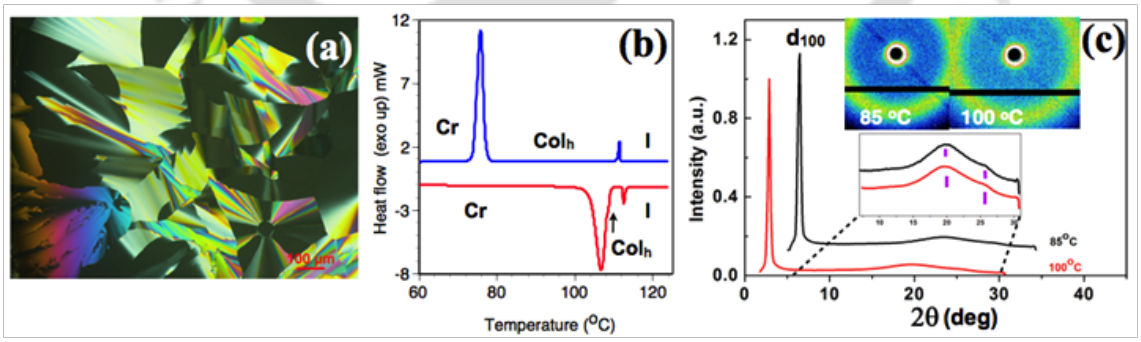


**Figure 4.4.** Photomicrograph of texture as seen by POM for the $Col_h$ phase of compound **SI2** at 85 °C (a); DSC traces obtained for the first cooling (upper trace) and second heating (lower trace) cycles of **SI2** at a rate of 5 °C min$^{-1}$ (b) and XRD profiles depicting the intensity against the $2\theta$ obtained for the $Col_h$ phase of compound **SI2** at 100 $^o$C and 85 $^o$C (inset shows the XRD image patterns obtained) (c).

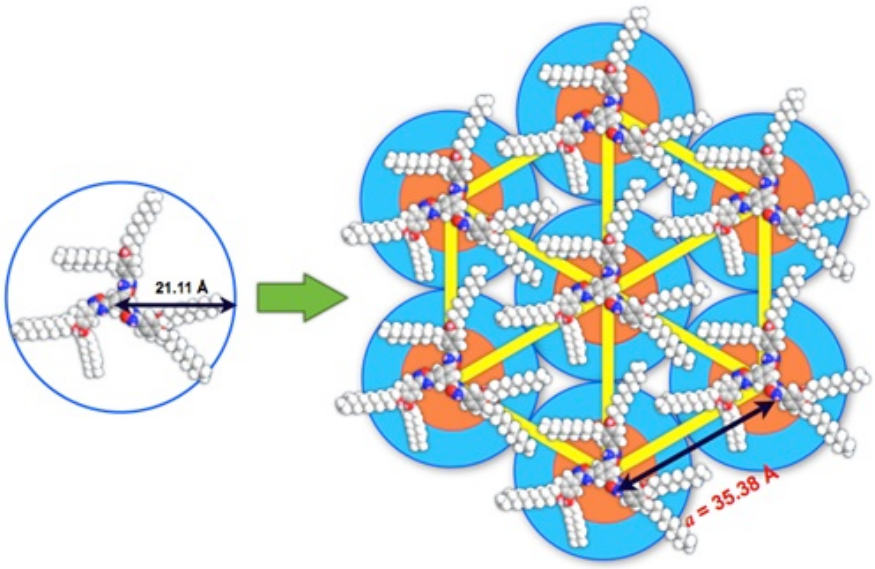


**Figure 4.5.** Self-organization of compound **SI2** in hexagonal columnar ($Col_h$) lattice. The space filling energy minimized (all-*trans*) molecular model of **SI2** derived from the molecular mechanics (MM2) method.

oxadiazole derivatives (**SI2-4**). This enhanced core-core interaction with low intracolumnar distance is beneficial to one-dimensional charge carrier mobility.[26] The sharp single peak points out that the phase under investigation is the $Col_h$ phase. Even though it is not unambiguous to assign hexagonal symmetry for the Col phase with a single peak at a low angle, there are many instances in the literature as well as in chapter 2, wherein the phase was assigned as $Col_h$ because of the minimum in the form factor.[34] Hexagonal cell parameter '*a*' was calculated from $d_{100}$ and was found to be 35.38 Å. The value of '*a*' is 15% less than the molecular diameter of compound **SI2** (Table 4.2) which may be due to the interdigitation of peripheral alkyl chains or folding of alkyl chains in mesophase (Fig. 4.5). The number of molecules forming the columnar slice, which is denoted as *Z*, was found to be 1.48. This is difficult to explain considering the star shaped molecular structure which is also observed in chapter 2. Such a *Z* value (Z >1) is often found in polycatenars and explained due to the side-by-side packing of two molecules to form a disc.[13d]

**Table 4.2.** Results of (hkl) indexation of XRD profiles of the compounds at a given temperature (T) of mesophase[a]

| Compoun<br>($D$/Å) | Phase<br>(T/°C) | $d_{obs}$(Å) | $d_{cal}$(Å) | Miller indices<br>*hkl* | Lattice parameters (Å), Lattice area S (Å$^2$), Molecular volume V (Å$^3$) |
|---|---|---|---|---|---|
| **SI2**<br>(42.21) | $Col_h$ (100) | 30.64<br>4.48($h_a$)<br>3.29($h_c$) | 30.64 | 100 | $a$ = 35.38, S = 1084.1, V = 3566.5, Z = 1.48 |
| | $Col_h$ (85) | 30.63<br>4.51 ($h_a$)<br>3.29 ($h_c$) | 30.63 | | $a$ = 35.37, S = 1084.4, V = 3564.3, Z = 1.48 |
| **SI3**<br>(42) | $Col_h$ (100) | 28.62<br>4.65<br>3.29 | 28.62 | 100 | $a$ = 33.05, S = 945.9, V = 3112, Z = 0.98 |
| | $Col_h$ (80) | 28.63<br>4.55($h_a$)<br>3.28($h_c$) | 29.63 | 100 | $a$ = 33.06, S = 946.5, V = 3114, Z = 0.98 |
| | $Col_h$ (25) | 29.60<br>4.40($h_a$)<br>3.29($h_c$) | 29.60 | 100 | $a$ = 34.18, S = 1011.7, V = 3328.6, Z = 1.05 |
| **SI4**<br>(42.8) | $Col_h$ (130) | 29.62<br>4.57($h_a$)<br>3.29($h_c$) | 32.83 | 100 | $a$ = 34.2, S = 1013, V = 3332.8, Z = 0.93 |
| | $Col_h$ (100) | 30.62<br>4.51($h_a$)<br>3.29($h_c$) | 28.63 | 100 | $a$ = 34.8, S = 1053.1, V = 3464.6, Z = 0.96 |
| | $Col_h$ (50) | 30.63<br>4.43($h_a$)<br>3.29($h_c$) | 29.60 | 100 | $a$ = 35.4, S = 1083.1, V = 3563.3, Z = 1 |
| | $Col_h$ (25) | 32.83<br>4.36($h_a$)<br>3.30($h_c$) | 32.83 | 100 | $a$ = 37.9, S = 1244.6, V = 4107.2, Z = 1.1 |

[a]The diameter (D) of the disk (estimated from Chem 3D Pro 8.0 molecular model software from Cambridge Soft). $d_{obs}$: spacing observed; $d_{cal}$: spacing calculated (deduced from the lattice parameters; $a$ for $Col_h$ phase). The spacings marked $h_a$ and $h_c$ correspond to diffuse reflections in the wide-angle region arising from correlations between the alkyl chains and core regions, respectively. $Z$ indicates the number of molecules per columnar slice of thickness $h_c$, estimated from the lattice area $S$ and the volume $V$.

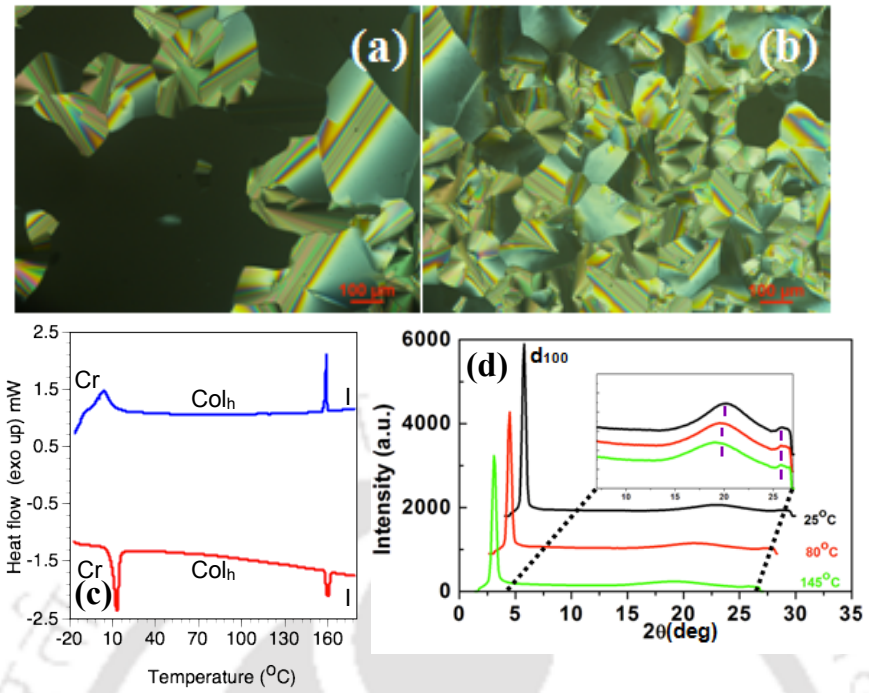


**Figure 4.6.** Photomicrographs of textures as seen by POM for the Col$_h$ phase of compound **SI3** at 135 °C (a); at 25 °C (b); DSC traces obtained for the first cooling (upper trace) and second heating (lower trace) cycles of compound **SI3** at a rate of 5°C min$^{-1}$ (c); and XRD profiles depicting the intensity against the 2$\theta$ obtained for the Col$_h$ phase of compound **SI3** at 145 °C, 80 °C and 25 °C (d).

Compound **SI3** with nine *n*-decyloxy tails showed an improved mesophase range with an isotropic temperature of around 160 °C. Upon cooling the isotropic liquid, mosaic texture develops from the homeotropic region (Fig. 4.6a). This is a regular textural pattern associated with Col phases in the literature. Most notably the compound crystallized at around 4 °C as confirmed by the DSC thermogams (Fig. 4.6c). The optical texture observed at room temperature (RT) also showed similar textural pattern showing no signs of crystallization at RT (Fig. 4.6b). Powder XRD studies carried out at higher temperature and room temperature showed a similar diffraction pattern (Table 4.2, Fig.4.6d), which shows that the Col$_h$ phase is stable for a temperature range of 155 degrees including room temperature. The number of molecules present in the unit cell '*Z*' in the case of compound **SI3** was found to be 1. It must be noted that in the case of compound **SI2**, which has six alkyl tails, the value of Z was 1.48. The molecular diameter is almost the same as that of compound **SI3**. This difference between the two molecules may be due to the increase in the number of peripheral alkyl chains in the case of compound **SI3** when

compared to compound **SI2**. The last compound of the series **SI4**, which is having nine dodecyloxy chains also exhibited the $Col_h$ phase but with a slight decrease in the mesophase range in comparison to its decyloxy homologue, due to an increase in the melting and a decrease in clearing temperature (Table 4.1 and Fig. 4.3). Thus the increase in the peripheral chain length decreased the thermal range of the mesophase. The POM image was characteristic of the $Col_h$ phase with large spherulites (Fig. 4.7a and b), which persisted up to room temperature. In DSC thermograms of the first cooling scan crystallization was seen at 12 $^oC$ (Fig. 4.7c). The XRD patterns obtained at different temperatures corroborated the POM and DSC observations confirming the type and thermal range of the $Col_h$ phase (Table 4.2)

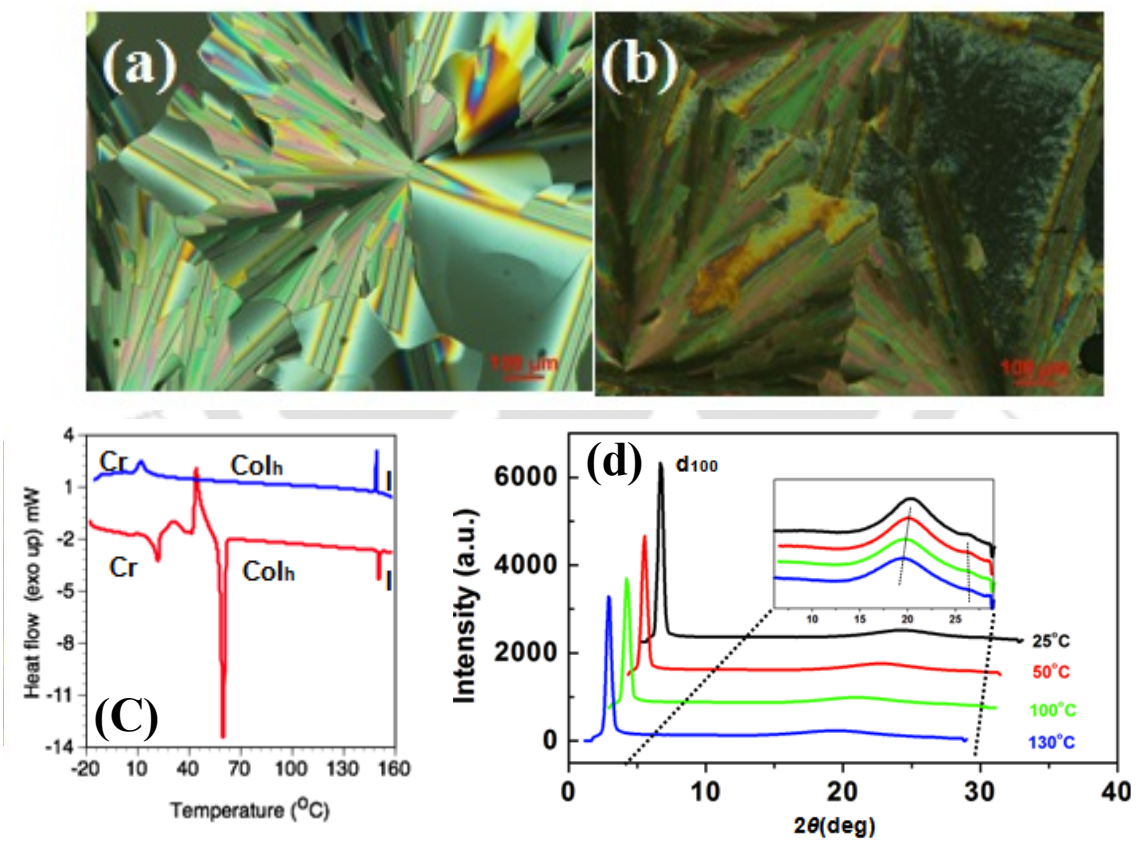


**Figure 4.7.** Photomicrographs of textures as seen by POM for the $Col_h$ phase of compound **SI4** at 125 °C (a); at 30 $^oC$ (b); DSC traces obtained for the first cooling (upper trace) and second heating (lower trace) cycles of compound **SI4** at a rate of 5$^oC$ $min^{-1}$ (c); and XRD profiles depicting the intensity against the 2$\theta$ obtained for the $Col_h$ phase of compound **SI4** at 130 $^oC$, 100 $^oC$, 50 $^oC$ and 25 $^oC$ (d).

### 4.2.3. Photophysical and electrochemical studies

The photophysical properties of the star-shaped molecules **SI1-4** in micromolar THF solution are depicted in Table 4.3. We expected a significant difference in their photophysical properties due to the difference in the substitution pattern. Absorbance and fluorescence spectra of compounds **SI1-4** were measured in micromolar THF solutions (Fig. 4.8). As can be seen, the absorption spectra of hekates **SI1-4** showed absorption maximum centered at around 278 nm, which was not dependant on their substitution pattern. The absorption maxima of hekates **SI1-4** with respect to their 1,3,4-oxadiazole counterparts **SO1-3** compounds of chapter 2 exhibited a hypsochromic shift (absorption maxima 312-324 nm).

**Table 4.3.** Photophysical[a] and electrochemical[c] properties of star-shaped molecules

| DLCs | Absorption (nm) | Emission[b] (nm) | Stoke's shift (nm) | $\lambda_{onset}$ (nm) | Emission[i] (nm) | $\Delta E_{g,opt}$ [d,e] | $E_{1ox}$ [f] | $E_{HOMO}$ [d,h] | $E_{LUMO}$ [d,g] |
|---|---|---|---|---|---|---|---|---|---|
| **SI1** | 278 | 299 | 21 | 294 | 410 | 4.23 | 1.97 | -6.31 | -2.08 |
| **SI2** | 278 | 314 | 36 | 295 | 484 | 4.21 | 1.83 | -6.17 | -1.96 |
| **SI3** | 279 | 311 | 32 | 294 | 502 | 4.22 | 1.97 | -6.31 | -2.09 |
| **SI4** | 278 | 309 | 31 | 294 | 496 | 4.23 | ------ | ----- | ----- |

[a]Micromolar solutions in THF. [b] Excited at the respective absorption maxima. [c] Experimental conditions: micromolar DCM solutions, $Ag/AgNO_3$ as the reference electrode, glassy carbon as the working electrode, platinum wire as the counter electrode, TBAP (0.1 M) as a supporting electrolyte, room temperature. [d] In electron volts (eV). [e] Band gap was determined from the red edge of the longest wave length ( $\lambda_{onset}$) in the UV-Vis absorption spectra using the relation $\Delta E_{g,opt} = 1242.37/ \lambda_{onset}$. [f] In volts (V). [g] Estimated from the formula $E_{LUMO} = E_{HOMO} + E_{g,opt}$. [h] Estimated from the onset reduction peak values by using $E_{HOMO} = -(4.8 - E_{1/2,Fc,Fc+} + E_{ox,onset})$ eV. [i] Emission obtained by exciting the thin films at their absorption maxima in solution.

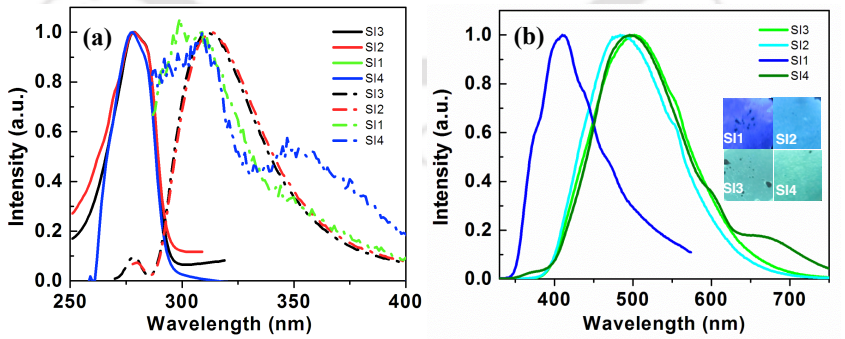


**Figure 4.8.** Normalized absorption (solid line) and emission spectra (dotted line) in micromolar THF solution obtained for **SI1-4** (a); normalized emission spectra of thin films of compounds **SI1-4** (excited at the absorption maxima obtained in the solution state), the inset shows the images of these thin films under UV light of long wavelength (365 nm) (b).

Based on the resemblance to the previously reported 1,2,4-oxadiazole derivatives[20] the single absorption band observed with these molecules could be due to the π-π* transition of the aromatic system. Optical bandgaps of these systems were estimated from the red edge of the absorption spectra. Compounds **SI1-4** showed a larger band gap of 4.2 eV, in comparison to their 1,3,4-oxadiazole derivatives (3.4-3.5 eV) of chapter 2. Emission spectra obtained by exciting the solutions of these compounds at their absorption maxima showed emission maxima centered at around 299-314 nm. The emission spectra were red shifted upon increasing the number of peripheral alkyl chains.

The emission intensity was lower in the solution state and we could not measure the relative quantum yield of these compounds with respect to the standard compound. We were interested in studying the emissive nature of these molecules in the solid state. The thin films of the compounds were prepared by slow cooling of the isotropic liquids of the samples sandwiched between the glass coverslips. They showed red-shifted emission and excitation spectra (Fig. 4.9; Table 4.4), which point to the formation of aggregates. The red-shifted excitation and emission spectra of the thin films in comparison to the respective spectra in the solution state at micromolar concentration point to the formation of J-aggregates[35]

Energy levels of frontier molecular orbitals (HOMO and LUMO) of the star shaped molecules were obtained by cyclic voltammetry (CV) and the data are tabulated in Table 4.3. We have chosen compounds **SI1-3** for carrying out CV studies. All the compounds exhibited irreversible oxidation and reduction waves (Fig. 4.10.). The optical band gap $E_{g,\ opt}$ was estimated from the red edge of the absorption spectra. The energy levels of the LUMO and the HOMO were determined by using the formulae $E_{LUMO} = E_{HOMO} + E_{g,opt}$ and $E_{HOMO} = -(4.8 - E_{1/2,Fc,Fc+} + E_{ox,onset})$ eV. Compounds **SI1-3** exhibited LUMO levels of -2.08 eV, -1.96 eV and -2.09 eV, and HOMO levels of -6.31 eV, -6.17 eV and -6.31 eV. In comparison to their 1,3,4-oxadiazole counterparts these compounds showed lower LUMO and HOMO levels and higher band gaps. The higher band gap is the most challenging material property pursued in the advancement of deep blue PHOLEDs.[36] Considering this the present series of compounds are good candidates

for such applications.

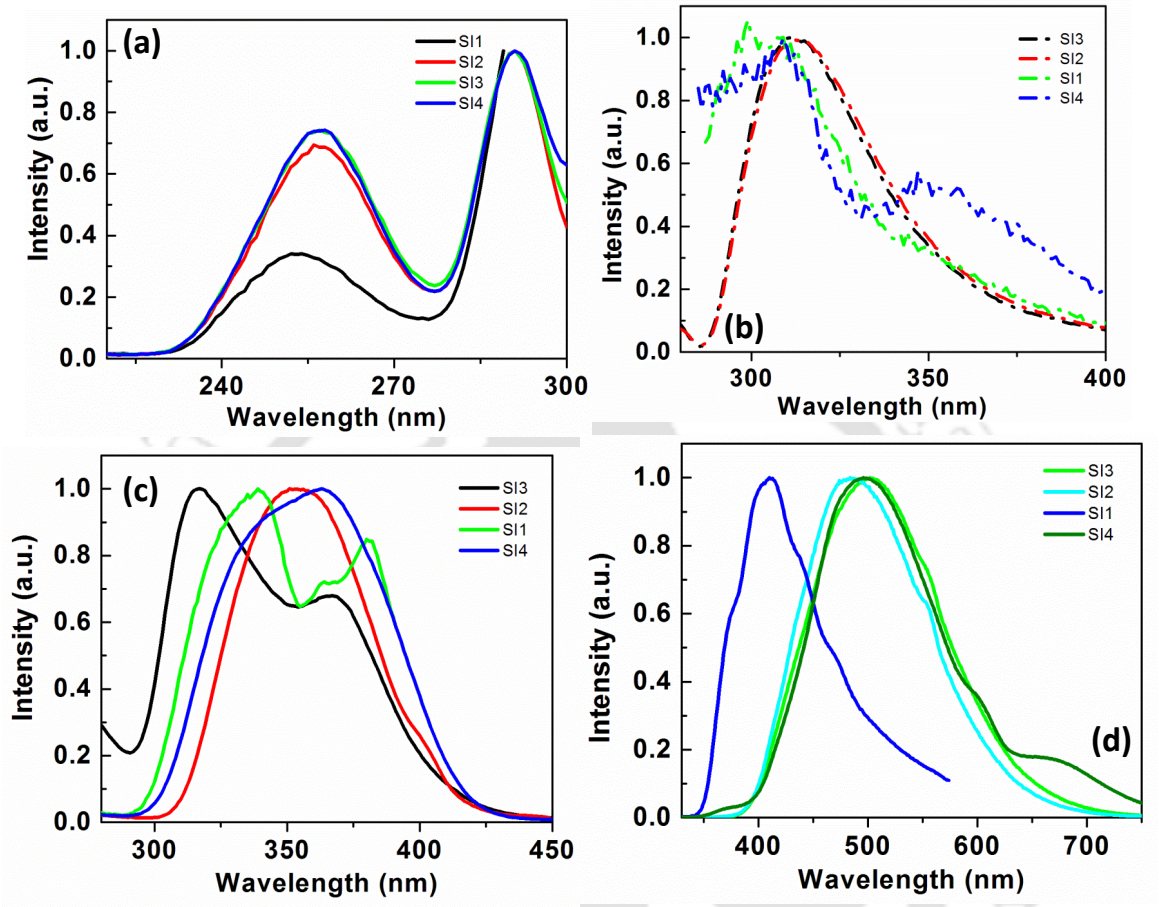


**Figure 4.9.** Excitation and emission spectra of compounds **SI1-4** in micromolar THF solution (a), (b) and Excitation and emission spectra of compounds **SI1-4** in thin film state (c), (d) respectively.

**Table. 4.4.** Photophysical properties of star-shaped molecules in solution and thin film

| | Solution[a] | | Thin film | |
|---|---|---|---|---|
| Entry | Excitation[b] (nm) | Emission (nm) | Excitation[b] (nm) | Emission[c] (nm) |
| **SI1** | 255 | 299 | 339, 380 | 410 |
| **SI2** | 255, 291 | 314 | 351 | 484 |
| **SI3** | 256, 291 | 311 | 317, 367 | 502 |
| **SI4** | 258, 291 | 309 | 363 | 496 |

[a]Micromolar THF solution; [b]Emission monitored at $\lambda_{max}$ ; [c]Excitation monitored at $\lambda_{max}$

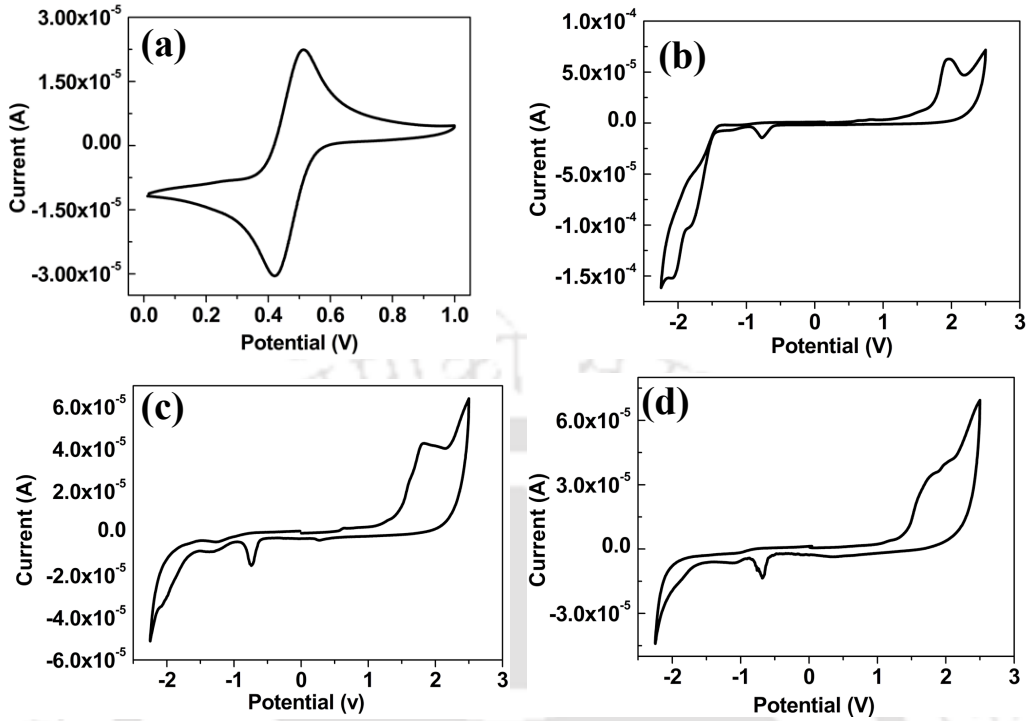


**Figure 4.10.** Cyclic voltammograms of ferrocene (a); compound **SI1** (b); **SI2** (c) and **SI3** (d) in anhydrous DCM solution of tetra-*n*-butylammonium perchlorate (0.1 M)(The half-wave potential of the ferrocene/ ferrocenium ($Fc/Fc^+$) redox couple ($E_{1/2,\ Fc,Fc^+}$) was found to be 0.46 V relative to the $Ag/Ag^+$ reference electrode).

### 4.2.4. Gelation studies

The compounds were investigated for their ability to aggregate in solutions of hexane, decane, dodecane, hexadecane, chloroform, dichloromethane, ethanol, dimethylsulfoxide (DMSO), *n*-butanol, tetrahydrofuran, benzene, toluene and *m*-xylene. Except for compound **SI2** with six decyloxy chains, none of the compounds exhibited gel-forming ability. Compound **SI2** formed gels in solvents like hexane, decane, dodecane and hexadecane and confirmed by the inversion of the glass vial (Fig. 4.11c, Table 4.5). This compound was soluble in chloroform, dichloromethane and tetrahydrofuran, while it was insoluble in DMSO. Compound **SI2** got precipitated in solvents like ethanol and *n*-butanol. Compound **SI1** with three decyloxy chains did not form any gel in dodecane and the same with the case of compounds **SI3** and **SI4** with nine alkoxy chains. Compound **SI2** with six decyloxy chains stabilized the gel formation

in dodecane with very low critical gelation concentration (CGC) of 0.52 wt %. In the literature it is well-known that the molecules which undergo gelation at concentrations lower than 1 wt% are usually classified as super gelators.[10] The supergelation capability of compound **SI2** was further confirmed by the formation of self-standing gels (Fig. 4.11e)

**Table 4.5.** Gelation properties of compound **SI2**

| Entry | Solvent | Properties | Critical Gel Concentration (wt.%) | $T_{gel}$ ($^{O}$C) |
|---|---|---|---|---|
| 1 | Hexane | G (O) | 0.67 | 66 |
| 2 | Decane | G (O) | 0.62 | 68 |
| 3 | Dodecane | G (O) | 0.52 | 70 |
| 4 | Hexadecane | G (O) | 0.47 | 75 |
| 5 | Toluene | S | ---- | --- |
| 6 | Benzene | S | ---- | --- |
| 7 | *m*-xylene | S | ---- | --- |
| 8 | DCM | S | ---- | --- |
| 9 | Chloroform | S | ---- | --- |
| 10 | THF | S | ---- | --- |
| 11 | *n*-butanol | P | ---- | --- |
| 12 | Ethanol | P | ---- | --- |
| 13 | DMSO | I | ---- | --- |

G = stable gel; S = soluble; P = precipitate; I = insoluble; O = opaque; The critical gelation concentration (wt. %) is the minimum concentration necessary for gelation; $T_{gel}$ ($^{o}$C) is the thermal stability of the gels determined by 'dropping ball' method (weight of the ball is 68.5 mg)

The organogel was formed within 150 seconds after dissolving in dodecane (Fig. 4.11c and d). The formation of gel was probed by fluorescence spectroscopy by plotting the fluorescence intensity at an emission maximum against the time taken for gelation in seconds. The emission intensity increases with time and reaches saturation at 220 seconds (Fig. 4.11 a, b and f). Visually this change is apparent upon irradiating the solution at these time intervals with the UV light of long wavelength (λ = 365 nm) (Fig. 4.11d). Normalized emission spectra showed a red shift in the emission maxima from 426 nm to 442 nm (Fig. 4.11b).

To the best of our knowledge, compound **SI2** is the first star shaped supergelator without any supportive H-bonding in its molecular structure. In the literature few metal-organic gels,[37] organic-inorganic hybrids,[38] polypeptides,[39] sugars [40] and polymers[41] show such super gelation properties. This can be explained as below. From the XRD data of the xerogel of compound **SI2** it is shown that the molecules self-assemble to form a rectangular columnar phase, while in the bulk state the molecules self-assemble to form a hexagonal columnar phase. In both cases π-π interactions play a major role in supporting columnar self-assembly. The H-bond that is observed in the case of crystalline compound **SI1** is between the aromatic hydrogen of one molecule and the heterocyclic nitrogen of the other molecule. This hydrogen bonding is only possible, if the molecules arrange in an antiparallel lamellar structure (Fig. 4.24a). Thus we can conclude that the H-bond does not play a role in the columnar self-assemblies found in liquid crystal and gel state. Apart from π-π interactions, other factors like the number and position of the peripheral alkyl chains also have a vital role in the gelation, aided by weak forces like van der Waals force. To date there has been a single report on supergelation, where π-π interactions play a major role and they are found in 1,3,4-oxadiazole based polycatenar.[12] We also like to point out that rod-like systems are more conducive to the formation of organogels than the star shaped molecules in the absence of supporting interactions like H-bonding and one can find many examples in the literature.[2]

The formation of organogels was also confirmed by measuring the emission spectra of the solution as a function of decreasing temperature. The emission intensity increased upon decreasing the temperature up to 40 $^{o}$C with a red shift from 426 nm to 452 nm (Fig. 4.12 a-c). There is a huge increase (four fold) in the luminescence intensity in the gel state in comparison to the solution state emission (Fig. 4.11a and 4.12a). But we should note that this increase in luminescence intensity is seen when the solution is above CGC (3.4 mM in dodecane). When the concentration of the solution is very less for example at 20 μM, where the monomers are greater in number in comparison to aggregates, the difference between the luminescence intensity is twelve fold (Fig. 4.13b). Thus this is a phenomenon of aggregation-induced emission. The emission spectra

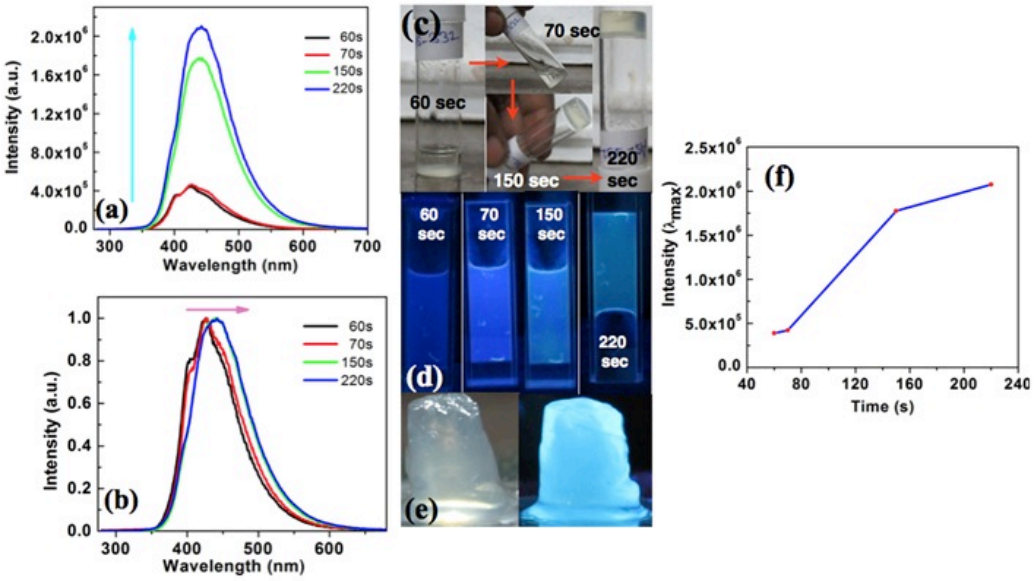


**Figure 4.11.** Emission spectra of compound **SI2** showing an increase in the emission intensity with time upon gelation (a); normalized emission spectra showing a red shift upon gelation (b); images showing the gel formation with respect to time in daylight (c); images showing the gel formation under the UV light (365 nm) with respect to time (d); self standing gel in daylight (left) and under UV light (365 nm) (e); plot showing the change in the emission intensity at emission maximum with respect to time (f).

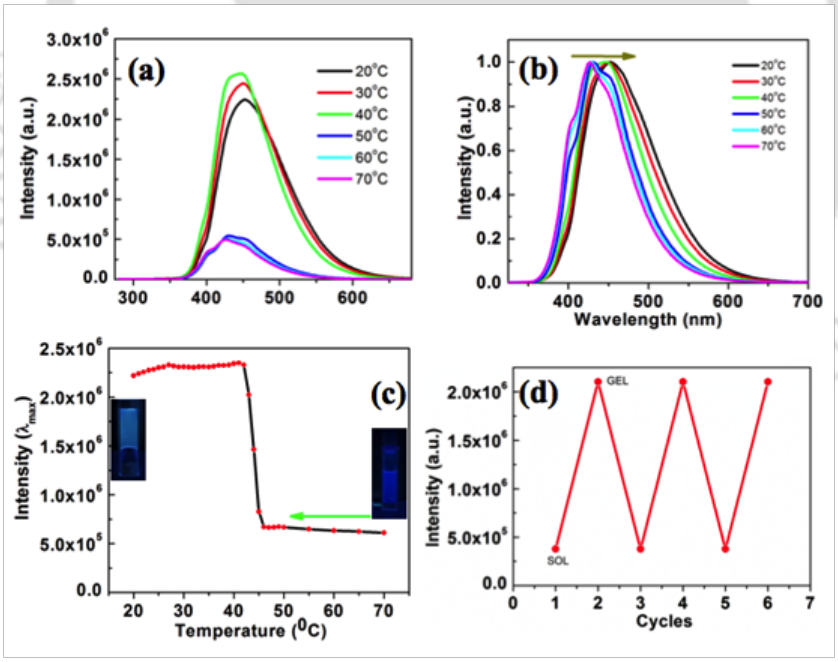


**Figure 4.12.** Emission spectra of compound **SI2** showing an increase in the emission intensity upon decreasing the temperature due to gelation (a); normalized emission spectra showing a red shift upon gelation (b); plot showing the change in emission intensity upon decreasing the temperature (inset shows the images of gel at 20°C and sol at 70°C under the UV light of long wavelength) (c); reproducible reversibility of emission intensity in solution to gel interconversion (d).

showed a red shift upon gelation (Fig. 4.12 b and c), which was similar to the observation in Fig. 4.11b. This gel formation was reversible for many cycles of heating and cooling as evidenced by the change in the emission intensity at emission maximum (Fig. 4.12d).

Fluorescence lifetimes of the excited species formed in the 20 μM and 4 mM dodecane solutions were measured by monitoring their emission maxima (426 nm for dilute solution and 442 nm for the concentrated solution). The solution with lower concentration showed biexponential decay with two excited species [$T_1$ = 3.4 ns (87%), $T_2$ = 15 ns (13%)]. The solution with higher concentration showed the same set of excited state species, where the excited state species with a higher lifetime was in a higher

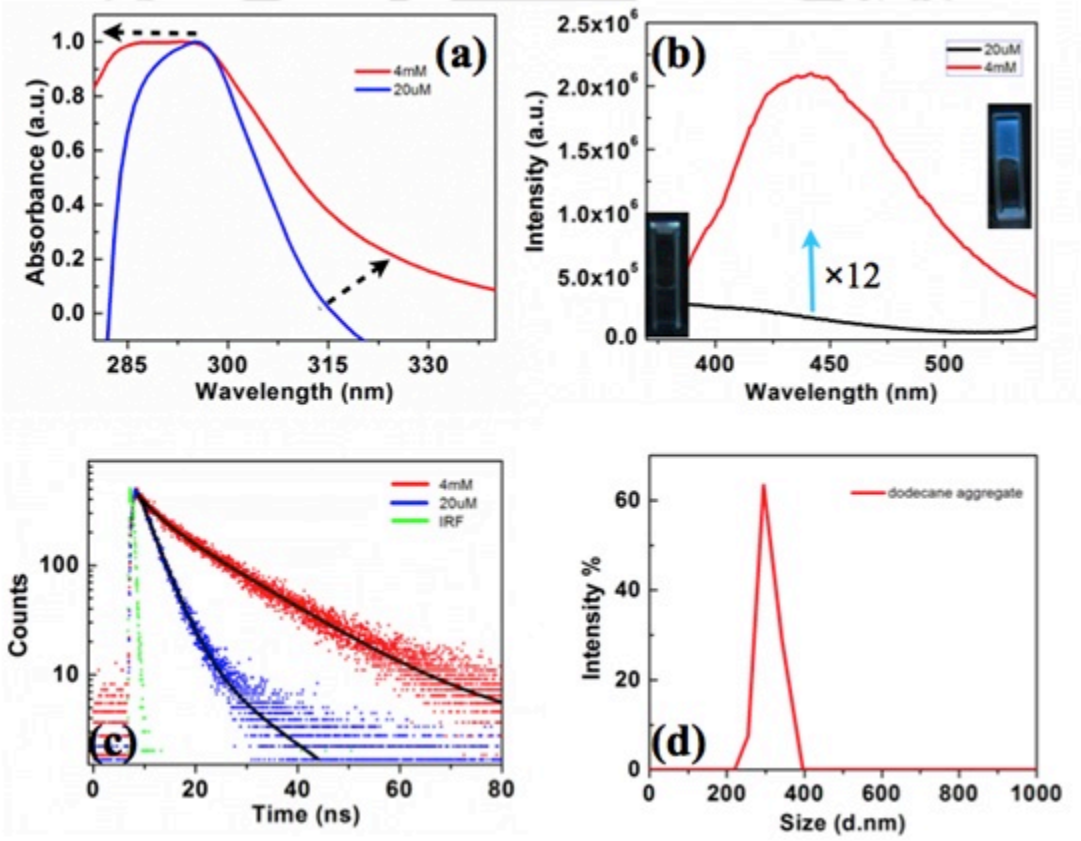


**Figure 4.13.** Normalized absorption spectra of compound **SI2** in dodecane at 4 mM (red trace) and 20 μM (blue trace) concentration (a); emission spectra of compound **SI2** in dodecane at 4 mM (red trace) and 20 μM (black trace) concentration (inset shows the images of gel at 4mM concentration and solution at 20 μM concentration under the UV light of long wavelength) (b); the fluorescence decay of compound **SI2** in dodecane at 4 mM (red trace) and 20 μM (blue trace) concentrations (green trace is instrument response function: IRF; $\lambda_{exc}$ = 290 nm) (c); dynamic light scattering curve observed for compound **SI2** in dodecane in micromolar concentration (d).

amount [$T_1$ = 3.4 ns (10%), $T_2$ = 15 ns (90%)] (Fig. 4.13c). The species with a lower lifetime was a solvated monomer, whereas the species with the higher lifetime is formed due to aggregation. Dynamic light scattering experiments carried out for compound **SI2** in dodecane in milimolar concentration showed the presence of aggregates of 300 nm size (Fig. 4.13d). The absorption spectrum obtained at higher concentration (4 mM) has shown a blue shift compared to the solution at lower concentration (20 μM) (Fig. 4.13a). This shows that the aggregates formed during gelation are H-type aggregates where the molecules are arranged one above the other in a cofacial or parallel manner. Excitonic splitting in these aggregates leads to a high-energy transition and a low energy forbidden transition. In such systems the absorption spectra are dominated by the high-energy band leading to a blue shifted absorption band with respect to the monomer absorption band. This also leads to a strong red shift in the fluorescence from a low energy band.[41] Even though H-aggregates are supposed to exhibit reduced luminescence compared to that in solution, here the situation is exactly opposite of the expected.[42] In the literature there are limited reports on luminescent H-aggregates.[43] Usually this luminescence by H-aggregates is accounted for the excimer species or due to a slight rotation of two exciton-coupled molecules in the excited state. We should note that the annealed thin films showed the formation of J-aggregates. Thus J- to H-type conversion was seen upon moving from the solid to the gel state. A similar H-type aggregation of star shaped molecules upon gelation in hydrocarbon solvents was reported by Das *et al.* [44]

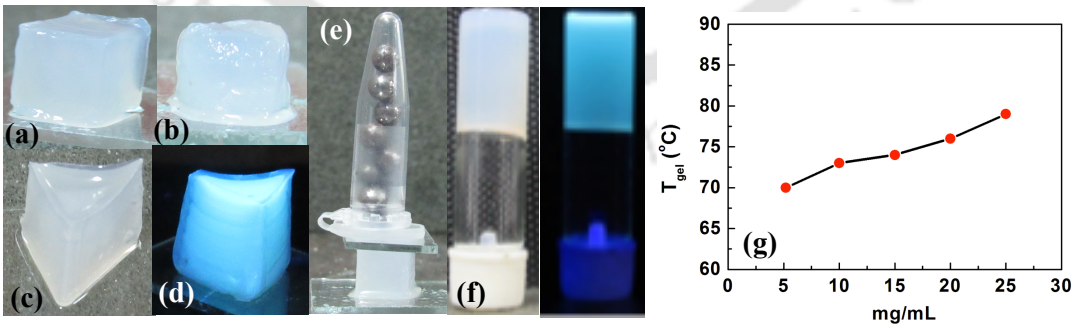


**Figure 4.14.** Moldability of organogel of **SI2** in dodecane (1.5 wt%) into different shapes like cube (a); cylinder (b); trigonal prism (c) seen under day light; under UV light (365 nm) (d); ability to sustain the weight (e); Photograph of gel after standing for 45 days in daylight and under UV light (365 nm) (f); plots of $T_{gel}$ *vs.* concentration for compound **SI2** in dodecane (g).

**Figure 4.15.** Photograph of the gel after keeping inverted for 25 days showing the formation of xerogel under daylight and UV light ($\lambda_{max}$ = 365 nm)

The self-standing gel showed an incredible stability when kept inverted for a period of more than a month (Fig. 4.14f). When we took the gel in a small amount and kept it inverted, shrinkage of the gel was observed over a period of 25 days but the shape was retained (Fig. 4.15). This indicated another level of self-organization of the xerogel architecture in the absence of solvent. The luminescence remained the same in spite of the change in the structure of the gel. We have investigated the thermal stability of the gel with respect to concentration by the 'dropping ball' method,[45] which showed a gradual increase (Fig. 4.14g) upon increasing the concentration. The gel prepared at 1.5 wt % concentration showed higher mechanical strength and could be molded into any shape as shown in Fig. 4.14a-d and the luminescence remained unchanged.

Extensive microscopy was carried out to understand the superstructure of the gel formed from compound **SI2**. The surface morphology of the xerogels of **SI2** obtained from the organogel in dodecane was studied with the help of field emission scanning electron microscopy (FE-SEM), atomic force microscopy (AFM) and transmission electron microscopy (TEM). Scanning electron microscopy (SEM) images of the xerogels obtained by evaporating the 1 mM dodecane solutions of compound **SI2** showed the entangled network of fibers (Fig. 4.16). AFM microscopy was carried out on a drop cast film (**SI2** in dodecane, 1mM) and the solvent was allowed to evaporate to get a xerogel film. The AFM images showed a very dense network of fibers (Fig. 4.17a). The same

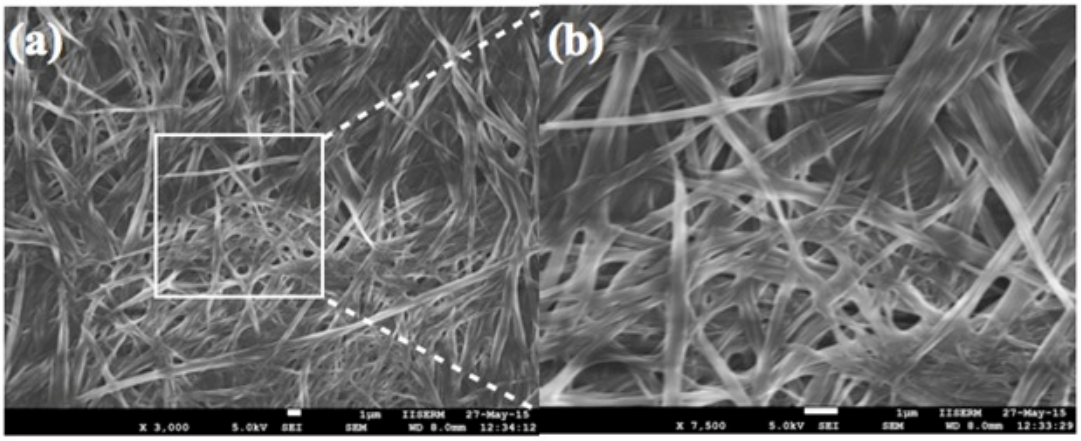


**Figure 4.16.** SEM images obtained for compound **SI2** at 1mM dodecane solution (a); an expanded region of the first image (b) (scale bar is 1µm).

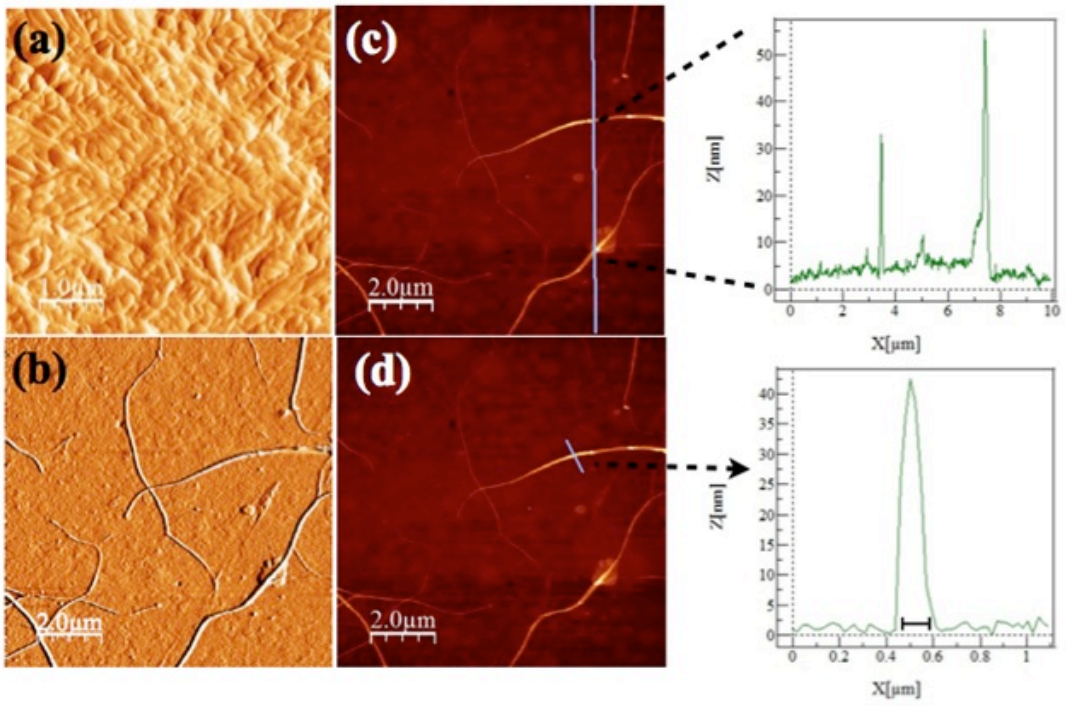


**Figure 4.17.** AFM images obtained for compound **SI2** at 1mM dodecane solution (scale bar is 1 µm) (a); at 1 x $10^{-5}$ M (scale bar is 2µm) (b); expanded regions of (b) showing the height profiles of the individual fibers (c); expanded regions of (b) showing the thickness of an individual fiber (d).

experiment carried out by drop casting a solution at lower concentration (1 × $10^{-5}$ M) helped us to look at the individual fiber in detail (Fig. 4.17b). The fibers are of several

micrometers in length, with heights of 30-40 nm and thickness of around 185 nm (Fig. 4.17c and d). Transmission electron microscopy (TEM) images of the gels (1mM dodecane solution) showed an interwoven network of fibers of diameter 30-40 nm (Fig. 4.18). These SEM, AFM and TEM images of the gels were further supported by fluorescence microscopy and optical microscopy studies (see the Fig. 4.19a and b).

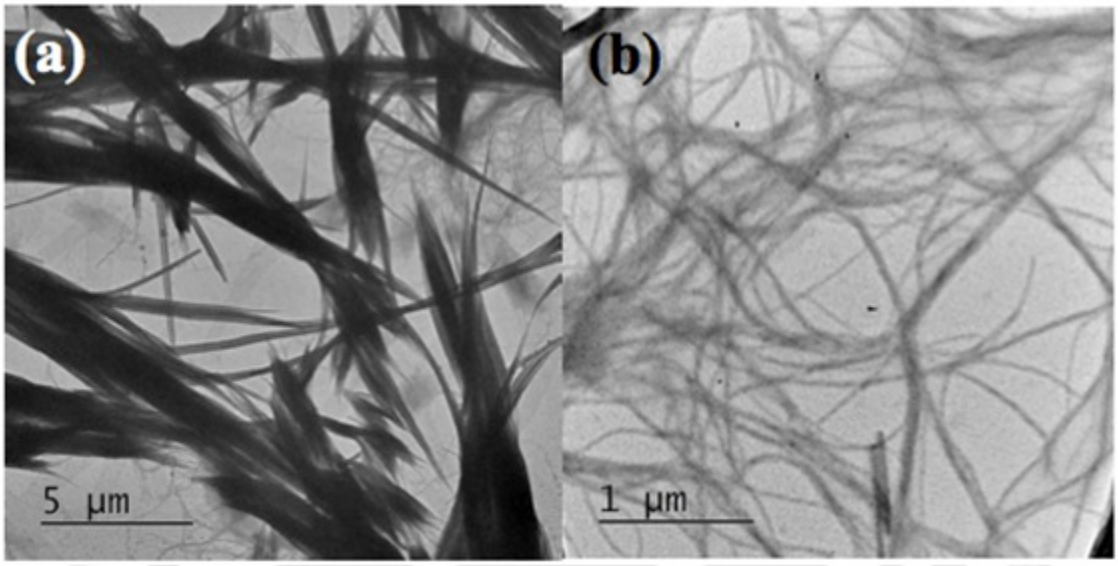


**Figure 4.18.** TEM images obtained for compound **SI2** at 1mM dodecane solution (scale bar is 5 µm) (a); an expanded regions of (a) showing entangled fibers (scale bar is 1 µm) (b).

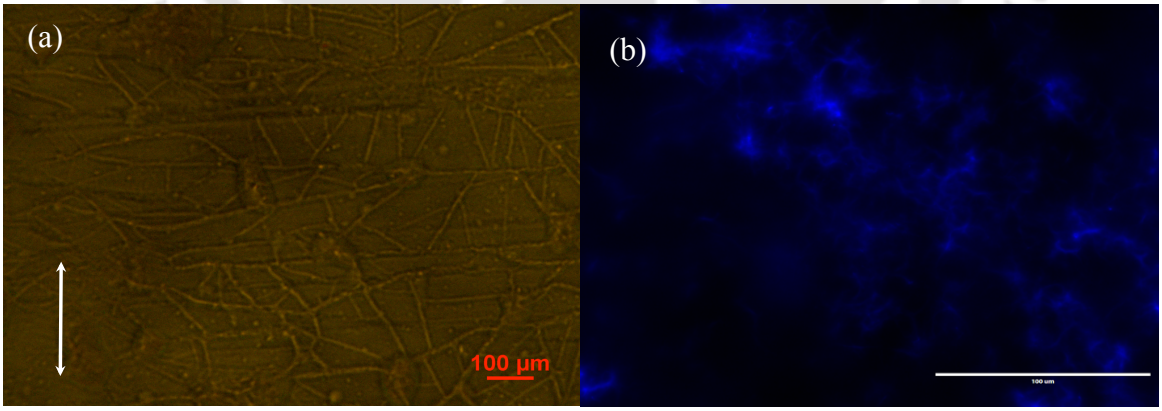


**Figure 4.19.** POM image of the thin film of compound **SI2** in xerogel state under parallel polarizers (obtained from the dropcasting of 4mM dodecane solution) (a); and Fluorescent Microscopy Image of the thin film of the xerogel obtained for compound **SI2** (4mM solution in dodecane, scale bar 100 µm) (b).

Furthermore, the structure of the xerogel was studied with the help of powder X-ray diffraction studies carried out on a thin film of compound **SI2** prepared by drop casting the 1 mM solution on a glass slide. The XRD pattern of the xerogel film (Fig. 4.20a) showed many peaks centered at 30.61, 24.91, 10.67, 9.11, 7.11 6.18, 5.96, 5.42, 5.05 and 3.79. This may be due to the strong intermolecular interactions of the adjacent

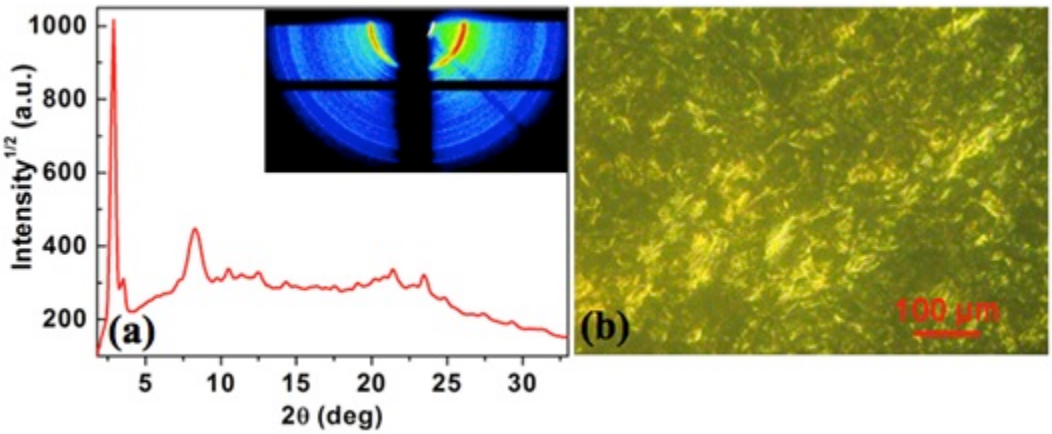


**Figure 4.20.** XRD profile depicting the intensity against the 2$\theta$ obtained for the $Col_r$ phase of compound **SI2** in xerogel state (inset shows the XRD image pattern obtained) (a) POM image of the xerogel showing a birefringent texture (b).

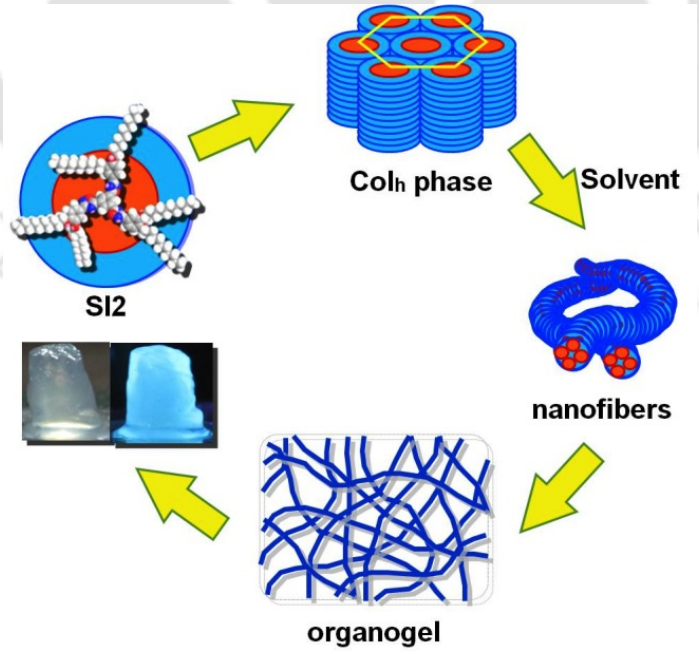


**Figure 4.21.** Schematic representation showing the supramolecular hierarchical organization of compound **SI2**.

molecules in the xerogel state. The ratio of reciprocal *d*-spacings clearly rules out a lamellar order of the molecules, but strongly suggests a columnar rectangular structure in particular. The lattice parameters '*a*' and '*b*' of the unit rectangular cell was found to be 61.22 and 27.26 Å, respectively as shown in Table 4.6. The columnar arrangement of

**Table 4.6.** Results of (hkl) indexation of XRD profiles of the compound **SI2** in xerogel state at room temperature

| Compounds (*D*/Å) | Phase (T/°C) | $d_{obs}$ (Å) | $d_{cal}$ (Å) | Miller indices *hkl* | Lattice parameters (Å) |
|---|---|---|---|---|---|
| **SI2** (42.21) | $Col_r$ (RT) | 30.61 | 30.61 | 200 | |
| | | 24.91 | 24.91 | 110 | $a$ = 61.22 |
| | | 10.67 | 11.33 | 320 | |
| | | 9.11 | 9.08 | 330 | $b$ = 27.26 |
| | | 7.11 | 6.65 | 240 | |
| | | 6.18 | 6.22 | 440 | |
| | | 5.96 | 5.95 | 540 | |
| | | 5.42 | 5.66 | 640 | |
| | | 5.05 | 4.98 | 500 | |
| | | 3.79 | 3.91 | 400 | |

these molecules in the nanofibers of the xerogel is also supported by the birefringent texture obtained for the xerogel state (Fig. 4.20b). Thus we can represent the hierarchical self-assembly of these star shaped molecules in bulk and gel states as shown in Fig. 4.21.

### 4.2.5. Rheological studies

To obtain further insights into the dynamic mechanical properties of the organogel formed from compound **SI2** in dodecane, we performed dynamic frequency sweep experiments (at constant stress) to measure the rheological response, as characterized by $G^*(\omega) = G'(\omega) + iG''(\omega)$, where $G'$ is the storage modulus, $G''$ is the loss modulus and $\omega$ is the angular frequency.[46] These measurements are advantageous as the final details of the gel structure remain perfect due to small dormation (*i.e.* small stress). Figure 4.22a, shows the measurements of $G'$ and $G''$ for the gels containing 0.52 wt% of compound **SI2** in dodecane as a function of $\omega$ (at 25 °C using 0.2 kPa stress). We make two observations from Fig. 4.22a.

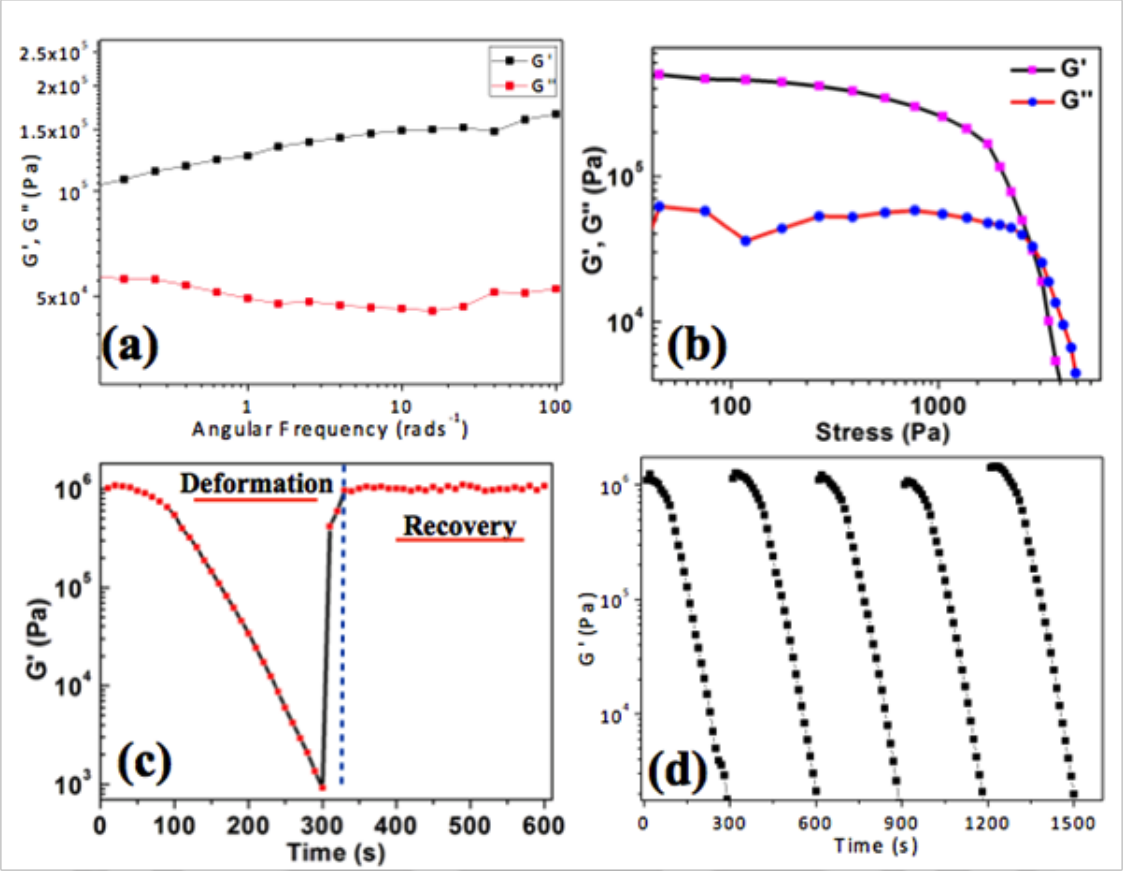


**Figure 4.22.** Angular frequency (rad $s^{-1}$) dependence of *G'* and *G"* obtained with small stress amplitudes: (a) 0.52 wt% of compound **SI2** in dodecane at 25 °C using 0.2 kPa stress. (b) Stress dependence of *G'* and *G"* of the same gel **SI2** measured at constant frequency (at 25 °C, and frequency at 0.1 Hz). (c) Thixotropic nature of organogel of **SI2** (3.4 mM) in *n*-dodecane at 25 °C (deformation; stress: 0.1 to 100 Pa, time: 300 s, angular frequency: 10 Hz; recovery; Stress: 1 Pa, time: 300 s; angular frequency: 10 Hz). (d) Five continuous cycles of measurement for **SI2** (3.4 mM) to prove that the gel is thixotropic.

First, *G'* is greater than *G"* over the entire range of frequency measurements, indicating that the LC gel behaves as a solid-like, viscoelastic material. Second, G' and G" are weakly dependent on frequency. It should also be noted that even at the lowest frequency (the limit of the instrument) we did not see liquid like behaviour of the gel (*i.e.* *G"*> *G'*). This confirms that gel nature of these materials in which structural relaxation is very large.

Past studies have also demonstrated that the dynamics of the sol-gels lead to characteristic features in non-linear rheological measurements. To establish this non-linear viscoelastic regime, we performed stress amplitude dependence of the storage and

loss moduli. Fig. 4.22b shows stress-dependent nonlinear measurements of the gel at a fixed frequency of 0.1 Hz. We note two features in Fig. 4.22b. First, at low strain amplitudes *G'* is nearly constant, suggesting a linear viscoelastic regime. In this regime, *G' > G"* which is consistent with the solid like behavior of the gel. Second, above a critical stress value (2.8 kPa), both *G'* and *G"* became strain dependent and leads ultimately to the observation of viscoelastic liquid-like behaviors at high stress (*G" > G'*). This signifies a deformation driven transition from a viscoelastic solid to viscoelastic liquid.

The thixotropic nature of the gel was also examined by studying the recovery of the destroyed gel. Two continuous processes, *i.e.* deformation and recovery, were followed step by step to understand the thixotropic nature (Fig. 4.22c). A varying stress from 0.2 to 3 kPa at an angular frequency of 10 Hz for 300 s was applied for the deformation step and the values of *G'* was monitored as a function of time for 300 s. In the recovery process, the storage modulus *G'* was monitored as a function of same time interval (300 s) for a low shear stress of 0.2 kPa while keeping the same angular frequency (10 Hz). This experiment was repeated five times and the results are shown in Fig. 4.22d. The results show that the gel recovered immediately after removing the applied stress.

### 4.2.6. Single crystal XRD studies

We were curious to know how these 1,2,4-oxadiazole based molecules self-assemble in the crystalline state. We thought that this knowledge would help us in unraveling the association of these molecules in liquid crystalline and gel self-assemblies. Even though we desired the crystallization of compound **SI2**, unfortunately except for compound **SI1**, none of the compounds in this series crystallized in any solvents. Nevertheless the crystal structure of compound **SI1** provided some valuable insights into the self-assembly of this series of molecules, as we discuss in the following (Table 4.7).

Slow evaporation of $CH_2Cl_2$ solution of **SI1** at room temperature afforded colorless rectangular prism like crystals suitable for single crystal X-ray diffraction

determination (Fig. 4.23b); the crystallographic data are summarized in the Table 4.7. The star-shaped molecule of **SI1** has a diameter of 43.11Å and its oxadiazole ring is roughly coplanar with central benzene rings and two peripheral benzene rings (Fig. 4.23a).

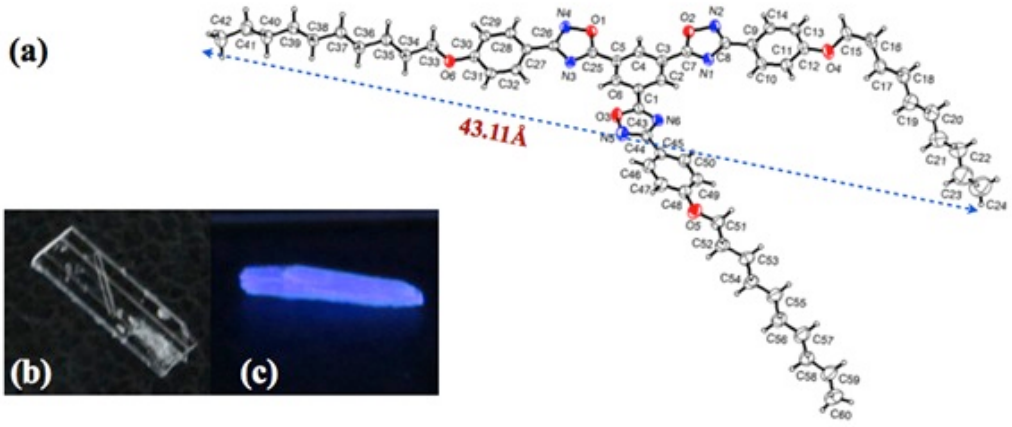


**Figure 4.23.** ORTEP representation of compound of **SI1** (a); the image of a crystal of **SI1** under day light (b); the image of a crystal under UV light (λ = 365 nm) (c).

The neighboring pair of molecules is aligned in an alternating anti-parallel manner augmented by two sets of π···π stacking interactions.[47] The first one is (stacking distance of 4.50Å) between the centroid of the oxadiazole ring of one molecule and the same of the neighboring molecule. The second one is between the centroid of the central benzene ring of one molecule and centroid of the peripheral benzene ring of other molecule (stacking distance of 4.03 Å) (Fig. 4.24b). Furthermore there is a lateral non covalent C-H···N interaction between the hydrogen atom (H29) of the peripheral benzene ring of one molecule and the nitrogen atom (N2) of the oxadiazole ring of another molecule ($d_{CH\ldots N}$ = 2.628 Å) (Fig. 4.24a). The intramolecular rotation would be restricted by the van der Waals interaction of long alkyl chains from the neighbouring molecule leading to interdigitation[48] (Fig. 4.25a). In addition there is hydrophobic interactions (2.394Å) between terminal *n*-decyl chains of the next row. As a result, this alternate packing of molecules, leads to a repeating lamellar distance of 26.95 Å (Fig 4.24a and Fig. 4.25b).

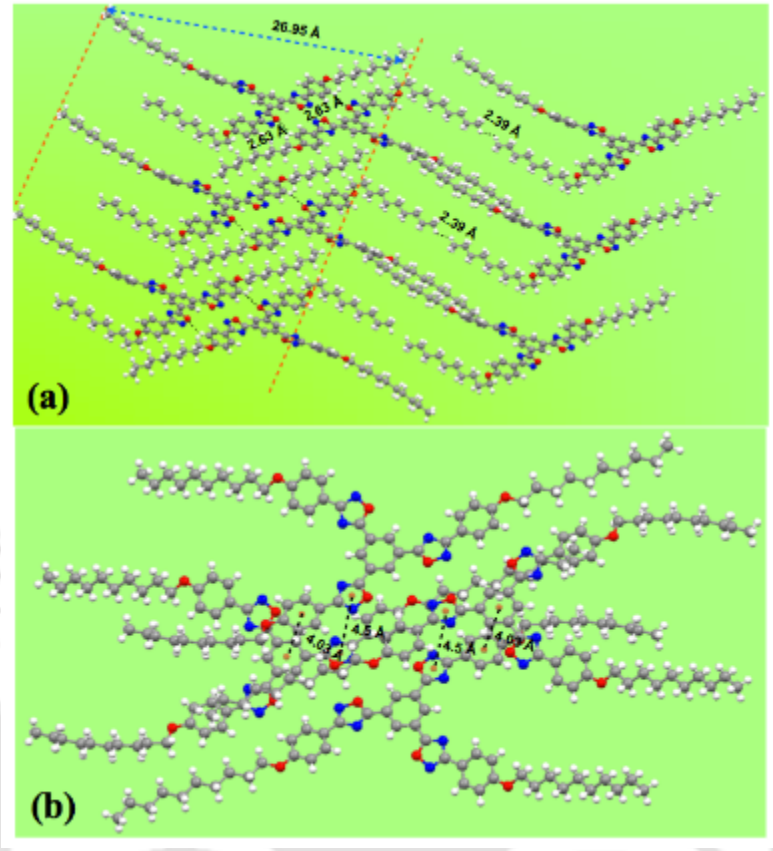


**Figure 4.24.** Crystallographic packing structure of compound **SI1**, the side view showing H-bonding, hydrophobic interactions and lamellar packing (a) and simplified top view showing π-stacking interactions (b).

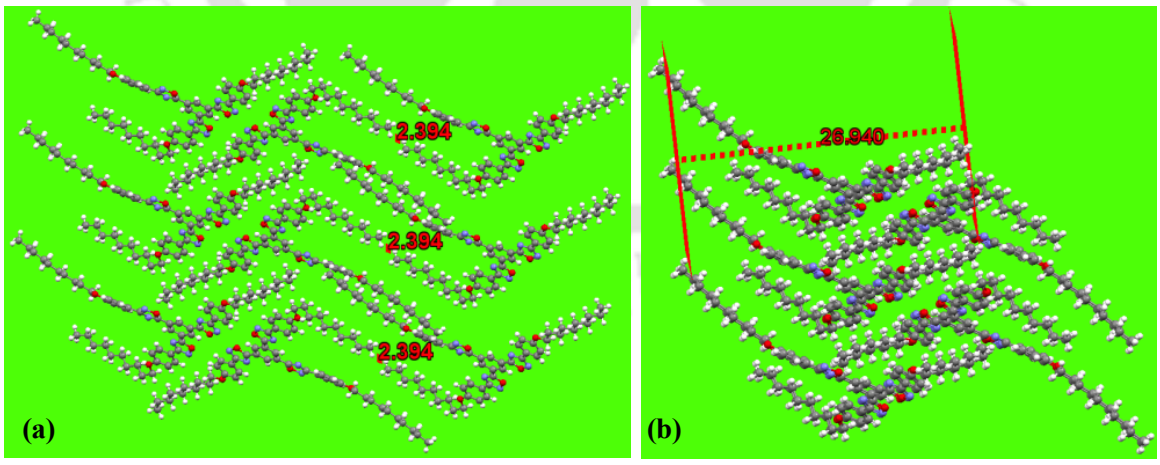


**Figure 4.25.** Vanderwaals' interaction between the peripheral alkyl chains of two molecules of compound **SI1** (a) and lamellar arrangement of molecules of compound **SI1** (b).

The heteroatoms in the five membered rings were preferentially co-planar with the carbon and nitrogen atoms to form a planar π-conjugation system. A comparison of C-O, N-O and C-N bond distances and angles of the heterocyclic ring of **SI1** has been made and the results are summarized in Table 4.7.

**Table 4.7.** Crystal data and structure refinement for **SI1,** [$C_{60}$ $H_{78}$ $N_6$ $O_6$].[32]

| | |
|---|---|
| Empirical formula | $C_{60}$ $H_{78}$ $N_6$ $O_6$ |
| Formula weight | 979.28 |
| Crystal habit, colour | needle, colorless |
| Crystal size, $mm^3$ | 0.36 × 0.20 × 0.18 |
| Temperature, $T$ | 296(2) K |
| Wavelength, $\lambda$ | 0.71073 Å |
| Crystal system | triclinic |
| Space group | $P$ –1 |
| Unit cell dimensions | $a$ = 9.5084(6) Å<br>$b$ = 10.1887(6) Å<br>$c$ = 29.8085(17) Å<br>$\alpha$ = 87.885(4)°<br>$\beta$ = 83.205(4)°<br>$\gamma$ = 80.832(4)° |
| Volume, $V$ | 2830.4(3) $Å^3$ |
| $Z$ | 2 |
| Calculated density, $Mg \cdot m^{-3}$ | 1.149 $Mg/m^3$ |
| Absorption coefficient, $\mu$ | 0.074 $mm^{-1}$ |
| $F$(000) | 1056 |
| $\theta$ range for data collection | 0.69° to 25.00° |
| Limiting indices | $-11 \leq h \leq 11$, $-11 \leq k \leq 11$, $-35 \leq l \leq 35$ |
| Reflection collected / unique | 41914/ 9375 [$R$(int) = 0.0694] |
| Completeness to $\theta$ | 0.941 % |
| Max. and min. transmission | 0.987 and 0.982 |
| Refinement method | Full–matrix least–squares on $F^2$ |
| Data / restraints / parameters | 9375 / 0 / 652 |
| Goodness–of–fit on $F^2$ | 1.029 |
| Final $R$ indices [$I$>2sigma($I$)] | $R1$ = 0.0674, $wR2$ = 0.1695 |
| $R$ indices (all data) | $R1$ = 0.1543, $wR2$ = 0.2203 |
| Largest diff. peak and hole | 0.232 and –0.249 $e.Å^{-3}$ |

| **Bond distances** | | | | | | | |
|---|---|---|---|---|---|---|---|
| Bond distance | (Å) | Bond distance | (Å) | Bond distance | (Å) | Bond distance | (Å) |
| C1−C2 | 1.388(4) | C2−C3 | 1.389(4) | C3 −C4 | 1.408(4) | C4−C5 | 1.382(4) |
| C5 −C6 | 1.395(4) | C6 −C1 | 1.395(4) | C3 −C7 | 1.471(4) | C7 −N1 | 1.294(4) |
| C7 −O2 | 1.345(3) | N1− C8 | 1.382(4) | O2− N2 | 1.424(3) | N2− C8 | 1.305(4) |
| C8−C9 | 1.465(4) | C9−C10 | 1.387(4) | C10−C11 | 1.373(4) | C11−C12 | 1.390(4) |
| C12−C13 | 1.379(4) | C13−C14 | 1.381(4) | C14−C9 | 1.385(4) | C12−O4 | 1.362(4) |
| O4−C15 | 1.440(4) | C5−C25 | 1.459(4) | C25−O1 | 1.344(3) | C25−N3 | 1.296(4) |
| O1−N4 | 1.427(3) | N3−C25 | 1.296(4) | C26−N3 | 1.390(3) | C26−N4 | 1.311(4) |
| C26−C27 | 1.458(4) | C27−C28 | 1.379(4) | C28−C29 | 1.376(4) | C29−C30 | 1.387(4) |
| C30−C31 | 1.394(4) | C31−C32 | 1.372(4) | C27−C32 | 1.388(4) | C30−O6 | 1.366(3) |
| O6−C33 | 1.436(3) | C1−C43 | 1.460(4) | C43−O3 | 1.338(4) | C43−N6 | 1.294(4) |
| N5−C44 | 1.300(4) | N6−C44 | 1.378(4) | C44−C45 | 1.472(4) | C45−C46 | 1.379(4) |
| C46−C47 | 1.369(5) | C47−C48 | 1.381(5) | C48−C49 | 1.368(4) | C49−C50 | 1.390(4) |
| C50−C45 | 1.369(4) | C48−O5 | 1.371(4) | O5−C51 | 1.422(4) | | |

| **Bond angles** | | | | | |
|---|---|---|---|---|---|
| Bond angle | ( ◦ ) | Bond angle | ( ◦ ) | Bond angle | ( ◦ ) |
| C2− C1− C6 | 119.0(3) | C2− C1− C43 | 119.1(3) | C1− C2− C3 | 121.1(3) |
| C2 −C3− C4 | 119.7(3) | C2−C3 −C7 | 117.0(3) | C4 −C3− C7 | 123.2(3) |
| C5 −C4 −C3 | 119.2(3) | C4− C5 −C6 | 120.7(3) | C4−C5−C25 | 122.3(3) |
| C6 −C5 −C25 | 117.0(3) | C1 −C6− C5 | 120.3(3) | N1 - C7 - O2 | 113.7(3) |
| N1− C7− C3 | 126.3(3) | O2 −C7− C3 | 119.9(3) | C7 −N1− C8 | 102.6(3) |
| N2 −C8−N1 | 114.6(3) | N2 −C8− C9 | 124.2(3) | N1− C8 −C9 | 121.2(3) |
| C7− O2− N2 | 105.8(2) | C14−C9−C10 | 117.8(3) | C14 −C9− C8 | 122.6(3) |
| C10− C9− C8 | 119.6(3) | C11−C10−C9 | 121.3(3) | C10−C11−C12 | 120.1(3) |
| O4 −C12−C13 | 125.3(3) | O4− C12−C11 | 115.2(3) | C13−C12−C11 | 119.5(3) |
| C12−C13−C14 | 119.6(3) | C13− C14− C9 | 121.7(3) | C12− O4−C15 | 119.1(3) |
| N3 −C25−O1 | 113.5(3) | N3− C25− C5 | 126.7(3) | O1 −C25− C5 | 119.8(3) |
| C25− O1− N4 | 105.9(2) | C26− N4− O1 | 103.8(2) | N4− C26− N3 | 113.5(3) |
| N4− C26−C27 | 124.3(3) | N3 −C26−C27 | 122.2(3) | C25− N3−C26 | 103.3(3) |
| C28−C27−C32 | 118.1(3) | C28−C27−C26 | 121.6(3) | C32−C27−C26 | 120.3(3) |
| C29−C28−C27 | 121.6(3) | C28−C29−C30 | 119.6(3) | O6 −C30−C29 | 125.1(3) |
| O6 −C30−C31 | 115.3(3) | C29−C30−C31 | 119.6(3) | C32−C31−C30 | 119.5(3 |
| C31−C32−C27 | 121.5(3) | C30− O6−C33 | 117.8(2) | N6− C43− O3 | 113.5(3) |
| N6− C43−C1 | 128.8(3) | O3 −C43− C1 | 117.7(3) | C43− O3− N5 | 105.8(2) |
| C44− N5− O3 | 103.7(3) | N5− C44− N6 | 114.0(3) | N5 −C44−C45 | 121.9(3) |
| N6− C44−C45 | 124.0(3) | C43− N6−C44 | 103.0(3) | C50−C45−C46 | 118.3(3) |
| C50−C45−C44 | 120.7(3) | C46−C45−C44 | 120.8(3) | C47−C46−C45 | 121.3(4) |
| C46−C47−C48 | 120.2(3) | C49− C48−O5 | 125.8(4) | C49−C48−C47 | 119.1(3) |
| O5− C48−C47 | 115.0(3) | C48−C49−C50 | 120.2(3) | C45−C50−C49 | 120.9(3) |
| C48− O5−C51 | 118.8(3) | | | | |

Compound **SI1** is almost nonfluorescent in solution but a significant enhancement in the emission intensity in thin film was observed, emitting blue fluorescence (Fig. 4.8b) upon exposure to UV light ($\lambda_{ex}$= 365nm). Interestingly, similar behavior was observed with the single crystal too (Fig. 4.23c). Presumably, inhibition of the intramolecular rotation helps in the planarization of the molecule in the crystalline state of compound **SI1**, thus enhancing the fluorescence due to push-pull mechanism. In addition, this arrangement prevents aggregation quenching. Thus π···π stacking, lateral H-bonding, van der Waal's interaction and hydrophobic interactions of alkyl tails as a whole lead to lamellar packing in the crystal structure. In the case of compound **SI2** with six alkyl tails, the increased number of alkyl chains enhances the disorder at the periphery, while maintaining the planarity of the central aromatic core; which allows the columnar stacking. An increase in the number of alkyl tails helps in the stabilization of liquid crystallinity and organogelation in hydrocarbons due to increased fluidity (Fig. 4.26). Thus with the

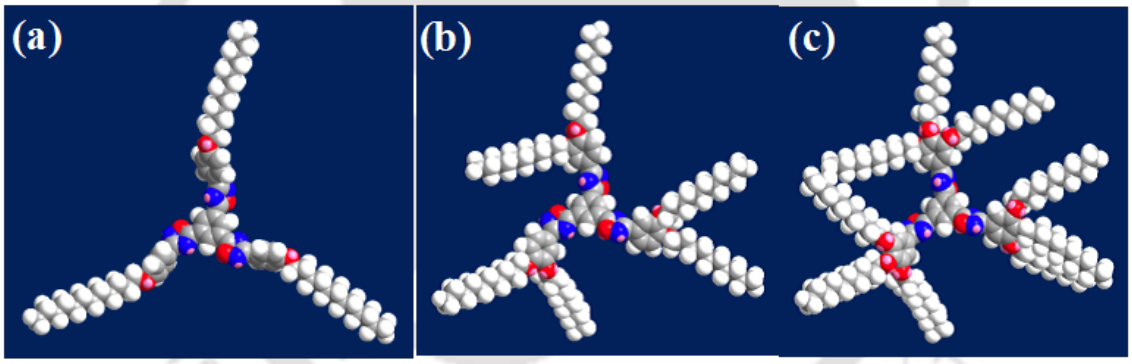


**Figure 4.26.** Energy minimized structures of compounds **SI1** (a); **SI2** (b) and **SI3** (c)

increase in the number of alkyl chains, molecules move from lamellar packing in the crystalline state to columnar packing in liquid crystalline and gel state as in the case of **SI2**. A further increase in the number of alkyl tails disrupts this subtle balance, as in the case of compounds **SI3** and **SI4**, which exhibit only a columnar LC phase, but lose the ability to undergo gelation. A similar behavior was observed in the recently reported series of macrocycles, where the number of peripheral tails played a major role in deciding the type and thermal range of the mesophase.[49]

### 4.3. Conclusions

We have reported a new class of star shaped 1,2,4-oxadiazole derivatives stabilizing the hexagonal columnar phase over a broad temperature range. Their thermal behavior was analyzed with the help of polarizing optical microscopy, differential scanning calorimetry and X-ray diffraction studies. The number and length of the peripheral chains affected the mesophase stability and the thermal range. Compounds with three peripheral tails was crystalline and showed the lamellar packing as evidenced from single crystal XRD studies. The compounds required at least six alkyl tails at the periphery to stabilize the columnar hexagonal mesophase. The thermal range of the mesophase increased with the number of alkyl chains. An increase in the chain length reduced the thermal range of the columnar hexagonal phase. All the compounds showed weak fluorescence in the solution state but strong emission in the solid state. In the solid-state emission the compounds showed a red shift with the increase in the number of peripheral chains. Compounds with six alkyl chains showed the ability to self-assemble into freestanding gels in nonpolar solvents. This is the first example of star-shaped supergelators, which form self-standing gels where attractive π-π interactions play a major role. At higher concentrations these compounds forms a mechanically stable, moldable gel. Another property of technological importance is that these compounds shows aggregation-induced blue light emission, which is twelve times greater than the monomer emission. By photophysical studies of thin films and gels it is revealed that in the former case these compounds form J-aggregate, while in the later case they form H-aggregates. Rheological studies confirmed the thixotropic nature of the gels. The xerogels were characterized with the help of scanning electron microscopy, transmission electron microscopy, atomic force microscopy, fluorescence microscopy and polarizing optical microscopy. These microscopic techniques confirmed a highly interwoven network of fibers. Fluorescence microscopy revealed that these fibers were fluorescent due to the aggregation-induced emission phenomenon. Polarizing optical microscopy of the xerogel films showed a birefringent texture, which is evidence to the anisotropic nature of self-assembly. X-ray diffraction studies revealed that the molecules are organized to form a

Col phase with rectangular symmetry. Considering the dearth of wide band gap, solid-state blue light emitting organic materials, these star shaped molecules are promising, due to their emissive nature in the aggregated state and columnar self-assembly. They have great potential in the field of solid-state emissive displays.

### 4.4. Experimental Section

In this section the detailed synthetic procedures and the molecular structural characterization data have been presented for the intermediates and target compounds mentioned in the scheme 4.1. Some intermediates **1c** and **4b** are reported and described in earlier chapters 2 and 3.

Procedure for the synthesis of (3,4,5-tris(decyloxy)phenyl)methanol (**8c**):[29b]

To a stirred suspension of lithium aluminium hydride (LAH) (18.2 mmol, 1.5 equiv.) in dry THF (20 ml) under nitrogen atmosphere, added the solution of ethyl 3,4,5-tris(decyloxy) benzoate (12.13 mmol, 1 equiv.) drop wise at 0 $^{o}$C. Then the reaction mixture was allowed to reach room temperature and stirred for 2 h. Excess LAH present was quenched by the addition of moist sodium sulphate. Reaction mixture was extracted with EtOAc (5 × 50 ml). The combined extracts were washed with water, dried over anhyd $Na_2SO_4$ and concentrated *in vaccuo*. Purification was done by column chromatography over silica gel (60-120) with 10% EtOAc-hexanes as eluent.

$R_f$ = 0.12 (10% EtOAc-hexanes), white solid, m.p: 44 – 46$^{o}$C; yield: 75%; IR (KBr pellet): $\nu_{max}$ in cm$^{-1}$ 3412.64, 2922.60, 2852.97, 1592.66, 1466.88, 1440.35, 1335.89, 1233.54, 1121.80, 811.98, 723.09 and 455.56; $^1$H NMR ($CDCl_3$, 400 MHz): δ 6.55 (s, 2H, Ar), 4.58 (s, 2H, $ArCH_2$), 3.91- 3.98 (m, 6H, 3 × $OCH_2$), 1.27-1.82 (m, 48H, 24 × $CH_2$), 0.86 – 0.89 (m, 9H, 3 × $CH_3$); $^{13}$C NMR ($CDCl_3$, 100 MHz): 153.46, 137.75, 136.27, 105.52, 73.65, 69.30, 65.84, 63.30, 33.01, 32.15, 32.12, 30.53, 29.95, 29.89, 29.86, 29.83, 29.80, 29.76, 29.63, 29.57, 26.34, 26.31, 25.94, 22.89, 14.31; HRMS (ESI+) exact mass calculated for $C_{37}H_{69}O_4$(M+1): 577.5190, Found: 577.5185.

Procedure for the synthesis of (3,4,5-tris(dodecyloxy)phenyl) methanol (**8d**): [29b]

To a stirred suspension of lithium aluminium hydride (LAH) (21.33 mmol, 1.5 equiv.) in dry THF (20 ml) under nitrogen atmosphere, added the solution of ethyl 3,4,5-tris(dodecyloxy) benzoate (14.22 mmol, 1 equiv.) drop wise at 0 $^{o}$C. Then the reaction mixture was allowed to reach room temperature and stirred for 2 h. Excess LAH present was quenched by the addition of moist sodium sulphate. Reaction mixture was extracted with EtOAc (6 × 30 ml). The combined extracts were washed with water, dried over

anhyd $Na_2SO_4$and concentrated *in vaccuo*. Purification was done by column chromatography over silica gel (60-120) with 10% EtOAc-hexanes as eluent.

$R_f$= 0.15 (10% EtOAc-hexanes), white solid, m.p: 52 – 54°C;yield: 80%; IR (KBr pellet): $\nu_{max}$ in $cm^{-1}$ 3417.27, 2922.36, 2852.51, 1590.29, 1467.09, 1438.45, 1334.39, 1231.90, 1124.64, 806.80, 722.27, and 466.28; $^1$H NMR ($CDCl_3$, 400 MHz): δ 6.55 (s, 2H, Ar), 4.59 (s, 2H, $ArCH_2$), 3.91- 3.98 (m, 6H, 3 × $OCH_2$), 1.26- 1.81 (m, 60H, 30 × $CH_2$), 0.86 – 0.89 (m, 9H, 3 × $CH_3$);$^{13}$C NMR ($CDCl_3$, 100 MHz): 153.46, 137.75, 136.27, 105.52, 73.65, 69.29, 65.86, 32.16, 32.14, 30.53, 29.97, 29.95, 29.92, 29.87, 29.84, 29.63, 29.58, 26.35, 26.32, 22.91, 14.33;HRMS (ESI+) exact mass calculated for $C_{43}H_{81}O_4$(M+1): 661.6129, Found: 661.6128.

Procedure for the synthesis of 3,4- bis(decyloxy)benzaldehyde (**9b**):

A mixture of 3,4-dihydroxybenzaldehyde (14.48 mmol, 1equiv.), anhyd. $K_2CO_3$ (60.82 mmol, 4.2 equiv.), *n*-bromodecane (31.86 mmol, 2.2 equiv.) were taken in dry DMF (20 ml) and heated at 80 °C for 17 h under nitrogen atmosphere. Then the reaction mixture was poured into ice-water and extracted with $CH_2Cl_2$. The combined extract was washed with water and brine. Dried over anhyd. $Na_2SO_4$ and concentrated. The crude product was recrystallised with ethanol to get the pure product.

$R_f$ = 0.5 (10% EtOAc-hexanes); white solid, m.p: 62 – 64°C;yield: 80%; IR (KBr pellet): $\nu_{max}$ in $cm^{-1}$ 3341.99, 3086.82, 2953.59, 2921.42, 2850.54, 2754.45, 1687.44, 1591.37, 1438.55, 1394.40, 1345.49, 1235.46, 1132.99, 723.43, 657.51, and 586.51; $^1$H NMR ($CDCl_3$, 400 MHz): δ 9.83(s, 1H, CHO), 7.41 (d, 1H, *J* = 8 Hz, Ar), 7.39 (s, 1H, Ar), 6.95 (d, 1H, *J* = 8 Hz, Ar), 4.03-4.09 (m, 4H, 2× $OCH_2$), 1.27-1.87 (m, 32H, 16 × $CH_2$), 0.86 - 0.89 (m, 6H, 2 × $CH_3$); $^{13}$C NMR ($CDCl_3$, 100 MHz): 191.24, 154.89, 149.64, 130.07, 126.82, 111.95, 111.15, 69.33, 32.12, 29.83, 29.80, 29.78, 29.76, 29.59, 29.56, 29.28, 29.18, 26.19, 26.16, 22.89, 14.32; HRMS (ESI+) exact mass calculated for $C_{27}H_{47}O_3$(M+1): 419.3520, Found: 419.3517.

Procedure for the synthesis of 3,4,5-tris(decyloxy)benzaldehyde **(9c)**:[29b]

An appropriate (3,4,5-tris(decyloxy) phenyl)methanol (8.7 mmol,1 equiv.) was taken in $CH_2Cl_2$ (10 vol.). To this pyridinium chlorochromate (8.7 mmol, 1 equiv.) adsorbed over equal amount of silica gel is added and stirred at room temperature for 1h. The reaction mixture was filtered over celite bed and concentrated to get the crude product, which was further purified by column chromatography on silica gel (60-120) with 10% EtOAc-hexanes as eluent.

$R_f$ = 0.51(10% EtOAc-hexanes), low melting white solid, yield: 70%; IR (KBr pellet): $\nu_{max}$ in $cm^{-1}$ 3369.16, 2950.81, 2923.70, 2852.91, 2728.30, 1742.75, 1695.63, 1585.77, 1439.72, 1382.43, 1332.61, 1228.57, 1117.47, 720.99, 645.56 and 580.35; $^1$H NMR ($CDCl_3$, 400 MHz): δ 9.82 (s, 1H, CHO), 7.08 (s, 2H, Ar), 4.01 - 4.07(m, 6H, 3 × $OCH_2$), 1.27 -1.84 (m, 48H, 24 × $CH_2$), 0.86 – 0.89 (m, 9H, 3 × $CH_3$); $^{13}$C NMR ($CDCl_3$, 100

MHz): 191.55, 153.72, 144.00, 131.63, 108.01, 73.84, 69.41, 32.15, 32.12, 30.54, 29.93, 29.88, 29.84, 29.79, 29.76, 29.59, 29.56, 29.45, 26.28, 26.23, 22.90, 14.33; HRMS (ESI+) exact mass calculated for $C_{37}H_{67}O_4$(M+1): 575.5034, Found: 575.5033.

Procedure for the synthesis of 3,4,5-tris(dodecyloxy)benzaldehyde (**9d**): [29b]

An appropriate (3,4,5-tris(dodecyloxy) phenyl)methanol (11.3 mmol,1 equiv.) was taken in $CH_2Cl_2$ (10 vol.). To this pyridinium chlorochromate (11.3 mmol, 1 equiv.) adsorbed over equal amount of silica gel is added and stirred at room temperature for 1h.The reaction mixture was filtered over celite bed and concentrated to get the crude product, which was further purified by column chromatography on silica gel (60-120) with 10% EtOAc-hexanes as eluent.

$R_f$ = 0.53 (10% EtOAc-hexanes), white solid, m.p: 49 – 51$^o$C; yield: 81%; IR (KBr pellet): $\nu_{max}$ in cm$^{-1}$ 3441.06, 2956.36, 2919.21, 2849.30, 2729.23, 1695.12, 1584.10, 1439.42, 1381.82, 1336.74, 1226.84, 1119.30, 720.33, 645.33 and 579.48; $^1$H NMR ($CDCl_3$, 400 MHz): δ 9.83(s, 1H, CHO), 7.08 (s, 2H, Ar), 4.01 - 4.07(m, 6H, 3 × $OCH_2$), 1.18-1.84 (m, 60H, 30 × $CH_2$), 0.86 – 0.89 (m, 9H, 3 × $CH_3$); $^{13}$C NMR ($CDCl_3$, 100 MHz): 191.52, 153.74, 144.08, 131.66, 108.07, 73.85, 69.45, 32.14, 30.56, 29.97, 29.94, 29.92, 29.88, 29.85, 29.76, 29.60, 29.47, 26.29, 26.25, 22.92, 14.33; HRMS (ESI+) exact mass calculated for $C_{43}H_{79}O_4$(M+1): 659.5973, Found:659.5975.

Procedure for the synthesis of 4-decyloxy benzonitrile (**10a**):

A mixture of 4-dihydroxybenzaldehyde (41.97 mmol, 1equiv.), anhyd. $K_2CO_3$ (92.34 mmol, 2.2 equiv.), *n*-bromodecane (46.17 mmol, 1.1 equiv.) were taken in dry DMF (20 ml) and heated at 80 $^o$C for 17 h under nitrogen atmosphere. Then the reaction mixture was poured into ice-water and extracted with $CH_2Cl_2$. The combined extract was washed with water and brine. Dried over anhyd. $Na_2SO_4$ and concentrated. The crude product was recrystallised with ethanol to get the pure product.

$R_f$ = 0.53 (10% EtOAc-hexanes), low melting white solid, yield: 80%; IR (KBr pellet): $\nu_{max}$ in cm$^{-1}$ 2920.38, 2851.64, 2556.48, 2218.96, 1606.75, 1573.82, 1508.08, 1470.06, 1396.50, 1258.77, 1118.93, 832.93, 808.98 and 715.49; $^1$H NMR ($CDCl_3$, 600 MHz): δ 7.57 (d, 2H, *J* = 6 Hz, Ar), 6.93 (d, 2H, *J* = 6 Hz, Ar), 3.99 (t, 2H, *J* = 6 Hz, 1 × $OCH_2$), 1.24-1.81 (m, 16H, 8 × $CH_2$), 0.88 (t, 3H, *J* = 6 Hz, 1 × $CH_3$); $^{13}$C NMR ($CDCl_3$, 100 MHz): 162.67, 134.16, 119.55, 115.37, 103.82, 68.63, 32.08, 29.73, 29.51, 29.18, 26.13, 22.88, 14.31; HRMS (ESI+) exact mass calculated for $C_{17}H_{26}NO$(M+1): 260.2009, Found: 260.1999.

Procedure for the synthesis of 3,4-bis(decyloxy) benzonitrile (**10b**): [30]

3,4-bis(decyloxy) benzaldehyde (9.55mmol, 1equiv.) was added to a solution of hydroxyl amine hydrochloride (17.68mmol, 1.85equiv.) in DMSO (19.1mL), and the resulting reaction solution was stirred and heated for 3hrs at 100 $^o$C. After cooling to room

temperature, water was added to the reaction mixture, which was then extracted with chloroform (5× 20mL). The combined chloroform layers were washed with water (4× 20mL) and dried with sodium sulfate. Removal of chloroform by rotatory evaporation and high vacuum yielded the desired product which was then recrystallised with ethanol to get the pure product.

$R_f$ = 0.6 (10% EtOAc-hexanes), white solid, m.p: 77 – 78°C; yield: 70%; IR (KBr pellet): $\nu_{max}$ in $cm^{-1}$ 2920.20, 2850.27, 2220.44, 1597.05, 1518.72, 1467.71, 1422.67, 1278.38, 1242.48, 1138.03, 988.18, 808.27 and 722.14;$^1$H NMR ($CDCl_3$, 400 MHz): δ 7.23 (dd, 1H, *J* = 1.2 Hz, *J* = 8Hz, Ar), 7.06-7.07 (m, 1H, Ar), 6.86 (d, 1H, *J* = 8 Hz, Ar), 3.96-4.04(m, 4H, 2 × $OCH_2$), 1.27-1.85 (m, 32H, 16 × $CH_2$), 0.86-0.89(m, 6H, 2 × $CH_3$); $^{13}$C NMR ($CDCl_3$, 100MHz):153.30, 149.28, 126.52, 119.66, 116.27, 112.94, 103.71, 69.67, 69.33, 32.12, 29.80, 29.76, 29.55, 29.24, 29.16, 26.14, 22.89, 14.32; HRMS (ESI+) exact mass calculated for $C_{27}H_{46}NO_2$(M+1): 416.3523, Found: 416.3419.

Procedure for the synthesis of 3,4,5-tris(decyloxy) benzonitrile (**10c**): [30]

3,4,5-tris(decyloxy) benzaldehyde (5.9mmol, 1equiv.) was added to a solution of hydroxyl amine hydrochloride (10.92mmol, 1.85equiv.) in DMSO( 11.8mL), and the resulting reaction solution was stirred and heated for 3hrs at 100 °C. After cooling to room temperature, water was added to the reaction mixture, which was then extracted with chloroform (5× 20mL). The combined chloroform layers were washed with water (4× 20mL) and dried with sodium sulfate. Removal of chloroform by rotatory evaporation and high vacuum yielded the desired product which was then recrystallised with ethanol to get the pure product.

$R_f$ = 0.65 (10% EtOAc-hexanes), white solid, m.p: 50 – 52°C; yield: 80%; IR (KBr pellet): $\nu_{max}$ in $cm^{-1}$ 2922.87, 2852.85, 2225.51, 1580.96, 1500.88, 1465.41, 1431.78, 1239.49, 1121.99, 813.75 and 720.49; $^1$H NMR ($CDCl_3$, 600 MHz): δ 6.81(s, 2H, Ar), 4.00(t, 2H, *J* = 6 Hz, 1 × $OCH_2$), 3.95 (t, 4H, *J* = 6 Hz, 2 × $OCH_2$), 1.24-1.82 (m, 48H, 24 × $CH_2$), 0.88(t, 9H, *J* = 6 Hz, 3 × $CH_3$); $^{13}$C NMR ($CDCl_3$, 150MHz): 153.65, 142.71, 119.44, 110.69, 106.37, 73.90, 69.61, 32.12, 32.10, 30.48, 29.90, 29.85, 29.79, 29.76, 29.72, 29.57, 29.53, 29.37, 26.20, 22.88, 14.29; HRMS (ESI+) exact mass calculated for $C_{37}H_{66}NO_3$(M+1): 572.5037, Found:572.5037.

Procedure for the synthesis of 3,4,5-tris(dodecyloxy) benzonitrile (**10d**): [30]

3,4,5- tris(dodecyloxy)benzaldehyde (3.03mmol, 1equiv.) was added to a solution of hydroxyl amine hydrochloride (5.614mmol, 1.85equiv.) in DMSO (6mL), and the resulting reaction solution was stirred and heated for 3hrs at 100°C. After cooling to room temperature, water was added to the reaction mixture, which was then extracted with chloroform (5× 20mL). The combined chloroform layers were washed with water (4× 20mL) and dried with sodium sulfate. Removal of chloroform by rotatory evaporation and high vacuum yielded the desired product which was then recrystallised with ethanol to get the pure product.

$R_f$ = 0.67 (10% EtOAc- hexanes), white solid, m.p: 62 – 63 $^oC$; yield: 78%;IR (KBr pellet): $\nu_{max}$ in $cm^{-1}$ 2921.22, 2851.17, 2225.45, 1580.94, 1502.67, 1467.20, 1431.38, 1239.70, 1122.57, 832.19 and 720.40; $^1H$ NMR ($CDCl_3$, 600 MHz): δ 6.81(s, 2H, Ar), 4.00(t, 2H, $J$ = 6 Hz, 1 × $OCH_2$), 3.94 – 3.97 (m, 4H, 2 × $OCH_2$), 1.23-1.82 (m, 60H, 30 × $CH_2$), 0.88 (t, 9H, $J$ = 6 Hz, 3 × $CH_3$); $^{13}C$ NMR ($CDCl_3$, 100MHz): 153.63, 142.62, 119.49, 110.61, 106.35, 73.91, 69.57, 32.14, 30.48, 29.95, 29.92, 29.89, 29.86, 29.82, 29.73, 29.60, 29.57, 29.55, 29.35, 26.21, 22.90, 14.32; HRMS (ESI+) exact mass calculated for $C_{43}H_{78}NO_3$(M+1): 656.5976, Found:656.5853.

Procedure for the synthesis of 4-(decyloxy)-*N'*-hydroxybenzimidamide(**11a**): [31b]

To a stirred solution of 4 -decyloxy benzonitrile (30.84 mmol, 1equiv.) in ethanol (20ml) was added hydroxylamine hydrochloride (67.85 mmol, 2.2 equiv.) and then triethylamine (70.94 mmol, 2.3 equiv.) was added. The solution was stirred under reflux for 18h and then diluted with water. Ethanol was removed under reduced pressure and the aqueous layer extracted 2 times with DCM. The combined organic phases were dried over $Na_2SO_4$, evaporated under reduced pressure as the residue purified by recrystallization (ethanol) to afford the title compound as a white solid.

$R_f$ = 0.5 (40% EtOAc-hexanes), white solid, m.p: 112 – 114$^oC$, yield: 85%; IR (KBr pellet): $\nu_{max}$ in $cm^{-1}$ 3448.41, 3350.58, 2921.52, 2852.69, 1652.88, 1610.28, 1519.12, 1390.54, 1251.93 and 826.64;$^1H$ NMR ($CDCl_3$, 600 MHz): δ 7.55(d, 2H, $J$ = 6 Hz, Ar), 6.90 (d, 2H, $J$ = 12 Hz, Ar), 4.82 (s, 2H, $NH_2$), 3.97(t, 2H, $J$ = 6 Hz, 1 × $OCH_2$), 1.25 - 1.81 (m, 16H, 8 × $CH_2$), 0.88(t, 3H, $J$ = 6Hz, 1 × $CH_3$); $^{13}C$ NMR ($CDCl_3$, 100MHz): 160.78, 152.80, 127.37, 124.82, 114.73, 68.32, 32.11, 29.79, 29.60, 29.54, 29.40, 26.23, 22.90, 14.34; HRMS (ESI+) exact mass calculated for $C_{17}H_{29}N_2O_4$(M+1): 293.2224, Found: 293.2220.

Procedure for the synthesis of 3,4-bis(decyloxy)-*N'*-hydroxybenzimidamide(**11b**): [31b]

To a stirred solution of 3,4-bis(decyloxy) benzonitrile ( 6.01 mmol, 1equiv.) in ethanol (10ml) was added hydroxylamine hydrochloride (13.23 mmol, 2.2 equiv. ) and then triethylamine ( 13.82 mmol, 2.3 equiv.) was added. The solution was stirred under reflux for 18h and then diluted with water. Ethanol was removed under reduced pressure and the aqueous layer extracted 2 times with DCM. The combined organic phases were dried over $Na_2SO_4$, evaporated under reduced pressure as the residue purified by recrystallization (ethanol) to afford the title compound as a white solid.

$R_f$ = 0.58 (40% EtOAc-hexanes), white solid, m.p: 77 – 78$^oC$; yield: 82%; IR (KBr pellet): $\nu_{max}$ in $cm^{-1}$ 3452.31, 2953.80, 2922.91, 2852.18, 1638.91, 1522.08, 1384.51, 1264.04 and 807.26; $^1H$ NMR ($CDCl_3$, 400 MHz): δ 7.18(s, 1H, Ar), 7.12 (d, 1H, $J$ = 8 Hz, Ar), 6.86 (d, 1H, $J$ = 8.4 Hz, Ar) 4.85 (s, 2H, $NH_2$), 3.99 - 4.02 (m, 4H, 2 × $OCH_2$), 1.26-1.81 (m, 32H, 16 × $CH_2$), 0.86 – 0.89 (m, 6H, 2× $CH_3$); $^{13}C$ NMR ($CDCl_3$, 100MHz):153.05, 150.97, 149.33, 125.32, 118.67, 113.37, 111.63, 69.56, 69.44, 32.13,

29.85, 29.80, 29.63, 29.57, 29.47, 29.41, 26.25, 26.22, 22.90, 14.31; HRMS (ESI+) exact mass calculated for $C_{27}H_{49}N_2O_3$(M+1): 449.3738, Found:449.3661.

Procedure for the synthesis of 3,4,5-tris(decyloxy)-*N'*-hydroxybenzimidamide (**11c**):[31b]

To a stirred solution of 3,4,5–tris(decyloxy)benzonitrile ( 3.5 mmol, 1equiv.) in ethanol (5ml) was added hydroxylamine hydrochloride ( 7.69 mmol, 2.2 equiv. ) and then triethylamine ( 8.05 mmol, 2.3 equiv.) was added. The solution was stirred under reflux for 18h and then diluted with water. Ethanol was removed under reduced pressure and the aqueous layer extracted 2 times with DCM. The combined organic phases were dried over $Na_2SO_4$, evaporated under reduced pressure as the residue purified by recrystallization (ethanol) to afford the title compound as a white solid.

$R_f$ = 0.6 (40% EtOAc-hexanes), white solid, m.p: 66 - 68°C; yield: 72%; $\nu_{max}$ in $cm^{-1}$ 3440.43, 2922.26, 2851.53, 1633.54, 1583.77, 1512.26, 1379.12, 1239.39 and 942.71; $^1$H NMR ($CDCl_3$, 400 MHz): δ 6.80 (s, 2H, Ar), 4.83 (s, 2H, $NH_2$), 3.94-3.99 (m, 6H, 3 × $OCH_2$), 1.27-1.81(m, 48H, 24 × $CH_2$), 0.86 – 0.89 (m, 9H, 3 × $CH_3$);$^{13}$C NMR ($CDCl_3$, 100MHz):153.43, 153.28, 139.99, 127.69, 104.79, 73.69, 69.44, 32.15, 32.12, 30.52, 29.95, 29.89, 29.86, 29.81, 29.63, 29.57, 26.30, 22.90, 14.32; HRMS (ESI+) exact mass calculated for $C_{37}H_{69}N_2O_4$(M+1): 605.5252, Found: 605.5289.

Procedure for the synthesis of 3,4,5-tris(dodecyloxy)-*N*'-hydroxybenzimidamide (**11d**):[31b]

To a stirred solution of 3,4,5–tris(dodecyloxy) benzonitrile ( 2.29 mmol, 1equiv.) in ethanol (5ml) was added hydroxylamine hydrochloride ( 5.04 mmol, 2.2 equiv. ) and then triethylamine ( 5.27 mmol, 2.3 equiv.) was added. The solution was stirred under reflux for 18h and then diluted with water. Ethanol was removed under reduced pressure and the aqueous layer extracted 2 times with DCM. The combined organic phases were dried over $Na_2SO_4$, evaporated under reduced pressure as the residue purified by recrystallization (ethanol) to afford the title compound as a white solid.

$R_f$ = 0.62(40% EtOAc-hexanes), white solid, m.p: 74 – 75°C; yield: 70%; $\nu_{max}$ in $cm^{-1}$3440.88, 3354.89, 2945.26, 2921.07, 2850.12, 1634.03, 1582.24, 1511.82, 1371.52, 1240.11, 941.74; 1H NMR ($CDCl_3$, 600 MHz): δ 6.81 (s, 2H, Ar), 4.81 (s, 2H, $NH_2$), 3.95-3.99 (m, 6H, 3 × $OCH_2$), 1.23 - 1.82 (m, 60H, 30 × $CH_2$), 0.88 (t, 9H, $J$ = 6 Hz, 3 × $CH_3$); $^{13}$C NMR ($CDCl_3$, 100MHz): 153.44, 153.26, 139.98, 127.69, 104.78, 73.69, 69.44, 32.16, 32.14, 30.53, 29.97, 29.95, 29.92, 29.87, 29.82, 29.63, 29.61, 29.59, 26.32, 22.91, 14.34; HRMS (ESI+) exact mass calculated for $C_{43}H_{81}N_2O_4$(M+1): 689.6191, Found: 689.6191.

Procedure for the synthesis of 5-(3,5-bis(3-(4-(decyloxy)phenyl)-1,2,4-oxadiazol-5-yl)phenyl)-3-(4-(decyloxy)phenyl)-1,2,4-oxadiazole **(SI1)** [20a]

A mixture of 4-(decyloxy)-N'-hydroxybenzimidamide (1.11mmol, 3.1 equiv.) and dry pyridine (8ml) was stirred under Ar atmosphere at 0 $^{o}$C. To this, a solution of benzene-1,3,5-tricarboyl trichloride (0.36 mmol, 1 equiv.) in dry THF was added drop wise. The reaction mixture was refluxed for 12 h and then poured into cold water. The whole mass (a mixture of solid and water) was extracted with chloroform (2 × 100 ml). The combined extracts were washed with water, brine, dried over anhyd. $Na_2SO_4$ and concentrated under reduced pressure. The crude product was purified by column chromatography on neutral alumina. Elution with 20% $CH_2Cl_2$ hexanes yielded the desired product. Recrystallization with ethylacetate gives the pure product.

$R_f$ = 0.5 (60%$CH_2Cl_2$-hexane), colorless crystals, m.p: 128 – 130$^{o}$C; yield: 60%; $\nu_{max}$ in $cm^{-1}$ 2922.62, 2851.59, 1609.91, 1543.21, 1471.52, 1355.16, 1252.64, 1171.24, 759.28; $^1$H NMR ($CDCl_3$, 400 MHz): δ 9.15 (s, 3H, Ar), 8.13 (d, 6H, *J* = 8.8 Hz, Ar), 7.01 (d, 6H, *J* = 8.8 Hz, Ar), 4.02(t, 6H, *J* = 6.4 Hz, 3 × $OCH_2$), 1.23-1.84(m, 48H, 24 × $CH_2$), 0.89(t, 9H, *J* = 6.4 Hz, 3 × $CH_3$); $^{13}$C NMR ($CDCl_3$, 100MHz): 173.28, 169.31, 162.06, 130.71, 129.46, 126.85, 118.72, 115.05, 68.43, 32.12, 29.79, 29.63, 29.55, 29.41, 26.25, 22.91, 14.34; MALDI-TOF exact mass calculated for $C_{60}H_{81}N_6O_6$(M+3H): 981.6207, Found:981.6210.

Procedure for the synthesis of 3-(3,4-bis(decyloxy)phenyl)-5-(3,5-bis(3-(3,4-bis(decyloxy)phenyl)-1,2,4-oxadiazol-5-yl)phenyl)-1,2,4-oxadiazole (**SI2**): [20a]

A mixture of 3,4-bis(decyloxy)-*N'*-hydroxybenzimidamide (1.11mmol, 3.1 equiv.) and dry pyridine (8ml) was stirred under Ar atmosphere at 0 $^{o}$C. To this, a solution of benzene-1,3,5-tricarboyl trichloride (0.36 mmol, 1 equiv.) in dry THF was added drop wise. The reaction mixture was refluxed for 12 h and then poured into cold water. The whole mass (a mixture of solid and water) was extracted with chloroform (2 × 100 ml). The combined extracts were washed with water, brine, dried over anhyd. $Na_2SO_4$ and concentrated under reduced pressure. The crude product was purified by column chromatography on neutral alumina. Elution with 20% $CH_2Cl_2$ hexanes yielded the desired product. Recrystallization with ethylacetate gives the pure product.

$R_f$ = 0.58 (60%$CH_2Cl_2$-hexane), white solid, yield: 60%; $\nu_{max}$ in $cm^{-1}$ 2922.30, 2851.61, 1607.97, 1546.77, 1462.74, 1386.22, 1262.72, 1131.83 and 752.12; $^1$H NMR ($CDCl_3$, 400 MHz): δ 9.24(s, 3H, Ar), 7.80 – 7.82 (m, 3H, Ar), 7.70 (s, 3H, Ar), 7.00 (d, 3H, *J* = 8.4 Hz, Ar), 4.13 – 4.16(m, 6H, 3× $OCH_2$), 4.09(t, 6H, *J* = 8Hz, 3 × $OCH_2$), 1.29-1.91(m, 96H, 48 × $CH_2$), 0.86-0.89(m,18H, 6 × $CH_3$); $^{13}$C NMR ($CDCl_3$, 100MHz): 173.30, 169.47, 152.25, 149.52, 130.75, 126.82, 121.35, 118.86, 113.18, 112.30, 69.59, 69.32, 32.15, 29.88, 29.84, 29.71, 29.66, 29.60, 29.51, 29.40, 26.31, 26.25, 22.92, 14.33. MALDI-TOF exact mass calculated for $C_{90}H_{141}N_6O_9$(M+3H): 1450.0744, Found: 1450.0170.

Procedure for the synthesis of 3-(3,4,5-tris(decyloxy)phenyl)-5-(3,5-bis(3-(3,4,5-tris(decyloxy)phenyl)-1,2,4-oxadiazol-5-yl)phenyl)-1,2,4-oxadiazole (**SI3**): [20a]

A mixture of 3,4,5-tris(decyloxy)-*N'*-hydroxybenzimidamide (0.9 mmol, 3.1 equiv.) and dry pyridine (8ml) was stirred under Ar atmosphere at 0 $^{o}$C. To this, a solution of benzene-1,3,5-tricarboyl trichloride (0.29 mmol, 1 equiv.) in dry THF was added drop wise. The reaction mixture was refluxed for 12 h and then poured into cold water. The whole mass (a mixture of solid and water) was extracted with chloroform (2 × 100 ml). The combined extracts were washed with water, brine, dried over anhyd. $Na_2SO_4$ and concentrated under reduced pressure. The crude product was purified by column chromatography on neutral alumina. Elution with 20% $CH_2Cl_2$ hexanes yielded the desired product. Recrystallization with ethylacetate gives the pure product.

$R_f$ = 0.6 (60%$CH_2Cl_2$-hexane), white solid, yield: 56%; $\nu_{max}$ in $cm^{-1}$ 2921.00, 2850.86, 1603.26, 1551.65, 1441.02, 1396.59, 1353.69, 1235.95, 1125.41 and 750.74; $^{1}$H NMR ($CDCl_3$, 400 MHz): δ 9.27(s, 3H, Ar), 7.43 (s, 6H, Ar), 4.11 – 4.14(m, 12H, 6× $OCH_2$), 4.04 – 4.07(m, 6H, 3 × $OCH_2$), 1.28-1.89 (m, 144H, 72 × $CH_2$), 0.86-0.88(m, 27H, 9 × $CH_3$);$^{13}$C NMR ($CDCl_3$, 150MHz): 173.49, 169.76, 153.88, 141.42, 131.03, 126.93, 121.14, 106.26, 73.83, 69.59, 32.16, 30.61, 29.89, 29.84, 29.64, 29.39, 26.39, 22.91, 14.32. MALDI-TOF exact mass calculated for $C_{120}H_{200}N_6O_{12}$(M+2H): 1917.5213, Found:1917.285.

Procedure for the synthesis of 3-(3,4,5-tris(dodecyloxy)phenyl)-5-(3,5-bis(3-(3,4,5-tris(dodecyloxy)phenyl)-1,2,4-oxadiazol-5-yl)phenyl)-1,2,4-oxadiazole(**SI4**): [20a]

A mixture of 3,4,5-tris(dodecyloxy)-*N*'-hydroxybenzimidamide (0.91 mmol, 3.1 equiv.) and dry pyridine (8ml) was stirred under Ar atmosphere at 0 $^{o}$C. To this, a solution of benzene-1,3,5-tricarboyl trichloride (0.29 mmol, 1 equiv.) in dry THF was added drop wise. The reaction mixture was refluxed for 12 h and then poured into cold water. The whole mass (a mixture of solid and water) was extracted with chloroform (2 × 100 ml). The combined extracts were washed with water, brine, dried over anhyd. $Na_2SO_4$ and concentrated under reduced pressure. The crude product was purified by column chromatography on neutral alumina. Elution with 20% $CH_2Cl_2$ hexanes yielded the desired product. Recrystallization with ethylacetate gives the pure product.

$R_f$ = 0.65 (60%$CH_2Cl_2$-hexane), white solid, yield: 55%; $\nu_{max}$ in $cm^{-1}$ 2920.97, 2850.96, 1603.54, 1551.60, 1466.76, 1396.15, 1235.37, 1125.00 and 750.33; $^{1}$H NMR ($CDCl_3$, 400 MHz): δ 9.27(s, 3H, Ar), 7.43 (s, 6H, Ar), 4.06 – 4.14(m, 18H, 9× $OCH_2$), 1.27-1.88 (m, 180H, 90 × $CH_2$), 0.86-0.89 (m, 27H, 9 × $CH_3$); $^{13}$C NMR ($CDCl_3$, 100MHz): 173.47, 169.73, 153.84, 141.28, 126.89, 121.12, 110.23, 106.11, 73.81, 69.51, 32.15, 30.60, 29.99, 29.95, 29.93, 29.89, 29.84, 29.69, 29.60, 26.39, 26.34, 22.92, 14.34. MALDI-TOF exact mass calculated for $C_{138}H_{237}N_6O_{12}$(M+3H): 2170.8109, Found: 2170.6540.

## 4.5. References


1. (a) J. W. Goodby, P. J. Collings, T. Kato, C. Tschierske, H. Gleeson and P. Raynes, *Handbook of Liquid Crystals: Fundamentals*, *Wiley-VCH, Weinheim, Germany*, 2014, vol. **1**; (b) T. Wöhrle, I. Wurzbach, J. Kirres, A. Kostidou, N. Kapernaum, J. Litterscheidt, J. C. Haenle, P. Staffeld, A. Baro, F. Giesselmann, and S. Laschat, *Chem. Rev.*, 2016, **116** (3), 1139–1241; (c) X. Li, B. Li, L. Chen, J. Hu, C. Wen, Q. Zheng, L. Wu, H. Zeng, B. Gong and L. Yuan, Angew.Chem. Int.Ed., 2015, **54**,11147 –11152.
2. (a) P. Dastidar, *Chem. Soc. Rev.*, 2008, **37**, 2699-2715; (b) S. S. Babu, V. K. Praveen and A. Ajayaghosh, *Chem. Rev.*, 2014, **114** (4), 1973-2129.
3. (a) S. S. Babu, S. Prasanthkumar and A. Ajayaghosh, *Angew. Chem., Int. Ed.*, 2012, **51**, 1766-1776; (b) S. Diring, F. Camerel, B. Donnio, T. Dintzer, S. Toffanin, R. Capelli, M. Muccini and R. Ziessel, *J. Am. Chem. Soc.*, 2009, **131**, 18177-18185.
4. (a) J. H. Jung, Y. Ono and S. Shinkai, *Angew. Chem., Int. Ed.*, 2000, **39**, 1862-1865; (b) S. Kobayashi, N. Hamasaki, M. Suzuki, M. Kimura, H. Shirai and K. Hanabusa, *J. Am. Chem. Soc.*, 2002, **124**, 6550-6551; (c) E. D. Sone, E. R. Zubarev and S. I. Stupp, *Angew. Chem., Int. Ed.*, 2002, **41**, 1705-1709; (d) G. Gundiah, S. Mukhopadhyay, U. G. Tumkurkar, A. Govindaraj, U. Maitra and C.N.R. Rao, *J. Mater. Chem*., 2003, **13**, 2118-2122.
5. C. Wang, Q. Chen, F. Sun, D. Zhang, G. Zhang, Y. Huang, R. Zhao and D. Zhu, *J. Am. Chem. Soc*., 2010, **132**, 3092-3096.
6. (a) Z. Zhao, J. W. Y. Lam and B. Z. Tang, *J. Mater. Chem.*, 2012, **22**, 23726-23740; (b) Z. Zhao, J. W. Y. Lam and B. Z. Tang, *Soft Matter* 2013, **9**, 4564-4579; (c) Y. Zhang, C. Liang, H. Shang, Y. Ma and S. Jiang, *J. Mater. Chem. C*, 2013, **1**, 4472-4480; (d) P. Xue, R. Lu, G. Chen, Y. Zhang, H. Nomoto, M. Takafuji and H. Ihara, *Chem. - Eur. J.* 2007, **13**, 8231-8239.
7. (a) R. Hu, N. L. C. Leung and B. Z. Tang, *Chem. Soc. Rev.*, 2014, **43**, 4494-4562; (b) Y. Hong, J. W. Y. Lam and B. Z. Tang, *Chem. Soc. Rev.*, 2011, **40**, 5361-5388; (c) B. Z. Tang and A. Qin, *Wiley-VCH Verlag GMBH: Weinheim*, 2013; (d) Y. Hong, J. W. Y. Lama and B. Zhong Tang, *Chem. Commun.*, 2009, 4332-4353.
8. (a) P. I. Shih, C. Y. Chuang, C. H. Chien, E. W. G. Diau and C. F. Shu, *Adv. Funct. Mater.*, 2007, **17**, 3141-3146; (b) H. C. Li, Y. P. Lin, P. T. Chou, Y. M. Cheng and R. S. Liu, *Adv. Funct. Mater.*, 2007, **17**, 520-530; (c) C. J. Tonzola, A. P. Kulkarni, A. P. Gifford, W. Kaminsky and S. A. Jenekhe, *Adv. Funct. Mater.*, 2007, **17**, 863-874.
9. (a) Z. Zhao, S. Chen, J. W. Y. Lam, P. Lu, Y. Zhong, K. S. Wong, H. S. Kwok and B. Z. Tang, *Chem. Commun.*, 2010, **46**, 2221-2223; (b) Z. Zhao, J. W. Y. Lam and B. Z. Tang, *J. Mater. Chem.*, 2012, **22**, 23726-23740.
10. (a) I. Abu Bin, S. Takahiro and T. Yukikazu, *Polym. J.*, 2010, **42**, 839-851; (b) A. Harada, R. Kobayashi, Y. Takashima, A. Hashidzume and H.Yamaguchi, *Nat. Chem.*, 2011, **3**, 34-37; (c) T. Yamamoto and M. Yoshida, *Langmuir*, 2012, **28**, 8463-8469; (d) K. Yuichiro, T. Yoshinori, H. Akihito, Y. Hiroyasu and H. Akira,

*Sci. Rep.* 2013, **3**, 1243; (e) M. Zhang, D. Xu, X. Yan, J. Chen, S. Dong, B. Zheng and F. Huang, *Angew. Chem., Int. Ed*., 2012, **51**, 7011-7015; (f) *R.* Yoshida, *Adv. Mater.*, 2010, **22**, 3463-3483.
11. L. E. Buerkle and S. Rowan, *J. Chem. Soc. Rev*., 2012, **41**, 6089-6102.
12. A. P. Sivadas, N. S. S. Kumar, D. D. S. Varghese, S. K. Prasad, D. S. S. Rao and S. Das, *J. Am. Chem. Soc.*, 2014, **136**, 5416-5423.
13. (a) A. J. Attias, C. Cavalli, B. Donnio, D. Guillon, P. Hapiot and J. Malthête, *Chem. Mater.*, 2002, **14**, 375-384; (b) B. Roy, N. De and K. C. Majumdar, *Chem. Eur. J.*, 2012, **18**, 14560-14588; (c) C. V. Yelamaggad, A. S. Achalkumar, D. S. Shankar Rao, and S. Krishna Prasad, *J. Org. Chem*., 2009, **74**, 3168–3171; (d) K. P. Gan, M. Yoshio and T. Kato, *J. Mater. Chem. C*., 2016, **4**, 5073-5080.
14. (a) Y. Shirota, *J. Mater. Chem.*, 2000, **10**, 1-25; (b) D. Apreutesei and G. H. Mehl, *J. Mater. Chem.*, 2007, **17**, 4711-4715.
15. M. L. Parra, P. I. Hidalgo, E. A. Soto-Bustamante, J. Barbera´, E. Y. Elgueta and V. H.Trujillo-Rojo, *Liquid Crystals*, 2008, **35**, 1251-1262.
16. (a) Q. Li, L. S. Cui, C. Zhong, X. D. Yuan, S. C. Dong, Z. Q. Jiang and L. S. Liao, *Dyes and Pigments*, 2014, **101**, 142-149; (b) Q. Li, L.S. Cui, C. Zhong, Z. Q. Jiang and L. S. Liao, *Org. Lett.*, 2014, **16**, 1622-1625.
17. H. Gallardo, R. Cristiano, A. A. Vieiraa, R. A. W. N. Filho, R. M. Srivastava and I. H. Bechtold, *Liquid Crystals*, 2008, **35**, 857-863.
18. S. I. Torgova, L. A. Karamysheva, T. A. Geivandova, A. Strigazzi, *Mol. Cryst. and Liq.Cryst.*, 2001, **365**, 99-106.
19. (a) G. S. Shanker, M. Nagaraj, A. Kocot, J. K. Vij, M. Prehm and C. Tschierske, *Adv. Funct. Mater.*, 2012, **22**, 1671-1683; (b) G. S. Shanker, M. Prehm, M. Nagaraj, J. K. Vij, M. Weyland, A. Eremin and C. Tschierske, *ChemPhysChem*., 2014, **15**, 1323-1335.
20. (a) H. Gallardo, M. Ferreira, A. A. Vieira, E. Westphal, F. Molin, J. Eccher and I. H. Bechtold, *Tetrahedron*, 2011, **67**, 9491-9499; (b) T. E. Frizon, D. S. Rampon, H. Gallardo, A. A. Merlo, P. H. Schneider, O. E. D. Rodrigues, A. L. Braga, *Liquid Crystals*, 2012, **39**, 769-777.
21. H. Gallardo, G. Conte, P. A. Tuzimoto, B. Behramand, F. Molin, J. Eccher and I. H. Bechtold, *Liquid Crystals*, 2012, **39**, 1099-1111.
22. (a) S. V. Subrahmanyam, P. V. Chalapathi, S. Mahabaleswara, M. Srinivasulu and D. M. Potukuchi, *Liquid Crystals*, 2014, **41**, 1130-1151; (b) H. Gallardo, R. Cristiano, A. A. Vieira, R. A. W. N. Filho, R. M. Srivastav and I. H. Bechtold, *Liquid Crystals*, 2008, **35**, 857-863; (c) M. Parra, P. Hidalgo, E. Carrasco, J. Barbera´ and L. Silvino, *Liquid Crystals*, 2006, **33**, 875-882.
23. (a) M. Parra, P. Hidalgo and J. Alderete, *Liquid Crystals*, 2005, **32**, 449-452; (b) M. A. Parra, P. Hidalgo, J. N. Barbera´ and J. Alderete, *Liquid Crystals*, 2005, **32**, 573-577.
24. (a) M. L. Parra, P. I. Hidalgo and E. Y. Elgueta, *Liquid Crystals*, 2008, **35**, 823-832; (b) M. L. Parra, P. I. Hidalgo, E. A. Soto-Bustamante, J. Barbera´, E. Y. Elgueta and V. H. Trujillo-Rojo, *Liquid Crystals*, 2008, **35**,1251-1262.
25. S. Chandrasekhar, B. K. Sadashiva and K. A. Suresh, *Pramana*, 1977, **9**, 471-480.

26. Q. Li, *Self-Organized Organic Semiconductors: From Materials to Device Applications*, John Wiley & Sons: New York, 2011.
27. (a) M. Lehmann, *Chem. -Eur. J.*, 2009, **15**, 3638-3651; (b) M. Lehman, *Top Curr. Sci.*, 2012, **318**, 193−224; (c) M. Lehmann and M. Jahr, *Chem. Mater.*, 2008, **20** (17), 5453-5456; (d) M. Lehmann, R. I. Gearba, M. H. J. Koch and D. A. Ivanov, *Chem. Mater.*, 2004, **16**, 374– 376.
28. V. Percec, M. Glodde, T. K. Bera, Y. Miura, I. Shiyanovskaya, K. D. Singer, V. S. K. Balagurusamy, P. A. Heiney, I. Schnell, A. Rapp, H. -W. Spiess, S. D. Hudson and H. Duan, *Nature*, 2002, **417**, 384-387.
29. (a) A. S. Achalkumar, U. S. Hiremath, D. S. S. Rao, S. K. Prasad and C. V. Yelamaggad, *J. Org. Chem*., 2013, **78**, 527-544; (b) A. S. Achalkumar and C. V. Yelamaggad, *Tetrahedron Lett.*, 2012, **53**, 7108; (c) A. S. Achalkumar, B. N. Veerabhadraswamy, Uma S. Hiremath, D. S. Shankar Rao, S. Krishna Prasad and C. V. Yelamaggad, *Dyes and Pigments*, 2016, **132**, 291-305.
30. S. T. Chill and R. C. Mebane, *Synthetic Commun.*, 2009, **39**, 3601-3606.
31. (a) D. Conole, T. M. Beck, M. Jay-Smith, M. D. Tingle, C. T. Eason, M. A. Brimble and D. Rennison, *Bioorganic & Medicinal Chemistry* 2014, **22**, 2220-2235; (b) A. Kivrak and M. Zora, *Tetrahedron*, 2014, **70**, 817- 831.
32. CCDC 1058790 contains the supplementary crystallographic data for compound **SI1.** These data can be obtained free of charge at www.ccdc.cam.ac.uk/conts/retrieving.html.
33. R. I. Gearba, M. Lehmann, J. Levin, D. A. Ivanov, M. H. J. Koch, J. Barbera, M. G. Debije and J. Piris, Y. H. Geerts, *Adv. Mater*., 2003, **15**, 1614-1618.
34. a) S. Ito, M. Ando, A. Nomura, N. Morita, C. Kabuto, H. Mukai, K. Ohta, J. Kawakami, A. Yoshizawa and A. Tajiri, *J. Org. Chem.*, 2005, **70**, 3939-3949; b) A. Hayer, V. D. Halleux, A. Kohler, A. El-Garoughy, E. W. Meijer, J. Barbera, J. Tant, J. Levin, M. Lehmann, J. Gierschner, J. Cornil and Y. H. Geets, *J. Phys. Chem. B*, 2006, **110** (15), 7653-7659; (c) C. V. Yelamaggad, A. S. Achalkumar, D. S. S. Rao and S. K. Prasad, *J. Mater. Chem.*, 2007, **17**, 4521-4529; (d) C. V. Yelamaggad, A. S. Achalkumar, D. S. S. Rao and S. K. Prasad, *J. Org. Chem.*, 2007, **72** (22), 8308-8318; (e) C. V. Yelamaggad, A. S. Achalkumar, D. S. S. Rao, M. Nobusawa, H. Akutsu, J. Yamada and S. Nakatsuji, *J. Mater. Chem*., 2008, **18**, 3433-3437; (f) A. S. Achalkumar, U. S. Hiremath, D. S. S. Rao, S. K. Prasad and C. V. Yelamaggad, *J. Org. Chem.*, 2013, **78** (2), 527-544; (g) R. K. Gupta, S. K. Pathak, B. Pradhan, M. Gupta, S. K. Pal and A. S. Achalkumar, *ChemPhysChem*., 2016, **17**, 859-872.
35. (a) F. Wu¨rthner, T. E. Kaiser and C. R. Saha-Mu¨ller, *Angew. Chem., Int. Ed*., 2011, **50**, 3376-3410; (b) F. Wu¨rthner, C. Bauer, V. Stepanenko and S. A Yagai, *Adv. Mater*., 2008, **20**, 1695-1698; (c) F. Wu¨rthner, C. Thalacker, S. Diele and C. Tschierske, Dyes. *Chem.–Eur. J*., 2001, **7**, 2245-2253.
36. (a) K.-R. Wee, Y. –J. Cho, S. Jeong, S. Kwon, J. D. Lee, I. H. Suh and S. O Kang, *J. Am. Chem. Soc*., 2012, **134** (43), 17982-17990; (b) P. Venkatakrishnan, P. Natarajan, J. N. Moorthy, Z. Lin and T. J. Chow, *Tetrahedron*, 2012, **68**, 7502-7508.
37. S. Suman and B. Kumar, *Chem. Mater*., 2012, **24** (6), 1165-1173.

38. Q. Wang, J. Mynar, M. Yoshida, E. Lee, M. Lee, K. Okuro, K. Kinbara and T. Aida, *Nature*, 2010, **463,** 339-343.
39. E. R. Zubarev, M. U. Pralle, E. D. Sone and S. I. Stupp, *Adv. Mater*., 2002, **14**, 198-203.
40. (a) D. Gao, M. Xue, J. Peng, J. Liu, N. Yan, P. He and Y. Fang, *Tetrahedron*, 2010, **66**, 2961-2968; (b) Y. Kenji, A. Natsuki, O. Yoshiyuki, A. Tetsuyuki, S. Hideyuki, T. Masayuki, S. Seiji and N. R. David, *Chem. -Eur. J*., 1999, **5**, 2722-2729; (c) A. Vidyasagar, K. Handore and K. M. Sureshan, *Angew.Chem. Int. Ed*., 2011, **50**, 8021-8024.
41. (a) A. Mahler, M. Reches, M. Rechter, S. Cohen and E. Gazit, *Adv. Mater*., 2006, **18**, 1365-1370; (b) L. E. R. O'Leary, J. A. Fallas, E. L. Bakota, M. K. Kang and J. D. Hartgerink*, Nat. Chem*., 2011, **3**, 821-828.
42. (a) B.W. Messmore, J. F. Hulvat, E. D. Sone and S. I. Stupp, *J. Am. Chem. Soc*., 2004, **126** (44), 14452-14458; (b) M. Kasha, H. R. Rawls and M. A. El-Bayoumi, *Pure Appl. Chem*., 1965, **11**, 371-392; (c) D. G. Whitten, *Acc. Chem. Res*., 1993, **26** (9), 502-509; (d) K. C. Hannah and B. A. Armitage, *Acc. Chem. Res*., 2004, **37** (11), 845-853; (e) S. Y. Ryu, S. Kim, J. Seo, Y. -W. Kim, O. –H. Kwon, D. -J. Jang and S. Y. Park, *Chem. Commun*., 2004, 70-71; (f) H. H. Yao, K. Domoto, T. Isohashi, K. Kimura, *Langmuir*, 2005, **21**, 1067-1073.
43. (a) S. Basak, S. Bhattacharya, A. Datta and A. Banerjee, *Chem.– Eur. J*., 2014, **20**, 5721-5726; (b) F. Alexandre, D. J. Marc, G. D. Todor, I. G. Nikolai, A. V. Aleksey and V. Eric, *J. Am. Chem. Soc*., 2006, **128**, 7661-7669; (c) M. Cigan, J. Donovalova, V. Szocs, J. Gaspar, K. Jakusova and A. Gaplovsky, *J. Phys. Chem. A*, 2013, **117**, 4870-4883; (d) Q. Fang, F. Wang, H. Zhao, X. Liu, R. Tu, D. Wang and Z. Zhang, *J. Phys. Chem. B*, 2008, **112**, 2837-2841; (e) V. Lau and B. Heyne, *Chem. Commun*., 2010, **46**, 3595-3597; (f) U. Rosch, S. Yao, R. Wortmann and F. Wurthner, *Angew. Chem., Int. Ed*., 2006, **45**, 7026-7030; (g) L. Liangde, J. L. Rene, L. P. Thomas, P. Jerry and G. W. *J. Am. Chem. Soc*., 1999, **121**, 8146-8156; (h) Y. Seong-Jun, C. Jong Won, G. Johannes, K. Kil Suk, C. Moon-Gun, K. Dongho and P. Soo Young, *J. Am. Chem. Soc*., 2010, **132**, 13675-13683; (i) Y. Seong-Jun and P. SooYoung, *J. Mater. Chem*., 2011, **21**, 8338-8346; (j) C. Jiajia, L. Yan, H. Song, L. Chang, Z. Liancheng and Z. Xianshun, *Chem. Commun*., 2013**, 49**, 6259-6261.
44. D. D. Prabhu, A. P. Sivadas and S. Das, *J. Mater. Chem.*, 2014, **2**, 7039-7046.
45. A. Takahashi, M. Sakai and T. Kato, *Polym. J*., 1980, **12**, 335-341.
46. (a) C. G. Robertson and X. Wang, *Phys. Rev. Lett.*, 2005**, 95**, (7), 075703-075703-6; (b) P. Sollich, F. Lequeux, P. Hebraud and M. E. Cates, *Phys. Rev. Lett.*, 1997**, 78**, (10), 2020-2023; (c) H. M. Wyss, K. Miyazaki, J. Mattsson, Z. Hu, D. R. Reichman and D. A. Weitz, *Phys. Rev. Lett.*, 2007**, 98**, (23), 238303-238303-4; (d) S. K. Pal, A. Agarwal and N. L. Abbott, *Small*, 2009**, 5**, (22), 2589-2596.
47. J. Han, X. -Y. Chang, L. -R. Zhu, Y. -M. Wang, J. -B. Ji-Ben Meng, S. -W. Lai and S. –Y. C. Stephen, *Liquid Cryst.*, 2008, **35**, 1379-1394.
48. D. Lopez and E. M. García-Frutos, *Langmuir*, 2015, **31**, 8697-8702.
49. S. Kawano, Y. Ishida and K. Tanaka, *J. Am. Chem. Soc*., 2015, **137**, 2295−2302.

# Chapter V

# 1,2,4-Oxadiazole based polycatenar mesogens

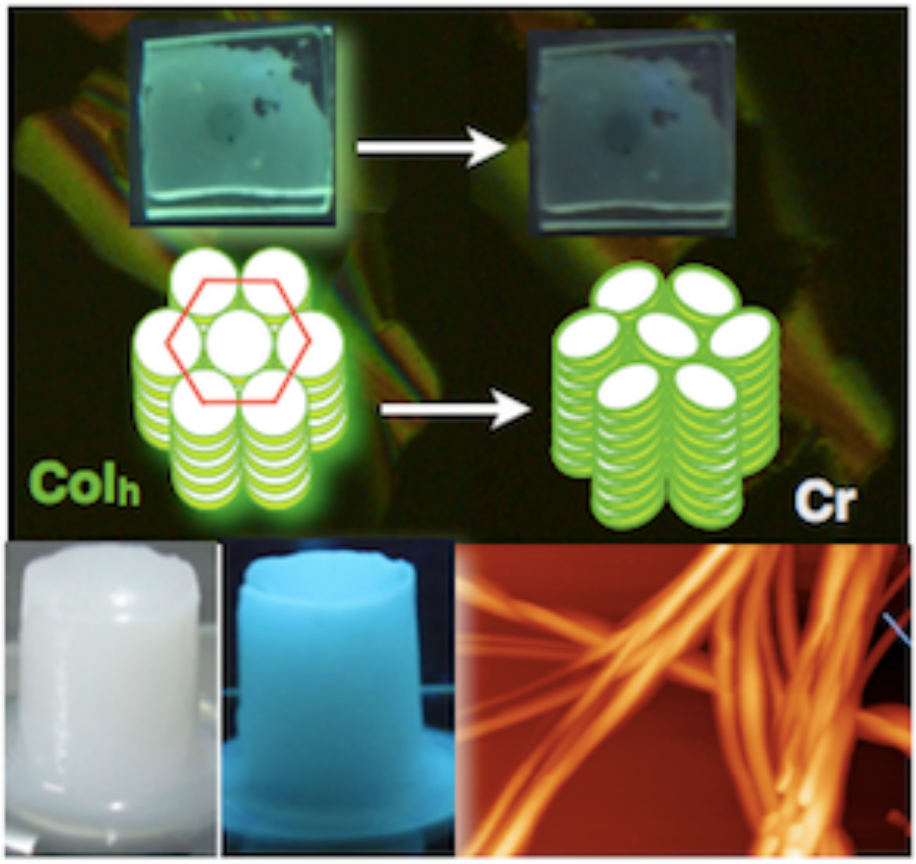


Results have been published in *Chemistry Select*, 2016, **1**, 5107 – 5120.

## 5.1. Introduction

The self-assembly of organic molecules into well-defined macroscopic self-assemblies that perform desired functions requires careful molecular engineering keeping in mind that, how these functional molecules behave in bulk or in a medium. Liquid crystals (LC) are one such example of engineered molecular materials formed from the spontaneous self-assembly of shape anisotropic molecules. This is an exceptional combination of order and mobility, which provides stimuli responsive, self-healing and adaptive behavior, leading to their technological importance in the present era. [1] Columnar LCs created by the stacking of disc like molecules are receiving increasing interest nowadays due to their potential application in organic electronics.[2] This is due to the strong overlap of π-π orbitals, ability to form large domain free thin films, absence of grain boundaries due to self-healing ability, solution processability and tunable surface alignment resulting from their columnar organization. Over the years there are many unconventional designs that stabilize Col LC phases have been reported that vary from the conventional disc like design. Polycatenar mesogens or phasmids are regarded as the connecting link between conventional rod like (calamitics) and disc like (discotics) mesogens as they possess the structural features and exhibit rich mesomorphic behavior common to both class of conventional LCs.[1] With regard to the stabilization of Col phase this class of molecules are advantageous due to their lower melting/clearing point which helps in the alignment and the inherent synthetic flexibility to incorporate various functionalities, in comparison to discotics.

Col LCs are making way in the area of organic light emitting diodes (OLEDs), basically as materials for hole/electron transport or emissive layers.[3a] Especially the interest in light-emitting Col LCs for the applications in OLEDs is increasing from their compatibility for large area, low cost processing[2,3a] and also the possibility to generate the polarized emission.[3b-d] There is a surge in the interest in the development of high-performance white OLEDs in recent years due to their importance in wide area displays and solid-state lighting. White light emission is realized by having two or three complementary color emitters or by using three primary color emitters. This requires the

doping or combination of several components.[4] Blue light emitters form an integral part of the full color display devices and also for white light emitting devices.[5] Hence there are lot of efforts on building solid-state blue light emitters by the introduction of functional moieties which will help to generate aggregation induced emission (AIE).[6] The scarcity of blue emitters is due to the requirement of high band gap and instability.[7] Introduction of heterocyclic units in the molecular structure of mesogens greatly contributed in the design of luminescent LCs.[8] Among heterocyclic units, the compounds based on 2,5-diphenyl-1,3,4-oxadiazole units are particularly found importance in OLED fabrication due to their high thermal stability, electron transporting and/or hole blocking nature, blue luminescence and high quantum yield.[9] In spite of having similar structure, compounds based on 2,5-diphenyl-1,2,4-oxadiazole units are not much explored either in the area of liquid crystals or in the area of OLEDs in comparison to substituted 1,3,4-oxadiazole derivatives.[22] Asymmetrical nature of 2,5-diphenyl-1,2,4-oxadiazole derivatives provide a strong lateral dipole, which stabilizes different LC phases in comparison to their 1,3,4-oxadiazole isomer.[10a.] In addition, the bent angle is 141$^{o}$ which is more than that of 1,3,4-oxadiazole derivative (bent angle of 134$^{o}$), which in turn provides a much linear structure, thus helping in the mesophase stabilization. It has been reported that ferroelectric switching and biaxiality occur in the nematic phase formed by a bent core molecule based on central 2,5-diphenyl-1,2,4-oxadiazole.[10b] Presence of polar clusters in these nematic phases was reported,[10c] and further studies were done to widen the thermal range of these compounds.[10d] Usually these molecules possess moderate thermal stability than their 1,3,4-isomers[11] but known to exhibit lower melting point and a wider mesophase range.[12] It is also known to possess high S1 and T1 energy which is beneficial for the design of high triplet energy host material for efficient phosphorescent OLEDs (PHOLEDs).[13] PHOLEDs are known for their higher efficiency in comparison to OLEDs as they harvest both the singlet and triplet excitons.

Supramolecular gels are another class of molecules with specific structural features, which immobilize large amount of solvents when they self-assemble.[14] They may gelate organic or aqueous solvents. The self-assembly of such molecules to form gels is assisted

by weak forces like H-bonding, π-π interactions, hydrophobic-hydrophilic or van der Waals interactions. This class of materials is showing promise for the application in optoelectronics,[15] templates for the growth of inorganic nanostructures,[16] fluorescent sensors[17] and controlled release systems.[14] From the view point of application in OLEDs the compounds exhibiting blue light emission in gel state are much privileged. This provide a possibility to bring white light emission by doping other emitters.[18]

In this paper, we report two series of novel polycatenars comprising five rings, among which two are 1,2,4-oxadiazoles. These two oxadiazole rings are interconnected by a *para*- and *meta*-substituted benzene rings, and having four or six-alkyl chains attached equally to two terminal benzene rings. Their thermal behavior and gelation properties were studied thoroughly. Among these molecules, *para*-substituted polycatenars exhibited superior mesomorphic behavior in comparison to *meta*-substitued polycatenars. One of the molecules in *para*-series showed transition from hexagonal columnar to soft crystal phase. This compound showed a weak emission in the solution state (solvated monomers) and exhibited technologically important aggregation induced blue light emission.

## 5.2. Results and discussion

### 5.2.1. Synthesis and Characterization

The synthetic method for the preparation of the target molecules (Fig. 5.1) is presented in scheme 5.1. The synthetic methods for ethyl gallate, 3,4,5-trialkoxyethyl gallates and 3,4-bis(decyloxy) ethyl benzoate are same as reported earlier.[19a] 3,4,5-trialkoxy ethyl gallates **1c**, **4b**, **12c** and 3,4-didecyloxy benzaldehyde **(9b)** were obtained by the *O*-alkylation of ethyl gallate and 3,4-dihydroxy benzaldehyde respectively following Williamson's protocol. Compounds **1c**, **4b**, **12c** were reduced to respective 3,4,5-trialkoxy benzyl alcohols **8c, 8d, 13c** by lithium aluminium hydride (LAH) in dry THF. Further oxidation of 3,4,5- trialkoxy benzyl alcohols **8c, 8d, 13c** using pyridinium chlorochromate (PCC) gave 3,4,5-trialkoxy benzaldehydes **9c, 9d, 14c**.[19b] These benzaldehyde derivatives **(9b-d), 14c** converted to their respective nitriles **(10b-d), 15c** upon heating with

hydroxylamine hydrochloride in DMSO at 100 °C for 3 h.[20] Further reflux of nitrile **(10b-d), 15c** with hydroxylamine hydrochloride and triethylamine in ethanol led to benzamidoxime intermediates **(11b-d), 16c**, which on further refluxing with 1,4- or 1,3-benzene dicarboxylic acid chlorides in pyridine afforded *p*-substituted polycatenars **(PO1-4)** and *m*-substituted polycatenars **(MO1-4)**.[21] The structures of all the intermediates and target molecules were confirmed using $^{1}$H NMR, $^{13}$C NMR, IR spectroscopy and ESI-HRMS or MALDI-TOF analysis. (See the experimental part presented in section 5.4 for the details and Fig. 5.1). As representative cases from each series, $^{1}$H NMR and $^{13}$C NMR spectra of the *para*-1,2,4-oxadiazole **PO2** and *meta*-1,2,4-oxadiazole **MO2** are presented in Fig. 5.2.

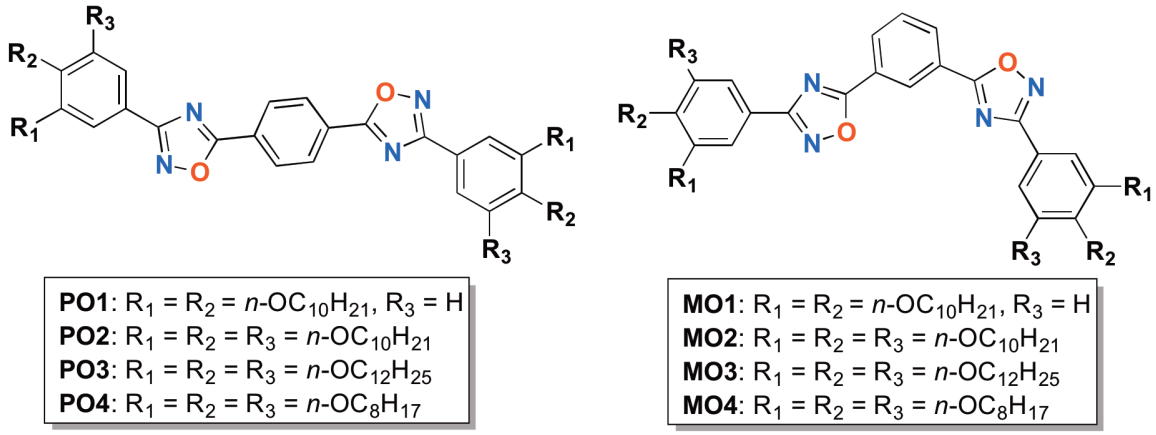


**Figure 5.1.** The molecular structures of compounds **PO1-4** and **MO1-4**.

### 5.2.2. Thermal behavior

The target molecules were probed for their thermal behavior with the help of Polarizing Optical Microscopy (POM) and Differential Scanning Calorimetry (DSC). The thermotropic LC behavior of the compounds is summarized in Table 5.1. Compound **PO1** with four *n*-decyloxy tails turned out to be a crystalline compound. The flexibility provided by four alkoxy tails was not sufficient to induce liquid crystallinity. Compound **PO2** with six *n*-decyloxy tails exhibited an enantiotropic thermal behavior. The isotropic melt on cooling exhibited, a mosaic texture mixed with large homeotropic domains (Fig.

5.4a). The presence of homeotropic domains suggests the uniaxial nature of the mesophase. This is in line with the proposed columnar hexagonal ($Col_h$) phase.

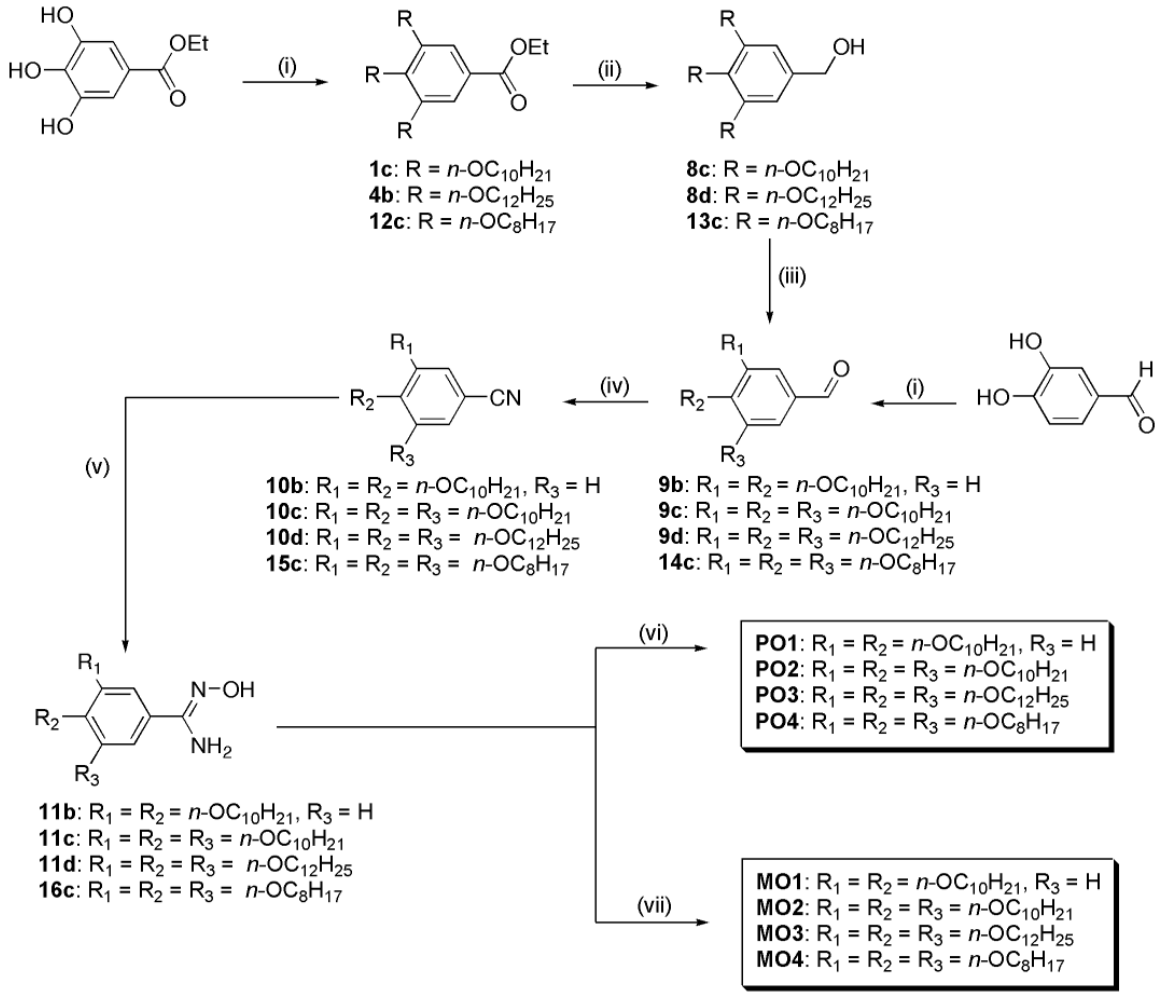


**Scheme 5.1.** Synthesis of star-shaped 1,2,4-oxadiazole polycatenars. Reagents and conditions: (i) 1-Bromoalkanes, anhyd. $K_2CO_3$, DMF, 80 $^oC$, 17 h (70-95%); (ii) LAH, THF, 0 $^oC$ to rt, 2 h (75-86%); (iii) PCC, DCM, rt, 1 h (70-85%); (iv) $NH_2OH{\cdot}HCl$, DMSO, 100 $^oC$, 3 h (70-80%); (v) $NH_2OH{\cdot}HCl$, triethylamine, $C_2H_5OH$, reflux, 24 h (70-82%); (vi) 1,4-benzene dicarboxylic acid chloride, pyridine, 6 h, reflux (56-61%); (vii) 1,3-benzene dicarboxylic acid chloride, pyridine, 6 h, reflux (54-57%).

The mosaic texture on further cooling showed a change in color, while the homeotropic domains fused together, which persisted till the crystallization (as seen in Fig. 5.4b.), while DSC did not show any peak corresponding to this transition. This prompted us to investigate the mesophase at two different temperatures, *i.e.* at 75 $^oC$ and 65 $^oC$ (Fig. 5.4d) with the help of XRD studies. The XRD patterns obtained were almost similar,

showing a single reflection at low angle followed by two diffused reflections at wide angle.

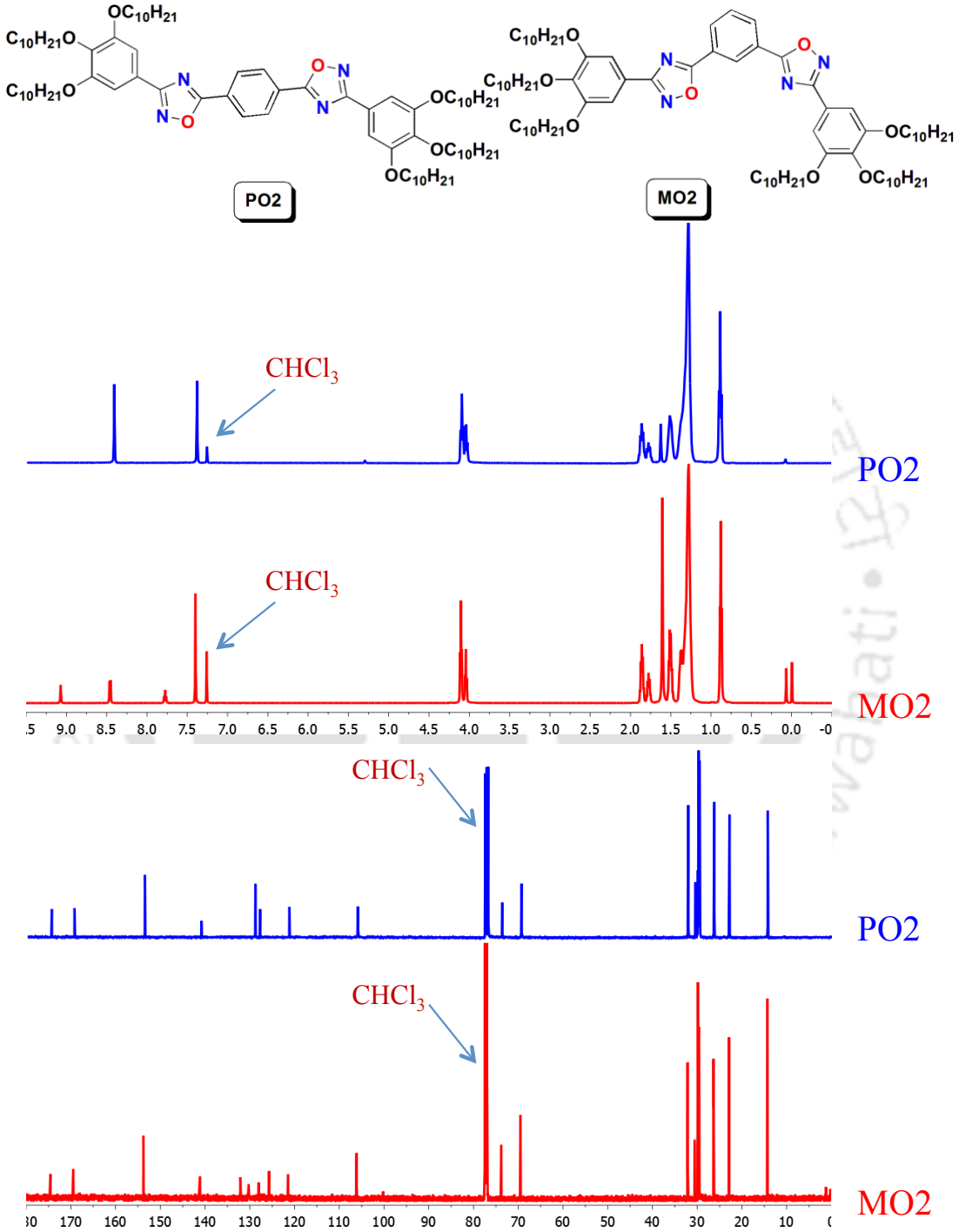


**Figure 5.2.** $^{1}$H NMR (400 MHz) and $^{13}$C NMR (150 MHz) spectra of compound **PO2**; $^{1}$H NMR (600MHz) and $^{13}$C NMR (150MHz) spectra of compound **MO2** in $CDCl_3$.

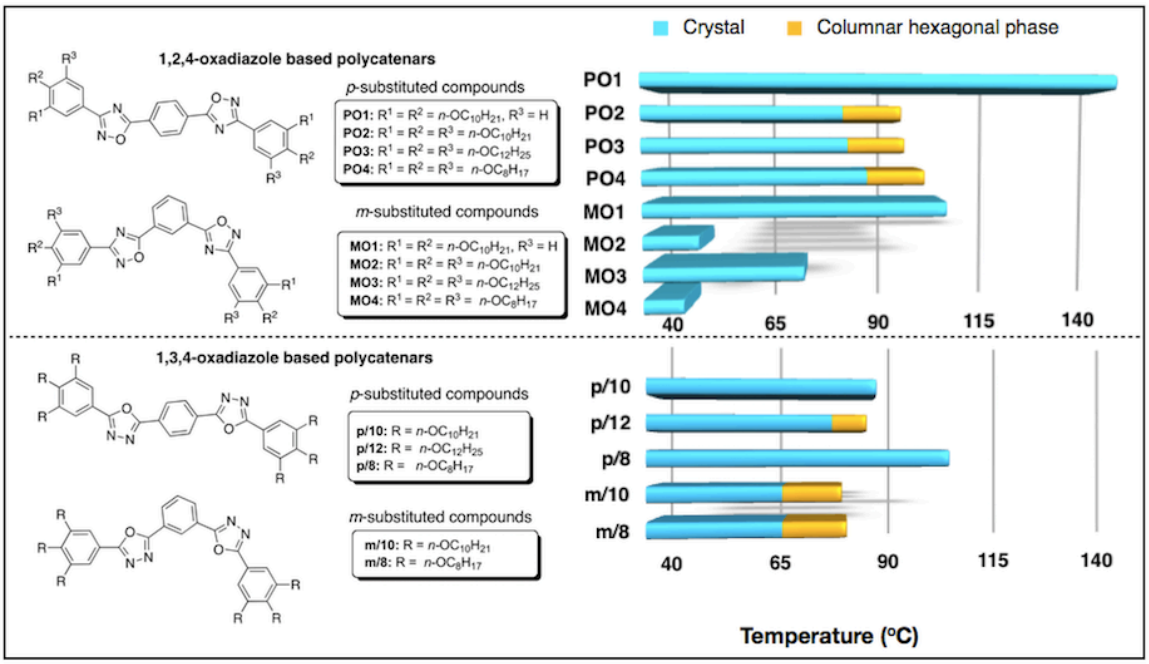


**Figure 5.3.** Bargraph summarizing the thermal behavior of compounds **PO1-4** and **MO1-4** (second heating cycle)

**Table 5.1.** Phase transition temperatures [a] (°C) and corresponding enthalpies (kJ/mol) of DLCs

| | Phase sequence | |
|---|---|---|
| | 2nd Heating | 1st Cooling |
| **PO1** | Cr 138.4 (246.3) I | I 117 (319.6) Cr |
| **PO2** | $Cr_1$ 41.7 (7.4) $Cr_2$ 51.6 (74) $Cr_3$ 80.9 (198.1) $Col_h$ 93 (16.3) I | I 89.3 (17.7) $Col_h$ 58.5 (98.7) $Cr_2$ 38.3 (9.2) $Cr_1$ |
| **PO3** | $Cr_1$ 70.8 (213.7) $Cr_2$ 81.9 (239.4) $Col_h$ 93.7 (22) I | I 90.6 (23.6) $Col_h$ 65.6 (99.3) $Cr_2$ 29.6 (31.2) $Cr_1$ |
| **PO4** | $Cr_1$ 32.3 (28.9) $Cr_2$ 49.9 (32.9) $Cr_3$ 85.9 (162.9) $Col_h$ 97.9 (21) I | I 94.7 (20.4) $Col_h$ 54.9 (1.9) $Cr_3$ 49.5 (68.2) $Cr_2$ 12.3 (26.1) $Cr_1$ |
| **MO1** | Cr 102.6 (321.4) I | I 84.7 (325.7) Cr |
| **MO2** | $Cr_1$ 22.4 (5.5) $Cr_2$ 51.4 (53.5) I | I 51 $Col_h$ [b] 42.6 (2.2) $Cr_2$ 30.5 (21.1) $Cr_1$ |
| **MO3** | Cr 72.9 (97.4) I | I 52.2 (3.9) $Col_h$ 39.7 (32.1) Cr |
| **MO4** | $Cr_1$ 40.9 (40.4) $Cr_2$ 48.2 (2.6) I | I 44.4 (5.9) $Cr_2$ 19.7 (64.8) $Cr_1$ |

[a] Peak temperatures in the DSC thermograms obtained during the second heating and first cooling cycles at 5 °C/min. [b] The transition observed only under microscope. Cr = Crystal phase; $Col_h$ = Columnar hexagonal phase; I = Isotropic phase.

The XRD pattern obtained at 75 °C showed a single sharp reflection at low angle, from which the distance between the adjacent (100) lattice planes $d_{10}$, *i.e.* the lattice

parameter '*a*' can be calculated, assuming a hexagonal lattice. The presence of a single maximum at low angle region prevents an unequivocal structural assignment to $Col_h$ phase; but it is often found in the literature and such a pattern assigned to the Col phase has been ascribed to a minimum in the form factor.[23] The value of '*a*', *i.e.* intercolumnar distance was found to be 40.6 Å, which is smaller than the calculated molecular diameter, *i.e.* 45 Å (in all *trans* conformation estimated from the Chem 3D Pro 8.0 molecular model software from Cambridge Soft, Fig. 5.9). This is due to the interdigitation of peripheral alkyl tails or alkyl chain melting (Table 5.2). The diffused peaks at wide-angle region

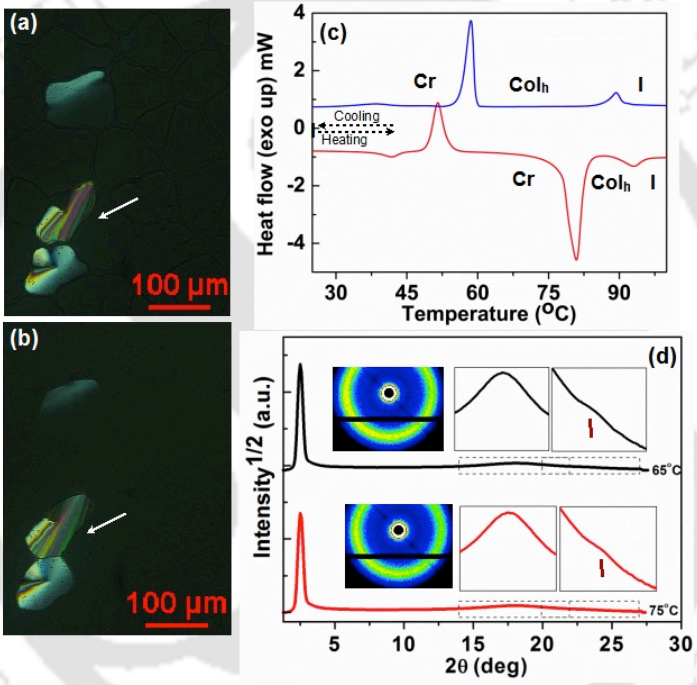


**Figure 5.4.** Photomicrograph of texture as seen by POM for the $Col_h$ phase of compound **PO2** at 85 °C (a); and at 65 °C (the arrow shows the change in the color of mosaic pattern) (b); DSC traces obtained for the first cooling and second heating cycles of **PO2** at a rate of 5 °C $min^{-1}$ (c) and XRD profiles depicting the intensity against the 2$\theta$ obtained for the $Col_h$ phase of compound **PO2** at 75 °C and 65 °C (inset shows the XRD image patterns obtained) (d).

correspond to the packing of flexible tails and the aromatic cores within the column. This typical XRD pattern along with the optical texture confirms the hexagonal symmetry of the columnar phase. The number of molecules packed in a unit cell, *i.e.* denoted as '*Z*' was found to be 2.5. In polycatenars, it is very common to observe the *Z* value more than

2. Here it is expected that two or more molecules pack side by side to form a columnar slice, which further self-organize to form columnar phases which is also observed in chapter 3.[22] The XRD pattern obtained at 65 °C was very much similar to the high temperature diffraction pattern and showed that $Col_h$ phase prevailed till crystallization.

Compound **PO3** with six *n*-dodecyloxy tails on cooling from the isotropic melt exhibited mosaic texture intermixed with homeotropic regions with a dark field of view (Fig. 5.5a). The sharp patterns became blurred after a transition at 66 °C ($\Delta H$ =99.3 kJ/mol) as noticed from DSC scans (Fig. 5.5b and 5.5d). Eventhough the texture did not show any signs of crystallization, the high enthalpy change reaffirm that it may be a soft crystal. Another Cr-Cr transition was observed at ≈ 30 °C ($\Delta H$ =31.2 kJ/mol). But the optical texture at 30 °C did not show any signs of crystallization (Fig. 5.5c). The next heating scan showed the crystal to mesophase transition at ≈ 71 °C ($\Delta H$ =213.7 kJ/mol) showing that the mesophase has crystallized during the cooling process.

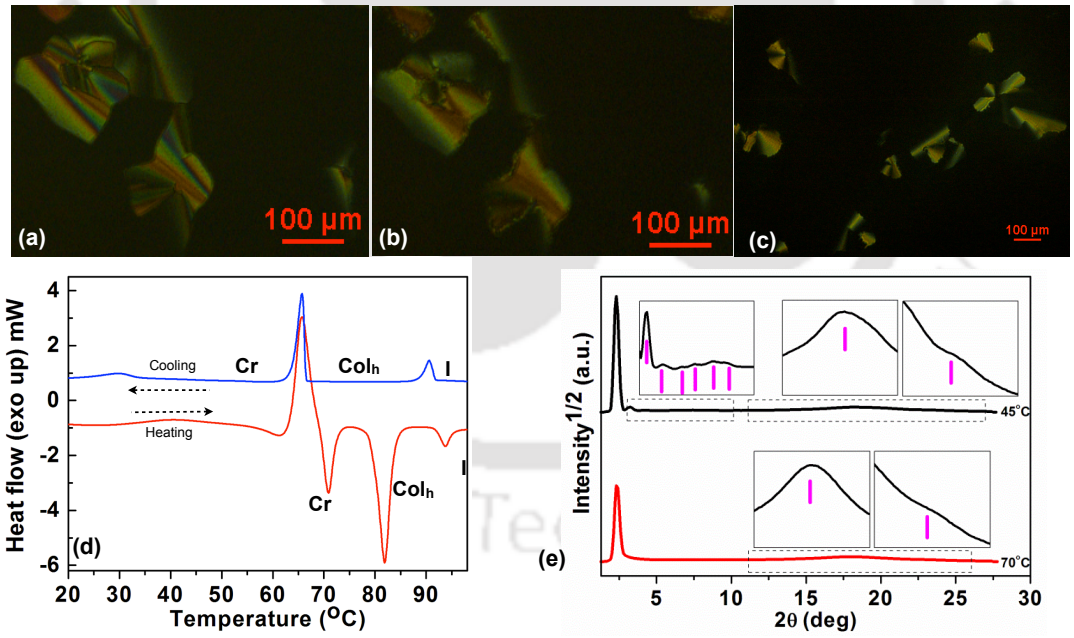


**Figure 5.5.** Photomicrograph of texture as seen by POM for the $Col_h$ phase of compound **PO3** at 70 °C (a); Soft crystal phase at 45 °C (b) and at 30 °C (c); DSC traces obtained for the first cooling and second heating cycles of **PO3** at a rate of 5 °C $min^{-1}$ (d) and XRD profiles depicting the intensity against the $2\theta$ obtained for the $Col_h$ phase of compound **PO3** at 70 °C and Cr phase at 45 °C (e).

The XRD pattern obtained at 70 °C shown a single peak at low angle region along with two diffused peaks in the wide angle. Assuming a hexagonal lattice as in the case of compound **PO2**, the value of the lattice parameter obtained from the corresponding *d* spacing (38.1 Å), was found to be 43.9 Å and the number of molecules in the hexagonal unit cell was 2.6. Powder XRD studies carried out at 45 °C and (Fig. 5.5e, Table 5.2) have shown a sharp single peak at low angle ($2\theta \approx 2.3^{o}$), along with several weak reflections at middle angle region ($2\theta \approx 3\text{-}9^{o}$) and two diffused peaks at wide angle region ($2\theta \approx 18\text{-}23^{o}$). The first diffused peak corresponding to the *d*-spacing of 4.84 Å is related to the packing of flexible tails, while the second relatively sharp peak corresponds to the stacking of cores with a *d*-spacing of 3.78 Å. The *d*-spacings observed in the low and mid angle region suggests that the phase in question is a kind of soft crystal or the mesophase has undergone a partial crystallization (Fig. 5.5e and Table 5.2).

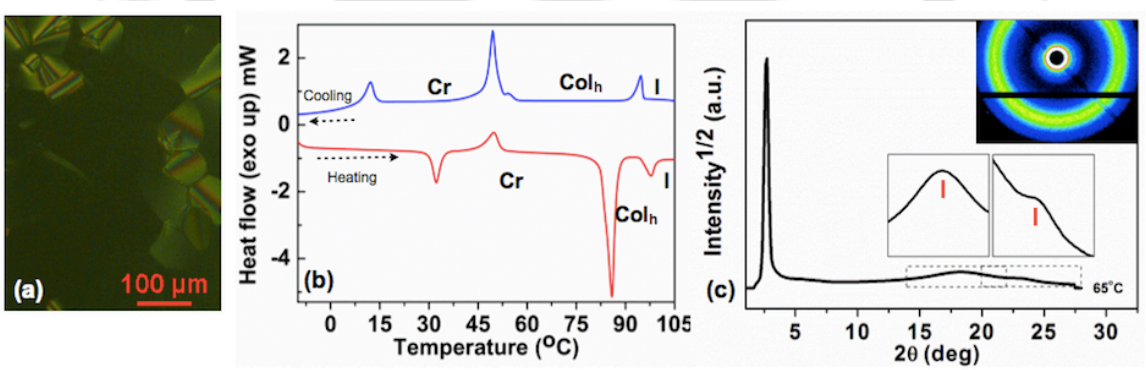


**Figure 5.6.** Photomicrograph of texture as seen by POM for the Col$_h$ phase of compound **PO4** at 65 °C (a); DSC traces obtained for the first cooling and second heating cycles of **PO4** at a rate of 5 °C min$^{-1}$ (b) and XRD profiles depicting the intensity against the 2$\theta$ obtained for the Col$_h$ phase of compound **PO4** at 65 °C (XRD image patterns obtained are shown on the right side) (c).

Compound **PO4** with six *n*-octyloxy tails exhibited Col$_h$ phase with the similar POM texture and XRD pattern as observed in the case of previous compounds (Fig. 5.6a and c). The DSC thermograms were concurrent with the POM observations (Fig. 5.6b). Thus the decrease in the length of the peripheral chains showed an increase in the clearing point, maintaining the same mesophase width in the heating cycle, but showed an increase of 14 degrees in the cooling scan. *m*-Substituted compound **MO1-4** showed relatively poor

mesomorphic behavior in comparison to *p*-substituted derivatives **PO1-4**. Compound **MO1** with four *n*-decyloxy tails turned out to be crystalline compound.

**Table 5.2.** Results of (hkl) indexation of XRD profiles of the compounds at a given temperature (T) of mesophase

| Compounds [a](*D*/Å) | Phase (T/°C) | $d_{obs}$ (Å) | $d_{cal}$ (Å) | Miller indices *hkl* | Lattice parameters (Å), Lattice area *S* (Å$^2$), Molecular volume *V* (Å$^3$) |
|---|---|---|---|---|---|
| **PO2** (43.08) | $Col_h$ (75) | 35.22<br>4.90 ($h_a$)<br>3.86 ($h_c$) | 35.22 | 100 | *a* = 40.64, S = 1430.29, V = 5520.92, Z = 2.55 |
| | $Col_h$ (65) | 35.21<br>4.89 ($h_a$)<br>3.82 ($h_c$) | 35.21 | 100 | *a* = 40.63, S = 1429.59, V = 5461.03, Z = 2.52 |
| **PO3** (47.74) | $Col_h$ (70)<br>Cr (45) | 38.08<br>4.94 ($h_a$)<br>3.79 ($h_c$)<br>38.10<br>27.09<br>21.03<br>16.18<br>14.05<br>11.91<br>10.93<br>4.84 ($h_a$)<br>3.78 ($h_c$) | 38.08 | 100 | *a* = 43.94, S = 1672.01, V = 6336.92, Z = 2.59. |
| **PO4** (38.46) | $Col_h$ (65) | 32.78<br>4.86 ($h_a$)<br>3.84 ($h_c$) | 32.78 | 100 | *a* = 37.83, S = 1239.34, V = 4759.07, Z = 2.52. |
| **MO2** (41.42) | $Col_h$ (50) | 32.77<br>4.87 ($h_a$) | 32.77 | 100 | *a* = 37.82, S = 1238.69, V = 6032.42, Z = 2.79. |
| **MO3** (46.25) | $Col_h$ (50) | 36.62<br>4.90 ($h_a$) | 36.62 | 100 | *a* = 42.26, S = 1546.60, V = 7578.34, Z = 3.1. |

[a]The diameter (D) of the disk (estimated from Chem 3D Pro 8.0 molecular model software from Cambridge Soft). $d_{obs}$: spacing observed; $d_{cal}$: spacing calculated (deduced from the lattice parameters; *a* for $Col_h$ phase). The spacings marked $h_a$ and $h_c$ correspond to diffuse reflections in the wide-angle region arising from correlations between the alkyl chainsand core regions, respectively. *Z* indicates the number of molecules per columnar slice of thickness $h_c$ ($h_a$ is considered when $h_c$ was not observed), estimated from the lattice area *S* and the volume *V*.

The flexibility provided by four alkoxy tails was not sufficient to stabilize liquid crystallinity as in the case of **PO1**. Compound **MO2** with six *n*-decyloxy tails showed monotropic $Col_h$ phase (Fig. 5.7). Increasing the chain length to *n*-dodecyloxy chains **MO3** did not improve the mesomorphic behavior, which also exhibited monotropic

$Col_h$ phase (Fig. 5.8), whereas the reduction of chain length to *n*-octyloxy **MO4** turned the compound to be crystalline.

Overall the thermal range and mesophase stability of these compounds are less than the corresponding star shaped molecules as given in chapter 4. *p*-substituted polycatenars exhibited higher mesophase stability than their *m*-substituted counterparts. In the case of isomeric 1,3,4-oxadiazole based polycatenars[22c-e] an opposite trend is observed, with the *m*-substituted compounds exhibiting enhanced mesophase stability (Fig. 5.3). This may be explained by the bending angle of these regioisomeric heterocyclic cores. 1,3,4-oxadiazole unit with a bent angle of 134° does not support the packing of linear structures, as we can see from the crystalline behavior of **p/10** and **p/8**, in comparison to LC analogues **PO2** and **PO3**.

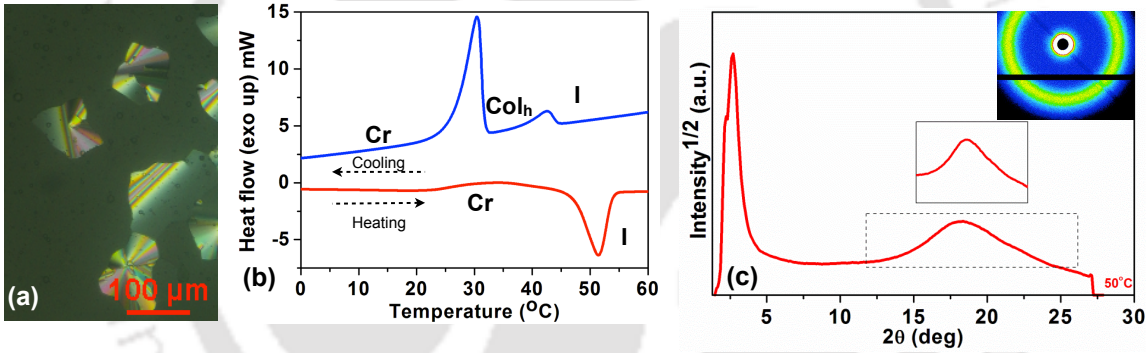


**Figure 5.7.** Photomicrograph of texture as seen by POM for the $Col_h$ phase of compound **MO2** at 50 °C (a); DSC traces obtained for the first cooling and second heating cycles of **MO2** at a rate of 5 °C $min^{-1}$ (b) and XRD profiles depicting the intensity against the $2\theta$ obtained for the $Col_h$ phase of compound **MO2** at 50 °C (XRD image patterns obtained are shown in the inset) (c).

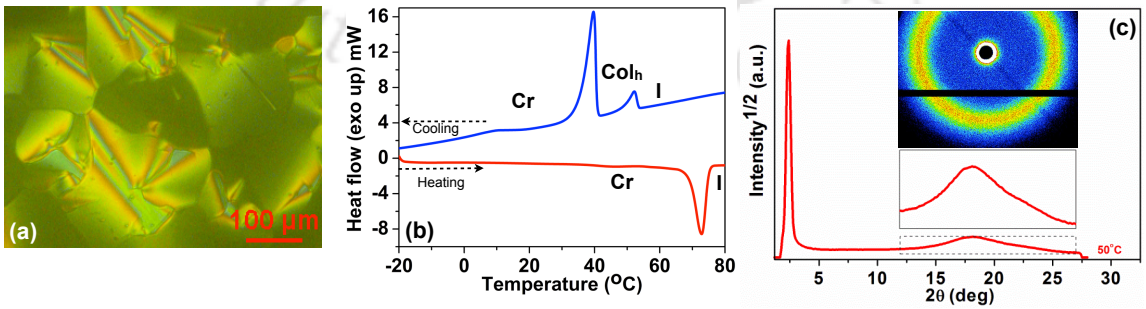


**Figure 5.8.** Photomicrograph of texture as seen by POM for the $Col_h$ phase of compound **MO3** at 50 °C (a); DSC traces obtained for the first cooling and second heating cycles of **MO3** at a rate of 5 °C $min^{-1}$ (b) and

XRD profiles depicting the intensity against the 2$\theta$ obtained for the $Col_h$ phase of compound **MO3** at 50 $^oC$ (XRD image patterns obtained are shown in the inset) (c).

based on 1,2,4-oxadiazoles. The wider bending angle of 141$^o$ in the case of 1,2,4-oxadiazole unit make the molecule more linear in comparison to its regioisomeric analogues based on 1,3,4-oxadiazoles. Similarly the *m*-substituted compounds based on 1,3,4-oxadiazole show liquid crystallinity (for example, **m/10** and **m/8**) in comparison to the 1,2,4-oxadiazole analogues (for example, **MO2** and **MO4)**, which may be due to the efficient space filling achieved by the more bent structure.

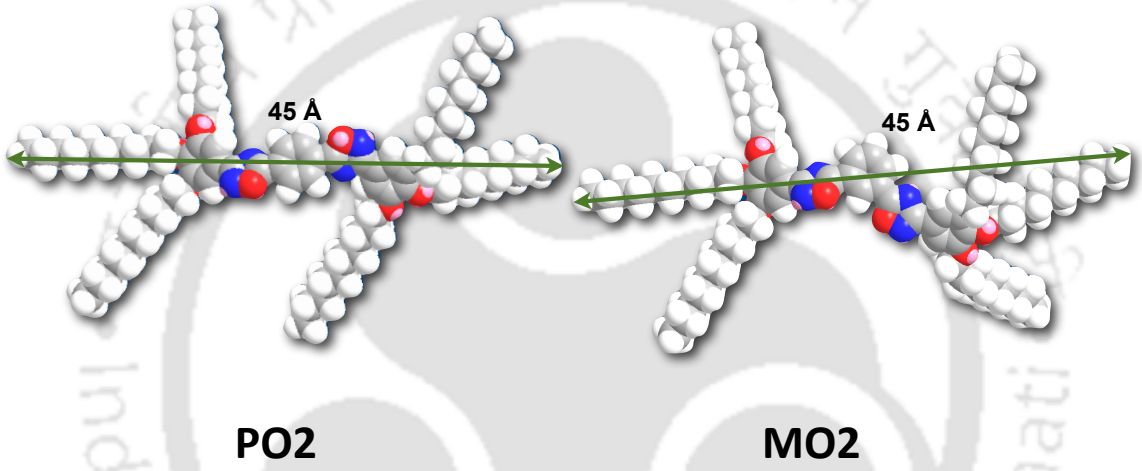


**Figure 5.9.** Molecular models obtained for polycatenars **PO2** and **MO2** (in all *trans* conformation estimated from the Chem 3D Pro 8.0 molecular model software from Cambridge Soft)

### 5.2.3. Photophysical and electrochemical studies

We were interested to study the effect of the regioisomerism on the photophysical properties of the polycatenars. The micromolar soutions of *p*-substituted hexacatenars in chloroform showed single absorption maximum at around 289 nm, while the tetracatenar exhibited two bands in absorption spectra centered at 282 and 303 nm of almost equal intensity. Similarly *m*-substituted hexacatenars exhibited single absorption maximum centered at 268 nm, while the tetracatenar **MO1** exhibited an absorption maximum centered at 265 nm with a broad shoulder at 290 nm (Fig. 5.9a, Table 5.3). It should be noted that in the case of star shaped 1,2,4-oxadiazole derivatives only single band was observed at 278 nm as shown in chapter 4. *m*-substituted compounds exhibited blue shifted absorption maximum in comparison to *p*-substituted compounds. Observation of

high molar extinction coefficients (ε: 24000-57000 $M^{-1}cm^{-1}$) confirms that these molecules are highly conjugated systems. The emission spectra of *p*-substituted hexacatenars exhibited a single emission maximum centered around 536-540 nm, while the tetracatenar exhibited a blue shifted emission maximum at 488 nm (Fig. 7b, Table 5.3). Similarly the *m*-substituted hexacatenars showed an emission maximum centered at 469 nm, while the *m*-substituted tetracatenar, showed a blue shifted emission maximum centered at 444 nm. The Stoke's shift was in a range of 11960-16203 nm. The optical band gap calculated for these systems from the red edge of the absorption spectra were found to be in the range of 3.87-3.92 eV.

**Table 5.3.** Photophysical[a] and electrochemical[a, c] properties of polycatenars (**PO1-4** and **MO1-4**)

| Entry | Absorption (nm) | Emission [b] (nm) | Stoke's shift ($cm^{-1}$) | $\lambda_{onset}$ (nm) | Emission[i] (nm) | $\Delta E_{g,opt}$ [d, e] | $E_{1ox}$ [f] | $E_{HOMO}$ [d, h] | $E_{LUMO}$ [d, g] | ε ($M^{-1}cm^{-1}$) |
|---|---|---|---|---|---|---|---|---|---|---|
| **PO1** | 282, 303 | 488 | 12511 | 319 | 440 | 3.89 | 1.76 | -6.10 | -2.21 | 30058 |
| **PO2** | 288 | 540 | 16203 | 321 | 477 | 3.87 | 1.71 | -6.05 | -2.22 | 24026 |
| **PO3** | 290 | 536 | 15826 | 319 | Weak Emission | 3.89 | ----- | ------ | ------ | 30261 |
| **PO4** | 289 | 539 | 16049 | 319 | 474 | 3.89 | ------ | ------- | --------- | 32002 |
| **MO1** | 265, 290 | 444 | 11960 | 319 | 433 | 3.89 | 1.78 | -6.12 | -2.31 | 56872 |
| **MO2** | 268 | 469 | 15991 | 317 | 482 | 3.92 | 1.70 | -6.04 | -2.21 | 31650 |
| **MO3** | 268 | 471 | 16082 | 317 | 473 | 3.92 | ------- | ------- | ------ | 26108 |
| **MO4** | 268 | 469 | 15991 | 319 | 467 | 3.89 | ------- | ------- | -------- | 52975 |

[a]Micromolar solutions in chloroform. [b]Excited at the respective absorption maxima. [c]Experimental conditions: $Ag/AgNO_3$ as reference electrode, glassy carbon as working electrode, platinum rod as counter electrode, TBAP (0.1 M) as a supporting electrolyte, room temperature. [d]In electron volts (eV). [e]Band gap was determined from the red edge of the longest wave length in the UV-Vis absorption spectra. [f] In volts (V). [g] Estimated from the formula $E_{LUMO} = E_{HOMO} + E_{g,opt}$. [h]Estimated from the onset oxidation peak values by using $E_{HOMO} = -(4.8 - E_{1/2,Fc,Fc+} + E_{ox,onset})$ eV. [i]Emission obtained by exciting the thin films at their absorption maxima in solution.

The emission intensity was less in solution state and we could not measure the relative quantum yield of these compounds with respect to standard compound. We were interested to study the emissive nature of these molecules in solid state. The thin films of the compounds were prepared by slow cooling of the isotropic liquids of the samples sandwiched between the glass coverslips. Except compound **PO3** all the compounds showed good emission in the film state. They showed a red-shifted emission and excitation spectra (Fig. 5.10c and d; Table 5.3. and Fig. 5.11), which points to the

formation of aggregates. The red-shifted excitation and emission spectra of the thin films in comparison to the respective spectra in solution state at micromolar concentration points to the formation of J-aggregates.[24] We were curious to know the reason behind the low emission intensity of compound **PO3** in thin film state. This sample was heated to its

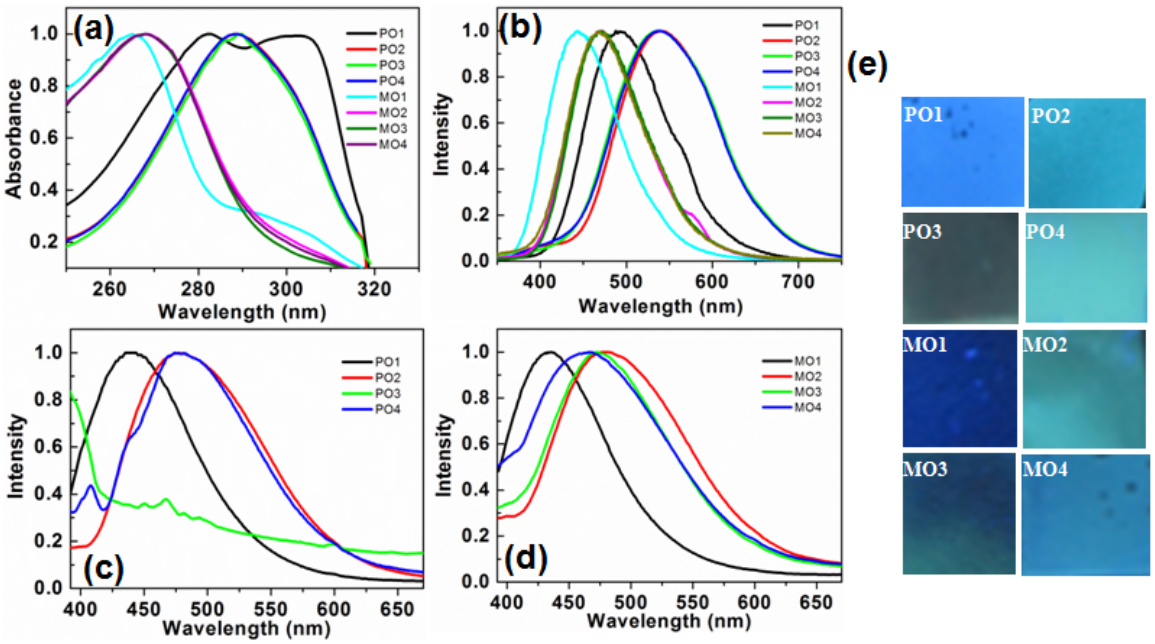


**Figure 5.10.** Absorption spectra (a) and emission spectra (b) in micromolar THF solution obtained for **PO1-4** and **MO1-4**; normalized emission spectra of thin films of compounds **PO1-4** (excited at the absorption maxima obtained in solution state) (c) and **MO1-4** (excited at the absorption maxima obtained in solution state) (d) images of the thin films of **PO1-4** and **MO1-4** under UV light of long wavelength (365 nm) (e).

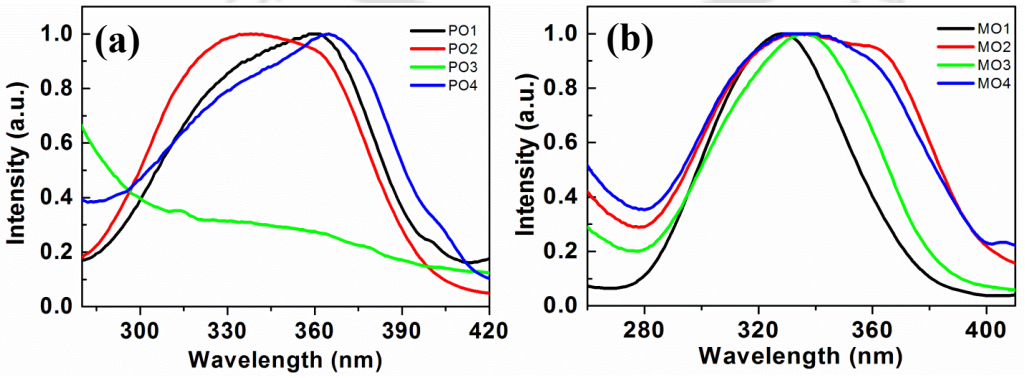


**Figure 5.11.** Excitation spectra for compounds **PO1-4** and **MO1-4** in thin film state.

**Table 5.4.** Data obtained from the Fig. 5.11.

| Compounds | Excitation (nm) | Compounds | Excitation (nm) |
|---|---|---|---|
| **PO1** | 362 | **MO1** | 329 |
| **PO2** | 340 | **MO2** | 335 |
| **PO3** | Weakly excited | **MO3** | 336 |
| **PO4** | 365 | **MO4** | 340 |

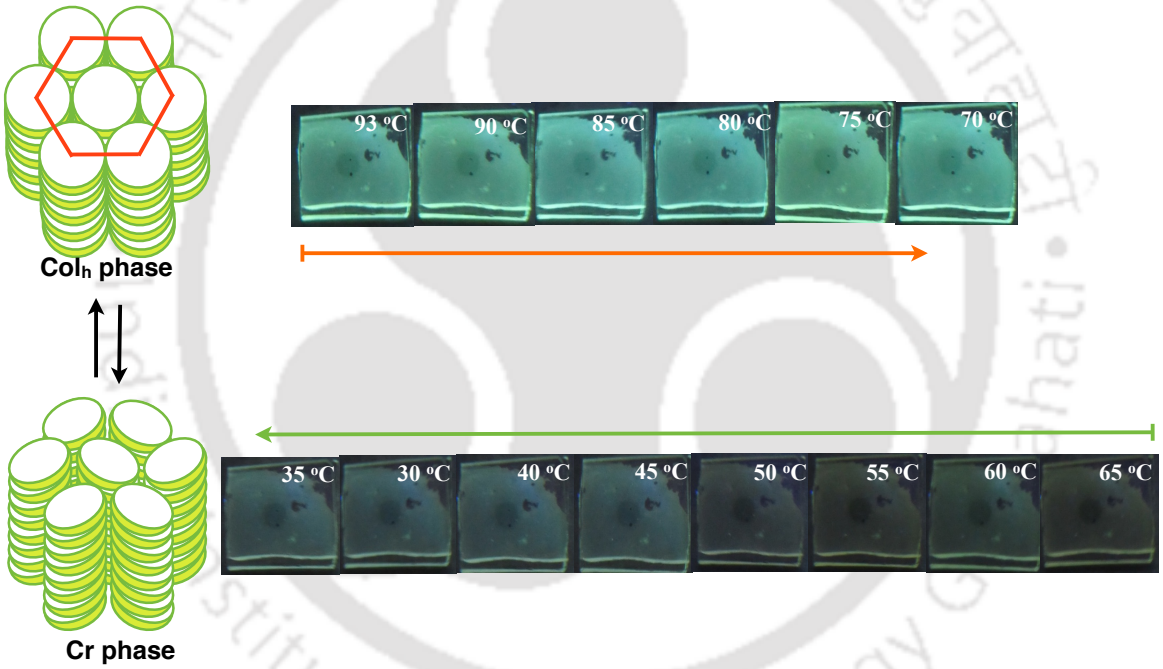


**Figure 5.12.** Thin films of the compound **PO3** on cooling from the isotropic state as observed under the UV light of long wavelength (365 nm). The upper row shows the films in Col$_h$ phase, while the lower row shows the films in soft crystal phase.

isotropic state and cooled slowly. For every 5$^{o}$ temperature interval the emission spectra were taken (Fig. 5.13a). The film was irradiated with UV light of long wavelength (365 nm) to visualize these changes (Fig. 5.12). As can be seen the thin film showed bright green emission from 93 $^{o}$C to 70 $^{o}$C. The emission suddenly diminished from 65 $^{o}$C and it did not show any increase up to room temperature. This was in accordance with the emission spectra measured in the thin film state. From the DSC and XRD studies it is evident that at 65 $^{o}$C there is a transition from $Col_h$ to Cr phase.

From this observation, it is evident that, the packing of molecules in the $Col_h$ phase is more supportive to the emission than their arrangement in Cr phase. In other words, $Col_h$ phase promotes aggregation induced enhanced emission (AIEE), while Cr phase shows the aggregation induced quenching (ACQ) (Fig. 5.13a,b). This explained the weak emission we observed in the case of the thin film at room temperature (Fig. 5.10e). The emission in the $Col_h$ phase is six times more than the emission in Cr phase (Fig. 5.13a). From the plot showing the emission maxima *vs* temperature it is clear that the emission maxima is red shifted with the decrease in temperature (Fig. 5.13c). We were interested to understand the type of aggregation in these two different structures, which are responsible for different emission behavior. The excitation spectra obtained at different temperatures has shown a red shift in comparison to the solution spectrum (Fig. 5.14). This suggested that in both Columnar and crystal phases, the molecules prefer to form J-aggregates. The J-aggregate formed in the case of $Col_h$ phase is emissive, while that in Cr phase is not.[24] Although it is difficult to explain the molecular packing arrangements in these two phases, it can be assumed that in the case of high temperature $Col_h$ phase, the molecules are far apart to avoid the ACQ, while at low temperature Cr phase they come closer leading to ACQ. Thus the compound **PO3** exhibit thermochromism, as a result of the change in the type of aggregation. Considering the different conformations possible it is difficult to specify the exact packing structure of the molecules in these different phases.

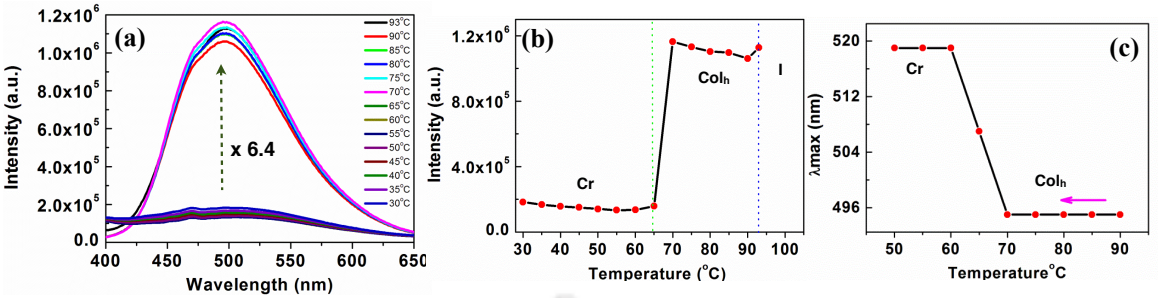


**Figure 5.13.** Emission spectra obtained for the thin film of compound **PO3** on cooling from the isotropic temperature (a); plot showing the variation in the emission intensity *vs* temperature (b); plot showing the shift in the emission maxima with respect to temperature (c).

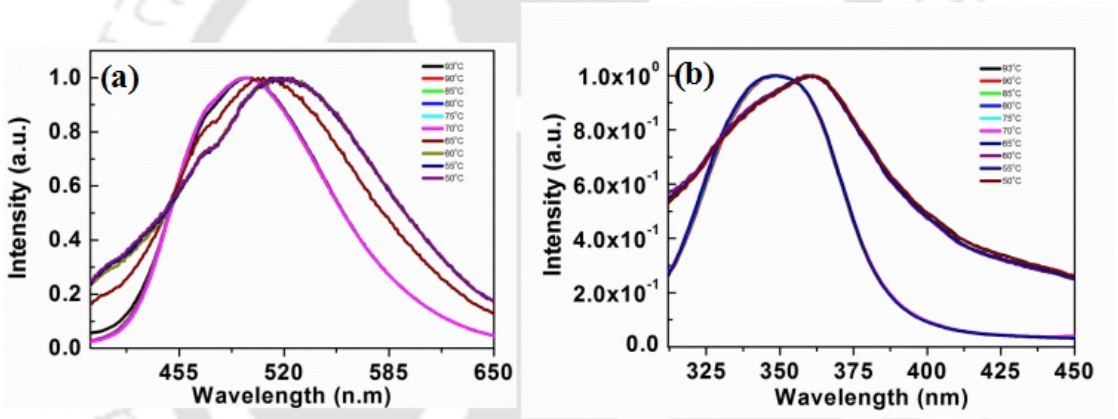


**Figure 5.14.** Normalised emission spectra obtained for the thin film of compound **PO3** with respect to temperature (a); excitation spectra obtained for the same (b).

Energy levels of frontier molecular orbitals (HOMO and LUMO) of the polycatenars were acquired by cyclic voltammetry (CV) and the data are presented in Table 5.3. We have chosen compounds **PO1-2** and **MO1-2** for carrying out CV studies. These compounds exhibited irreversible oxidation and reduction waves (Fig. 5.15.). The optical band gap $E_{g,\ opt}$ was estimated from the red edge of the absorption spectra. Cyclic Voltammograms showed that these molecules exhibit comparable HOMO, LUMO values irrespective of the position of the substitution to the central benzene ring (HOMO: -6.04 to -6.12 eV; LUMO: -2.21 to -2.31eV). In comparison to the star shaped derivatives these

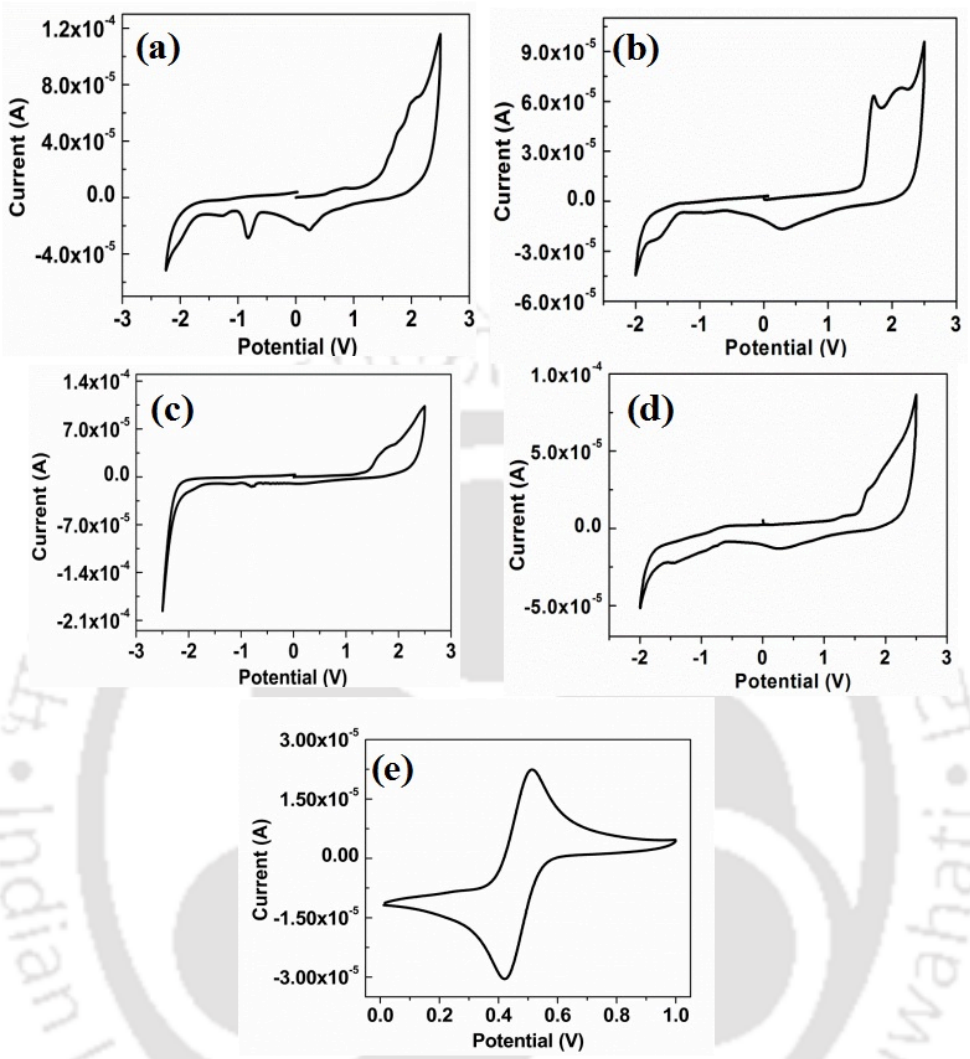


**Figure 5.15.** Cyclic voltammograms of compound **PO1** (a); **PO2** (b); **MO1** (c); **MO2** (d) and ferrocene (e) in anhydrous DCM solution of tetra-*n*-butylammonium perchlorate (0.1 M) (The half-wave potential of the ferrocene/ ferrocenium ($Fc/Fc^+$) redox couple ($E_{1/2,\ Fc,Fc^+}$) was found to be 0.46 V relative to the $Ag/Ag^+$ reference electrode).

molecules exhibit higher HOMO and lower LUMO levels (HOMO: -6.17 to -6.31 eV; LUMO: -1.96 to -2.09 eV) as given in chapter 4. Though the band gaps of these compounds are high ($E_{g,opt}$ = 3.87-3.89 eV), they were found to be lower than the band gaps of the corresponding star shaped molecules ($E_{g,opt} \approx 4.22$ eV) as given in chapter 4. The higher band gap is the most challenging material property pursued in the advancement of deep blue PHOLEDs.[25] Considering this the present series of compounds are good candidates for such applications.

### 5.2.4. Gelation studies

The compounds were investigated for their ability to aggregate in solutions of hexane, decane, dodecane, chloroform, ethanol, dimethylsulfoxide (DMSO), tetrahydrofuran, benzene, toluene and *m*-xylene (Table 5.5). As shown in Table 5.6, *p*-connected polycatenars (**PO1-4**) shows good gelation properties in *n*-dodecane, which was confirmed by the inversion of the glass vial. Among these compounds, compound **PO1-2** and **PO4** showed gelation at a concentration less than 1 wt. %, thus qualifying themselves as 'supergelators'.[26] There are many reports on supergelators, which are assisted by strong intermolecular attractive forces likes H-bonding,[27,28] but supergelation exclusively promoted by π-π interaction is very rare.[29] *m*-Connected polycatenars (**MO1-4**) did not show gelation in hydrocarbon solvents, the reason behind this observation may be their bent structure and high solubility in the aliphatic solvents.

The gels of compound **PO1**, **PO3** and **PO4** also showed similar photophysical behavior, with the emission maxima did not vary much (450-465 nm) (Fig. 5.16, 5.17). Compound **PO2** after dissolving in dodecane at a CGC of 0.8 wt% formed the gel on standing for a time interval of 30 min (Fig. 5.18d). The gelation was followed by taking the emission spectra with a regular interval of time showed a gradual increase in the emission intensity (Fig. 5.18a, c). The gelation also showed a slight red shift in the emission maxima on gelation (Fig. 5.18b). The gel showed a blue light emission on irradiation of the UV light of long wavelength (365 nm) (Fig. 5.18d). Formation of organogel was also confirmed by measuring the emission spectra of the solution as a function of decreasing temperature (Fig. 5.19a). The gel formation was reversible for any number of heating and cooling cycles (Fig. 5.19b). The absorption spectra measured for 6.1 mM dodecane solutions showed a blue shift of 5 nm with respect to the absorption spectrum observed in solution at 20 μM concentration, whereas the emission spectra at higher concentration showed a red shift of 19 nm (Fig. 5.20a). Fluorescence lifetimes of the excited species formed in the 20 μM and 6.1 mM dodecane solutions were measured by monitoring at their emission maxima (415 nm for dilute solution and 470 nm for the concentrated solution). The solution with lower

concentration showed biexponential decay with two excited species [$T_1$ = 2.7 ns (66 %), $T_2$ = 5.4 ns (34 %)]. The solution with higher concentration showed two different set of excited state species, where the excited state species with higher lifetime was in

**Table 5.5.** Gelation properties of compound **PO2**

| Entry | Solvent | Properties | Critical Gel Concentration (wt.%) | $T_{gel}$ ($^{O}$C) |
|---|---|---|---|---|
| 1 | Hexane | S | ------- | ------- |
| 2 | Decane | PG | ------ | ------ |
| 3 | Dodecane | G(O) | 0.8 | 55 |
| 4 | Toluene | S | ---- | --- |
| 5 | Benzene | S | ---- | --- |
| 6 | *m*-xylene | S | ---- | --- |
| 7 | DCM | S | ---- | --- |
| 8 | Chloroform | S | ---- | --- |
| 9 | THF | S | ---- | --- |
| 10 | Ethanol | P | ---- | --- |
| 11 | DMSO | P | ---- | --- |

G = stable gel; PG = partial gel; S = soluble; P = precipitate; O = opaque; The critical gelation concentration (wt. %) is the minimum concentration necessary for gelation; $T_{gel}$ ($^{o}$C) is the thermal stability of the gels determined by 'dropping ball' method (weight of the ball is 68.5 mg)

higher amount [$T_1$ = 1.5 ns (10%), $T_2$ = 21.8 ns (90%)] (Fig. 5.20b). The species with lower lifetime was solvated monomer, whereas the species with the higher lifetime is formed due to aggregation. The dynamic light scattering studies on the solution state has shown that the solution is containing aggregates of approximately 459 nm size (Fig. 5.21). Thus, the six-fold increase in the emission intensity is due to the aggregation induced emission effect. The blue shifted absorption spectra at higher concentration showed that the aggregates formed during gelation are of H-type aggregates where the molecules are arranged one above the other in cofacial or parallel manner. Excitonic splitting in these aggregates leads to a high-energy transition and a low energy forbidden transition. In such systems the absorption spectra is dominated by the high-energy band leading to a blue shifted absorption band with respect to monomer absorption band. This

**Table 5.6.** Gelation properties of compound **PO1-4** and **MO1-4** in hydrocarbon solvents

| Compound | Hexane | Decane | Dodecane |
|---|---|---|---|
| **PO1** | Insoluble | G(O) (0.45)[a] | G(O) (0.61)[a] |
| **PO2** | Soluble | PG | G(O) (0.80)[a] |
| **PO3** | Soluble | PG | G(O) (1.2)[a] |
| **PO4** | P | PG | G(O) (0.65)[a] |
| **MO1** | PG | PG | PG |
| **MO2** | S | S | S |
| **MO3** | S | S | S |
| **MO4** | S | S | S |

G = stable gel; PG = partial gel; S = soluble; P = precipitate; I = insoluble; O = opaque; [a]The critical gelation concentration (wt.%) is the minimum concentration necessary for gelation.

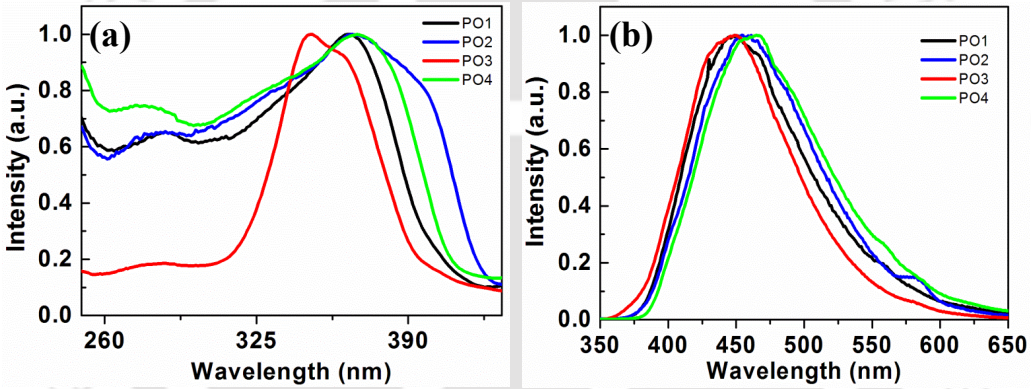


**Figure 5.16.** Normalized excitation (a) and emission spectra (b) in micromolar dodecane solution for compounds **PO1-4**.

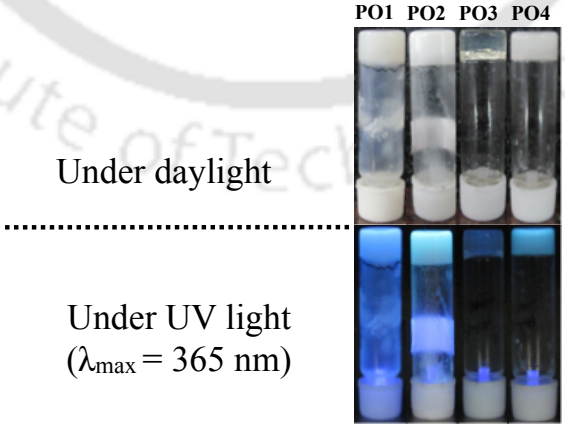


**Figure 5.17.** Photographs of dodecane gels obtained for compounds **PO1-4** as seen in day light and UV light of long wavelength.

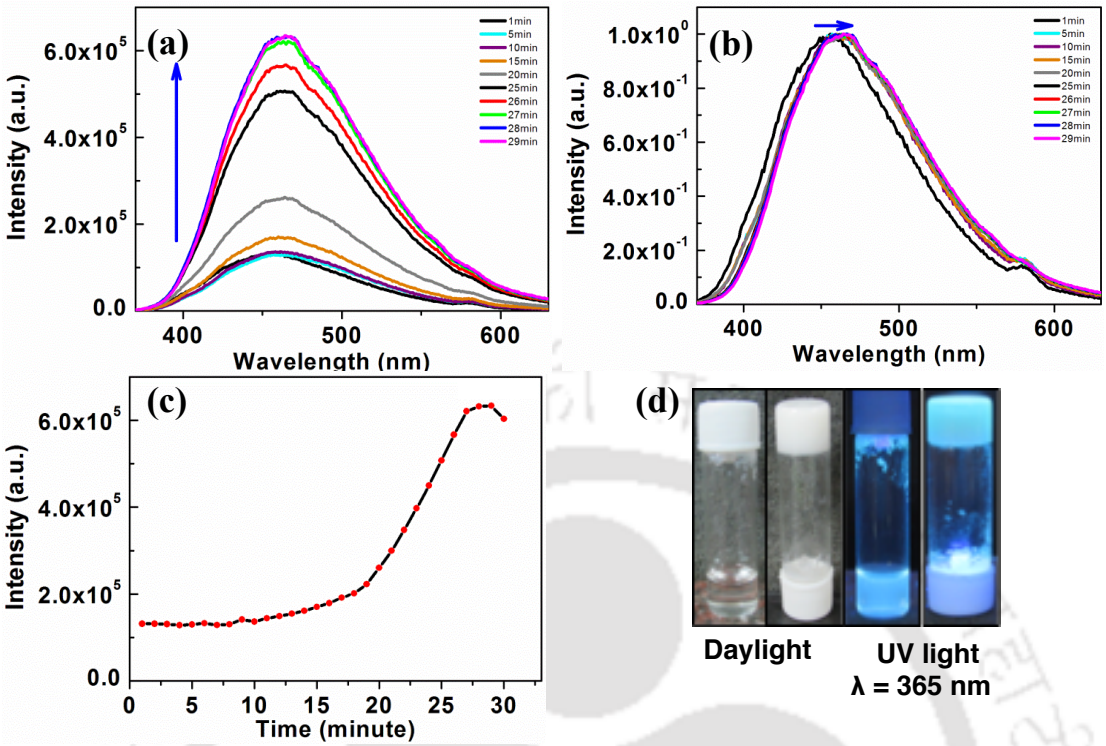


**Figure 5.18.** Emission spectra of compound **PO2** showing an increase in the emission intensity with time on gelation (Concentration: 6.1 mM) (a); normalized emission spectra showing a red shift on gelation (b); plot showing the emission intensity *vs* time (c); images showing the compound **PO2** as a solution in dodecane and as a gel in dodecane in day light as well as UV light of long wavelength (365 nm) (d).

also leads to strong red shift in the fluorescence from low energy band.[30] Eventhough H-aggregates are supposed to exhibit reduced luminescence than in solution, here the situation is exactly opposite of the expected. In literature there are limited reports on luminescent H-aggregates.[31]

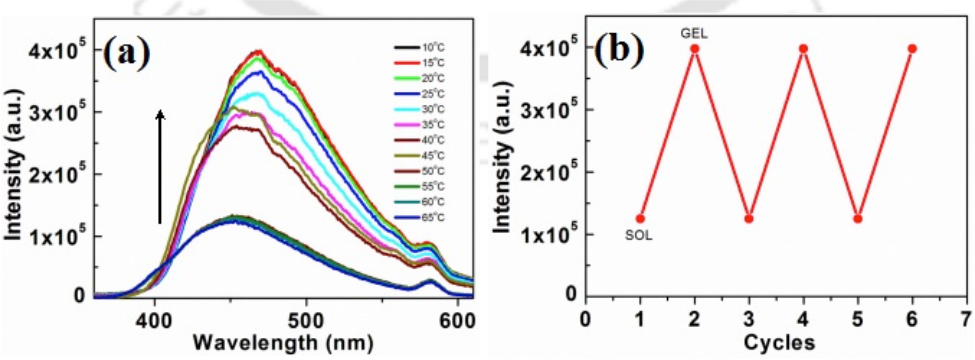


**Figure 5.19.** Emission spectra of compound **PO2** showing an increase in the emission intensity on decreasing the temperature due to gelation (Concentration: 6.1 mM)(a); reproducible reversibility of emission intensity in solution to gel interconversion (b).

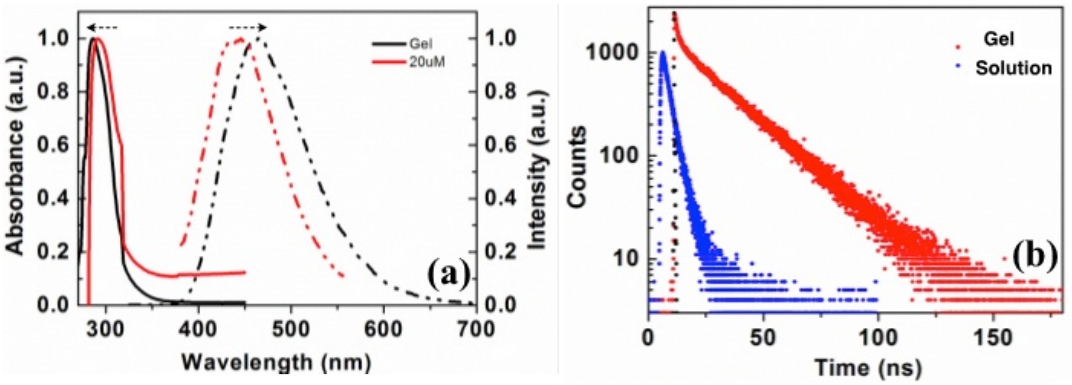


**Figure 5.20.** Normalized absorption (solid trace) and emission spectra (broken trace) of compound **PO2** in dodecane (Concentration: 6.1 mM) (black trace) and 20 μM (red trace) concentration (a); the fluorescence decay of compound **PO2** in dodecane at 6.1 mM (red trace) and 20 μM (blue trace) concentrations (black trace is instrument response function: IRF; $\lambda_{exc}$ = 290 nm) (b).

Usually this luminescence by H-aggregates is accounted for the excimer species or due to a slight rotation of two exciton-coupled molecules in the excited state. We should note that the annealed thin films showed the formation of J-aggregates. Thus there is a J- to H-type conversion was seen on moving from solid to gel state. Similar H-type aggregation of star shaped molecules on gelation in hydrocarbon solvents was reported by Das *et al.*[32]

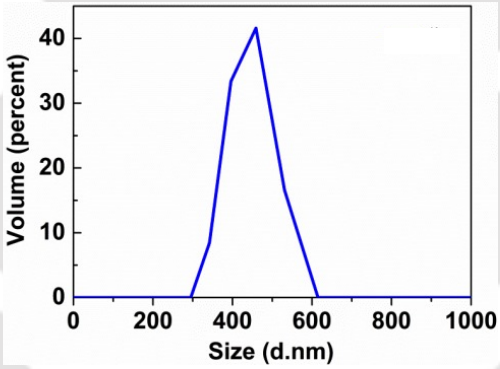


**Figure 5.21.** Dynamic light scattering curve observed for compound **PO2** in dodecane in micromolar concentration.

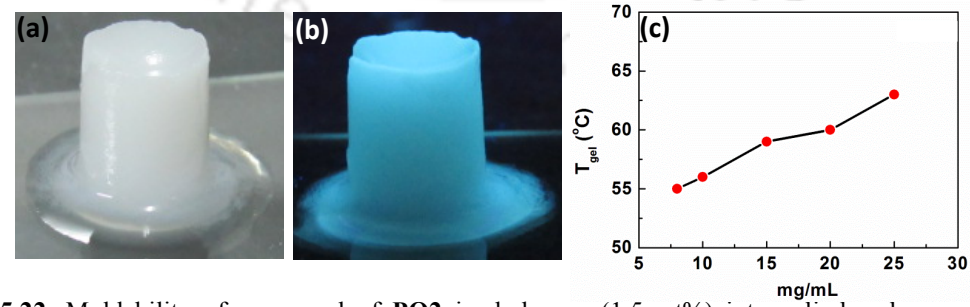


**Figure 5.22.** Moldability of organogel of **PO2** in dodecane (1.5 wt%) into cylinder shape as seen in daylight (a); under UV light (365nm) (b); plots of $T_{gel}$ *vs* concentration for compound **PO2** in dodecane (c).

The self-standing gel showed an incredible stability on keeping inverted for a period of more than a month (Fig. 5.18d). We have investigated the thermal stability of the gel with respect to concentration by 'dropping ball' method,[33] which showed a gradual increase (Fig. 5.22c) on increasing the concentration. The gel prepared at 1.5 wt % concentration showed higher mechanical strength and could be molded into any shape as shown in Fig. 5.22a and the luminescence remained unchanged (Fig. 5.22b).

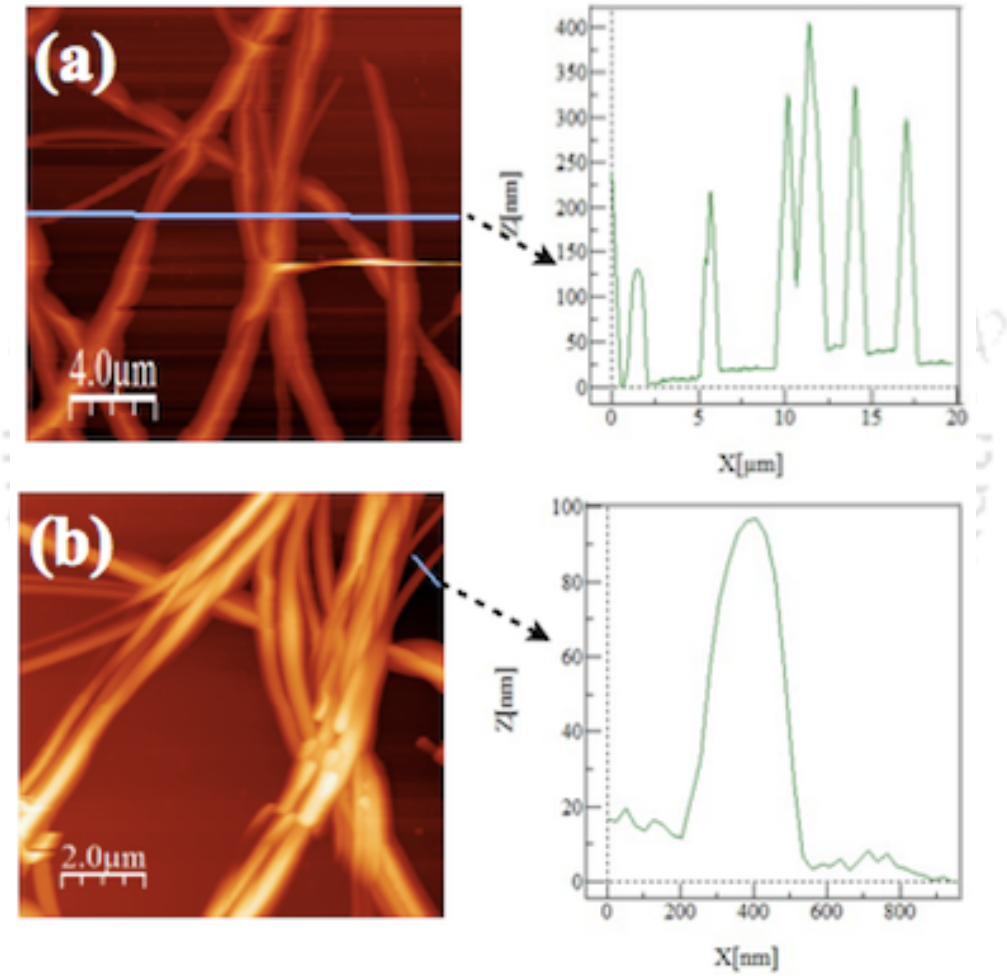


**Figure 5.23.** AFM images obtained for compound **PO2** at 10 μM dodecane solution (scale bar is 4 μm) showing the height profiles of the individual fibers (scale bar is 4 μm) (a); AFM showing the thickness of an individual fiber (scale bar is 2 μm) (b).

Atomic force microscopy (AFM) was carried out to understand the superstructure of the gel formed from compound **PO2**. The surface morphology of the xerogels of **PO2**

obtained by drying the dropcasted solution (1 mM) in dodecane showed an entangled network of fibers (Fig. 5.23). The fibers are of several micrometers in length, heights of 100-400 nm with the thickness of 200 nm (Fig. 5.23b). The tip of the fiber in Fig 5.23b shows branching indicating that the thick fiber is a bundle of primary thin fibers, while each fiber in turn is made up from the cofacial self-assembly of molecules.

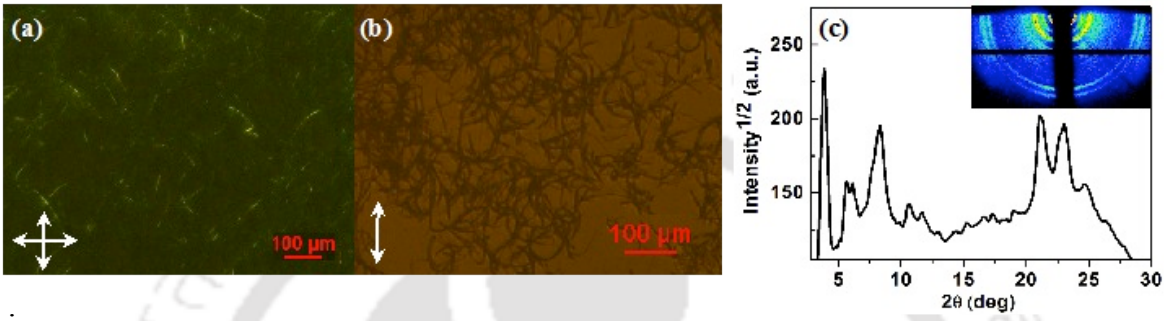


.

**Figure 5.24.** POM image with crossed polarizers (a); with parallel polarizers (b); XRD profile depicting the intensity against the 2$\theta$ obtained for the compound **PO2** in xerogel state (inset shows the XRD image pattern obtained) (c).

**Table 5.7.** Data obtained from XRD profile of the compound **PO2** in xerogel state at room temperature

| Compounds | $d_{obs}$ (Å) |
|---|---|
| **PO2** | 23.12<br>15.65<br>14.51<br>10.69<br>8.96<br>8.36<br>7.61<br>6.80<br>6.14<br>5.82<br>5.34<br>5.13<br>4.92<br>4.80<br>4.65<br>4.50<br>4.22<br>3.86<br>3.61<br>3.38 |

Further the structure of the dry xerogel was studied with the help of powder X-ray diffraction studies carried out on a thin film of the compound **PO2** prepared by drop casting the 1 mM solution on a glass slide. The XRD pattern of the xerogel film (Fig. 5.24c and Table 5.7) showed many peaks centered at low and wide angle regions, which may be due to the crystalline order arising from the strong intermolecular interactions of the adjacent molecules in the xerogel state. A birefringent texture was seen on looking at the xerogel under polarizing optical microscope (Fig. 5.24a) confirming the anisotropic organization of the molecules in gel state. The presence of entangled fibres of several micrometer length was seen when the xerogel was observed with the polarizers of the POM were parallel to each other (Fig. 5.24b).

### 5.3. Conclusions

We have reported two series of polycatenars comprising five rings, among which two are 1,2,4-oxadiazoles. These two series vary from each other with respect to the position at which these unsymmetrically substituted 1,2,4-oxadiazole moieties are connected to the central benzene ring. It is interesting to note that the number of flexible tails in the periphery dictated the self-assembly (liquid crystallinity and gelation) and the photophysical behavior. Their thermal behavior was analyzed with the help of polarizing optical microscopy, differential scanning calorimetry and X-ray diffraction studies.

The compound with four *n*-decyloxy tails was crystalline in both series. In the *para*-substituted series, all the hexacatenars exhibited columar hexagonal phase. It is noteworthy that the hexacatenar with *n*-dodecyloxy chains showed thermochromism. The emissive nature of this compound exhibited a crossover on moving from $Col_h$ phase to Cr phase, where the $Col_h$ phase was highly emissive, while the Cr phase showed quenching of fluorescence. All the compounds of the *p*-substituted series exhibited an ability to gelate in longer chain hydrocarbons. Three of the compounds in this series exhibited supergelation, exclusively promoted by π-π interactions. This is very rare, in comparison to earlier reports where the supergelation is supported by H-bonding interactions. Besides the capability to form self-standing, moldable gel, the hexacatenar with decyloxy chains

exhibited aggregation-induced blue light emission. In the *meta*-substituted series, tetracatenar with *n*-decyloxy tails was crystalline and the same is true for the compound with six *n*-octyloxy tails. Compounds with six *n*-decyloxy and *n*-dodecyloxy tails exhibited columnar hexagonal phase. The *meta*-substituted series exhibited reduced tendency to stabilize the mesophase in comparsion to *p*-substituted series. In comparison to hexacatenars based on 1,3,4-oxadiazoles, *p*-substituted hexacatenars exhibit higher ability to show mesophase, while *m*-substituted hexacatenars exhibit lower ability to form the mesophase. This observation shows the impact of the bend angle of these two regioisomeric heterocycles affects liquid crystallinity. The columnar order and emissive nature in the aggregated state makes these molecules promising for the application in emissive displays. This report emphasizes the importance of various non-covalent interactions in deciding the nature of self-assembly. Additionally this report also highlights the beneficial effect of *p*-substitution in this class of molecules on the stabilization of supramolecular self-assemblies.

### 5.4. Experimental Section

In this section the detailed synthetic procedures and the molecular structural characterization data have been presented for the intermediates and target compounds mentioned in the scheme 5.1. Some of the intermediates such as **1c**, **4b**, **8c-d**, **9b-d**, **10b-d** and **11b-d** are reported and characterized in the earlier chapters.

Procedure for the synthesis of ethyl 3,4,5-tris(octyloxy)benzoate (**12c**)

A mixture of ethyl gallate (25.23 mmol, 1equiv), anhyd. $K_2CO_3$ (166.52 mmol, 6.6 equiv), *n*-bromoctane (83.26 mmol, 3.3 equiv) were taken in dry DMF (20 ml) and heated at 80 $^oC$ for 17 h under nitrogen atmosphere. Then the reaction mixture was poured into ice-water and extracted with $CH_2Cl_2$. The combined extract was washed with water and brine. Dried over anhyd. $Na_2SO_4$ and concentrated. The crude product was purified by column chromatography on neutral alumina. Elution with hexanes followed by 5 - 10% ethylacetate - hexanes yielded the desired product.

$R_f$ = 0.52 (10% EtOAc - hexanes); colorless liquid; yield: 95%; IR (KBr pellet): $\nu_{max}$ in $cm^{-1}$ 2956.0, 2928.0, 2855.0, 1719.0, 1587, 1501.0, 1430.0, 1333.0, 1218.0, 1114.0; $^1H$ NMR ($CDCl_3$, 600 MHz): δ 7.25 (s, 2H, Ar), 4.33 – 4.37 (m, 2H, $COOCH_2$), 4.01 (t, 6H, $J$ = 6Hz, 3 × $OCH_2$), 1.24 - 1.83 (m, 36H, 18 × $CH_2$), 0.87 - 0.89 (m, 12H, 4 × $CH_3$); $^{13}C$ NMR ($CDCl_3$, 150 MHz): 166.68, 152.97, 142.45, 125.23, 108.13, 73.68, 69.35, 69.17,

32.03, 30.52, 29.72, 29.56, 29.49, 26.25, 22.88, 14.61, 14.30; HRMS (ESI+) exact mass calculated for $C_{33}H_{59}O_5$ (M+1): 535.4357, Found: 535.4310.

Procedure for the synthesis of (3,4,5-tris(octyloxy)phenyl)methanol (**13c**):

To a stirred suspension of lithium aluminium hydride (LAH) (25.24 mmol, 1.5 equiv) in dry THF (20 ml) under nitrogen atmosphere, added the solution of ethyl 3,4,5-tris(octyloxy)benzoate (16.83 mmol, 1 equiv) drop wise at 0 $^oC$. Then the reaction mixture was allowed to reach room temperature and stirred for 2 h. Excess LAH present was quenched by the addition of moist sodium sulphate. Reaction mixture was extracted with EtOAc (6 × 30 ml). The combined extracts were washed with water, dried over anhyd $Na_2SO_4$ and concentrated *in vaccuo*. Purification was done by column chromatography over silica gel (60 - 120) with 10% EtOAc - hexanes as eluent.

$R_f$ = 0.10 (10% EtOAc - hexanes); low melting white solid; m.p: 32 – 33 $^oC$; yield: 86%; IR (KBr pellet): $\nu_{max}$ in $cm^{-1}$ 3447.0, 2951.0, 2921.0, 2851.0, 1601.0, 1469.0, 1437.0, 1356.0, 1233.0, 1123.0, 799.0, 722.0 ; $^1H$ NMR ($CDCl_3$, 600 MHz): δ 6.55 (s, 2H, Ar), 4.58 (s, 2H, $ArCH_2$), 3.92- 3.97 (m, 6H, 3 × $OCH_2$), 1.24 - 1.80 (m, 36H, 18 × $CH_2$), 0.88 (t, 9H, $J$ = 6 Hz, 3 × $CH_3$); $^{13}C$ NMR ($CDCl_3$, 150 MHz): 153.44, 137.70, 136.24, 105.48, 73.65, 69.28, 65.86, 32.12, 32.05, 30.52, 29.77, 29.61, 29.51, 22.89, 14.32; HRMS (ESI+) exact mass calculated for $C_{31}H_{57}O_4$ (M+1): 493.4251, Found: 493.4206.

Procedure for the synthesis of 3,4,5-tris(octyloxy)benzaldehyde (**14c**):

An appropriate (3,4,5-tris(octyloxy)phenyl)methanol (16.44 mmol, 1 equiv) was taken in $CH_2Cl_2$ (10 vol.). To this pyridinium chlorochromate (16.44 mmol, 1 equiv) adsorbed over equal amount of silica gel is added and stirred at room temperature for 1 h. The reaction mixture was filtered over celite bed and concentrated to get the crude product, which was further purified by column chromatography on silica gel (60 - 120) with 10% EtOAc - hexanes as eluent.

$R_f$ = 0.5 (10% EtOAc - hexanes); yellow viscous liquid; yield: 85%; IR (KBr pellet): $\nu_{max}$ in $cm^{-1}$ 3444.8, 2953.8, 2923.1, 2852.9, 1742.5, 1632.6, 1586.9, 1466.2, 1435.5, 1384.6, 1357.5, 1233.2, 1124.5, 721.5, 653.7; $^1H$ NMR ($CDCl_3$, 600 MHz): δ 9.82 (s, 1H, CHO), 7.08 (s, 2H, Ar), 4.02 - 4.06(m, 6H, 3 × $OCH_2$), 1.24 - 1.85 (m, 36H, 18 × $CH_2$), 0.87 – 0.89 (m, 9H, 3 × $CH_3$); $^{13}C$ NMR ($CDCl_3$, 150 MHz): 191.51, 153.73, 144.07, 131.65, 108.08, 73.86, 69.46, 32.10, 32.03, 30.55, 29.70, 29.55, 29.48, 26.29, 26.23, 22.88, 14.31; HRMS (ESI+) exact mass calculated for $C_{31}H_{55}O_4$ (M+1): 491.4095, Found: 491.4067.

Procedure for the synthesis of 3,4,5-tris(octyloxy)benzonitrile (**15c**):

3,4,5-tris(octyloxy)benzaldehyde (2.04 mmol, 1equiv) was added to a solution of hydroxyl amine hydrochloride (3.77 mmol, 1.85equiv ) in DMSO (4 mL), and the

resulting reaction solution was stirred and heated for 3 h at 100 $^{o}$C. After cooling to room temperature, water was added to the reaction mixture, which was then extracted with chloroform (5 × 20 mL). The combined chloroform layers were washed with water (4 × 20 mL) and dried with sodium sulfate. Removal of chloroform by rotatory evaporation and high vacuum yielded the desired product, which was then recrystallised with ethanol to get the pure product.

$R_f$ = 0.63 (10% EtOAc-hexanes); white solid; m.p: 33 – 36 $^{o}$C; yield: 70%; IR (KBr pellet): $\nu_{max}$ in cm$^{-1}$ 2953.8, 2923.1, 2853.4, 2225.2, 1694.5, 1580.5, 1501.6, 1467.7, 1427.9, 1239.4, 1124.8, 835.9, 722.9; $^{1}$H NMR ($CDCl_3$, 600 MHz): δ 6.81 (s, 2H, Ar), 4.00(t, 2H, $J$ = 6 Hz, 1 × $OCH_2$), 3.94 – 3.97 (m, 4H, 2 × $OCH_2$), 1.25 - 1.83 (m, 36H, 18 × $CH_2$), 0.87 – 0.90(m , 9H, 3 × $CH_3$); $^{13}$C NMR ($CDCl_3$, 150MHz): 153.66, 142.70, 119.50, 110.69, 106.37, 73.94, 69.63, 32.10, 32.02, 30.49, 29.68, 29.51, 29.38, 26.22, 22.90, 22.88, 14.31, 14.29. HRMS (ESI+) exact mass calculated for $C_{31}H_{54}NO_3$ (M+1): 488.4098, Found: 488.4091.

Procedure for the synthesis of 3,4,5-tris(octyloxy)-N'-hydroxybenzamidine **(16c):**

To a stirred solution of 3,4,5 – tris(octyloxy) benzonitrile (1.46 mmol, 1 equiv) in ethanol (5ml) was added hydroxylamine hydrochloride (3.21 mmol, 2.2 equiv) and then triethylamine (3.36 mmol, 2.3 equiv). The solution was stirred under reflux for 6 h and then diluted with water. Ethanol was removed under reduced pressure and the aqueous layer extracted two times with DCM. The combined organic phases were dried over anhyd. $Na_2SO_4$, evaporated under reduced pressure as the residue purified by recrystallization (ethanol) to afford the compound as a white solid.

$R_f$ = 0.54 (40% EtOAc-hexanes); white solid; m.p: 58 – 60 $^{o}$C; yield: 80%; $\nu_{max}$ in cm$^{-1}$ 3444.4, 2953.8, 2924.8, 2854.1, 1696.9, 1582.6, 1507.5, 1381.9, 1236.5, 1017.7 and 722.1; $^{1}$H NMR ($CDCl_3$, 600 MHz): δ 6.80 (s, 2H, Ar), 4.83 (s, 2H, $NH_2$), 3.95 - 4.01 (m, 6H, 3 × $OCH_2$), 1.24 - 1.82 (m, 36H, 18 × $CH_2$), 0.88 (t, 9H, $J$ = 6 Hz, 3 × $CH_3$); $^{13}$C NMR ($CDCl_3$, 150MHz): 153.46, 140.05, 127.66, 106.41, 104.84, 73.71, 69.48, 32.12, 32.05, 30.52, 29.58, 29.50, 26.30, 22.91, 22.88, 14.31; HRMS (ESI+) exact mass calculated for $C_{31}H_{57}N_2O_4$ (M+1): 521.4313, Found: 521.4316.

Procedure for the synthesis of 3-(3,4-bis(decyloxy)phenyl)-5-(4-(3-(3,4-bis(decyloxy)phenyl)-1,2,4-oxadiazol-5-yl)phenyl)-1,2,4-oxadiazole **(PO1)**

A mixture of 3,4-bis(decyloxy)-N'-hydroxybenzamidine (1.81 mmol, 2.1 equiv.) and dry pyridine (8 ml) was stirred under Ar atmosphere at 0 $^{o}$C. To this, a solution of terephthaloyl dichloride (0.86 mmol, 1 equiv.) in dry THF was added drop wise. The reaction mixture was refluxed for 12 h and then poured into cold water. The whole mass (a mixture of solid and water) was extracted with chloroform (2 × 50 ml). The combined extracts were washed with water, brine, dried over anhyd. $Na_2SO_4$ and concentrated under reduced pressure. The crude product was purified by column chromatography on

neutral alumina. Elution with DCM yielded the desired product. Recrystallization with ethyl acetate gives the pure product.

$R_f$ = 0.51 (70%$CH_2Cl_2$ - hexane); white solid; m.p: 137 – 139 $^oC$; yield: 61%; $\nu_{max}$ in $cm^{-1}$ 2949.9, 2921.9, 2851.3, 1605.9, 1564.7, 1442.4, 1333.0, 1262.0, 1264.8, 1125.6 and 751.1; $^1H$ NMR ($CDCl_3$, 400 MHz): δ 8.40 (s, 4H, Ar), 7.76 (d, 2H, $J$ = 8 Hz, Ar), 7.67 (s, 2H, Ar), 6.98 (d, 2H, $J$ = 8 Hz, Ar), 4.06 - 4.13 (m, 8H, 4 × -$OCH_2$), 1.25 - 1.90 (m, 64H, 32 × $CH_2$), 0.87 - 0.90(m, 12H, 4 × $CH_3$); $^{13}C$ NMR ($CDCl_3$, 100MHz): 174.47, 169.35, 152.12, 149.46, 128.97, 128.00, 121.26, 119.15, 113.23, 112.38, 69.58, 69.34, 32.15, 29.92, 29.87, 29.85, 29.82, 29.81, 29.67, 29.65, 29.60, 29.58, 29.47, 29.38, 26.28, 26.24, 22.92, 14.35; MALDI-TOF exact mass calculated for $C_{62}H_{95}N_4O_6$ (M+H): 991.7246, Found: 991.6606.

Procedure for the 3-(3,4-bis(decyloxy)phenyl)-5-(3-(3-(3,4-bis(decyloxy)phenyl)-1,2,4-oxadiazol-5-yl)phenyl)-1,2,4-oxadiazole **(MO1)**

A mixture of 3,4-bis(decyloxy)-N'-hydroxybenzamidine (0.88 mmol, 2.1 equiv) and dry pyridine (8ml) was stirred under Ar atmosphere at 0 $^oC$. To this, a solution of isophthaloyl dichloride (0.42 mmol, 1 equiv) in dry THF was added drop wise. The reaction mixture was refluxed for 12 h and then poured into cold water. The whole mass (a mixture of solid and water) was extracted with chloroform (2 × 50 ml). The combined extracts were washed with water, brine, dried over anhyd. $Na_2SO_4$ and concentrated under reduced pressure. The crude product was purified by column chromatography on neutral alumina. Elution with DCM yielded the desired product. Recrystallization with ethylacetate gives the pure product.

$R_f$ = 0.49 (70% $CH_2Cl_2$ - hexane); white solid; m.p: 101 – 103 $^oC$; yield: 54%; $\nu_{max}$ in $cm^{-1}$ 2920.3, 2851.0, 1605.5, 1554.8, 1410.0, 1373.3, 1224.6, 1144.0 and 750.9; $^1H$ NMR ($CDCl_3$, 400 MHz): δ 9.06(s, 1H, Ar), 8.44 (d, 2H, $J$ = 8 Hz, Ar), 7.75 - 7.79 (m, 3H, Ar), 7.68 (s, 2H, Ar), 6.99 (d, 2H, $J$ = 4 Hz, Ar), 4.13(t, 4H, $J$ = 8 Hz, 2× $OCH_2$), 4.08 ( t, 4H, $J$ = 8 Hz, 2× $OCH_2$), 1.27 -1.91(m, 64H, 32 × $CH_2$), 0.87 - 0.90(m, 12H, 4 × $CH_3$); $^{13}C$ NMR ($CDCl_3$, 100MHz): 174.40, 169.29, 152.10, 149.98, 131.98, 130.20, 127.92, 125.75, 121.26, 119.21, 113.26, 112.40, 69.58, 69.35, 32.14, 29.85, 29.81, 29.67, 29.58, 29.48, 29.39, 26.29, 26.24, 22.91, 14.33; MALDI-TOF exact mass calculated for $C_{62}H_{95}N_4O_6$ (M+H): 991.7246, Found: 991.6578.

Procedure for the synthesis of 3-(3,4,5-tris(decyloxy)phenyl)-5-(4-(3-(3,4,5-tris(decyloxy)phenyl)-1,2,4-oxadiazol-5-yl)phenyl)-1,2,4-oxadiazole **(PO2)**

A mixture of 3,4,5-tris(decyloxy)-N'-hydroxybenzamidine (0.69 mmol, 2.1 equiv) and dry pyridine (6ml) was stirred under Ar atmosphere at 0 $^oC$. To this, a solution of terephthaloyl dichloride (0.33 mmol, 1 equiv) in dry THF was added drop wise. The reaction mixture was refluxed for 12 h and then poured into cold water. The whole mass (a mixture of solid and water) was extracted with chloroform (2 × 50 ml). The combined

extracts were washed with water, brine, dried over anhyd. $Na_2SO_4$ and concentrated under reduced pressure. The crude product was purified by column chromatography on neutral alumina. Elution with DCM yielded the desired product. Recrystallization with ethylacetate gives the pure product.

$R_f$ = 0.75 (70% $CH_2Cl_2$ - hexane); white solid; yield: 57%; $\nu_{max}$ in $cm^{-1}$ 2923.6, 2853.8, 1746.1, 1593.0, 1505.9, 1437.9, 1392.1, 1334.4, 1116.1 and 723.3; $^1H$ NMR ($CDCl_3$, 400 MHz): δ 8.41(s, 4H, Ar), 7.38 (s, 4H, Ar), 4.08 - 4.11(m, 8H, 4× $OCH_2$), 4.04 (t, 4H, $J$ = 8 Hz, 2 × $OCH_2$ ), 1.27 - 1.89(m, 96H, 48 × $CH_2$), 0.88 (t, 18H, $J$ = 8 Hz, 6 × $CH_3$); $^{13}C$ NMR ($CDCl_3$, 150MHz): 174.57, 169.49, 153.74, 141.10, 129.01, 127.95, 121.41, 106.07, 73.78, 69.46, 32.17, 32.15, 30.58, 29.98, 29.91, 29.88, 29.83, 29.65, 29.59, 26.34, 22.92, 14.35. MALDI-TOF exact mass calculated for $C_{82}H_{135}N_4O_8$ (M+H): 1304.0274, Found: 1304.041.

Procedure for the synthesis of 3-(3,4,5-tris(decyloxy)phenyl)-5-(3-(3-(3,4,5-tris(decyloxy)phenyl)-1,2,4-oxadiazol-5-yl)phenyl)-1,2,4-oxadiazole **(MO2)**

A mixture of 3,4,5-tris(decyloxy)-N'-hydroxybenzamidine (1.22 mmol, 2.1 equiv) and dry pyridine (5ml) was stirred under Ar atmosphere at 0 $^oC$. To this, a solution of isophthaloyl dichloride (0.58 mmol, 1 equiv) in dry THF was added drop wise. The reaction mixture was refluxed for 12 h and then poured into cold water. The whole mass (a mixture of solid and water) was extracted with chloroform (2 × 50 ml). The combined extracts were washed with water, brine, dried over anhyd. $Na_2SO_4$ and concentrated under reduced pressure. The crude product was purified by column chromatography on neutral alumina. Elution with DCM yielded the desired product. Recrystallization with ethyl acetate gives the pure product.

$R_f$ = 0.65 (70% $CH_2Cl_2$-hexane); white solid; yield: 55%; $\nu_{max}$ in $cm^{-1}$ 2956.5, 2923.14, 2853.0, 1744.5, 1588.2, 1492.1, 1357.5, 1124.4 and 722.3; $^1H$ NMR ($CDCl_3$, 600 MHz): δ 9.07 (s, 1H, Ar), 8.46 (d, 2H, $J$ = 6Hz, Ar), 7.76 - 7.79 (m, 1H, Ar), 7.40 (s, 4H, Ar), 4.10 (t, 8H, $J$ = 6 Hz, 4× $OCH_2$), 4.04 (t, 4H, $J$ = 6 Hz , 2 × $OCH_2$ ), 1.25 - 1.88( m, 96H, 48 × $CH_2$), 0.88 (t, 18H, $J$ = 6Hz , 6 × $CH_3$); $^{13}C$ NMR ($CDCl_3$, 150MHz): 174.55, 169.47, 153.77, 141.15, 132.11, 130.26, 127.98, 125.70, 121.46, 106.14, 73.80, 69.51, 32.14, 30.58, 29.97, 29.91, 29.88, 29.83, 29.81, 29.66, 29.61, 26.36, 26.33, 22.91, 14.33. MALDI-TOF exact mass calculated for $C_{82}H_{135}N_4O_8$ (M+H): 1304.0274, Found: 1304.106.

Procedure for the synthesis of 3-(3,4,5-tris(dodecyloxy)phenyl)-5-(4-(3-(3,4,5-tris(dodecyloxy)phenyl)-1,2,4-oxadiazol-5-yl)phenyl)-1,2,4-oxadiazole **(PO3)**

A mixture of 3,4,5-tris(dodecyloxy)-N'-hydroxybenzamidine (0.73 mmol, 2.1 equiv) and dry pyridine (5ml) was stirred under Ar atmosphere at 0 $^oC$. To this, a solution of terephthaloyl dichloride (0.35 mmol, 1 equiv) in dry THF was added drop wise. The

reaction mixture was refluxed for 12 h and then poured into cold water. The whole mass (a mixture of solid and water) was extracted with chloroform (2 × 50 ml). The combined extracts were washed with water, brine, dried over anhyd. $Na_2SO_4$ and concentrated under reduced pressure. The crude product was purified by column chromatography on neutral alumina. Elution with DCM yielded the desired product. Recrystallization with ethylacetate gives the pure product.

$R_f$ = 0.79 (70% $CH_2Cl_2$ - hexane); white solid; yield: 56%; $\nu_{max}$ in $cm^{-1}$ 2921.8, 2851.0, 1745.8, 1605.4, 1563.7, 1436.6, 1357.6, 1231.5 and 750.5; $^1H$ NMR ($CDCl_3$, 600 MHz): δ 8.41 (s, 4H, Ar), 7.39 (s, 4H, Ar), 4.09 (t, 8H, *J* = 6 Hz, 4× $OCH_2$), 4.04 (t, 4H, *J* = 6 Hz, 2 × $OCH_2$ ), 1.24 -1.88 (m, 120H, 60 × $CH_2$), 0.87 - 0.89(m, 18H, 6 × $CH_3$); $^{13}C$ NMR ($CDCl_3$, 150MHz): 174.60, 169.52, 153.77, 141.19, 129.03, 127.99, 121.44, 106.16, 73.80, 69.51, 32.17, 30.59, 29.99, 29.95, 29.89, 29.84, 29.66, 29.63, 29.61, 26.35, 22.93, 14.35. MALDI-TOF exact mass calculated for $C_{94}H_{159}N_4O_8$ (M+H): 1472.2152, Found: 1472.163.

Procedure for the synthesis of 3-(3,4,5-tris(dodecyloxy)phenyl)-5-(3-(3-(3,4,5-tris(dodecyloxy)phenyl)-1,2,4-oxadiazol-5-yl)phenyl)-1,2,4-oxadiazole **(MO3)**

A mixture of 3,4,5-tris(dodecyloxy)-N'-hydroxybenzamidine (0.5 mmol, 2.1 equiv) and dry pyridine (5ml) was stirred under Ar atmosphere at 0 $^oC$. To this, a solution of isophthaloyl dichloride (0.24 mmol, 1 equiv) in dry THF was added drop wise. The reaction mixture was refluxed for 12 h and then poured into cold water. The whole mass (a mixture of solid and water) was extracted with chloroform (2 × 50 ml). The combined extracts were washed with water, brine, dried over anhyd. $Na_2SO_4$ and concentrated under reduced pressure. The crude product was purified by column chromatography on neutral alumina. Elution with DCM yielded the desired product. Recrystallization with ethylacetate gives the pure product.

$R_f$ = 0.76 (70% $CH_2Cl_2$ - hexane); white solid; yield: 54%; $\nu_{max}$ in $cm^{-1}$ 2954.3, 2919.7, 2850.3, 1619.4, 1593.3, 1434.0, 1354.8, 1259.7, 1235.0 and 748.3; $^1H$ NMR ($CDCl_3$, 600 MHz): δ 9.07 (s, 1H, Ar), 8.46 (d, 2H, *J* = 12Hz, Ar), 7.76 - 7.79 (m, 1H, Ar), 7.40 (s, 4H, Ar), 4.10 (t, 8H, *J* = 6Hz, 4 × -$OCH_2$), 4.04 (t, 4H, *J* = 6 Hz, 2× $OCH_2$), 1.25 - 1.88 (m, 120H, 60 × $CH_2$), 0.86 - 0.89 (m, 18H, 6 × $CH_3$); $^{13}C$ NMR ($CDCl_3$, 150MHz): 174.53, 169.46, 153.76, 141.11, 132.10, 130.25, 127,97, 125.69, 121.45, 106.10, 73.78, 69.48, 32.16, 30.59, 29.94, 29.89, 29.84, 29.67, 29.63, 29.60, 26.36, 22.92, 14.34. MALDI-TOF exact mass calculated for $C_{94}H_{159}N_4O_8$ (M+H): 1472.2152, Found: 1472.2060.

Procedure for the synthesis of 3-(3,4,5-tris(octyloxy)phenyl)-5-(4-(3-(3,4,5-tris(octyloxy)phenyl)-1,2,4-oxadiazol-5-yl)phenyl)-1,2,4-oxadiazole **(PO4)**

A mixture of 3,4,5-tris(octyloxy)-N'-hydroxybenzamidine (0.94 mmol, 2.1 equiv) and dry pyridine (5ml) was stirred under Ar atmosphere at 0 $^oC$. To this, a solution of terephthaloyl dichloride (0.45 mmol, 1 equiv.) in dry THF was added drop wise. The

reaction mixture was refluxed for 12 h and then poured into cold water. The whole mass (a mixture of solid and water) was extracted with chloroform (4 × 30 ml). The combined extracts were washed with water, brine, dried over anhyd. $Na_2SO_4$ and concentrated under reduced pressure. The crude product was purified by column chromatography on neutral alumina. Elution with DCM yielded the desired product. Recrystallization with ethylacetate gives the pure product.

$R_f$ = 0.7 (70% $CH_2Cl_2$ - hexane); white solid; yield: 59%; $\nu_{max}$ in $cm^{-1}$ 2922.4, 2853.8, 1634.7, 1602.3, 1503.5, 1436.8, 1356.6, 1231.0 and 749.0; $^1$H NMR ($CDCl_3$, 400 MHz): δ 8.41 (s, 4H, Ar), 7.39 (s, 4H, Ar), 4.03 - 4.11(m, 12H, 6× $OCH_2$), 1.25 - 1.89(m, 72H, 36 × $CH_2$), 0.88 -0.91(m, 18H, 6 × $CH_3$); $^{13}$C NMR ($CDCl_3$, 150MHz): 174.58, 169.49, 153.75, 141.15, 129.01, 127.96, 121.42, 106.12, 73.79, 69.49, 32.13, 32.07, 30.57, 29.77, 29.60, 29.53, 26.34, 22.90, 14.33. MALDI-TOF exact mass calculated for $C_{70}H_{111}N_4O_8$ (M+H): 1135.8396, Found: 1135.9560.

Procedure for the synthesis of 3-(3,4,5-tris(octyloxy)phenyl)-5-(3-(3-(3,4,5-tris(octyloxy)phenyl)-1,2,4-oxadiazol-5-yl)phenyl)-1,2,4-oxadiazole **(MO4)**

A mixture of 3,4,5-tris(octyloxy)-N'-hydroxybenzamidine (0.94 mmol, 2.1 equiv) and dry pyridine (6ml) was stirred under Ar atmosphere at 0 $^oC$. To this, a solution of isophthaloyl dichloride (0.45 mmol, 1 equiv) in dry THF was added drop wise. The reaction mixture was refluxed for 12 h and then poured into cold water. The whole mass (a mixture of solid and water) was extracted with chloroform (4 × 50 ml). The combined extracts were washed with water, brine, dried over anhyd. $Na_2SO_4$ and concentrated under reduced pressure. The crude product was purified by column chromatography on neutral alumina. Elution with DCM yielded the desired product. Recrystallization with ethylacetate gives the pure product.

$R_f$ = 0.64 (70% $CH_2Cl_2$ - hexane); white solid; yield: 57%; $\nu_{max}$ in $cm^{-1}$ 2955.5, 2922.6, 2850.0, 1598.0, 1554.5, 1359.9, 1236.0, 1133.4 and 723.0; $^1$H NMR ($CDCl_3$, 400 MHz): δ 9.08 (s, 1H, Ar), 8.46 (d, 2H, *J* = 8Hz, Ar), 7.78 (t, 1H, *J* = 12Hz, Ar), 7.40 (s, 4H, Ar), 4.09 – 4.12 (m, 8H, 4× $OCH_2$), 4.03 - 4.06 (m, 4H, 2 × $OCH_2$ ), 1.25 - 1.90(m, 72H, 36 × $CH_2$), 0.87 - 0.90 (m, 18H, 6 × $CH_3$); $^{13}$C NMR ($CDCl_3$, 100MHz): 174.54, 169.45, 153.75, 141.09, 132.10, 125.67, 121.45, 106.06, 73.79, 69.48, 32.14, 32.07, 30.58, 29.92, 29.77, 29.61, 29.53, 26.35, 26.32, 22.93, 22.91, 14.34; MALDI-TOF exact mass calculated for $C_{70}H_{111}N_4O_8$ (M+H): 1135.8396, Found: 1135.7360.

## 5.5. References

1. (a) J. W. Goodby, P. J. Collings, T. Kato, C. Tschierske, H. Gleeson and P. Raynes, *Wiley-VCH, Weinheim, Germany*, 2014, **1**. *Handbook of Liquid Crystals: Fundamentals*, ed. (b) C. Tschierske, *Angew. Chem. Int. Ed.*, 2013, **52**, 8828 –

8878.
2. (a) *Self-organized Organic Semiconductors – From Materials to Device Applications (Ed.: Q. Li), Wiley, Hoboken,* 2011; (b) *Anisotropic Nanomaterials: Preparation, Properties and Applications (Ed.: Q. Li) Springer,* 2015; (c) B. R. Kaafarani, *Chem. Mater.* 2011, **23**, 378−396.
3. M. O'Neill and S. M. Kelly, *Adv. Mater.*, 2011, **23**, 566–584
4. W. Xie, Z. Wu, S. Liu and S. T. Lee, *J. Phys. D: Appl. Phys.*, 2003, **36**, 2331-2334; (b) W. Xie, Z. Wu and S. Liu, *Opt. Quantum Electron.*, 2004, **36**, 635-640; (c) H. Bi, K. Ye, Y. Zhao, Y. Yang, Y. Liu and Y. Wang, *Org. Electron.*, 2010, **11**, 1180-1184; (d) X. Gong, S. Wang, D. Moses, G. C. Bazan and A. J. Heeger, *Adv. Mater.*, 2005, **17**, 2053-2058.
5. (a) P. I. Shih, C. Y. Chuang, C. H. Chien, E. W. G. Diau and C. F. Shu, *Adv. Funct. Mater.*, 2007, **17**, 3141-3146; (b) H. C. Li, Y. P. Lin, P. T. Chou, Y. M. Cheng and R. S. Liu, *Adv. Funct. Mater.*, 2007, **17**, 520-530; (c) C. J. Tonzola, A. P. Kulkarni, A. P. Gifford, W. Kaminsky and S. A. Jenekhe, *Adv. Funct. Mater.*, 2007, **17**, 863-874.
6. (a) Z. Zhao, S. Chen, J. W. Y. Lam, P. Lu, Y. Zhong, K. S. Wong, H. S. Kwok and B. Z. Tang, *Chem. Commun.*, 2010, **46**, 2221-2223; (b) Z. Zhao, J. W. Y. Lam and B. Z. Tang, *J. Mater. Chem.*, 2012, **22**, 23726-23740.
7. (a) S. Tao, Z. Peng, P. Wang, C.-S. Lee and S.-T. Lee, *Adv. Funct. Mater.*, 2005, **15**, 1716–721; (b) N.-X. Hu, M. Esteghamatian, S. Xie, Z. Popovic, Ah.-M. Hor, O. Beng and S. Wang, *Adv. Mater.*, 1999, **11**, 1460–1463.
8. B. Roy, N. De and K. C. Majumdar, *Chem. Eur. J.*, 2012, **18**, 14560-14588.
9. F. Dumur and F. Goubard, *New J. Chem*, 2014, **38**, 2204-2224.
10. M. L. Parra, P. I. Hidalgo, E. A. Soto-Bustamante, J. Barbera´, E. Y. Elgueta and V. H. Trujillo-Rojo, *Liquid Cryst.*, 2008, **35**, 1251-1262.
11. H. Gallardo, R. Cristiano, A. A. Vieiraa, R. A. W. N. Filho, R. M. Srivastava and I. H. Bechtold, *Liquid Cryst.*, 2008, **35**, 857-863.
12. S. I. Torgova, L. A. Karamysheva, T. A. Geivandova and A. Strigazzi, *Mol. Cryst. and Liq.Cryst.*, 2001, **365**, 99-106.
13. Q. Li, L.S. Cui, C. Zhong, Z. Q. Jiang and L. S. Liao, *Org. Lett.*, 2014, **16**, 1622-1625.
14. (a) P. Dastidar, *Chem. Soc. Rev.*, 2008, **37**, 2699-2715; (b) S. S. Babu, V. K. Praveen and A. Ajayaghosh, *Chem. Rev.*, 2014, **114**, 1973-2129.
15. (a) S. S. Babu, S. Prasanthkumar and A. Ajayaghosh, *Angew. Chem., Int. Ed.*, 2012, **51**, 1766-1776; (b) S. Diring, F. Camerel, B. Donnio, T. Dintzer, S. Toffanin, R. Capelli, M. Muccini and R. Ziessel, *J. Am. Chem. Soc.*, 2009, **131**, 18177-18185.
16. (a) J. H. Jung, Y. Ono and S. Shinkai, *Angew. Chem., Int. Ed.*, 2000, **39**, 1862-1865; (b) S. Kobayashi, N. Hamasaki, M. Suzuki, M. Kimura, H. Shirai and K. Hanabusa, *J. Am. Chem. Soc.*, 2002, **124**, 6550-6551; (c) E. D. Sone, E. R. Zubarev and S. I. Stupp, *Angew. Chem., Int. Ed.*, 2002, **41**, 1705-1709; (d) G. Gundiah, S. Mukhopadhyay, U. G. Tumkurkar, A. Govindaraj, U. Maitra and C.N.R. Rao, *J. Mater. Chem.*, 2003, **13**, 2118-2122.
17. C. Wang, Q. Chen, F. Sun, D. Zhang, G. Zhang, Y. Huang, R. Zhao and D. Zhu, *J.*

*Am. Chem. Soc*., 2010, **132**, 3092-3096.
18. V. K. Praveen, C. Ranjith and N. Armaroli, *Angew. Chem. Int. Ed.*, 2013, **53**, 365–368.
19. (a) A. S. Achalkumar, U. S. Hiremath, D. S. Shankar Rao, S. Krishna Prasad, and C. V. Yelamaggad, *J. Org. Chem.*, 2013, **78**, 527−544; (b) A. S. Achalkumar and C. V. Yelamaggad, *Tetrahedron Letters*, 2012, **53**, 7108-7112; (c) Achalkumar, A. S.; Veerabhadraswamy, B. N.; Hiremath, U. S.; Shankar Rao, D. S.; Krishna Prasad, S.; Yelamaggad, C. V. *Dyes and Pigments*, 2016, **132**, 291-295.
20. S. T. Chill and R. C. Mebane, *Synthetic Communications*, 2009, **39**, 3601-3606.
21. D. Conole, T. M. Beck, M. Jay-Smith, M. D. Tingle, C. T. Eason, M. A. Brimble and D. Rennison, *Bioorganic & Medicinal Chemistry*, 2014, **22**, 2220-2223.
22. X. Yang, H. Dai, Q. He, J. Tang, X. Cheng, M. Prehm, and C. Tschierske, *Liq. Cryst.*, 2013, **40**, 8, 1028-1034.
23. (a) F. Liu, R. Kieffer, X. Zeng, K. Pelz, M. Prehm, G.Ungar and C. Tschierske, *Nature Communications*, 2012, **3:1104**, 1-7; (b) H. F. Gao, Y. F. Ye, L. Y. Kong, X. H. Cheng, M. Prehm, H. Ebert and C. Tschierske, *Soft Matter*, 2012, **8**, 10921– 10931; (c) X. H. Cheng, H. F. Gao, X. P. Tan, X. Y. Yang, M. Prehm, H. Ebert and C. Tschierske, *Chem. Sci*., 2013, **4**, 3317–3331; (d) H. F. Gao, H. Cheng, Z. Yang, M. Prehm, X. Cheng and C. Tschierske, *J. Mater. Chem. C*, 2015, **3**, 1301-1308.
24. (a) F. Wu¨rthner, T. E. Kaiser and C. R. Saha-Mu¨ller, *Angew. Chem., Int. Ed*., 2011, **50**, 3376-3410; (b) F. Wu¨rthner, C. Bauer, V. Stepanenko and S. A Yagai, *Adv. Mater*., 2008, **20**, 1695-1806; (c) F. Wu¨rthner, C. Thalacker, S. Diele and C. Tschierske, *Chem.–Eur. J*., 2001, **7**, 2245-2253.
25. (a) K.-R. Wee, Y. –J. Cho, S. Jeong, S. Kwon, J. D. Lee, I. H. Suh and S. O Kang, *J. Am. Chem. Soc*., 2012, **134**, 17982-17990; (b) P. Venkatakrishnan, P. Natarajan, J. N. Moorthy, Z. Lin and T. J. Chow, *Tetrahedron*, 2012, **68**, 7502-7508.
26. (a) I. Abu Bin, S. Takahiro and T. Yukikazu, *Polym. J*., 2010, **42**, 839-851; (b) A. Harada, R. Kobayashi, Y. Takashima, A. Hashidzume and H. Yamaguchi, *Nat. Chem.* 2011, **3**, 34-37; (c) T. Yamamoto and M. Yoshida, *Langmuir*, 2012, **28**, 8463-8469; (d) K. Yuichiro, T. Yoshinori, H. Akihito, Y. Hiroyasu and H. Akira, *Sci. Rep.*, 2013, **3,** 1243-1243-4. (e) M. Zhang, D. Xu, X. Yan, J. Chen, S. Dong, B. Zheng and F. Huang, *Angew. Chem., Int. Ed*., 2012, **51**, 7011-7015; (f) R.Yoshida, *Adv. Mater.*, 2010, **22**, 3463-3483.
27. E. R. Zubarev, M. U. Pralle, E. D. Sone and S. I. Stupp, *Adv. Mater*., 2002, **14**, 198-203.
28. (a) G. Di, X. Min, P. Junxia, L. Jing, Y. Ni, H. Panli and F. Yu, *Tetrahedron*, 2010, **66**, 2961-3142; (b) Y. Kenji, A. Natsuki, O. Yoshiyuki, A. Tetsuyuki, S. Hideyuki, T. Masayuki, S. Seiji and N. R. David, *Chem.Eur. J*., 1999, **5**, 2722-2729; (c) A. Vidyasagar, K. Handore and K. Sureshan, *Angew.Chem. Int. Ed*., 2011, **50**, 8021-8024.
29. A. P. Sivadas, N. S. S. Kumar, D. D. Prabhu, S. Varghese, S. K. Prasad, D. S. S. Rao and S. Das, *J. Am. Chem. Soc.*, 2014, **136**, 5416–5423.

30. (a) A. Mahler, M. Reches, M. Rechter, S. Cohen and E. Gazit, *Adv. Mater*., 2006, **18**, 1365-370; (b) L. O'Leary, J. Fallas, E. Bakota, M. Kang and J. Hartgerink, *Nat. Chem*., 2011, **3**, 821-828.
31. (a) S. Basak, S. Bhattacharya, A. Datta and A. Banerjee, *Chem.– Eur. J.*, 2014, **20**, 5721-5726; (b) F. Alexandre, D. J. Marc, G. D. Todor, I. G. Nikolai, A. V. Aleksey and V. Eric, *J.Am. Chem. Soc*., 2006, **128**, 7661-7669; (c) M. Cigan, J. Donovalova, V. Szocs, J. Gaspar, K. Jakusova and A. Gaplovsky, *J. Phys. Chem. A*, 2013, **117**, 4870-4883; (d) Q. Fang, F. Wang, H. Zhao, X. Liu, R. Tu, D. Wang and Z. Zhang, *J. Phys. Chem. B*, 2008, **112**, 2837-2841; (e) V. Lau and B. Heyne, *Chem. Commun*., 2010, **46**, 3595-3597; (f) U. Rosch, S. Yao, R. Wortmann and F. Wurthner, *Angew. Chem., Int. Ed*., 2006, **45**, 7026-7030; (g) L. Liangde, J. L. Rene, L. P. Thomas, P. Jerry and G. W. David, *J. Am. Chem. Soc*., 1999, **121**, 8146-8156; (h) Y. Seong-Jun, C. Jong Won, G. Johannes, K. Kil Suk, C. Moon-Gun, K. Dongho and P. Soo Young, *J. Am. Chem. Soc*., 2010, **132**, 13675-13683; (i) Y. Seong-Jun and P. SooYoung, *J. Mater. Chem*., 2011, **21**, 8338-8346; (j) C. Jiajia, L.Yan, H. Song, L. Chang, Z. Liancheng and Z. Xianshun, *Chem. Commun*., 2013**, 49**, 6259-6261.
32. D. D. Prabhu, A. P. Sivadas and S. Das, *J. Mater. Chem.*, 2014, **2**, 7039-7046.
33. A. Takahashi, M. Sakai and T. Kato, *Polym. J*., 1980, **12**, 335-341.

# Chapter VI

# Stilbene amide based star-shaped mesogens

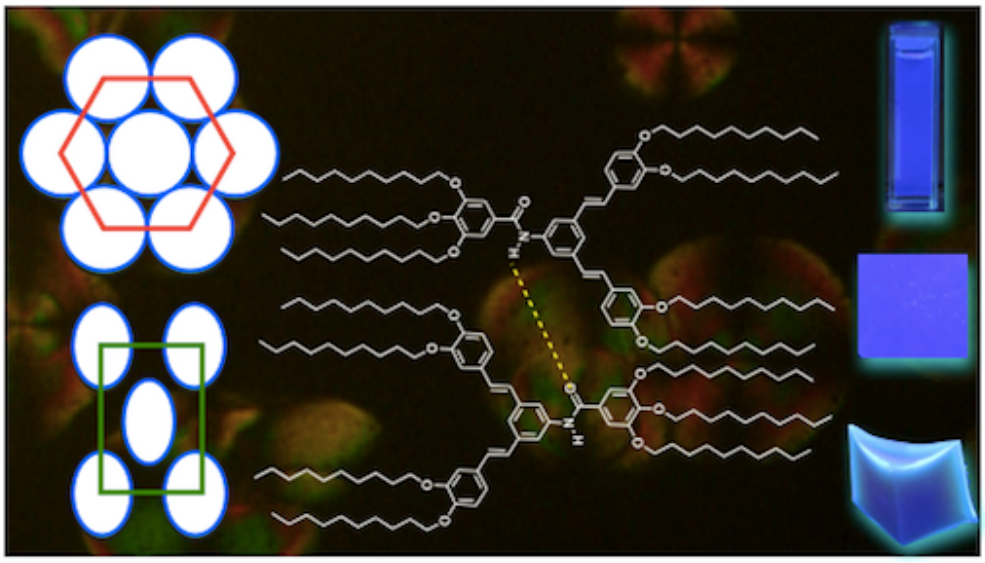

## 6.1. Introduction

Molecular self-assembly plays a crucial role in the development of functional soft materials.[1] There are various functional supramolecules such as dendrimers, peptosomes, microcapsules, micelles, organogels and liquid crystalline materials that are formed through molecular self-assembly. Organogels and liquid crystals are one such example where the engineered molecules exhibit the desired functions in the self-assembled state. Columnar liquid-crystalline (Col LC) self-assembly of disc shaped molecules was discovered in 1977,[2] and this unique one-dimensional (1D) self-assembly has potential in the development of organic light emitting diodes (OLED),[3] organic field-effect transistors (OFETs),[4] organic photovoltaics (OPVs),[5] gas sensors and lubricants.[6] The efficiency of these devices depends on the intermolecular order, which help in the charge migration along the columnar phases.[6,7] Thus, the molecular design principle of Col LCs involves the utilization of various secondary interactions such as H-bonding, π-π, ionic, hydrophilic and hydrophobic interactions apart from the molecular shape anisotropy that leads to the nanoseggregation of incompatible molecular subunits.[8,9] After the discovery of the Col phase in disc-shaped molecules, there were many different nonconventional molecular designs to stabilize Col phases. Shape-persistent star-shaped mesogens[10-13] or hekates,[11,12] are one of the nonconventional LCs formed by the covalent linking of three rigid arms symmetrically to a central core through linkers. Their lack of shape anisotropy to exhibit mesophases is compensated by the nanophase segregation of chemically/physically different molecular subunits and their tendency toward efficient space filling. More recently, propeller-like 1,3,5-triphenyl benzenes exhibiting ordered columnar phases have been reported.[13] Inherent synthetic flexibility and the easy incorporation of properties such as hole/electron transport, nonlinear optical activity, fluorescence and the ability to exhibit a rich variety of mesophases such as nematic, columnar, cubic or soft crystals comprise the uniqueness of hekates in comparison to discotics. The presence of the voids between the arms of these star-shaped molecules promotes the glassy state.[11,12] Columnar phases with a glassy nature are important because they allow the movement of charge carriers with a simultaneous restriction on

ionic impurities.[14] In the context of the application of Col phases towards OLEDs, it is important to stabilize the Col phase along with the preserved solid-state luminescence. This is because aggregation quenching of luminescence is detrimental to device performance. Similarly, organogels comprise the three-dimensional network of entangled supramolecular fibers that is formed by the self-assembly of a low-molecular weight gelator, entrapping a large volume of the solvent.[15,16] The 1D self-assembly of the molecules in the form of fibers has great potential in the area of optoelectronics, controlled drug release, [17] energy transfer, [18,19] sensing,[20] and security.[21,22]

Both self-assemblies, i.e., Col LCs and organogels, can be designed and tuned to have properties such as long-range order and high charge-carrier mobility in addition to their inherent properties such as self-healing ability, ease of processing, high solubility to enhance their application in the fabrication of electronic devices.[8,9,15,16] These self-assemblies bring about anisotropies in the physical properties; for example, the conductivity along the column is greater whereas that across the column is smaller by many orders. The emission may be more in the bulk state if the molecules form slip-stacked or J-type aggregates, whereas it gets quenched when they form cofacial or H-type aggregates.[2,3] The aggregation-caused quenching (ACQ) due to the nonradiative decay of the excited state is a notorious problem in decreasing the luminescence efficiency in aggregates, which have strong π-π interactions. Because the planar structure of the molecule is a prerequisite for the stabilization of the Col phase and vital for charge migration, this is a delicate problem to address. Thus, the design should include an option to preserve both the columnar order and the emissive nature.

There is a class of molecules that show the phenomenon of aggregation-induced emission (AIE), where luminescence quenching is avoided because of the restricted rotation of the fluorophores. Hence, there is a flurry of activity to synthesize molecules that exhibit the AIE phenomenon over the whole visible region[24] and eventually target their application in solid-state emissive displays. In spite of these efforts, the molecules that exhibit aggregation-induced blue light emission are very rare. Further columnar self-assembly of such molecules is a challenging task. Considering the scarcity and the vital

role in the construction of a full color display and white light emission[25-27] while developing such molecules, which combine columnar self-assembly, blue emission and the AIE phenomenon, is of foremost importance. Again, the absence of a general protocol makes molecular design complicated and demanding.

It will be ideal if a molecule exhibits LC behavior and the ability to undergo gelation while maintaining the same order. Such compounds are suitable candidates for the applications in optoelectronic devices.[28,29] To achieve this, the molecule should have the ability to self-assemble into columnar aggregates, and the interaction of these aggregates with the solvents must not destabilize the columnar self-assembly. The incorporation of functionalities such as amide, hydroxyl, acid, large aromatic units and steroid moieties often known to support gelation and in few case less than 1 weight % of a molecule is sufficient to gelate a large volume of slovents. Such compounds are known as supergelators.[30] There are some reports on fluorescent amide derivatives that employ the hydrogen bonding to form large 3D entangled networks, which help in entrapping the solvent.[31,32]

Though some reports on the mesogens containing amide units are reported, their gelation properties are not explored in detail. It should be noted that such molecules with amide units stabilized a wide mesophase range including room temperature.[33] Stabilizing room-temperature Col phase is also another factor that will enhance the performance of the semiconductor because most of them crystallize at room temperature, leading to defects that might act as charge traps. Amide units are incorporated as linking units between the central core and peripheral tails in the case of discotics to overcome the Coulombic repulsion between the cores, resulting in a reduced intracolumnar distance and hence a high charge-carrier mobility.[34] Recently, there has been a report where the introduction of amide units stabilized a ferroelectrically switching Col phase.[35]

The *trans*-Stilbene unit has been known for its excellent photochemical/photophysical properties,[36] and has found many commercial applications *viz.*, optical brightener, laser dyes, the fabrication of OLEDs, photoresists,

photoconductive devices, optical switching and non linear optics (NLO). Coya *et. al.* fabricated a blue OLED from 1,3,5-tris(3,4,5-tris(dodecyloxy)styryl benzene, but the molecules were crystalline at room temperature.[37] Lehman *et. al.* reported a star shaped stilbene based molecule that stabilized the Col phase over a thermal range of 37°.[38] Yelamaggad *et. al.* reported the star-shaped molecules based on *trans*-stilbene stabilizing the $Col_h$ phase; however, the compound is a green light emitter in solution, and a further red shift was seen in the solid state.[39,40]

In this chapter, we have designed a star-shaped molecule where the central benzene ring is connected to two *trans*-stilbene fluorophores at alternate positions, and the other meta position is occupied by a peripherally substituted alkoxybenzene connected through an amide linkage. Peripherally substituted *trans*-stilbenes were chosen for their emissive nature, and the amide linkage was introduced as a possible means to achieve room-temperature liquid crystallinity and gelation. Further variation in the structure was carried out by varying the number of alkyl tails in these peripheral rings to tune the thermal and gelation behavior (Fig. 6.2).

## 6.2. Results and discussion

### 6.2.1. Synthesis and Characterization

The synthesis route for the preparation of the target molecules is depicted in schemes 6.1 and 6.2 (See the experimental and characterization data). *m*-Xylene was subjected to oxidation by refluxing in an alkaline aqueous solution of $KMnO_4$ to obtain isophthalic acid (**24**), which was nitrated by heating with the nitration mixture to get 5-nitro benzene-1,3-dioic acid (**23**). This compound was reduced with $NaBH_4$ in presence of Lewis acid $BF_3{\cdot}Et_2O$ to get 3,5-bis-(hydroxymethyl) nitrobenzene (**22**). This alcohol was further reacted with $PBr_3$ to obtain 3,5-bis–(bromomethyl)nitrobenzene **(21)**. The Michaelis–Arbuzov reaction of compound **(21)** with the triethylphosphite furnished 1,3-bis((diethoxyphosphoryl)methyl)-5-nitrobenzene (**20**). The requisite aldehyde (**9b-c**) were prepared in quantitative yields by different methods as follows; (i) 3,4,-decyloxy benzaldehyde (**9b**) was prepared by the *O*-alkylation of 3,4-dihydroxybenzaldehyde with

*n*-bromodecane following Williamson's etherification protocol; (ii) 3,4,5-tridecyloxy benzaldehyde (**9c**) was synthesized by the oxidation of 3,4,5-tridecyloxy benzyl alcohol (**8c**) using pyridiniumchlorochromate that in turn was obtained by the reduction of ethyl 3,4,5-tridecyloxy benzoate (**1c**). The Wittig-Horner reaction of these benzaldehydes **(9b-c)** with the phosphonate ester (**20**) in the presence of NaH in THF at 0 $^{o}$C furnished (*E*)-1,3-bis(3,4-bis(decyloxy)styryl)-5-nitrobenzene **(18a)** and (*E*)-5-(3-(3,4,5-tris(decyloxy)styryl)-5-nitrostyryl)-1,2,3-tris(decyloxy)benzene **(18b)** respectively. These nitro products were converted to corresponding key amines, (*E*)-3,5-bis(3,4-bis(decyloxy)styrl) benzenamine (**19a**) and (*E*)-3,5-bis(3,4,5-tris(decyloxy)styrl) benzenamine (**19b**) respectively. Finally, aminostyryl compound **19a** was reacted with 3,4-didecyloxy benzoyl chloride and 3,4,5-tridecyloxybenzoyl chloride to obtain target molecules (**SA1**) and (**SA2**) respectively. These acid chlorides were obtained by refluxing corresponding acids **17b** and **17c** with $SOCl_2$ in the presence of a catalytic amount of anhydrous DMF. The reaction mixture was subjected to distillation to remove excess thionyl chloride to furnish the acid chlorides, and the residue obtained was used as such for the next step. Similarly, aminostyryl compound **19b** was reacted with 3,4-didecyloxy benzoyl chloride and 3,4,5-tridecyloxy benzoyl chloride to obtain the target molecules **SA4** and **SA5** respectively. 4-decyloxybenzoyl chloride was reacted with aminostyryl compound **19b** to give the target molecules **SA3**. Representative $^{1}$H and $^{13}$C NMR spectra of molecules are presented in Fig. 6.1.

### 6.2.2. Thermal behavior

The target molecules were probed for their thermal behavior with the help of polarizing optical microscopy (POM) and differential scanning calorimetry (DSC). Furthermore, the nature of the mesophase is confirmed with the help of X-ray diffraction (XRD) studies. The thermotropic LC behavior of the compounds is summarized in Table 6.1. A comparison between the thermal behaviors of the compounds of the present series is furnished in Fig. 6.2. Compound **SA1** containing two styrene units with a total of four alkoxy chains and one 3,4-di-*n*-decyloxybenzenecarboxamide connected to the central benzene ring (effectively six peripheral chains) turned out to be crystalline. Compound

**SA2**, where the benzene carboxamide is derived from 3,4,5-tri-*n*-decyloxy benzene carboxylic acid (seven peripheral chains in total), melts into a fluidic birefringent pattern at ≈ 89 $^{o}$C ($\Delta H$ = 65.3 kJ/mol), after passing through a crystal-to-crystal transitions (Fig. 6.3c). This spanned a temperature range of 14$^{o}$ before transforming into another mesophase at ≈ 102 $^{o}$C ($\Delta H$ = 10.5 kJ/mol). This birefringent texture then turns into an isotropic liquid at 126 $^{o}$C. Slow cooling of the isotropic liquid shows the emergence of spherulites from the dark field of view and further cooling showed the widening and merging of these arms with each other (Fig. 6.3a) to form a mosaic texture. Such textures are observed for phases with reduced flexibility such as smectic and columnar phases. The presence of homeotropic domains points to the uniaxial nature of the mesophase, which is in line with the proposed columnar hexagonal ($Col_h$) phase as below. Powder XRD studies on the sample was carried out at different temperature intervals on cooling

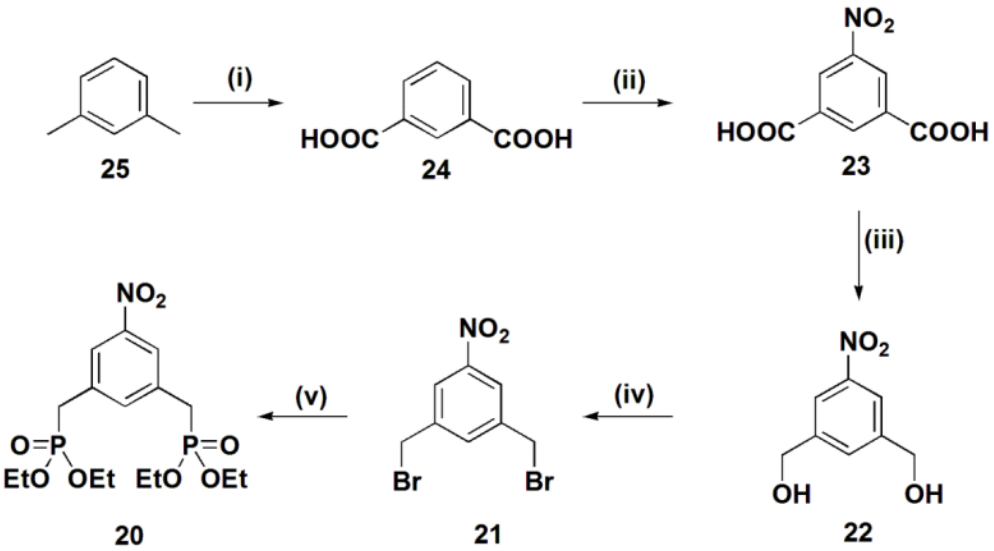


**Scheme 6.1.** Synthesis of key-intermediate1,3-bis(diethoxyphosphoryl)methyl)-5-nitro benzene (**20**). Reagents and conditions: i) $KMnO_4$, aq. NaOH, reflux, 6 days (58%); ii) $HNO_3$, $H_2SO_4$, reflux, 24 h (73%); iii) $NaBH_4$, $BF_3{\cdot}Et_2O$, dry THF, 16h, rt (89%); iv) $PBr_3$, dry THF, 24 h (97%); v) Triethylphosphite, 130$^{o}$C, 6 h, $N_2$ (70%).

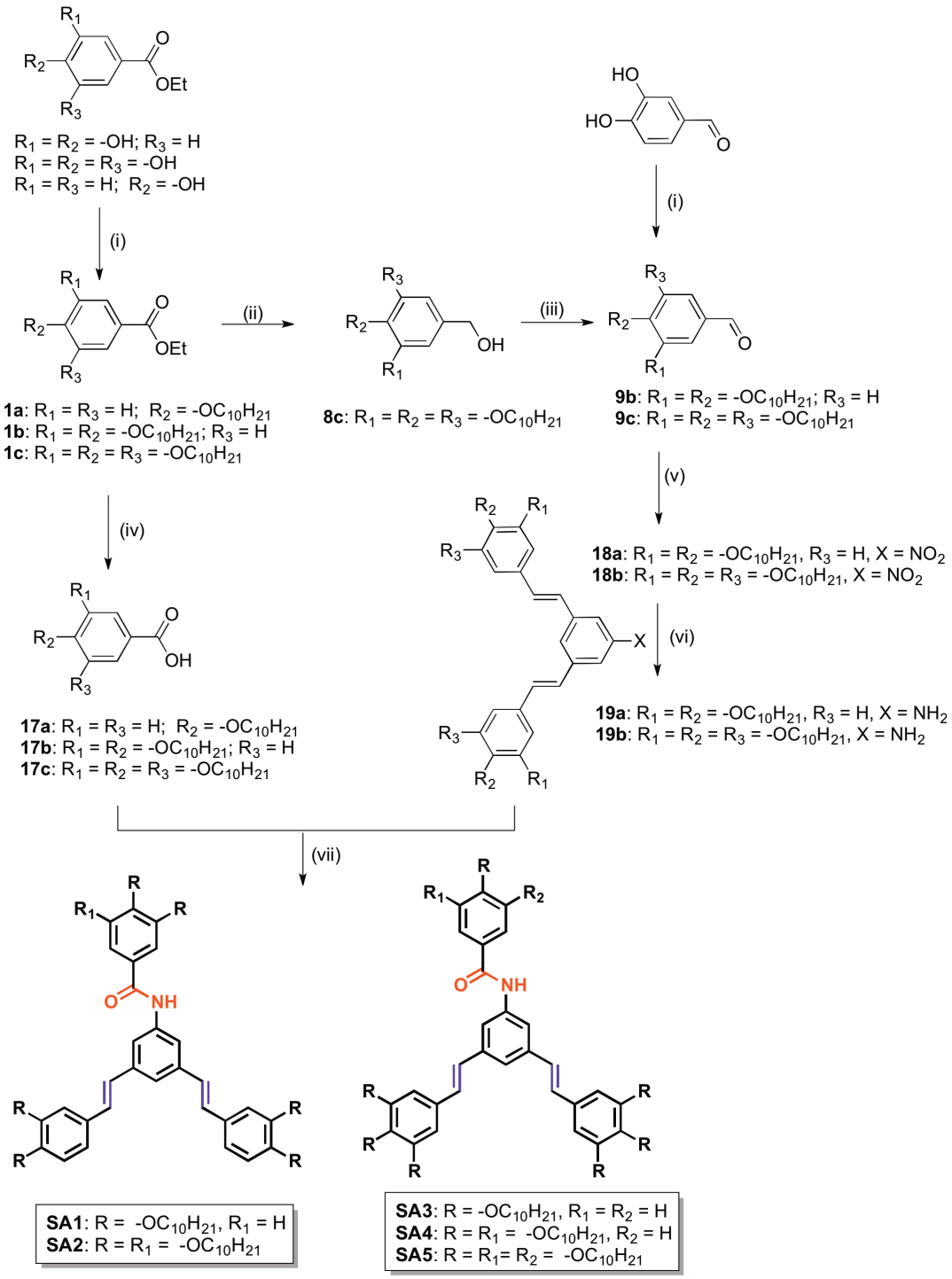


**Scheme 6.2.** Reagents and Conditions: i)1-Bromodecane, anhyd. $K_2CO_3$, DMF, 80 $^oC$, 24h (70-80%) ii) LAH, THF, 0 $^oC$ to rt, 12 h (75%); iii) PCC, DCM, rt, 4h (70-80%); iv) 10% NaOH(aq), Ethanol, reflux, 6 h (76 - 80%); v) 3,5(bis((diethoxyphosphoryl)methyl)1-nitrobenzene, NaH, dry THF, 0 $^oC$ - rt (53-60%); vi) Zn, $HCOONH_4$, THF + Methanol (1:1), 1 h, rt (80-90%); vii) (a) (**17a-c**), $SOCl_2$, DMF (catalytic), 4 h, reflux; (b) acid chlorides of **17a-c**, dry THF, $Et_3N$, 6 h, reflux (52 - 76%).

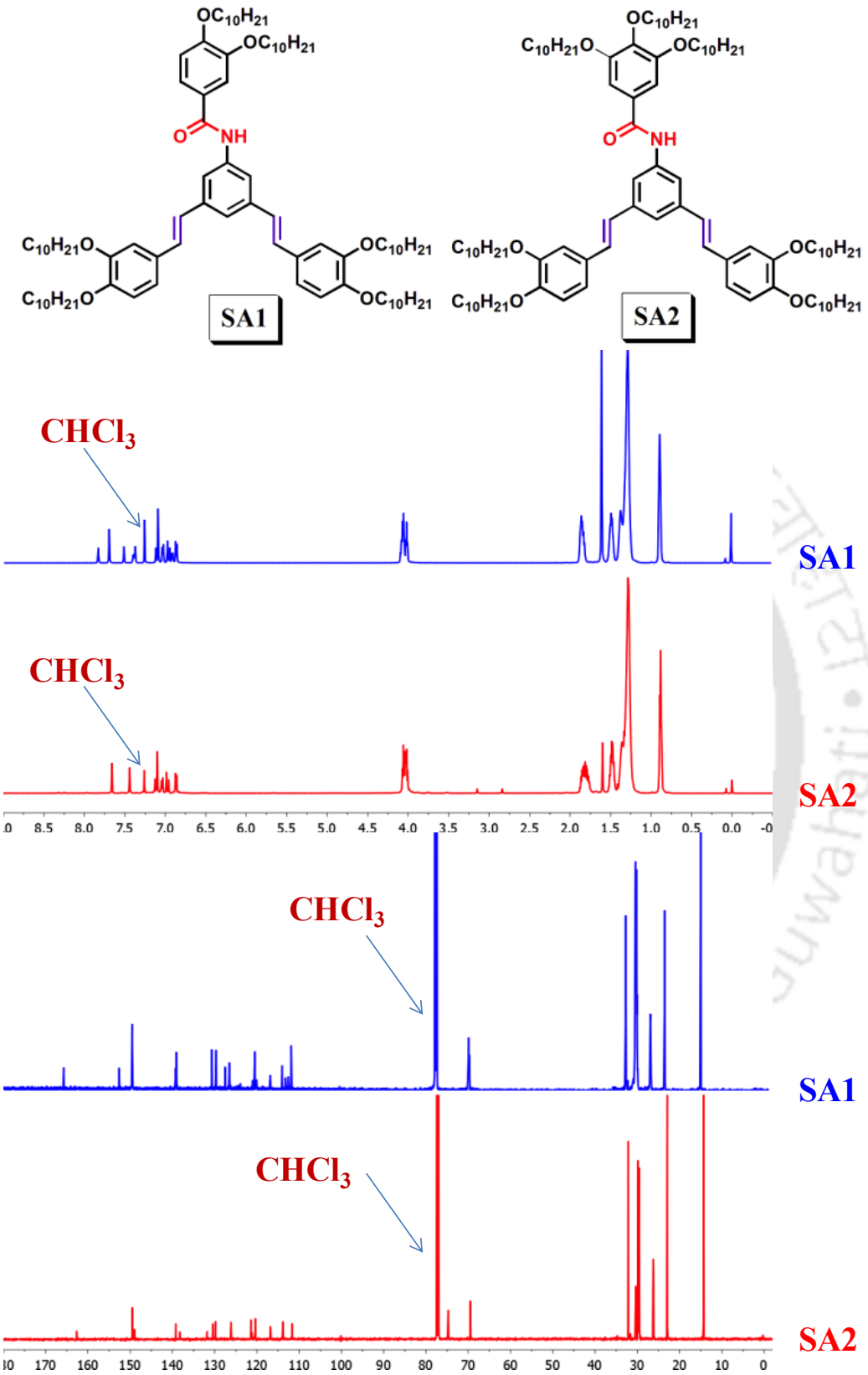


**Figure 6.1.** $^{1}$H NMR (600MHz) and $^{13}$C NMR (150MHz) spectra of **SA1 and SA2** in $CDCl_3$.

**Table 6.1.** Phase transition temperatures [a] (°C) and corresponding enthalpies (kJ/mol) of DLCs

| | Phase sequence | |
|---|---|---|
| | 2nd Heating | 1st Cooling |
| **SA1** | Cr 65 (155.7) I | I 24.7 (168.1) Cr |
| **SA2** | Cr[c] 88.6 (65.3) $Col_r$ 102 (10.5) $Col_h$ 126 (39.3) I | I 117.1 (43.5) $Col_h$ 93 $Col_r$ 79.1 (3.2) Cr[d] |
| **SA3** | $Col_h$ 111.9 (22.3) I | I 110.2 (22.5) $Col_h$[b] |
| **SA4** | $Col_h$ 109.1 (52.5) I | I 107 (52) $Col_h$[b] |
| **SA5** | $Col_h$ 77.5 (39.4) I | I 75 (36.4) $Col_h$[b] |

[a]Peak temperatures in the DSC thermograms obtained during the second heating and cooling cycles at 5 °C/min. [b]The mesophase is not crystallizing up to -20 °C. Cr = Crystal phase; $Col_h$ = Columnar hexagonal phase; $Col_r$= Columnar rectangular phase; I = Isotropic phase. [c]This crystalline state is preceded by the following Cr-Cr transitions at 82.8 (18.7); [d]Below this temperature there is another Cr-Cr transition at 72.3 (75) Cr.

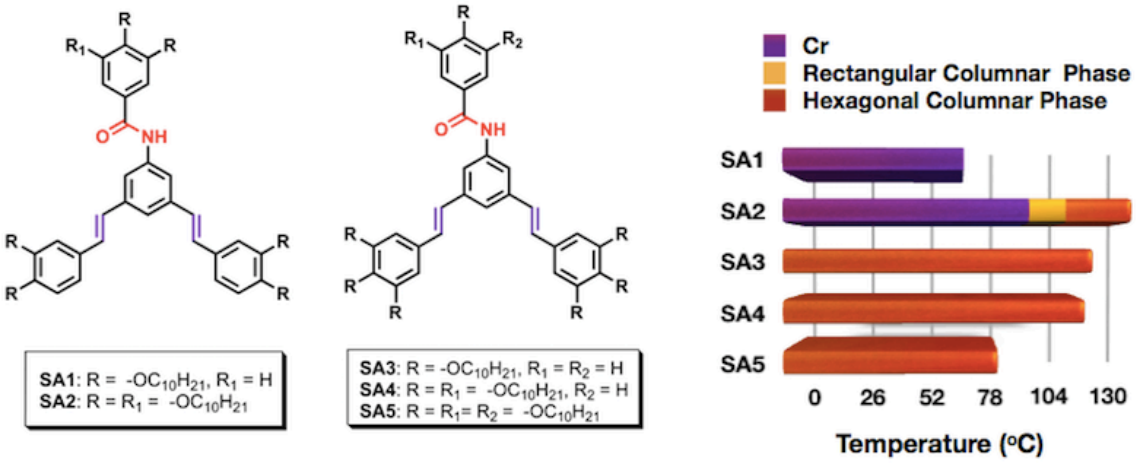


**Figure 6.2.** Bargraph summarizing the thermal behavior of compounds **SA1-5** (second heating cycle).

from isotropic liquid to understand the symmetry of the Col phase (Fig. 6.4). For the sake of explanation we describe here the XRD patterns obtained at 110 and 90 °C (Fig. 6.3d and Table 6.2). The XRD pattern obtained at 110 and 90 °C showed a single diffused peak at wide angle ($19^o < 2\theta < 26^o$) s corresponding to *d*-spacings of ~ 5.1 Å. This diffused peak corresponds to the packing of flexible peripheral tails in the liquid-crystalline phase. Considering the presence of an amide linkage, which often leads to a decreased core-core distance as a result of intermolecular H-bonding, the absence of a core-core stacking reflection is quite surprising.[34] The diffraction pattern obtained at 110 °C showed a single sharp reflection in the low angle region ($2^o < 2\theta < 7^o$) at a *d*-spacing of 28.7 Å. This can be

assigned to 100 reflection of a hexagonal lattice with a lattice parameter $a$ = 33.1 Å. This corresponds to the intercolumnar distance and is found to be smaller than the calculated molecular diameter 41.9 Å. This points to an interdigitation of the peripheral alkyl tails or chain melting in the liquid-crystalline state.

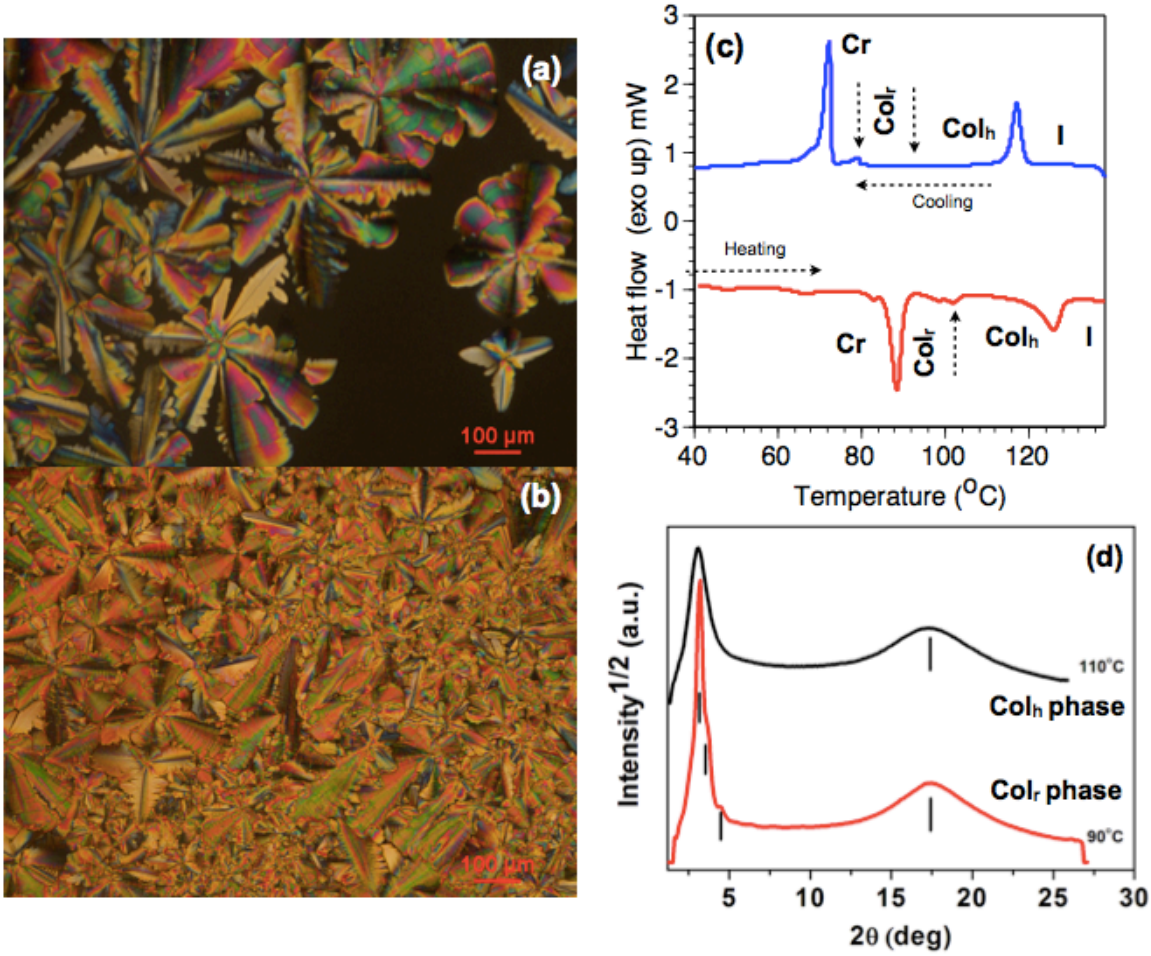


**Figure 6.3.** POM photograph of compound **SA2** at 95 °C (a) and at 90 °C (b); DSC scans of first cooling (blue trace) and second heating (red trace) cycles of compound **SA2** (c); XRD pattern obtained for compound **SA2** at 110 °C and 90 °C (d).

The XRD patterns showed a transition at 93 °C, where the 100 peak of the Col$_h$ phase splits into 200 and 110 reflections (Fig. 6.4). It should be noted that the transition was hard to detect by POM or DSC (Fig. 6.3c and Fig. 6.4). For example, the XRD pattern at 90 °C (Fig. 6.3d) showed *d*-spacings of be 27.51, 23.81, and 19.62 Å, which can be fitted into a rectangular lattice with Miller indices of 200, 110, and 210. The lattice

parameters of the rectangular unit cell was found to be $a$ = 55 Å, $b$ = 26.4 Å. The mesophase crystallizes at around 80 °C (Fig. 6.4).

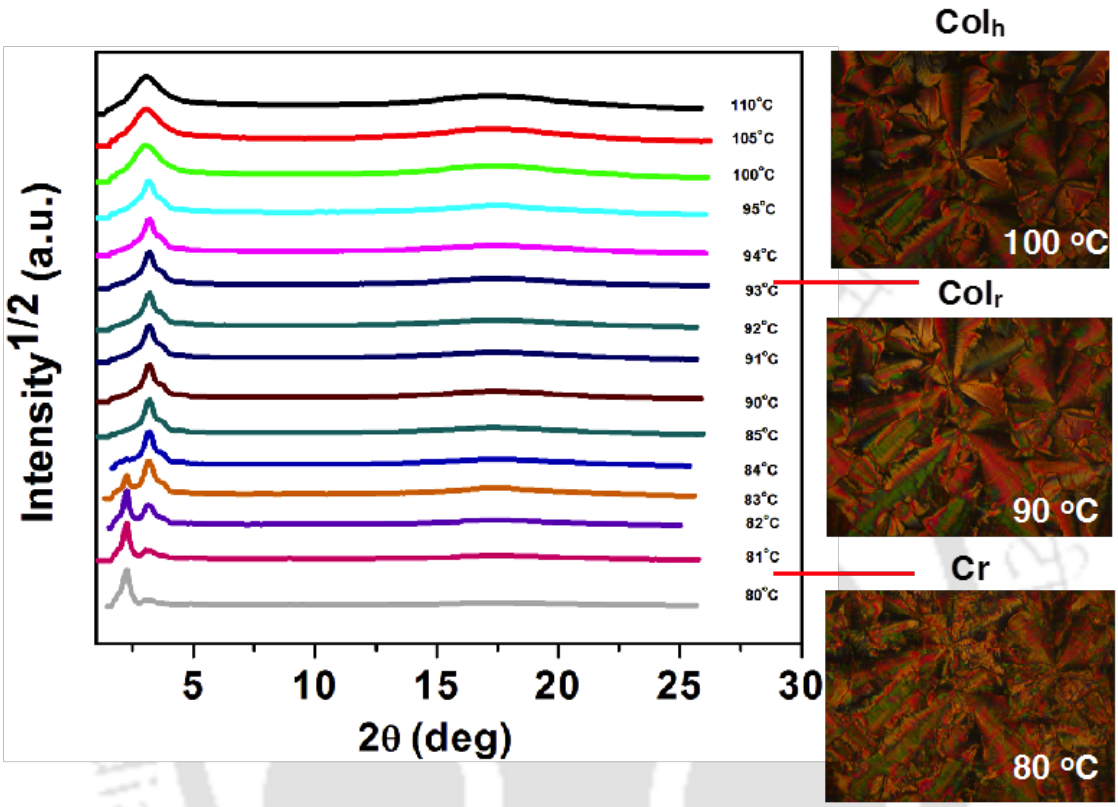


**Figure 6.4.** XRD pattern obtained for compound **SA2** on cooling from isotropic melt to crystallization (corresponding POM textures are shown in the side).

Star shaped molecule **SA3** with two styrene units with a total of six alkoxy chains and one 4-*n*-decyloxybenzenecarboxamide connected to the central benzene ring (effectively seven peripheral chains as in the case of compound **SA2**) exhibits a room-temperature mesophase, as identified by its fluid birefringent texture, sticky nature of the sample, and DSC. The mesophase converts to an isotropic liquid at a temperature of ~112 °C ($\Delta H$ = 22.3 kJ/mol). Slow cooling of the isotropic liquid yields a mosaic texture that is characteristic of the $Col_h$ phase (Fig. 6.5a). The texture remains unchanged untill room temperature (Fig. 6.5b), and DSC scans did not show any sign of crystallization untill -20 °C and also in the subsequent heating cycles (Fig. 6.5c). Powder XRD patterns obtained at 80 °C and room temperature (Fig. 6.5d) showed that the symmetry of the Col phase is

hexagonal in nature. The low-angle region of the XRD patterns obtained at 80 $^{o}$C showed one intense reflection at a *d*-spacing of 31.6 Å and two weak reflections centered at 18.5 and 15.7 Å. There was a diffused peak corresponding to a *d* spacing of 4.9 Å that arises from the packing of flexible chains. The first three reflections at the low angle region can be indexed into 100, 110, and 200 reflections of a hexagonal lattice, and the ratio of these

**Table 6.2.** Results of (hkl) indexation of XRD profiles of the compounds at a given temperature (T) of the mesophase

| Compounds ($D$/Å)[a] | Phase (T/$^{o}$C) | $d_{obs}$(Å) | $d_{cal}$(Å) | Miller indices *hkl* | Lattice parameters (Å) |
|---|---|---|---|---|---|
| **SA2** (41.9) | $Col_h$ (110) | 28.7<br>5.1 ($h_a$) | 28.7 | 100 | $a$ = 33.1 |
| | $Col_r$ (90) | 27.5<br>23.8<br>19.3<br>5.1 ($h_a$) | 27.5<br>23.8<br>19.1 | 200<br>110<br>210 | $a$ = 55<br>$b$ = 26.4 |
| **SA3** (40.9) | $Col_h$ (80) | 31.6<br>18.5<br>15.7<br>4.9 ($h_a$) | 31.6<br>18.2<br>15.8 | 100<br>110<br>200 | $a$ = 36.5 |
| | $Col_h$ (28) | 32.2<br>18.8<br>16<br>4.84 ($h_a$) | 32.2<br>18.6<br>16.1 | 100<br>110<br>200 | $a$ = 37.1 |
| **SA4** (41.6) | $Col_h$ (80) | 31.7<br>18.2<br>15.7<br>4.9 ($h_a$) | 31.7<br>18.3<br>15.8 | 100<br>110<br>200 | $a$ = 36.5 |
| | $Col_h$ (28) | 32.7<br>18.9<br>16.5<br>4.8 ($h_a$) | 32.7<br>18.9<br>16.4 | 100<br>110<br>200 | $a$ = 37.8 |
| **SA5** (41) | $Col_h$ (50) | 30.6<br>17.7<br>15.4<br>4.9 ($h_a$) | 30.6<br>17.7<br>15.3 | 100<br>110<br>200 | $a$ = 35.4 |
| | $Col_h$ (28) | 31.6<br>18.3<br>15.7<br>4.8 ($h_a$) | 31.6<br>18.3<br>15.8 | 100<br>110<br>200 | $a$ = 36.5 |

[a]The diameter (D) of the disk (estimated from Chem 3D Pro 8.0 molecular model software from Cambridge Soft). $d_{obs}$: spacing observed; $d_{cal}$: spacing calculated (deduced from the lattice parameters; $a$ for the $Col_h$ phase). The spacings marked $h_a$ correspond to diffuse reflections in the wide-angle region arising from correlations between the alkyl chains.

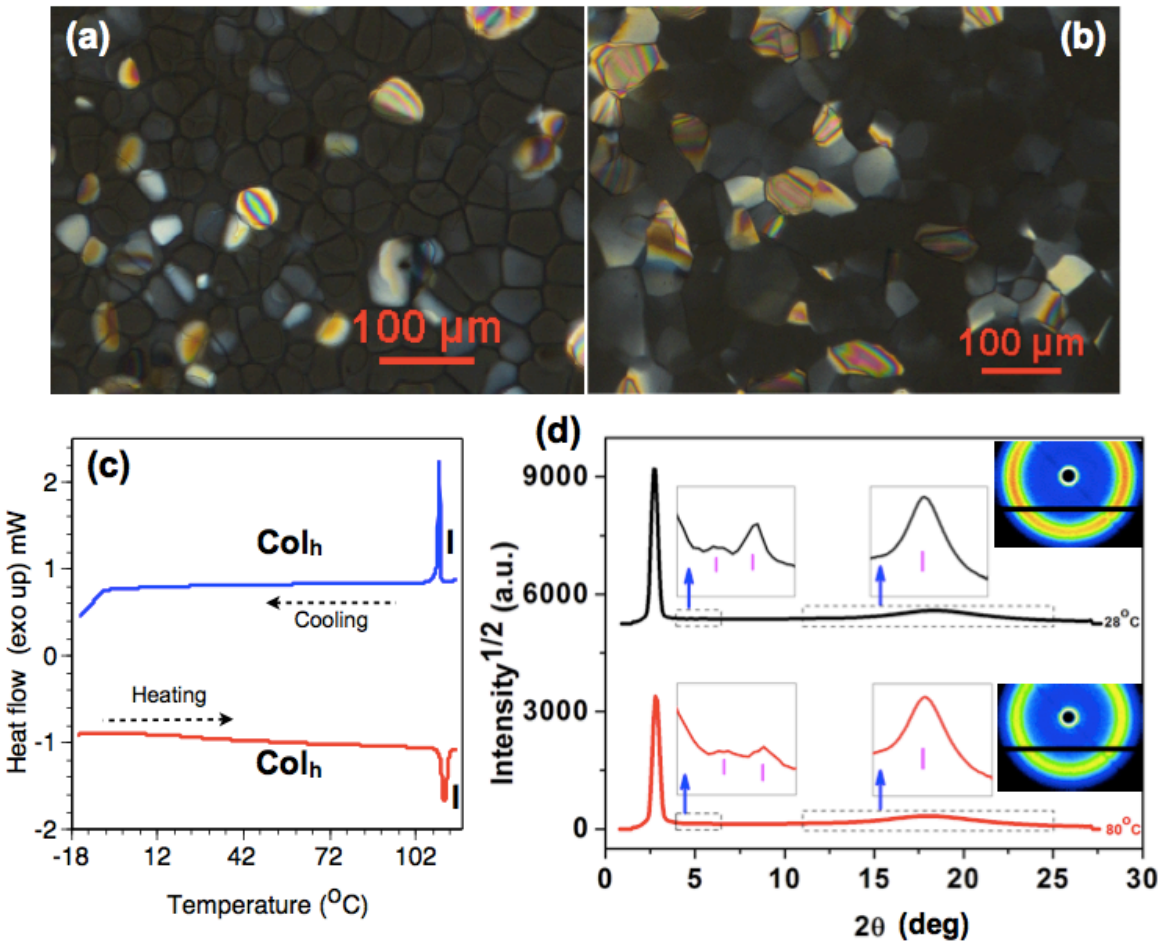


**Figure 6.5.** POM photograph of compound **SA3** at 104 °C (a) and at 28 °C (b); DSC scans of first cooling (blue trace) and second heating (red trace) cycles of compound **SA3** (c); XRD pattern obtained for compound **SA3** at 80 °C (red trace) and at 28 °C (black trace), the inset shows the image patterns obtained (d).

spacing was 1:1/√3:1/√2. The hexagonal lattice constant, *a*, was 36.5 Å, which is approximately 10% less than the molecular diameter, suggesting an interdigitation of peripheral alkyl tails. The XRD pattern observed at room temperature was similar to the one observed at high temperature with a marginal increase in the value of *a*. This must accounted for the stretching of alkyl tails on lowering the temperature. Compounds **SA4** and **SA5** with eight and nine alkyl tails, respectively, stabilized the room-temperature $Col_h$ phase as evidenced from POM textures (Fig. 6.6), DSC and XRD studies (See Fig. 6.7, 6.8, 6.9 and Table 6.2).

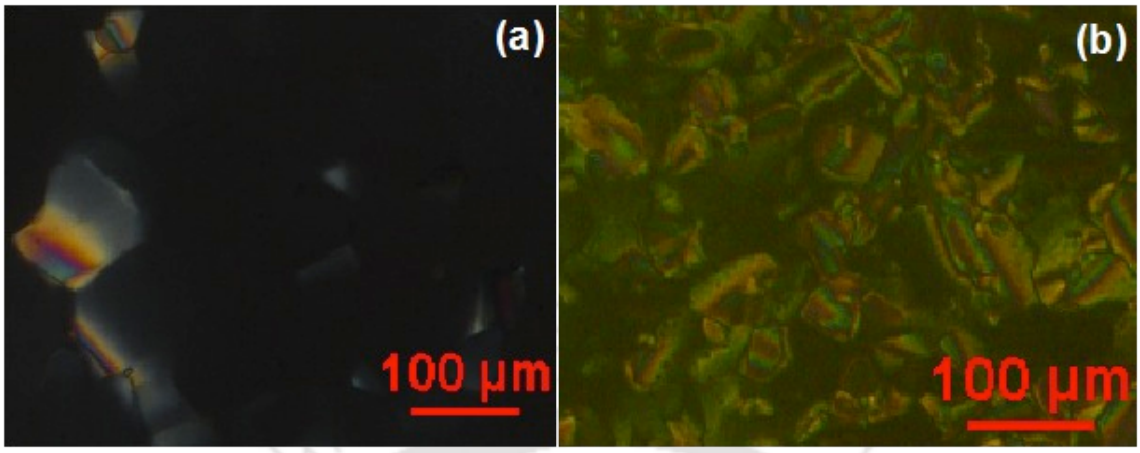


**Figure 6.6.** POM photographs of $Col_h$ phases of compound **SA4** at 28 $^oC$ (a); and compound **SA5** at 28 $^oC$ (b).

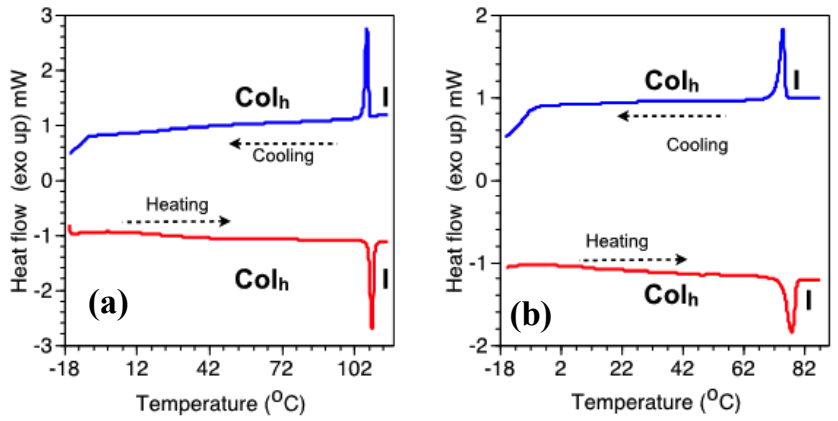


**Figure 6.7.** DSC scans of compounds in first cooling (blue trace) and second heating (red trace) cycles for compounds **SA4** (a) and **SA5** (b)

A small decrease in the thermal range of the $Col_h$ phase was seen on moving from **SA3** to **SA4** (from seven to eight alkyl chains), but a drastic decrease in the clearing temperature was observed in the case of compound **SA5** with nine alkyl chains. Thus, on comparing the mesomorphic behavior of compounds **SA2** and **SA3**, it is evident that even though both molecules have the same number of alkyl chains, compound **SA2** exhibit higher melting and clearing points in comparison to compound **SA3**. Further increases in the number of alkyl tails on the benzene carboxamide moiety (for compounds **SA4** and **SA5**)

lead to a reduction in clearing temperature because it may reduce the core-core interaction of the star-shaped molecule. It is interesting that a minimum of seven flexible tails are necessary to exhibit liquid crystallinity as seen from the thermal behavior of **SA1**, **SA2** and **SA3**, where compounds **SA2** and **SA3**, both with seven flexible tails, are liquid crystalline.

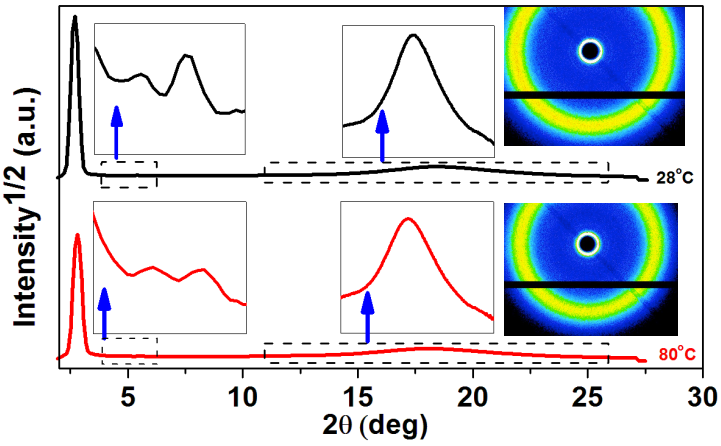


**Figure 6.8.** XRD pattern obtained for compound **SA4** at 80 °C (red trace) and at 28 °C (black trace), the inset shows the image patterns obtained.

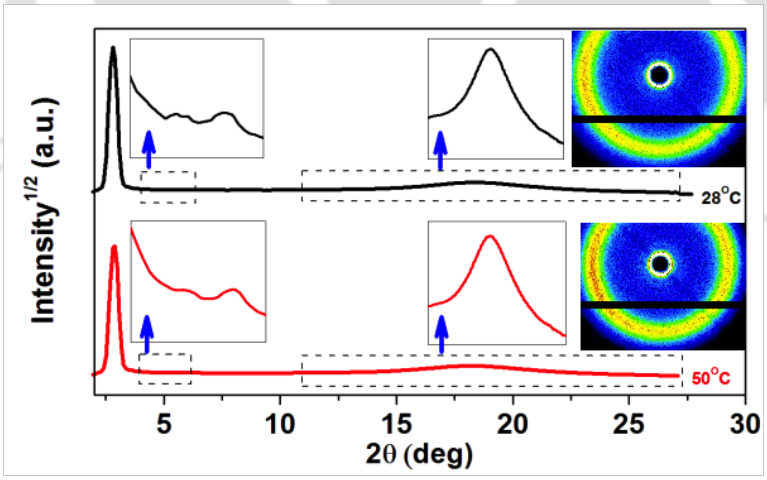


**Figure 6.9.** XRD pattern obtained for compound **SA5** at 50 °C (red trace) and at 28 °C (black trace), the inset shows the image patterns obtained.

### 6.2.3. Photophysical and Electrochemical studies

Photophysical properties of star-shaped stilbene amides **SA1-5** in micromolar THF solution are represented in Table 6.3. Absorption and fluorescence spectra of compounds **SA1-5** were taken in THF (Fig. 6.10). As can be seen, the absorption spectra for the solutions of hekates **SA1-5** showed a small variation in absorption maxima varying from 317 to 333 nm, which may be due to their substitution pattern. The series of molecules shows large values of the molar absorption coefficients, implying that these are highly conjugated systems ($\varepsilon \geq 39110\ M^{-1}cm^{-1}$). The single absorption band of these systems is attributed to $\pi$-$\pi^*$ transition of the double bond conjugated with an aromatic system. Optical bandgaps of these systems calculated from the red edge of the absorption spectra were in the range of 3.17 – 3.24 eV. Emission spectra obtained by exciting the micromolar solutions of these compounds at their absorption maxima did not show much variation, and the emission maxima were centered around 406-412 nm.

**Table 6.3.** Photophysical[a] and electrochemical [c] properties of star shaped compounds **SA1-5**

| | Absorption (nm) | Emission [b] (nm) | Stoke's shift (nm) | Quantum yield[j] | Absorption[i] | Emission[i] (nm) | $\Delta E_{g,opt}$ [d, e] | $E_{1ox}$ [f] | $E_{HOMO}$ [d, h] | $E_{LUMO}$ [d, g] |
|---|---|---|---|---|---|---|---|---|---|---|
| **SA1** | 332 | 406 | 74 | 0.25 | 339 | 422 | 3.19 | 1.77 | -6.11 | -2.92 |
| **SA2** | 333 | 407 | 74 | 0.39 | 339 | 414 | 3.23 | 1.71 | -6.05 | -2.82 |
| **SA3** | 327 | 407 | 80 | 0.27 | 334 | 439 | 3.17 | 1.79 | -6.13 | -2.96 |
| **SA4** | 317 | 407 | 90 | 0.35 | 337 | 426 | 3.24 | 1.79 | -6.13 | -2.89 |
| **SA5** | 328 | 412 | 84 | 0.24 | 332 | 427 | 3.20 | 1.78 | -6.12 | -2.92 |

[a]Micromolar solutions in THF. [b]Excited at the respective absorption maxima. [c]Experimental conditions: Micromolar DCM solutions, $Ag/AgNO_3$ as reference electrode, glassy carbon as working electrode, platinum rod as counter electrode, TBAP (0.1 M) as a supporting electrolyte, room temperature. [d]In electron volts (eV). [e]Band gap was determined from the red edge of the longest wave length in the UV-Vis absorption spectra $E_g$ (eV) = 1240/(wavelength in nm), **SA1**: 389 nm, **SA2**: 385 nm, **SA3**: 392 nm, **SA4**: 383 nm; **SA5**: 388 nm. [f]In volts (V). [g]Estimated from the formula $E_{LUMO} = E_{HOMO} + E_{g,opt}$. [h] Estimated from the onset reduction peak values by using $E_{HOMO} = -(4.8 - E_{1/2,Fc,Fc+} + E_{ox,onset})$ eV. [i]in thin film. [j]Relative quantum yield calculated with respect to quinine sulphate solution in 0.1 M $H_2SO_4$ with a quantum yield of 0.54.

We were interested to study the emissive nature of these molecules in the solid state. The thin films of the compounds were prepared by annealing the isotropic liquids of the samples sandwiched between the glass cover slips. They showed red-shifted absorption and emission spectra (Table 6.3, Fig. 6.10b and Fig. 6.11), which points to the formation of aggregates. The red-shifted absorption and emission spectra of the annealed thin films in comparison to the respective spectra in the micromolar solution state point to the

formation of J-aggregates.[28] The solution and thin films exhibited blue emission under long wavelength UV light (λ = 365 nm) (Fig. 6.10c).

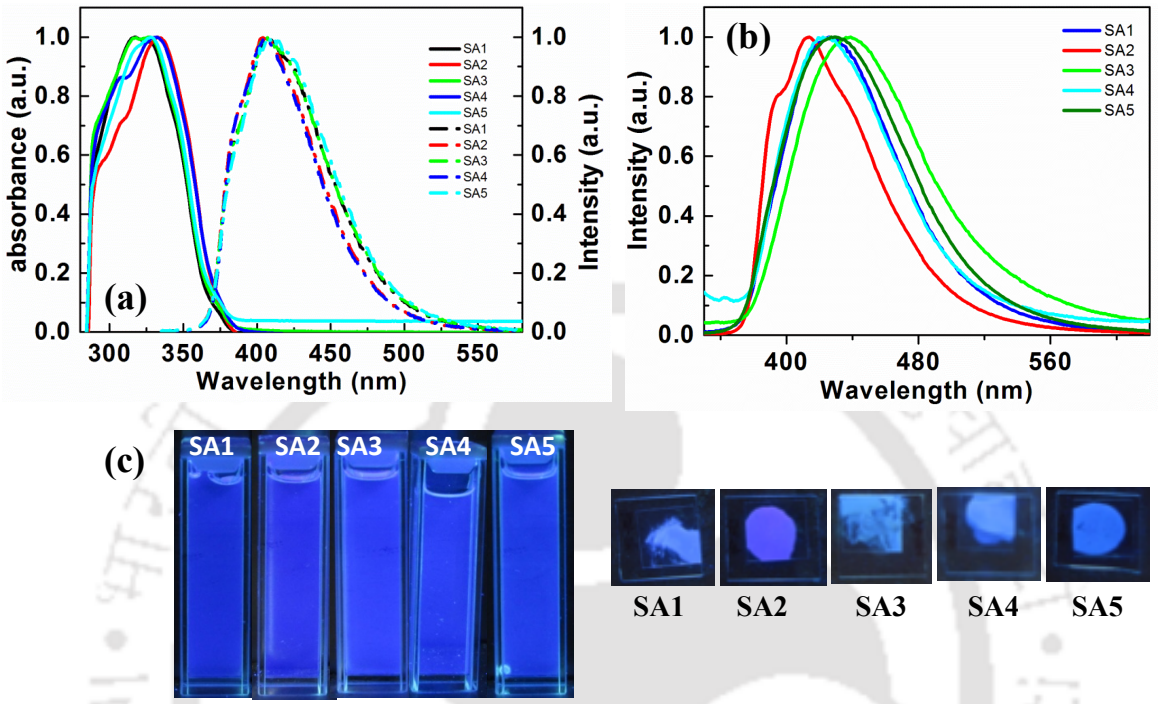


**Figure 6.10.** Normalized absorption (solid line) and emission spectra (dotted line) in micromolar THF solution obtained for **SA1-5** (a); Normalized emission spectra of thin films of compounds SA1-5 (excited at the absorption maxima obtained in solution state) (b); Images of the micromolar solutions (Left panel) and thin films (Right panel) of compounds **SA1-5** under UV light of long wavelength (365 nm) (c).

The quantum yields of these compounds measured with respect to that of quinine sulphate solution (in 0.1 M $H_2SO_4$, with quantum yield of 0.54) were found to be in the range 0.25 to 0.39 (Table 6.3 and Fig. 6.12). Quantum yield was measured according to established procedure by using quinine sulfate in 0.1 M $H_2SO_4$ solution as the standard. Absolute values were calculated according to the following equation: $Q_S = Q_R \times (m_S / m_R) \times (n_S / n_R)^2$; where Q: Quantum yield, m: Slope of the plot of integrated fluorescence intensity *vs* absorbance n: refractive index (1.407 for THF and 1.33 for distilled water). The subscript R refers to the reference fluorophore *i.e.* quinine sulphate solution in 0.1 M $H_2SO_4$ and subscript S refers to the sample under investigation. In order to minimize re-absorption

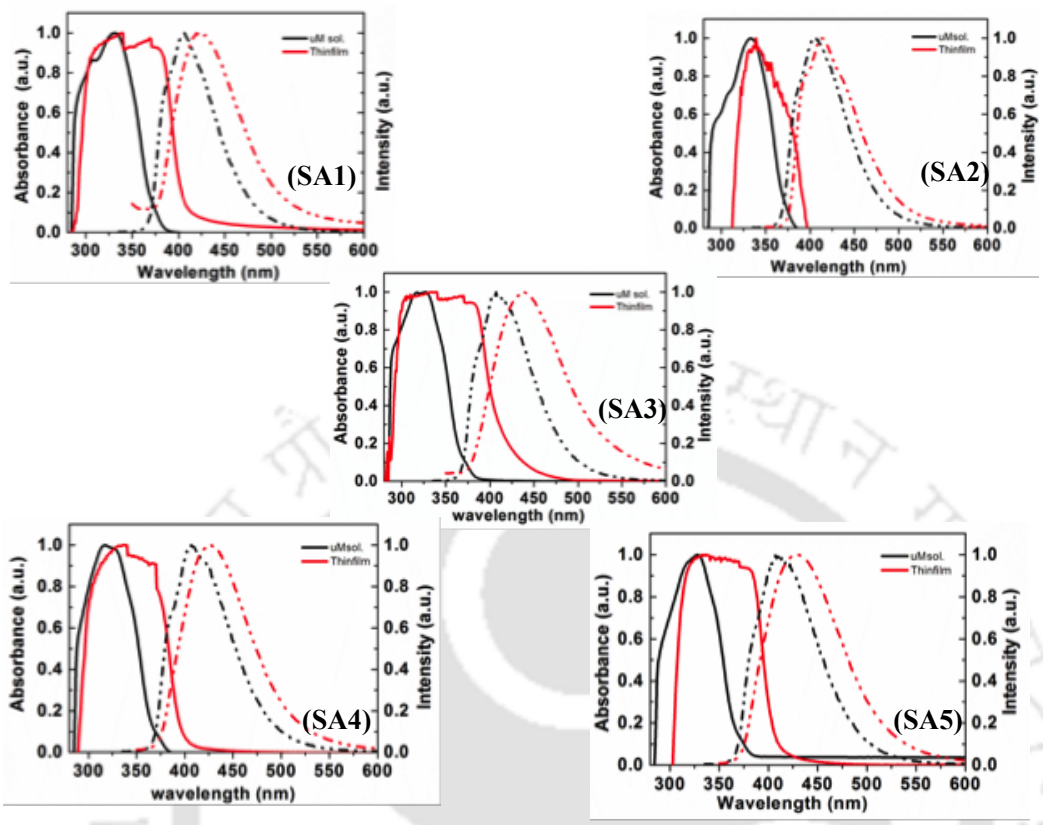


**Figure 6.11.** Absorption spectra in micromolar THF solution (black solid line), in thin film state (red solid line), emission in micromolar THF solution (black broken line) and emission spectra in thin film state (red broken line) of compounds **SA1-5**.

effects, absorbance was kept below 0.15 at the excitation wavelength of 347 nm. Quantum Yield of quinine sulphate is 0.54. Simplified equation for the calculation after substituting the appropriate values is given below and values obtained are given in Table 6.4. $Q_S = 0.54 \times (m_S / 2.71\times10^9) \times (1.407/1.33)^2 = 0.223 \times m_S$

**Table 6.4.** Quantum yield of star shaped compounds **SA1-5**

| Entry | $m_S$ | $m_R$ | $Q_s^{a,b,c}$ |
|---|---|---|---|
| **SA1** | $1.14\times10^9$ | $2.71\times10^9$ | 0.25 |
| **SA2** | $1.76\times10^9$ | $2.71\times10^9$ | 0.39 |
| **SA3** | $1.23\times10^9$ | $2.71\times10^9$ | 0.27 |
| **SA4** | $1.56\times10^9$ | $2.71\times10^9$ | 0.35 |
| **SA5** | $1.07\times10^9$ | $2.71\times10^9$ | 0.24 |

[a] Measured in THF solution.[b]Excited at absorption maxima . [c]Standard quinine sulphate ($Q_f$ = 0.54) in 0.1M $H_2SO_4$.

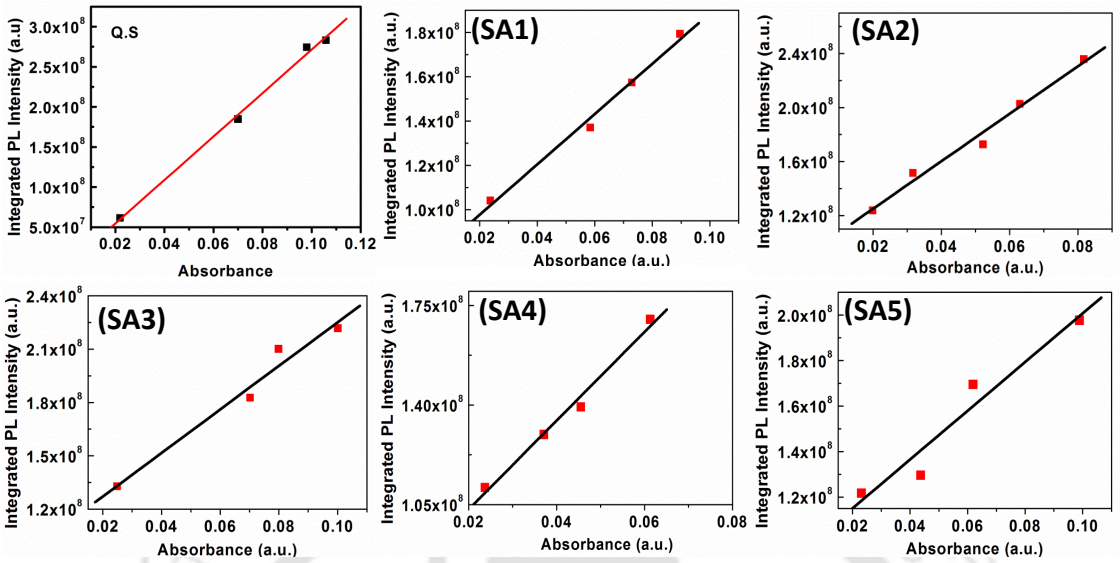


**Figure 6.12.** Plots of integrated photoluminescence intensity vs absorbance of Quinine sulphate (0.1M $H_2SO_4$ solution), compounds **SA1, SA2, SA3, SA4** and **SA5** (micromolar THF solution).

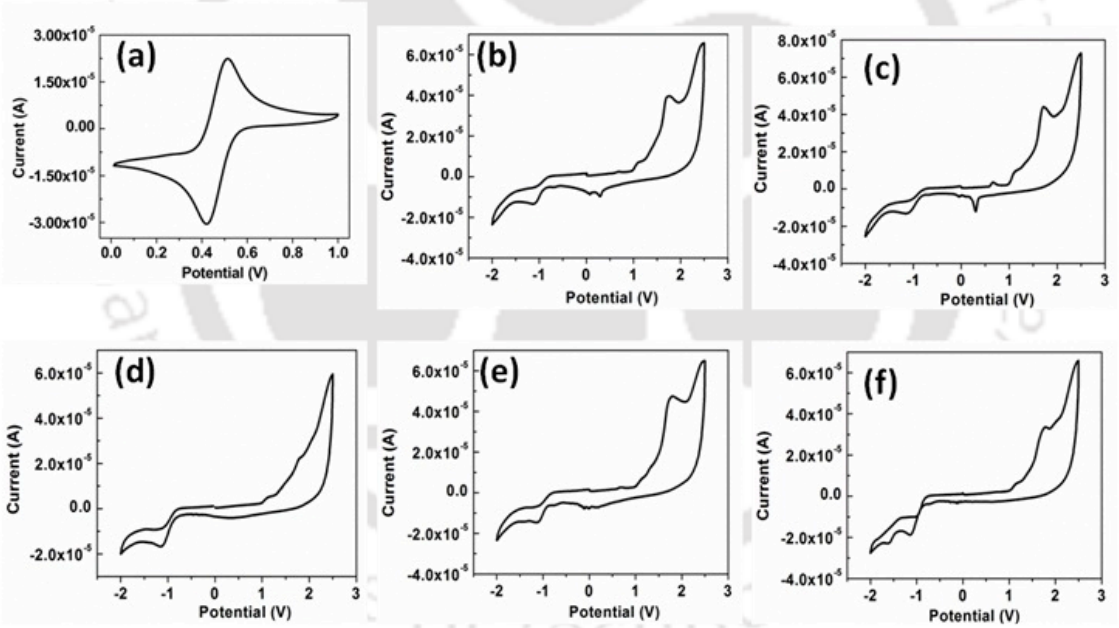


**Figure 6.13.** Cyclic voltammograms of ferrocene (a); compound **SA1** (b); **SA2** (c); **SA3** (d); **SA4** (e) and **SA5** (f) in anhydrous DCM solution of tetra-*n*-butylammonium perchlorate (0.1 M)(The half-wave potential of the ferrocene/ ferrocenium ($Fc/Fc^+$) redox couple ($E_{1/2,\ Fc,Fc^+}$) was found to be 0.46 V relative to the $Ag/Ag^+$ reference electrode).

Energy levels of frontier molecular orbitals (HOMO and LUMO) of the star-shaped molecules were obtained by cyclic voltammetry (CV), and the data are tabulated

in Table 6.3. All of the compounds exhibited irreversible oxidation and reduction waves (Fig. 6.13). The optical band gap, $E_{g,opt}$ estimated from the red edge of the absorption spectra was found to be around 3.2 eV. Energy levels of LUMO and HOMO were determined by using the formulae $E_{LUMO} = E_{HOMO} + E_{g,\ opt.}$ and $E_{HOMO} = -(4.8 - E_{1/2,Fc,Fc+} + E_{ox,\ onset})$ eV. Compounds **SA1-5** exhibited LUMO levels ranging from -2.82 to -2.96 eV and HOMO levels ranging from -6.05 to -6.13 eV.

### 6.2.4 Gelation studies

The compounds were investigated for their ability to aggregate in solutions of *n*-hexane, *n*-decane, *n*-dodecane, *n*-hexadecane, chloroform, dichloromethane, ethanol, dimethylsulfoxide (DMSO), tetrahydrofuran, benzene, toluene and *m*-xylene. Compound **SA1** with six decyloxy chains and **SA2** with seven decyloxy chains (where the amide part contains three decyloxy chains), exhibited gelation in hexadecane, whereas other compounds in this series did not exhibit gelation. It should be noted that compound **SA1** is crystalline, **SA2** is liquid crystalline at higher temperature, and **SA3-5** are room temperature liquid crystals, which relates to the delicate balance of rigidity and fluidity required for gelation. The number and position of the alkoxy chains also matter in this self-assembly process. This can be understood from the fact that compound **SA2** with seven decyloxy chains stabilized the gel formation in *n*-hexadecane whereas compound **SA3**, which also possess seven alkyl chains but at different positions, was soluble. The gelation of compound **SA2** was confirmed by the inversion of the glass vial (Fig. 6.14d, 6.15c, Table 6.5 and 6.6).This compound was soluble in chloroform, dichloromethane, and tetrahydrofuran, and it precipitated in ethanol and DMSO. Compound **SA2** shows a low critical gelation concentration (CGC) of 0.75 wt %. In the literature, it is well known that the molecules which undergo gelation at concentrations lower than 1 wt% are usually classified as super gelators.[30,31] The organogel was formed within 20 minutes after dissolving in *n*-hexadecane (Fig.6.14c-e). The formation of the gel was proven by fluorescence spectroscopy by plotting the fluorescence intensity at $\lambda_{max}$ against the time taken for gelation in minutes. The emission intensity increases with time and reaches saturation at 20 minutes (Fig. 6.14a-c). Visually, this change is apparent on irradiating the

solution at these time intervals with long wavelength UV light (λ = 365 nm) (Fig. 6.14e). Normalized emission spectra showed a red shift in the emission maxima from 437 nm to 449 nm (a shift of 12 nm, Fig. 6.14b). Organogel formation was also confirmed by recording the emission spectra of the solution for decreasing temperature. The emission

**Table 6.5.** Gelation properties of compound **SA2**

| Entry | Solvent | Properties | Critical Gel Concentration (wt.%) | $T_{gel}$ ($^{O}$C) |
|---|---|---|---|---|
| 1 | Hexane | S | ------- | ------- |
| 2 | Decane | S | ------ | ------ |
| 3 | Dodecane | S | ----- | ----- |
| 4 | Hexadecane | G (O) | 0.75 | 50 |
| 5 | Toluene | S | ---- | --- |
| 6 | Benzene | S | ---- | --- |
| 7 | *m*-xylene | S | ---- | --- |
| 8 | DCM | S | ---- | --- |
| 9 | Chloroform | S | ---- | --- |
| 10 | THF | S | ---- | --- |
| 11 | Ethanol | P | ---- | --- |
| 12 | DMSO | P | ---- | --- |

G = stable gel; S = soluble; P = precipitate; I = insoluble; O = opaque; The critical gelation concentration (wt. %) is the minimum concentration necessary for gelation; $T_{gel}$ ($^{o}$C) is the thermal stability of the gels determined by 'dropping ball' method (weight of the ball is 68.5 mg)

**Table 6.6.** Gelation properties of compound **SA1-5** in hydrocarbon solvents

| Compound | Hexane | Decane | Dodecane | Hexadecane |
|---|---|---|---|---|
| **SA1** | S | S | PG | G(O)(0.63) |
| **SA2** | S | S | S | G(O)0.75) |
| **SA3** | S | S | S | S |
| **SA4** | S | S | S | S |
| **SA5** | S | S | S | S |

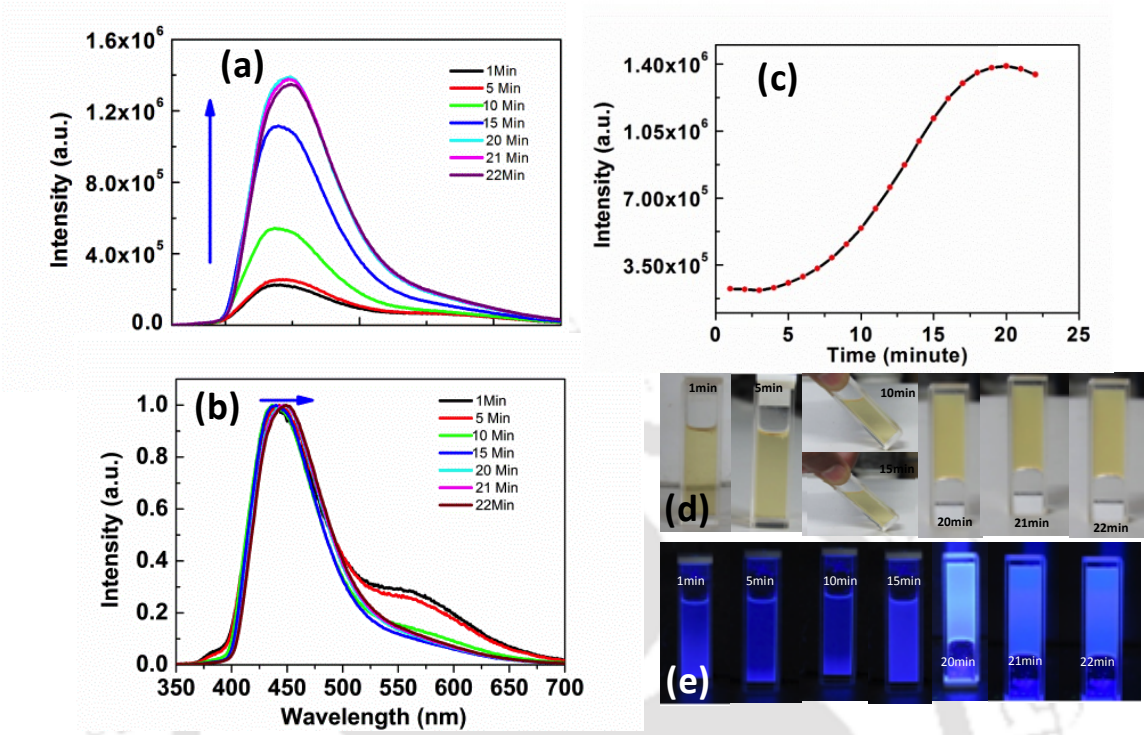


**Figure 6.14.** Emission spectra of compound **SA2** showing an increase in the emission intensity with time on gelation (5mM)(a); Normalized emission spectra of compound **SA2** showing a red shift on gelation (b); Plot showing the change in the emission intensity of compound **SA2** at $\lambda_{max}$ with respect to time (c); Images showing the gel formation with respect to time in daylight (d); Images showing the gel formation under the UV light (365 nm) with respect to time (e).

intensity increased on decreasing the temperature, with a red shift from 435 to 456 nm (Fig. 6.15a-c). There is a huge increase (six fold) in the luminescence intensity with a red-shifted emission maximum in gel state in comparison to the solution state emission with same CGC concentration (5 mM) (Fig. 6.15a). To have a clear understanding, we have overlapped the emission spectra of compound **SA2** at 20 μM , 5 mM (in solution state), and 5 mM (in gel state) solutions in *n*-hexadecane. This solution at 5 mM concentration, showed a red-shifted emission maximum in comparison to that of the 20 μM solution (Fig.6.16). On gelation, there is a huge increase (six fold) in the luminescence intensity with a red-shifted emission maximum in comparison to the solution state emission (Fig.6.15a and Fig. 6.16).Thus, this is a phenomenon of aggregation-induced emission in which the increase in concentration leading to the aggregation of fluorophores with the desired configuration to prevent aggregation quenching. The desired configuration could

be achieved by restricted intramolecular rotation (RIR) or by a favorable packing of molecules as a result of gelation. This can be explained as follows. For the solution in CGC at room temperature (at 5 mM), the molecules are present as aggregates, but with a very little restriction imposed on their intramolecular rotation, which leads to the efficient annihilation process associated with the active intramolecular rotation. Gel formation and the decrease in temperature reinforce the RIR process, enhance the strength of the H-bonding, and activate the radiative decay leading to the AIE effect.[42] Another possibility is that the aggregates formed in the gel state have the molecules arranged in a favorable packing to exhibit this phenomenon. This gel formation was reversible for many cycles of heating and cooling as evidenced by the change in the emission intensity (Fig. 6.15d).

We were interested to study the emissive nature of compound **SA2** in the gel state. The solution at this concentration showed a red-shifted excitation and emission spectra (Fig. 6.17a), in comparison to the respective spectra obtained in micromolar solution state. This points to the formation of *J*-aggregates where the molecules are arranged in a slip-stacked arrangement.[41] Fluorescence lifetime studies to confirm the presence of different species at these different concentrations (20 μM and 5 mM hexadecane solutions) were carried out by monitoring at their emission maxima (407 nm for dilute solution and 450 nm for concentrated solution). The solution at lower concentration showed an exponential decay with one excited species [$T_1$ = 3.07 ns]. The solution at higher concentration showed the different excited-state species, with a lifetime of $T_1$ = 4.11 ns (Fig. 6.17b). The species with a lower lifetime was a solvated monomer, whereas the species with the longer lifetime was formed as a result of aggregation. Dynamic light scattering studies at this concentration showed that the solution contained aggregates of 100-110 nm size (Fig. 6.17c). We have investigated the thermal stability of the gel with respect to concentration by the "dropping ball" method,[43] which showed a gradual increase (Fig. 6.18i) on increasing the concentration. The gel prepared at 1.5 wt% concentration had greater mechanical strength and was found to be moldable into any shape as shown in Fig. 6.18a-f and the luminescence remained unchanged. The gel that remained in an inverted position over a period of 15 days showed enormous stability

without showing any solvent leaching or collapse of architecture. The gel under long-wavelength UV light exhibited blue emission (Fig. 6.18h).

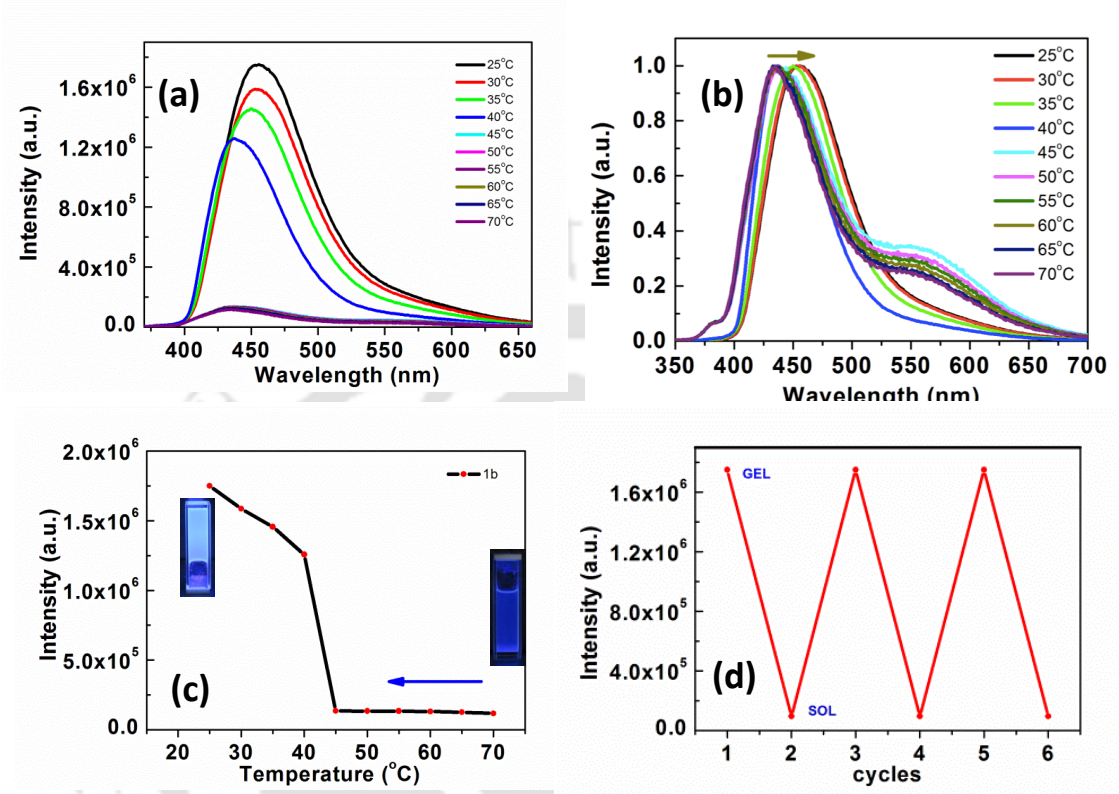


**Figure 6.15.** Emission spectra showing an increase in the emission intensity on decreasing the temperature due to gelation (5mM in hexadecane) (a); Normalized emission spectra showing a red shift on gelation (b); Plot showing the change in emission intensity on decreasing the temperature (c); Reproducible reversibilityof emission intensity in solution to gel interconversion (d).

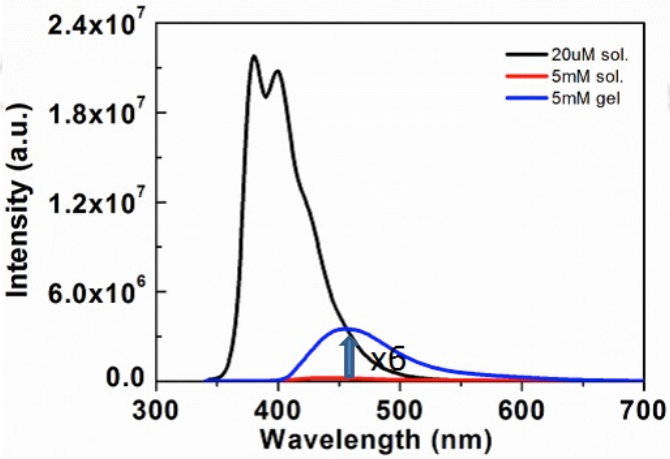


**Figure 6.16.** Emission spectra of compound **SA2** in hexadecane at different concentrations.

**Table 6.6.** Data obtained from Figure 6.16.

| Concentration | Emission maximum | Comments |
|---|---|---|
| 5 mM Solution | 452 nm | Low fluorescence intensity, weak blue light emission |
| 5 mM Gel | 456 nm | Enhancement of fluorescence intensity by six times and blue light emission in gel state |
| 20 μM Solution | 380 nm, 400 nm | Although the intensity is higher, much of the emission does not lie in the visible region. |

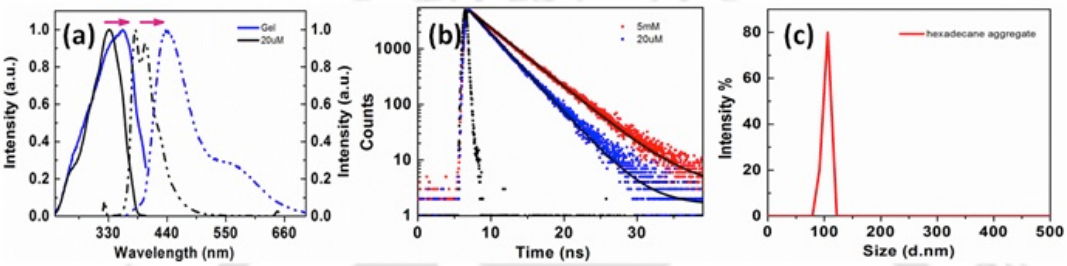


**Figure 6.17.** Normalized excitation and emission spectra of compound **SA2** in hexadecane at 5mM (blue trace) and 20 μM (black trace) concentration (a); The fluorescence decay of compound **SA2** in hexadecane at 5mM (red trace) and 20 μM (blue trace) concentrations (black trace is instrument response function; $\lambda_{exc}$ = 290 nm) (b); Dynamic light scattering curve observed for compound **SA2** in hexadecane in micromolar concentration (c).

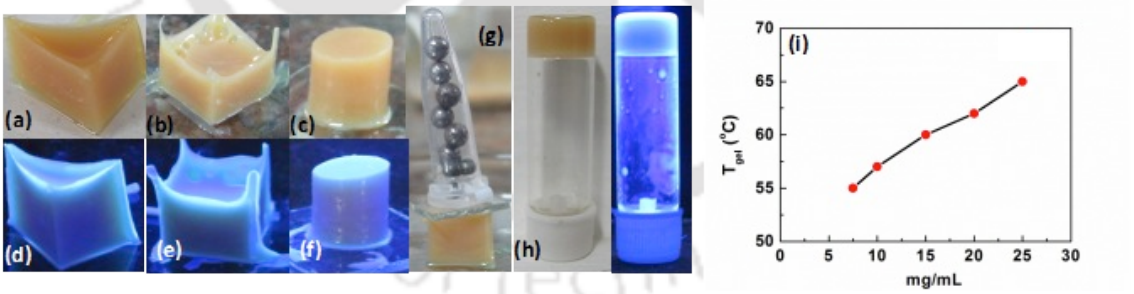


**Figure 6.18.** Moldability of organogel of **SA2** in hexadecane (1.5 wt%) into different shapes as seen in day light: trigonal prism (a); cube (b); cylinder (c); the same shapes under UV light (λ = 365 nm) (d), (e) and (f); ability to sustain the weight (g); Photograph of gel after standing for 1 month in daylight and under UV light (λ = 365 nm) (h); Plots of $T_{gel}$ *vs* concentration for compound **SA2** in hexadecane (i).

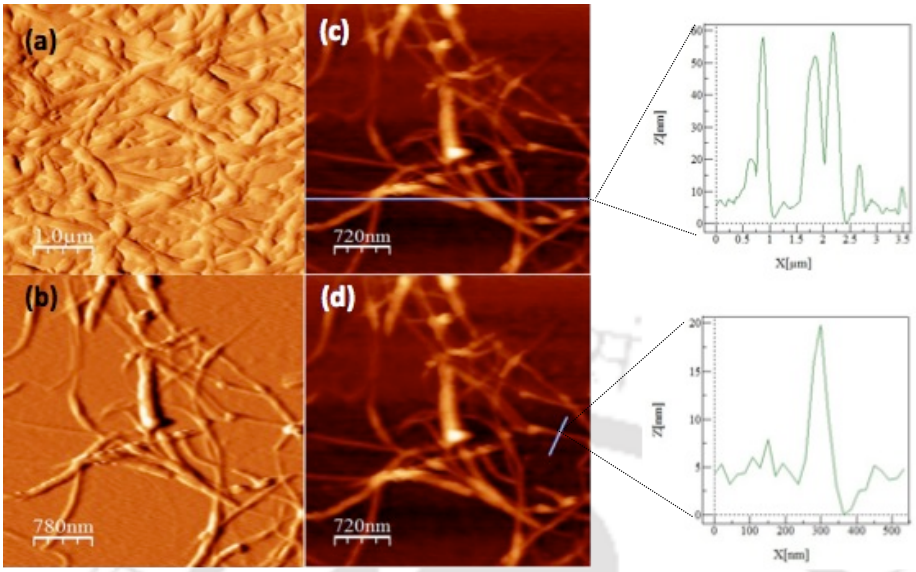


**Figure 6.19.** AFM images obtained for compound **SA2** at 1mM hexadecane solution (scale bar is 1 μm) (a); at 1 x $10^{-5}$ M (scale bar is 780 nm) (b); Expanded regions of figure 6.19a and showing the height profiles of the individual fibers (c); Expanded regions of figure 6.19a and showing the thickness of an individual fiber (d).

Atomic force microscopy (AFM) carried out to understand the surface morphology revealed that the entangled network of nanofibres with an average height of 60 nm and a thickness of 60-100 nm forms the gel (Fig. 6.19). The polarizing optical image of the organogel showed a birefringent texture (Fig. 6.20a). This motivated us to characterize its xerogel by powder X-ray diffraction studies to characterize the mode of self-assembly. The thin film of the xerogel was formed by drop casting a 1 mM solution on a glass slide. The diffraction pattern in the thin film state did not provide the data that is helpful for the analysis of the self-assembly of molecule **SA2** in the xerogel state. Thus, the film was scratched and the powder obtained was used to fill the capillary tube and was analyzed with XRD. The XRD pattern of the xerogel (Fig. 6.20b, Table 6.7) showed two small peaks in the small-angle region ($2\theta < 3^{o}$) corresponding to *d* spacings of 63.1 and 33.3 Å. The ratio of these two peaks is close to 1:0.5 and can be fitted into 100 and 200 reflections arising from the lamellar ($D_L$) phase, which is rarely observed.[44-47] Further into

the middle-angle region (2θ ≈ 8°), a small peak corresponding to a *d*-spacing of 10.51 Å was observed which can be assigned to the 600 reflection from the lamellar phase. Additionally, a diffuse peak at wide-angle region (2θ = 20.3°) corresponding to a *d* spacing of 4.38 Å was observed that corresponds to the packing of alkyl tails (Fig. 6.20b). The *d* spacing corresponding to the 100 reflection is almost 50% more than the molecular length (Fig. 6.21). This corresponds to the intercalation of alkyl tails from the neighboring layers. The molecular arrangement is reinforced by the intermolecular H-bonding as shown in Fig. 6.21.

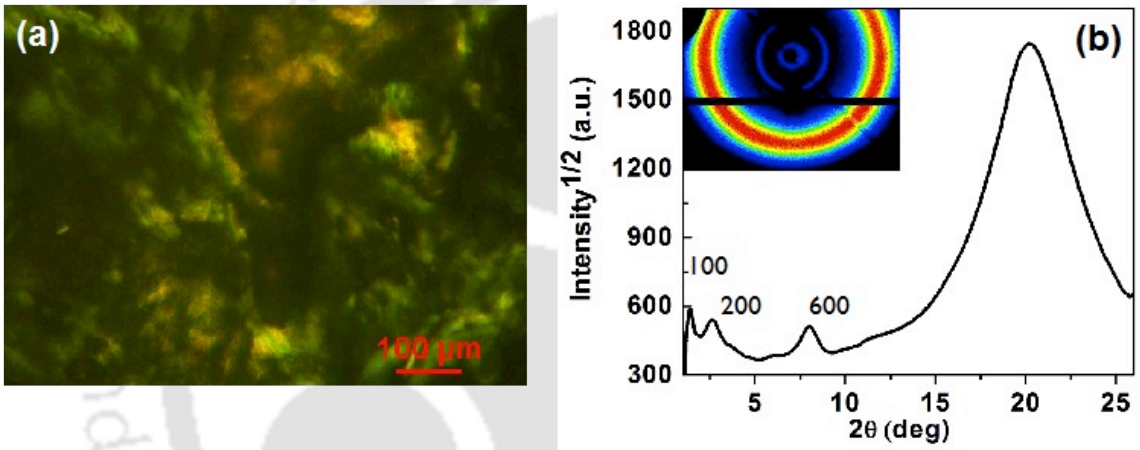


**Figure 6.20.** POM image of the xerogel obtained for compound **SA2** (a); XRD pattern obtained for the xerogel of compound **SA2** (b).

**Table 6.7.** Data obtained from XRD studies of the xerogel of compound **SA2** in hexadecane

| | 2$\theta$ | $d_{obs}$ | $d_{cal}$ | hkl | Phase |
|---|---|---|---|---|---|
| Xerogel of **SA2** at RT | 1.398 | 63.10 | 63.10 | 100 | Lamellar arrangement |
| | 2.65 | 33.28 | 31.55 | 200 | |
| | 8.02 | 11.03 | 10.51 | 600 | |
| | 20.27 | 4.38 ($h_a$) | | | |

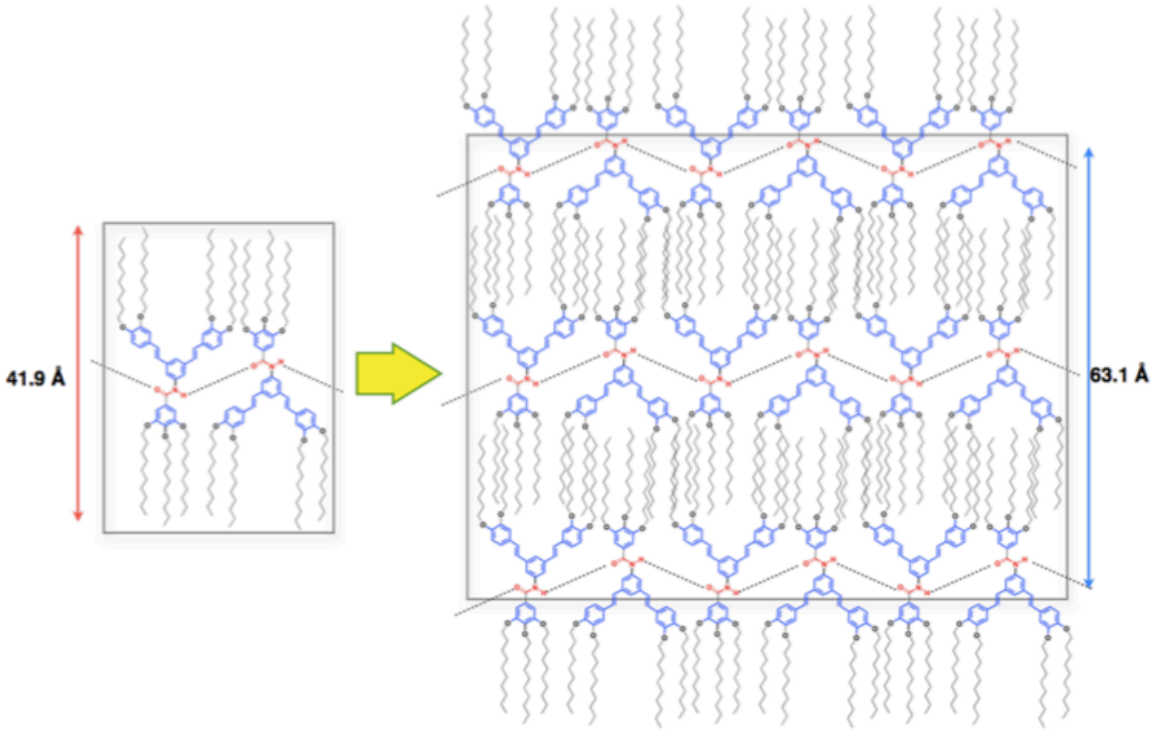


**Figure 6.21.** Schematic showing the arrangement of compound **SA2** in the discotic lamellar phase, which is reinforced by intermolecular hydrogen bonding.

## 6.3. Conclusion

We have reported a new class of star-shaped stilbene derivatives containing an amide linkage that varies with respect to the number and position of the flexible tails. This structural variation has had a tremendous effect on the mode of self-assembly. The compounds formed by the connection of dialkoxy styrene with a benzene at 3 and 5 positions and a single amide linkage at the 1 position of the central benzene ring exhibited either a crystalline phase or a columnar phase, which depended on the number of alkoxy tails in the amide unit. The compound with six alkoxy tails (two alkoxy tails on the amide unit) was crystalline, and the compound with seven alkoxy tails (three alkoxy tails on the amide unit) was bimesomorphic, showing hexagonal and rectangular columnar phases. These two compounds exhibited gelation at very low concentration in *n*-hexadecane, to qualify them as supergelators. The next set of compounds formed by connecting two trialkoxy styrene units and an amide unit to a central benzene ring exhibited improved

thermal behavior. All of the compounds in this subset had a room-temperature hexagonal phase, whereas the increase in the number of flexible chains reduced the clearing temperature. These compounds did not exhibit gelation in hydrocarbon solvents as did the first two compounds. All of the compounds exhibited blue luminescence in solution and in the thin-film state. Red-shifted absorption and emission of compounds in thin films suggested the formation of *J*-type aggregates. A similar observation was made in the case of the compound with seven alkoxy tails (three alkoxy tails on the amide unit), confirming the presence of *J*-aggregates in the gel state. Gel formation was reversible for any number of cycles. This compound at higher CGC formed a self-standing gel that can be molded into any shape. More interestingly, this compound exhibited aggregation-induced blue-light emission.

The microscopic characterization of the gel showed a highly interwoven network of fibers. Polarizing optical microscopy of the xerogel films showed a birefringent texture, which is evidence of the anisotropic nature of self-assembly. From XRD studies, it was found that these molecules self-assembled into an intercalated lamellar phase. Considering the scarcity of wide-band-gap, solid-state blue-light emitting organic materials, these star-shaped molecules are promising because of their emissive nature in the aggregated state and columnar self-assembly. They are promising for the development of solid-state displays.

## 6.4. Experimental Section

In this section the detailed synthetic procedures and the molecular structural characterization data have been presented for the intermediates and target compounds mentioned in the scheme.

Procedure for the synthesis of Isophthalic acid (**24**)[48]

A mixture of (94.3 mmol, 1 equiv.) of *m*-Xylene, (122.6 mmol, 1.3 equiv.) of NaOH, (478.3 mmol, 5.1 equiv.) of $KMnO_4$ and 471 ml of water was heated under reflux for 7 days. The excess $KMnO_4$ was decomposed with ethanol and $MnO_2$ was removed by filtration. The filtrate was acidified with conc. HCl and the precipitate was removed by filtration and dried under high vacuum.

$R_f$ = 0.51 (50% $CH_3OH$-$CHCl_3$); white solid; m.p: 345 – 348 $^oC$; yield: 58%; IR (KBr pellet): $\nu_{max}$ in $cm^{-1}$ 3088.4, 2821.6, 2668.1, 2549.1, 1690.7, 1580.2, 1486.3, 1282.6, 728.7, 689.8; $^1H$ NMR (DMSO-$d_6$, 400 MHz): δ 8.65 (s, 1H, Ar), 8.23 (d, 2H, *J* = 8Hz, Ar), 7.60 (t, 1H, *J* = 8Hz, Ar); $^{13}C$ NMR (DMSO-$d_6$, 150 MHz): δ 166.62, 133.41, 131.22, 129.99, 129.17; HRMS (ESI+) exact mass calculated for $C_8H_7O_4$(M+1): 167.0339, Found: 167.0844.

Procedure for the synthesis of 5-nitro benzene -1,3-dioic acid (**23**) [49]

Compound **24** (42.1 mmol, 1 equiv.) was dissolved in 8.4 ml of conc. $H_2SO_4$ at 80 $^oC$. A mixture of $HNO_3$ (29.1 mmol, 0.7 equiv.) and $H_2SO_4$ (18.5 mmol, 0.4 equiv.) was added and heated at 110 $^oC$ for 1h. After that conc. $HNO_3$ (124.7 mmol, 3 equiv.) was added and further heated at 110 $^oC$ for 2 h. Allowed the reaction mixture to stand overnight and poured it into 300 ml of cold water contained in a beaker. The precipitate was removed by filtration and dried. The crude product was further purified by recrystallization with boiling water.

$R_f$ = 0.52 (50% $CH_3OH$-$CHCl_3$); white solid; m.p: 254 – 258 $^oC$; yield: 73%; IR (KBr pellet): $\nu_{max}$ in $cm^{-1}$ 3500.0, 3199.3, 3090.6, 2925.1, 1716.2, 1534.4, 1353.5, 1218.5, 782.1, 667.8; $^1H$ NMR ($CD_3OD$, 400 MHz): δ 8.96 (s, 2H, Ar), 8.93 (s, 1H, Ar); $^{13}C$ NMR ($CD_3OD$, 150 MHz): δ 164.81, 148.08, 135.10, 133.13, 127.28; HRMS (ESI+) exact mass calculated for $C_8H_6NO_6$(M+1): 212.0190, Found: 212.0218.

Procedure for the synthesis of 3,5-bis-(hydroxymethyl) nitro benzene (**22**) [50]

Sodium borohydride (90.3 mmol, 3 equiv.) was added in portions to a solution of compound **23** (30.1 mmol., 1equiv.) in dry THF. The contents were cooled to 0 $^oC$ and $BF_3.Et_2O$ (90.3 mmol, 3 equiv.) was added dropwise over 1 h. The mixture was allowed to warm to room temperature and stirred for 16 h. The reaction mixture was then cooled to 0 $^oC$ and cautiously quenched with aqueous NaOH (1N, 178 mL). The contents were stirred for 3 h and the THF was removed under vacuum. The resulting aqueous suspension was extracted with EtOAc. The combined extract was washed with water and brine. Dried over anhydrous sodium sulfate and concentrated.

$R_f$ = 0.4 (70% EtOAc-hexanes); light yellowish solid; m.p: 91 – 92$^oC$; yield: 89%; IR (KBr pellet): $\nu_{max}$ in $cm^{-1}$ 3280.5, 2924.7, 2857.4, 1537.1, 1345.4, 1062.0, 1036.5, 773.8, 746.4, 676.7; $^1H$ NMR ($CD_3OD$, 400 MHz): δ 8.14 (s, 2H, Ar), 7.72 (s, 1H, Ar), 4.72 (s, 4H, 2× Ar-$CH_2$); $^{13}C$ NMR ($CD_3OD$, 100 MHz): 150.42, 145.99, 132.17, 121.39, 64.43; HRMS (ESI+) exact mass calculated for $C_8H_9NO_4$ ($M^+$): 183.0532, Found: 183.0797.

Procedure for the synthesis of 3,5-bis-(bromomethyl)nitro benzene (**21**)[49]

Compound **22** (19.1 mmol, 1 equiv.) was dissolved in THF (20 ml) with stirring and cooled to 0 $^oC$. $PBr_3$ (44.0 mmol, 2.3 equiv.) was added to the above reaction mixture and

stirred at the same temperature for 6 h and then at ambient temperature for 12 h. The reaction mixture was poured into crushed ice and extracted with $CHCl_3$ (30 ml × 5). The organic layer was washed with $Na_2CO_3$ solution and water, and dried over $Na_2SO_4$. The crude oily liquid was obtained on concentration. The crude product was purified by column chromatography over silica gel with 10-15% EtOAc-hexane as eluent.

$R_f$ = 0.4 (10% EtOAc-hexanes); white solid; m.p: 102 – 103 $^oC$; yield: 97%; IR (KBr pellet): $\nu_{max}$ in $cm^{-1}$ 3069.5, 3036.2,1530.6, 1359.2, 1320.5, 1212.2, 970.9, 899.7, 685.8; $^1H$ NMR ($CDCl_3$, 400 MHz): δ 8.19 (s, 2H, Ar), 7.75 (s, 1H, Ar), 4.52 (s, 4H, Ar-$CH_2$); $^{13}C$ NMR ($CDCl_3$, 100MHz): δ 148.73, 140.59, 135.42, 123.97, 30.85; HRMS (ESI+) exact mass calculated for $C_8H_9Br_2NO_2$(M+2): 308.8989, Found: 308.9739.

Procedure for the synthesis of 1,3-bis ((diethoxy phosphoryl) methyl)-5-nitro benzene (**20**)[51]

A solution of compound **21** (16.2 mmol, 1equiv.) in triethylphosphite (64.8 mmol, 4 equiv.) was refluxed for 17 h. Excess solvent was removed under reduced pressure and the residue obtained was taken in EtOAc (50 ml) and washed with water (50 ml × 3), brine (50 ml × 3), dried over anhydrous $Na_2SO_4$ and concentrated. The resulting oil was purified by column chromatography over silica gel, starting with 50% $CHCl_3$-hexane and 100% $CHCl_3$ to remove the excess triethylphosphite and then 2-10% $CH_3OH$-$CHCl_3$ to obtained the pure product.

$R_f$ = 0.3 (5%$CH_3OH$-DCM); low melting white solid; yield: 70%; IR (KBr pellet): $\nu_{max}$ in $cm^{-1}$ 2984.9, 2924.6, 2854.3, 1535.4, 1355.2, 1324.3, 1245.6, 1053.1, 1025.7, 967.0, 798.2; $^1H$ NMR ($CDCl_3$, 600 MHz): δ 8.05 (s, 2H, Ar), 7.58 (s, 1H, Ar), 4.03-4.08 (m, 8H, 4×$OCH_2$), 3.21 (d, 4H, $J$ = 24Hz, 2×Ar-$CH_2$), 1.27 (t, 12H, $J$ = 6Hz, 4×$CH_3$); $^{13}C$ NMR ($CDCl_3$, 150 MHz): δ 148.52, 137.50, 134.47, 123.48, 62.67, 62.41, 34.11, 33.19, 16.66 ; HRMS (ESI+) exact mass calculated for $C_{16}H_{28}NO_8P_2$ (M+1): 424.1285 , Found: 424.1295.

Procedure for the synthesis of ethyl 4-(*n*-decyloxy)benzoate (**1a**)

A mixture of ethyl 4-hydroxybenzoate (18.1 mmol, 1equiv.), anhyd. $K_2CO_3$ (119.2 mmol, 6.6 equiv.), *n*-bromodecane (21.7 mmol, 1.2 equiv.) were taken in dry DMF (20 ml) and heated at 80 $^oC$ for 17 h under nitrogen atmosphere. Then the reaction mixture was poured into ice-water and extracted with $CH_2Cl_2$. The combined extract was washed with water and brine. Dried over anhyd. $Na_2SO_4$ and concentrated. The crude product was purified by column chromatography on neutral alumina. Elution with hexanes followed by 5% ethyl acetate-hexanes yielded the desired product.

$R_f$ = 0.46 (10% EtOAc-hexanes); colorless liquid; yield: 80%; IR (KBr pellet): $\nu_{max}$ in $cm^{-1}$ 2981.0, 2928.0, 2856.0, 1715.0, 1579.0, 1511.0, 1468.0, 1436.0, 1366.0, 1313.0, 1254.0,1167.0, 1103.0, 770.0, 647.0; $^1H$ NMR ($CDCl_3$, 400 MHz): δ 7.97 (d, 2H, $J$ = 11.6 Hz, Ar), 6.89 (d, 2H, $J$ = 4.8 Hz, Ar), 4.31 – 4.37 (m, 2H, $COOCH_2$), 3.98 – 4.01 (m, 2H, $J$ = 6.8 Hz, $OCH_2$), 1.77 – 1.81 (m, 2H, $CH_2$), 1.27-1.47 ( m, 14H, 7 × $CH_2$), 0.86-0.89

(m, 6H, 2 × $CH_3$); $^{13}$C NMR ($CDCl_3$, 100 MHz): 166.69, 163.12, 131.72, 122.90, 114.24, 68.43, 60.80, 32.11, 29.76, 29.58, 29.52, 29.34, 26.20, 22.89, 14.60, 14.31; HRMS (ESI) exact mass calculated for $C_{19}H_{31}O_3$ (M+1) : 307.2268, Found: 307.2276

Procedure for the synthesis of ethyl 3,4,-bis(decyloxy)benzoate (**1b**)

A mixture of ethyl 3,4-dihydroxybenzoate (16.5 mmol, 1 equiv.), anhyd. $K_2CO_3$ (108.9 mmol, 6.6 equiv.), *n*-bromodecane (36.2 mmol, 2.2 equiv.) were taken in dry DMF (20 ml) and heated at 80 $^oC$ for 17 h under nitrogen atmosphere. Then the reaction mixture was poured into ice-water and extracted with $CH_2Cl_2$. The combined extract was washed with water and brine. Dried over anhyd. $Na_2SO_4$ and concentrated. The crude product was purified by column chromatography on neutral alumina. Elution with hexanes followed by 5-10% ethylacetate-hexanes yielded the desired product.

$R_f$ = 0.54 (10% EtOAc-hexanes); Low melting white solid; yield: 70%; IR (KBr pellet): $\nu_{max}$ in $cm^{-1}$ 2921.0, 2850.0, 1710.0, 1596.0, 1517.0, 1466.0, 1424.0, 1338.0, 1212.0, 1104.0, 761.0, 628.0; $^1$H NMR ($CDCl_3$, 400 MHz): δ 7.63 (dd, 1H, $J_1$= 2 Hz, $J_2$= 2 Hz, Ar), 7.53 (d, 1H, $J$ = 2 Hz, Ar), 6.85 (d, 1H, $J$ = 8Hz, Ar), 4.32 – 4.37 (m, 2H, $COOCH_2$), 4.02-4.05 (m, 4H, 2 × $OCH_2$), 1.81 – 1.85 (m, 4H, 2 × $CH_2$), 1.27 - 1.48 (m, 28H, 14 × $CH_2$), 0.86-0.89 (m, 9H, 3 × $CH_3$). $^{13}$C NMR ($CDCl_3$, 100 MHz): 166.79, 153.38, 148.74, 123.69, 123.02, 114.60, 112.20, 69.55, 69.26, 60.92, 32.14, 29.85, 29.82, 29.80, 29.63, 29.60, 29.56, 29.43, 29.31, 26.23, 26.19, 22.91, 14.63, 14.32; HRMS (ESI) exact mass calculated for $C_{29}H_{51}O_4$ (M+1): 463.3782, Found: 463.3708.

Procedure for the synthesis of ethyl 3,4,5-tris(decyloxy) benzoate (**1c**)

A mixture of ethyl gallate (15.1 mmol, 1 equiv.), anhyd. $K_2CO_3$ (99.9 mmol, 6.6 equiv.), *n*-bromodecane (48.4 mmol, 3.2 equiv.) were taken in dry DMF (20 ml) and heated at 80 $^oC$ for 17 h under nitrogen atmosphere. Then the reaction mixture was poured into ice-water and extracted with $CH_2Cl_2$. The combined extract was washed with water and brine. Dried over anhyd. $Na_2SO_4$ and concentrated. The crude product was purified by column chromatography on neutral alumina. Elution with hexanes followed by 5-10% ethylacetate-hexanes yielded the desired product.

$R_f$ = 0.58 (10% EtOAc-hexanes); Low melting white solid; yield: 70%; IR (KBr pellet): $\nu_{max}$ in $cm^{-1}$ 2920.0, 2850.0, 1710.0, 1597.0, 1516.0, 1466.0, 1424.0, 1347.0, 1213.0, 1103.0, 760.0, 613.0; $^1$H NMR ($CDCl_3$, 400 MHz): δ 7.26 (s, 2H, Ar), 4.35-4.36 (m, 2H, $COOCH_2$), 4.01 (m, 6H, 3 × $OCH_2$), 1.27-1.81 (m, 48H, 24 × $CH_2$), 0.89 (m, 12H, 4 × $CH_3$), $^{13}$C NMR ($CDCl_3$, 100 MHz): 166.67, 152.99, 145.31, 125.24, 108.19, 73.68, 69.37, 61.14, 32.12, 30.53, 29.93, 29.84, 29.79, 29.60, 29.56, 26.29, 22.89, 14.30; HRMS (ESI+) exact mass calculated for $C_{39}H_{71}O_5$ (M+1): 619.5296, Found: 619.5218.

Procedure for the synthesis of 4-(decyloxy)benzoic acid **(17a)** [52]

The compound ethyl 4-(decyloxy)benzoate (8.6 mmol, 1 equiv.) was dissolved in ethanol (50 ml). A solution of NaOH (17.2 mmol, 2 equiv.) in minimum amount of water and

heated. Froth formed during heating was dissolved by the addition of water and refluxed for 17 h. Excess of the solvent was removed and the residue was added to the ice water. This solution was acidified with HCl and extracted with EtOAc. The Extract was dried over anhydrous $Na_2SO_4$ and concentrated. The crude solid was recrystallised with ethanol to get a white solid.

$R_f$ = 0.2 (50% EtOAc-hexanes); off brown solid; clearing point: 141 - 143 $^oC$; yield: 76%; IR (KBr pellet): $\nu_{max}$ in $cm^{-1}$ 3445.1, 2920.7, 2851.2, 1686.4, 1605.6, 1575.3, 1511.5, 1469.2, 1429.9, 1256.0, 1169.1, 1125.6, 1108.4, 1062.7, 771.0, 646.9; $^1H$ NMR ($CDCl_3$, 600 MHz): δ 8.06 (d, 2H, *J* = 6Hz, Ar), 6.93 (d, 2H, *J* =12Hz, Ar), 4.02 (t, 2H, *J* = 6Hz, 1 × -$OCH_2$), 1.26 - 1.83 (m, 16H, 8×$CH_2$), 0.87-0.90 (m, 3H, 1×$CH_3$) ; $^{13}C$ NMR ($CDCl_3$, 150 MHz): δ 172.03, 163.91, 132.55, 121.61, 114.42, 68.53, 32.11, 29.77, 29.57, 29.53, 29.32, 26.20, 22.90, 14.32 ; HRMS (APCI+) exact mass calculated for $C_{17}H_{27}O_3$ (M+1):279.1955, Found: 279.1972.

Procedure for the synthesis of 3,4-bis(decyloxy)benzoic acid **(17b)**[52]

The compound ethyl 3,4-bis(decyloxy)benzoate (9 mmol, 1 equiv.) was dissolved in ethanol (50 ml). A solution of NaOH (18 mmol, 2 equiv.) in minimum amount of water and heated. Froth formed during heating was dissolved by the addition of water and refluxed for 17 h. Excess of the solvent was removed and the residue was added to the ice water. This solution was acidified with HCl and extracted with EtOAc. The Extract was dried over anhydrous $Na_2SO_4$ and concentrated. The crude solid was recrystallised with ethanol to get a white solid.

$R_f$ = 0.3 (50% EtOAc-hexanes); white solid; m.p: 117 – 119 $^oC$; yield: 76%; IR (KBr pellet): $\nu_{max}$ in $cm^{-1}$ 3445.0, 2955.1, 2922.9, 2850.1, 1674.4, 1592.5, 1519.7, 1441.0, 1307.7, 1275.5, 1226.4, 1144.0, 769.8; $^1H$ NMR ($CDCl_3$, 600 MHz): δ 7.72 (d, 1H, *J* = 6Hz, Ar), 7.58 (s, 1H, Ar), 6.89 (d, 1H, *J* =12Hz, Ar), 4.04-4.07 (m, 4H, 2 × -$OCH_2$), 1.24 - 1.87 (m, 32H, 16×$CH_2$), 0.87 – 0.89 (m, 6H, 2×$CH_3$) ; $^{13}C$ NMR ($CDCl_3$, 150 MHz): δ 171.80, 154.10, 148.69, 124.75, 121.50, 114.57, 112.02, 69.45, 69.23, 32.13, 29.80, 29.59, 29.34, 29.23, 26.21, 22.92, 14.35; HRMS (APCI+) exact mass calculated for $C_{27}H_{47}O_4$ (M+1): 435.3469, Found: 435.3498.

Procedure for the synthesis of 3,4,5-tris(decyloxy)benzoic acid **(17c)** [52]

The compound ethyl 3,4,5-tris(decyloxy)benzoate (8 mmol, 1 equiv.) was dissolved in ethanol (50 ml). A solution of NaOH (16 mmol, 2 equiv.) in minimum amount of water and heated. Froth formed during heating was dissolved by the addition of water and refluxed for 17 h. Excess of the solvent was removed and the residue was added to the ice water. This solution was acidified with HCl and extracted with EtOAc. The Extract was dried over anhydrous $Na_2SO_4$ and concentrated. The crude solid was recrystallised with ethanol to get a white solid.

$R_f$ = 0.31(50% EtOAc-hexanes); white solid; m.p: 52 – 53 $^oC$; yield: 76%; IR (KBr pellet): $\nu_{max}$ in $cm^{-1}$ 3447.4, 2955.3, 2922.4, 2852.2, 1688.1, 1587.7, 1547.9, 1504.8, 1432.8, 1276.8, 1228.8, 1118.6, 1008.9, 722.9; $^1H$ NMR ($CDCl_3$, 400 MHz): δ 7.32 (s, 2H, Ar), 4.01 - 4.06 (m, 6H, 3× -$OCH_2$), 1.27 - 1.86 (m, 48H, 24×$CH_2$), 0.88 (t, 9H, *J* = 8Hz, 3×$CH_3$); $^{13}C$ NMR ($CDCl_3$, 150 MHz): δ 171.60, 153.05, 143.28, 123.77, 108.74, 73.77, 69.38, 32.14, 30.54, 29.82, 29.62, 29.57, 29.48, 26.29, 22.91, 14.35; HRMS (APCI+) exact mass calculated for $C_{37}H_{67}O_5$ (M+1):591.4983, Found: 591.5065.

Procedure for the synthesis of (3,4,5-tris(decyloxy)phenyl)methanol (**8c**)[39,40]

To a stirred suspension of lithium aluminium hydride (LAH) (18.2 mmol, 1.5 equiv.) in dry THF (20 ml) under nitrogen atmosphere, added the solution of ethyl 3,4,5-tris(decyloxy) benzoate (12.1 mmol, 1 equiv.) drop wise at 0 $^oC$. Then the reaction mixture was allowed to reach room temperature and stirred for 2 h. Excess LAH present was quenched by the addition of moist sodium sulphate. Reaction mixture was extracted with EtOAc (5 × 50 ml). The combined extracts were washed with water, dried over anhyd. $Na_2SO_4$ and concentrated *in vaccuo*. Purification was done by column chromatography over silica gel (60-120) with 10% EtOAc-hexanes as eluent.

$R_f$ = 0.12 (10% EtOAc-hexanes); white solid; m.p: 47 – 48 $^oC$; yield: 75%; IR (KBr pellet): $\nu_{max}$ in $cm^{-1}$ 3412.6, 2922.6, 2853.0, 1592.7, 1466.9, 1440.4, 1335.9, 1233.5, 1121.8, 812.0, 723.1 and 455.6; $^1H$ NMR ($CDCl_3$, 400 MHz): δ 6.55 (s, 2H, Ar), 4.58 (s, 2H, Ar-$CH_2$), 3.91- 3.98 (m, 6H, 3 × $OCH_2$), 1.27-1.82 (m, 48H, 24 × $CH_2$), 0.86 – 0.89 (m, 9H, 3 × $CH_3$); $^{13}C$ NMR ($CDCl_3$, 100 MHz): 153.46, 137.75, 136.27, 105.52, 73.65, 69.30, 65.84, 63.30, 33.01, 32.15, 32.12, 30.53, 29.95, 29.89, 29.86, 29.83, 29.80, 29.76, 29.63, 29.57, 26.34, 26.31, 25.94, 22.89, 14.31; HRMS (ESI+) exact mass calculated for $C_{37}H_{69}O_4$ (M+1): 577.5190, Found: 577.5185.

Procedure for the synthesis of 3,4-bis(decyloxy)benzaldehyde (**9b**)[53]

A mixture of 3,4-dihydroxybenzaldehyde (14.5 mmol, 1equiv.), anhyd. $K_2CO_3$ (60.9 mmol, 4.2 equiv.), *n*-bromodecane (31.9 mmol, 2.2 equiv.) were taken in dry DMF (20 ml) and heated at 80 $^oC$ for 17 h under nitrogen atmosphere. Then the reaction mixture was poured into ice-water and extracted with $CH_2Cl_2$. The combined extract was washed with water and brine. Dried over anhyd. $Na_2SO_4$ and concentrated. The crude product was recrystallised with ethanol to get the pure product.

$R_f$ = 0.5 (10% EtOAc-hexanes); white solid; m.p: 62 – 64 $^oC$; yield: 80%; IR (KBr pellet): $\nu_{max}$ in $cm^{-1}$ 3342.0, 3086.8, 2953.6, 2921.4, 2850.5, 2754.5, 1687.4, 1591.4, 1438.6, 1394.4, 1345.5, 1235.5, 1133.0, 723.4, 657.5, and 586.5; $^1H$ NMR ($CDCl_3$, 400 MHz): δ 9.83 (s, 1H, CHO), 7.41 (d, 1H, *J* = 8Hz, Ar), 7.39 (s, 1H, Ar), 6.94 (d, 1H, *J* = 8Hz, Ar), 4.03-4.09 (m, 4H, 2× $OCH_2$), 1.32 - 1.87 (m, 32H, 16 × $CH_2$), 0.86 - 0.89 (m, 6H, 2 × $CH_3$); $^{13}C$ NMR ($CDCl_3$, 100 MHz): 191.24, 154.89, 149.64, 130.07, 126.82, 111.95,

111.15, 69.33, 32.12, 29.83, 29.80, 29.78, 29.76, 29.59, 29.56, 29.28, 29.18, 26.19, 26.16, 22.89, 14.32; HRMS (ESI+) exact mass calculated for $C_{27}H_{47}O_3$ (M+1): 419.3520, Found: 419.3517.

Procedure for the synthesis of 3,4,5-tris(decyloxy)benzaldehyde (**9c**) [53]

The compound (3,4,5-tris(decyloxy)phenyl)methanol (8.7 mmol, 1 equiv.) was taken in $CH_2Cl_2$ (10 vol.). To this pyridinium chlorochromate (8.7 mmol, 1 equiv.) adsorbed over equal amount of silica gel is added and stirred at room temperature for 1 h. The reaction mixture was filtered over celite bed and concentrated to get the crude product, which was further purified by column chromatography on silica gel (60-120) with 10% EtOAc-hexanes as eluent.

$R_f$ = 0.51 (10% EtOAc-hexanes); low melting white solid; yield: 70%; IR (KBr pellet): $\nu_{max}$ in $cm^{-1}$ 3369.2, 2950.8, 2923.7, 2852.9, 2728.3, 1742.8, 1695.6, 1585.8, 1439.7, 1382.4, 1332.6, 1228.6, 1117.5, 721.0, 645.6 and 580.4; $^1$H NMR ($CDCl_3$, 400 MHz): δ 9.82 (s, 1H, CHO), 7.08 (s, 2H, Ar), 4.01 - 4.07 (m, 6H, 3 × $OCH_2$), 1.27 - 1.84 (m, 48H, 24 × $CH_2$), 0.86 – 0.89 (m, 9H, 3 × $CH_3$); $^{13}$C NMR ($CDCl_3$, 100 MHz): 191.55, 153.72, 144.00, 131.63, 108.01, 73.84, 69.41, 32.15, 32.12, 30.54, 29.93, 29.88, 29.84, 29.79, 29.76, 29.59, 29.56, 29.45, 26.28, 26.23, 22.90, 14.33; HRMS (ESI+) exact mass calculated for $C_{37}H_{67}O_4$ (M+1): 575.5034, Found: 575.5033.

Procedure for the synthesis of 1,3-bis(3,4-bis(decyloxy)styryl)-5-nitrobenzene (**18a**)[53]

A suspension of sodium hydride (10.8 mmol, 12 equiv.) in dry THF was prepared and compound **20** (0.9 mmol, 1equiv.) in dry THF was added at 0 °C. After stirring for 15 minutes, compound **9b** (1.8 mmol, 2 equiv.) in dry THF was added dropwise and the reaction mixture stirred for 3 h under argon atmosphere. The excess THF was distilled off and the reaction mixture was washed with water and neutralized with 1:1 HCl. It was then extracted with DCM and dried over anhydrous sodium sulfate. The product was purified by column chromatography using 2% ethyl acetate-hexane as eluent and silica as packing material.

$R_f$ = 0.4 (10% EtOAc-hexanes); yellow solid; m.p: 94 – 96 °C; yield: 53%; IR (KBr pellet): $\nu_{max}$ in $cm^{-1}$ 3445.3, 2953.9, 2921.8, 2849.9, 1630.2, 1534.4, 1294.9, 1263.2, 1236.8, 1136.6, 1071.4, 1022.5, 959.8 ; $^1$H NMR ($CDCl_3$, 600 MHz): δ 8.18 (s, 2H, Ar), 7.82 (s, 1H, Ar), 7.19 (d, 2H, $J$ =18Hz, =CH-), 7.11 (s, 2H, Ar), 7.07 (d, 2H, $J$ =12Hz, Ar), 6.99 (d, 2H, $J$ =18Hz, =CH-), 6.89 (d, 2H, $J$ = 6Hz, Ar), 4.06 (t, 4H, $J$ = 6Hz, 2 × -$OCH_2$), 4.03 (t, 4H, $J$ = 6Hz, 2×-$OCH_2$), 1.26 - 1.88 (m, 64H, 32 × $CH_2$), 0.87-0.90 (m, 12H, 4×$CH_3$); $^{13}$C NMR ($CDCl_3$, 150 MHz): δ 150.15, 149.55, 149.45, 139.86, 131.88, 129.73, 129.58, 124.25, 120.83, 118.95, 113.80, 111.91, 69.64, 69.47, 32.14, 29.87, 29.81, 29.68, 29.65, 29.58, 29.48, 26.29, 26.26, 22.91, 14.33; MALDI-TOF exact mass calculated for $C_{62}H_{97}NO_6$ ($M^+$): 951.7316, Found: 951.7040.

Procedure for the synthesis of 5-(3-(3,4,5-tris(decyloxy)styryl)-5-nitrostyryl)-1,2,3-tris(decyloxy)benzene **(18b)** [53]

A suspension of sodium hydride (14.4 mmol, 12 equiv.) in dry THF was prepared and compound **20** (1.2 mmol, 1 equiv.) in dry THF was added at 0 $^{o}$C. After stirring for 15 minutes, compound **9c** (2.4 mmol, 2 equiv.) in dry THF was added dropwise and the reaction mixture stirred for 3h under Ar - atmosphere. The excess THF was distilled off and the reaction mixture was washed with water and neutralized with 1:1 HCl. It was then extracted with DCM and dried over sodium sulfate. The product was purified by column chromatography using 2% ethyl acetate-hexane as eluent and silica as packing material.

$R_f$ = 0.4 (5% EtOAc-hexanes); yellow solid; m.p: 81 – 83 $^{o}$C; yield: 60%; IR (KBr pellet): $\nu_{max}$ in cm$^{-1}$ 3444.6, 2956.6, 2922.8, 2852.1, 1581.7, 1535.6, 1506.3, 1341.7, 1240.5, 1125.8, 1020.08, 957.5 ; $^{1}$H NMR ($CDCl_3$, 400 MHz): δ 8.20 (s, 2H, Ar), 7.83 (s, 1H, Ar), 7.16 (d, 2H, *J* =16Hz, =CH-), 7.00 (d, 2H, *J* =16Hz, =CH-), 6.75 (s, 4H, Ar), 4.02 – 4.05 (m, 8H, 4 × $OCH_2$), 3.99 (t, 4H, *J* = 8Hz, 2×$OCH_2$), 1.24 - 1.87 (m, 96H, 48 × $CH_2$), 0.88 (t, 18H, *J* = 8Hz, 6×$CH_3$) ; $^{13}$C NMR ($CDCl_3$, 100 MHz): δ 153.63, 149.45, 139.67, 139.32, 132.24, 131.63, 129.93, 125.29, 119.25, 105.77, 73.82, 69.48, 69.44, 32.17, 32.14, 30.58, 29.99, 29.97, 29.91, 29.88, 29.85, 29.83, 29.74, 29.67, 29.66, 28.63, 29.60, 29.58, 26.35, 22.95, 22.93, 22.91, 14.36, 14.33 ; HRMS (ESI+) exact mass calculated for $C_{82}H_{138}O_8$ (M+1): 1265.0417, Found: 1265.0342.

Procedure for the synthesis of 3,5-bis((*E*)-3,4-bis(decyloxy)styryl)aniline (**19a**)[54]

A solution of compound **18a** (0.4 mmol, 1equiv.) in THF and $CH_3OH$ (2:1) 9 ml. Adding $HCOONH_4$ (2.4 mmol, 6.1 equiv.) and Zn powder (2.4 mmol, 6.1 equiv.) simultaneously and left for stirring at room temperature for 1 hr. After completion of reaction, the crude solution was filtered through a celite bed. The filtrate was concentrated to remove methanol and THF. Then it was extracted with DCM, washed with water and dried over anhydrous $Na_2SO_4$ and concentrated in vacuo. The product was purified by column chromatography using 5-10% ethylacetate-hexane as eluent and neutral alumina as packing material.

$R_f$ = 0.3 (20% EtOAc-hexanes); off white solid; m.p: 88 – 90 $^{o}$C; yield: 90%; IR (KBr pellet): $\nu_{max}$ in cm$^{-1}$ 3442.2, 2956.3, 2922.0, 2851.4, 1629.6, 1589.5, 1516.0, 1465.6, 1268.4, 1231.5, 1136.2, 1070.5, 1021.5, 955.8; $^{1}$H NMR ($CDCl_3$, 600 MHz): δ 7.08 (s, 2H, Ar), 7.05 (s, 1H, Ar), 7.01-7.04 (m, 4H, 2 × =CH-, 2 × Ar), 6.85 - 6.90 (m, 4H, 2 × =CH-, 2 × Ar), 6.73 (s, 2H, Ar), 4.05 (t, 4H, *J* = 6Hz, 2 × -$OCH_2$), 4.01 (t, 4H, *J* = 6Hz, 2 × -$OCH_2$), 1.26-1.87 (m, 64H, 32×$CH_2$), 0.87-0.90 (m, 12H, 4×$CH_3$); $^{13}$C NMR ($CDCl_3$, 150 MHz): δ 149.47, 149.36, 146.94, 139.14, 130.75, 128.84, 126.89, 120.23, 116.02, 113.97, 112.16, 111.80, 69.57, 69.52, 32.14, 29.87, 29.82, 29.68, 29.65, 29.58, 29.51, 26.29, 26.26, 22.91, 14.33; HRMS (ESI+) exact mass calculated for $C_{62}H_{100}NO_4$ (M+1): 922.7647, Found: 922.7443.

Procedure for the synthesis of 3,5-bis((*E*)-3,4,5-tris(decyloxy)styryl)aniline (**19b**) [54]

A solution of compound **18b** (0.56 mmol, 1 equiv.) in THF and $CH_3OH$ (2:1) 10ml was made. To this added $HCOONH_4$ (2.26 mmol, 6.1 equiv.) and Zn powder (2.26 mmol, 6.1 equiv.) simultaneously and left for stirring at room temperature for 1 h. After completion of the reaction, the crude solution was filtered through a celite bed. The filtrate was concentrated to remove methanol and THF. Then it was extracted with DCM, washed with water and dried over anhydrous $Na_2SO_4$ and concentrated in vacuo. The product was purified by column chromatography using 5-10% ethylacetate-hexane as eluent and neutral alumina as packing material.

$R_f$ = 0.31 (5% EtOAc-hexanes); off white solid; m.p: 63 – 65 $^oC$; yield: 80%; IR (KBr pellet): $\nu_{max}$ in $cm^{-1}$ 3441.3, 2959.3, 2924.6, 2853.0, 1630.3, 1587.0, 1505.2, 1330.9, 1241.1, 1124.4, 1025.1, 800.1; $^1H$ NMR ($CDCl_3$, 400 MHz): δ 7.06 (s, 1H, Ar), 7.00 (d, 2H, *J* = 16Hz, =CH-), 6.9 (d, 2H, *J* = 16Hz, =CH-), 6.74 (s, 2H, Ar), 6.71 (s, 4H, Ar), 4.01 – 4.03 (m, 8H, 4 × -0$CH_2$), 3.96 – 3.99 (m, 4H, 2×-$OCH_2$), 3.71 (bs, 2H, -$NH_2$), 1.27 - 1.86 (m, 96H, 48 × $CH_2$), 0.87 – 0.90 (m, 18H, 6 × $CH_3$); $^{13}C$ NMR ($CDCl_3$, 100 MHz): δ 153.50, 147.03, 138.95, 138.55, 132.75, 129.18, 127.92, 116.16, 112.39, 105.44, 73.77, 69.40, 32.17, 32.14, 30.57, 29.97, 29.90, 29.88, 29.84, 29.82, 29.73, 29.68, 29.66, 29.62, 29.58, 26.36, 22.92, 22.91, 14.33 ; HRMS (APCI+) exact mass calculated for $C_{82}H_{141}NO_6$ (M+2): 1236.0748, Found: 1236.2715.

Procedure for the synthesis of *N*-(3,5-bis(3,4-bis(decyloxy)styryl)phenyl)-3,4-bis(decyloxy) benzamide (**SA1**)

Compound **17b** (0.24 mmol, 1 equiv.) in 6 ml of thionyl chloride and DMF (catalytic amount) was refluxed for 4 h. The excess of thionyl chloride was removed by distillation and the crude acid choride (0.24 mmol, 1.1 equiv.) in THF was added dropwise to a solution of compound **19a** (0.22 mmol, 1 equiv.) and $Et_3N$ (0.43 mmol, 2 equiv.) in THF (10 ml). The reaction mixture was refluxed for 12 h. After cooling, THF was evaporated under reduced pressure and the residue was extracted with DCM. The extract was washed with water and brine. Dried over anhydrous $Na_2SO_4$ and concentrated. The crude product was further purified through column chromatography on neutral alumina. Elution with 5-10% ethylacetate-hexane yielded the desired product.

$R_f$ = 0.2 (10% EtOAc-hexanes); off brown solid; yield: 52%; IR (KBr pellet): $\nu_{max}$ in $cm^{-1}$ 3440.3, 3284.7, 2955.3, 2923.5, 2853.0, 1660.1, 1598.0, 798.7, 723.9 ; $^1H$ NMR ($CDCl_3$, 600 MHz): δ 7.83 (s, 1H, NH), 7.70 (s, 2H, Ar), 7.52 (s, 1H, Ar), 7.38-7.40 (m, 2H, Ar), 7.11 (m, 4H, 2× = CH-, 2×ArH), 7.04 (d, 2H, *J* = 6Hz, Ar), 6.97 (d, 2H, *J* =18Hz, Ar), 6.92 (d, 1H, *J* = 6Hz, Ar), 6.87 (d, 2H, *J* = 6Hz, Ar), 4.04 - 4.09 (m, 8H, 4 × -$OCH_2$), 4.00 - 4.03 (m, 4H, 2 × -$OCH_2$), 1.25-1.88 (m, 96H, 48×$CH_2$), 0.87 - 0.89 (m, 18H, 6×$CH_3$); $^{13}C$ NMR ($CDCl_3$, 150 MHz): δ 165.67, 152.46, 149.38, 149.26, 139.09, 138.92, 130.46, 129.43, 127.29, 126.30, 120.83, 120.26, 119.83, 116.59, 113.77, 112.96, 112.88, 112.29, 111.59, 69.47, 32.13, 29.85, 29.57, 26.24, 22.90, 14.33; MALDI-TOF exact mass calculated for $C_{89}H_{143}NO_7Na$ ($M+Na^+$): 1361.0757, Found: 1361.464.

Procedure for the synthesis of *N*-(3,5-bis(3,4-bis(decyloxy)styryl)phenyl)-3,4,5-tris(decyloxy) benzamide (**SA2**)

Compound **17c** (0.18 mmol, 1.1 equiv.) in 5 ml of thionyl chloride and DMF (catalytic amount) was refluxed for 4 h. The excess of thionyl chloride was removed by distillation and the crude acid chloride (0.18 mmol, 1.1 equiv.) in THF was added dropwise to a solution of compound **19a** (0.16 mmol, 1 equiv.) and $Et_3N$ (0.33 mmol, 2 equiv.) in THF (9 ml). The reaction mixture was refluxed for 12 h. After cooling, THF was evaporated under reduced pressure and the residue was extracted with DCM. The extract was washed with water and brine and dried over anhydrous $Na_2SO_4$ and concentrated. The crude product was further purified through column chromatography on neutral alumina. Elution with 5-10% ethylacetate-hexane yielded the desired product.

$R_f$ = 0.4 (10% EtOAc-hexanes); off brown solid; yield: 53%; IR (KBr pellet): $\nu_{max}$ in $cm^{-1}$ 3444.1, 3280.7, 2964.0, 2923.5, 2853.1, 1660.0, 1598.1, 724.2, 682.9 ; $^1$H NMR ($CDCl_3$, 600 MHz): δ 7.66 (s, 2H, Ar), 7.44 (s, 2H, Ar), 7.26 (s, 1H, Ar), 7.10-7.12 (m, 4H, 2 × =CH-, 2 × Ar-H), 7.04 (d, 2H, *J* = 12Hz, Ar ), 6.97 (d, 2H, *J* = 12Hz, 2 × =CH-), 6.87 (d, 2H, *J* = 6Hz, Ar), 4.01-4.07 (m, 14H, 7×$OCH_2$), 1.22 - 1.87 (m, 112H, 56×$CH_2$), 0.87 - 0.90 (m, 21H, 7×$CH_3$) ; $^{13}$C NMR ($CDCl_3$, 150 MHz): δ 162.64, 149.50, 149.47, 149.00, 139.19, 138.22, 131.79, 130.43, 129.80, 126.13, 121.42, 121.22, 120.55, 130.36, 116.80, 113.87, 111.68, 74.74, 69.49, 32.13, 30.46, 30.39, 29.87, 29.85, 29.82, 29.71, 29.67, 29.57, 29.49, 26.28. 26.25, 26.16, 22.91, 14.33; MALDI-TOF exact mass calculated for $C_{99}H_{162}NO_8$ ($M\text{-}H^+$): 1493.2306, Found: 1493.123.

Procedure for the synthesis of *N*-(3,5-bis(3,4,5-tris(decyloxy)styryl) phenyl)-4-(decyloxy) benzamide (**SA3**)

Compound **17a** (0.16 mmol, 1.3 equiv.) in 4 ml of thionyl chloride and DMF (catalytic amount) was refluxed for 4 h. The excess of thionyl chloride was removed by distillation and the crude acid chloride (0.16 mmol, 1.3 equiv.) in THF was added dropwise to a solution of compound **19b** (0.12 mmol, 1 equiv.) and $Et_3N$ (0.24 mmol, 2 equiv.) in THF (8 ml). The reaction mixture was refluxed for 12 h. After cooling, THF was evaporated under reduced pressure and the residue was extracted with DCM. The extract was washed with water and brine and dried over anhydrous $Na_2SO_4$ and concentrated. The crude product was further purified through column chromatography on neutral alumina. Elution with 5-10% ethylacetate-hexane yielded the desired product.

$R_f$ = 0.39 (10% EtOAc-hexanes); off brown solid; yield: 54%; IR (KBr pellet): $\nu_{max}$ in $cm^{-1}$ 3441.2, 3280.7, 2952.9, 2853.0, 1660.0, 1598.1, 798.8, 723.3; $^1$H NMR ($CDCl_3$, 600 MHz): δ 7.86 (d, 2H, *J* = 12Hz, Ar), 7.80 (bs, 1H, NH), 7.71 (s, 2H, Ar), 7.39 (s, 1H, Ar), 7.08 (d, 2H, *J* = 12Hz, 2 × =CH-), 6.97 - 6.99 (m, 4H, 2 × =CH-, 2 × Ar-H), 6.73 (s, 4H, Ar), 4.02 (t, 10H, *J* = 6Hz, 5 × -$OCH_2$), 3.98 (t, 4H, *J* = 6Hz, 2 × -$OCH_2$) 1.21 - 1.88 (m, 112H, 56×$CH_2$), 0.88 (t, 21H, *J* = 6Hz, 7×$CH_3$); $^{13}$C NMR ($CDCl_3$, 150 MHz): δ 165.52,

162.46, 153.51, 139.09, 138.83, 138.60, 132.51, 129.89, 129.06, 127.33, 126.90, 120.94, 116.91, 114.74, 105.42, 73.79, 69.39, 68.54, 32.15, 30.57, 29.98, 29.91, 29.89, 29.84, 29.79, 29.68, 29.59, 29.54, 29.36, 26.36, 22.91, 14.34 ; MALDI-TOF exact mass calculated for $C_{99}H_{163}NO_8Na$ ($M+Na^+$): 1517.2271, Found: 1517.654.

Procedure for the synthesis of of *N*-(3,5-bis(3,4,5-tris(decyloxy)styryl) phenyl)-3,4-bis(decyloxy) benzamide (**SA4**)

Compound **17b** (0.10 mmol, 1.3 equiv.) in 4 ml of thionyl chloride and DMF (catalytic amount) was refluxed for 4 h. The excess of thionyl chloride was removed by distillation and the crude acid chloride (0.10 mmol, 1.3 equiv.) in THF was added dropwise to a solution of compound **19b** (0.08 mmol, 1 equiv.) and $Et_3N$ (0.16 mmol, 2 equiv.) in THF (8 ml). The reaction mixture was refluxed for 12 h. After cooling, THF was evaporated under reduced pressure and the residue was extracted with DCM. The extract was washed with water and brine. Dried over anhydrous $Na_2SO_4$ and concentrated. The crude product was further purified through column chromatography on neutral alumina. Elution with 5-10% ethylacetate-hexane yielded the desired product.

$R_f$ = 0.45 (10% EtOAc-hexanes); offbrown solid; yield: 76%; IR (KBr pellet): $\nu_{max}$ in $cm^{-1}$ 3444.6, 3285.9, 2955.3, 2853.1, 1660.0, 1598.0, 965.6, 798.9; $^1H$ NMR ($CDCl_3$, 600 MHz): δ 7.91 (s, 1H, NH), 7.73 (s, 2H, Ar), 7.52 (s, 1H, Ar), 7.40 (d, 1H, *J* = 6Hz, Ar), 7.37 (s, 1H, Ar), 7.08 (d, 2H, *J* =18Hz, Ar), 6.98 (d, 2H, *J* = 18Hz, Ar), 6.90 (d, 1H, *J* = 6Hz, Ar), 6.72 (s, 4H, Ar), 3.97 - 4.08 (m, 16H, 8 × -$OCH_2$), 1.22 - 1.87 (m, 128H, 64 × $CH_2$), 0.87- 0.90 (m, 24H, 8 × $CH_3$); $^{13}C$ NMR ($CDCl_3$, 150 MHz): δ 165.66, 153.49, 152.62, 149.39, 139.12, 138.80, 138.60, 132.51, 129.86, 127.32, 120.99, 119.71, 116.85, 113.05, 112.42, 105.40, 73.78, 69.62, 69.37, 32.17, 32.14, 30.57, 29.97, 29.89, 29.83, 29.80, 29.68, 29.67, 29.63, 29.58, 29.43, 29.34, 26.35, 26.34, 26.22, 22.91, 14.33; MALDI-TOF exact mass calculated for $C_{109}H_{184}NO_9$ (M+1): 1651.3966, Found: 1651.2780.

Procedure for the synthesis of *N*-(3,5-bis(3,4,5-tris(decyloxy)styryl)phenyl)-3,4,5-tris(decyloxy)benzamide (**SA5**)

Compound **17c** (0.04 mmol, 1.1 equiv.) in 4 ml of thionyl chloride and DMF (catalytic amount) was refluxed for 4 h. The excess of thionyl chloride was removed by distillation and the crude acid chloride (0.09 mmol, 1.1 equiv.) in THF was added dropwise to a solution of compound **19b** (0.08 mmol, 1 equiv.) and $Et_3N$ (0.16 mmol, 2 equiv.) in THF (8 ml). The reaction mixture was refluxed for 12 h. After cooling, THF was evaporated under reduced pressure and the residue was extracted with DCM. The extract was washed with water and brine. Dried over anhydrous $Na_2SO_4$ and concentrated. The crude product was further purified through column chromatography on neutral alumina. Elution with 5-10% ethylacetate-hexane yielded the desired product.

$R_f$ = 0.5 (10% EtOAc-hexanes); off brown solid; yield: 70%; IR (KBr pellet): $\nu_{max}$ in $cm^{-1}$ 3444.1, 3274.8, 2955.3, 2923.4, 2853.0, 1660.1, 1597.9, 798.6, 723.6; $^1H$ NMR ($CDCl_3$,

600 MHz): δ 8.25 (s, 1H, NH), 7.75 (s, 2H, Ar), 7.47 (s, 1H, Ar), 7.28 (d, 2H, *J* = 24Hz, Ar), 7.13, (d, 2H, *J* =12Hz, =CH-), 7.03 (d, 2H, *J* = 12Hz, =CH-), 6.78 (s, 4H, Ar), 4.01 - 4.12 (m, 18H, 9×$OCH_2$), 1.29-1.90 (m, 144H, 72×$CH_2$), 0.92 (t, 27Hz, 9×$CH_3$); $^{13}$C NMR ($CDCl_3$, 150 MHz): δ 164.41, 153.52, 150.02, 145.45, 138.93, 138.67, 132.46, 130.04, 129.68, 127.23, 121.19, 117.37, 116.91, 110.04, 105.46, 74.59, 74.30, 73.79, 69.40, 69.32, 32.17, 32.14, 30.57, 30.51, 30.44, 29.98, 29.91, 29.89, 29.83, 29.74, 29.68, 29.66, 29.63, 29.58, 29.41, 26.35, 26.27, 26.24, 22.91, 14.33; MALDI-TOF exact mass calculated for $C_{119}H_{203}NO_{10}$ ($M^+$): 1806.5407, Found: 1806.233.

## 6.5. References


1. P. Terech and R. G. Weiss, *Chem. Rev.*, 1997, **97**, 3133-3160.
2. S. Chandrasekhar, B. K. Sadashiva and K. A. Suresh, *Pramana*, 1977, **9**, 471-480.
3. M. O'Neill and S. M. Kelly, *Adv. Mater.*, 2011, **23**, 566–584.
4. B. A. Jones, M. J. Ahrens, M.-H. Yoon, A. Facchetti, T. J. Marks and M. R. Wasielewski, *Angew. Chem., Int. Ed.*, 2004, **43**, 6363–6366.
5. H. C. Hesse, J. Weickert, M. Al-Hussein, L. Do¨ssel, X. Feng, K. Mullen and L. S. Mende, *Sol. Energy Mater. Sol. Cells*, 2010, **94**, 560–567.
6. Q. Li, Self-Organized Semiconductors: From Materials to Device Applications, John Wiley & Sons, New York, 2011.
7. L. Schmidt Mende, A. Fechtenkotter, K. Mullen, E. Moons, R. H. Friend and J. D. Mackenzie, *Science*, 2001, **293**, 1119-1122.
8. T. Wöhrle, I. Wurzbach, J. Kirres, A. Kostidou, N. Kapernaum, J. Litterscheidt, J. C. Haenle, P. Staffeld, A. Baro, F. Giesselmann, S. Laschat, *Chem Rev*., 2016, **116**, 1139–1241.
9. S. Sergeyev, W. Pisula, Y. H. Geerts, *Chem Soc Rev*., 2007, **36**, 1902–1929.
10. H. Detert, M. Lehmann and H. Meier, *Materials*, 2010, **3**, 3218–3330.
11. M. Lehman, *Chem. Eur. J*. 2009, **15**, 3638−3651.
12. M. Lehman, Handbook of Liquid Crystals, 2nd ed. Vol. 5, p. 243.
13. T. Wöhrle, S. J. Beardsworth, C. Schilling, A. Baro, F. Giesselmann, S. Laschat, *Soft Matter*, 2016, **12**, 3730-3736.
14. V. Percec, M. Glodde, T. K. Bera, Y. Miura, I. Shiyanovskaya, K. D. Singer, V. S. K. Balagurusamy, P. A. Heiney, I. Schnell, A. Rapp, H. W. Spiess, S. D. Hudson, H. Duan, *Nature* 2002, **419**, 384−387.
15. S. S. Babu, V. K. Praveen and A. Ajayaghosh, *Chem Rev*., 2014, **114**, 1973.
16. S. Ghosh, V. K. Praveen, A. Ajayaghosh, *Annu. Rev. Mater. Res.*, 2016, **46**, 235–262.
17. A. Friggeri, B. L. Feringa and J. Esch, *J. Controlled Release*, 2004, **97**, 241–248.
18. V. K. Praveen, S. J. George, R. Varghese, C. Vijayakumar, A. Ajayaghosh, *J. Am. Chem. Soc.*, 2006, **128**, 7542–7550.
19. A. Ajayaghosh, V. K. Praveen, C. Vijayakumar, *Chem Soc Rev*., 2008, **37**, 109–122.
20. S. Basak, J. Nanda and A. Banerjee, *Chem. Commun*., 2014, **50**, 2356-2359.

21. K. K. Kartha, A. Sandeep, V. K. Praveen, A. Ajayaghosh, *Chem. Rec.*, 2015, 15, 252–265.
22. R. Thirumalai, R. D. Mukhopadhyay, V. K. Praveen, A. Ajayaghosh, *Sci. Rep.*, 2015, **5**, 9842.
23. F. Würthner, C. Thalacker, S. Diele and C. Tschierske, *Chem. Eur. J.*, 2001, **7**, 2245–2253.
24. R. Hu, N. L. C. Leung and B. Z. Tang, *Chem. Soc. Rev.*, 2014, **43**, 4494.
25. V. K. Praveen, C. Ranjith, N. Armaroli, *Angew. Chem. Int. Ed.*, 2014, **53**, 365–368.
26. S. Mukherjee, P. Thilagar, *Dyes and Pigments*, 2014, **110**, 2–27.
27. C. J. Tonzola, A. P. Kulkarni, A. P. Gifford, W. Kaminsky and S. A. Jenekhe, *Adv. Funct. Mater.*, 2007, **17**, 863-874.
28. F. Camerel, R. Ziessel, B. Donnio, C. Bourgogne, D. Guillon, M. Schmutz, C. Iacovita and J.-P. Bucher, *Angew. Chem., Int. Ed.*, 2007, **46**, 2659–2662.
29. S. S. Babu, V. K. Praveen, K. K. Kartha, S. Mahesh, A. Ajayaghosh, *Chem. Asian J.*, 2014, **9,** 1830–1840.
30. R. Yoshida, *Adv. Mater.*, 2010, **22**, 3463–3483.
31. A. Gopal, R. Varghese, A. Ajayaghosh, *Chem. Asian J.*, 2012, **7**, 2061–2067.
32. R. Ziessel, G. Pickaert, F. Camerel, B. Donnio, D. Guillon, M. Cesario, and T. Prange, *J. Am. Chem. Soc*., 2004, **126**, 12403-12413.
33. E. Westphal, M. Prehm, I. H. Bechtold, C.Tschierske and Hugo Gallardo, *J. Mater. Chem. C*, 2013, **1**, 8011-8022.
34. M. Palma, J. Levin, V. Lemaur, A. Liscio, V. Palermo, J. Cornil, Y. Geerts, M. Lehmann, and P. Samorì, *Adv. Mater.*, 2006, **18**, 3313–3317.
35. D. Miyajima, F. Araoka, H. Takezoe, J. Kim, K. Kato, M. Takata and T. Aida, *Science*, 2012, **336**, 209–213.
36. H. Bleier, *Organic Materials for Photonics, Ed.: G. Zerbi, Elsevier*, *Amsterdam*, 1993, 77-101.
37. C. Coya, A. de Andrés, C. Zaldo, A. L. Álvarez, B. Arredondo, R. Gómez, J. L. Segura, and C. Seoane, *Journal Of Applied Physics*, 2009, **105**, 044510 – 044510-6.
38. M. Lehmann, I. Fischbach, H. W. Spiess, and H. Meier, *J. Am. Chem. Soc.*, 2004, **126**, 772-784.
39. A. S. Achalkumar, C. V. Yelamaggad, *Tetrahedron Letters*, 2012, **53**, 7108–7112.
40. A. S. Achalkumar, B. N. Veerabhadraswamy, U. S. Hiremath, D. S. Shankar Rao, S. K. Prasad, C. V. Yelamaggad, *Dyes and Pigments,* 2016, **132,** 291-305.
41. D. Huang, M. Prehm, H. Gao, X. Cheng, Y. Liu and C. Tschierske*, RSC Adv.*, 2016, **6**, 21387-21395.
42. Y. Hong, J. W. Y. Lama and B. Z. Tang, *Chem. Commun*., 2009, 4332–4353.
43. A. Takahashi, M. Sakai and T. Kato, *Polym. J*., 1980, **12**, 335-341.
44. H. Sakashita, A. Nishitani, Y. Sumiya, H. Terauchi, K. Ohta, I. Yamamoto, *Mol. Cryst. Liq. Cryst. Inc. Nonlinear Opt*. 1988, **163 (1)**, 211−219.
45. M. Mansueto, S. Sauer, M. Butschies, M. Kaller, A. Baro, R. Woerner, N. H. Hansen, G. Tovar, J. Pflaum and S. Laschat, *Langmuir*, 2012, **28(22),** 8399-8407.
46. V. Prasad, A. Roy, N. G. Nagaveni and K. Gayathri, *Liq. Cryt*. 2011, **38(10)**, 1301-1314.

47. C. W. Ong, Y. C. Chan, M. –C. Yeh, H. –Y. Lin and H. –F. Hsu, *RSC Adv.* 2013, **3** (23), 8657-8659.
48. W. J. Bailey and J.Economy, *J. Org. Chem*., 1958, **23**, 1002-1004.
49. B. S. Chhikara, N. Kumar, V. Tandon and A. K. Mishra, *Bioorganic and Medicinal Chemistry*, 2005, **13**, 4713 – 4720.
50. S-D. Cho, Y-D. Park, J-J. Kim, J. R. Falck and Y-J. Yoon, *Bull. Korean Chem. Soc*. 2004, **25**, 407-409.
51. M. Arendt, W. Sun, J. Thomann, X. Xie and T. Schrader, *Chem. Asian J.,* 2006, **1**, 544 – 554.
52. K. Kaneko and N. Nakamura, *Liquid Crystals*, 2007, **34**, 229–234.
53. S. Varghese, N. S. Saleesh Kumar, A. Krishna, D. S. S. Rao, S. K. Prasad and S. Das, *Adv. Funct. Mater.,* 2009, **19**, 2064–2073.
54. D. C. Gowda, B. Mahesh and S. Gowda, *Indian Journal of Chemistry*, 2001, **40B**, 75-77.